Transcription dynamics during metabolic changes

Meredith Wouters

A thesis submitted for the degree of Doctor of Philosophy

Supervisor: Prof. Jane Mellor

Department of Biochemistry, University of Oxford

Green Templeton College, Hilary Term, 2023

Acknowledgements

Over the past four years, I have been honoured to work and interact with many great human beings.

First, I would like to thank my supervisor, Prof. Jane Mellor, for the regular uplifting meetings, scientific discussions, and for her supervision. Many thanks to Dr. Andrew Angel for his collaboration. This project would not have been possible without his “RNA-FISH analytical pipeline”. Thank you for taking the time and effort and for the mathematics and bioinformatics advice. As a novice, embarking on this coding journey has truly transformed me.

To Prof. Catherine Pears and Dr. Folkert van Werven, thank you for acting as my examiners, taking the time to read my thesis and for your critical evaluation of my work.

My gratitude to Darragh Ennis, Joshua Titlow, and Jeff Lee from the Davis lab for sharing their protocol of the enzymatic synthesis of smRNA-FISH probes with me.

To Assoc. Prof. Lothar Schermelleh, thank you for taking the time to show me how to use the 3D SIM, the exciting microscopy discussions, and for their evaluation of my work together with Assoc. Prof. Lidia Vasilieva.

To the Micron facility team, your help has been much appreciated over the years.

To the Furger lab members, in particular to Assoc. Prof. Andre Furger, I have appreciated our lab meetings and I am grateful for your advice.

To the Kornmann lab, especially Agnes Michel, Christian Covill-Cooke, and Matthew Karadzas, thank you for your presence in the lab, it brightened my days.
Special thanks to Manuel Vinluan for checking on me when I was alone in the lab during the pandemic. His positive attitude helped a lot.

To my former and current colleagues: Françoise Howe, Anitha Nair, Thomas Brown, Struan Murray, Harry Fischl, Philip Lorenz, thank you for making the Mellor lab such an enjoyable working environment. A special thanks to Julian Urdiain for his internship work on the YMC. To Salva Casani for his advice on spheroplasting. To Shidong Xi and Jack Feltham for teaching me how to use the fermenters. To Umut Gerlevik, David Aitken, and Noah Crook for reigniting the scientific spark in me. To Sibyl Bertrand, Anna Lamstaes, and Ülkü Uzun for their problem solving skills, moral support and encouragements. To Silvia Raineri for inspiring me to push through the hard PhD times and introducing me to Suria and Chiara, whose friendships, together with hers, mean a lot. You all bring so much fun in my life.

To the amazing members of the Predictive Epigenetics Network (PEP-NET ITN), thank you for always reminding me why I decided to work in research and how fun the study of epigenetics can be. I have had brilliant discussions with you all.
A particular acknowledgement to the European Union's Horizon 2020 research and innovation programme for funding my research project through the Marie Skłodowska-Curie grant.

I would also like to thank the members of the Oxford University Underwater Exploration Group (OUUEG) for electing me as their president for the year 2022. Blowing bubbles

in your company brought me great joy. Also, special thanks to members of YogaVenue and Oxford University Pole Sports for providing enjoyable training and contributing to my mental well-being. To Elena W. I really appreciated your help during the final year of my PhD.

To my former and current housemates, in particular Chiara, Judith, Hadiqa, Paloma, Mary, and Alex, thank you for making our house a place I could call home. Your encouragement, fun spirits and laughs filled me with happiness. I will miss you.

To my friends Marine, Julien, and Antoine, I have appreciated your constant cheering. Especially to Dr. Ariane Mwema, thank you for the regular check-ups, occasional fire emojis, and the long life updates. I hope one day the MWAM scientific team will be reunited. In the meantime, thank you for being an amazing friend.

To my dear friend Vânia, your presence during our long writing sessions has meant the world to me. Thank you for your kindness. You have been the best online buddy ever! Bit by bit we have done it. Cheers to the post-PhD, in-person life.

To my family, in particular Stephanie, many thanks for your help and emotional support. To my mum Véronique and my sister Gabrielle, thank you for your persistent encouragement. Mum, I am forever grateful for the loving environment and education you provided for us.

Finally, to my extraordinary partner Emile, thank you for your continuous support despite sometimes living in different time zones, for your patience, your unconditional love, and all the fun you bring into my life. And a special thank you for always encouraging me to pursue my scientific dreams.

Abstract

Temporal control of processes in cells such as metabolism, gene expression, and cell growth and division are ubiquitous in nature but how they are coordinated in single cells is poorly understood. The yeast *Saccharomyces cerevisiae* offers a tractable system in which to address these relationships, as growth rates, the number of cells in the cell division cycle (CDC), and their metabolism can be varied and linked to patterns of gene expression. Precise numbers of nascent and mature transcripts can be monitored in single cells using single-molecule RNA fluorescence *in-situ* hybridisation (smRNA-FISH). The Yeast Metabolic Cycle (YMC) is a model system of temporal compartmentalisation of cellular and metabolic processes in slow-growing synchronous cultures and can be compared with data from asynchronous cultures at different growth rates (exponential mid-log versus slow growth) and metabolic states.

These studies reveal that single cells from mid-log and YMC cultures possess an intrinsic metabolic and gene expression clock. Remarkably, individual cells are found to possess a high degree of variability in levels of expression of individual transcripts yet the oscillations in mean transcript levels over time are similar to those described at the population level using RNA-seq. Furthermore, although most yeast genes are proposed to show a constitutive mode of transcription initiation, the transcript distribution of oscillating transcripts along the YMC do not fit those predicted by a one-state mathematical model of constitutive transcription. Instead, the predicted “bursty” mode of expression could explain the variability in transcript levels in single cells. Cell-to-cell transcript heterogeneity was also observed for pre-rRNA transcripts during the YMC, despite population levels oscillating with periods of cell growth and ribosome

biogenesis. The link to cell growth is supported by the observation that ribosomal RNA production is found to be temporally coordinated to TORC1-controlled Rps6 phosphorylation.

The examination of DNA content and cell diameters together with transcript numbers in single cells of YMC and mid-log populations indicates distinct sub-populations with different relationships between gene expression, proliferation and growth. In synchronous YMC cultures, metabolism and patterns of gene expression are proposed to alternate synchronously between phases of growth and quiescence, linked to metabolism by high or lower levels of oxygen consumption respectively. This study suggests that the organization of the culture is far more nuanced. It supports at least three distinct co-existing states in the population over each metabolic cycle, including small quiescent-like cells, slow-growing cells, and larger cells whose metabolism is remodelled, with increased oxygen consumption, to facilitate their entry and progression through the cell division cycle.

Experimental delays were experienced due to the Covid 19 pandemic

Funding

This project has received funding from the European Union's Horizon 2020 research and innovation programme under the Marie Skłodowska-Curie grant agreement No. 813282, H2020-MSCA-ITN "PEP-NET: Predictive Epigenetics".

Acknowledgements

I gratefully acknowledge the Micron Advanced Bioimaging Facility (supported by Wellcome Strategic Awards 091911/B/10/Z and 107457/Z/15/Z) for their support & assistance in this work.

Publications

Brown, T., Howe, F. S., Murray, S. C., Wouters, M., Lorenz, P., Seward, E., Rata, S., Angel, A., & Mellor, J. (2018). Antisense transcription-dependent chromatin signature modulates sense transcript dynamics. *Molecular Systems Biology*, *14*(2), e8007. https://doi.org/10.15252/msb.20178007

Waiting to be published;

Feltham, J. E., Xi, S., Murray, S. C., Wouters, M., Urdiain-Arraiza, J., Heilig, R., George, C.,Townley, A. F., Roberts, E., Kessler, B. M., Liberatori, S., Charles, P. D., Angel, A., Fischer, R., & Mellor, J. (2020). Transcriptional changes are regulated by metabolic pathway dynamics but decoupled from protein levels. *BioRxiv*, 833921. https://doi.org/10.1101/833921

Declaration of Authorship

I hereby confirm that except where stated explicitly to the contrary in the text, the work presented here is my own and has been generated by me as the result of my own original research.

Part of this work also includes and discuss data found in Feltham et al., *BioRxiv.*, (2020). I have received permission from the authors to use this material in my thesis.

Word count : 56810

Abbreviations

YMC	Yeast metabolic cycle
HOC	High oxygen consumption
LOC	Low oxygen consumption
CDC	Cell division cycle
OX	Oxidative
RB	Reductive building
RC	Reductive charging
dO_2	Dissolved oxygen levels in the medium
Mid-Log	Mid logarithmic phase
DT	Doubling time
smRNA-FISH	Single molecule RNA *in-situ* hybridization
NET-seq	Native elongating transcript sequencing
RNA-seq	RNA sequencing
WT	WILD TYPE
Tp	Time point
ATO3	Transcript of the Ammonia transporter outward gene
SHM2	Transcript of the cytoplasmic serine hydroxymethyl transferase
IDH1	Transcript of the NAD+ dependent isocitrate dehydrogenase 1
ACT1	Transcript of the gene coding for Actin
nt	nucleotide
µm	micrometre
A.U.	Arbitrary Units
rRNA	Ribosomal RNA
mtDNA	Mitochondrial DNA
TF	Transcription factor

Table of Contents

Acknowledgements *2*

Abstract *5*

Abbreviations *9*

Chapter 1 ..... *16*

Introduction *16*

1.1 Addressing the knowledge gaps in the field **17**

1.2 1st Gap; A need for gene expression studies through intermediate and extreme metabolic changes **17**

1.2.1 The Yeast Metabolic Cycle a model of temporal compartmentalization of metabolic changes 18

1.2.2 Oscillating features of the YMC 23

1.2.3 Gene expression levels in YMC cultures 26

1.2.4 The YMC is a model system for the study of quiescence and growth 39

1.2.5 Two (or more) sub-populations compose the YMC cultures 54

1.3 2nd Gap; A need for quantitative gene expression single cell studies **61**

1.3.1 Metabolic oscillations in single cells 61

1.3.2 An intrinsic metabolic clock 63

1.3.3 Single-cell transcripts in asynchronous cell population 64

1.4 3rd Gap; A need for single cell gene expression studies at the transcript level **66**

1.4.1 Single-cell protein levels in synchronous cell population 66

1.4.2 Limitations of protein reporter assays 67

1.4.3 Using smRNA-FISH on YMC populations 68

1.5 Aims of research **71**

Chapter 2 ..... *72*

Materials and Methods *72*

2.1 Experimental Models/Strains **73**

2.2 Strain construction **73**

2.2.1 Cloning PCR 74

2.2.2 Yeast transformation 74

2.2.3 Non-phenol genomic DNA extraction 75

2.2.4 Checking PCR 75

2.3 Yeast cultures **75**

2.3.1 Mid-logarithmic growth 75

2.3.2 Chemostat continuous cultures 76

2.4 Experimental settings for synchronized cultures **76**

2.4.1 Solutions 78

2.5 RNA fluorescence *in-situ* hybridization, RNA-FISH experimental design **78**

2.5.1 Probe designs 78

2.5.2 Enzymatic synthesis of probes 79

2.5.3 Labelling strategy 82

2.5.4 Negative Controls 82

2.5.5 Fluorophore Swap 83

2.5.6 Sampling 84

2.6 RNA fluorescence *in-situ* hybridization, RNA-FISH Wet-lab Workflow 84
2.6.1 Fixing or Cross-linking 84
2.6.2 Cell wall removal or Spheroplasting 84
2.6.3 Spheroplasting optimization 85
2.6.4 Attachment on coverslips and membrane permeabilization 86
2.6.5 Hybridization 87
2.6.6 Testing probe concentration 87
2.6.7 Washing and Nucleus Staining 88
2.6.8 Mounting 88
2.6.9 Image acquisition 88
2.6.10 Deconvolution 89
2.6.11 Visual examination of the data 89
2.6.12 Images presented in this study 89

2.7 Data processing, RNA-FISH Dry-lab Workflow 90

'In-house automated quantification pipeline' 90
2.7.1 Software 90
2.7.2 Background substraction 90
2.7.3 Automated Nuclei Detection 90
2.7.4 Automated Cell Detection 91
2.7.5 Foci identification 91
2.7.6 Thresholding 92
2.7.7 Foci classification 93
2.7.8 pre-rRNAs quantification 94
2.7.9 Single molecule quantification 94
2.7.10 Nuclear DNA content quantification 95
2.7.11 Mitochondrial DNA nucleoids and total mitochondrial content quantification 95
2.7.12 Scripts 96

2.8 Downstream analysis 96
2.8.1 Cell size 96
2.8.2 Statistical tests 96
2.8.3 Data filtering 97
2.8.4 Sample size 99
2.8.5 Cell categories 100

2.9 Limitations of the techniques used in this study 101

2.9.1 Pre-rRNA-FISH, a semi-quantitative method 101

Chapter 3 102

smRNA-FISH on YMC samples in a nutshell 102

3.1 Inducing and recording the Yeast Metabolic Cycle 103

3.2 Overview of experimental design and analytical pipelines for smRNA-FISH 106
3.2.1 At the bench 106
3.2.2 At the microscope 107
3.2.3 On the computer 107

Chapter 4 110

Ribosomal RNA production is globally coordinated to Rps6 phosphorylation during the YMC, yet heterogenous in single cells of YMC populations 110

4.1 Introduction 111
4.1.1 Signalling pathways and phosphorylation cascades 111
4.1.2 Linking metabolites and ribosomal protein activities 112
4.1.3 Rps6 phosphorylation oscillates during the cycle 113

4.1.4 Rps6 activity regulates Ribosomal RNA biogenesis ... 114

4.2 Experimental design and method development ... **115**
4.2.1 Probe design ... 115
4.2.2 pre-rRNA-FISH, a semi-quantitative method. ... 116

4.3 Results ... **118**
4.3.1 Pre-rRNA production peaks in the middle of the HOC-phase ... 119
4.3.2 More cells in the population have high pre-rRNA levels during the HOC phase of the YMC ... 120
4.3.3 RNA Polymerase I transcription is heterogeneous in cells from YMC populations ... 120
Figure 4.8 Pre-rRNA foci total volumes increase in HOC phase of the YMC ... 123

4.4 Discussion ... **125**
4.4.1 Pre-rRNA production peaks in the HOC phase of the YMC ... 125
4.4.2 TORC1 phosphorylation cascades might regulate growth along the YMC ... 125
4.4.3 Three-state sub-populations compose the YMC cultures ... 128
4.4.4 Evidence of cell-to-cell gene expression variability in YMC cultures ... 129

4.5 Conclusion ... **129**

Chapter 5 ... ***131***

Chapter 5 Part I ... ***132***

Single-molecule RNA-FISH data recapitulates the overall cycling of transcripts throughout the YMC ... ***132***

5.I.1 Experimental design and method development ... **133**
5.I.1.1 Multiplex smRNA-FISH of antagonistically oscillating transcripts ... 133
5.I.1.2 Probe design and synthesis ... 133
5.I.1.3 The target transcripts chosen for this study ... 135
5.I.1.4 A brief comparison of metrics between target transcripts ... 142

5.I.2 Overview of smRNA-FISH experimental design ... **145**
5.I.2.1 Single and dual label (multiplex) smRNA-FISH of transcripts during the YMC ... 145

5.I.3 Preliminary results and analysis ... **148**
5.I.3.1 Controls to optimize the quality of experimental data ... 148
5.I.3.2 Variability between experimental replicates ... 148
5.I.3.3 Microscopy images ... 149
5.I.3.4 Downstream data analysis ... 156
5.I.3.5 Cell categories ... 156

5.I.4 Results ... **157**
5.I.4.1 The smRNA-FISH data recapitulates the cycling of population-averaged transcript levels ... 157
5.I.4.2 Mean steady-state transcripts levels in single cells reflect differences in metabolic state between the YMC and mid-log phase cells ... 161

5.I.5 Conclusions ... **165**

Chapter 5 Part II ... ***166***

Transcript levels of genes transcribed by RNA polymerase II vary between single cells from synchronized cultures ... ***166***

5.II.1 Introduction ... **167**
5.II.1.1 Gene expression noise ... 167

5.II.2 Results ... **170**
5.II.2.1 Yeast cells show low RNA Pol II transcriptional noise in synchronous population ... 170

5.II.2.2 Gene expression noise oscillates over the YMC ... 175
5.II.3 Conclusions ... 179
5.II.4 Results ... 180
5.II.4.1 The fraction of expressing cells oscillates over the YMC ... 180
5.II.4.2 At all times during the YMC a small proportion of cells is detected without transcripts ... 189
5.II.5 Conclusions ... 190
5.II.6 Discussion ... 191
5.II.6.1 Fast changes of ON-OFF transcription state along the YMC ... 191
5.II.6.2 Changing degradation rates are likely to be involved in the regulation of transcript levels over the YMC ... 192
5.II.7 Conclusions ... 193
5.II.8 Results ... 194
5.II.8.1 Individual cells possess a high degree of variability in levels of expression of individual transcripts ... 194
5.II.9 Discussion ... 205
5.II.9.1 Different modes of regulation of transcripts along the YMC ... 205
5.II.10 Conclusions ... 208
Chapter 6 ... 211
Transcription dynamics alter upon metabolic changes ... 211
6.1 Introduction ... 212
6.1.1 Sources of gene expression stochasticity ... 212
6.1.2 Modes of transcription ... 214
6.2 Preliminary results ... 215
6.2.1. Poisson distributions do not fit cytoplasmic RNA distributions from the FISH data ... 215
6.3 Conclusions ... 217
6.4 Future directions ... 221
6.4.1 Using a two-state model of transcription ... 221
Chapter 7 ... 223
Single cells from high-growth asynchronous mid-log cultures and slow-growth synchronous cultures possess an intrinsic metabolic clock and YMC cultures are organised in sub-populations ... 223
7.1 Introduction ... 224
7.1.1 Investigation of the concept of an intrinsic gene expression clock ... 224
7.2 Results ... 227
7.3 High-growth asynchronous mid-log cultures ... 230
7.3.1 Cells co-express antagonist transcripts in high-growth asynchronous cell populations (mid-Log cells) ... 230
7.4 Discussion ... 231
7.4.1 The proportion of cells expressing only one transcript in asynchronous mid-log population returns the chronology of the transcriptional intrinsic clock ... 231
7.5 Conclusions ... 233

7.6 Slow-growth synchronous YMC cultures 234
7.6.1 Antagonistically oscillating transcripts are co-expressed in single cells of the synchronized YMC population 234
7.6.2 Transcript exclusivity rises as global transcript levels of antagonist drops 238

7.7 Conclusions 239

7.8 Discussion 239
7.8.1 The proportion of cells expressing target transcripts in the YMC synchronous population indicate an organisation in sub-populations 239
7.8.2 A proportion of cells remains in the LOC state during the HOC phase 240
7.8.3. A proportion of cells stay in a HOC state at all times during the YMC 242
7.8.4 Only a proportion of cells transition to a HOC state in HOC phase 242

7.9 Results 243
7.9.1 Cells that co-express HOC and LOC transcripts in HOC phase of the YMC show high expression levels of HOC transcripts and low expression levels of LOC transcripts 243

7.10 Conclusions 247
7.10.1 A three-state population model for the YMC 247

Chapter 8 250

Coordination of growth, proliferation and gene expression delineates distinct sub-populations in mid-Log and YMC cultures 250

8.1 Introduction 251
8.1.1 Coordination between Growth and CDC through Start 251
8.1.2 Cell size control and homeostasis 252
8.1.3 Cell size acts as a proxy for growth and proliferative states of cells 252
8.1.4 Cell size and a critical size threshold in nutrient limiting conditions 253

8.2 Discussing the organisation of YMC population 254
8.2.1 Organisation of yeast cells in synchronous population 254
8.2.1 Growth models 255
8.2.2 Alternating growth model 257
8.2.3 The need for a model considering both growth and quiescence 257
8.2.4 Quiescence models 259

8.3 Investigation of the relationship between cell cycle progression, cell size and gene expression in single cells of yeast cultures 261

8.4 Experimental design and method development 262
8.4.1 Identification of budded cells in YMC cultures 262
8.4.2 DAPI intensities in-nucleus accounts for the nuclear DNA content 262
8.4.3 Cell size distributions during the YMC 264
8.4.4 Mitochondrial DNA as a proxy for cell cycle progression 264

8.5 Results 266
8.5.1 Nuclear and mitochondrial DNA content in single cells 266
8.5.2 Cell size correlates with DNA content in the YMC and mid-log cultures 270
8.5.3 Cells from mid-log phase cultures are larger than YMC cells 270
8.5.4 A cell diameter threshold of ~4.2μm defines 2 sub-populations of cells in mid-log cultures 273
8.5.5 The cell diameter of YMC cells increase in mid-HOC and peak in late HOC 273
8.5.6 The proportion of cells with higher cell sizes increases in mid-HOC phase of the YMC but does not scale up with the nuclear and mtDNA content 275

8.6 Conclusions 276

8.7 Introduction to mitochondrial biology 277
8.7.1 A proportion of cell show signs of respiratory growth in mid-HOC phase 277

8.8 Results **279**
8.8.1 Transcript numbers poorly correlate with nuclear DNA, mtDNA content and cell size in the YMC and mid-log cultures 279
8.9 High-growth asynchronous mid-log cultures **283**
8.9.1 Gene expression and cell size are coordinated in mid-log phase 283
8.10 Discussion **286**
8.10.1 The cell size seems coordinated with the intrinsic metabolic clock 286
8.10.2 Cells with quiescent stationary phase characteristics are found in mid-log cultures 287
8.11 Slow-growth synchronous YMC cultures **288**
8.11.1 In YMC cultures gene expression, cell growth and proliferation are coordinated . 288
8.11.2 In YMC cultures sub-populations of cells show distinct gene expression, cell growth and proliferation profiles 296
8.12 Conclusions **304**
8.13 Discussion **309**
8.14 Future directions **311**
Chapter 9 ..... ***312***
Discussion ***312***
9.1 Summary of results **313**
9.2 The Yeast Metabolic Cycle in context of other biological systems **319**
9.3 Future directions **321**
9.4 Concluding remarks **325**
Chapter 10 ..... ***327***
Appendix ***327***
References ***351***

Chapter 1

Introduction

1.1 Addressing the knowledge gaps in the field

This study explores the behaviour of single cells in slow-growing synchronized cultures of the Yeast Metabolic Cycle (YMC). This work aims to address some of the gaps found in previous studies relating metabolism and gene expression in budding yeast: (i) the study of gene expression at steady-state rather than under changing conditions (iii) the lack of single cell studies and associated quantitative data analysis (iii) the relatively mis-use of protein levels to infer the behaviour of transcripts. In order to address these gaps, (i) the Yeast Metabolic Cycle is exploited as a tool to establish metabolic changes in yeast populations, (ii) the RNA fluorescence *in-situ* hybridization (RNA-FISH) technique is utilized to gather quantitative data at the transcript level in single cells of YMC cultures and (iii) analysis and interpretation of transcript numbers and cellular distributions are carried out along the metabolic cycle, focusing on cell population heterogeneity and sub-population organisation.

1.2 1st Gap; A need for gene expression studies through intermediate and extreme metabolic changes

The study of transcription regulation under metabolic changes often focus on drastic changes such as osmotic stress, heat shock, carbon source exchange, amino acid starvation, stationary phase and diauxic shift (Radonjic et al. 2005, DeRisi et al. 1997, Gash et al. 2000, Causton et al. 2001, Brauer et al. 2005), but also on changes such as cell-cycle arrest and progression (Cho et al. 1998), quiescence entry, maintenance and exit (Aragon et al.,2008, Miles et al. 2013, McKnight et al. 2015, Cucinotta et al. 2021).

Some of these changes are not fully reversible and these, and many other studies on gene expression, often focus on the extreme steady states (before and after metabolic changes), rather than looking at intermediate states. Thus, there is a need for

experimental settings providing slow changing and reoccurring conditions, allowing the study of gene expression under metabolic changes for extreme and intermediate states at a fine time resolution.

In order to address this gap, the Yeast Metabolic cycle (YMC), a system of temporal compartmentalization of cellular and metabolic processes is used in this project as a tool to study gene expression under cyclic changes in metabolism.

1.2.1 The Yeast Metabolic Cycle a model of temporal compartmentalization of metabolic changes

The Yeast Metabolic Cycle, was discovered in the 1950s, when researchers aimed to reproduce “budding yeast slow-growth natural conditions” in the lab using a chemostat (Monod. 1950, Novick & Szilard. 1950) to grow prototrophic strains of *Saccharomyces cerevisiae* under slow-growth rate in batch culture and at high cell density, such as found in yeast colonies (Chance et al. 1964, von Meyenburg. 1969,1973, Parelukar et al. 1986, Porro et al. 1988).

Typically, yeast cell populations undergo synchronized metabolic oscillations, called yeast metabolic cycles, after starvation and upon continuous glucose feeding in limiting concentration (von Meyenburg. 1973, Chen & McDonald. 1990, Chen et al. 1990, Borzani et al. 1977, Tu et al. 2005). One of the easiest way to monitor the yeast culture, its synchronization and further metabolic oscillations is by looking at the dissolved oxygen levels (dO_2) in the culture medium over time as presented at Figure 1.1. Accordingly, the YMC can be divided into two phases characterized by the level of oxygen consumption. On one hand, the Low Oxygen Consumption (LOC) phase, where dissolved oxygen levels in the medium are high, on the other hand the High Oxygen Consumption (HOC) phase, where dissolved oxygen levels in the medium are lower (Satroutdinov et al. 1992). Metabolic changes occur along the cycle; during the

LOC phase, cells possess low ATP levels (Machne & Murray. 2012) and build up their carbohydrate stores (Shi et al. 2010), while during the HOC phase, cells proceed to cell biosynthesis via nutrient consumption, respiration and thus possess higher energy states (Tu et al. 2005, Tu et al. 2007, Mellor. 2016, O'Neill et al. 2020).

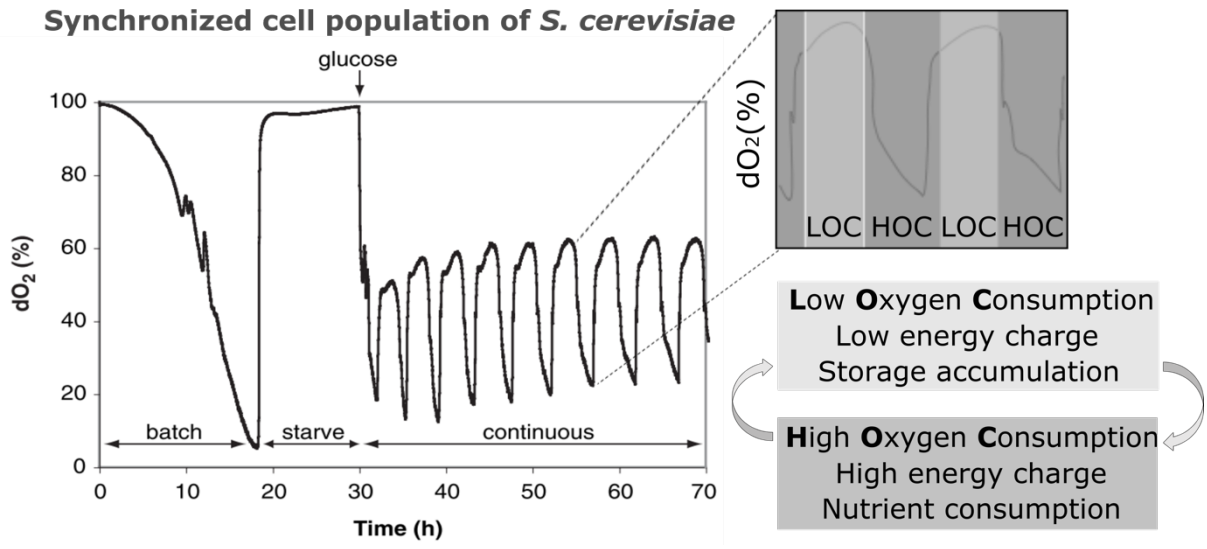

Figure 1.1. Typical dissolved oxygen trace recorded through time of a yeast cell population undergoing the YMC. *Modified from Tu et al. 2005.*

Before the synchronization and metabolic cycling starts, the *Saccharomyces cerevisiae* batch culture goes through distinct and well-known metabolic states. First the cells go through exponential growth, then diauxic shift to reach stationary phase. As cells go through the diauxic shift, the oxygen consumption increases and thus the dO_2 levels in media drop (end of the batch culture phase, Figure 1.1). Then a peak in oxygen levels is observed. At this stage, cells stop consuming oxygen via respiration and enter stationary phase (phase 2, starvation). Cells are then starved for a short period of time before the YMC is induced through constant feeding of the culture under limiting concentration of glucose (phase 3, feeding) (Tu et al. 2005, Xi. DPhil thesis.

2019). Next these states are briefly explained in light of previous studies on budding yeast batch cultures.

1.2.1.1 Exponential Growth

During the first phase of batch culture, yeast cells consume glucose at a high rate and grow through exponential phase via fermentation. Fermentation occurs even in presence of oxygen, as glucose is the budding yeast preferred carbon source (Johnston. 1999, Dickinson & Schweizer. 1999). When around half of the available glucose has been consumed by the cells, the glucose uptake is increased through the activation of a high-affinity transporter (Ye et al. 2001, Youk & Van Oudenaaden. 2009) but the glycolytic flux is slowly reduced through the downregulation of glycolytic proteins (Zampar et al. 2013). Meanwhile, glucose accumulates in some cells as carbohydrate stores namely; trehalose and glycogen (Lillie & Pringle. 1980) or even in cell walls (Orlean et al. 2012). As the glucose availability decrease, nutrient signalling pathways are down regulated; the TOR pathway is inactivated and the cAMP and PKA activity decreases (Boy-Marcotte et al. 1996, Slattery et al. 2008).

1.2.1.2 Diauxic shift

When the yeast culture reaches glucose depletion cells enter the so-called diauxic shift. At this stage, extracellular levels of ethanol and pyruvate levels are at their peak. The pace at which biomass and CO_2 accumulate slows down and cells transition from glycolytic fermentation to aerobic respiration. When shifting to respiration, cells consume extracellular ethanol and pyruvate (Zampar et al. 2013, Dickinson & Schweizer, 1999) and produce more energy than when fermenting. Indeed, respiration is a more efficient way to produce energy as it produces ˜18 ATP molecules per molecule of glucose compared to only 2 ATP molecules per molecule of glucose for

fermentation in *Saccharomyces cerevisiae* (Pfeiffer & Morley. 2014, Dickinson & Schweizer, 1999, Brauer et al. 2005).

Upon the diauxic shift, after glucose exhaustion, the metabolic flux of glycolysis is reduced while gluconeogenesis is highly increased through the upregulation of the enzymes of the glyoxylate cycle, and via the use of 2 carbon compounds and the production of oxaloacetate (Zampar et al. 2013). Cells metabolise fatty acids and use ethanol or acetate for the production of Acetyl CoA which will feed the glyoxylate cycle and increase respiration (Lorenz & Fink. 2001). Finally, later on, the pentose phosphate pathway is shut down. Thus, during the diauxic shift, many metabolite levels vary (Zampar et al. 2013). In parallel to these metabolic modifications, major transcriptional changes occur. These affect about a third of the genome, mostly before but also during and after glucose exhaustion (DeRisi et al. 1997, Gasch et al. 2000, Hanisch et al. 2022, Brauer et al. 2005, Radonjic et al. 2005). Indeed, transcripts levels of genes involved in the respiratory pathway, stress response (Gasch et al. 2000, Puig & Perez-Ortin. 2000) and accumulation of carbohydrates (Parrou et al. 1999) increase, while transcripts levels of genes involved in fermentation, translation and ribosomal proteins decrease (DeRisi et al. 1997). Finally, transcription factors Msn2p/Msn4p but also others such as Snf1p or Abf1p (Zampar et al. 2013) participate in the transcriptional regulation of many transcripts post diauxic shift (Boy-Marcotte et al. 1998, Causton et al. 2001). Similarly, protein levels but also isoforms ratios of metabolic enzymes change during the diauxic shift (Murphy et al. 2015).

1.2.1.3 Stationary phase

When ethanol is exhausted from the extra cellular media, and many cells have stopped their cell division cycle, the cells have entered the so-called stationary phase (Herman et al. 2002), under which the dO_2 levels remain constant (Figure 1.1).

At this stage, the culture is under starvation and both transcripts and proteins levels drop (Boucherie et al. 1985, Fuge et al. 1994, Paz et al. 1999). Transcript profiles change compared to those found in exponential cultures (DeRisi et al. 1997, Gasch et al. 2000, Gasch & Werner-Washburne. 2002, Martinez et al. 2004, Radonjic et al. 2005). Under starvation a decrease in transcript levels is reported for genes involved in signal transduction pathways such as the PKA and TOR pathways necessary for the switch to respiratory growth (Gray et al., 2004). Autophagy is induced through TORC1 and PKA inhibition (Kamada et al. 2004, Budovskaya et al. 2004, Furuta et al. 2004, Padilla et al. 2019), enabling amino acid pools to increase under nitrogen starvation (Waite et al. 2016). This process grants cells the ability to recycle macromolecular complexes to single amino acids and thus to re-allocate resources to survive longer (Alvers et al. 2009, Suzuki et al. 2011, Breeden & Tsukiyama. 2022). Thus prior to the induction of yeast metabolic cycles, yeast population in batch culture already undergoes major metabolic and gene expression changes.

1.2.1.4 Yeast Metabolic Oscillations

Next, to induce metabolic cycling, the starved yeast batch culture is fed with limiting concentration of glucose. The culture is continuously fed under chemostatic conditions maintaining constant environmental conditions; the volume of the culture, pH, temperature, aeration and agitation (Monod. 1950, Novick & Szilard. 1950). At this stage (beginning of stage 3, Figure 1.1) the dissolved oxygen levels in the media

decrease again while the cell density increases, until reproducible dO_2 oscillations start, characterizing changes in metabolism (Satroutdinov et al. 1992, Tu et al. 2005, thesis of Dr. Xi). The period of oscillation depends on the experimental settings ranging from 1 to 5 hours depending on the feeding rate (Tu et al. 2005, Klevecz et al. 2004).

1.2.2 Oscillating features of the YMC

During the YMC, the global metabolic flux observed for the yeast population changes (Tu et al. 2007, O'Neill et al. 2020). Cells oscillate from a state of autophagy in the low oxygen consumption phase (LOC) to a state of growth and protein synthesis in the high oxygen consumption phase (HOC) (O'Neill et al. 2020). Indeed, previous studies revealed many features such as metabolites, ions and osmolytes levels but also redox reactions fluctuate during the YMC. Figure 1.2 shows a model for YMC phases and their significant metabolic events developed by O'Neil et al. (2020).

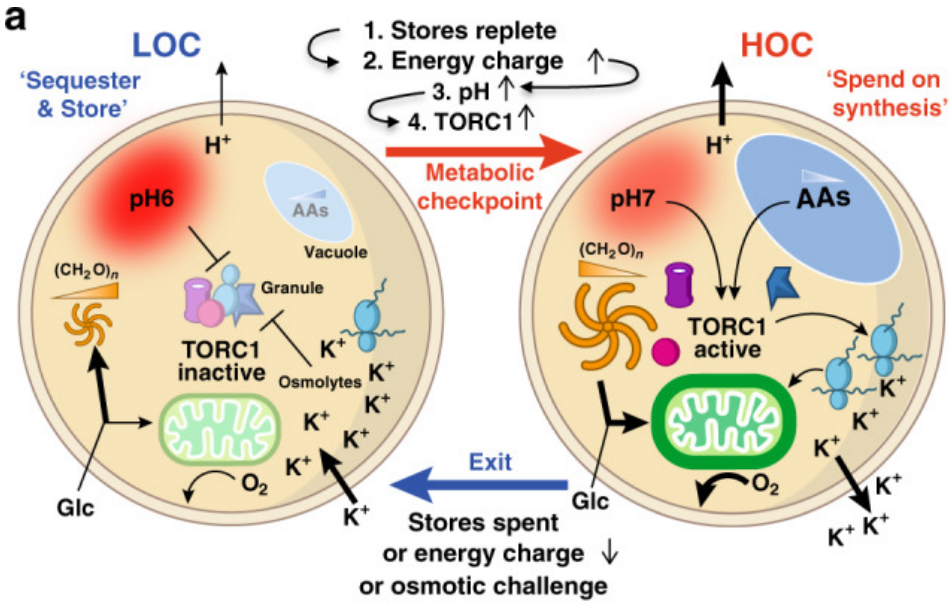

Figure 1.2 The YMC oscillates between autophagy and protein synthesis

During the Low Oxygen Consumption phase (LOC) cells accumulate intra-cellular energy, carbohydrate and amino acid stores, while during the High Oxygen Consumption phase (HOC) cells spend these to feed protein synthesis (O'Neill et al. 2020).

During the low oxygen consumption phase (LOC), trehalose and glycogen carbohydrate stores accumulate (Muller et al. 2003, Shi et al. 2010, O'Neill et al. 2020) while lipid and nucleotide biosynthesis increases (Tu et al. 2005). Osmolyte levels build up in cells. Proton export decreases, leading to lower intracellular pH (Keulers et al. 1996). Accordingly, the formation of biomolecular condensates was reported in this phase (O'Neill et al. 2020).

Upon transition to the high oxygen consumption phase (HOC), cells energy stores; cAMP and ATP (Muller et al. 2003, Machne & Murray. 2012) and carbohydrate stores are full. Next, during HOC, cells consume higher oxygen levels through increased respiration. Levels of Acetyl-CoA, NADPH and other metabolites involved in glycolysis and respiration increase through the TCA/Krebs cycle (Tu et al. 2005, Tu et al. 2007, Murray et al. 2011). Osmolytes are exported outside the cells. Proton export is higher than in LOC phase, and intracellular pH is thus increased. At the end of the HOC phase, levels of ATP, carbohydrate stores, amino acids and osmolytes are thus depleted (O'Neill et al. 2020).

In the model presented at Figure 1.2, the target of rapamycin TORC1 complex, is proposed to act as the final step of the metabolic checkpoint for the transition between the LOC and HOC phase (O'Neill et al. 2020). TORC1 is a nutrient sensing signalling pathway involving phosphorylation cascades and promoting growth and cell proliferation (Martin & Hall. 2005). It is proposed to be inactivated in LOC and activated in HOC through a pH dependent way (Delarue et al. 2018) and act at the transition between the 2 phases of the YMC, sensing intracellular carbohydrate and amino acids levels (O'Neill et al. 2020). When these are full, TORC1 is believed to promote the breakdown of carbohydrate stores and permits the passage of cells in HOC phase (O' Neill et al. 2020, Feltham et al. 2020).

Many redox reactions were also shown to cycle along the progression of the YMC. These involve targets such as cofactors (NAD+/NADH, NADP+/NADPH), flavin, (Murray et al. 1999, Murray et al. 2011) hydrogen sulphide (Sohn et al. 2000, 2001, Henson. 2004) and peroxiredoxin (Causton et al. 2015, Amponsah et al. 2021).

Finally, some metabolites were shown to induce the HOC phase of the YMC and were thus proposed as synchronization signals between cells for the beginning of metabolic oscillations. Among these, acetaldehyde (Murray et al. 2003, Robertson et al. 2008), and carbon sources such as ethanol and acetate (Cai et al. 2011, Kuang et al. 2017), H_2S (Sohn et al. 2000, 2001), CO_2 (Tu & McKnight. 2009, Machne et al. 2021) and H_2O_2 (Chen et al. 2007).

Together these studies and others indicate that the YMC allows temporal compartmentalization of cellular and metabolic processes. It is an oscillating system of metabolic states (Tu et al. 2005, Tu & McKnight. 2006, Mellor. 2016, O'Neill et al. 2020). The YMC is a cycle of metabolic changes and is *different* from the cell division cycle (CDC). The relationship between the two cycles; YMC and CDC is complex and is described later on.

1.2.3 Gene expression levels in YMC cultures

1.2.3.1 Global transcripts levels cycle

Remarkably, along the metabolic changes and progression through the YMC, gene expression also oscillates. Transcription and transcript levels of genes associated with particular pathways alternate during the YMC and up to 60% of transcripts cycle at the mRNA level (Klevecz et al. 2004, Li & Klevecz. 2006, Tu et al. 2005, Slavov et al. 2011, Kuang et al. 2014, Feltham et al, 2020). Next, details about the gene expression changes observed during the YMC are presented.

Genome-wide gene expression changes were reported during the Yeast Metabolic Cycle using Affymetrix chips microarrays, to investigate total RNA gene expression in synchronized yeast populations of different strains (Klevecz et al. 2004, Li & Klevecz. 2006, Tu et al. 2005). While Klevecz's team sampled the YMC culture every 4 minutes over short period yeast metabolic cycles (˜40min), McKnight's lab sampled the culture every 25 minutes, over long period yeast metabolic cycles (˜300min). Both research teams discovered temporal organisation of gene expression patterns along the YMC. Over 50% of the genes showed periodic gene expression with an average period that was similar to that of the YMC. However different genes were found to peak at different times of the YMC. Thus, genes were then clustered by their expression patterns by picking the most periodic genes and then looking for genes with similar profiles and using an unbiased k-means clustering method. The later method showed the data could be divided into 3 super-clusters (Tu et al. 2005). Similarly, genes were also grouped according to the time and phase of the YMC at which their respective gene expression was peaking by Klevecz et al.(2004, 2006) who also found 3 major gene expression clusters.

Gene expression clusters were characterized using Gene Ontology (GO) annotations of the transcripts grouped in each cluster (Klevecz et al. 2004, Li & Klevecz. 2006, Tu et al. 2005). Additional clusters and common gene expression pathways were found by other labs using the same data but with different clustering strategies (Soranzo et al. 2009, Machne & Murray. 2012).

Following the increased accessibility in sequencing tools, genome-wide transcript levels were then assessed along the YMC via sequencing techniques (Kuang et al. 2014). Kuang et al., processed 16 samples over one metabolic cycle (~4 h period) via RNA-seq. Finally, more recently, members of our laboratory gathered transcriptomic data throughout the YMC (Feltham et al. 2020, thesis of Dr. Xi). During his thesis, Dr. Shidong Xi, processed 22 YMC samples (˜3h20min period) through strand-specific 3'end RNA sequencing. Thus, both sequencing studies, for samples gathered at a higher time resolution, confirmed microarray results and allowed the discovery of a more detailed temporal organization of gene expression, in particular during the HOC phase of the YMC (Kuang et al. 2014, Feltham et al. 2020).

1.2.3.2 Detailed temporal organization of gene expression

The 3 super-clusters detected by both labs shared many genes in common. These clusters were named according to the time or phase of the YMC during which transcript levels were at their peak (Klevecz et al. 2004, Li & Klevecz 2006. Tu et al. 2005).

The **first cluster** corresponds to genes for which transcript levels peak in the early phase of **high oxygen consumption (early HOC)**. In other words, the time or phase for which the levels of dissolved oxygen sharply lower in the culture media. This cluster was named "**OX**" for **oxidative**. Genes for which transcript levels peak in the **late phase of high oxygen consumption phase (late HOC)** belong to the **second**

cluster named "**RB**" for **reductive building**. It corresponds to the time or phase in which the yeast population continues to consume oxygen but at a lower rate to then gradually reduce its oxygen consumption, i.e. the phase for which the levels of dissolved oxygen in the media start to increase until they stabilize. Finally, the **third cluster** comprises genes for which transcript levels peak during the **low oxygen consumption phase of the YMC (LOC)** during which yeast cells consume less oxygen than in the HOC phases. This cluster was named "**RC**" for **reductive charging**.

NB: After the discovery of these clusters, labs commonly adopted the following nomenclature and are to this day referring to the phases of the YMC by these clusters' names. However, as "phases or clusters" might differ slightly between studies, it might be of best practice to name the YMC phases according to the oxygen consumption taking place throughout the cycle. Therefore, the terms HOC and LOC (Satroutdinov et al. 1992) are used in this study to refer to YMC metabolic phases.

Figure 1.3 shows the main GO terms found for the 3 main gene expression clusters while Figure S.1.A, B & C in Appendix combines more of the GO terms found by the different labs over the years. It provides a more detailed view of the gene expression pathways for each cluster.

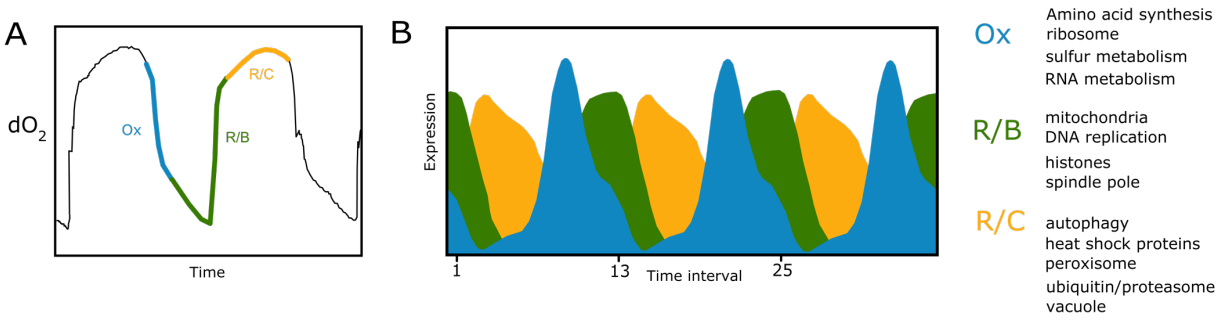

Figure 1.3 Gene expression clusters of the YMC

A. *The 3 Phases of the Yeast Metabolic Cycle (Oxidative, Reductive Building and Reductive Charging) for which gene-expression superclusters were described are indicated in color.* ***B.*** *Representation of the 3 super clusters of gene expression along the YMC. Modified from Tu et al., (2005).*

The first super-cluster, "**OX**", contains many genes coding for amino acid metabolism, RNA processing and ribosome synthesis. The second super-cluster, "**RB"**, is mostly composed of genes coding for proteins involved in the cell division cycle, mitochondria functions and biogenesis. The third super-cluster, "**RC",** comprises genes coding for proteins participating in cellular organization such as mitochondrion organization, cytokinesis and cytoskeleton, as well as proteins contributing to the function of the peroxisome, autophagy, fermentation and stress response (Klevecz et al. 2004, Li & Klevecz. 2006, Tu et al. 2005). To simplify even more, Machne & Murray., (2012) described 2 main clusters instead of 3. Similarly, HOC and LOC clusters were found by Feltham et al., (2020). Transcripts peaking in the HOC phase of the YMC constitute the first cluster and contribute overall to cell growth and anabolism. On the contrary, transcripts peaking in the LOC phase of the YMC mainly participate to stress response, mitochondrial growth and catabolism (Machne & Murray. 2012, Feltham et al. 2020).

1.2.3.3 Amplitude of oscillation

Remarkably, each lab's data contained many of the same genes/pathways in each cluster but also showed different numbers of genes in each cluster according to the method and analysis used. Recent RNA-seq analysis showed around 70% of genes present low cycling-amplitude during the YMC (Feltham et al. 2020). Many of these genes were considered as "non-periodic" by Tu et al., but were analyzed by Klevecz et al., who considered all expressed genes and classified their oscillations as high (>2. fold change) or low-amplitude (<2. fold change). By retaining the genes with low-amplitude oscillations throughout their analysis, another cluster of genes was found. These genes are highly expressed and coding for proteins such as actin, ribosomal proteins, intermediate of metabolism or structure maintenance proteins (Klevecz et al. 2004, Li & Klevecz.. 2006).

Overall these studies showed global oscillation in transcript levels as well as fine-tuned temporal regulation of gene expression patterns along the YMC. This discovery however raised the following questions: **How and why do transcript levels cycle?**

How do transcript levels cycle?

Steady-state transcript levels reflect the intricate balance between transcription and post-transcription processes (Rabani et al. 2014). Here some of the most important processes predicted and/or known to be involved in the regulation of RNA levels throughout the YMC are presented.

1.2.3.4 Global Transcription levels cycle during the YMC

Recently Nascent Elongating Transcripts sequencing (NET-Seq) was performed on 11 samples taken along the YMC (Feltham et al. 2020, Xi. DPhil thesis. 2019). NET-seq uses a co-immunoprecipitation technique allowing RNA Polymerase II to be pulled down together with nascent transcripts (Nojima et al. 2015; Churchman & Weissman. 2011). Nascent transcript levels were found to oscillate over the YMC, indicating global transcription also fluctuate along the cycle (Feltham et al. 2020, Xi. DPhil thesis. 2019). A significant overlap was found between transcription and steady-state transcript clusters; HOC, LOC and "low-amplitude cycling cluster". Figure 1.4 shows NET-Seq and RNA-Seq clusters. Moreover, a global transcription activation was reported in early-HOC phase, as a raise in global NET-seq (as well as RNA-seq) can be detected prior to "0", the point of maximal O_2 consumption, in early-HOC phase for all expressing genes (Figure 1.4) (Feltham et al. 2020, data from Dr. Xi) and GO terms for the early-HOC cluster show enrichment of the 3 RNA Polymerases, together with RNA processing (Soranzo et al. 2009). Therefore, transcription plays a major role in establishing oscillating transcript levels.

1.2.3.4.1 Factors influencing transcription levels along the YMC

Since transcription levels oscillate, other factors regulating transcription and or vice-versa might see their levels change over the YMC. In fact, many factors were found to vary along the metabolic cycle from transcription factors to chromatin architecture including changes in histone post-translational modifications and chromatin remodelling complexes levels. Indeed, different transcription factors are proposed enriched in different times of the cycle based on changing transcript levels (Rao & Pellegrini. 2011, Sanchez-Gaya et al. 2018, Kuang et al. 2014, Kuang et al. 2017).

Histone post transcriptional modifications patterns also change during the cycle, in particular histone lysine acetylation (H3K9, K14, K18, K23, K27 and H4K5, K8, K12) increase at growth genes during the HOC phase of the YMC, when Acetyl-CoA levels increase. Changes in histone lysine acetylation, observed during the YMC, were reported to result from the action of the Gcn5 in the SAGA chromatin remodelling complex (Cai et al. 2011, Cai & Tu. 2012, Shi & Tu. 2013, Kuang et al. 2014, Kuang et al. 2017).

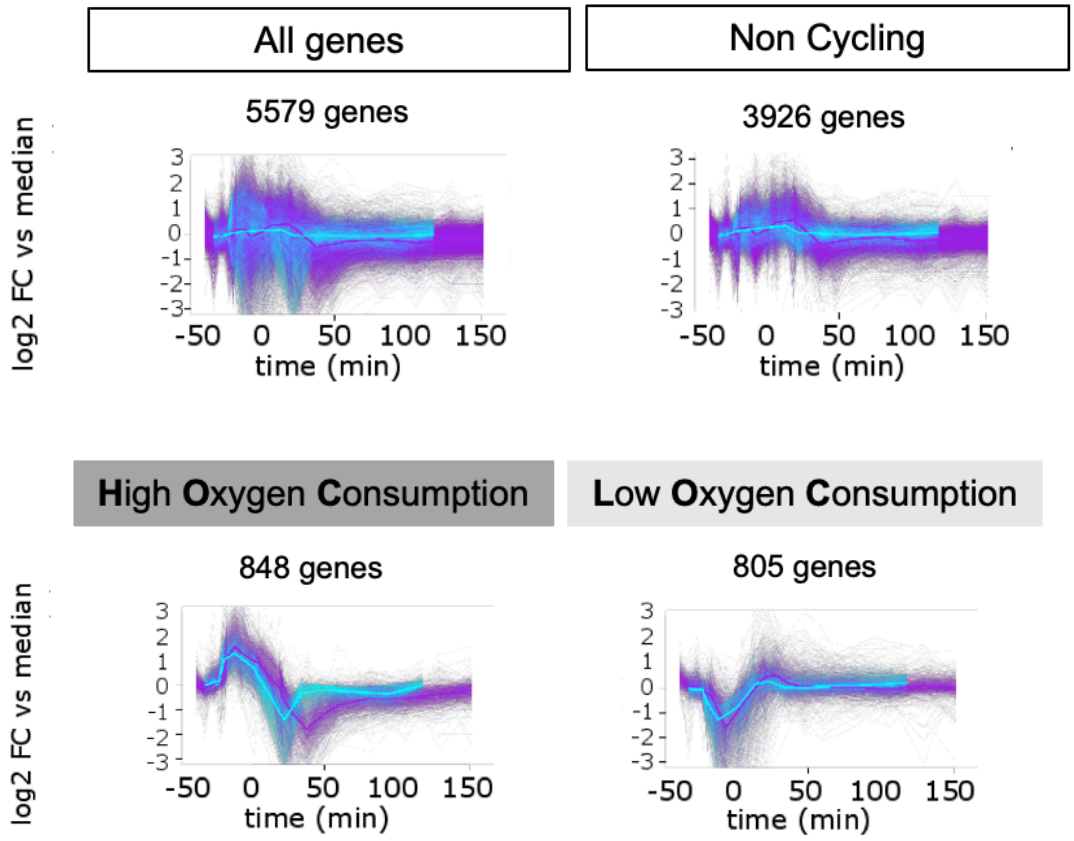

Figure 1.4 Nascent and steady-state transcript levels cycle

Log 2 fold-change of the counts vs median counts over the YMC (log2 FC vs median), respectively for NET-Seq and RNA-Seq counts, for all expressed genes and NET-Seq clusters found through k-means clustering; Non-cycling, HOC and LOC. In blue, NET-Seq : Measure of nascent transcript levels (from 11 timepoints across the YMC) , In purple, RNA-Seq : Measure of steady-state transcript levels (from 22 timepoints across the YMC). Modified from Feltham et al., (2020).

1.2.3.4.2 Transcription-independent regulation over the YMC

Surprisingly, not all genes from the data shown at Figure 1.4 were found to correspond between NET-seq and RNA-seq clusters. For example, 29% of genes found in the HOC RNA-Seq cluster, belonged to the “low-amplitude cycling” NET-seq cluster, while 7% of genes in the low-cycling amplitude cluster were found in the LOC-NET-seq cluster (Feltham et al. 2020, data from Dr. Xi). The results thus indicated that transcript stability is affected along the cycle and for different classes of genes and thus that transcription only can’t explain the steady state transcript profiles.

First, **RNA splicing** might be involved in transcript levels regulation as the examination of introns-exons junctions for transcript levels measured along the YMC, indicated splicing of Ribosomal Protein transcripts. Indeed, transcripts of RP genes are detected in early HOC phase, while spliced transcripts appeared a few minutes later (Kuang et al. 2014).

Second, it is likely that **mRNA degradation** plays a major role in establishing oscillating steady-state transcript levels. In fact, except for a few clusters and gene subclasses, a strong correlation was found between the average half-life of transcripts, the widths of the transcript level peaks and the phase of the YMC in which they are clustered. For example, transcripts involved with ribosome biogenesis, mRNA processing and rRNA metabolism showing a short expression peak in early HOC (Tu et al. 2005), are particularly short-lived (<10min) while transcripts of genes implicated in oxidative phosphorylation, showing wider expression peaks in late HOC (Tu et al. 2005) possess longer half-lives (>60min) (Soranzo et al. 2009). Transcript turnover was thus suggested to be a major way of gene expression regulation along the YMC. Nevertheless, transcript half-lives used in (Soranzo et al. 2009) might not reflect actual $T_{1/2}$ in YMC cultures as these were gathered from yeast logarithmic cultures (Kuai et

al. 2005, Grigull et al. 2004) and not directly from YMC cultures, in which transcript degradation rates might be altered as YMC cultures are growing at a slower rate.

Third, RNA binding proteins might be involved in the regulation of transcripts turnover. Binding motifs for Puf proteins (Pumilio RNA binding protein) (Gerber et al. 2004, Wang et al. 2018) were found at genes for which transcript levels peak in early HOC phase of the YMC. These proteins were thus suggested to affect the stability of some transcripts along the YMC **(**Tu et al. 2005, Soranzo et al. 2009, Machne & Murray. 2012). Thus, it seems that for some sub-classes of genes, constituting specific clusters of the YMC, post-transcriptional regulation acts upon transcript levels. mRNA stability seems to be a key component of global transcript oscillation, but detailed mechanistic explanations of temporal organization of mRNA turnover rates along the YMC are still missing.

Why do transcription and transcript levels cycle along the YMC?

1.2.3.5 Protein levels remain constant over the YMC

Up until recently, the oscillation of transcripts was assumed to lead to the oscillation of proteins over the metabolic cycle. Many described changes in transcript levels as “ways to anticipate the next phase of the YMC” (Klevecz et al. 2004 ,Kuang et al. 2014). As gene expression clusters group genes coding for proteins involved in similar functions (Klevecz et al. 2004, Tu et al. 2005, Kuang et al. 2014), some groups developed the concept of phase anticipation, with transcription and transcript levels peaking right before the time at which proteins coded for are needed. This hypothesis was raised under the assumption that the rate of protein production would be coordinated to the rate of transcription and that both processes of transcript and protein manufacturing would take place within a short temporal window (Klevecz et al.

2004). This idea of metabolism as a production line (Wells. 2004) to explain gene expression changes detected along the YMC was proposed by Kuang et al., with their "**Just-in-time supply chain model**" (Kuang et al. 2014).

However, recent proteomic data partly contradict this model. Indeed, although transcription and transcript levels cycle during the YMC, recent proteomic analysis revealed protein levels stay relatively constant over the YMC.

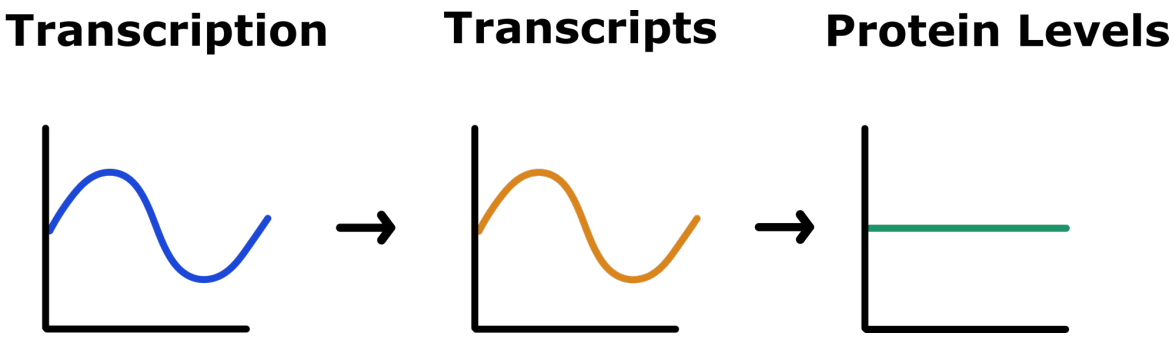

Figure 1.5. Protein levels are de-coupled from transcriptional changes along the YMC
Adapted from (Feltham et al. 2020)

Using puromycin incorporation array as an active measure of translation and Tandem Mass Tag labelling as a measure of protein abundance, translation was shown to cycle while proteins levels remain constant over the YMC (Figure 1.5) (Feltham et al. 2020). Similarly, recent TMT labelling experiments on YMC samples corroborated the labs findings and showed that most proteins (>96% of the proteome) present no significant oscillation in abundance over the YMC (O'Neill et al. 2020). Moreover, these experiments performed on YMC cultures, indicated that protein levels remain constant at different growth rates. These results raised the question of how global protein levels remain constant, when transcription and transcript levels change along the YMC.

Feltham et al., suggested that protein homeostasis detected along the YMC result from low protein turnover rates. Indeed, protein half-lives are high, with median protein $T_{1/2}$ corresponding to 17.2hr (Lahtvee et al. 2017) and median transcript $T_{1/2}$ corresponding to 32 min (Geisberg et al. 2014). Moreover, protein half-lives are also longer than the periods of the yeast metabolic cycles and their respective doubling time used in both studies (YMC periods of 4.9h, 6.4h, 8.3h , DT of ˜8.66h, 11.55h, 15.4h for O'Neill et al., 2020, YMC period of ˜3h20-3h30min, DT of ˜8.45h for Feltham et al., 2020). Therefore, it is likely that high protein half-lives or low protein degradation rate can buffer changes in the protein production rate. I.e. small increases in protein levels might occur every metabolic cycle but these changes are not significant enough to be detected when large protein pools are constantly present due to low turnover rate (Feltham et al. 2020). In conclusion, the hypothesis of a global and front-to-back gene-expression oscillation, including the tryptic "DNA->RNA->Protein" proved to be mostly wrong with recent studies demonstrating the lack of oscillation in global protein levels (Feltham et al. 2019, O'Neill et al. 2020).

1.2.3.5.1 Protein accessibility and activity is likely to change during the YMC

Nevertheless, the discovery of a flat proteome is particularly disconcerting from a mechanistic point of view. Indeed for metabolic states to evolve and change through time, reactions catalyzed by metabolic enzymes must occur. And if protein levels are not accounting for the metabolic changes than other processes must be involved. Thus, protein accessibility and/or activity were suggested to change along the YMC (O'Neill et al. 2020, Feltham et al. 2020). **First, protein accessibility** has been argued to play a major role in the regulation of protein activity along the YMC as a fraction of proteins was found to alternate between soluble and non-soluble states, together with

cytosolic pH change during the metabolic oscillations, indicating that biomolecular condensates (BMCs), could constitute a mean of regulation of the cycle's progression (O'Neill et al. 2020). **Second,** because some of the essential metabolites that oscillate during the YMC can induce **protein post-translational modifications** and PTMs constitute a very efficient way for cells to rapidly modify the activities of enzymes in order to transition to different states in a precise manner through space and time (Pawson & Scott. 2010), it was hypothesized that proteins PTMs take part in the regulation of the YMC progression (Feltham et al. 2020).

If transcription and transcript levels do not drive the YMC by changing proteins levels than how come these cycle?

The discovery of a flat proteome along the YMC refutes to some extent the "just-in-time model". With this arises the question of whether transcription and transcripts oscillation are merely a consequence of metabolic changes.

1.2.3.6 Gene expression oscillations is a global growth response

Here, some of the models and hypotheses as to why such partitioning of gene expression occurs through the YMC are presented. In fact, some studies indicate that gene expression profiles observed along the YMC might be due to more general gene expression response.

A correlation between gene expression and growth rate was found for a large proportion of genes for which transcript levels were found to oscillate along the YMC. Indeed, a global growth rate response (GRR) was identified for genes peaking along the YMC. HOC genes generally presented positive GR slopes while LOC genes showed negative correlations with growth rate (Brauer et al. 2008). Similarly, gene

expression was analyzed for its relationship to universal growth rate response (UGRR, independent from the limiting nutrient in culture) (Slavov and Botstein. 2011). As identified through microarray gene expression studies, 25% of the yeast genome show this characteristic. Genes involved in biosynthesis, ribosome biogenesis, translation and its regulation, post-transcriptional regulation of gene expression and mitochondrial translation show a positive response while genes involved in autophagy, vacuolar protein catabolic processes, cell differentiation and stress response present a negative UGRR. Remarkably, genes found to show a universal growth rate response all cycle during the YMC. UGRR genes for which transcript peak in HOC show a positive growth response as opposed to UGR genes for which transcripts peak in LOC (Slavov and Botstein. 2011). Next, the peak in transcript levels of environmental stress response (ESR) genes in LOC was suggested to result from a more global growth rate response, as gene expression of many environmental stress response (ESR) genes (Gasch et al. 2000) was found to correlate with growth rate, indicating that perhaps typical gene expression patterns arising from stress response might be due to a more general growth rate response of the cells under stress (Castrillo et al. 2007, Brauer et al. 2008). Finally, a “global delayed negative feedback mechanism” has been proposed to describe the relationship between the energetic states of the budding yeast cells and their gene expression patterns. Put simply, anabolic processes evoked for the different HOC clusters might be coupled to the HOC-phase as they require high energy states as opposed to catabolic processes found in LOC-clusters. Thus, energy state of the yeast culture could directly impact chromatin architecture via ATP-dependent chromatin remodeling complexes, regulate gene expression and lead to transcription and transcript levels oscillations along the YMC (Machne & Murray. 2012).

Together these findings indicate that oscillations in transcription and transcript levels within the context of metabolic cycling might arise from a more global transcriptional response linked to growth and nutrient starvation. Thus, the complex gene expression patterns detected along the YMC might simply reflect a global response to growth leading to a cascade of transcriptional activation (Soranzo et al. 2009). This implies that changes in transcription and transcript levels along the cycle are not driving the periodic metabolic changes throughout the YMC but are rather a consequence of it (Feltham et al. 2020., O'Neill et al. 2020).

1.2.4 The YMC is a model system for the study of quiescence and growth

According to gene expression studies of the YMC (Figure 1.3 & S.1 Appendix), during the LOC phase of the YMC, catabolic reactions take place enabling protein recycling and genes usually expressed in stationary phase**,** with gene ontology terms for autophagy and stress response, are up-regulated. On the opposite, during the HOC phase, hallmarks of anabolism are found. Aerobic respiratory growth occurs and proliferation follows with the commitment of some cells to the cell division cycle. Genes involved in biosynthesis, growth, DNA replication but also cellular respiration are up-regulated (Klevecz et al. 2004, Li & Klevecz. 2006, Tu et al. 2005, Slavov et al. 2011, Kuang et al. 2014, Felhtam et al. 2020). For these reasons, the YMC is often described as a system oscillating between Quiescence and Growth (Klevecz et al. 2004, Tu et al. 2005, Tu & McKnight. 2006, Cai et al. 2011, Kuang et al. 2014, Causton et al. 2015, Mellor et al. 2016, O'Neill et al. 2020).

Next, quiescence, growth and the cell division cycle (CDC) and their implication within the context of the yeast metabolic cycle (YMC) will be discussed.

1.2.4.1 YMC-CDC coupling

The YMC is a cycle of metabolic changes and is different than the cell division cycle (CDC). At all times during the YMC, most cells are in G1 and only a proportion of the cells progress through the CDC during a specific period of time during the YMC (Figure 1.6) (Klevecz et al. 2004, Tu et al. 2005, Slavov & Botstein. 2011, Burnetti et al. 2016). Metabolic cycles can be maintained in the absence of the cell division cycle (CDC) (Slavov et al. 2011), although the two cycles are known to be coordinated (Tu et al. 2005, Slavov & Botstein. 2011, Burnetti et al. 2016).

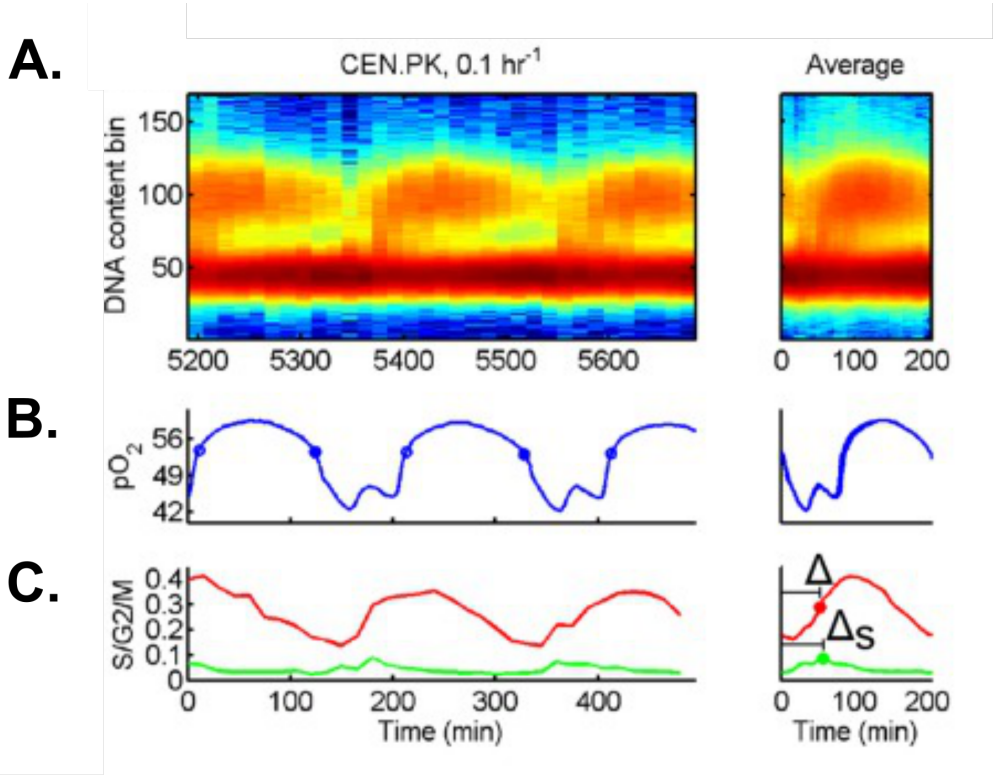

Figure 1. 6 DNA replication along the YMC

A. *DNA content along the YMC (assessed by DNA staining in cytox green an FACS).* ***B.*** *The blue line indicates the dissolved oxygen levels in the culture media of a YMC culture* ***C.*** *Fraction of cells in S/G2/M phases (in red) or in S phase only (in green) of the cell division cycle during the YMC. The right panel shows the average over multiple cycles and 0 indicates the time of entry into the HOC phase (Burnetti et al. 2016).*

1.2.4.1.1 The gating of DNA replication is an outdated model of the YMC

Although no perfect correlation could be detected between the YMC and CDC, experiments showed that DNA replication (S-phase of the cell division cycle) of a proportion of the cell population happened in a “single pulse” per YMC, only after the HOC peak, when the oxygen consumption is decreasing in late-HOC, when dissolved oxygen levels in the media increase (Kleveckz et al. 2004, Tu et al. 2005). This was observed by different labs, using propidium iodide or Cytox Green and fluorescence activated cell sorter (FACS) to monitor DNA replication (Figure 1.6) together with brightfield microscopy to identify and count budded cells along the cycle (Tu et al. 2005, Klevecz et al. 2004, Feltham et al. Laxman et al. 2010, Slavov & Botstein. 2011, Burnetti et al. 2016). This lead to the theory that evolutionary adaptations of metabolism together with respiration lead to time-segregation of oxidative metabolism and DNA replication (Kleveckz et al. 2004, Tu et al. 2005). This hypothesis was coherent with a temporal organization of redox processes (Murray et al. 1999). Undoubtedly, oxidative metabolism can lead to production of Reactive Oxygen Species. Increasing levels of ROS are detrimental for the cells (Murphy. 2009, Eleutherio et al. 2018) and can even lead to cell death in stationary phase (Fabrizio et al. 2004, Herker et al. 2004). In fact, CDC impaired mutants capable of cell division in all phases of the YMC (including the oxidative phase or early HOC) showed higher point mutation rates than WT cells under YMC conditions, implying DNA replication in oxidative environment could lead to DNA damage during the YMC (Chen et al. 2007). In light of these results, the hypothesis of a role for the YMC in “gating the DNA replication” was for long believed by many (Tu et al. 2006, Reinke & Gatfield. 2006, Chen et al. 2007), until some studies cast doubts on this theory. First, DNA replication was shown to happen at a time dependent on feeding rate of the culture; in the

oxidative phase in early HOC phase of the YMC, but also in LOC depending on the feeding rate (Slavov & Bostein. 2011). Second, metabolic cycles persisted even in absence of cell division when the fraction of cells in G1 among the population increases up to 99% (Slavov et al. 2011). The original hypothesis was further challenged, as Murray & Lloyd explained that past papers (von Meyenburg. 1969, Munch et al. 1992) actually showed DNA replication can take place in HOC and that Tu et al., (2005) also presented such data, but interpret it differently by defining new phases; OX, RB, RC which do not correspond to the HOC and LOC oxygen consumption phases defined by Satroutdinov et al., (1992). However, opinions on past experiments indicates that the relationship between the YMC and CDC is complex (Murray & Lloyd. 2021).

1.2.4.1.2 The relationship between growth and CDC

CDC and Growth are linked by nutrient availability, translation rate and cell size for the passage of cells through Start (Hartwell et al. 1974, Johnston et al. 1977, Hartwell & Unger. 1977, Moore. 1988, Futcher. 1996, Jorgensen et al. 2004). A linear relationship is observed between growth rate and the fraction of cells in G1 under batch culture in limiting concentration of any essential nutrients (Brauer et al. 2008), confirming cells growing slowly spend more time in G1 (Beck & von Meyenburg. 1968, Unger & Hartwell et al. 1974, Hartwell. 1976, Lorincz & Carter. 1979).

1.2.4.1.3 The transition from LOC to HOC and the exit from G1 is believed to be coordinated through the growth rate

The growth rate also impacts YMC synchronous cultures and the cell cycle progression (Slavov et al. 2011, Burnetti et al. 2016), as growth-retarded CDC mutants

show impaired metabolic oscillations providing evidence of a connection between the two cycles (Chen et al. 2007).

During the slow synchronous metabolic cycles of the YMC, the proportion of cells progressing through the CDC changes; cells are found in a G0/G1 state in LOC, while a proportion of the cell population progress through the CDC and transition to a S/G2 or M phase each YMC after passing through HOC (Tu et al. 2005, Klevecz et al. 2004, Feltham et al. 2020, Laxman et al. 2010, Slavov & Botstein. 2011, Burnetti et al. 2016). Importantly, the length of time spent in the G1 phase of the CDC can be coordinated to the growth rate of YMC cultures as presented at Figure 1.7 (Slavov & Botstein. 2011).

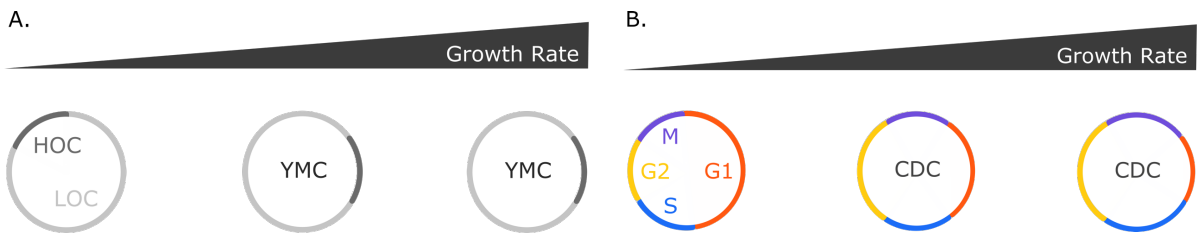

Figure 1.7 Model of the relationships between YMC and CDC phases and growth-rates
A. *The length of the LOC phase decreases as the growth rate increase while the length of the HOC phase stays constant over the YMC.* ***B.*** *The length of the G1 phase of the CDC decreases as the growth rate increases over the YMC. Modified from Slavov et al., (2011).*

Indeed, the YMC period shortens at higher feeding rate compared to lower feeding rate (the feeding rate (dilution rate) equals the growth rate in YMC cultures). This difference in periods result from shorter or longer LOC phases, while the HOC phases period stays relatively invariant when tuning the feeding rate (Figure 1.7. A). Accordingly, as the growth rate reduces and the time spent in LOC phase increases, the cell population show longer G1 phases, as most cells only bud after HOC phase

(Figure 1.7.B) (Slavov & Botstein. 2011). On one hand, time spent from the LOC to the transition point at which a maximum proportion of cells undergoes DNA replication in HOC stays constant regardless of the feeding rate of the YMC cultures. Indeed between dilution rates of 0.1 to 0.05 hr^{-1} (glucose minimal media), the strain CEN.PK shows a time interval of around 56.5 to 53.5 minutes between the start of HOC and the transition to S-phase (in mid HOC at these dilution rates), rising with levels of dissolved oxygen in the media (Burnetti et al. 2016). On the other hand, the LOC phases showed longer extent of time coupled to longer G1 phases, at lower feeding rates under phosphate starvation (Slavov et al. 2011). Moreover, the entry to HOC provoked by a pulse of ethanol in LOC, was shown to permit a passage to cell cycle (Robertson et al. 2008). It was then argued that the time cells spend to accumulate resources such as glycogen and trehalose is dependent of the dilution rate (in LOC), while the time spent to use the metabolic resources for growth, DNA replication and cell division is hardly affected (in HOC), suggesting a universal timing for energy expenditure (O'Neill et al. 2020). Note that time in HOC phase differs between strains, most likely due to the slightly different Growth-rate to CDC-rate proportional relationships of each strain (Burnetti et al. 2016).

1.2.4.1.4 The YMC gates protein synthesis

Evidence that the passage through Start and DNA replication is in fact joined to the transition from LOC to HOC through the use of stored carbohydrates (Muller et al. 2003) gave rise to a more convincing model; the "Finishing-kick to Start" or the gating of protein synthesis (Futcher et al. 2006). This theory implies that cells committing to the CDC during the YMC need to (i) accumulate enough resources in LOC to be able to transition to HOC, (ii) in HOC an extra boost of energy and protein is provided for

cells allowing the transition to Start. This explains why most cells in the YMC would transition to DNA replication only after going through respiration providing high energy for the cells to synthesize new proteins and allowing the cells to grow, DNA replication and cell division (Burnetti et al. 2016). With the “Finishing-kick to Start” hypothesis, a boost in protein synthesis was proposed to counter high turnover rates of cyclins, granting access through the Start checkpoint of the CDC (Futcher et al. 2006). This idea is supported by the existence of further metabolic checkpoints at Start through the assessment of nutrient availability, translation rate and cell size required for the passage of cells through Start (Hartwell et al. 1974, Jones et al. 2005, Saqcena et al. 2013, Takubo et al. 2013) as argued by Papagiannakis et al., (2017). Feedback mechanisms have also been suggested to act on metabolism in YMC cells, such as cyclin-mediated (Clb1-Cdk1) phosphorylation of mitochondrial proteins, which was found to upregulate mitochondrial respiration in cells, increasing energy levels in cells before G2/M transitions (Wang et al. 2014, Papagiannakis et al. 2017). Other studies corroborate the “finishing kick to Start” model and argue for a “gating of protein production” allowing cells to grow and proceed to catabolic reactions “at the right time”, saving energy costs (Slavov & Bostein. 2011) by only allowing a translational burst “when the cell is ready” notably through the activation of the TORC1 signaling pathway, eventually leading to protein homeostasis (Fetham et al. 2020., O’Neill et al. 2020, Machne et al. 2021).

1.2.4.1.5 The coupling model of independent cycles: YMC – CDC

The “simplified model” of YMC-CDC coupling by Burnetti et al. is presented at Figure 1.8. With this model, typical dissolved oxygen levels are represented over a population of cells. Orange lines represent LOC phases, while purple lines represent HOC

phases. Upon each transition to HOC, a fraction of the population progress from a “LOC-state” (quiescent-like in orange) to a “HOC-state” (growth + CDC like in purple). HOC-state cells catabolize stored carbohydrates and secrete metabolites. Through cell-to-cell communication, more cells are suggested to be recruited in this “growth state” (Robertson et al. 2008) though many cells will stay in a LOC-state because they have not reached the adequate levels of energy and/or carbohydrate stores (black dots) for a transition to Start. Thus, it is believed that these cells will continue to grow slowly during the next cycles (Roberston et al. 2008, Burnetti et al. 2016).

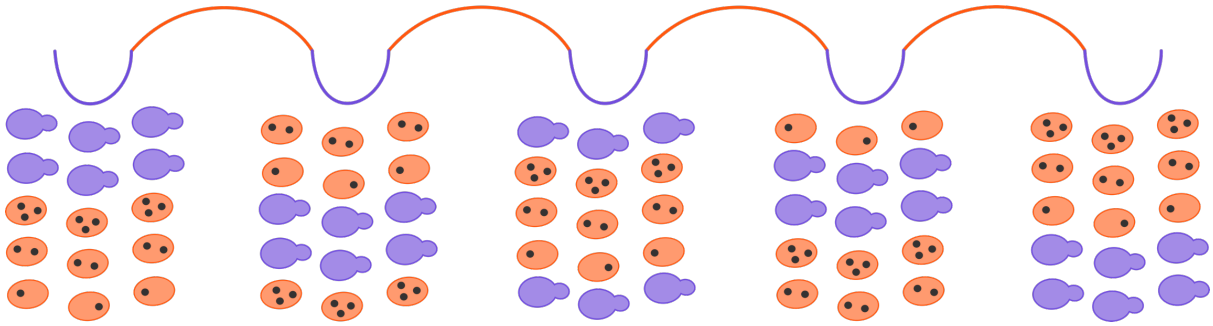

Figure 1.8 The coupling of YMC and CDC; a recruitment model

Typical dissolved oxygen levels are represented, LOC phase is presented in orange, HOC phase is represented in purple. The YMC population is represented; cells in a “LOC” state are orange while cells in a “HOC” state are purple. At each HOC phase, a proportion of cells break down their carbohydrate stores, transition to a HOC state (a state of growth) and progress through the cell cycle (purple budded cells). These cells were suggested to release metabolites and by doing so, recruit other cells with enough carbohydrate stores (black dots) to transition to a HOC state and exit G1. Modified from Burnetti et al. (2016).

In conclusion, metabolic states oscillate in cells in an autonomous manner, with a frequency regulated by nutrient availability. Such oscillations can lead to the passage through metabolic checkpoints, perhaps involving CDC proteins and metabolites interactions, allowing the transition through Start (Shi et Tu. 2013, Burnetti et al. 2016). After the passage through Start, the following CDC cascade itself could regulate the

metabolic state of the cells. Thus, while the YMC is an autonomous cycle, it can be coupled to the CDC (Papagiannakis et al. 2017).

1.2.4.2 The link between metabolic cycling and quiescence

For long it has been argued that the YMC reflects fluctuations of a yeast cell population between growth and quiescence, mostly because growth-related transcripts are only expressed during the HOC phase and stationary phase transcripts are expressed during the LOC phase, as measured at the population level (Klevecz et al. 2004, Tu et al. 2005, Tu & McKnight. 2006, Cai et al. 2011, Kuang et al. 2014, Causton et al. 2015, Mellor et al. 2016).

However, stationary phase populations are heterogenous and are not only composed of quiescent cells. Indeed, the stationary phase is characterised by cells that are no longer proliferating but the stationary phase population differentiate into at least four different cells types including quiescent, senescent and dead cells (Figure 1.9) (Li et al. 2015, Miles et al. 2020) and therefore do not represent one metabolic or transcriptional state (Garcia-Martinez et al. 2004, Aragon et al. 2008, Werner-Washburne et al. 2011, Li et al. 2015, Laporte et al. 2018, Miles et al. 2020).

Thus, based on the literature, as stationary phase cells include more than one cell type, YMC cell populations might be more complex than thought.

Next, sub-populations of stationary phase cultures and their characteristics are described.

1.2.4.2.1 Quiescence

Quiescence is a reversible non-proliferative state. It is common to some eukaryotic cell types such as stem cells but also to many microbes such as *Saccharomyces cerevisiae* (Werner-Washburne et al. 1993, Aragon et al. 2008). Quiescence can be induced in yeasts under stationary phase, when cells reach high density (Gray et al. 2004). It allows cells to survive to essential nutrient depletion (Lillie & Pringle. 1980, Valcourt et al. 2012). Cells that fail to enter a quiescent state will end up going through senescence and apoptosis (Terzi et al. 2016). Quiescence is characterized by reversible cell cycle and growth arrest. This means that upon improved conditions, cells can exit G0, resume the cell cycle (G1) and high growth (Gray et al. 2004). Figure 1.9 depicts the model for cell differentiation under stationary phase (Allen et al. 2006, Davidson et al. 2011, Werner-Wahsburne et al. 2012).

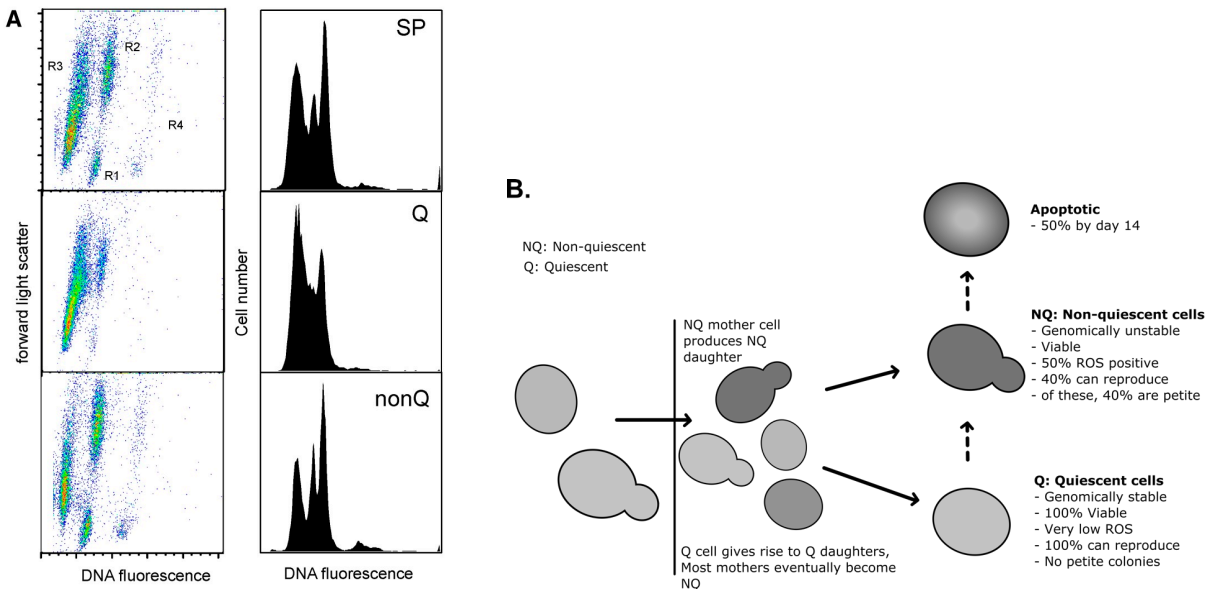

Figure 1.9 Model of cell differentiation in stationary phase cultures

A. *Identification of 4 sub-populations (R1, R2, R3, R4) in stationary phase cultures by Li et al., (2015).*

B. *Canonical view of the partition of cells taking place during stationary phase ; into 2 sub-populations; large non-quiescent mothers and small quiescent daughters, adapted from Davidson et al., (2011).*

1.2.4.2.2 Cell differentiation in stationary phase cultures

Transition to quiescence is initiated through a cascade of events in yeast cultures (grown in rich glucose media) that progress from exponential phase to stationary phase (Figure 1.9) (Allen et al. 2006, Davidson et al. 2011, Werner-Washburne et al. 2012). First, the metabolic process of quiescence arise before glucose exhaustion. When around half of the glucose present in the medium is consumed (Lillie & Pringle. 1980), the activity of glucose transporter is increased (Youk & Van Oudenaaden. 2009). As glucose accumulates in future quiescent cells, under the form of carbohydrate stores; trehalose and glycogen (Lillie & Pringle. 1980) or even in cell walls (Orlean et al.. 2012) cells become denser (Werner-Washburne.. 1993). When analysed, the Percoll density gradient of exponentially growing culture shows a somewhat homogeneous phase as opposed to the one of stationary phase culture, for which two phases are detected. The lower fraction of cells is composed of dense quiescent cells, while the upper fraction is composed of less dense non-quiescent cells (Allen et al. 2006). Both the accumulation and metabolization of carbohydrate stores are essential for the processes of quiescence entry and exit, respectively (Werner-Washburne. 1993, Shi et al. 2010). However, though necessary, trehalose is not sufficient for cells to transition to quiescence (Miles et al. 2020), as cells can enter quiescence despite low carbohydrate store levels (Li et al. 2013) and cells accumulating trehalose can also be light (Miles et al. 2019). Nevertheless, these two fractions have been for long an important criterion differencing quiescent and non-quiescent cells.

Next, before the diauxic shift, the cell growth arrest in G1 begins, with half of the yeast population transitioning to a G0/G1 state (Miles et al. 2013). The inhibition of the Cyclin-dependent Kinases (CdK) is required for this conversion (Miles et al. 2020).

After glucose exhaustion and post diauxic shift, when the culture transition from fermentation to aerobic respiration, the last cell division occurs (Allen et al. 2006). This division is asymmetric as mother and daughter cells will differ considerably (Figure 1.9) (Miles et al. 2020). Canonically, 50% of the cells will become **non-quiescent (NQ).** These are **mother** cells that are able to divide in post diauxic phase. These cells keep budding in an asynchronous way, as they are most likely unable to stop the cell cycle after starvation, thus the NQ population is made of both mother and daughters and is heterogeneous, in many ways (Li et al. 2013, Miles et al. 2019). On the opposite 50% of the population is arrested in G1. These are **quiescent** cells **(Q)**, mainly composed of unbudded **daughter cells** with no bud scars (Werner-Washburn et al. 1993, Gray et al. 2004, Allen et al. 2006, Aragon et al. 2008, Davidson et al. 2011, Werner-Washburne et al. 2012).

1.2.4.2.3 Characteristics of stationary phase cultures

Characteristics of quiescent and non-quiescent cells have been investigated over the years by many and were preciously gathered in recent reviews published on the study of quiescence in budding yeast (Miles et al. 2020, Breeden & Tsukiyama. 2022).

On one hand, quiescent cells are dense (Miles et al., 2020). Quiescent cells also present major morphological changes including highly glycosylated thicker cell walls (Allen et al. 2006, Orlean. 2012). Several organelles also undergo major reorganization upon entry into quiescence (Miles et al. 2020). These cells are resistant to stress such as heat shock but also desiccation. They remain viable under nutrient starvation and show a lower metabolic rate (Werner-Washburne. 1993, Allen et al. 2006). Many transcription factors are also implicated in the regulation of quiescence. G1 arrest is regulated through Msa1 and Msa2 transcription factors which repress

histones and regulates both SBF and MBF (G1 transcription) complexes (Miles et al. 2016). During quiescence, some TFs activate transcription while others repress it (McKnight et al. 2015). Together, transcription factors activities induce a global decrease in histone lysine acetylation levels via the Rpd3L histone deacetylase (McKnight et al. 2015., Miles & Breeden. 2016) leading to more condensed chromatin (Pinon et al. 1978). Accordingly, lower transcript and protein levels are measured as transcription and translation rates decrease massively. This occurs before glucose exhaustion and continues in stationary phase (Choder. 1991, Jona et al. 2000., McKnight et al. 2015, Boucherie et al.1985, Fuge et al. 1994). Next, while 90% of the splicing machinery is used for ribosome production under exponential growth, introns compete for spliceosomes and ribosome production slows down under nutrient starvation or limitation most likely through TORC1 inactivation or down-regulation (Warner et al. 1999, Morgan et al. 2019, Breeden & Tsukiyama. 2022). RNA and protein degradation is also increased upon quiescence (Breeden & Tsukiyama. 2022). Active mechanisms of regulation of RNA degradation take place upon starvation as Puf proteins, involved in RNA turnover (Gerber et al. 2004, Wang et al. 2018), are found at transcripts involved in growth mitochondrial and ribosome synthesis and activities (Foat et al. 2005). Finally, although proteasomes and ubiquitin were shown to be aggregated during stationary phase (Laporte et al. 2008, Shah et al. 2014, Marshall & Vierstra. 2018), these can also be degraded through autophagy. In fact, bulk autophagy is up-regulated upon nutrient starvation, stress (Huang et al. 2015) or only later upon quiescence exit if the population is under glucose exhaustion (Laporte et al. 2008).

Non quiescent cells on the other hand, are less dense, stress resistant and viable than quiescent cells (Allen et al. 2006). These cells possess many vesicles, thought to be resulting from enhanced autophagy. In the early stage of the stationary phase, only half of the non-quiescent population is able to transition to CDC, a process thought to be genetically regulated. The part of the population of NQ cells that is able to divide produce petite colonies (˜half of the NQ fraction; lacking mitochondrial DNA) (Allen et al. 2006). This was suggested as a mechanism to protect cells from high ROS levels (Miles et al. 2020). These cells also show different re-organisation of their mitochondrial network (Laporte et al. 2018). At a more advance stage of stationary phase however, a large proportion of the non-quiescent cells slowly lose through time their ability to divide (90%) and die via apoptosis or necrosis (50%) (Fabrizio et al. 2004, Herker et al. 2004). This was proposed to result from the asymmetric division taking place post diauxic shift, as mother cells from stationary phase cultures can accumulate and retain damages (Aguilaniu et al. 2003, Lai et al. 2002, Miles et al. 2020).

Finally, whether or not cells enter quiescence under nutrient starvation in stationary phase, seem to be highly linked to the metabolic status of the cell, with major signalling pathways such as TORC, Ras/cAMP dependent PKA and AMPK regulating nutrient response but also quiescence entry, maintenance and exit (Spain et al. 2018 Biorxiv, Breeden & Tsukiyama. 2022).

1.2.4.2.4 Entry and exit from quiescence during the YMC

Evidence other than gene expression (Klevecz et al. 2004, Tu et al. 2005, Tu & McKnight. 2006, Cai et al. 2011, Kuang et al. 2014, Causton et al. 2015, Mellor et al.

2016) seem to indicate that transition in and out of a quiescent-state occurs during the YMC. First, bulk levels of trehalose and glycogen raise upon entry into quiescence but also in LOC phase while they decrease upon exit from quiescence but also in early HOC phase of the YMC at the same time that carbohydrate stores are used for growth and proliferation (Li et al. 2013, Muller et al. 2003, Shi et al. 2010). It was thus argued that the accumulation of trehalose and its utilization permits the entry and exit from quiescence along the YMC (Muller et al. 2003, Shi et al. 2010, O'Neill et al. 2020). Second, major epigenetic changes were recorded during the metabolic cycle. Histone post-translational modifications (H-PTMs) in particular lysine acetylation, were shown to play a critical role in transcriptional regulation during quiescence entry, maintenance and exit (Friis et al. 2009, Mews et al.,2014) but also during the YMC (Cai et al. 2011, Kuang et al. 2011, Shi & Tu. 2013, Kuang et al. 2017, Sanchez-Gaya et al. 2018). Acetyl-CoA pools were suggested to feed histone acetylation at growth genes during the HOC phase of the YMC, granting a quiescence exit of YMC cells as acetyl CoA levels peak, at the same time then histone lysine acetylations do (Cai et al. 2011).

Together these findings indicate that cells from synchronous YMC cultures likely possess similar metabolic states as the ones found in stationary phase (quiescent and non-quiescent) and undergo similar transitions; entry/exit from quiescence.

1.2.4.2.5 The total biomass of the yeast culture seems essential for the establishment of yeast metabolic cycles and as well as for quiescence entry and exit

The link between YMC and quiescence is explored, although more experimental evidence is required. The transition to quiescence in batch cultures is similar to chemostat cultures when inducing the YMC: glucose exhaustion, a diauxic shift and a

starvation period of more than 6 hours take place in the prototrophic high-density yeast batch culture used to induce the YMC (Klevecz et al. 2004, Tu et al. 2005, Fetham et al. 2020). Indeed, quiescence in batch cultures starts upon limiting concentration of glucose, when glucose uptake is boosted in cells (Miles et al. in preparation, Miles et al. 2020, Li et al. 2013). Next, both entry into quiescence and entry into the YMC seem to depend on the total biomass of the culture. Both quiescence entry and the overall induction of the YMC require the cells progression through the diauxic shift, which happens when the yeast population reaches a high cell density (Zampar et al. 2013). In contrast, the initiation of the YMC, and the first HOC phase, is usually induced upon feeding of the culture (Klevecz et al. 2004, Tu et al. 2005, Fetham et al. 2020). Remarkably, HOC phase was also reported to start upon sampling of high volumes of culture during the LOC phase (Xi. DPhil thesis. 2019).

Thus, the transition into the HOC phase of the YMC culture, seems somewhat similar to the exit from quiescence which was shown to be induced by the addition of fresh glucose media to stationary phase cells, and also shows synchronous cell divisions (Allen et al. 2006).

Therefore, for both metabolic systems, YMC and quiescence, the ability to re-enter into growth and the cell cycle seems to be linked to the culture biomass, because addition of fresh media dilutes the cultures in both cases and thus reduce the cell density and increase available carbohydrate concentration as suggested by Krishna & Laxman (2018).

1.2.5 Two (or more) sub-populations compose the YMC cultures

Despite many findings, indicating that the YMC is a model system under which cells oscillate between a stationary phase (perhaps quiescent-like) state and a growth state (Klevecz et al. 2004, Tu et al. 2005, Tu & McKnight. 2006, Cai et al. 2011, Kuang et al.

2014, Causton et al. 2015, Mellor et al. 2016), it is not clear whether all cells from the synchronous population of the YMC transition between these 2 states; “Quiescence vs Growth” (LOC vs HOC) or whether only a subset of the population do so. Previous studies did not always consider this question, while others claimed “almost all cells” synchronize during the YMC (Tu et al. 2005, Silverman et al. 2010). Most recent studies, however, tend to argue only a proportion of the cells transition to growth in HOC phase, with good logic but with little evidence as most studies used bulk results to build up models on (Burnetti et al. 2016, Slavov & Botstein. 2011).

1.2.5.1 Cells that proliferate and cells that don’t

The existence of at least two different populations along the metabolic cycle has been demonstrated. That is to say, dividing and non-dividing cells have been identified in YMC populations (Slavov et al. 2011). Indeed, only a fraction of cells will transition through Start and bud along each yeast metabolic cycle. However, different proportions of dividing cells were reported. Studies showed that a maximum of 10 to 50% of the cells from YMC population transition to S/G2 or M phase each cycle after passing through HOC (10% Feltham et al. 2020, 33% Klevecz et al. 2004, 35% Slavov & Botstein. 2011, 40% Burnetti et al. 2016, 46% Laxman et al. 2010, 50% Tu et al. 2005). Nevertheless, it was also noted that some cells divide asynchronously at all times along the YMC although the fraction of cells doing so is relatively low with around 10% of the population found in this state. (Robertson et al. 2008). These results thus suggest that along the YMC, some cells divide synchronously in late HOC, some cells divide asynchronously all along the YMC and some cells do not divide. Furthermore, according to YMC-CDC coupling models, cells that are able to proliferate and thus divide are most likely cells who just experienced high-growth and for which ATP levels increased allowing anabolic reactions (Futcher et al. 2006, Slavov & Bostein. 2011).

In other words, cells that commit to the CDC must have committed to a growth or "HOC-state" beforehand (Burnetti et al. 2016).

Nonetheless, it is uncertain whether all cells transitioning to a growth state or HOC-state will commit to the CDC and divide. Certainly, it has been argued that cells entering a "growth state" during the HOC phase, will inevitably enter and complete the cell division cycle (Burnetti et al. Laxman et al. 2010). Yet some results and mathematical models point out that it might be otherwise. Metabolic oscillations have been shown to continue, even when the fraction of cells in the population transitioning to S-phase is less than 1% (Slavov et al. 2011), therefore implying that not all cell committing to HOC transition to CDC. However, oscillations of dissolved O_2 recorded by Slavov et al., seem to decrease in amplitude as the fraction of G1 cells increase in the population, hinting that perhaps only a few cells, undergoing CDC are responsible for the HOC phase.

1.2.5.2 Cells that become dense and cells that don't'

Remarkably, cells of the YMC can also be grouped according to their densities. Percoll density gradient time-course experiments along the YMC, showed a shift in cell density, with a proportion of the population becoming lighter in OX phase and the majority of cells becoming dense in late RC (Shi et al. 2010). Thus it was suggested that only a proportion of cells transition to growth and re-enter the cell division cycle at each HOC phase, while all or most cells re-enter a quiescent-like state in LOC (Shi et al. 2010). However, the relationship between cell densities and proliferative state has not been explored along the YMC.

Together these findings thus suggest that only a subset of the population transition in and out of a quiescent-like state, to a “growth state” and is thus responsible for the typical oxygen consumption trace rather than the whole yeast cell population.

1.2.5.3 A two-state mathematical model: Quiescent-state versus Growth-state

Mathematical models have been used to understand metabolic oscillations. As reviewed by Patnaik., 2003, many were constructed on feedback mechanisms, based on bulk extra-cellular parameters and results, and did not consider key aspects in the establishment and maintenance of the YMC. However, some could restate characteristic oscillations of yeast metabolic cycles or even of cell division cycles (Wolf et al. 2001, Ozsezen et al. 2019, Boczko et al. 2010, Morgan, Moses & Young. 2018, Stowers et al. 2011, Young et al. 2012).

More recently Krishna & Laxman, proposed mathematical models to characterize the shift between two cell states; a Quiescent “Q-state” and a Growth “G-state”, based on the assumption that in YMC cultures, only a sub-population of cells will enter a growth state, induce the HOC phase and commit to the CDC (Krishna & Laxman. 2018). Although other models might explain this transition in a more accurate manner (best-fit models), this simple mathematical model was sufficient to recapitulate the experimental output that is the oscillation of dissolved oxygen in medium over time, characteristic measure of the YMC.

The model assumes; a constant cell density (as established by chemostat cultures), the presence of a metabolic resource driving the oscillations and cell-to-cell communication between G-state cells, Q-state cells and the metabolic resource. Three

scenarios were investigated; first (i) one part of the population generates the resource needed for the growth of the other part of the population (as suggested in Futcher. 2006), second (ii) only a part of the population responds to a signal produced by all cells, third (iii) (the most realistic model) the metabolic resource is accumulated by some cells only and consumed after a certain threshold is reached within cells (as suggested by O'Neill et al. 2020 and Shi et al. 2010).

If no switch is possible between the 2 states (G and Q) or if the switch is random then no oscillations can be detected. In order to observe oscillations, the switch between the two states has to depend on the cell density or the level of the metabolic resource. This two-state model uses frustrated bi-stability, meaning (i) the growth rate depends on and is proportional to the metabolic resource, which therefore act as a negative feedback loop; (ii) The switching rate of Q to G, G to Q or both depends on the metabolic resource so that when the metabolic resource decreases the net rate of G to Q follows, leading to bi-stability in the fraction of cells in a quiescent or a growth state, when the metabolic resource is kept constant; (iii) Finally, the changes in both the growth rate and accumulation/consumption of the metabolic resource should be slower than the transitions in the proportion of cells (Q and G states), i.e. the switching rates (Krishna & Laxman. 2018).

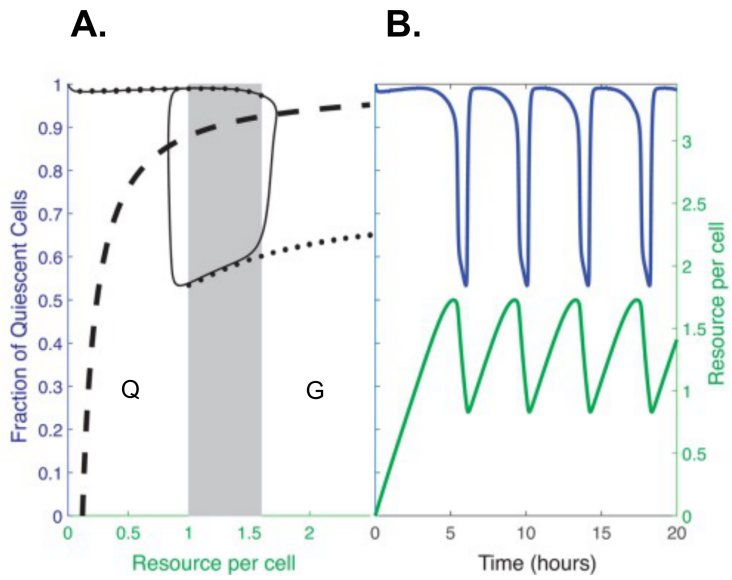

Figure 1.10 The push-pull" model explained

Frustrated bi-stability model between Quiescent-state and Growth-state. ***A.*** *When the resource per cell is low, all cells are under a quiescent-state (Q), when the resource per cell is high, cells are in a growth-state (G), when the resource per cell is limiting (grey area) the system is bi-stable. The thin black line shows the oscillation path and indicates cells cycle between a quiescent-state and a growth-state under limiting resource per cell (in the grey zone). The thick dashed black line indicates equal rate of production and rate of utilization or dilution of the resource. The solid black dot line indicate the proportion of cells in quiescent-state under steady-state conditions when the resource per cell does not vary.* ***B.*** *The fraction of cells in quiescent-state (blue) oscillates through time, it plummets right after the resources per cell (green) reaches a peak (Krishna & Laxman. 2018).*

Figure 1.10 shows the model. For small amount of metabolic resource, only the "Quiescent state" is possible. On the contrary when the amount of resource is high, then only a "Growth state" is possible. These predictions are reminiscent of single cell data and a model for which no coupling between YMC and CDC could be detected at low or high metabolic frequencies or feeding rates (Papagiannakis et al. 2017b, Ozsezen et al. 2019). For levels of metabolic resource in between these 2 extremes however, the system shows bi-stability. In this region, when the fraction of "quiescent" cells is high, the metabolic resource increases as the cells are unable to consume it,

thus the system follows the upper horizontal thin black line. Once it hits the upper right edge, 30 to 40% of the cells transition from a quiescent to a growth state (black thin vertical line on the right). Cells in a growth state consume the metabolic resource, leading to a decrease in its level, moving the system to the left (horizontal black line at the bottom) until it reaches the left edge, at which point cells transition back to a quiescent state. Simply, the metabolic resource is suggested to be slowly accumulated in cells until the levels of the resource reach a threshold which starts a cascade of events leading to the fast consumption of the metabolic resource (Krishna & Laxman. 2018).

This two-state mathematical model implies that the organisation of the yeast cell population is different in HOC and LOC phase. Most importantly, it provides an easy and convincing explanation as to how cells can transition between two metabolic states during the YMC, based on the available data provided for YMC populations. However, in order to confirm which biological scenario takes place during the YMC, biological data on single cell metabolism is required.

1.3 2nd Gap; A need for quantitative gene expression single cell studies

The examination of the relationship between metabolism and gene expression in general often miss an essential point of view as it rarely interrogates the nature and actions of individual cells. The lack of single cell studies is particularly true for synchronized cell populations of the YMC. Indeed, gene expression studies of the YMC focused on whole cell populations to study the connection with metabolism (Klevecz et al. 2004, Li & Klevecz. 2006, Tu et al. 2005, Slavov et al. 2011, Kuang et al. 2014, Felhtam et al. 2020). Many assumptions however were made about individual cell behavior in YMC populations (Klevecz et al. 2004, Tu et al. 2005, Futcher. 2006, Slavov et al. 2011, Slavov & Botstein. 2011, Kuang et al. 2014, Burnetti et al. 2016, Feltham et al. 2020, O'Neill et al. 2020, Robertson et al. 2010), although no real evidence followed as most experiments were and are still made on batch cultures whole cell population, except for a few perhaps using single cell techniques but only to gather population-averaged data. Thus, still little is known about single cell behaviour in yeast cell populations.

1.3.1 Metabolic oscillations in single cells

Only a handful of studies actually examine single cells in the context of metabolic cycling. These are presented next. Different type of Yeast Metabolic Oscillations (YMOs) have been observed and described at the population level. Fast oscillations of redox, pH and NADH levels were detected in single cells (Aon et al. 2007, Dodd & Krajl. 2017). YMOs happen within seconds to minutes as opposed to YMC oscillations showing dissolved oxygen oscillations with waveform shapes, and occurring within minutes to hours (Klevecz et al. 2004, Tu et al. 2005). Thus, faster oscillations (YMOs) have been described as glycolytic, respiratory and CDC independent.

Oscillations with longer period (YMCs) however, are characterized by the periodic change of metabolism; i.e. fermentation versus respiration and can be coupled to CDC and are the ones studied with the establishment of the YMC and the recording of the dissolved oxygen trace through time (Morgan, Moses & Young. 2018).

Nevertheless, recent studies demonstrated the existence of metabolic oscillations in single cells with longer periods (in the order of minutes to hours). Flavin oscillations were reported under four different nutrient conditions in single cells with periods of around 100 minutes (Baumgartner et al. 2018). Metabolic oscillations were also detected in single cells using NAD(P)H auto-fluorescence and Foster resonance energy transfer (FRET) to assess ATP levels combined with microfluidics (Papagiannakis et al. 2017). Coupling between the YMC and CDC was identified in single cells. Indeed, along the YMC, the transition into early cell cycle was detected to increase with NAD(P)H levels (in mid to late HOC), while the end of the mitotic phase was reported to occur when ATP levels are high and NAD(P)H are low in single cells. Although frequencies of both metabolic oscillations and CDC fluctuations always correlate and depend on the growth rate, the metabolic oscillations were demonstrated to be autonomous, with more cells exhibiting YMCs without CDC transitions at lower glucose concentration (Papagiannakis et al. 2017). Finally, recent data gathered using experiments and mathematical modelling suggest that the YMC-CDC coupling does not require YMC batch culture settings and synchronization of the cell population, as these oscillations can be identified in single cells from log-phase cultures, analysed with a microfluidics device (Litsios et al. 2019) and that cell undergo 2 protein synthesis pulses, one in G1 predicted to be associated with an increased glucose metabolic flux and oxygen consumption and one later in S/G2/M phase, together with a pulse in lipid and carbohydrate stores synthesis (Takhaveev et al. 2023).

1.3.2 An intrinsic metabolic clock

As metabolic oscillations can be detected in single cells, it is likely that individual cells possess an intrinsic metabolic clock. Indeed, it is presumed by some that single cells act as single oscillators and thus possess an intrinsic metabolic clock. The YMC and its population averaged oscillations is believed to be the result of the synchronization of each cell's intrinsic clock (Tu et al. 2005, Silverman et al. 2010). This means single cells go through different metabolic states through time in a cyclical manner. It is based on the concept of intrinsic biological clocks which has been discussed for different species within the context of circadian rhythms (Dunlap. 1999). Signs of intrinsic circadian clocks have been identified in single cells, in which transcriptional changes occur together with clear feedback loops between well studied proteins (Fleissner. 1992). For example; the FRQ/PERs/CRYs vs BMAL1/CLOCK proteins in cells of the syncytial fungi neurospora (Hurley et al. 2016, Wang et al. 2019, Bartholomai et al. 2022) also found in the superchiasmatic nucleus or liver of higher eukaryotes (Welsh et al. 1995, Herzog et al. 1998, Hastings et al. 2018), or the Kai system in cyanobacteria involving protein phosphorylation feedback loops rather than changes in proteins levels (Golden et al. 1997, Cohen & Golden. 2015). Still, in budding yeasts (i) no such protein feedback loop has been detected so far. The YMC is instead intrinsically linked to the chemostat conditions, the feeding rate and thus to the yeast growth rate (Slavov & Botstein. 2011). Therefore, the intrinsic clock discussed here is a metabolic clock, referring to interactions between metabolites and cell growth.

1.3.3 Single-cell transcripts in asynchronous cell population

Because gene expression and metabolism seem highly linked along the YMC, the hypothesis of the “intrinsic metabolic clock” was tested by Silverman et al., using population transcript levels along the YMC (data from Tu et al. 2005) and assessing single-cell transcript levels in unsynchronized slow-growing cultures. As presented at Figure 1.11, RNA fluorescence *in-situ* hybridization (RNA-FISH) was performed on 22 pairs of transcripts predicted to be co-expressed or not, at the global gene-expression levels throughout the YMC according to Tu et al., data. The single-cell technique was applied to yeast cells from unsynchronized exponentially slow-growing cultures (growth rate of $0.1h^{-1}$ and doubling time of ˜6.9h) (Silverman et al. 2010).

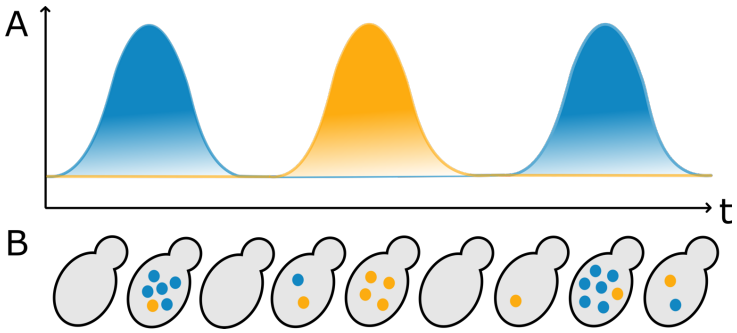

Figure 1.11 RNA-FISH of antagonist transcripts in asynchronous cell population

*Cartoon representing **A.** levels of expression through the YMC for two antagonist transcripts (detected to peak at opposed times during the YMC by Tu et al., (2005). **B.** mRNA numbers of these antagonist transcripts in single cells from RNA-FISH experiments on asynchronous cell populations. Modified from Silverman et al., (2010).*

According to the intrinsic clock concept, the following predictions for single cells from asynchronous cultures were tested and validated. (i) Most cell were expected to be in a metabolic state in which periodic transcripts are lowly expressed or not at all. (ii) If global gene expression of periodic transcripts is peaking at the same time or phase of

the YMC, then many cells were expected to co-express high mRNA numbers of these transcripts. (iii) Finally, if periodic transcripts peak at different times and phases of the YMC, then cells expressing high RNA numbers were expected to only do so for one or the other transcript but not for both.

To test these predictions, coefficient of correlations between pairs of transcripts were computed to compare transcripts synchronism in single cells from asynchronous populations to those of synchronous cell populations (at the global level). Briefly the paper reports, (i) a high proportion of non-expressing cells, (ii) positive Pearson correlation coefficients between transcripts globally co-expressed in the YMC and (iii) negative correlation coefficients between transcripts antagonistically expressed in the YMC. The study concluded that single cells from asynchronous populations show similar correlations to those observed in the population of synchronised cells in the YMC, thus suggesting that yeast cells undergo metabolic cycling in asynchronous populations due to their intrinsic clock, which are simply not synchronized (Silverman et al. 2010). The reconstruction of gene expression dynamics using mathematical modelling and employing mRNA correlations from Silverman et al., data, also advocated for the existence of an intrinsic metabolic clock in budding yeasts (Wyart et al. 2010).

Next, following the concept of an intrinsic clock, it was predicted that in slow asynchronous cultures the fraction of cells found in a HOC or LOC state was proportional to the length of these phase in synchronous cultures of the YMC. Indeed, higher feeding rates give rise to shorter LOC phases and thus relatively longer HOC phases in synchronous population of the YMC (Figure 1.7.B) (Slavov & Botstein. 2011,

Slavov et al. 2011). Thus, in asynchronous cultures, at a higher growth rate fewer cells are expected to be in LOC and more cells should be in HOC. Finally, as the fraction of cells in HOC or LOC state rises, the population average transcript levels of genes for which the gene expression levels peak in the corresponding phase also increases. This relationship was called “ensemble average over phase” or EAP (Wyart et al. 2010., Slavov et al. 2011).

Together these results indicated that budding yeast cells most likely possess an intrinsic metabolic clock, connected to intrinsic transcriptional patterns and that the state and proportion of the yeast population found in each phase depends on the metabolic resource and growth rate. Most importantly, it shows that the study of the single-cell gene expression can be exploited as a mean to understand organisation of yeast cell populations. Yet, as of today, gene expression levels of the synchronous cell population of the YMC were only assessed at the population level (Klevecz et al. 2004, Li & Klevecz. 2006, Tu et al. 2005, Slavov et al. 2011, Kuang et al, 2014, Feltham et al. 2020), therefore leaving a breach in the understanding of the mechanisms behind the YMC.

1.4 3rd Gap; A need for single cell gene expression studies at the transcript level

1.4.1 Single-cell protein levels in synchronous cell population

Single-cell gene expression reporter assays were used within the context of the YMC (Laxman et al. 2010). Indeed, fluorescent proteins were used to analyze the expression of a few genes in YMC populations at the single cell level but in a qualitative way only as results from this work were defined as “determined visually”. Nonetheless, the study revealed significant cell heterogeneity with regard to fluorescent signals,

indicating that cells from synchronized populations are not showing the same gene-expression profiles and might not all be “synchronized” (Laxman et al. 2010).

1.4.2 Limitations of protein reporter assays

Assessing single-cell protein levels through the use of fluorescent reporters nonetheless includes limitations. First, the introduction of a tag at the end of a gene of interest modifies the content of its sequence, its chromatin environment perhaps, the length of its transcript, as well as the length, conformation, and even sometimes maturation and oligomerization of its protein (Balleza et al. 2017, Craggs. 2009). Thus the introduction of a reporter could potentially disrupt transcription, transcript, and protein dynamics. In fact, many processes affecting transcripts and proteins levels could be impacted by it, such as turnover rates as it was shown for GFP (increased protein half-lives) (Mateus & Avery. 2000) or even the ability of a transcript or protein to aggregate into biomolecular condensates if length, GC content or secondary structure are changed (Khong et al. 2017, Courel et al. 2019, Roden & Gladfelter. 2020, Parker et al. 2022). Next, molecular cloning is required to obtain gene constructs for the gene reporter essays but these could be problematic in particular for the study of the YMC. On one hand, modifying a gene of interest could impact the yeast metabolic cycle itself and change the typical dissolved oxygen output, resulting in unpredicted metabolic changes, as observed for some Knock Out strains used to induce the YMC (thesis of Dr. Xi). On the other hand, transformation of the CEN.PK WT strain proves to be challenging as more unsuccessful attempts were counted when compared to the BY WT strain (lab experiments). Finally, unless using special fluorescent molecules together with super-resolution microscopy techniques (Prakash et al. 2022), single molecule imaging of protein is not possible with the essential

Immuno-Fluorescence technique. IF is therefore a semi-quantitative technique that only delivers mean protein levels rather than discrete protein numbers. Nevertheless, the fluorescent toolbox is now enriched (Giepmans et al. 2006) and recent technologies such as the coupling of small fluorophores to small ligands, i.e. small protein tags such as Halo-tags for live-cell microscopy (Los et al. 2008, Grimm et al. 2015) or even small antibodies such as nanobodies when performing immunoblotting alleviate some of the well-known limitations of these techniques (Fridy et al. 2014, Kaplan & Ewers. 2015, Traenkle & Rothbauer. 2017, de Beer & Giepmans. 2020). Thus new techniques now allow more precise localization and quantification of proteins.

Nevertheless, inferring “global gene expression levels” from protein levels, i.e. considering protein levels to reflect transcription and transcript levels is incorrect in many instances as only a week correlation is observed between mRNA and protein abundance and as far as 60% of the variation in protein levels can’t be explained by transcripts levels (Vogel & Marcotte. 2012). In particular, in the context of the YMC, most protein levels stay constant and thus do not follow transcriptional changes at the population level (Feltham et al. 2020, O’Neill et al. 2020). Therefore protein reporter assays are not adequate to study single-cell transcription dynamics and transcript processes in YMC populations and *vice versa*.

1.4.3 Using smRNA-FISH on YMC populations

For this work, single-molecule RNA fluorescence *in-situ* hybridization (RNA-FISH) (Femino et al. 1998, Raj et al. 2006, Zenklunsen et al. 2010) is employed in order to assess transcript levels in single cells from synchronous culture of the YMC.

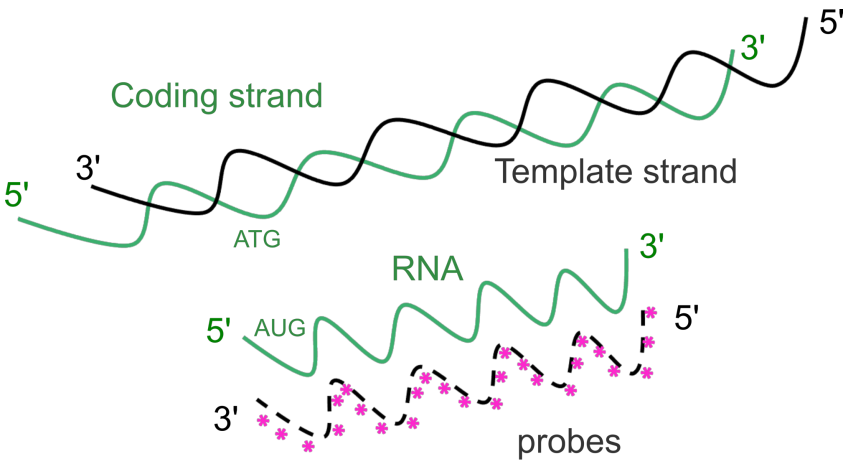

Figure 1.12 RNA-FISH probes annealing to the RNA target

RNA-FISH probes are designed to complement the RNA sequence. Probes possess the template strand sequence and are designed to be distributed evenly along it (black), while the RNA possess the same sequence as the coding strand (green). Inspired from Raj et al., (2006).

smRNA-FISH is a quantitative method used to assess gene expression in individual cells. The technique employs DNA fluorescent probe series that directly hybridize (bind) a specific endogenous RNA sequence in-situ/in-cells (Figure 1.12). The fluorescence signal emitted after excitation can thus be detected, imaged and recorded in single cells through fluorescence microscopy (Femino et al. 1998, Raj et al., 2006, Zenklunsen et al. 2010). Staining of the DNA with DAPI allows the detection of nuclei in cells, thus the localization of transcripts in-nucleus or in-cytoplasm, therefore providing a way to infer nascent and steady state RNA levels in single cells (Raj et al. 2008, Zenklunsen et al. 2010). Single-molecule RNA-FISH in particular, permits the detection and quantification of single transcripts, using a combination of short probes (˜20nt oligos) providing target specificity and a linear amplification of the fluorescent signal (Raj et al. 2008, Stellaris). Packages or pipelines then typically enable the semi-automated analysis of the microscopy data and quantification of single RNA molecules (Mueller et al. 2013). Nevertheless, the technique includes limitation as it requires fixation of samples and thus provides only snap-shots of RNA

numbers in single cells (as opposed to live-cell imaging). Furthermore, because the technique is time-consuming and the number of fluorescent channels limited, studies using RNA-FISH usually focus on a few loci only (Femino et al. 1998, Femino et al. 2003, Raj et al. 2006, Raj et al. 2008, Zenklunsen et al. 2008, Treck et al. 2012, Brown et al. 2018).

Importantly, smRNA-FISH provides quantitative data. In addition to summary statistics, distributions of RNA numbers give information about the gene expression heterogeneity within a cell population (Hocine et al. 2013). Detailed analysis of RNA distributions can also point out transcription and transcript dynamics (and processes), in particular when using mathematical modelling (Zenklunsen et al. 2008, Brown et al. 2018).

1.5 Aims of research

The overall aim of this work is to gain a better understanding of the relationship between gene expression and metabolism in *Saccharomyces cerevisiae*.

The goal is to address the gaps in the literature, particularly the shortcoming of data and interpretation on transcription dynamics during metabolic changes and the poor understanding of single cell behaviour and organisation of YMC cultures.

To do so; (i) the Yeast Metabolic Cycle is utilized to study continuous metabolic changes in budding yeasts, (ii) smRNA-FISH is employed to gather quantitative gene expression data at the transcript level in single cells of YMC cultures, (iii) quantitative data analysis is exploited to decipher levels of heterogeneity between cells and assess organisation and characteristics of potential sub-populations of cells in synchronous cell populations of the YMC.

In chapter 3, the experimental approach employed in this study is presented. Chapter 4 aims to address the question of whether protein post-translational modifications (as opposed to protein levels) play a role in the progression of the YMC by changing protein activities during the metabolic cycle. In chapter 5, the question of whether cells show similar gene expression levels in YMC population is assessed. Chapter 6 aims to identify further transcription dynamics along the YMC. In chapter 7, the question of whether an intrinsic metabolic and gene expression clock can be detected in YMC population is investigated. This chapters also aims to describe the organisation of sub-populations of cells in YMC cultures, using transcript levels in single cells as proxy for metabolic states. Finally, chapter 8 aims to identify sub-populations of YMC cultures looking at metabolic and proliferative characteristics of individual cells in these populations.

Chapter 2

Materials and Methods

Note: a brief overview of the experimental approach is described in chapter 3.

2.1 Experimental Models/Strains

Table 2.1 S. cerevisiae. haploid strains used in this study.

For each strain, a description of the standard name, genotype and source is provided.

Strain	Genotype	Source
CENPK113-7D WT	MATa URA3 HIS3 LEU2 TRP1 MAL2-8c SUC2	Gift from Boeke Lab. Euroscarf
BY4741 WT	MATa; his3Δ 1; leu2Δ 0; met15Δ 0; ura3Δ 0	Euroscarf
BY4741 *ATO3 KO* (ato3 Δ)	ato3D::LEU	This study
BY4741 *SHM2 KO* (shm2 Δ)	shm2D::LEU	This study
BY4741 *IDH1 KO* (idh1 Δ)	idh1D::LEU	This study

The strains used in this study are listed in Table 2.1.

2.2 Strain construction

Table 2.2 Primers used in this study.

Oligonucleotide	Sequence (5' -> 3')
ATO3del_leu_tag_F	AAAGATTTAGTAAGAATAAAAAATAAAAATACTGGTTAAAatcagagcagattgtactga
ATO3del_leu_tag_R	TTTTAATGTTTTATAAGTTTTGTTTTTCATTTCATACCCTacttccttgttcatgtgtgt
ATO3_chk_F	ATGAGCTTCGCTTGATTGCC
ATO3_chk_R	TACCTCTTTTCCCCTGTGACG
SHM2del_leu_tag_F	CATAGCAAAGCATAACAGCTTAAACCGAATCCTCCTTAACatcagagcagattgtactga
SHM2del_leu_tag_R	GTTTATTTTTTTGGGATTAAGTGTCGTTGTGGTGATTTCTacttccttgttcatgtgtgt
SHM2_chk_F	GGATCTGAACAGCCGGAGTC
SHM2_chk_R	TTCAGCGATGGTGACAAGGT
IDH1del_leu_tag_F	CTCATTCTTCTCCCTTTTCCTCCATAATTGTAAGAGAAAAatcagagcagattgtactga
IDH1del_leu_tag_R	CACTTAAGTTGCAGAACAAAAAAAAGGGGAATTGTTTTCAacttccttgttcatgtgtgt
IDH1_chk_F	CATCGGGCGTCATAGGTCAC
IDH1_chk_R	CCCCTGAGCAGACCAAAAGA

Knock out strains of the smRNA-FISH target genes were constructed. Deletion mutant strains of BY WT were produced*, using homologous recombination (Longtine et al. 1998). *Note: Transformation in CENPK113-7D WT proved to be challenging in the past. Primers were designed using *SnapGene Viewer,* NCBI design primer and BLAST. These are listed in Table 2.2. The construction of new strains includes the following steps.

2.2.1 Cloning PCR

Cloning was performed using the pRs305 plasmid containing the leucine marker (Addgene vector database) as PCR template. A first PCR amplification was performed to obtain products containing the selection marker flanked on each side by the 40bp found upstream or downstream of the gene to be deleted. Products were checked via gel electrophoresis.

2.2.2 Yeast transformation

After reaching Mid-log phase, yeast cultures were harvested (3000 rpm, 4') and resuspended in LiAc/TE 0.1M (4°C). The next day, 100µl of these competent cells were incubated (30°C, 30') with 700µl of 0.1M LiAc/TE in 40% PEG, 10µl calf thymus DNA (Sigma) and 10µl of cloning PCR products. The cells were then heat-shocked (42°C, 20') and harvested (7000rpm, 5'). Transformed cells were resuspended in Milli-Q water and plated onto YPD agar plates made with Complete Supplement Mixture without L-Leucine . After 3-4 days, yeast colonies were picked, streaked onto another plate for referencing and put to overnight culture in 500 µl YPD at 30°C.

2.2.3 Non-phenol genomic DNA extraction

Yeast cells were broken down, DNA was precipitated and washed. To do so, yeast cultures were harvested (7000 rpm, 1‘) and resuspended in 100µl LiOAc 200mM with 1% SDS (65°C, 5’). Then the mix was centrifuged (13000 rpm, 3’) and washed with 300µl of 100% EtOH, followed by 100µl 70% EtOH. Each time discarding the supernatant. Pellets were resuspended in 100µl of TE (65 C, 5’) and quickly spined (13000 rpm, 15’’) to pellet cell debris. Supernatant was used for PCR.

2.2.4 Checking PCR

DNA extracted was verified using checking primers, flanking the site of insertion i.e. the gene of interest (at least 250bp away). A PCR amplification of these products was performed and transformants were confirmed by gel electrophoresis. Primers were designed to detect a clear size difference between a negative control and the insertion of the selection marker.

2.3 Yeast cultures

Strains were streaked from glycerol stocks onto 2% agar YPD plates (1% yeast extract (Difco), 1% bactopeptone, 2% glucose) and grown for 2 days (30°C).

2.3.1 Mid-logarithmic growth

Cell pre-cultures were grown overnight in 5 ml YPD at 30°C. This culture was used to inoculate a volume of 50 ml of YPD (BY strains) or MD media (CEN.PK strain) with a pH adjusted to 6.8. The culture was grown at 30°C, 200 rpm to OD_{600} of 0.6. The doubling time of the culture is ˜2.08h.

2.3.2 Chemostat continuous cultures

Here the different steps and solutions needed to set up the fermentor and other devices to induce regular metabolic oscillations are described with details. These settings are highly similar to those found in Klevecz et al. 2004, Tu et al. 2005 and Feltham et al. 2020. Different experimental campaigns were completed, thus several “fermentor runs” were accomplished. An overview of the chemostatic device and how to induce the Yeast Metabolic Cycle is described at Figure 3.1.

2.4 Experimental settings for synchronized cultures

First the fermentor vessel is cleaned and autoclaved with Milli-Q water. Then the fermentor is assembled with the appropriate volume of MD media. After what, the vessel, including tubings, luer locks and air filters are autoclaved once again. The base solution is also prepared and autoclaved. The next day, MD media contained in the fermentor is supplemented under sterile conditions. The base correction and feed tubings are then connected to the base solution or to the bottle of feeding with MD media, respectively. The control unit is then switched on. The temperature, dissolved Oxygen (dO) and pH probes are set up and the system is connected to the water lines to cool off the chemostat. dO and pH probes are left to polarize overnight. Finally, cell pre-cultures are grown overnight in 10 ml YPD at 30°C, 200 rpm. On the day of inoculation, the Julabo chilled water circulator unit, the Bambi air compressor and the motor unit connected to the agitation device are switched on to ensure constant temperature and aeration of the system. Once these conditions are reached, the dO probe is calibrated. Next, high-density overnight cultures are checked for the absence of contamination under the microscope. Cultures are used to inoculate a volume of 200ml or 1l of YMC Minimal Defined (MD) media, depending on the fermentor used;

either the 400ml vessel Minifor (Lambda) or the 2L vessel Fermentor Bioflo320 (New Brunswick Eppendorf). Cultures are kept at constant temperature of 30°C and pH of 3.5 (via the pH probe and base correction tubing). Aeration and agitation are also maintained constant, with rates of 0.15l/min and 3.0Hz for Minifor runs and rates of 1 l/min and 1000 rpm for Bioflo320 runs. Yeast cells are grown to maximal density (OD_{600} 4.0-5.0). During this time, the dO levels decrease to 0% (exponential phase). After what the diauxic shift occurs and the dO levels are back to 100%. Next, the culture is starved for more than 6 hours. When this period is over, the cultures are fed, under chemostatic conditions, with fresh MD media, at a dilution rate of 0.072 h^{-1} (1.2ml/min Bioflo320 or 0.24ml/min Minifor). This induces the metabolic cycling. At this dilution rate, the doubling time calculated for the culture is of ˜9.62h. At all time, when the feeding pump is on, the harvest pump is also activated ensuring a constant flow through the chemostat and therefore a constant volume of culture. Once, metabolic cycling is established and shows a regular period of ~3h20min, the culture can be collected through the sample port. Sampling timepoints are calculated using records of previous cycles. Samples were harvested every 10 minutes, aiming to always get one sample at the lowest dissolved oxygen point of the YMC and focusing on the HOC phase of the YMC. After sampling, dO levels are saved as CSV files. Finally, when the time-course experiment is over, the pumps and units of the fermentor system are turned off and the fermentor vessel is disassembled, cleaned and autoclaved with Milli-Q water once again. At all time, when handling of the fermentor and tubings, ethanol is sprayed on gloves and around the area of work if possible and records of fermentor runs are kept in log sheets.

2.4.1 Solutions

Large volumes of MD media* are prepared in advance to allow the growth and feeding of the cultures. First a MD solution is prepared and autoclaved (calcium chloride dihydrate 0.1 g/l, magnesium sulphate heptahydrate 0.5 g/l, potassium dihydrogen monophosphate 2 g/l, ammonium sulphate 5 g/l, sulphuric acid 0.0067 %, glucose 2.5 g/l, Milli-Q water). Then the solution is supplemented with antifoam-204 0.05% (Sigma-Aldrich), iron sulphate heptahydrate 20 mg/l, 100μl/l of trace salt solution and 1ml/l of vitamin solution under sterile conditions. The trace solution of 10ml is kept at room temperature and is composed of zinc sulphate heptahydrate 1g, copper sulphate pentahydrate 0.5g, manganese chloride tetrahydrate 0.1g and filtered sterilized Milli-Q water. The vitamin solution* of 500 ml is first autoclaved to dissolve powders and then kept a 4°C. It consists of biotin 1mg, calcium pantothenate 200mg, folic acid 1mg, inositol 1000mg, niacin 200mg, p-aminobenzoic acid 100mg, pyridoxine HCl 200mg, riboflavin 100mg, thiamine HCl 200mg and Milli-Q water. Finally a strong base solution is made using NaOH 10g/l. *Vitamin solution and MD media once supplemented are kept away from light.

2.5 RNA fluorescence *in-situ* hybridization, RNA-FISH experimental design

RNA-FISH experiments performed for this study followed to some extent conventional protocols used in Femino et al. 1998, Femino et al. 2003, Raj et al. 2006, Raj et al. 2008, Zenklunsen et al. 2008, Treck et al. 2012 and Brown et al. 2018. An overview of the RNA-FISH workflow is described at Figure 3.2.

2.5.1 Probe designs

Single Molecule RNA-FISH probes were designed as single strand DNA primers of ~20 nucleotides. Each one of the oligo possess at its 3'end a ddUTP labelled with a

fluorophore. A combination of 25 to 48 probes is recommended to insure target specificity, decrease signal variability while offering a good signal-to-noise ratio and a linear amplification of the fluorescent signal.

DNA sequences were obtained from the *Saccharomyces* Genome Database (SGD). Multiple sequence alignment was ruled out using BLAST. Probes were designed using Snap Gene viewer and the Stellaris probe designer from Biosearch Technologies. Oligos were designed to complement the coding strand of the target sequence i.e. the RNA sequence as described at Figure 1.12.

2.5.1.1 Pre-rRNA-FISH probes

The pre-ribosomal RNA-FISH probes were obtained from Stellaris. 46 DNA probes of ~20 nt, labelled with Quasar 570, were designed to bind both external and internal transcribed spacers regions of the pre-35S rRNAs (RDN37-2: SGD) (Table S.1, Appendix).

2.5.1.2 Multiplex smRNA-FISH probes

The smRNA-FISH probes used for the study of genes transcribed by RNA Pol II were designed and synthesized “in-house”. Between 32 to 48 DNA oligos of ~20 nt were ordered from Eurofins Genomics and labelled with Cy5 or Cy3 fluorophores for each of the following targets; *ATO3* or YDR384C, *SHM2* or YLR058C, *IDH1* or YNL037C, and *ACT1* or YFL039C (Table S.2 & S.3, Appendix). Probes are kept away from light.

2.5.2 Enzymatic synthesis of probes

This protocol was kindly shared by Prof. Ilan Davis’ s lab and is adapted from Gaspar et al. 2017. First NH_2-ddUtP were labelled with a 2 fold molar excess of NHS ester dye

or fluorophores; here ATTO633N-NHS-ester (Cy5) or ATTO565N-NHS-ester (Cy3) (Atto-tec). The reaction took place in the dark at room temperature for 3h before quenching unreacted NHS-ester groups with TrisHCl. Finally probe concentration was adjusted with Nuclease-free water (final stock solution 60μl 5mM). It is also possible to order already labelled ddUTP. Second, a single labelled ddUTP was added at the end of each single strand oligo. To do this oligos were pooled together and diluted to 200μm and then mixed with labelled ddUTP and Terminal Deoxynucleotidyl Transferase (TDT) catalyzing the addition of the nucleotide at the 3' hydroxyl terminus of each probe (overnight, 37°C). The next day, labelled oligonucleotides were purified using a kit (Oligo Clean and Concentrator kit, Zymo Research) and eluted in 20μl of nuclease-free water. This step ensures that any free dyes or oligos will be discarded. Finally assessment through imaging, RNA-FISH fluorescence microscopy and quantification, was performed on control yeast culture samples prior to each experimental campaign. To validate the degree of labelling and nucleotide incorporation, denaturing Urea Polyacrylamide Gel Eletrophoresis (Urea PAGE) were performed for different concentrations of the probe mixes. Figure 2.1 shows a degree of labelling of more than 75% is detected for the different probes synthesized.

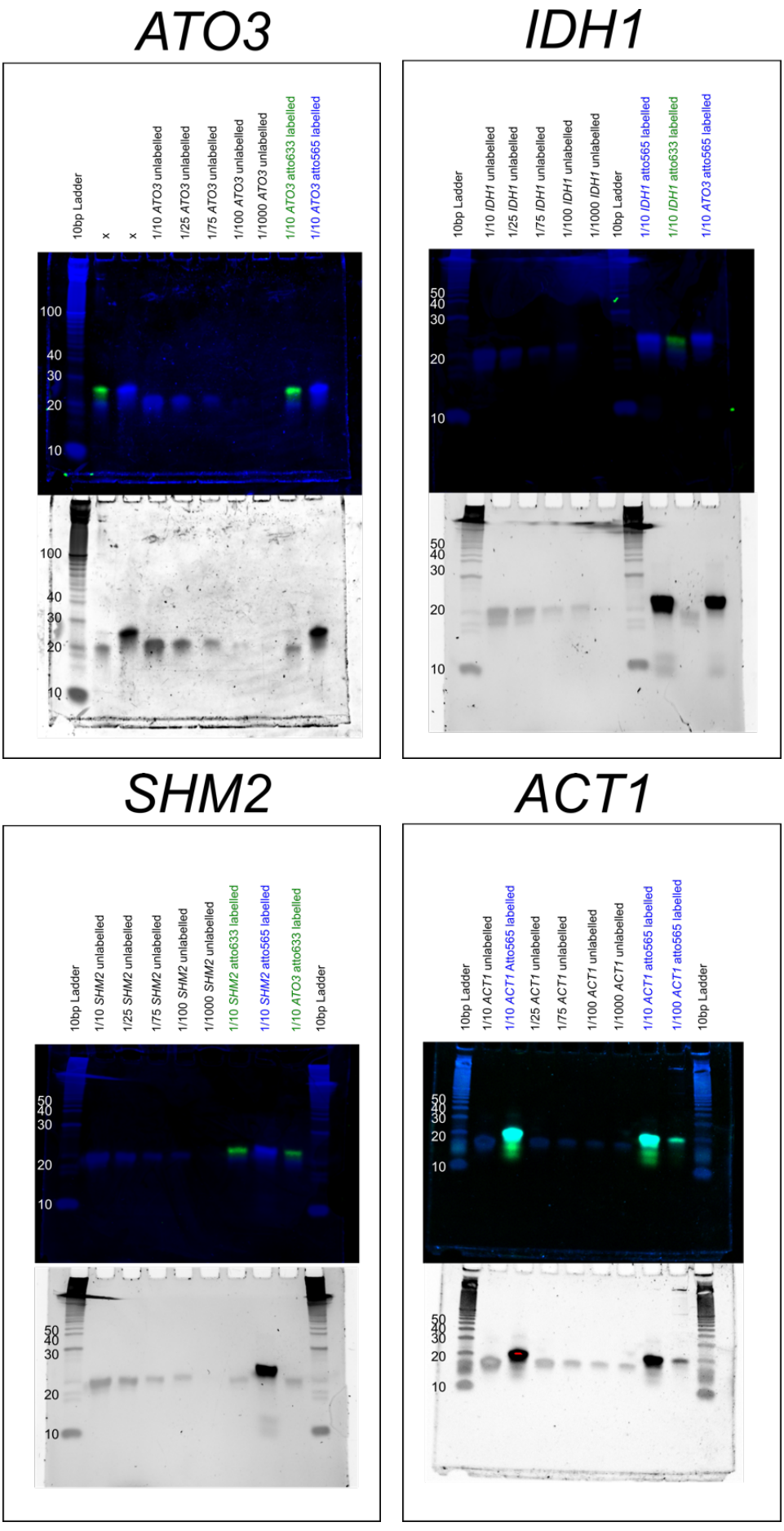
ATO3
10bp Ladder
x
x
1/10 ATO3 unlabelled
1/25 ATO3 unlabelled
1/75 ATO3 unlabelled
1/100 ATO3 unlabelled
1/1000 ATO3 unlabelled
1/10 ATO3 atto633 labelled
1/10 ATO3 atto565 labelled
100
40
30
20
10
IDH1
10bp Ladder
1/10 IDH1 unlabelled
1/25 IDH1 unlabelled
1/75 IDH1 unlabelled
1/100 IDH1 unlabelled
1/1000 IDH1 unlabelled
10bp Ladder
1/10 IDH1 atto565 labelled
1/10 IDH1 atto633 labelled
1/10 ATO3 atto565 labelled
50
40
30
20
10
SHM2
10bp Ladder
1/10 SHM2 unlabelled
1/25 SHM2 unlabelled
1/75 SHM2 unlabelled
1/100 SHM2 unlabelled
1/1000 SHM2 unlabelled
1/10 SHM2 atto633 labelled
1/10 SHM2 atto565 labelled
1/10 ATO3 atto633 labelled
10bp Ladder
50
40
30
20
10
ACT1
10bp Ladder
1/10 ACT1 unlabelled
1/10 ACT1 Atto565 labelled
1/25 ACT1 unlabelled
1/75 ACT1 unlabelled
1/100 ACT1 unlabelled
1/1000 ACT1 unlabelled
1/10 ACT1 atto565 labelled
1/100 ACT1 atto565 labelled
10bp Ladder
50
40
30
20
10

Figure 2.1. smRNA-FISH probes incorporated labelled ddUTPs with a high degree of labelling. *Urea PAGEs of unlabelled and labelled oligo mix imaged with a Li-Cor system at different excitation wavelength. Atto633 (Cy5) fluorophore is shown in green, Atto565 (Cy3) fluorophore is shown in blue and gray, as well as the SYBR GOLD staining the single strand DNA probes. (Maximum emission wavelength are for the different fluorophores are; atto633: 651nm, atto565: 590nm, SYBER GOLD: 537nm). Top images show gels imaged at 700nm. Bottom images show gels imaged at 600nm. Unlabelled oligos were loaded at different concentrations to provide a visual reference. This for the ATO3, IDH1, SHM2 and ACT1 probe mix. (x indicates other probes that were not used in this study). As expected, a slight shift in size is observed between unlabelled and labelled oligos (+ 1 labelled ddUTP) and a degree of labelling of more than 75% is observed.*

2.5.3 Labelling strategy

The labelling of probes and different target transcripts was performed as described;

(i) For the pre-rRNA-FISH; pre-35S rRNAs ETS and ITS probes were labelled with Quasar 570. (ii) For the single-RNA-FISH; probes targeting *ATO3* were labelled with atto565. (iii) For the dual-RNA-FISH; first *ATO3* was labelled with ato633 and *SHM2* with atto565, second *SHM2* with atto633 and *IDH1* with atto565, third *IDH1* with atto633 and *ATO3* with atto565. (iv) Finally for the control dual RNA-FISH; *ATO3* was labelled with atto633 and *ACT1* with atto565. Quasar 570 and atto565 emit in the Cy3 channel while, atto633 emits in the Cy5 channel.

2.5.4 Negative Controls

Negative controls were used in order to assess fluorescence Signal-to-Noise ratio and reinforce the computation of fluorescent foci and the quantification of single molecule transcripts. RNAseA treated samples were used for the pre-rRNA experiments to simply degrade all RNA present in cells. Knock Out strains for genes encoding target transcripts were used for the other single molecule RNA-FISH experiments. Figure 2.2, shows histograms of the fluorescent signal intensities between WT and KO strains for *ATO3*, *SHM2* and *IDH1* in both fluorescent channels. Since ACT1 is an essential

gene, no KO strain could be constructed for it. Therefore a “no probe” negative control (hybridization buffer without probes) was used for the control dual-RNA-FISH (*ATO3* - *ACT1*). Yeast samples for negative controls were grown to mid-log phase and processed at the same time with the rest of the samples for each experiment campaign.

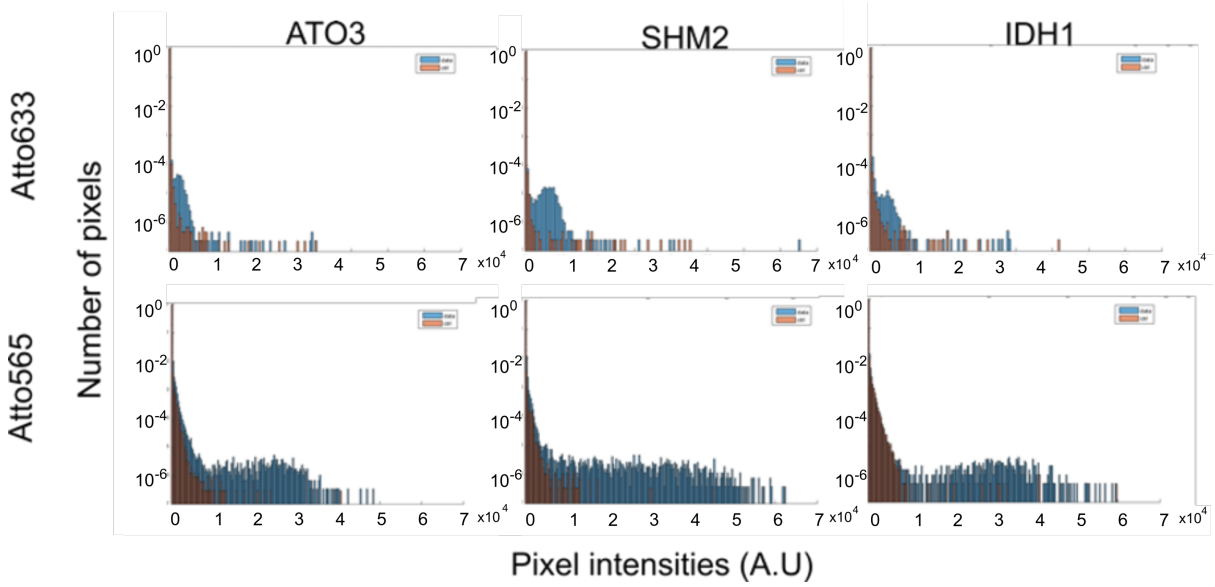

Figure 2.2. Histograms of the fluorescent signal intensities of the data vs control

Number of detected pixels against the pixel intensities of the fluorescent signal for the different target transcripts in Cy5 (atto633 fluorophore) or Cy3/TRITC (atto565 fluorophore) channel. The colours indicate data from WT yeast cells (blue) or from KO cells (brown). The inflection point between the brown and blue distribution indicate the typical threshold.

2.5.5 Fluorophore Swap

Intensity histograms at Figure 2.2. show a difference in fluorescence signal range between the 2 fluorescence channels used for this study; Cy5 (Atto633) and Cy3 (atto565). Despite this difference, the dynamic range is sufficient to detect fluorescent spots from noise as a clear separation between data (blue) and control (brown) can be seen. However, because of its shorter signal range, the use of the Cy5 channel perhaps increases the risk of false positives or negatives. Therefore, to prevent

labelling artifacts, fluorophores were swapped between smRNA-FISH targets (*ATO3*, *SHM2* and *IDH1*).

2.5.6 Sampling

Appropriate volumes of both mid-logarithmic (50 ml) and chemostat cultures (2 ml) were harvested. For both culture conditions, three biological repeats of the sampling and further procedures were carried out on different days. Each time, between 12 and 22 samples were taken along one YMC cycle. Figure 4.4, chapter 4 and figure 5.3, chapter 5 indicate sampling timepoints for each biological replica.

2.6 RNA fluorescence *in-situ* hybridization, RNA-FISH Wet-lab Workflow

This protocol was adapted from Zenklusen *et al.,* 2010 and Brown *et al.*, 2018.

2.6.1 Fixing or Cross-linking

The samples were pelleted and fixed with 4% (v/v) paraformaldehyde in PBS (45 min, 80 rpm, RT). Fixed cells were washed twice with buffer B (1.2 M sorbitol, 100 mM K_2HPO_4, pH 7.5) and re-suspended in 1 ml of buffer B. Samples were then split into 4-5 1.5 ml Eppendorf tubes, pelleted and left on ice to facilitate sampling.

2.6.2 Cell wall removal or Spheroplasting

Once gathered, pellets were re-suspended in 500 µl of Spheroplast buffer (buffer B, 36 µM B-ME) and kept at 30°C, 20 min. Cells were then washed without resuspension in 500 µl of Wash buffer (buffer B, 5 µM B-ME). Cells were centrifuged again and spheroplasted using Zymolyase (20.000 U/g , MP Biomedicals) in Wash buffer (10 mg/ml final concentration) at 30°C for 4 min with shaking, until the majority of the cells

was spheroplasted, as observed by microscopy. Cells were pelleted (4°C) and washed with cold buffer B.

2.6.3 Spheroplasting optimization

The step of spheroplasting or cell removal had to be optimized, as YMC cells were first found under-spheroplasted when compared to mid-log phase cells. Cell walls of stationary phase cells are enriched in proteins and are thus ticker and more resistant to B-glucanase enzyme such as zymolyase (Lesage & Bussey. 2006, De Virgilio. 2012). In particular quiescent cells possess thicker cells walls (Allen et al. 2006, Orlean. 2012), explaining perhaps why such difference is noticed between the two types of cultures (mid-log vs YMC). Because different metabolic phases are encountered during the YMC, it is possible that the cell wall composition of cells vary between the phases of the YMC but also between cells if these differ considerably, as zymolyase treatment was also found to vary between mutants for which the cell wall was most likely impaired (Hameed et al. 2020).

Spheroplasting was checked for YMC samples using Zymolyase in wash buffer (10mg/ml) and left at 30°C either for 4, 8, 12 or 60 min with shaking (150 rpm) as shown at Figure 2.3. A negative control without Zymolyase was prepared. Samples were checked under microscope just after treatment. Samples were then stained with DAPI and the integrity of the cells was checked, using brightfield microscopy. The DAPI incorporation was found to be similar for the different treatment with Zymolyase. The 4 minutes treatment was sufficient to spheroplast the majority of the cells (> 70% estimate) without causing aggregation as opposed to longer periods of treatment. Thus a spheroplasting time of 4 min was picked to remove the cell walls of yeast

samples while keeping the integrity of the cells. Among others, Okada et al. 2016 " Examination and disruption of the yeast cell wall" served as a visual guideline.

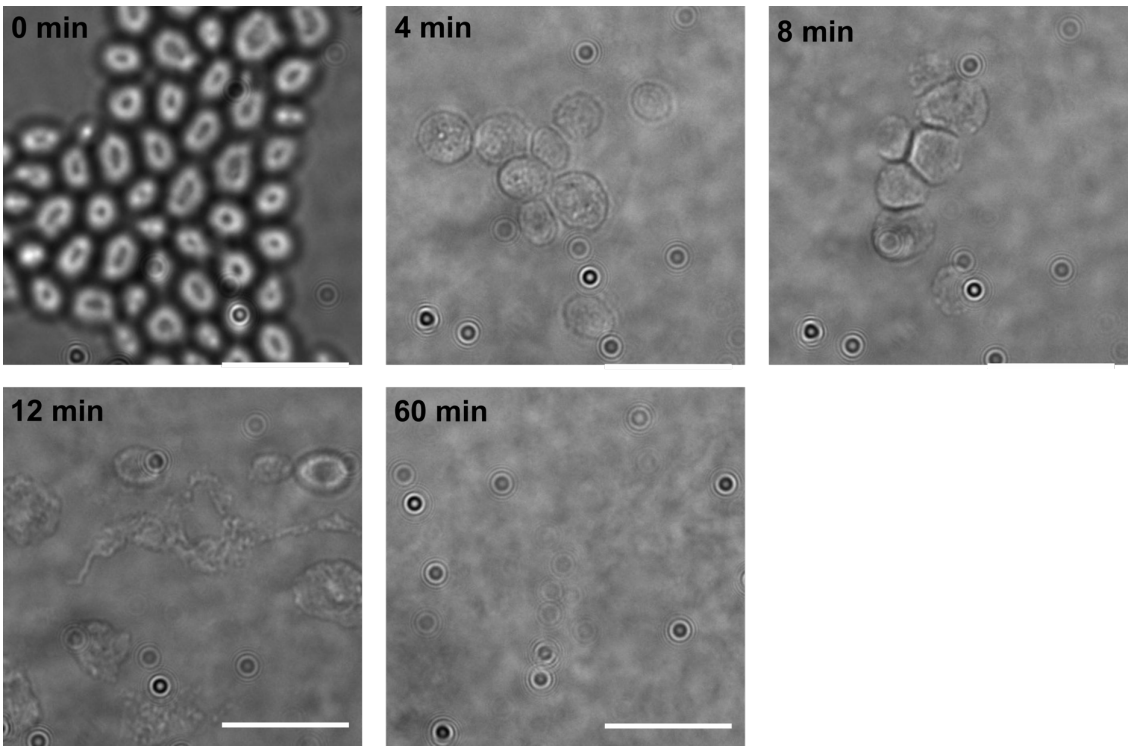

Figure 2.3 Examples of microscopy images gathered for the study of spheroplasting efficiency *Examples of entire fields of view. Detection of cells using brightfield. The spheroplasting time (incubation time with zymolyase) is indicated on the top left corner of each image; At 0 min (mock treatment with Buffer B and wash buffer without zymolyase) cell walls are clearly detected. After 4 min of treatment, the cell walls are removed and the membrane of cells are intact. After 8 min, the membranes are intact but some cells seem to be crushed (example top cell). At 12 min, some cells are intact, while some cells are bursted and spread on the coverslip. At 60 min only cell debris remain on coverslips. Scale bar is 10um.*

2.6.4 Attachment on coverslips and membrane permeabilization

After spheroplasting, ~200 µl of cells were left to settle (30 min, 4°C) on poly-L-lysine treated coverslips in 12-well tissue culture dishes. Coverslips were then washed with cold Buffer B and covered in 2 ml 70% ethanol and kept at -20°C overnight.

2.6.5 Hybridization

For each biological repeat, samples of both culture conditions were treated at the same time. Samples were rehydrated with 2 ml of 2x SSC (5 min, RT).

For the pre-rRNA FISH experiments only (chapter4), negative controls, i.e. coverslips destined to be treated with RNAse A (Merck) were then transferred to new culture dishes to avoid contamination. Samples were treated (90 min, 37°C) with 2 ml of pre-warmed 2x SSC with or without RNAse A (50 µg/ml final concentration).

Samples were washed with 2 ml of pre-warmed 2x SSC then washed with 2 ml of Wash buffer (10% formamide, 2x SSC). Coverslips were placed onto 50 µl of hybridization mix, with the cells facing down. Probes were used at a final concentration of 10 nM for pre-rRNA probes and 50nM for smRNA-FISH probes in hybridization buffer (10% formamide, 2x SSC, Dextran sulphate 100 mg/ml, *E. coli* tRNA 1 mg/ml, VRC 2 mM, BSA 0.02 mg/ml) per coverslips. Hybridization was performed in a parafilm-sealed chamber (16h, 30°C).

2.6.6 Testing probe concentration

Prior to experiments, RNA-FISH was performed on cells from Mid-logarithmic cultures with different probe concentrations. A 10nM and a 50nM concentration for pre-rRNA and smRNA-FISH probes respectively, gave the best signal above background and best signal above the negative control threshold, without showing filter saturation.

2.6.7 Washing and Nucleus Staining

The next day, coverslips were washed twice with Wash buffer and stained with a PBS solution containing DAPI (0.5 ug/ml). Coverslips were washed with PBS and dipped into H_2O.

2.6.8 Mounting

After allowing coverslips to dry, these were mounted onto microscope slides using ProLong Gold (Diamond Antifade Mountant, Life Technologies) without DAPI and kept in the dark over-night to allow polymerization. Coverslips were sealed with nail polish the following day.

2.6.9 Image acquisition

Cells were imaged using a DeltaVision CORE wide-field epi-fluorescence deconvolution microscope using a 100×/1.40 objective lens. Each experiment campaign was imaged using the same settings.

For the pre-ribosomal RNA FISH; 15 images were taken with an exposure time of 0.035 s (50 %T) and 0.05 s for TRITC and DAPI channels, respectively.

For the smRNA-FISH on antagonistically oscillating transcripts; for all experiment campaings; single-FISH, dual-FISH and control dual-FISH, 21 images were taken with an exposure time of 2s (1000 %T) for Cy5, 1s (100 %T) for TRITC and 0.05s (100 %T) for DAPI channels. 21 0.2 µm z-stacks were taken for all images of all samples. The last image of each set was a field of view without cells to assess the background noise.

2.6.10 Deconvolution

Images were deconvolved directly after imaging with a conservative deconvolution method and 15 cycles using DeltaVision Softworx software as in (Brown et al. 2018). Deconvolution (a Fourier transformation method) is applied on the “raw microscopy image” in order to resolve contrast and resolution and therefore allows precise location of single molecules in cells. Examples of microscopy images are presented at Figure 5.4. Fluorescent signals of raw and deconvolved RNA-FISH as well as brightfield signals are presented.

2.6.11 Visual examination of the data

Each “raw” and deconvolved image was looked at using FIJI (https://imagej.net/Miji) to control the quality of the samples. Mainly to qualitatively evaluate the spheroplasting efficiency, level of background fluorescence and spot detection in the “raw” data.

2.6.12 Images presented in this study

Brightness and contrast of all fluorescence images shown in chapter 4 were adjusted to the same levels using FIJI. Background was removed from the bright-field images by subtracting a “reference image” of the field taken without any cells.

2.7 Data processing, RNA-FISH Dry-lab Workflow

'In-house automated quantification pipeline'

The RNA quantification pipeline is performed using Matlab scripts and include; Background subtraction, Automated Nuclei Detection, Automated Cell Detection, Foci classification and RNA quantification. It was produced by Dr. Andrew Angel. Matlab quantification scripts were based in part on elements of FISH-quant (Mueller et al. 2013) and CellProfiler (Carpenter et al. 2006), allowing greater automization. The quantification pipeline was adapted from Brown *et al*. 2018, to allow for the detection of larger foci in the case of the pre-ribosomal RNAs quantification. The pipeline was also adapted for the quantification of DAPI foci in cytoplasms (mtDNA nucleoids) and the quantification of DAPI intensity in nuclei for the smRNA-FISH data.

2.7.1 Software

Identical set of software packages are used as in Brown et al. 2018; MATLAB (MATLAB Statistics and Image Toolboxes Release 2015a, The MathWorks, Inc., Natick, MA, USA). FIJI (https://imagej.net/Miji).

2.7.2 Background substraction

DAPI, Cy5 and Cy3 channels are processed separately. Images are background-corrected with the same procedure, as performed as in Brown et al. 2018.

2.7.3 Automated Nuclei Detection

The nuclei are identified in 3D using the DAPI channel of the images. The protocol followed here is described in (Feltham et al. 2020) and differed most significantly from (Brown et al. 2018).

2.7.4 Automated Cell Detection

The 2D nuclei identified in the previous step are used as seed points to identify cell outlines.The cell detection is performed as in Brown et al. 2018, using a combination of the DAPI signal, fluorescence signal from FISH probes and autofluorescence of the cells observed in the FISH channel. For the smRNA-FISH data sets the brightfield signal which enables the visualisation of cell outlines is also used. Figure 2.4 shows an example of nucleus and cell outlining using the automated pipeline.

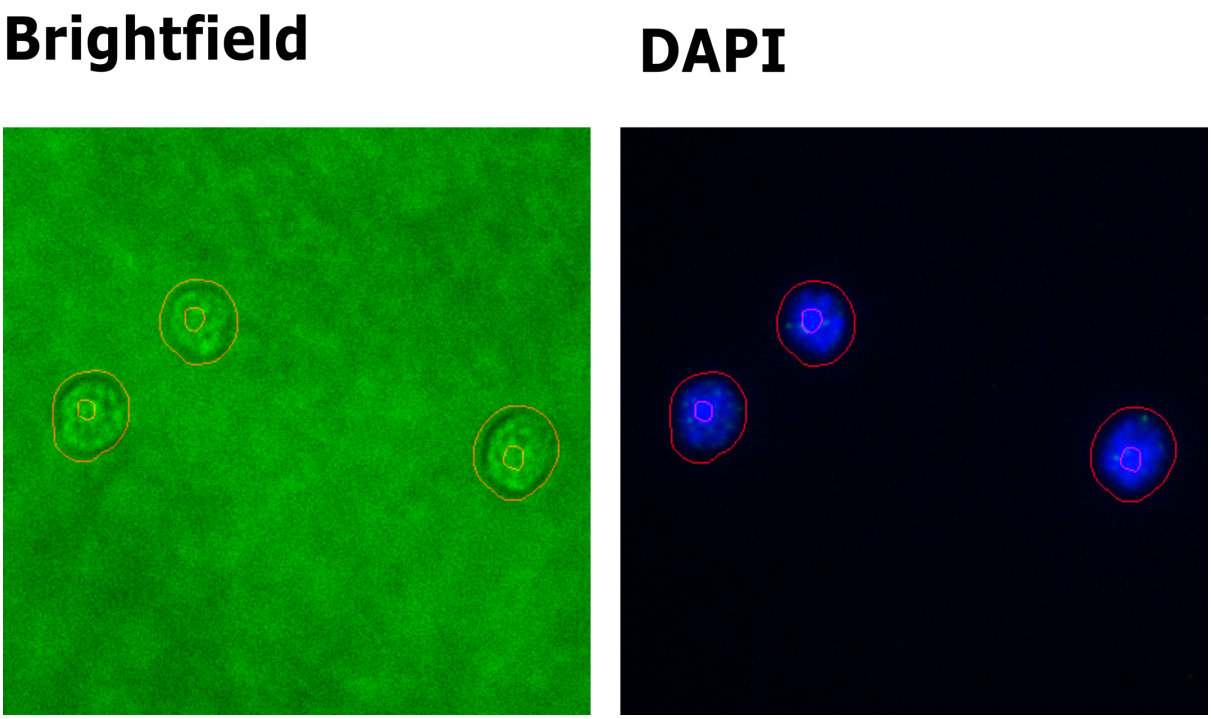

Figure 2.4 An example of nucleus and cell outlining

A. *Brightfield* ***B.*** *DAPI and fluorescent channel (of 1 z-stack only). Images are cropped and enlarged.*

2.7.5 Foci identification

Potential foci are identified as in Brown et al. 2018.

2.7.6 Thresholding

In order to identify “real” fluorescent signal from noise, a threshold is applied to the data to remove low signal intensities arising from background fluorescent signal in cells and on coverslips. Thresholding is typically done by looking at the fluorescence intensity histograms of the data. The ideal threshold usually sits between the exponentially decreasing curve and the plateau/increasing curve (Imbert et al. 2022) as presented at Figure 2.2. In other words; the threshold sits just after the decrease in signal that arise from a high number of pixel with low intensity, essentially background noise. For this study, negative controls were used to help with the determination of this Signal-to-Noise threshold, comparing foci intensities between data and controls. Figure 2.2 shows histograms of fluorescent intensities for CENPK113-7D WT strains vs CENPK113-7D WT KO strains, for *ATO3*, *SHM2* and *IDH1*, using atto633 or atto565 labeled smRNA-FISH probes. These show that passed the exponentially decreasing curve, most of the noise signal is lost, indicating that passed that point the signal emerges from FISH probes on targets and indicate a satisfying difference between fluorescence signals from WT and KO strains for each target transcript. For each sampling timepoint of each experiment, histograms of all foci intensities were produced (see figure S.2, S.3, S.4. Appendix). For each experiment campaign a threshold was applied to lie at the point for which fluorescence signal from the “data” was 10 times higher than the one from the “control”.

Finally, contiguous regions found with greater fluorescent intensities than the threshold are identified as foci. Figure 2.5 show the automated detection of fluorescent foci after applying the appropriate threshold.

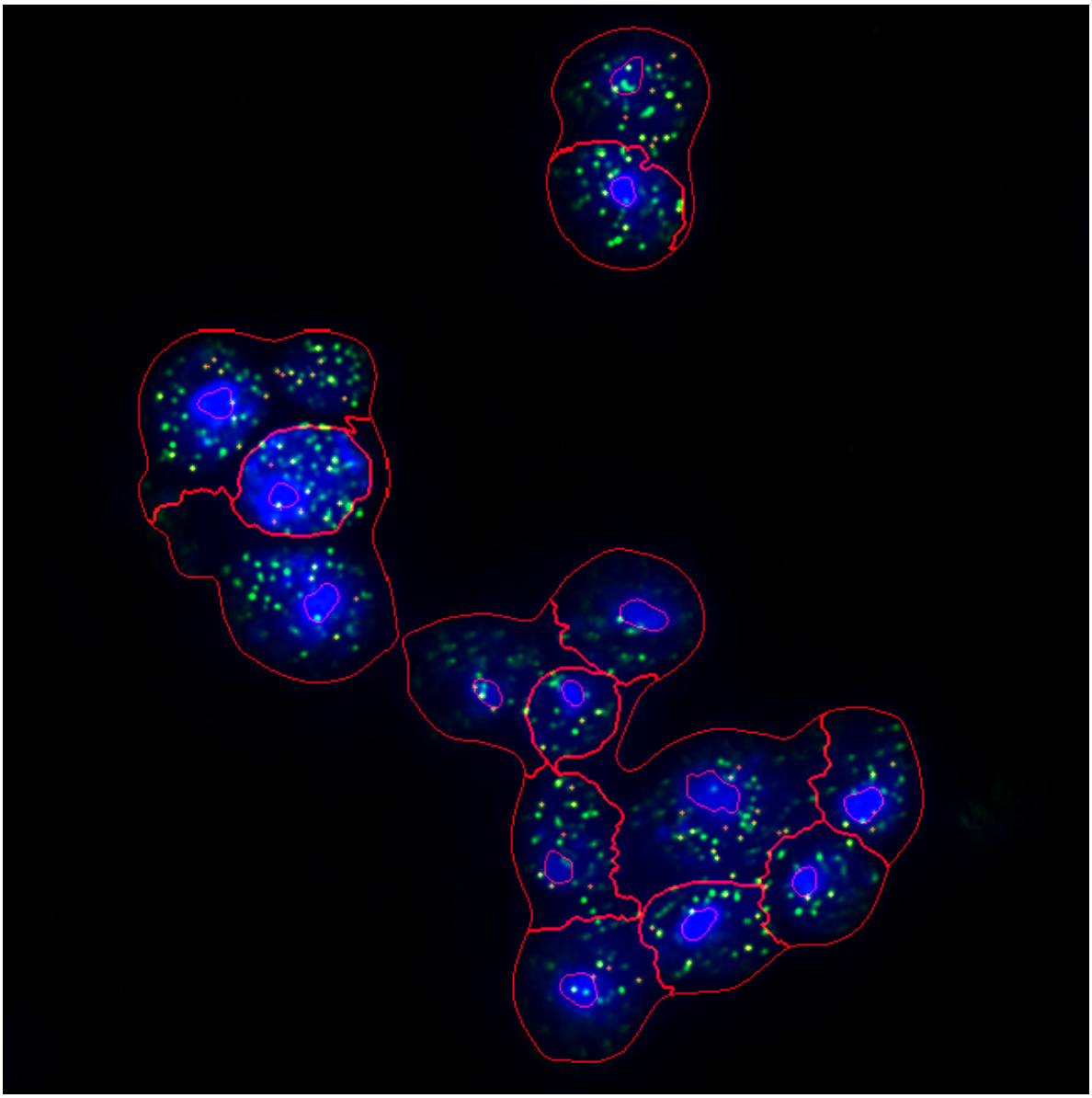

Figure 2.5. Detection of fluorescent foci

Z-stack of a microscopy image passed through the quantification pipeline. The RNA-FISH fluorescent signal is visible in green, while small red diamonds indicate the detected of foci.

2.7.7 Foci classification

Foci were classified as nuclear or cytoplasmic using the DAPI signal to determinate nuclear and cytoplasmic regions as described in Brown *et al*. 2018.

2.7.8 pre-rRNAs quantification

The sum intensities of all pre-rRNA foci pixels in each cell were computed and used to estimate pre-ribosomal RNA production levels.

2.7.9 Single molecule quantification

As described in Brown et al. 2018; in order to obtain absolute RNA numbers in cells, the mean intensity of all foci is calculated by computing the mean intensities of the 27 pixels found around the central pixel of the foci. Then the median of the foci intensities is computed and assigned to correspond to a single molecule RNA. Finally, the intensity of each focus is divided by the median intensity in order to quantify the numbers of single molecules per foci.

Importantly, this quantification method differs from the method commonly used in FISH-quant which uses a Gaussian Fitting method to identify and quantify single molecules (Mueller et al. 2013). The quantification method employed in this study however was determined to work best with yeast cell samples (Brown et al. 2018). The method is based on the fact that although foci can contain more than one transcripts, in particular at transcription sites in-nucleus, most foci were shown to contain a single RNA molecule in yeasts (Femino et al. 1998, Raj et al. 2006, Zenklunsen et al. 2011). Furthermore, cross-validation of the quantification technique was performed using Big-FISH (a more recent version of FISH-quant, Imbert et al. 2022) on a few microscopy images from previous RNA-FISH data sets on yeast cells (Meredith Wouters. Master's internship in Mellor LAB, 2017). The data was kindly analyzed by Arthur Imbert from the Mueller lab and similar RNA numbers were obtained using Big-FISH, validating the method used in this study. An example of the detection of spots/single RNA molecules (red circles) and foci (blue circles) is shown at Figure 2.6.

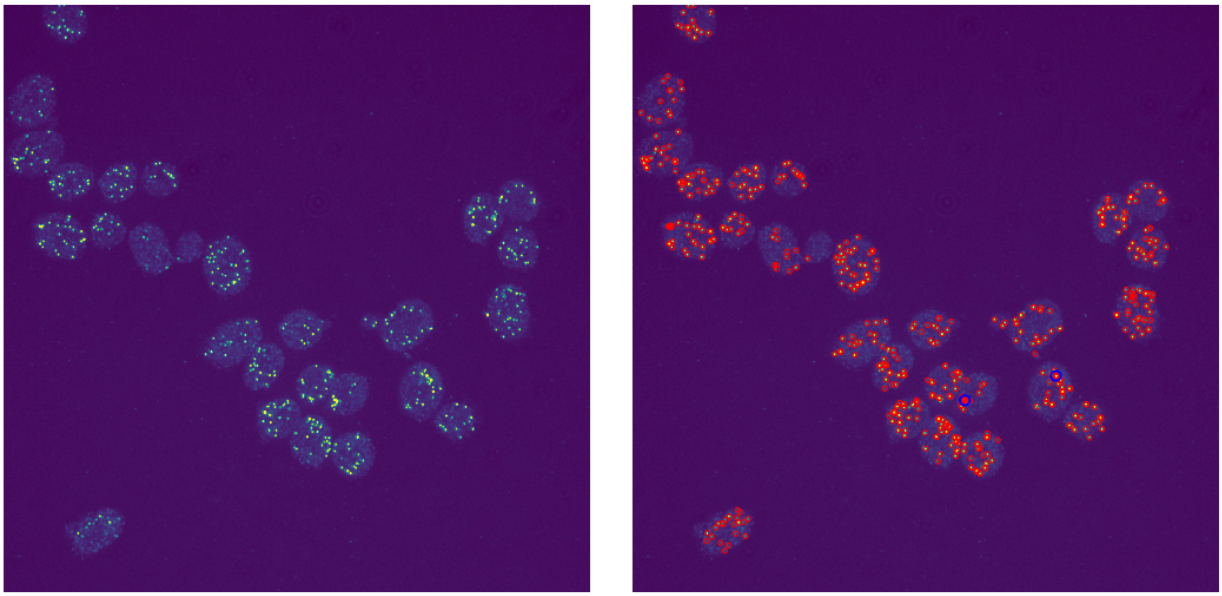

Figure 2.6 Example of single molecule detection using Big-FISH

Example of an entire field of view of a microscopy image from a sample of S. cerevisiae (BY Dset1) cells, expressing PDA1-GFP transcripts. Each mRNA is hybridized with GFP-FISH probes (Cy3). ***A.*** *Maxiumum intensity projection of the RNA-FISH fluorescent signal,* ***B.*** *Detection of single molecule/spots in red and foci in blue using Big-FISH (Images and analysis from Arthur Imbert, Mueller Lab).*

2.7.10 Nuclear DNA content quantification

The sum intensities of all DAPI pixels in-nucleus were computed and used to estimate nuclear DNA content in single cells. Figure 8.1 shows the detection and outline of nuclear DNA content (nucleus).

2.7.11 Mitochondrial DNA nucleoids and total mitochondrial content quantification

The single molecule quantification was applied to the DAPI signal found in cytoplasm. DAPI foci were detected, quantified and the sum of foci intensities was calculated for each cell. Figure 8.2 shows the mitochondrial DNA foci in yeast cells. NB: the possibility of nuclear membrane breakage (DNA leaking from the nucleus) was ruled out as the integrity of the cells was visually validated. All nuclei stained with DAPI

possessed a somewhat spherical shape (visualised through z-stacks) while cells membranes were intact as confirmed with brightfield microscopy.

2.7.12 Scripts

(i) The **Parameter Set-Up** and **First Pass scripts** comprise the Background subtraction, Automated, Nuclei Detection and Automated Cell Detection. (ii) The **Second Pass** script allows the foci identification. (iii) The **Determine Cutoffs** script produces the intensity histograms between the data and control. (iv) The **Third Pass** script enables to set a Signal-to-Noise threshold, identify foci, quantify single RNA molecules and compute quantification metrics.

2.8 Downstream analysis

The downstream analysis and plots were performed in MATLAB and R (R Core Team., 2019), using ggpubr, tidyverse and stats R packages (Kassambara. 2019, Wickham et al. 2019).

2.8.1 Cell size

Along the quantification pipeline, nucleus and cell areas are calculated in pixels. Then nucleus and cell rayons, diameters and areas are calculated in microns (15.4543 pixels/micron) and cell volumes in um^3.

2.8.2 Statistical tests

Wilcoxon tests (non-parametric equivalents of the t-test, working with unequal sample sizes) and Spearman correlations coefficients (non-parametric correlation test) are computed as the data gathered for the different samples is not normally distributed.

Finally, Kolmogorov-Smirnov or K-S tests are non-parametric tests used to compare probability distributions and RNA distributions from the FISH data.

2.8.3 Data filtering

All detected cells are filtered according to the sum of RNA numbers detected in each cell and to cell size in order to remove outliers.

2.8.3.1 RNA number filtering

A few cells of the smRNA-FISH datasets (single, dual and dual-control FISH) were detected with surprisingly high RNA numbers per cell (>50). The detection and quantification of high RNA numbers might arise from FISH probes forming cluster on some areas of the sticky Poly-L-lysine coverslips or on some cells and most likely do not reflect the biological data. Indeed, the RNA copy numbers vary between genes with mRNA numbers reaching up to a hundred copies for some genes (Miura et al. 2008). However, it was shown that for most genes between 0.1 to 2 mRNA copies of a gene were present per budding yeast cell (Holstege et al. 1998). In particular, previous studies evaluated absolute transcripts numbers to a maximum of 21.1 for the target transcripts picked for this study in mid-log WT cultures (Table 5.1.B, chapter 5, Holstege et al. 1998). Nevertheless, transcript copy number vary under growth conditions (Holstege et al. 1998, Lahtvee et al. 2017) and transcripts such as *ATO3* are expected to be expressed more highly in stationary phase but not in mid-Log phase.

Therefore, here a threshold of 50 RNAs/cell was applied to remove outliers (only a few cells were detected with higher numbers than 50 RNAs).

2.8.3.2 Cell size filtering

The computed cell size of a few cells also seemed aberrant. This is believed to be the result of the cell detection process, that very rarely leads to the outlining of multiple cells together. *Saccharomyces cerevisiae* cells possess an ovoid shape but can be thought of as spheres with a cell diameter of roughly 3 to 6 µm, the volume range for standard WT lab strains is between 30 to 100 μm^3 or fL (femtoliter) and haploid WT cells possess a lower median cell diameter than diploids (˜4um vs 6um) (Jorgensen et al, 2002). Importantly, cell size can vary depending on strains, growth, stress, environmental conditions, progression through the cell division cycle. The data was thus filtered accordingly to remove these outliers. For all datasets, cells for which the diameter was strictly above 6.2 um corresponding to a cell volume of $124um^3$ have been discarded from further analysis.

NB1: As the cell wall of the cells is removed by spheroplasting, the cell size reported here might be slightly smaller than found in literature for non-spheroplasted cell size. Moreover because the nucleus and cell sizes are computed from the automated cell detection, it is possible this induces some inaccuracies. NB2: some of the cells and nuclei detected are particularly small. This could result from the outlining and detection of the overall DAPI signal in cell as nuclei. However because new born cells and quiescent cells might be particularly small, no threshold was applied on lower cell sizes.

2.8.3.3 Samples filtering

Pre-rRNA-FISH: Some samples, for which most of the pellet was lost (during the crosslinking step of the RNA-FISH experiment), were removed from the final analysis.

smRNA-dual-FISH: Samples showing particularly low fluorescent probe levels in both channels at timepoints for which expression was expected and detected in other replica were suspected to represent products of experimental errors and were thus removed from the analysis; dual-FISH 2 (*SHM2* – *IDH1*); Tp -10, dual-FISH 3 (*IDH1*-*ATO3*) ; Tp +90 and control-dual-FISH (*ATO3* – *ACT1*); Tp +80.

2.8.4 Sample size

For the pre-ribosomal RNA FISH; a median of 102 cells was detected per time point. The number of detected cells per sm-dual-RNA-FISH experiment before and after filtering is displayed at Table 2.3.A & B respectively.

Table 2.3.A Number of detected cells per FISH experiment

Experiment	Target transcript (atto633 labelled)	Target transcript (atto565 labelled)	Mean	St.dev.	Median	Range	Total
DualFISH 1	ATO3	SHM2	155	35	147	98 - 219	2020
DualFISH 2	SHM2	IDH1	131	46	123	58 - 210	1704
DualFISH 3	IDH1	ATO3	140	70	123	56 - 295	1822
SingleFISH	x	ATO3	210	71	202	127 - 374	2943
DualFISH 4	ATO3	ACTIN1	484	226	439	184 - 964	11133
DualFISH 5	ATO3	ACTIN1	290	99	253	183 - 508	6685
DualFISH 6	ATO3	ACTIN1	546	207	580	191 - 967	12573

Table 2.3.B Number of detected cells per FISH experiment after filtering

Experiment	Target transcript (atto633 labelled)	Target transcript (atto565 labelled)	Mean	St.dev.	Median	Range	Total
DualFISH 1	ATO3	SHM2	145	41	130	84 - 217	1893
DualFISH 2	SHM2	IDH1	119	45	117	32 - 196	1547
DualFISH 3	IDH1	ATO3	130	73	102	28 - 291	1701
SingleFISH	x	ATO3	203	74	200	84 - 371	2855
DualFISH 4	ATO3	ACTIN1	324	179	278	79 - 675	7455
DualFISH 5	ATO3	ACTIN1	187	86	182	61 - 392	4301
DualFISH 6	ATO3	ACTIN1	414	188	449	130 - 827	9538

The number of cells captured through microscopy and then detected using the cell detection pipeline varies between repeats and timepoints (range Table 2.3.A & B). This is because a list of field of views containing yeast cells is selected for imaging rather than a precise number of cells. Despite the variability in sample size between the FISH experiments and sampling timepoints (range Table 2.3.A & B), the number of yeast cells detected are expected to be sufficient to represent the yeast population at the sampling timepoint they were taken. However, this variability was considered when analysing and plotting the data.

2.8.5 Cell categories

Cells were analysed and grouped according to their expression status based on the (i) absence or presence of transcripts in cells, (ii) the fluorescent channel in which transcript were imaged, (iii) the transcript localisation; in-nucleus, in-cytoplasm or in-cell (iv) the RNA numbers per cell.

2.9 Limitations of the techniques used in this study

2.9.1 Pre-rRNA-FISH, a semi-quantitative method

The signal intensity of smRNA-FISH probes is expected to positively correlates with the number of fluorescent probes hybridizing (Stellaris), thus the number of pre-rRNAs. However, in the case of the pre-rRNA-FISH experiment, because of the unusual size of the foci, the detection of “non-associated hybridization” signal can’t be completely ruled out. Nevertheless, the changes detected in pre-rRNA production levels were found within the range of what has been demonstrated before (Kief & Warner. 1981).

Chapter 3

smRNA-FISH on YMC samples in a nutshell

In this chapter, the experimental approach taken in this study is introduced and some of the key aspects of the materials and methods employed are discussed (Figure 3.1, 3.2).

3.1 Inducing and recording the Yeast Metabolic Cycle

The synchronisation of a yeast culture happens under specific and controlled laboratory conditions and experimental settings. Typically, yeast cells of a prototrophic strain of *Saccharomyces cerevisiae* (here wild type haploid CENPK) are grown in batch culture, to a high cell density, at a high-growth rate. After the nutrients are exhausted, the yeast culture is starved for several hours, until the cells are finally fed media with limiting concentration of glucose (Figure 3.1). At all times, the culture is kept at a constant volume. Therefore, as the culture is continuously fed, a part of the culture and media is also constantly discarded. Lastly, the yeast culture is kept at constant temperature, pH, and aeration, and is also constantly mixed. Together, continuous feeding with steady-state conditions lead to the synchronisation of the yeast cell population and regular metabolic oscillations (Klevecz et al. 2004, Tu et al. 2005).

Chemostats or fermenters are used to regulate these precise growth conditions (Monod. 1950, Novick & Szilard. 1950). These bioreactors, as their names indicate, ensure a static chemical environment. They are used in microbiology but also in brewing and bioengineering industries. Two types of chemostats were used for this research project; the LAMBDA Minifor and the Eppendorf Bioflo320. Although the two devices differ slightly, both fermenters are composed of the same parts (Figure 3.1). First a vessel contains the culture of interest. Second, a control unit or computer

enables the command of the system. Pumps permit the circulation of fresh media (feeding pump) and of a base solution (pH correction pump) to the culture, as well as the removal of the culture media from the vessel (harvest pump). Aeration of the culture is made via the use of an air compressor. Constant agitation is maintained with a motor combined to a pump or agitation blades. The volume of the culture is fixed through the use of a level sensor or weighing scale. Finally, the temperature of the vessel is kept constant using a water chiller. The maintenance of these particular conditions is made by way of different probes connected to the vessel (pH, temperature, dissolved oxygen) and reporting information to the control unit. This last allows the regulation of the whole system but also the recording of the parameters (Feltham et al. 2019, Xi. DPhil thesis. 2019).

The different stages of growth of the yeast culture are monitored through the dissolved oxygen levels (dO_2) in the culture medium over time (Figure 3.1). Most importantly, the dO_2 levels indicate the metabolic phase of the cell population. The experimental settings used in this study induce YMCs with a period of oscillation of around 3 hours and 20 minutes. The High Oxygen Consumption (HOC) phase lasts less than a third of the cycle (around 60 minutes), while the rest of the cycle is characterised by the Low Oxygen Consumption (LOC) phase. Finally, sampling from the YMC culture is made through time and relative to the dO_2 levels recorded for the population (Figure 3.1), while the harvest pump rate lowers to maintain a constant culture volume.

A.

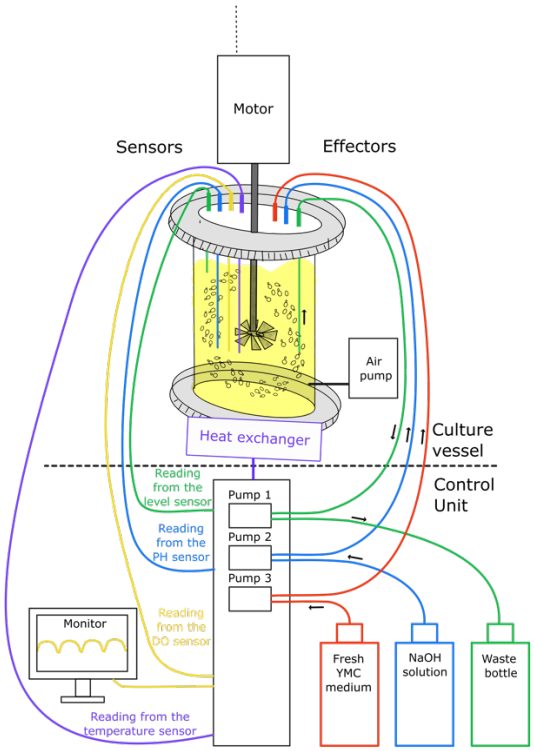

B.

C.

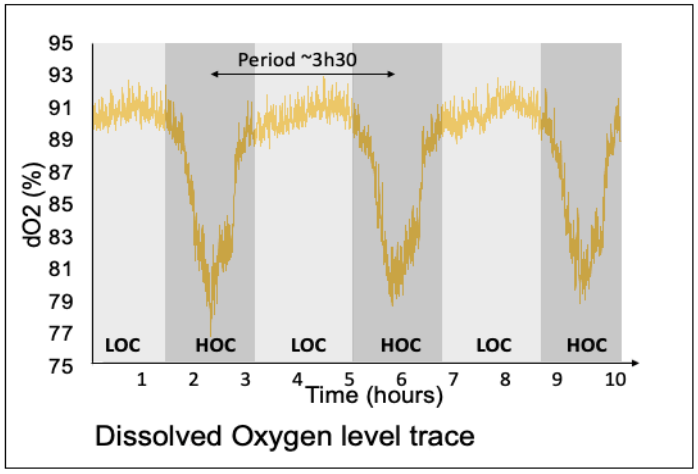

Figure 3.1. Inducing and recording the Yeast Metabolic Cycle under chemostatic conditions

A. *Schematic of the chemostat/fermenter is presented. Adapted from Xi. DPhil. 2019.* ***B.*** *Photos of the fermenters (i) the Eppendorf Bioflo320 and (ii) the LAMBDA Minifor. Images from https://www.eppendorf.com/IN-en/bioflo-320/ and https://www.lambda-instruments.com/fermenter-bioreactor/ .* ***C.*** *An example of the typical trace of dissolved oxygen levels obtained after the inducing the YMC for one of the experiments realised for this study. These were recorded by the control unit. Samples taken over time along the YMC for the time-course RNA-FISH experiments realised in this study are shown at Figures 4.4, 5.3 and S5.*

In this study, time-course smRNA-FISH experiments were carried out along the Yeast Metabolic Cycle. Samples were collected every 10 minutes, providing high time-resolution and permitting application of splining methods to the interval data that was collected. An emphasis was made on the HOC phase of the cycle. More samples were collected around this phase, as it is known to be a time-period of many metabolic and gene expression changes.

3.2 Overview of experimental design and analytical pipelines for smRNA-FISH

This study aims to use smRNA-FISH to explore the single-cell expression of rRNA transcripts transcribed by RNA polymerase I and four transcripts transcribed by RNA polymerase II. Details of the experiments, dO_2 traces and exact sampling time points along the YMC are given in chapter 4, and chapter 5 respectively.

3.2.1 At the bench

Once sampled, the yeast cells are directly processed through the smRNA-FISH experimental pipeline (Figure 3.2) (Femino et al. 1998, Raj et al. 2006, Zenklunsen et al. 2011). Briefly, the method of smRNA-FISH permits the detection and quantification of single transcripts, while the staining of the DNA with DAPI allows localisation of transcripts in-nucleus or in-cytoplasm as depicted in Figure 3.2.A. Thus, this technique allows inferences to be made about the nascent and steady state RNA levels in single cells (Raj et al., 2008, Zenklunsen et al. 2008). Cells are fixed with paraformaldehyde, a cross-linking agent, granting the capture of the cells' state in their original cultures and yeast populations. Next, the yeast cell walls are spheroplasted (digested). Following recovery, spheroplasts are attached on coverslips and their membranes are permeabilised with ethanol. Then follows the *in-situ* hybridization of the smRNA-FISH probes to the target transcripts, by inverting coverslips onto the hybridisation mixture

containing formamide, which reduces the temperature at which the single strand RNA (target transcript) and DNA (probes) melt. Hybridisations are completed overnight at 30 °C securing the preservation of the yeast cells. DNA is stained with DAPI before mounting the coverslips and cells onto slides. Labelling DNA with DAPI allows the further detection and outlining of the cell's nuclei and the localisation of transcripts. Many washes are performed in between the steps described above, with the purpose to decrease background fluorescent noise. Finally, negative controls were produced to assess signal-to-noise ratios.

3.2.2 At the microscope

Yeast cells are imaged using a wide-field epi-fluorescence deconvolution microscope, allowing the capture of many cells through the x, y and z planes in the different fluorescent channels and corresponding excitation and emission wavelength commonly named: Cy5, Cy3 and DAPI. Images are also taken with the brightfield to detect cell outlines. To capture enough yeast cells to permit quantitative analysis of the data, 15 to 20 images are taken for each YMC sampling timepoint.

3.2.3 On the computer

The data is processed as follows; first preliminary analysis and quantification of transcripts is performed using an "in-house" automated quantification pipeline constructed by Dr. Andrew Angel and adapted from Brown et al. 2018 (Figure 3.2.B). Through the pipeline, the MATLAB scripts use the imaging program FIJI (Image J). Different versions of the pipeline are used to either detect larger foci (to assess pre-rRNA levels) or single transcripts (to assess absolute transcript numbers). In summary, the pipeline allows the subtraction of background signal, the detection of nuclei, cells and candidate foci. Then a threshold is applied to the data to separate the data and

“real” fluorescent signal from the noise. This threshold is set with the help of negative controls; RNAseA treated samples (used here for the rRNA detection) or Knock Out strains (for the RNA polymerase II transcripts). Only foci or spots for which the intensity is greater than this threshold are retained for further analysis.

Next, the single molecule quantification is processed. Put simply, the mean intensity of each focus is computed. Then the median of the foci intensities is calculated and designated as a single molecule or transcript. Of course, foci can contain more than one transcripts, but previous work showed that most foci contain a single RNA molecule (Femino et al. 1998, Raj et al. 2006, Zenklunsen et al. 2011). Finally the number of transcripts in each focus is computed by dividing each focus intensity by the median intensity of 1 RNA molecule. Many metrics are then computed in addition to sum intensities of foci and single molecule quantification. Finally, after collecting information on the data, downstream analysis is performed in MATLAB and R to interrogate the data.

A considerable amount of time and effort was put into optimisation of the wet and dry parts of these experiments, particularly the optimisation of the removal of the yeast cell walls, finding the appropriate intensity thresholds, endorsing the quantification method. These optimization steps, but also the limitations of the techniques used in this study, together with the details of experimental settings, are described in Materials and Methods.

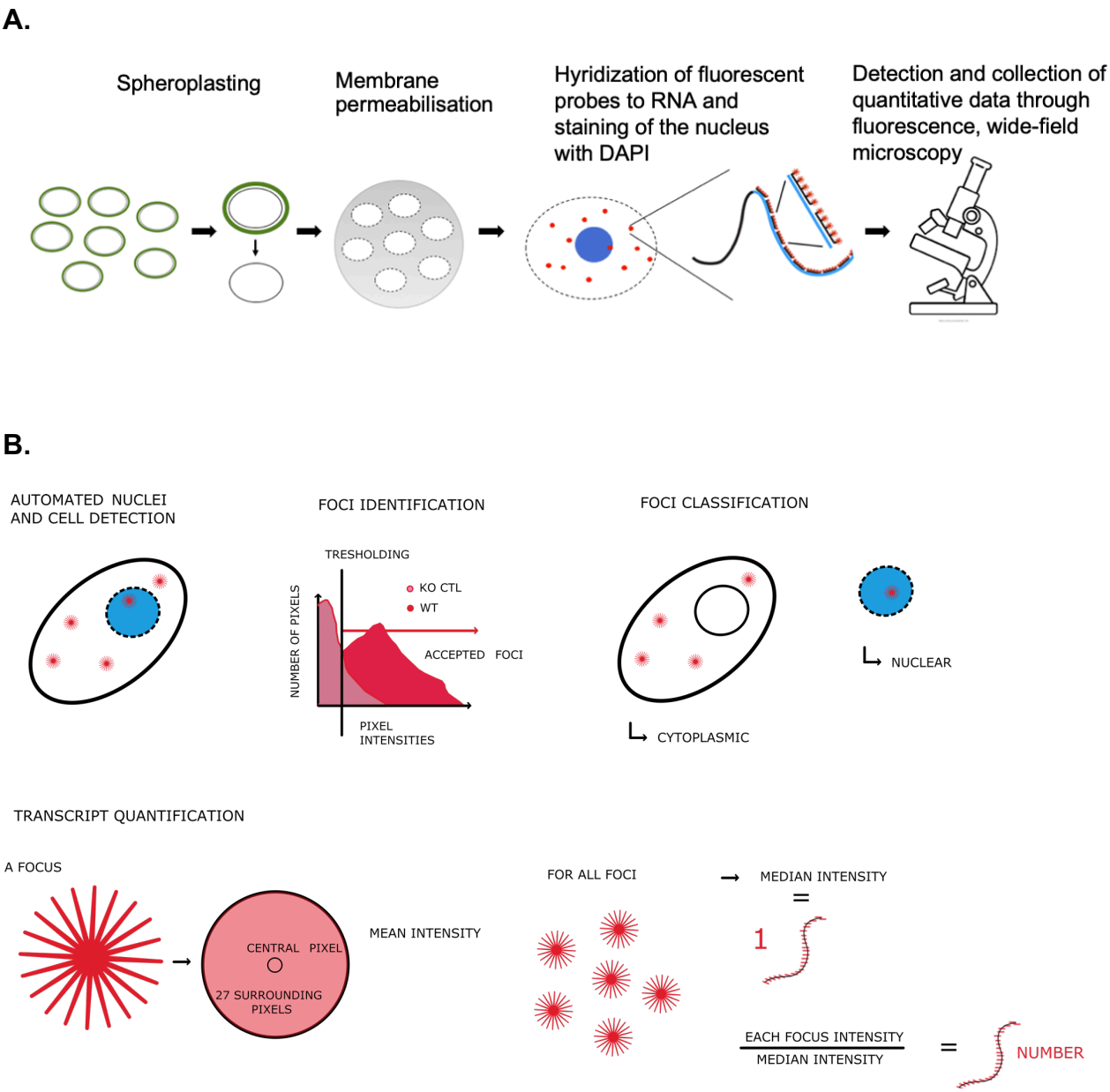

Figure 3.2 Experimental design and analytical pipelines for smRNA-FISH

A. *The main steps of RNA-FISH in budding yeasts are; the cell wall removal/spheroplasting, the membrane permeabilization, the hybridisation of the fluorescent probes to the target transcript, the staining of the nucleus with DAPI and the following detection and acquisition of quantitative data via fluorescence, wide-field microscopy.* ***B.*** *Next, the microscopy data is processed using a transcript quantification pipeline. Steps include; the automated detection of nuclei and cells, the identification of foci using thresholding, the classification of the foci and finally the quantification of transcripts using the foci mean intensities (details are found in chapter 2).*

Chapter 4

Ribosomal RNA production is globally coordinated to Rps6 phosphorylation during the YMC, yet heterogenous in single cells of YMC populations

4.1 Introduction

Recent transcriptomic and proteomic data gathered throughout the YMC (Feltham et al. 2020) corroborated previous reports showing transcription and transcript levels of genes associated with particular pathways were found to alternate during the YMC (Klevecz et al. 2004, Tu et al. 2005, Kuang et al. 2014). However, while oscillations were detected for translation, protein levels were found to remain stable throughout the cycle (Feltham et al. 2020). These findings contradict the “Just in time model” by Kuang et al. 2014 and lead to question as to how cells manage with constant protein levels in a changing rhythmic environment. Several hypotheses have been explored. These include metabolic flux, protein accessibility and post-translational modifications (PTMs) (O’Neill et al. 2020).

Here, the role of protein post-translational modifications during the YMC is explored. Protein phosphorylation is a predominant modification (Johnson & Barford. 1993, Vlastaridis, Papakyriakou, et al. 2017) which could orchestrate their cycling activity, providing a “fast-response to environmental changes” within the context of metabolic cycling.

4.1.1 Signalling pathways and phosphorylation cascades

Many highly conserved kinases and phosphatases function at the nexus between proliferation and quiescence. The target of rapamycin (TOR), protein kinase (PK) A, B, C, Sch9, as well as the mitogen-activated protein (MAP) Kinases and Snf1 are some of the most important kinases involved in promoting growth and proliferation from budding yeast to human cells (De Virgilio & Loewith. 2006). These kinases can sense and are regulated by nutrients and amino acid levels (Gonzalez & Hall. 2017).

Importantly, these nutrient signaling pathways lead to phosphorylation cascades involved in the regulation of many processes. Upon starvation, or limitation/depletion of essential nutrients, experienced by cells approaching the diauxic shift, for example, the kinase activities of pro-growth factors such as PKA, TORC1, Sch9 are downregulated. Activities of kinase such as Snf1 and Pho85 are upregulated to maximise the use of alternative nutrients. This generally leads to a decrease in ribosome biogenesis and protein synthesis, while the stress response and autophagy are up-regulated. Growth slows and cells arrest in G1 before transitioning to quiescence (G0) (De Virgilio. 2012).

Intra and extra-cellular metabolites regulate these nutrient signalling pathways during the diauxic shift and on entry into stationary phase (De Virgilio. 2012, Breeden & Tsukiyama. 2022). These pathways are expected to regulate the YMC, as growth under limiting concentrations of glucose is similar to the diauxic shift. However, during the HOC phase of the YMC, hallmarks of growth are found as genes involved in anabolic reactions are transcribed (Klevecz et al. 2004, Tu et al. 2005, Kuang et al. 2014, Feltham et al. 2020) and some cells progress through the cell division cycle (Burnetti et al. 2016). Therefore, in HOC phase up-regulation of growth-related nutrient-signalling pathways are expected.

4.1.2 Linking metabolites and ribosomal protein activities

Ribosome biogenesis is an important marker of cell growth (Johnston et al. 1977, Jorgensen et al. 2004) and is regulated by signalling pathways such as PKA, TORC1 and Sch9 (De Virgilio. 2012). Ribosomal protein (RP) and ribosome biogenesis (RiBi) genes are highly transcribed in the early HOC phase of the YMC (Klevecz et al. 2004,

Tu et al. 2005, Kuang et al. 2014, Feltham et al. 2020). However, like many other proteins, levels of ribosomal protein stay constant over the YMC (Feltham et al. 2020, Oneil et al. 2020). Thus it is likely that phosphorylation cascades and nutrient signalling pathways and protein PTMs could be orchestrating ribosome biogenesis and thus growth along the metabolic cycle.

4.1.3 Rps6 phosphorylation oscillates during the cycle

Rps6 is an evolutionary conserved ribosomal protein (Lecompte et al. 2002) found in the 40S-subunit of ribosomes (Planta et al. 1998). It plays a role in pre-ribosomal RNA processing and thus ribosome biogenesis (Phipps et al. 2011). Most importantly, Rsp6 is a downstream target of the TORC1/2 phosphorylation pathway, via the Ypk1-3 kinases as depicted in Figure 4.2 (Yerlikaya et al. 2016, Meyuhas et al. 2008, Magnuson et al. 2011).

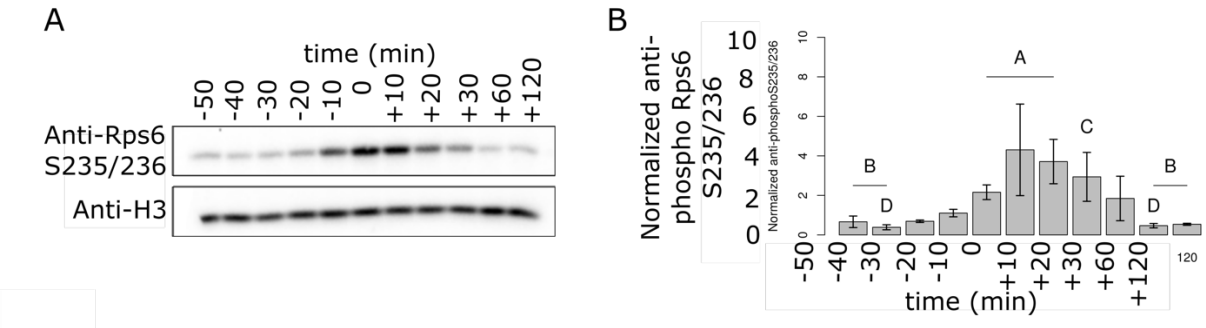

Figure 4.1 Levels of phosphorylated Rps6 in mid-HOC phase of the YMC

For different sampling timepoints taken along the YMC. Time is shown in minutes relative to the point of lowest dissolved oxygen levels in media (dO_2 %) found across the YMC, displayed as "0". ***A.*** *Western Blot of the Rps6(S235/S236) isoform and of histone H3 (acting as a control).* ***B.*** *Normalised levels of the doubly-phosphorylated Rps6 to H3 levels (ANOVA and Tukey's post hoc tests showed levels of group A are significantly greater than group B, and levels of group C are significantly greater than group D. Figure and data from Julian Urdian-Arraiza Master's internship. 2019, also found in Feltham et al., (2020).*

Phosphorylation of Rps6 is believed to regulate its activity, as an unbalanced ratio between the 40S and 60S ribosomal subunits is observed in absence of Rps6 phosphorylation (Yerlikaya et al. 2016). Phospho-Rps6p (S235/S236) levels were found to oscillate during the cycle, increasing in the early HOC phase and peaking during the mid-HOC phase of the YMC, as observed by Zn^{2+}-Phospho-Tag Western Blot and presented at Figure 4.1 (Julian Urdian-Arraiza Master's internship. 2019, Feltham et al. 2020; O' Neill *et al.* 2020).

4.1.4 Rps6 activity regulates Ribosomal RNA biogenesis

Fluctuating levels of phosphorylation of Rps6 along the YMC indicate that its activity is regulated during the cycle. Accordingly, ribosomal RNA biogenesis and the 40S ribosomal subunit assembly are expected to follow Rps6 phosphorylation during the YMC. Ribosomal RNA biogenesis takes place in the nucleolus, where RNA Polymerase I transcribes some tandem repeats (~150) of the *RDN1* locus into 35S pre-ribosomal RNAs (Figure 4.2). Different RNAs, factors and complexes, such as the SSU processome, mediate the cleavage and folding of these polycistronic pre-rRNAs into rRNAs and their assembly into mature ribosomes (Phipps et al. 2011). Rps6 is directly involved with pre-rRNAs processing since it is a component of the SSU processome. Therefore, during the YMC, changes in phosphorylation status of Rps6 leading to a coordinated production of the pre-ribosomal RNA (rRNA) are anticipated. In order to test this hypothesis, pre-ribosomal RNA (rRNA) production levels were assessed throughout the YMC.

4.2 Experimental design and method development

For this project, RNA-FISH (Femino et al. 1998, Raj et al. 2008) was used to quantify pre-ribosomal RNA (rRNA) production levels along the YMC.

4.2.1 Probe design

~20 nt RNA-FISH probes (Stellaris) were designed to target both external and internal transcribed spacers regions (TSRs) of the 35S pre-rRNAs (Figure 4.2).

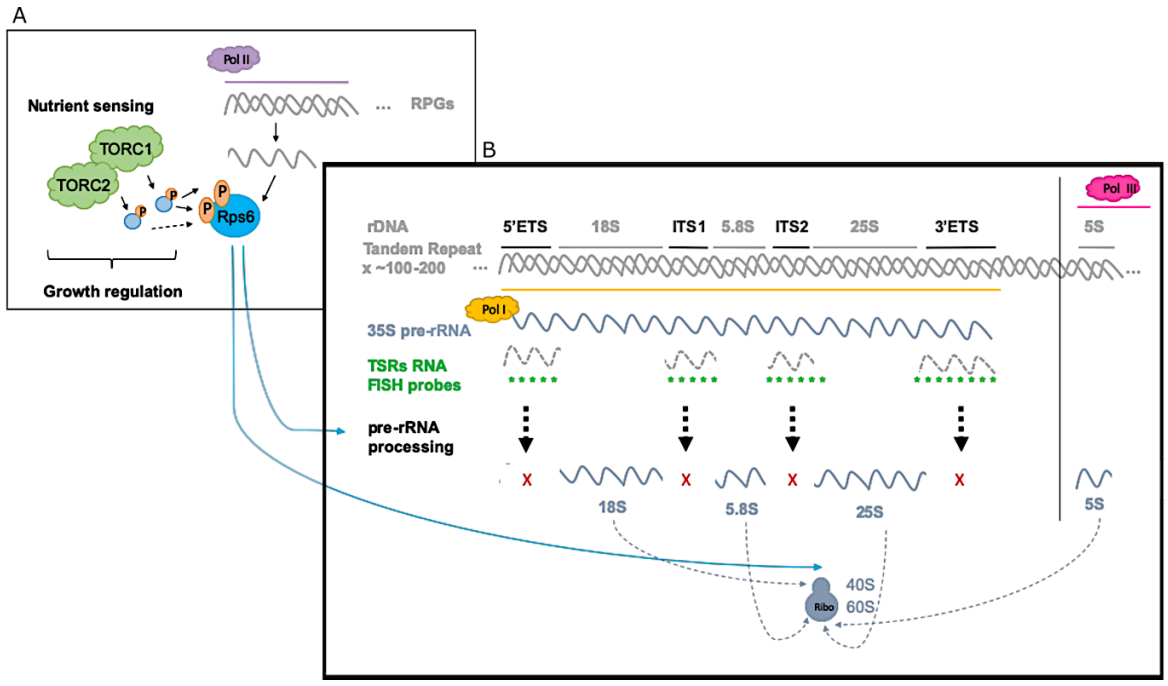

Figure 4.2 *Ribosomal RNA biogenesis, pre-rRNAs processing by Rps6 and RNA-FISH targeting of pre-rRNAs TSRs*

A. *The RNA Polymerase II transcribes the Rps6 coding gene. The TORC1 signaling pathway leads to Rps6 phosphorylation. B. RNA Polymerase I transcribes the RDN1 locus. Transcribed spacers regions (TSRs), from the polycistronic 35S pre-rRNAs (nascent transcripts), are probed using RNA-FISH. Pre-rRNAs processing, including co- and post-transcriptional cleavages of the TSRs, give rise to rRNAs. (RNA Polymerase III is involved in the 5S rRNA production). 18S, 5.8S, 25S and 5S rRNAs assemble with ribosomal proteins to form ribosomal subunits. Rps6 contributes to pre-rRNA processing and 40S-ribosomal subunit assemblage. Inspired by Yerlikaya et al. 2016, and Phipps et al. 2011.*

4.2.2 pre-rRNA-FISH, a semi-quantitative method.

Fluorescent FISH probes labelled with Quasar 570 allow the detection of pre-rRNA TSRs in single cells (Figure 4.3). Staining of the DNA with DAPI allows the detection of nuclei and cells and the localisation of transcripts in the nucleolus. Although the method of smRNA-FISH usually permits the detection and quantification of single transcripts, here the quantification of single molecules is not possible as transcription of the many rDNA repeats by RNA polymerase I produces high transcript levels. The pre-rRNAs form a cluster in the nucleolus of cells. Indeed, fluorescent foci are visible in each cell, at one side of the nucleus (Figure 4.3). Thus, instead of quantifying absolute RNA numbers, the method employed in this study quantifies the sum intensities of all pre-rRNA foci pixels in each cell, acting as proxies for pre-ribosomal RNA production levels.

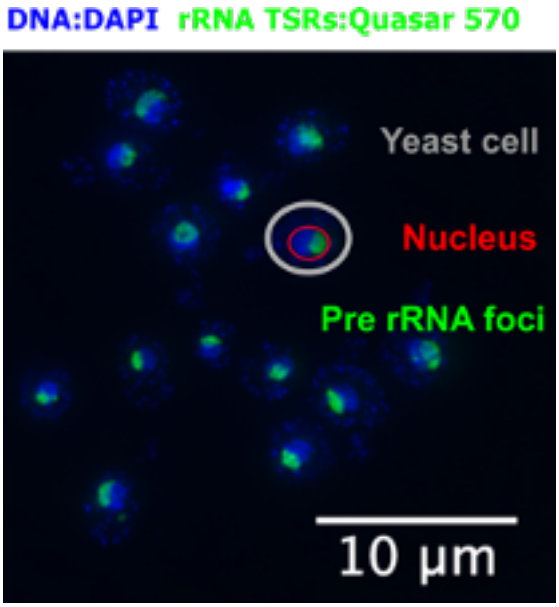

Figure 4.3 RNA-FISH targeting of pre-rRNAs TSRs, a semi-quantitative method acting as a proxy for ribosomal RNA transcription

Microscopy image cropped and enlarged of a sampling timepoint taken during the YMC. Fluorescent labeling; DNA is stained with DAPI (blue); Probes binding to Transcribed spacers regions of the 35S pre-rRNAs are labelled with Quasar 570 (green). Crescent shaped pre-rRNA foci are visible in nucleoli (green). The nucleus and the yeast cell are outlined for one cell.

4.2.3 Sampling timepoints along the YMC for pre-rRNA-FISH experiments

RNA-FISH experiments were carried out on around 20 samples taken along the YMC in triplicate (n=3) and for comparison from mid-log exponentially growing cells. The sampling timepoints relative to the dissolved oxygen traces of the cycles are presented at Figure 4.4. Details of the materials and methods and data analysis are described in chapters 2 & 3.

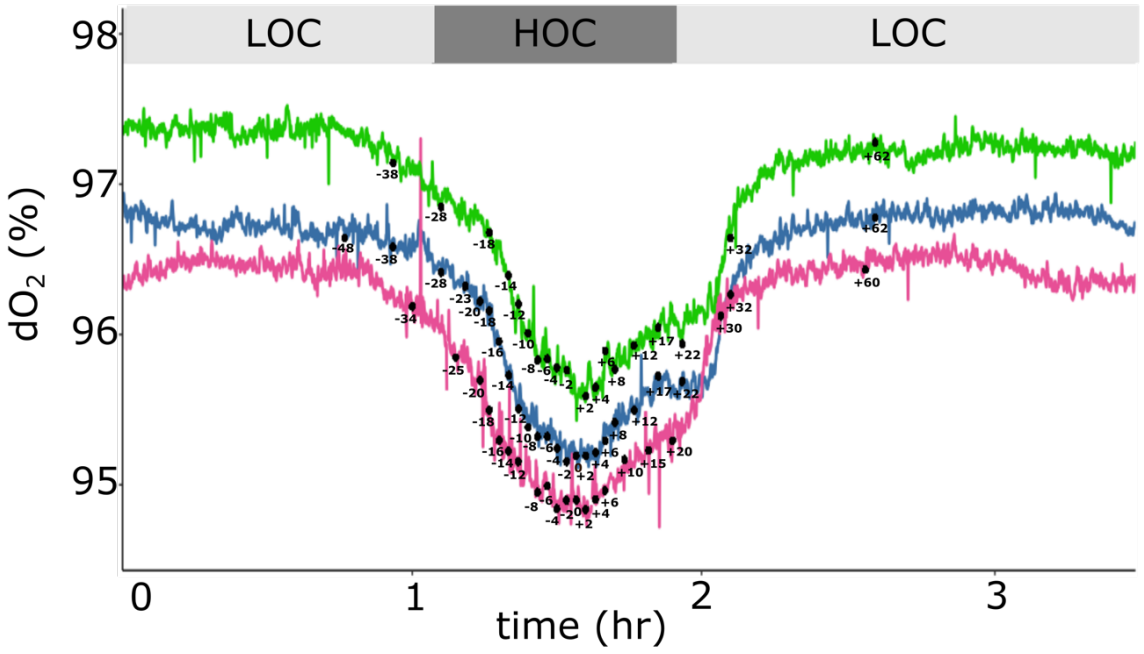

Figure 4.4 Sampling timepoints along the YMC for pre-rRNA-FISH experiments

Dissolved oxygen levels fermenter traces, sampling time points (time shown in minutes relative to the point of lowest dissolved oxygen levels in media (dO_2 %) found across the YMC, displayed as "0") and biological replicates of the different FISH experiment campaigns (n=3; 3 biological repeats or YMC sampling, 3 technical repeats or smRNA-FISH experiments). A: Blue, B: Pink, C: Green.

4.3 Results

Figure 4.5 shows an example of yeast cells stained with DAPI and presenting crescent shaped bright pre-rRNA foci in green in the nucleolus of cells.

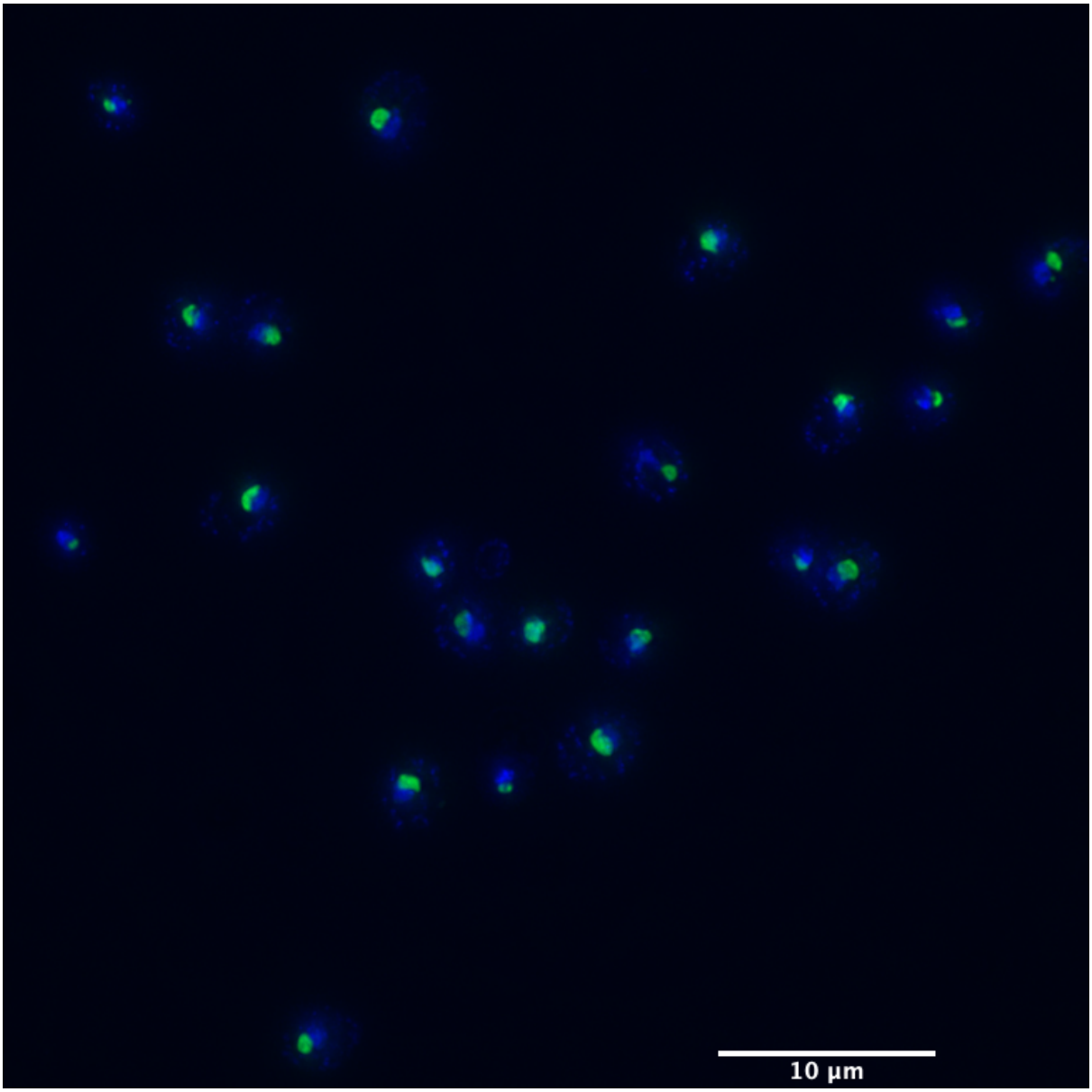

Figure 4.5 An example of microscopy image used in this work, here showing a field of view from a sample of the YMC culture for the pre-rRNA FISH experiments

Microscopy image cropped of a sampling timepoint taken during the YMC. Fluorescent labeling; DNA is stained with DAPI (blue); Probes binding to Transcribed spacers regions of the 35S pre-rRNAs are labelled with Quasar 570 (green). Crescent shaped pre-rRNA foci are visible in nucleoli (green). Scale bar: 10 µm.

4.3.1 Pre-rRNA production peaks in the middle of the HOC-phase

The distributions of pre-rRNA levels in single cells of YMC and mid-log cultures for the 3 biological replica are shown as violin plots (Figure 4.7). Violin plots indicate the range in signal intensities in the population and the frequency of the signal intensity (width of plot). Despite some variability between replica, all biological repeats show a significant increase in pre-rRNA production levels in the YMC, increasing significantly from the LOC phase to the early stage of the HOC-phase, reaching a peak in the middle of the HOC phase. Pre-rRNA sum intensities increase by a factor of ~3 from LOC to HOC phase. Finally, pre-rRNA production levels from exponentially growing mid-log cultures are substantially higher than those from YMC samples (~1.5x higher than HOC and ~4.6x higher than LOC).

Examples of representative images show pre-rRNA foci are brighter in HOC phase of the YMC (Figure 4.6). The increase in pre-rRNA production levels reflects, at least in part, an expansion in pre-rRNA foci volumes in nucleoli, which are larger in mid-logarithmic cultures than in the YMC, where HOC phase samples are larger than in the LOC phase of the YMC (at least 3.2x higher for mid-log and ~1.91x higher for HOC samples compare to LOC) (Figure 4.8). The differences observed between mid-log and YMC samples perhaps result from the number of gene copies of the *RDN1* locus being actively transcribed. Indeed, a higher number of active gene copies of the *RDN1* locus was reported in fast-growing cultures when compared to slow growing ones (Dammann et al. 1993).

4.3.2 More cells in the population have high pre-rRNA levels during the HOC phase of the YMC

Heatmaps were constructed in order to depict the fraction of cells where pre-rRNA production is high*, which means it is greater than the base mean of the sum intensities of all the time points, excluding the sample taken in mid-logarithmic cultures (Figure 4.9). During the late LOC phase only a small proportion of cells (15%) have high* pre-rRNA sum intensities. This fraction increases more than twice as cells enter the HOC-phase, with a peak around the mid-HOC phase, where more than 65% of cells (>4 fold change) have high* pre-rRNA sum intensities. This drops to 29% as cells enter the early LOC-phase. By contrast, most of the cells (89%) in mid-logarithmic phase exhibit high* pre-rRNA sum intensities.

4.3.3 RNA Polymerase I transcription is heterogeneous in cells from YMC populations

Violin plots in Figure 4.7 and 4.8, show single cells present a wide range of pre-rRNA production levels and pre-rRNA foci volume for each timepoint along the YMC and in mid-log phase. These results thus indicate that in mid-log and YMC populations RNA polymerase I gene expression is heterogenous among individual cells.

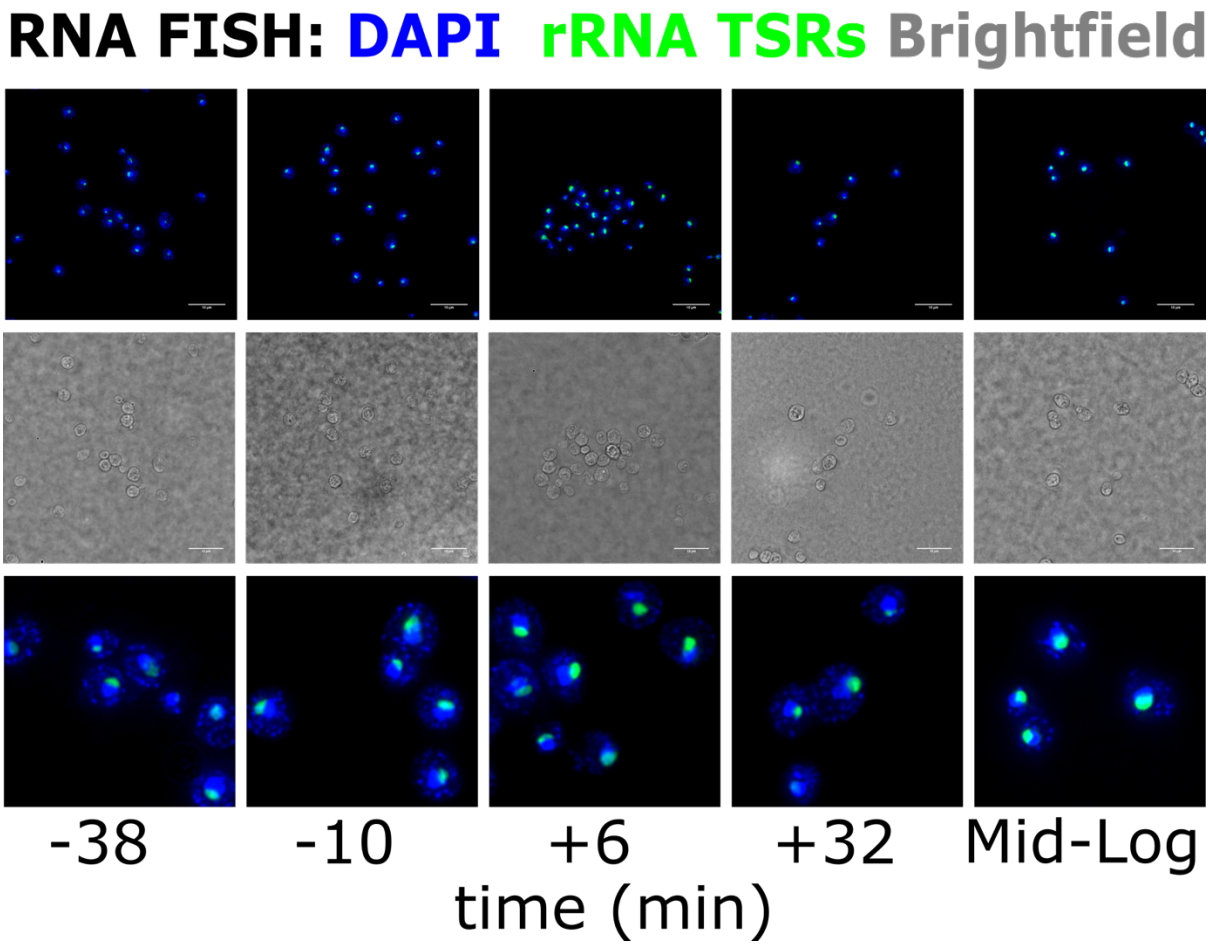

Figure 4.6 Pre-rRNA foci sum intensities vary between time and phases of the YMC

Representative pre-rRNA-FISH microscopy images of samples taken during the LOC-phase (-38, +32) and HOC-phase (-10, +6) of the YMC and in mid-logarithmic phase cultures. Images of the same field, using fluorescence (top and bottom cropped) and brightfield (middle). Fluorescent labeling; DNA is stained with DAPI (blue); Probes binding to TSRs of the 35S pre-rRNAs are labelled with Quasar 570 (green). Time shown in minutes relative to the point of lowest dissolved oxygen levels in media (dO_2 %) found across the YMC, displayed as "0". Scale bar: 10 μm.

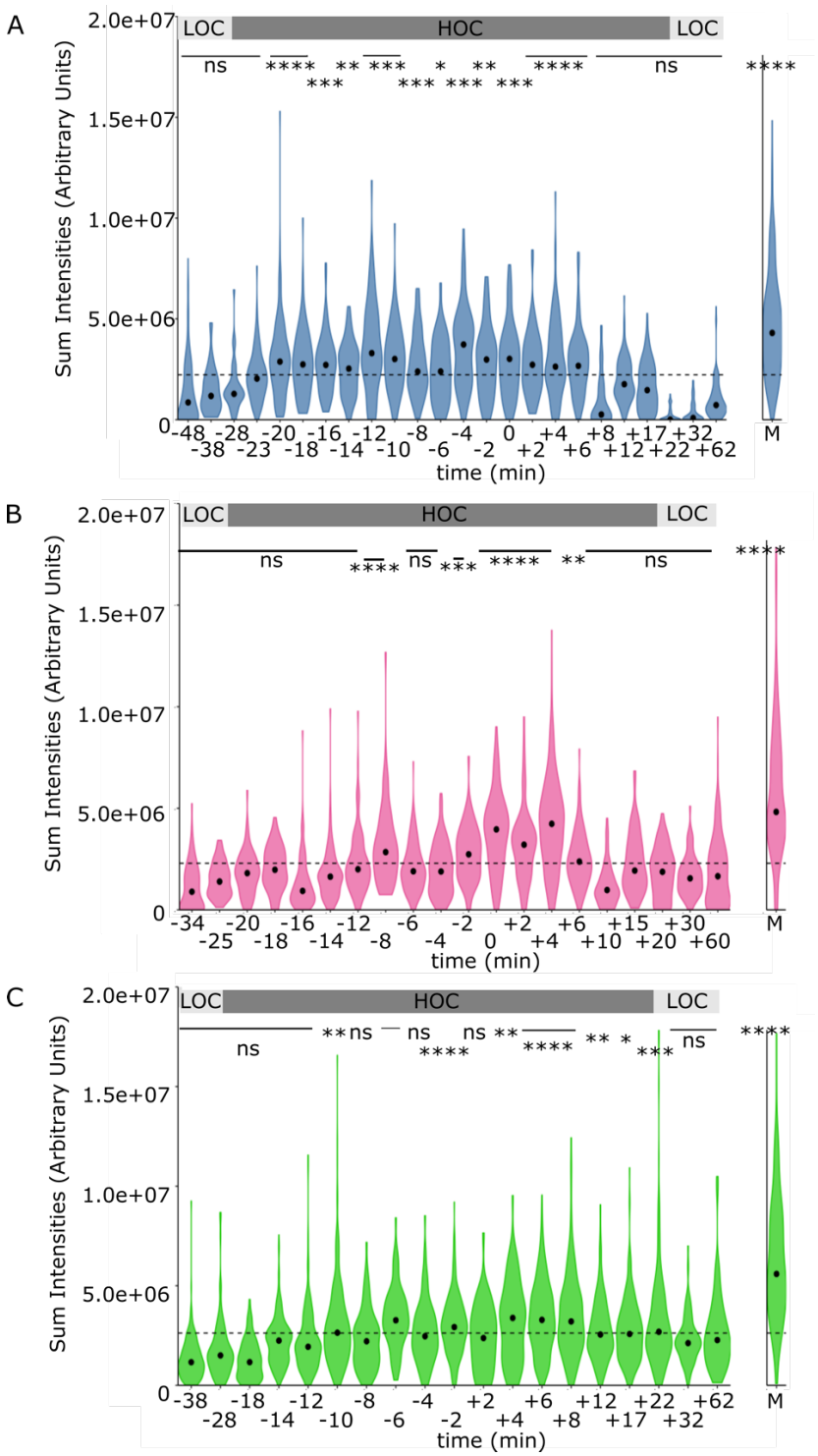

Figure 4.7 Pre-rRNA foci sum intensities peak in the middle of the HOC phase of the YMC

Violin plots of the pre-rRNA sum intensities in single cells for each sampling time points along the cycle. For the three biological replicates (A, B, C). Time shown in minutes relative to the point of lowest dissolved oxygen levels in media (dO_2 %) found across the YMC, displayed as "0", "M": Mid-logarithmic phase. The upper background colour indicates the phase of the YMC. Black dots: mean intensity for each time point. The dashed line: base mean of all the time points sum intensities. Asterisks indicate time points for which pre-rRNA sum intensities are significantly greater than the base mean* (p-value<0.05, Wilcoxon tests). *Excluding the sample taken in the Mid-logarithmic phase.*

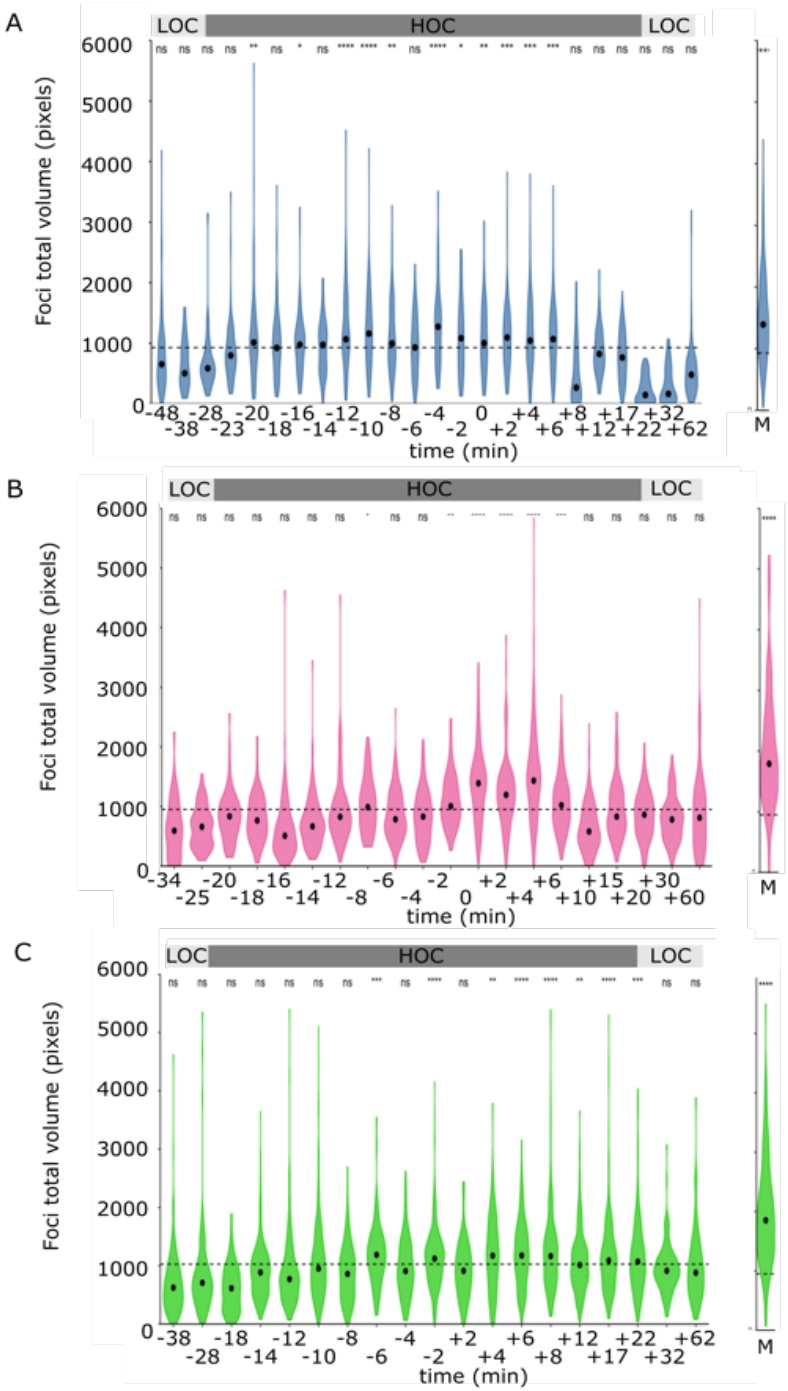

Figure 4.8 Pre-rRNA foci total volumes increase in HOC phase of the YMC

Violin plots of the total volume of pre rRNA foci in pixels in single cells (only expressing cells) for each time point. For the three biological replicates (A, B, C). Time shown in minutes relative to the point of lowest dissolved oxygen levels in media (dO_2 %) found across the YMC, displayed as "0", "M": Mid-logarithmic phase. The upper background color indicate the phase of the YMC. Black dots: mean intensity for each time point. The dashed line: base mean of all the time points sum intensities. Asterisks indicate time points for which pre-rRNA sum intensities are significantly greater than the base mean* (p-value<0.05, Wilcoxon tests). *Excluding the sample taken in the Mid-logarithmic phase.*

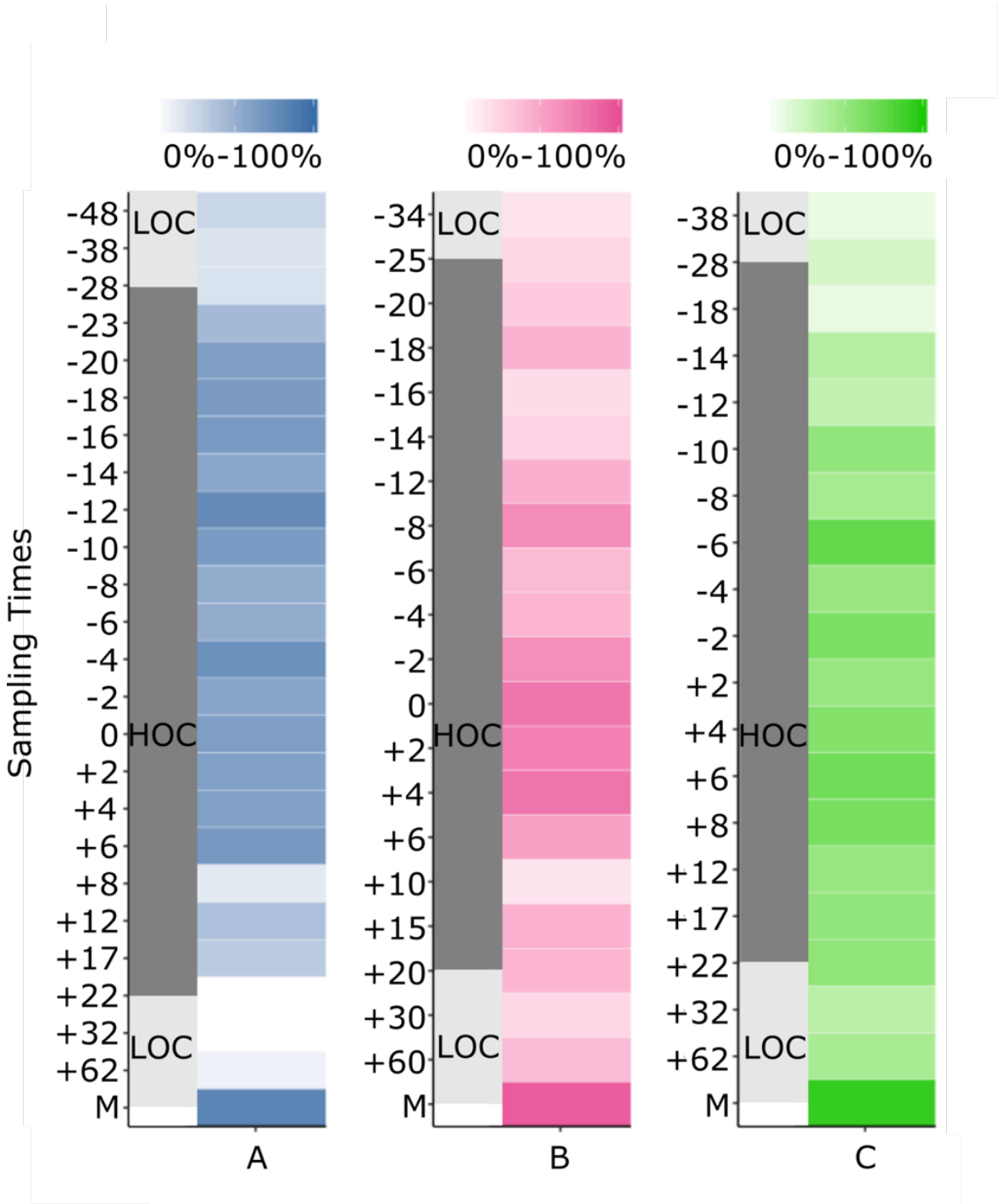

Figure 4.9 The proportion of cells expressing high* pre-rRNA production levels increase during the HOC-phase

Heat maps presenting the fraction of cells (0 to 100%) showing greater rRNA transcription levels (pre-rRNA sum intensities) than the base mean of all the time points sum intensities over the total number of cells detected. Each row of the heatmaps represents a sampling time point. Each heatmap corresponds to a biological replica (A, B, C). *Excluding the sample taken in the mid-logarithmic phase. Time shown in minutes relative to the point of lowest dissolved oxygen levels in media (dO_2 %) found across the YMC, displayed as "0", "M": Mid-logarithmic phase.*

4.4 Discussion

4.4.1 Pre-rRNA production peaks in the HOC phase of the YMC

By monitoring pre-rRNA transcript levels using RNA-FISH, this work reveals that levels of ribosomal RNA production vary during the YMC with low levels in the LOC compared to the HOC phase. Pre-rRNA levels reflect ribosomal RNA transcription. Ribosomal RNA synthesis is determined by the RNA Polymerase I initiation and elongation rates and, in specific conditions, by the number of active tandem repeats of the rDNA transcribed (Woolford et al., 2013). Therefore, changes observed along the YMC, particularly the decrease in pre-rRNA levels can reflect down-regulation of rRNA transcription rates, a decrease in the number of repeats transcribed and/or changes in rates of Rps6 processing of the polycistronic 35s pre-rRNA. As Rps6 phosphorylation, and RNA polymerase I activity and pre-rRNA transcription, are regulated by TORC1 and change coordinately through the YMC, they are likely to be linked (Feltham et al. 2020). Together these results support a key role for changes in the levels of protein post-translational modifications, in coordinating the YMC. Here Rps6 activity seems to be regulated by its phosphorylation across the metabolic cycle, rather than by its protein levels.

4.4.2 TORC1 phosphorylation cascades might regulate growth along the YMC

Here the data shows Rps6 phosphorylation (Feltham et al. 2020), and pre-rRNA production and processing oscillate over the YMC. Moreover, transcription and transcript levels of RiBis and RP increases in the HOC phase of the YMC suggesting they might be coordinated with TORC1-dependent activity. Ribosome biogenesis and protein production are essential for growth (Maaloe. 1979, Warner. 1999, Warner et al. 2001). In fact, ribosomal content and rRNA synthesis rates correlate with growth

rate and thus are highly depend on environmental conditions (Kief & Warner. 1981). Thus, in general, growth must be regulated along the YMC (Klevecz et al. 2004, Tu et al. 2005, Kuang et al. 2014, Feltham et al. 2020). Many signalling pathways and phosphorylation cascades could play a role in the regulation of growth in YMC cultures. However, because Rps6, as well as ribosome biogenesis more globally, are downstream targets of TORC1 (Honma et al. 2006, Li et al. 2006, Mayer & Grummt. 2006), the results suggest TORC1 activity in particular cycles along the YMC.

The targets of rapamycin (TOR) complex is composed of a Ser/Thr kinase that controls and promotes cell growth and proliferation (Martin & Hall. 2005). The kinase is found in multi-protein complexes TORC1 and TORC2, which possess different functions. TORC1 possess an ortholog in higher eukaryotes called mTORC1 (Gonzalez & Hall. 2017) and is sensitive to the growth inhibitor rapamycin. TORC2 is not and regulates cellular polarity instead of growth (Heitman et al. 1991, Loewith et al. 2002, De Virgilio & Loewith. 2006). When active, TORC1/2 phosphorylates various substrates including Sch9 (Pearce et al. 2010). These phosphorylation cascades can lead to the regulation of many processes such as transcription, ribosome biogenesis, translation initiation, amino acid synthesis and protein synthesis. TORC1 also inhibits stress responses through the inhibition of the retrograde pathway (RTG), Msn2 regulation of genes or even autophagy (Wullschleger et al. 2006, Loewith and Hall. 2011, Kaerbelein et al. 2005, Hughes Hallet et al. 2014, Li et al. 2017). In particular, TORC1 promotes ribosome biogenesis through transcription up-regulation of many genes regulating the gene expression of rRNA, tRNA, RP and RiBi transcripts. Most importantly, rDNA transcription by RNA Pol I is enhanced by TORC1, through the formation of the Rrn3-RNA Pol I complex and the recruitment of the chromatin factor

HmoI and RNA Pol I at the 35S rDNA repeats. RP and RiBi gene expression is up-regulated via the formation of Ifh1 and fhl1 complexes, the nuclear localisation of Sfp1, the inhibition of transcription factors blocking RiBi gene expression, and by the recruitment of Nua4 histone acetyl transferase at RP promoters (Jorgensen et al. 2002, 2004). However, upon inhibition of TORC1 by rapamycin, the coordination between nutrient sensing and growth is lost and ribosome biosynthesis is no longer stimulated when cells are stimulated to grow (Powers & Walter. 1999).

TORC1 is activated by carbon sources in particular glucose, but also by nitrogen. While limitation of these nutrients, oxidative and osmotic stress lead to inhibition of TORC1 activity (leading to reduced phosphorylation of Sch9) and similar changes in metabolism to those observed after rapamycin treatment. Moreover, the intracellular pool of amino acids also regulates TORC1 activity. Amino acid levels are sensed by the EGO complex and transmitted to TORC1 at the vacuole membrane and TORC1 is activated when aa levels are high (Alfatah et al. 2021, Hughes Hallett et al. 2014, Deprez et al. 2018, De Virgilio. 2012). Finally, TORC1 was shown to promote the transition through Start and thus cell cycle progression by upregulating Cln3 protein levels through the regulation of translation initiation and by destabilisation of Sic1, a CDK inhibitor (De Virgilio & Loewith. 2006, De Virgilio. 2012). For these reasons and due to its role as direct mediator between rRNA production and cellular growth, the TORC1 phosphorylation pathway could play a role in growth coordination along the YMC.

In addition to that, the TORC1 pathway was suggested to be regulated by pH levels and to act as a checkpoint for growth along the YMC, by allowing carbohydrate stores to be used, with the breakdown of trehalose and glycogen into glucose permitting the

transition of cells to the HOC phase (O' Neill *et al.* 2020, Feltham et al. 2020). This process is observed during the YMC (Shi et al. 2010) but also in stationary phase cultures during the exit of cells from quiescence (Allen et al. 2006, Miles et al. 2020), indicating perhaps a common response and regulation of growth in YMC cultures.

4.4.3 Three-state sub-populations compose the YMC cultures

As the proportion of cells expressing high pre-rRNAs levels vary along the YMC (Figure 4.9), the results suggest a partition of the YMC culture in sub-populations. First, according to the recent YMC-CDC coupling model (Burnetti et al. 2016) and the finishing kick to start model (Futcher et al. 2006), YMC cells that commit to the HOC phase, i.e. enter a growth state in HOC, are able to re-enter the cell division cycle. This thus imply that cells in which ribosome biogenesis is boosted during the HOC phase, should exit quiescence and progress through the cell division cycle, and divide synchronously.

Here results show that up to ˜50% of cells show high pre-rRNA production levels in mid-HOC compare to LOC. This thus suggests that around half of the yeast cells transition from a quiescent to a growth state in HOC. The pulse in ribosome production is then expected to aid transition of cells through the cell division cycle (Futcher et al. 2006). Nevertheless, because the proportion of cells reported to divide each yeast metabolic cycle varies between ˜10 to 50% depending on the studies (Tu et al. 2005, Klevecz et al. 2004, Feltham et al. 2020, Laxman et al. 2010, Slavov & Botstein. 2011, Burnetti et al. 2016), it is possible that some cells of the YMC culture enter a growth state in HOC but do not commit to the CDC. Second, some cells show low levels of pre-rRNA production during the YMC. Up to 85% in LOC and 35% in HOC, indicating that most of the cells show a quiescent state in LOC, but more importantly suggesting

that not all cells transition to a growth state in HOC. Thus a proportion of the YMC population seems to remain in a quiescent state in HOC. Finally, some cells (˜15%) show high pre-rRNA levels in late LOC phase. This indicates that even in LOC phase some cells are under a high-growth state. It thus suggests that not all cells are quiescent in LOC.

4.4.4 Evidence of cell-to-cell gene expression variability in YMC cultures

Population averaged techniques previously showed a global increase in transcript levels of RiBis and RP genes occurs in early and mid-HOC phase of the YMC (Klevecz et al. 2004, Tu et al. 2005, Kuang et al. 2014, Feltham et al. 2020). Here results corroborate these findings as ribosomal RNA production increases in HOC. Nevertheless the results also highlight RNA Pol I gene expression heterogeneity among the cell population. This indicates that although the YMC population is considered as synchronous, individual cells show distinct expression levels of pre-rRNAs, most likely show different growth status and perhaps behave differently.

4.5 Conclusion

The data indicates ribosome biogenesis and perhaps growth in general might be regulated by metabolic fluxes and proteins PTMs throughout the YMC rather than protein levels, since most of the protein levels remain constant. Remarkably, the data indicates preliminary evidence for at least 3 sub-population of cells within synchronised YMC cultures; a proportion of cells exiting quiescence in HOC, a proportion of cells staying in a quiescent state at all times, and a proportion of cells in a growth state at all times, even in LOC. Finally, the results support extensive cell-to-cell heterogeneity in rRNA expression in the YMC. This leads to the question as to

whether similar heterogeneity in expression levels and distribution in the population could be detected for genes transcribed by RNA polymerase II.

Chapter 5

This chapter aims to assess whether individual cells from YMC cultures behave synchronously and similarly. In particular whether cells show similar gene expression levels or not. To do so, single-molecule RNA-FISH (smRNA-FISH) is employed to gather mRNA numbers of four genes transcribed by RNA polymerase II, in single cells along the YMC.

Part I of this chapter acts as a proof of concept. It presents the experimental approach and development of the time-course smRNA-FISH experiments realized for this study, throughout the YMC. Preliminary results are presented and discussed.

Part II of this chapter focuses on the analysis of gene expression noise and RNA distributions.

Chapter 5 Part I

Single-molecule RNA-FISH data recapitulates the overall cycling of transcripts throughout the YMC

Part I of this chapter introduces the rationale followed for the establishment of the experimental plan and shows preliminary results that validate the approach taken in this work.

5.I.1 Experimental design and method development

5.I.1.1 Multiplex smRNA-FISH of antagonistically oscillating transcripts

Single molecule RNA-FISH experiments were performed on synchronous yeast cell populations of the YMC. The single-cell technique grants the detection and quantification of single transcripts. DNA DAPI staining permits the detection and outline of nuclei and the further characterization of transcripts as “nuclear” or “cytoplasmic”. These respectively act as proxies for nascent and steady state RNA numbers in single cells (Raj et al. 2008, Zenklunsen et al. 2008). Figure 5.1 shows the detection of both kinds of transcripts.

5.I.1.2 Probe design and synthesis

Probe synthesis for the smRNA-FISH experiments was performed using a protocol adapted by the Davis lab from the Gaspar et al. 2017 paper. Here, a mix of 32 to 48 single strand DNA probes were designed to bind across the entire length of each target transcript. Single molecule RNA FISH probes are relatively short oligos of around 20 nucleotides (Raj et al. 2008). Each oligo is coupled to a single fluorophore, through an enzymatic synthesis utilizing a Terminal Deoxynucleotidyl Transferase (TDT) which catalyzes the addition of a labelled ddUTP at the 3’ hydroxyl terminus of each probe. Probes were labelled with ATTO633 or ATTO565, more commonly known to emit fluorescence in the Cy5 or Cy3 channel respectively. Note: “In-house probe synthesis”

allows to label the same target transcripts with different fluorophores ensuring the absence of labelling artefacts and greatly reduces the costs of experiments.

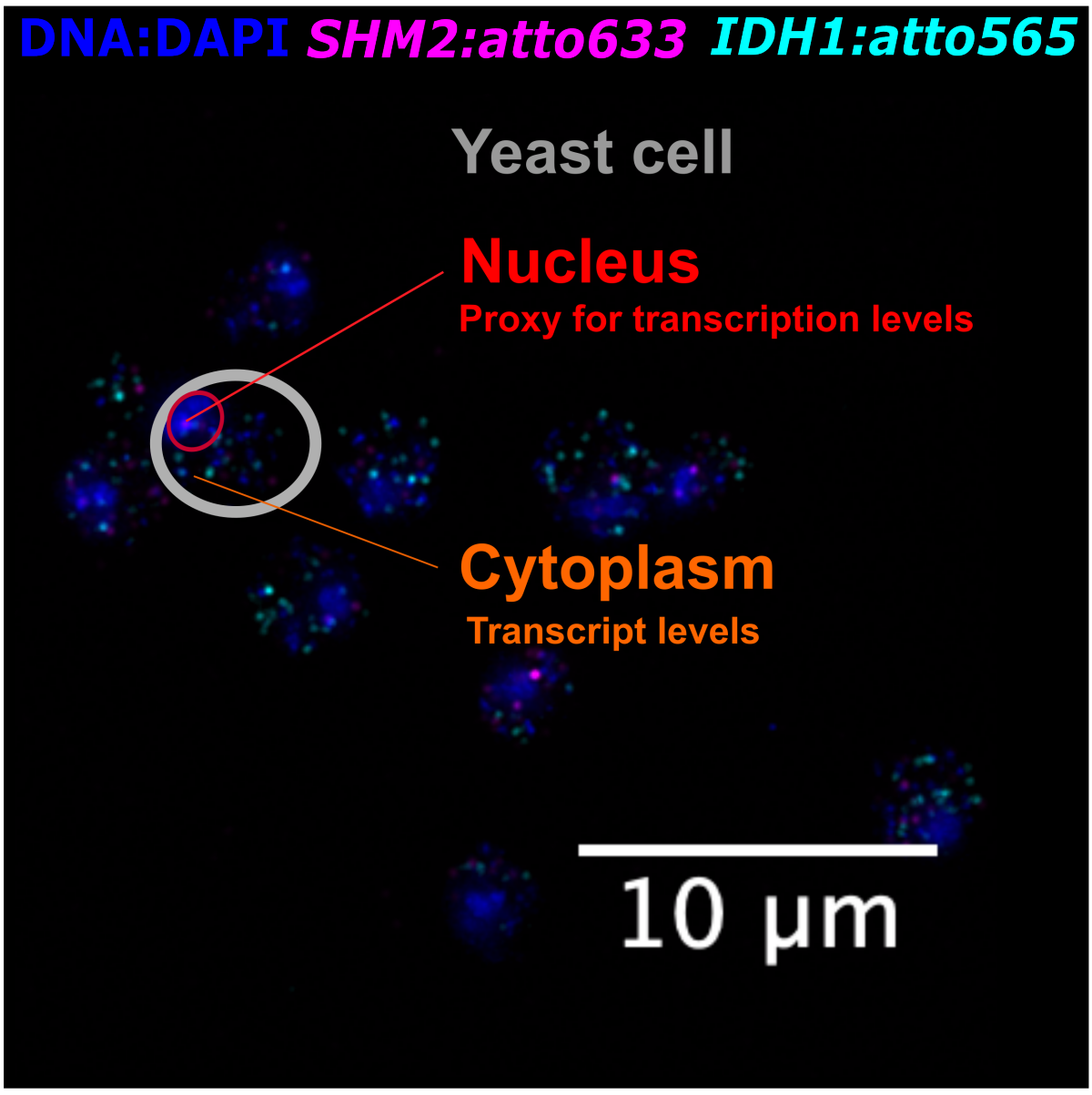

Figure 5.1 Multiplex (dual-label) smRNA-FISH, a quantitative method for the detection of single transcript from two different genes in nucleus and cytoplasm of yeast cells, acting as proxy for nascent and steady-state transcript levels. *Microscopy image cropped and enlarged of a sampling timepoint taken during the YMC, for which DNA was stained with DAPI, transcripts were probed with atto633 (Cy5 in magenta) for SHM2 and atto565 (Cy3 in Cyan) for IDH1. The nucleus and the yeast cell are outlined for one cell.*

5.I.1.3 The target transcripts chosen for this study

The criteria for the selection of target genes transcribed by RNA Polymerase II is described next.

Antagonistic oscillating transcripts of three recognized periodic genes of the YMC were picked in order to capture expression patterns for genes transcribed by RNA Polymerase II, under metabolic changes in the YMC. Initially, target transcripts were picked from the top 100 most periodic genes lists provided in Tu et al. 2005 supplementary data.

In this, and other studies (e.g. Kuang et al. 2014), a (log2FC vs mean)/(standard deviation) transformation was used. This transformation standardizes the data in order to identify common shapes between transcription and transcript profiles. However, it masks differences in the amplitude of these shapes and can lead to noisy but lowly expressed genes being included in the list of periodic genes. Thus, additional criteria were applied to pick adequate targets.

Genes were selected to (i) produce high enough mRNA levels to be detected using smRNA-FISH, (ii) not have paralogues that might also hybridize to the probes (iii) have similar global expression ranges and (iv) produce high levels of mRNA in three distinct phases of the YMC according to microarray (Tu et al. 2005) and strand-specific 3' RNA sequencing data (Feltham et al. 2020). In addition, except the gene coding for actin, *ACT1*, the genes selected for analysis are not essential for yeast cell survival (SGD). This enabled the construction of knock-out strains, employed as negative controls through the RNA-FISH quantification pipeline. These control strains are important to help differentiate fluorescent signal arising from single molecules of RNA from fluorescent background noise.

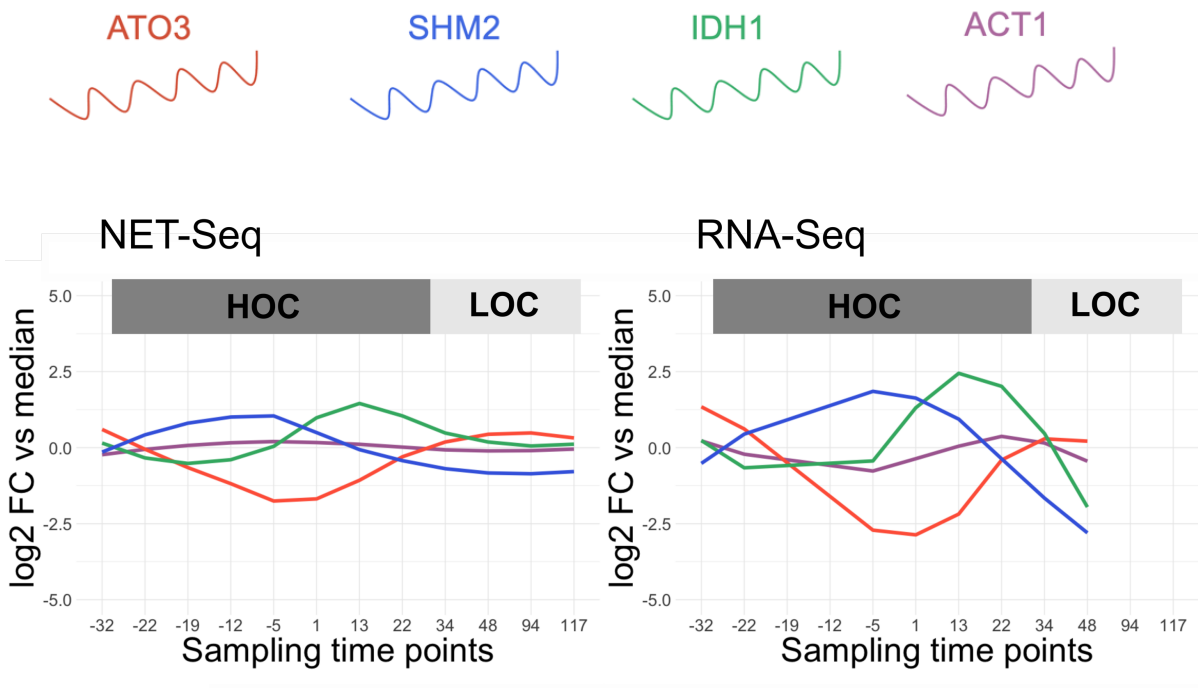

Figure 5.2 mRNA targets, their transcription and transcript averaged-population levels along the YMC.

Top. *Schematic of the transcript of interests. Colours indicate the different targets; ATO3 in orange, SHM2 in dark blue, IDH1 in green and ACT1 in purple.*

Bottom. *Smoothed conditional means of the log_2 fold-change of the average read number vs median average read number (LFCM) over the YMC.* ***1.*** *Measured by NET-seq.* ***2.*** *Measured by RNA-seq. The average read number is the average number of sense reads per bp within a 300 bp window placed immediately downstream of the Transcription Start Site. Upper panels indicate the HOC and LOC phases of the YMC. Time shown in minutes relative to the point of lowest dissolved oxygen levels in media (dO_2 %) found across the YMC, displayed as "0". Data from Dr. Xi. DPhil thesis. 2019 and Feltham et al. (2020).*

Thus, based on these criteria, three antagonistically oscillating transcripts and one transcript considered constant over time at the averaged-level were chosen for analysis: ***ATO3***, ***SHM2***, ***IDH1*** and ***ACT1***. The profiles of the four mRNA targets were plotted over the YMC (Figure 5.2), using data from Feltham et al. 2020, generated by Shidong Xi (DPhil thesis. 2019). Here, the smoothed conditional means of the log_2 fold-change of the average read number vs median average read number (LFCM)

over the YMC are plotted over time, first for calibrated global nascent transcription levels, derived from NET-Seq, and second for transcript levels derived from 3' RNA-Seq.

According to these recent sequencing data (Feltham et al. 2020), but also to previous microarray and other sequencing studies (Tu et al. 2005, Kuang et al. 2014); nascent transcript levels peak in the Low Oxygen Consumption or LOC phase for *ATO3*, the early to mid-High Oxygen Consumption or HOC phase for *SHM2*, in the mid to late HOC phase for *IDH1* and stays relatively constant over the YMC for *ACT1* (Fig.5.2.1). Similar patterns are observed for cytoplasmic transcripts levels along the YMC, though higher fold-changes are detected (Fig.5.2.2). Finally, although *ACT1* is mostly described and considered as a transcript with flat levels over the YMC (Tu et al. 2005, Kuang et al. 2014), it has also been described as a low-amplitude oscillating transcript, peaking in each phase of the YMC (3 peaks, between 1.3 and 1.4 fold change) (Klevecz et al. 2004). Here the nascent transcript levels of *ACT1* are flat along the YMC (Fig.5.2.1), while a modest increase is detected in the late HOC phase of the cycle when focusing on RNA-Seq levels of *ACT1* (Fig.5.2.2). This may reflect post-transcriptional stabilisation of the *ACT1* mRNA.

5.I.1.3.1 *ATO3* (YDR384C) is a LOC (or Reductive Charging) phase transcript

ATO stands for Ammonia Transporter Outward. *ATO* genes code for Ato proteins (1,2,3), which are transmembrane proteins; specifically, ammonium/proton antiporters. These are believed to play a role in ammonium extra-cellular export. Ato3p localise principally at the plasma membrane (Guaragnella & Butow. 2003), while both Ato1p and Ato2p have also been described as yeast mitochondrial proteins, therefore enabling the export of ammonium outside the mitochondria (Reinders et al. 2007).

Transcription of *ATO3* is strongly activated in the stationary phase of exponential cultures (Gash et al. 2000, Martinez et al. 2004, Radonjic et al. 2005) and during the LOC phase of the YMC (Tu et al. 2005). The expression of *ATO3* is believed to be raised under starvation by the Gcn4p transcription factor which acts as an intermediate in the general amino acid control pathway (Guaragnella & Butow. 2003, Hinnebush. 1992) and its expression was reported to increase in starved colonies (Palkova et al. 2002).

ATO3 seems to be among the few genes (164/3235) for which protein levels significantly change along the YMC. Indeed, a fold change of more than 1.33 in Ato3p level was observed along the YMC* (O'Neill et al. 2020; Feltham et al. 2020). Furthermore, Ato3p levels were reported to peak at the transition point between late LOC and HOC via Western Blot (Laxman et al. 2010).

Finally, gene expression profiles of *ATO3* are of particular interest in the context of metabolic oscillations, as volatile ammonia has been suggested to act as a cell-to-cell communication signal of starvation and perhaps even programmed cell death (Váchová & Palková. 2005).

5.I.1.3.2 *SHM2* (YLR058C) is an early HOC (or Oxidative) phase transcript

Shm2p together with Shm1p are serine hydroxymethyl transferases or SHMT. While Shm1p localizes in the mitochondria, Shm2p is the cytosolic enzyme catalysing the conversion of serine to glycine. During this reaction, the hydroxy methyl group of the serine is transferred as a methyl group to tetrahydrofolate (THF) to produce 5,10-methyleneTHF and glycine with the release of H_2O. Shm2p is a key enzyme in one-carbon metabolism, involved in the production of precursors of DNA building blocks (purine biosynthesis) (McNeil et al. 1994, Denis & Daignan-Fornier. 1998). It is

therefore, at the crossroads of metabolic decisions. One-carbon units are essential for anabolic metabolism, thus growth. Serine has been suggested to act as a growth-limiting factor (May et al. 2020). Moreover, *SHM2* together with other genes of one-carbon metabolism are up-regulated upon the addition of glycine to yeast cells under glucose minimal media, which leads to major transcriptional metabolic shifts (Gelling et al. 2004). Finally, Shm2p provides precursors for the production of methionine. Indeed, as amino-acid and nucleotide synthesis, depend on methionine levels through the pentose phosphate pathway, the synthesis of glutamate/glutamine, the pyridoxal-5 phosphate-dependent transamination processes and transcripts levels of genes involved in these pathways were found up-regulated after a methionine pulse given to starved cells. Methionine may allow these cells to transition to a “growth state”, again in a Gcn4p-dependent way. Thus, methionine availability has been suggested to act as a key mediator in the activation of an “anabolic switch” under starvation (Walvekar et al. 2018, Hinnebush. 2005). Therefore, Shm2p has a major role in the anabolic response to starvation too. Together these findings show Shm2p plays an essential role in metabolism integration and that transcription of *SHM2* is highly regulated and involved in global growth or anabolic response.

5.I.1.3.3 *IDH1* (YNL037C) is a late HOC (or Reductive Building) phase transcript

IDH1 and *IDH2* genes are coding for the 2 different subunits of the NAD+ dependent isocitrate dehydrogenase and both enzymes are essential for the octameric complex functionality. The budding yeast mitochondrial isocitrate dehydrogenase (Idhp) uses the cofactor NAD+ to oxidize isocitrate into alpha-ketoglutarate while releasing NADH. The reaction catalysed by the Idhp complex is the number one rate-limiting step of the Tricarboxylic Acid Cycle (TCA) (Cupp & McAlister-Henn. 1991 and 1992).

Among other transcription factors, *Rtg3p,* involved in the retrograde pathway, a signalling pathway between mitochondria and nucleus involving major metabolic re-organisations, regulates gene expression of *IDH1* and *IDH2* genes (Tate & Cooper. 2003, Liu & Butow. 2006). Past and recent findings, indicate that Idh1p expression is crucial for high-growth rate in yeast cells as the protein activity is activated in response to low energy status and is determinant for the TCA cycle which takes part in aerobic respiration, a process that produces more energy than fermentative growth (Pfeiffer & Morley. 2014). Both sub-units are essential for yeast respiratory growth, as *idh1* or *idh2* deleted strains show reduced growth rates on glycerol and lactate and do not grow on acetate (all non-fermentable sources) (Cupp & McAlister-Henn. 1991 and 1992). Moreover, deletion of *IDH1* in the opportunistic and pathogenic yeast *Candida albicans*, also leads to respiratory-deficient and smaller colonies, decreased cell cycle and slower growth. (Hameed et al. 2020, Tao et al. 2017). Finally, the production of ∝-ketoglutarate by Idhp is also important for growth, as the glutamate dehydrogenase catalyses the reaction between ∝-ketoglutarate and ammonia to produce glutamate an important precursor for amino acid synthesis (Cupp & McAlister-Henn. 1992).

Remarkably, the Idhp activity is regulated through different ways. It is responsive to low energy levels, as it is activated by AMP via allosteric regulation (Hathaway & Atkinson. 1963) and it is NAD+ dependent. Another way of regulation is via cooperativity with its substrate, isocitrate (Panisko & McAlister-Henn. 2001). It has also been proposed that proteins of the TCA cycle interact together, thus directing TCA substrates into the cycle (Kim & Guarente. 1986).

5.I.1.3.4 *ACT1* (YFL039C) is a transcript with constant or low-amplitude oscillating levels along the YMC

ACT1 is an essential gene (Shortle et al. 1982) and code for the actin protein (Gallwitz & Seidel. 1980, Ng & Abelson. 1980). *ACT1* gene expression is regulated by *Gcn5p* (Venters et al. 2011) among other transcription factors and is strongly associated with the cell division cycle and growth (Slavov et al. 2011).

The intrinsically polarized monomeric proteins can form filaments through ATP-dependent multimerization (Pruyne & Bretscher. 2000). Actin filaments can form different structures such as patches, cables and rings, for which structural re-arrangements play various roles along the cell cycle of yeasts (Kilmartin & Adams. 1984). First, actin cortical patches are involved in the polarization of the cell growth (Ayscough et al. 1997, Pruyne & Bretscher. 2000), together with the nucleation factors Arp2/3 (Winter et al. 1997, Evangelista et al. 2002). Actin patches also provide structure for endocytosis and cell wall integrity (Munn et al. 2001, Kaksonen et al. 2003). Next, actin cables, which follow the same direction as the mother-to-bud axis, provides transport tracks to growth sites (Sagot et al. 2002) while allowing mitotic spindle alignment (Schott et al. 2002). Finally, contractile rings composed of actin and myosin, enable cytokinesis or cell division between the mother and daughter cells (Tolliday et al. 2001). More recently, the role of nuclear Act1p has been investigated and the presence of monomeric Act1p has been detected in the INO80 complex, thus implying a role in chromatin remodelling (Kapoor et al. 2013). Finally, while sufficient Act1p levels are necessary for cell growth (Liu et al. 1992), overexpression of Act1p can lead to growth arrest (Espinet et al. 1995).

It is worth noting that, as opposed to Ato3p, protein levels of Shm2p, Idh1p and Act1p are found to be relatively constant during the YMC, with a fold change below 1.33 along the YMC* (O'Neill et al. 2020). Therefore, a global increase in transcript levels along the YMC does not lead to a noticeable increase in protein levels for these genes. Nevertheless, although protein pools are constant along the cycle, it is likely that (as discussed in chapter 1 and 4): (i) protein accessibility and protein activities change along the cycle via protein post-translational modifications, protein interactions, allosteric regulation, substrate cooperativity or other mechanisms, (ii) levels of metabolites found upstream of the reactions catalysed by Shm2p and Idh1p, such as serine and THF or isocitrate, respectively direct metabolic reactions and fluxes.

*Proteomic data from O'Neill et al. 2020, analysed by Dr. Feltham.

5.I.1.4 A brief comparison of metrics between target transcripts

Next, different metrics such as transcript and protein abundances, transcriptional frequencies and turnover rates, in high and slow-growing cultures, are compared between the different target transcripts picked for this study. Table 5.1 regroups these metrics gathered from different studies.

First, protein abundance in untreated WT cells differs between the targets. Higher protein levels are found for Act1p compared to Shm2p, itself showing greater levels than Idh1p, which presents levels above those found for Ato3p (SGD).

Table 5.1 Metrics of genes and their transcripts studied in this work

SGD *shows the standard name, systematic name, gene length, protein length, protein abundance for the four genes (SGD).* ***A.*** *Average transcript count from high throughput single-molecule sequencing Digital Gene Expression (smsDGE) technology (Lipson et al. 2009).* ***B.*** *Transcript expression levels detected via high-density oligonucleotide arrays for mid-log phase WT cultures, transcript half-lives and transcriptional frequency (Holstege et al. 1998).* ***C.*** *Transcript half-lives for mid-log phase WT cultures, of transcript levels assessed by time-course RNA-seq after RNA Pol II depletion from nucleus via Anchor-away (Geisberg et al. 2014).* ***D.*** *Transcript levels (absolute abundance from RNA-seq samples calibrated using 18 mRNAs with known absolute concentration), protein abundance from Mass Spectrometry, proxy for translation rate and protein half-lives from steady-state chemostat cultures (Lahtvee et al. 2017). N/A; data not available*

Standard Name	**ATO3**	**SHM2**	**IDH1**	**ACT1**	
Systematic Name	YDR384C	YLR058C	YNL037C	YFL039C	
Gene length (bp)	828	1410	1083	1437	**SGD**
Protein length (a.a)	275	469	360	375	
Protein abundance (molecules/cell)	2211 +/- 1152	47330 +/- 17495	12930 +/- 5858	59660 +/- 31382	
Average count	100.95	837.48	312.7	1297.93	**A**
Transcript levels (molecules/cell)	2	14.9	2	21.1	
Half Life (min)	12	12	19	17	**B**
Transcriptional frequency (mRNA/hr)	6.1	46	4	45.5	
Half-Life (min)	8	40	25	44	**C**
Transcript levels (molecules/cell)	3.69	3.19	1.78	5.91	
Protein abundance	NA	14929.96	23045.10	37643.34	
Translation rate proxy (protein/mRNA abundance)	NA	4679.25	12919.43	6372.42	**D**
Protein half-life (hr)	NA	28.4	24.0	32.3	

Second, when comparing the average transcript counts between transcripts (Table 5.1.A, Lipson et al. 2009), again higher transcript levels are found for *ACT1* compared to *SHM2* which presents higher levels than *IDH1*, itself showing greater levels than *ATO3*. This indicates that, for these four transcripts, in WT cells under exponential growth, protein levels follow to some extent transcript levels. The transcript levels detected via high-density oligonucleotide arrays for WT cells in mid-log phase cultures (Table 5.1.B, Holstege et al. 1998), however show higher numbers of mRNA molecules per cell for *ACT1* followed by *SHM2*, itself showing higher levels than both

IDH1 and *ATO3* which show similar levels. The variability of order between the 2 datasets most likely arises from the difference of technique used.

The estimated transcriptional frequency indicates that relatively similar, though slightly higher, numbers of transcripts are produced per hour for *SHM2* compared to *ACT1*. Both of these transcripts however show a frequency at least 7-fold greater than the ones for *ATO3* and *IDH1* (Table 5.1.B, Holstege et al. 1998). This indicates that in WT exponentially growing cultures, the transcription rate is higher for both *SHM2* and *ACT1* compared to *ATO3* and *IDH1*.

Surprisingly, while findings detected a higher transcript half-life for *IDH1*, compared to the one of *ACT1*, itself being greater than the ones of *ATO3* and *SHM2* (Table 5.1.B, Holstege et al. 1998), recent results indicate a higher half-life for *ACT1*, followed by the one for *SHM2*, then *IDH1* and finally *ATO3* (Table 5.1.C, Geisberg et al. 2014). Recent findings are more credible as the method used is less likely to perturb global cell states.

Finally, transcript levels acquired from steady-state chemostat cultures at a growth rate of $0.1hr^{-1}$ (Table 5.1.D, Lahtvee et al. 2017) show differences when compared to previous dataset (Table 5.1.B, Holstege et al. 1998). Higher levels of *ACT1* are still detected when compared to other transcripts, but *ATO3* present greater levels compared to *SHM2*, itself showing higher levels than *IDH1*. This is thus consistent with the characterization of *ATO3* as a stationary phase transcript (Gash et al. 2000, Martinez et al. 2004, Radonjic et al. 2005). Moreover, the translation rate and protein abundance detected in cells growing at steady-state also shows Act1p at higher abundance than Idh1p, which in turn has higher protein levels than Shm2p. However, *IDH1* has higher translation rates than *ACT1* and *SHM2*. Finally, protein half-lives are

higher than the median protein half-life (17.2 hr) with greater half-life for Act1p compared to Shm2p, which also possesses a higher half-life than Idh1p (Table 5.1.D, Lahtvee et al. 2017). Most importantly, these results (Table 5.1) indicate that at steady state, protein levels do not seem to follow transcript levels when comparing target genes.

5.I.2 Overview of smRNA-FISH experimental design

5.I.2.1 Single and dual label (multiplex) smRNA-FISH of transcripts during the YMC

Three different types of experiments were performed. Samples for smRNA-FISH were prepared from both fermenters. The approach used to develop a rigorous strategy of investigation is depicted in Figure 5.3.

(i) First, a complete assessment of the feasibility of the study was undertaken, together with optimization of the quantification pipeline. For this a "single-label RNA-FISH" experiment was performed on ***ATO3*** mRNA using a set of probes labelled with a fluorophore emitting in Cy3 (n=1; 1 biological repeat or sampling across the YMC presented at figures 5.3.i & S.5.A and 1 technical repeat or smRNA-FISH experiment).

(ii) Second, the controls for FISH experiments over the YMC were done to confirm; proper spheroplasting (cell wall removal), incorporation of the probes into cells and to assess noise levels. 3 repeats of the "control dual-label RNA FISH" experiment were performed; labelling the "oscillating transcript" ***ATO3*** and the "flat transcript" ***ACT1,*** with Cy5 and Cy3 fluorophore respectively (n=3; 3 biological repeats or sampling across the YMC presented at figures 5.3.ii & S.5.B.1,2,3 and 3 technical repeats or smRNA-FISH experiments).

(iii) Finally, after validation of the method, experiments investigated the behaviours of antagonistically oscillating transcript in single cells from synchronized populations. Three dual-label RNA-FISH experiments were done using the following combinations of transcripts: ***ATO3*** and ***SHM2***, ***SHM2*** and ***IDH1*** and finally ***IDH1*** and ***ATO3*** (n=2, for each transcript; 1 biological repeat or sampling across the YMC presented at figures 5.3.iii & S.5.C, 3 technical repeats or smRNA-FISH experiments = 2 technical repeats for each transcript). Probes were labelled with the opposite fluorophore in the different experiments.

For each experiment, the Yeast Metabolic Cycle was induced and between 12 to 22 samples were taken along different cycles at approximately 10 min intervals permitting a high temporal resolution along the O_2 consumption profile (black dots along the dissolved oxygen traces in Figure 5.3).

In addition to samples taken throughout the YMC, for each experiment and repeat, yeast cells grown to mid-exponential phase (mid-log cells) were subject to the same labelling protocol. This allows a comparison of asynchronous yeast cell population at high-growth rate (generation time 2.08h) relative to the synchronous population of the YMC at a slow-growth rate (generation time 9.62h, period 3h20min).

All samples were processed through the single molecule RNA-FISH wet and dry pipelines developed in the laboratory as part of this work, allowing the confident detection of fluorescent spots and quantification of single molecules as described in chapter 3. Specific experimental settings are described in chapter 2.

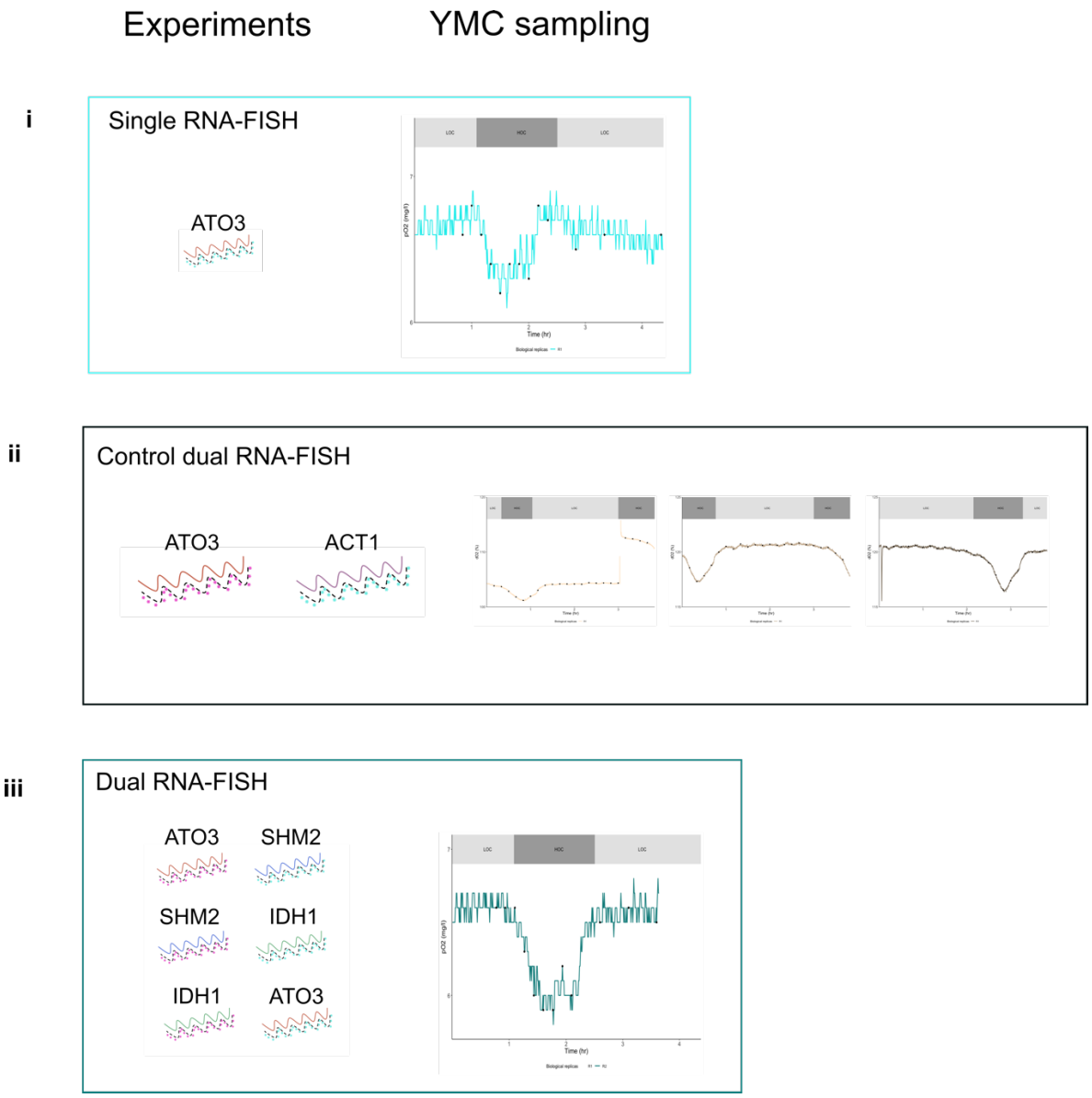

Figure 5.3 Outline of the design of the three smRNA-FISH experiments

Dissolved oxygen levels fermenter traces, sampling time points (time shown in min relative to the point of lowest dO_2 % in the YMC, displayed as "0") and biological replicates of the different FISH experiments. ***(i). Single- label RNA-FISH;*** *Minifor dO_2 traces, ATO3 in Cy3, (n=1; 1 biological repeat or YMC sampling and 1 technical repeat or smRNA-FISH experiment).* ***(ii) Control dual-RNA-FISH;*** *Bioflo320 dO_2 traces, ATO3 in Cy5 vs ACT1 in Cy3, (n=3; 3 biological repeats or YMC sampling and 3 technical repeats or smRNA-FISH experiments).* ***(iii) Dual-RNA-FISH;*** *Minifor dO_2 traces, ATO3 in Cy5 vs SHM2 in Cy3, SHM2 in Cy5 vs IDH1 in Cy3, IDH1 in Cy5 vs ATO3 in Cy3, (n=2; 1 biological repeat or YMC sampling, 3 technical repeats or smRNA-FISH experiments, 2 technical repeats for each transcript). A detailed view of the YMC dO2 traces presented here are provided in the Appendix in Figures S5.*

5.I.3 Preliminary results and analysis

5.I.3.1 Controls to optimize the quality of experimental data

The following controls were performed, leading to the conclusion that the labelling efficiency in all experiments is high and that the fraction of cells without transcripts is genuine. First, the spheroplasting (cell removal) step of the RNA-FISH experiment was optimized to ensure a high labelling efficiency (> 70% estimate). Images of yeast cells under different spheroplasting treatments are shown in Figure 2.3, in chapter 2. Second, negative controls were employed to threshold the fluorescent signal detected guaranteeing the detection of transcripts (chapter 2). Third, almost all cells express *ACT1*, the internal control, showing constant transcript levels across the YMC as presented at Figure 5.5, 5.7 and 5.14.5 chapter 5 Part II. Finally, results will show that a high percentage of expressing cells is detected also for the other target transcripts at some timepoints of the YMC (Figure 5.4 and 5.5). i.e. mainly arises from the yeast cell population rather than experimental noise.

5.I.3.2 Variability between experimental replicates

Despite using appropriate controls, there are some differences between the different experimental replicates. These differences are noticed between biological repeats (samplings across the YMC) but also between technical repeats (smRNA-FISH experiments). Thus, these may result from small changes to the composition and organisation of YMC populations. Other factors may include differences in the cell population (the number of cells) on coverslips, which are expected to some extent, even for samples taken at the same timepoints along the YMC. This variability may be reduced by increasing the number of cells captured. Other experimental variations might also explain this variability such as the use of different fermenter vessels and

computing devices, the use of Cy3 or Cy5 fluorophores which show different dynamic fluorescence signal ranges (chapter2), the use of somewhat different quantification methods and finally involuntary changes in microscope settings between experiments, leading to adjustments of the thresholds for single fluorescent molecule detection. A higher variability between repeats is noticed in nuclear transcript levels compared to cytoplasmic ones; most likely explained by the stochastic nature of transcription and the use of a fixed microscopy technique to capture RNA numbers.

Finally, some samples (smRNA-FISH dual-FISH 2; Tp -10, dual-FISH 3; Tp +90 and control-dula-FISH; Tp +80) showed suspectedly low fluorescent probe levels in both channels, at timepoints for which expression was expected and detected in other replica. Because these samples showed sufficient number of cells, low probe levels most likely arose from experimental artefacts arising during hybridization and/or microscopy. Thus, these samples were removed from the analysis, as they most likely represented experimental artefacts.

5.I.3.3 Microscopy images

Images were successfully acquired and examined to assess qualitatively the state of the yeast cells and hybridization. The images discussed and analysed in this study (after optimization) passed this qualitative control.

Figures 5.4, 5.5, 5.6, 5.7 and 5.8 show some examples of the FISH images gathered for this study. Figure 5.4 shows an example of images from an entire field of view. Image A. shows the membranes of the cells as detected using brightfield microscopy. Image B. shows a fluorescence microscopy “raw RNA-FISH image” of a yeast sample taken during the YMC, for which *ATO3* is labelled in Cy5, *ACT1* in Cy3 and DNA is stained with DAPI. Image C. shows the same data after deconvolution. Figure 5.5

shows the same image C. over an entire page for a better visualisation. Figure 5.6 shows examples of RNA-FISH images of the first experiment; the single-RNA-FISH with *ATO3* in Cy3, for a sample taken during the YMC and in mid-log phase. Figure 5.7 shows examples of RNA-FISH images of the second experiment; the control dual RNA-FISH for which *ATO3* is labelled in Cy5 and *ACT1* in Cy3; for samples taken during the YMC showing co-expression of transcripts (t=+10) but also antagonistic expression (or low co-expression t=-10). Finally, an example of a sample taken during the mid-log phase is presented on the right panel. Next, Figure 5.8 shows examples of dual RNA-FISH images; samples of yeast cells co-expressing (top row) or showing antagonistic expression (middle row) transcripts during the YMC and yeast sampled from high-growth (mid-log; bottom row) cultures. For these dual RNA-FISH experiments (i) *ATO3* is labelled in Cy5 and *SHM2* in Cy3; (ii) *SHM2* is labelled in Cy5 and *IDH1* in Cy3; *IDH1* is labelled in Cy5 and *ATO3* in Cy3.

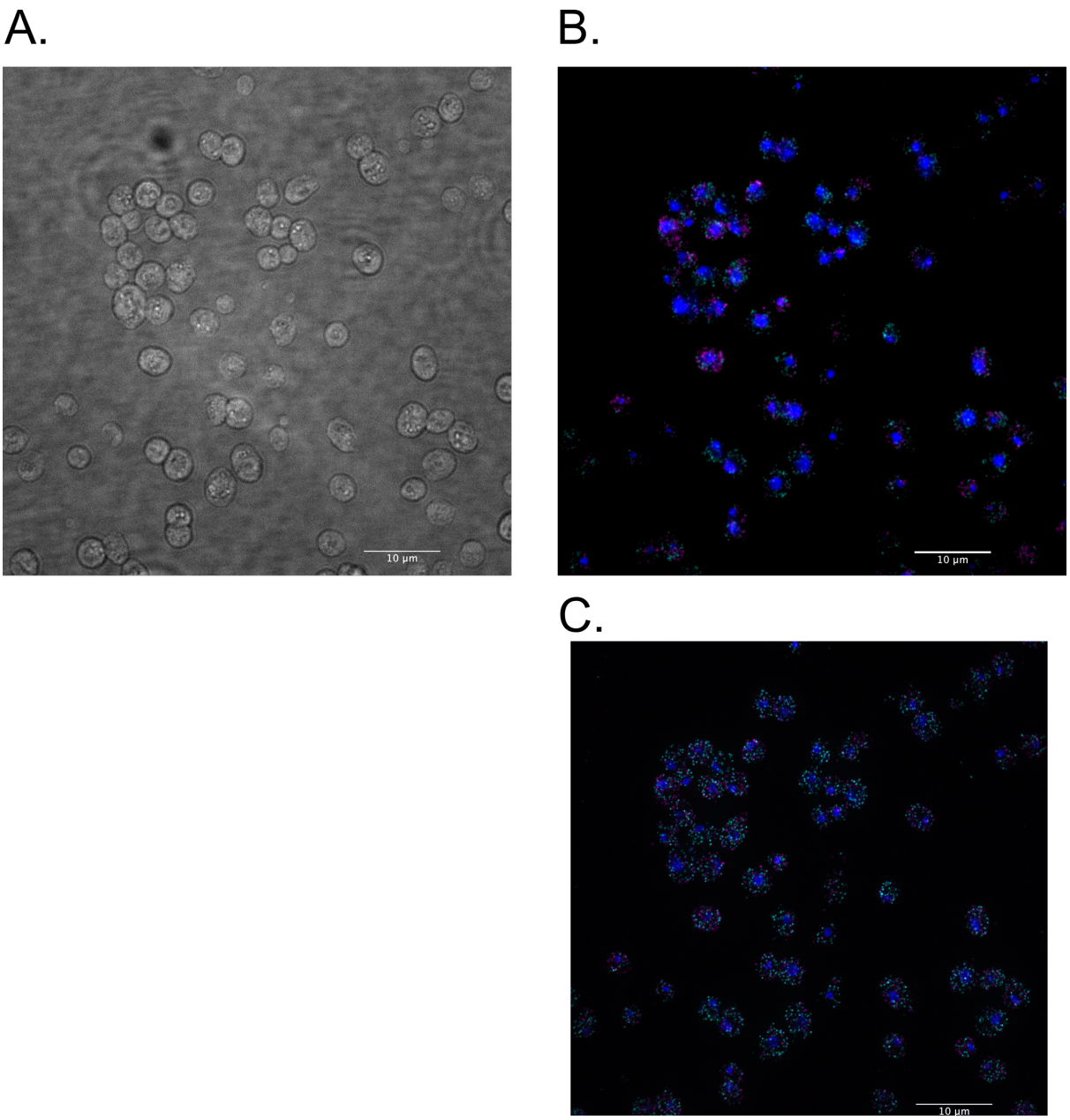

Figure 5.4 An example of brightfield and fluorescent signal from raw and deconvolved image

A. *Detection of cells using brightfield,* ***B.*** *"raw RNA-FISH data",* ***C.*** *"deconvolved data", (type ii dual label control experiment YMC sample (t=+20), ATO3 is labelled in Cy5 and ACT1 in Cy3,). Images are cropped. Bar is 10μm*

C.

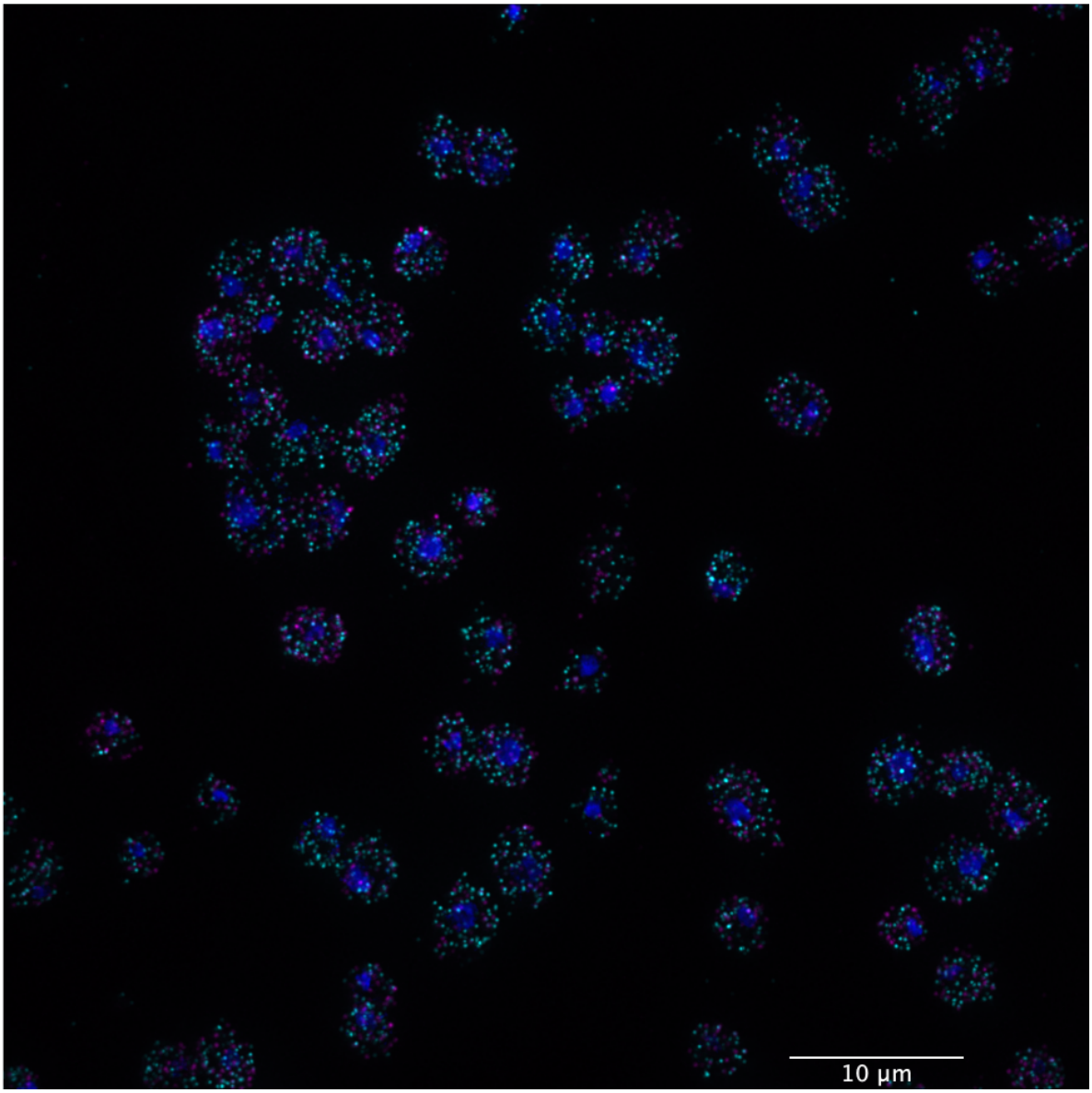

Figure 5.5. An example of microscopy images used in this work, here showing an entire field of view from a type ii dual label control experiment.

Control dual RNA-FISH with ATO3 is labelled in Cy5 and ACT1 in Cy3; for a sample taken during the YMC (t=+20). Image cropped and enlarged. Bar is 10μm

Single RNA-FISH

ATO3

YMC Tp12

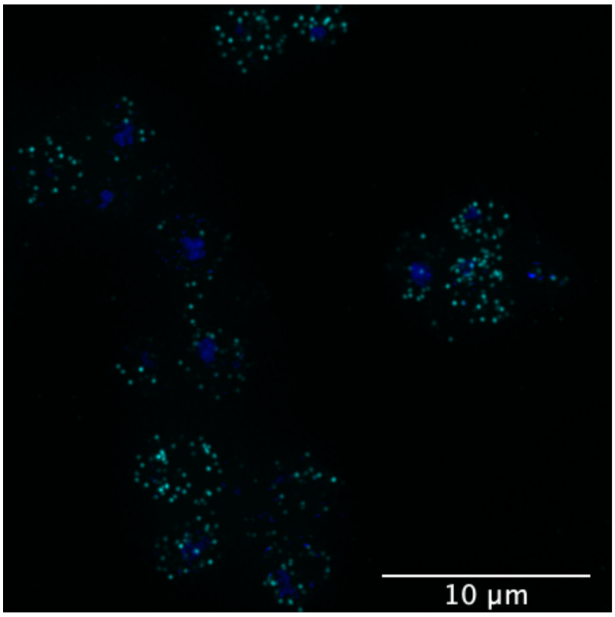

Mid-log

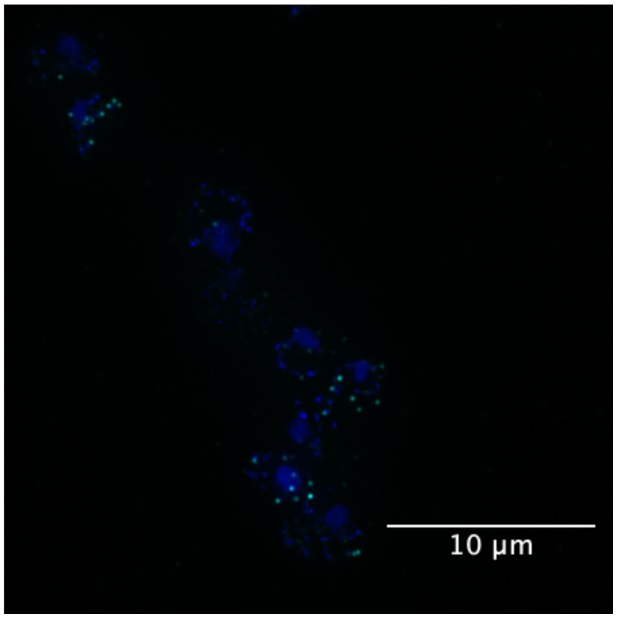

Figure 5.6. Examples of microscopy images used in this work showing a field of view from a type i single label *RNA-FISH with ATO3 in atto565 in Cy3, for a sample taken during the YMC (Time point 12) and in mid-log phase.*

Control dual RNA-FISH

ATO3* vs *ACT1

YMC Tp +10 co-expression

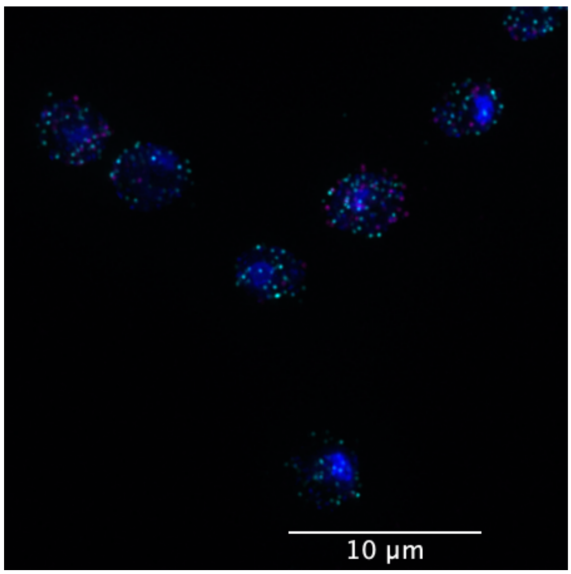

Mid-log

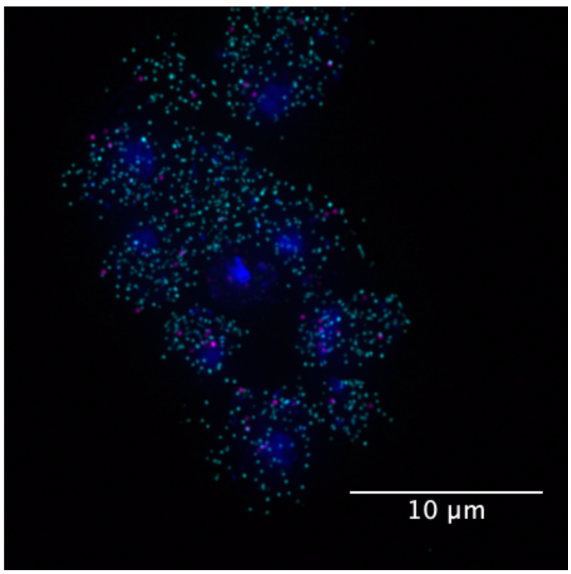

YMC Tp -10 antagonistic expression

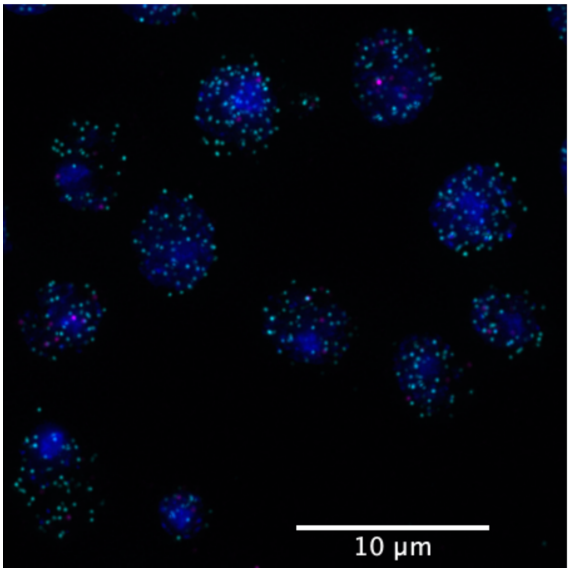

Figure 5.7 Examples of microscopy images used in this work showing a field of view from a type ii dual label *Control dual RNA-FISH with ATO3 is labelled in Cy5 and ACT1 in Cy3; for samples taken during theYMC (left) at timepoints of agonist (co-expression) (top) or antagonist expression (bottom) and in mid-log phase (right).*

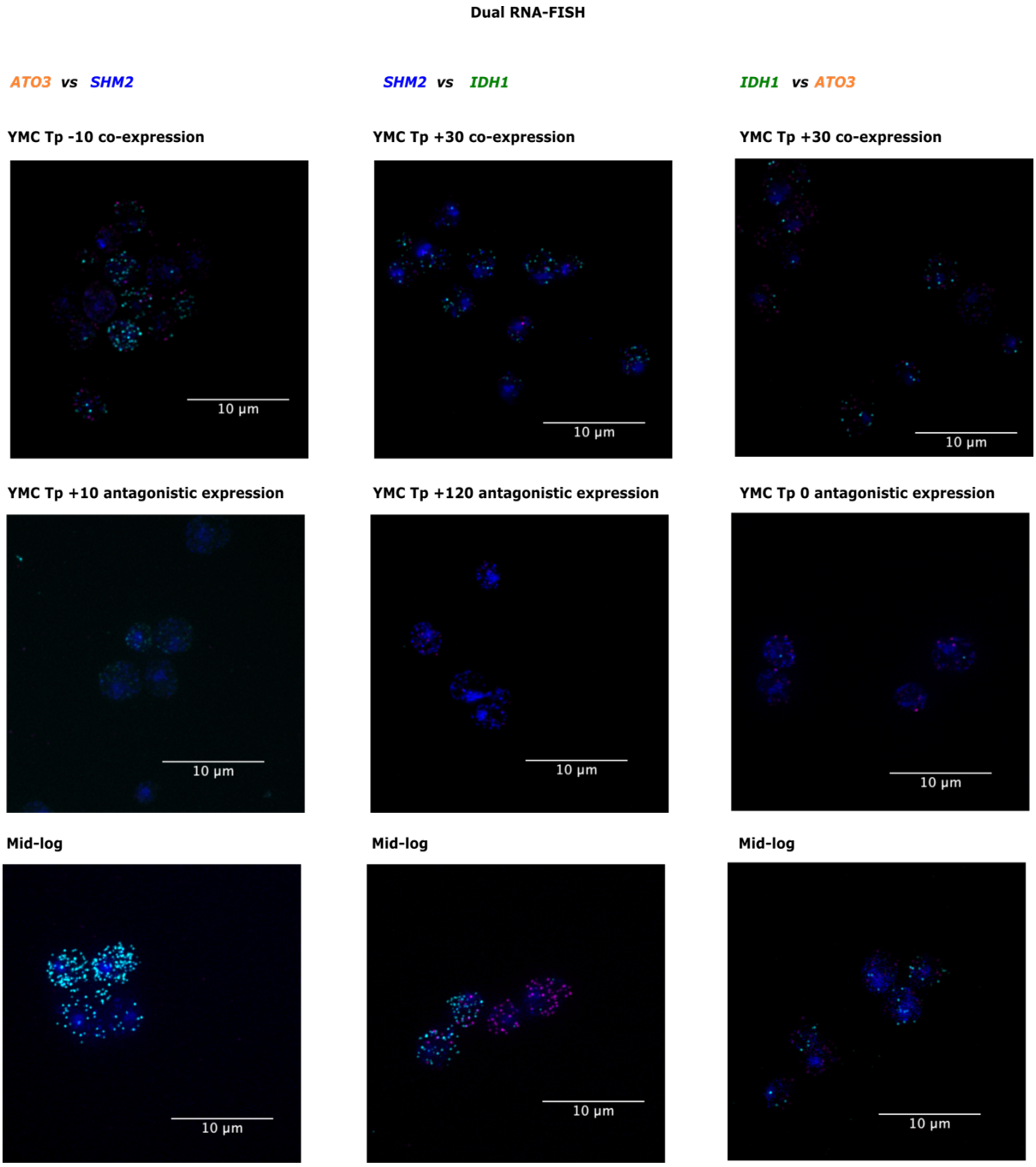

Figure 5.8 Examples of microscopy images gathered for this study.

*Type iii Dual-labelled RNA-FISH experiment for samples taken during the YMC at timepoints of co-expression (top) or antagonist expression (middle) and during the mid-log phase (bottom). ATO3 is labelled in Cy5 and SHM2 in Cy3 (**left column**), SHM2 in Cy5 and IDH1 in Cy3 (**middle column**) and IDH1 in Cy5 and ATO3 in Cy3 (**right column**). Here and for images in figures 5.4, 5.5, 5.6, 5.7, DNA is stained with DAPI and is represented in dark blue while the Cy5 (atto633) and Cy3 (atto565) channels are represented in magenta and cyan, respectively. Here also images* are cropped and enlarged.

5.I.3.4 Downstream data analysis

Once imaged, the smRNA-FISH data was analyzed following a dry-lab workflow, using the RNA quantification pipeline. Further steps were taken to prepare the datasets before analysis such as the filtering of outliers from the data. Cells for which the sum of RNA numbers and/or the cell size was too high, according to literature, were removed from the data set (see details in chapter 2).

5.I.3.5 Cell categories

The cells were analysed and partitioned into groups based on different metrics, including the presence or absence of transcripts in cells. To ascertain the transcription and transcript status of cells from the synchronized population during the YMC, different cell categories were defined according to the following criteria;

(i) The presence or absence of transcripts in a cell.

(ii) The fluorescent channel in which transcript were imaged. This is a simple a way to distinguish transcripts from each other, based on the fluorophore that was chosen to target them.

(iii) The localisation of transcripts; i.e. if transcripts are nuclear, cytoplasmic or if they are just considered to be part of the entire cell.

(iv) Finally, data subsets were also created effectively dividing cells into groups based on the sum of RNA numbers quantified in each of them.

5.I.4 Results

The first question addressed here is whether the sum of the transcript levels in individual cells recapitulates the oscillating pattern observed in NET-seq or RNA-seq data, or on microarrays, at the population level during the YMC. This was done for each transcript of interest and the data obtained was related to growth rate and culture conditions.

5.I.4.1 The smRNA-FISH data recapitulates the cycling of population-averaged transcript levels

The overall transcript levels gathered from the FISH experiments in individual cells for *ATO3*, *SHM2, IDH1* and *ACT1* are illustrated in Figure 5.9. The $\log_2$ fold-change of the mean RNA numbers compared to the median RNA number over the YMC was computed and a smoothing interpolation method was applied to it.

Transformation methods applied to the raw data confer a smooth oscillation to the transcript number profiles. As mentioned, these transformations are common in the field and have been applied to all data gathered so far for the YMC (Tu et al. 2005, Kleveck et al. 2004 Kuang et al. 2014, Feltham et al. 2020). However here transcript levels were transformed by a $\log_2$ fold-change vs median (LFCM) but not divided by the standard deviation, as was done for the RNASeq libraries in the Feltham et al (2020) paper. In contrast to the bioinformatic approach used by Tu and Kuang (2005, 2014) the transformation used here conserves the magnitude of fold changes. This allows comparison according to the amplitude of cycling behavior, as well as the period and phase. Finally, although transformations illustrate patterns, one should keep in mind that raw transcript levels from microarray and sequencing data appear a lot more irregular. It is also the case for FISH data, for which plots of mean RNA numbers are displayed in Figure S6 in the appendix.

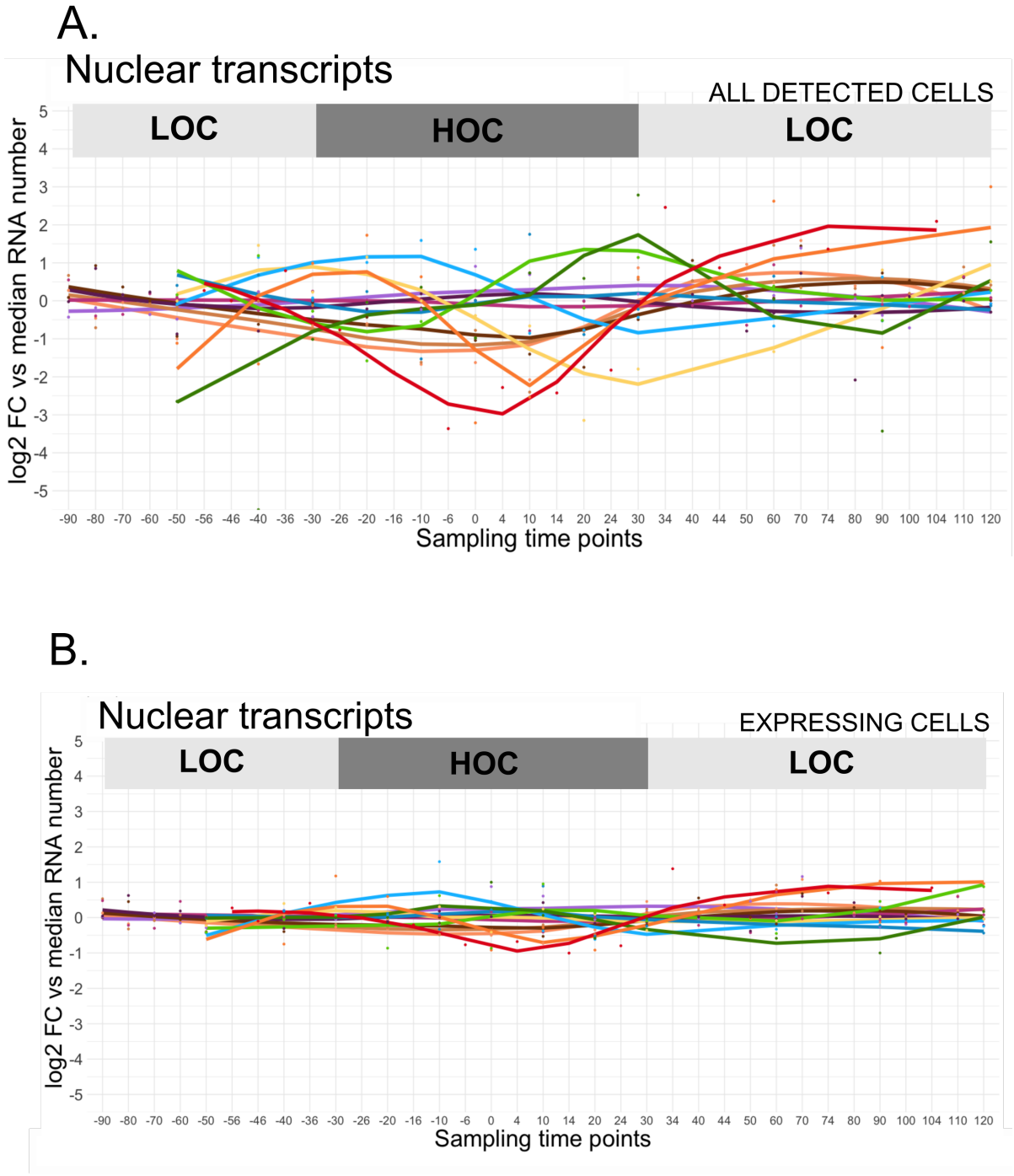
A.
Nuclear transcripts
ALL DETECTED CELLS
LOC
HOC
LOC
log2 FC vs median RNA number
Sampling time points
B.
Nuclear transcripts
EXPRESSING CELLS
LOC
HOC
LOC
log2 FC vs median RNA number
Sampling time points

Figure 5.9.1

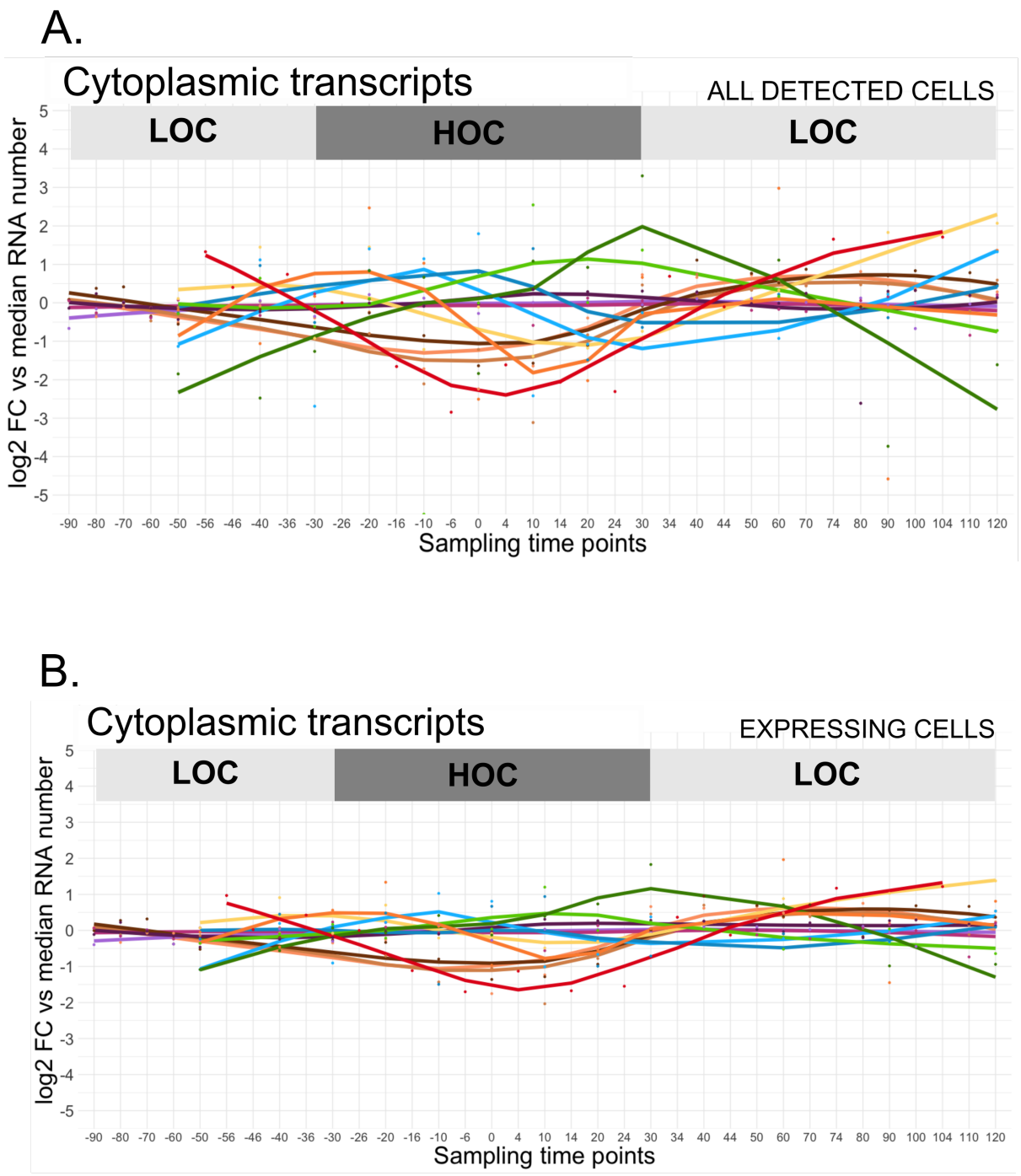
A.
Cytoplasmic transcripts
ALL DETECTED CELLS
LOC
HOC
LOC
log2 FC vs median RNA number
Sampling time points
B.
Cytoplasmic transcripts
EXPRESSING CELLS
LOC
HOC
LOC
log2 FC vs median RNA number
Sampling time points

Figure 5.9.2

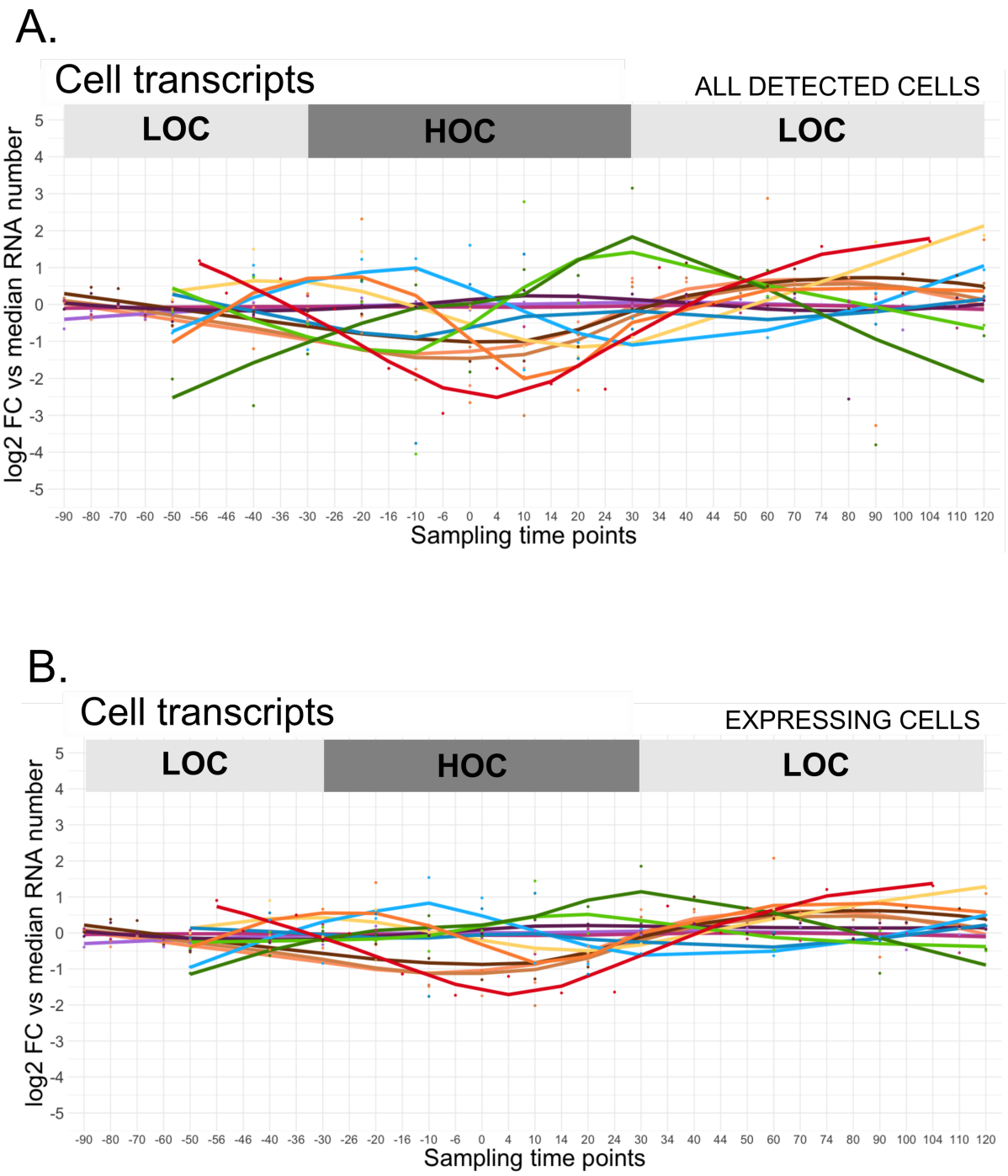

Figure 5.9.3

Figure 5.9.1,2 & 3 Overall transcript levels cycle along the YMC

Smoothed conditional means of the log_2 fold-change of the mean RNA numbers vs median RNA number (LFCM) over the YMC. Time shown in minutes relative to the point of lowest dissolved oxygen levels in media (dO_2 %) found across the YMC, displayed as "0". ***A.*** *In all detected cells.* ***B.*** *In expressing cells only. For nuclear (1), cytoplasmic (2) and cell (3) transcripts. Colors indicate the different experimental repeats; ATO3 levels are in yellow, orange, red and shades of brown; SHM2 levels are in light and dark blue; IDH1 levels are in light and dark green and ACT1 levels are shades of purple.*

Figure 5.9 reveals that the trends in mean transcript levels over time, in the nucleus, in the cytoplasm or in the whole cell, are similar to those observed in the population using a microarray, NET-Seq or 3' RNA-Sequencing techniques as presented at Figure 5.2 (Tu et al. 2005, Kleveck et al. 2004 Kuang et al. 2014, Feltham et al. 2020, Xi. DPhil thesis. 2019). Indeed, despite variability between biological replica, mean RNA levels for *ATO3* (in shades of yellow to brown), *SHM2* (in shades of blue) and *IDH1* (in shades of green) show oscillations over time while for *ACT1* they stay more even over the YMC (in shades of purple). *ATO3* levels increase in LOC and decrease in HOC, *SHM2* levels increase in early to mid-HOC and decrease in late-HOC, *IDH1* levels increase in late HOC and decrease in LOC, while *ACT1* levels stay flat over the YMC with perhaps a slight increase in late HOC, as expected. This relationship is observed when the data for all cells (Figure 5.9A) or just expressing cells (Figure 5.9B) are pooled.

5.I.4.2 Mean steady-state transcripts levels in single cells reflect differences in metabolic state between the YMC and mid-log phase cells

The means of mean RNA numbers were computed for each transcript, between replica RNA-FISH experiments in all the cells detected from high-growth asynchronous cultures (mid-log phase; generation time =˜2.08h). These are shown at Table 5.2 (DATA=Mid-log). These levels were compared to transcript levels found in previous studies.

First, the mean number of transcripts per cell for all cells detected from the mid-log phase samples reveal higher mean RNA levels for *ACT1* (22) and *SHM2* (21) compared to *IDH1* (8) and *ATO3* (3). We note that absolute transcript levels are within the possible range of mRNA copy numbers per cell (Miura et al. 2008) and that

transcript levels from the RNA-FISH data follow the same numerical ranking than the one from previous studies on mid-log phase samples (Table 5.2.A & B) (Lispon et al. 2009, Holstege et al. 1998). However, particularly for *SHM2* and *IDH1*, levels are slightly higher than previously estimated for mid-log phase samples from Holstege et al., (*ACT1* (21) *SHM2* (15), *IDH1* (2) and *ATO3* (2) (Table 5.2.B) (Holstege et al. 1998). Distinct growth rates, strain and cell sizes between the 2 mid-log phase WT cultures might explain some of these differences (data not available for Holstege et al. 1998). But this could also be explained by the differences in experimental procedures, as this observation is consistent with the one made by Zenklunsen et al. 2008, who reported higher transcript copy numbers when conducting RNA-FISH in yeast cells under exponentially growth, compared to previously recorded numbers via microarrays or RNA-seq sequencing studies.

Next, the means of mean RNA numbers per cell were computed for each transcript, between replica RNA-FISH experiments in all the cells detected for each time points from slow-growth synchronous YMC cultures (generation time = 9.62h, YMC period =3h20min). The range (minima and maxima of these metrics) of the RNA numbers per cell were considered. These are shown in Table 5.2 (DATA=YMC).

Mean RNA levels oscillate with a higher amplitude throughout the YMC for *ATO3* compared to *SHM2* and then *IDH1* (as observed in Fig 5.9 and Figure S6 appendix). The maxima of mean RNA numbers are 16, 11 and 8 for each transcript respectively. For the control transcript *ACT1*, the RNA numbers range from 16 to 29 along the YMC.

Next, the effect of growth rate on mean transcript levels was considered by comparing the data from fast growing mid-log cultures (generation time =˜2.08h) and the slow growing YMC (growth rate = $0.072h^{-1}$, generation time = 9.62h, YMC period

=3h20min), with other fast growing mid-log cultures from Holstege et al., (generation time =N/A) Table 5.2.B (Holstege et al. 1998), and other slow growing but asynchronous batch cultures using data obtained by RNA-seq estimates from Lahtvee et al., (growth rate = $0.1h^{-1}$, generation time =˜6.93h) in Table 5.2.C (Lahtvee et al. 2017).

First, transcript levels for *IDH1*, *SHM2* and *ACT1* were found to be higher in RNA-FISH data from fast growing mid-log cultures (generation time =˜2.08h, Table 5.2, mid-Log) than in data from slow growing asynchronous batch cultures from Lahtvee et al. (growth rate = $0.1h^{-1}$, generation time =˜6.93h), indicating an effect of growth rate on gene expression for these transcripts. This effect is not detected for ATO3 for which levels are the same between the two cultures.

Next, *ATO3* shows peak expression in the LOC phase of the YMC (n=+40) (Fig 5.9 and Fig.S6 appendix). These peak expression levels are higher than for both high-growth cultures from the FISH data and from Holstege et al., (Table 5.2.YMC & B). These results are consistent with the conclusions from population-averaged studies, indicating LOC transcript levels are always higher in slow-growth rates asynchronous cultures when compared to in high-growth asynchronous cultures (batch phosphate-starved, growth rates = $0.05h^{-1}$ vs $0.25h^{-1}$, generation times =˜13.86h vs ˜2.77h) suggesting more cells transition to a “LOC-state” and/or increase the expression levels of LOC transcripts, such as the stationary phase transcript *ATO3*, in the LOC phase of the YMC than in mid-log phase (Slavov et al. 2011).

Next, to separate the effects of growth rate from the mode of growth, transcripts whose expression peaks in the HOC phase of the slow growing YMC cultures (growth rate = $0.072h^{-1}$, generation time = 9.62h, YMC period =3h20min) were compared with

asynchronous slow growing batch cultures. Maximum levels of *SHM2* and *IDH1* in the YMC are higher than levels in a slow-growth batch culture (growth rate = $0.1h^{-1}$, generation time =˜6.93h, Lahtvee et al, 2017) as presented at Table 5.2.YMC vs C. One explanation is that more cells are found in a HOC state along the YMC, as opposed to in slow-growth batch cultures, as suggested previously (Slavov et al. 2011). This analysis thus suggests that the growth rate *per se* is not the main determinant of relative differences in transcript levels. Instead, different metabolic states (HOC and LOC) between batch grown cells and the YMC samples seem to reflect the differences in relative mean RNA levels.

Table 5.2 Metrics of genes and their transcripts analysed with smRNA-FISH experiments
Mid-log. *Means of mean RNA numbers between replica RNA-FISH experiments in all the cells detected in high-growth asynchronous cultures (mid-log phase; generation time = 2.08h).*
YMC. *Range; minima and maxima of means of the mean RNA numbers between replica RNA-FISH experiments in all the cells detected along the YMC. (generation time = 9.62h, YMC period =3h20min).* ***A.*** *Average transcript count from high throughput single-molecule sequencing Digital Gene Expression (smsDGE) technology (Lipson et al. 2009).* ***B.*** *Transcript expression levels detected via high-density oligonucleotide arrays for mid-log phase WT cultures (Holstege et al. 1998).* ***C.*** *Transcript levels (absolute abundance from RNA-seq samples calibrated using 18 mRNAs with known absolute concentration) (Lahtvee et al. 2017).*

Standard Name	**ATO3**	**SHM2**	**IDH1**	**ACT1**	**DATA**
Means of mean RNA numbers	3	21	8	22	**Mid-log**
Range (minima – maxima) of means of mean RNA numbers	0 - 16	0 - 11	0 - 8	16 - 29	**YMC**
Average count	100.95	837.48	312.7	1297.93	**A**
Transcript levels (molecules/cell)	2	14.9	2	21.1	**B**
Transcript levels (molecules/cell)	3.69	3.19	1.78	5.91	**C**

5.I.5 Conclusions

First, mean steady-state transcripts numbers in single cells from mid-log phase cultures follow the same numerical ranking identified between transcripts in previous studies using high-growth mid-log asynchronous cultures; higher transcripts levels for *ACT1* and *SHM2* than for *ATO3* and *IDH1*. This indicates mean RNA levels gathered through smRNA-FISH in this study comply with previous bulk data (Lipson et al. 2009, Holstege et al. 1998, Lahtvee et al. 2017).

Second, results from the RNA-FISH data along the YMC indicate high and relatively constant levels for *ACT1* (despite variability), and higher fluctuations in RNA numbers along the YMC for *ATO3* compared to *SHM2* and then *IDH1*. Averaged transcript levels from smRNA-FISH data show similar oscillations over the YMC compared to what was previously observed with microarrays or sequencing studies (Tu et al. 2006, Kleveck et al. 2004 Kuang et al. 2014, Feltham et al. 2020),

Third, when comparing asynchronous batch cultures, the effect of growth rate on transcript levels can be detected for *IDH1*, *SHM2* and *ACT1* (at higher growth-rates, mean RNA numbers increase) but not for *ATO3*.

Fourth, when comparing slow-growth synchronous cultures of the YMC, with other types of cultures, the metabolic state and thus phase of the YMC; HOC vs LOC rather than the constant growth-rate of the culture is found to be related to the transcripts levels.

In conclusion, the smRNA-FISH data acquired recapitulates well the cycling of overall transcript levels and reports authentic absolute transcript numbers therefore validating the approach taken in this study and the quality of the data acquired. Furthermore, mean transcript levels reflect the metabolic status of cells in YMC cultures.

Chapter 5 Part II

Transcript levels of genes transcribed by RNA polymerase II vary between single cells from synchronized cultures

Part II of this chapter aims to address whether all cells in the synchronous population of the YMC show similar oscillations in transcript levels over time.

Concretely (i) whether differences in gene expression heterogeneity can be identified and described between target transcripts and along the YMC and (ii) whether these can be explained by transcription dynamics and/or transcripts regulation processes. To do so; (i) The amount of variation (stochasticity) or noise in transcript levels is investigated across the synchronized population during the YMC, (ii) the fractions of expressing cells together with RNA distributions are compared between target transcripts during the YMC, (iii) alongside, predictions are made on the modes and rates of transcription and degradation for the different target transcripts picked for this study.

5.II.1 Introduction

5.II.1.1 Gene expression noise

Noise or stochasticity in gene expression has first been described for the expression of β-galactosidase (Novick & Weiner. 1957). Simply, it was demonstrated that upon increase of the β-galactosidase gene expression in cell population, gene expression between cells varies. The term “noise” is represented in Figure 5.10. It describes the stochastic variation in gene expression across a genetically identical population (Blake *et al*. 2003; Kaern *et al.* 2005; Raser & O’Shea. 2005). Gene expression stochasticity is present in every organism from prokaryotes to eukaryotes. It has been reported using reporters of protein levels in single cells but it is also described for transcript levels in various organisms including budding yeast in high-growth asynchronous cultures (Elowitz et al, 2002, Raj et al. 2006., Raj & van Oudenaarden. 2008, Sanchez et al. 2013).

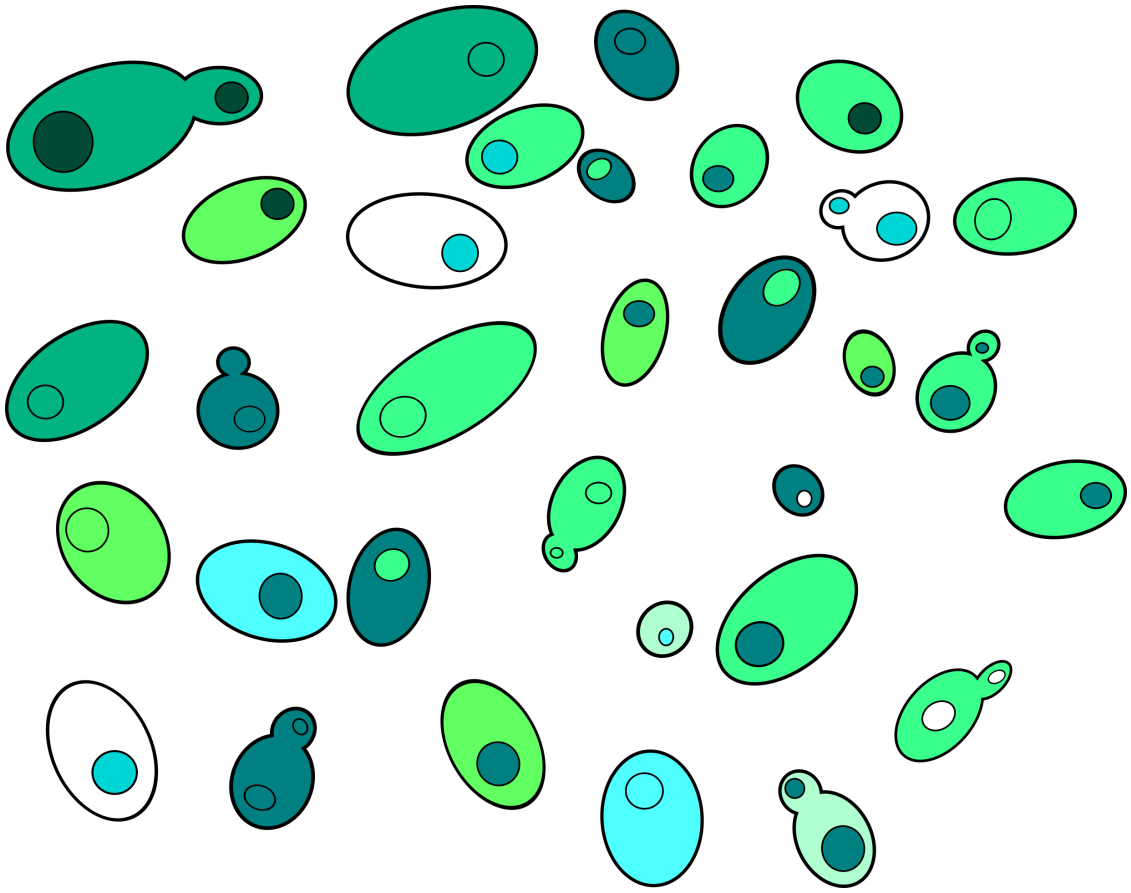

Figure 5.10 Representation of noise in a clonal population

Colours represent the level of expression in each cell. Different levels of transcripts are identified between cells, for nascent and steady-state transcripts. Modified from Dr. Struan Murray, (2016), unpublished.

Gene expression noise is typically measured by the Coefficient Of Variation (COV) and sometimes by the Fano Factor (variance divided by the mean) (Golding et al. 2005, Sanchez et al. 2013). As a COV of 1 indicates an equal standard deviation to mean ratio, genes with a COV above 1 are considered to show “noisier” gene expressions. On the contrary genes with COV below 1 or with lower Fano Factors are considered less noisy as shown at Figure 5.11 (Thattai & van Oudenaarden. 2001).

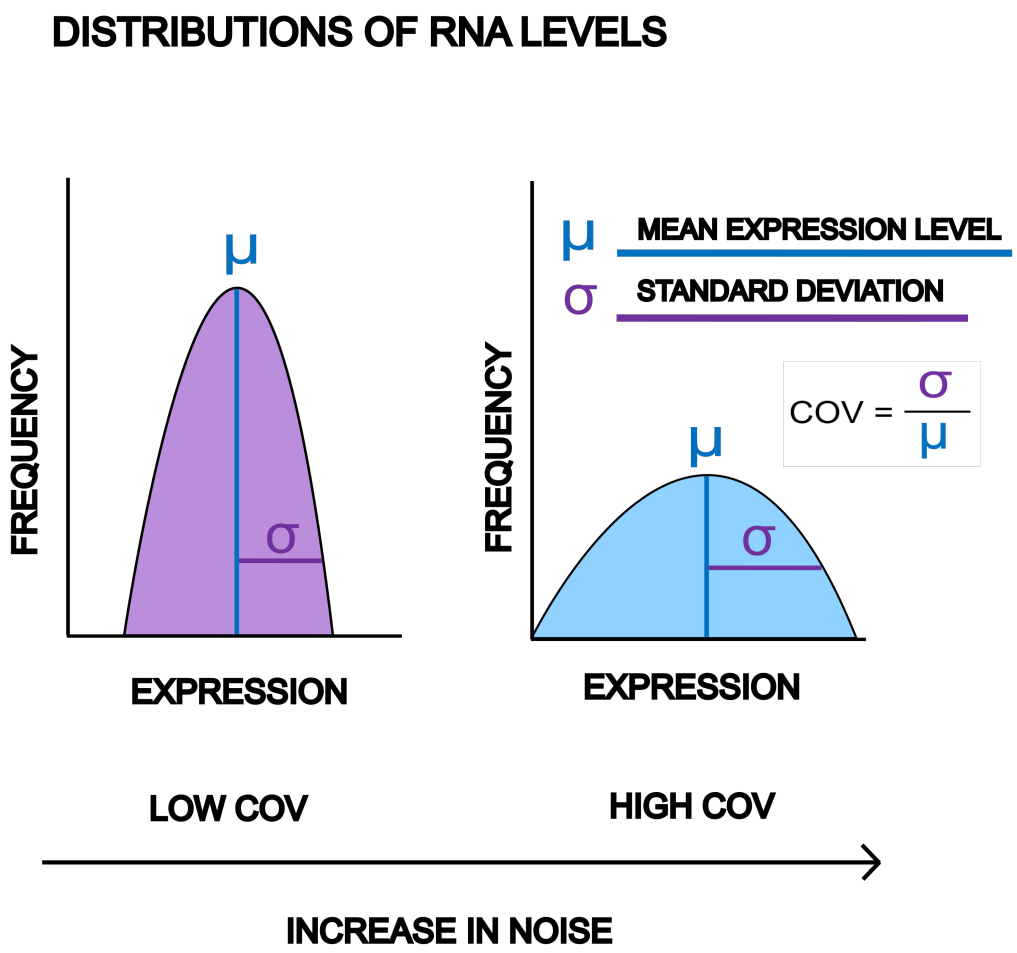

Figure 5.11 Measures of Noise

Distribution of RNA levels for a "quiet" gene, showing a high mean and a low standard deviation, therefore a low coefficient of variation and Fano factor (left) and a "noisy" gene, showing a lower mean and a higher standard deviation, therefore a higher coefficient of variation and Fano factor (right). Modified from Dr. Philipp. Lorenz, (2017), unpublished.

5.II.2 Results

5.II.2.1 Yeast cells show low RNA Pol II transcriptional noise in synchronous population

Next, the level of stochasticity is investigated for the four target transcripts picked for this study, looking at gene expression noise of these mRNAs transcribed by RNA polymerase II (smRNA-FISH data set).

The scatter plots in Figure 5.12 indicate the correlation between the standard deviation and mean RNA numbers for YMC (left panel) and mid-log (right panel) samples (Figure 5.12.A for all detected cells and Figure 5.12.B for expressing cells). An increase in noise is characterized by an increase in standard deviation compared to the mean (higher COV). Therefore, points on the left side of the diagonal of each plot can be interpreted as sampling timepoints for which gene expression is noisier than points found on the right side of the diagonal showing no noise.

There are three general points to be made about the data. First, gene expression noise is detected for all detected cells (Fig.5.12.A) as well as for expressing cells (Fig. 5.12.B). Second, variability is more prevalent in cells from the YMC time course when transcript levels are low. This is particularly evident for the nuclear transcripts in the YMC, where the majority of cells show 5 or fewer transcripts. For the cytoplasmic transcripts, once levels are >10, levels of variability (noise) across the population rapidly reduces. Third, the samples from the YMC time course tend to show more variability than observed in the mid-log cells, even at low transcript numbers (compare left and right panels in Figure 5.12.A and B).

When the variability for transcripts from the four different genes studied here are examined in YMC samples, some timepoints deviate from the diagonal while others don't, indicating that noise is present for these transcripts in YMC cultures. The variability in *ACT1* (purples) transcripts distribution in cells in the YMC is generally less than observed for *ATO3*, *SHM2* and then *IDH1.*

In high growth asynchronous mid-log population, noise levels directly reflect the overall expression levels of the transcripts; expression is noisier for *ATO3* than for *IDH1* followed by *SHM2* and *ACT1*, reflecting the higher transcript numbers for *SHM2* and *ACT1.*

Together these results indicate the presence of low gene expression noise for budding yeast cells in asynchronous population under high-growth (mid-log) but also in synchronous slow growing cell populations of the YMC. This data confirms previous reports, indicating the presence of relatively low gene expression heterogeneity in either YMC populations, through Immuno-Fluorescence of a few proteins (Laxman et al. 2010), or in slow-growth rate asynchronous yeast cultures (Silverman et al. 2010). Furthermore, the results obtained here are consistent with observations of lower gene expression noise in budding yeast compare to other more complex eukaryotic model systems such as mammalian cells (Golding et al. 2005; Sanchez et al. 2013). Finally, different levels of stochasticity are observed for the different target transcripts in both types of culture growth.

A.

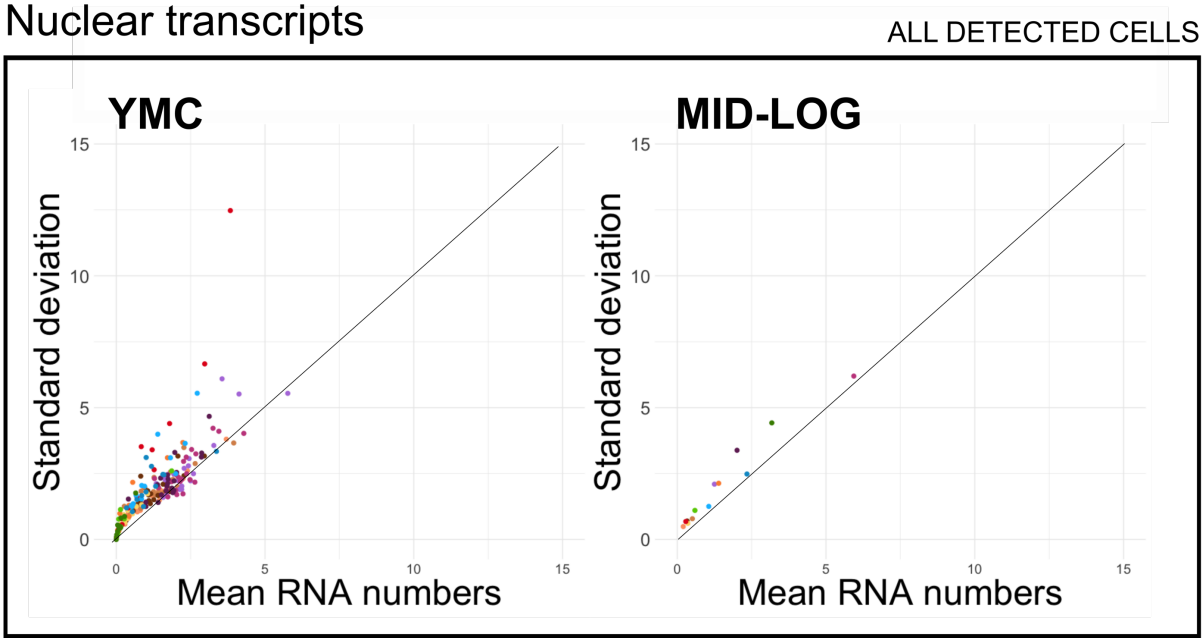

B.

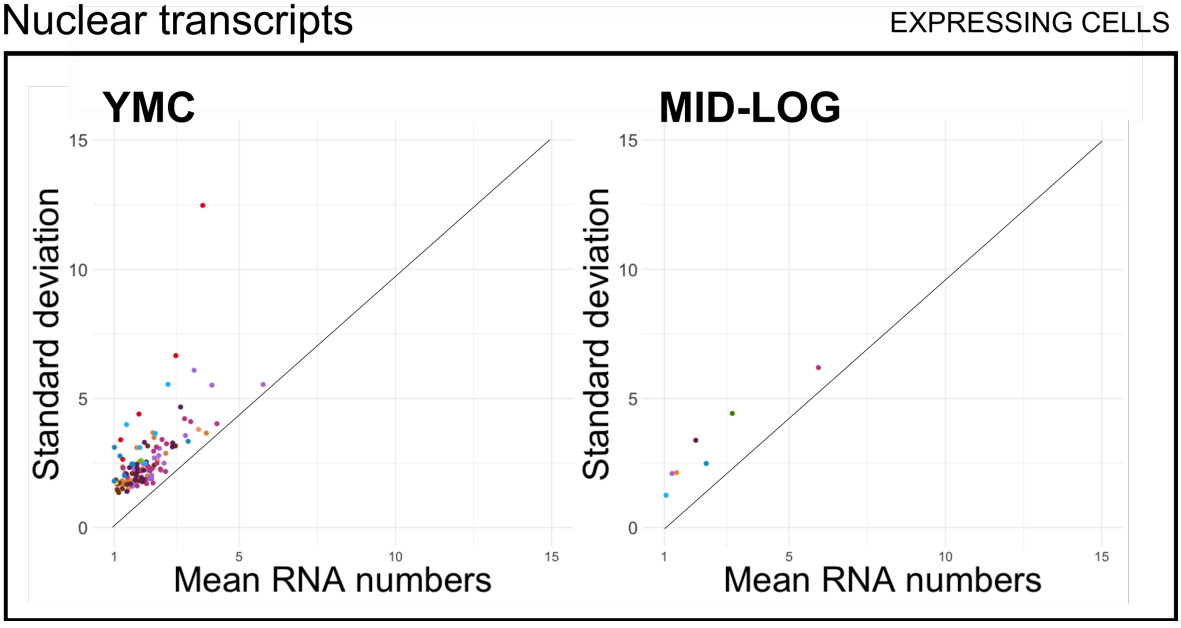

Figure 5.12.1

A.

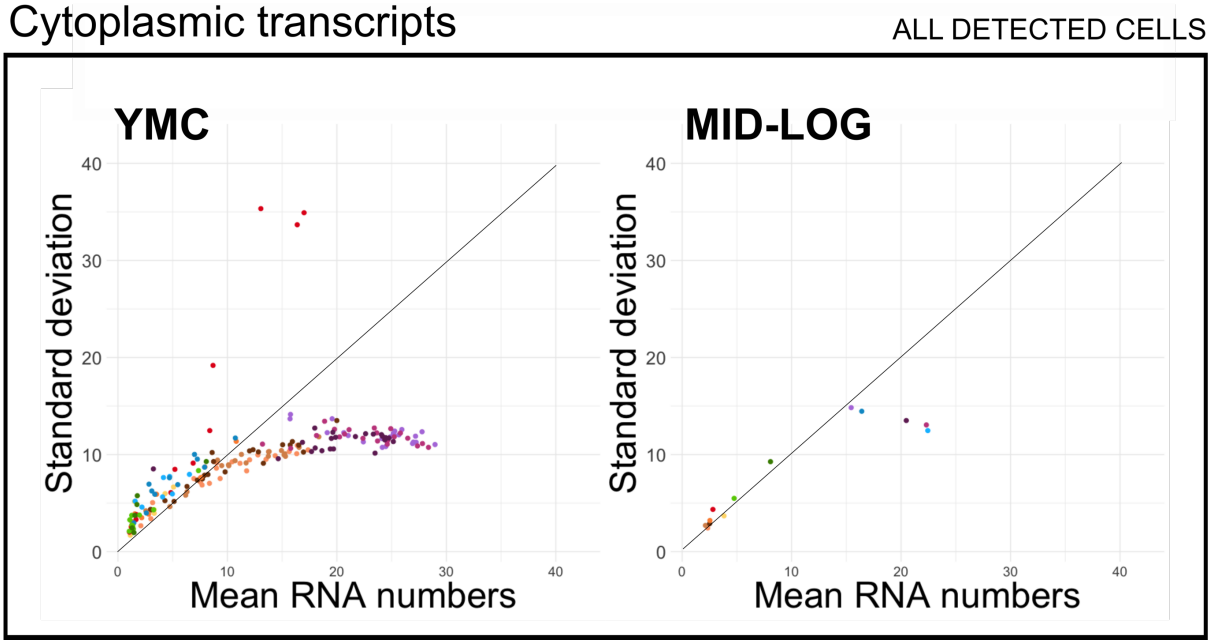

B.

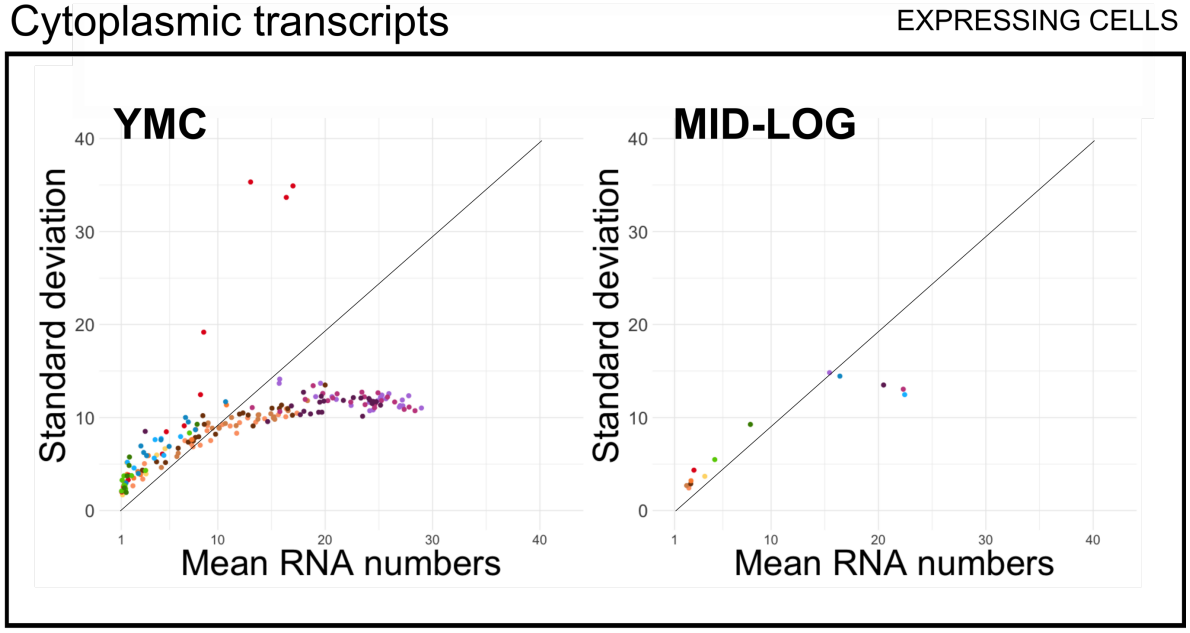

Figure 5.12.2

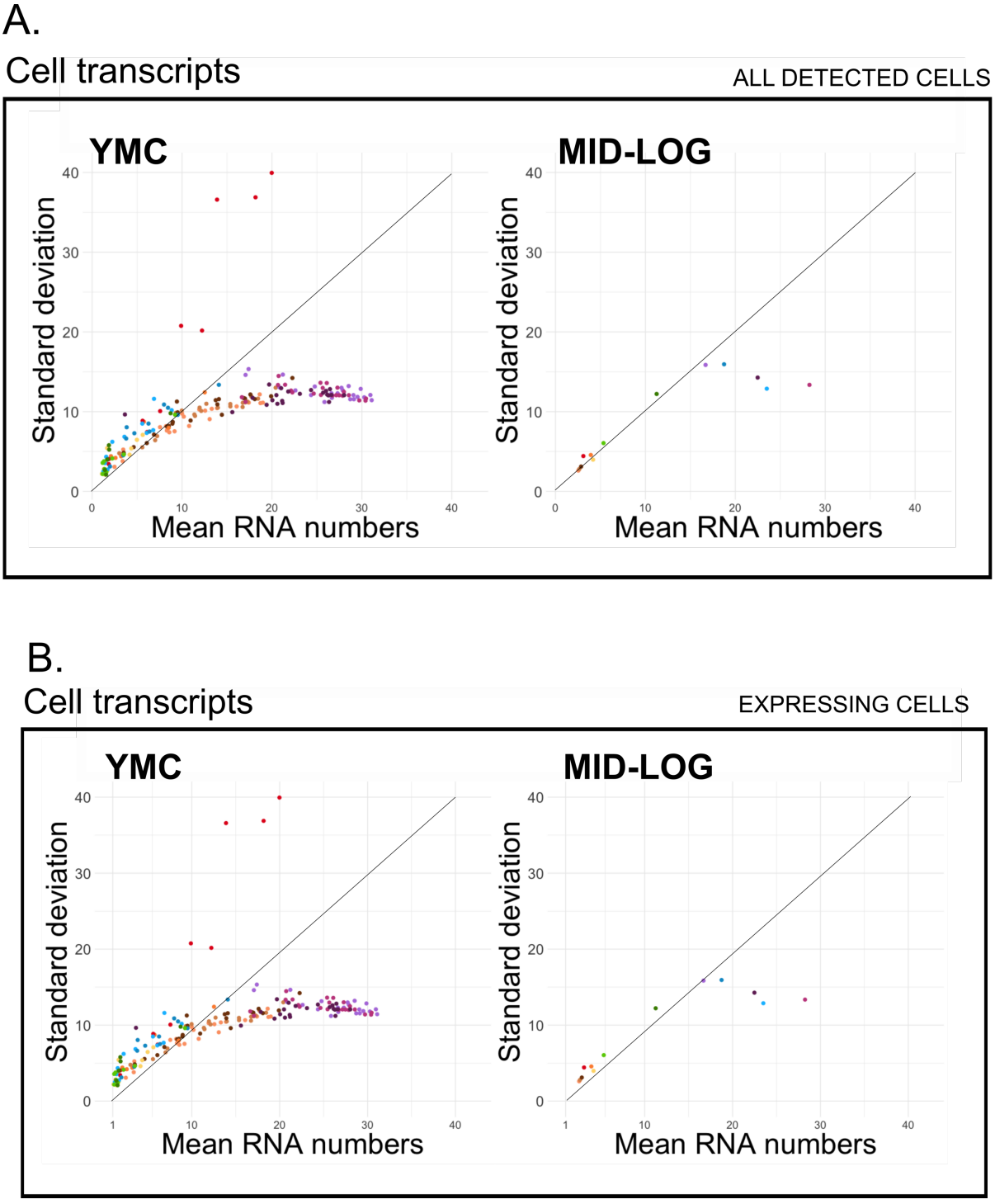

Figure 5.12.3

Figure 5.12.1,2 & 3 Standard deviation vs mean RNA numbers for all detected cells.

For all sampling timepoints taken, ***Left.*** *along the YMC (regardless of time of sampling),* ***Right.*** *in Mid-log cultures. For nuclear (1), cytoplasmic (2) and cell (3) transcripts.* ***A.*** *In all detected cells,* ***B.*** *In expressing cells. Colors indicate the different experimental repeats; ATO3 levels are in yellow, orange, red and shades of brown; SHM2 levels are in light and dark blue; IDH1 levels are in light and dark green and ACT1 levels are in shades of purple.*

It is notable that the scatter plots show some outliers and deviations from the diagonal for YMC samples (Figure 5.12.A and 5.12.B, left panels), hinting that noise levels differ between sampling timepoints taken along the YMC, and for each target transcript. This leads to the question as to whether the levels of gene expression stochasticity change throughout the YMC. To investigate this, noise measures were computed for the different mRNA targets and their transcript levels over the YMC.

5.II.2.2 Gene expression noise oscillates over the YMC

The coefficient of variation (COV) for RNA numbers (standard deviation/mean) was calculated and plotted as smoothed conditional means of the $\log_2$ fold-change of these COV vs median COV (LFCM) over the YMC (Figure 5.13). These plots demonstrate that noise levels cycle along the YMC. The ranges of values are 1.5 to 4.7 for all detected cells, compared to 0.62 to 1.04 for expressing cells only. By contrast, mid-log cultures show ranges of 0.68 to 1.84 for all detected cells compared to 0.56 to 0.96 for expressing cells.

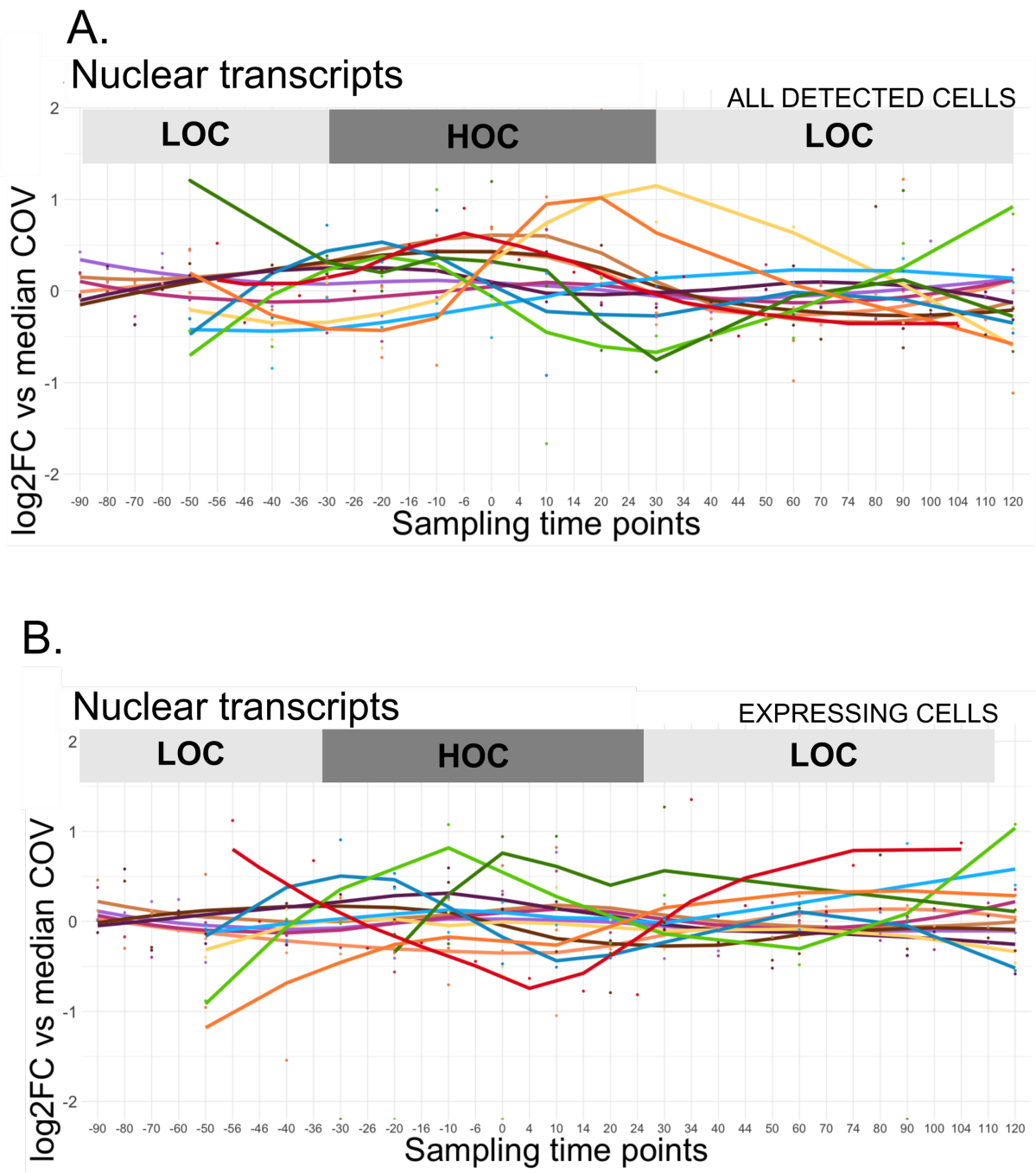
A.
Nuclear transcripts
ALL DETECTED CELLS
LOC
HOC
LOC
log2FC vs median COV
Sampling time points
B.
Nuclear transcripts
EXPRESSING CELLS
LOC
HOC
LOC
log2FC vs median COV
Sampling time points

Figure 5.13.1

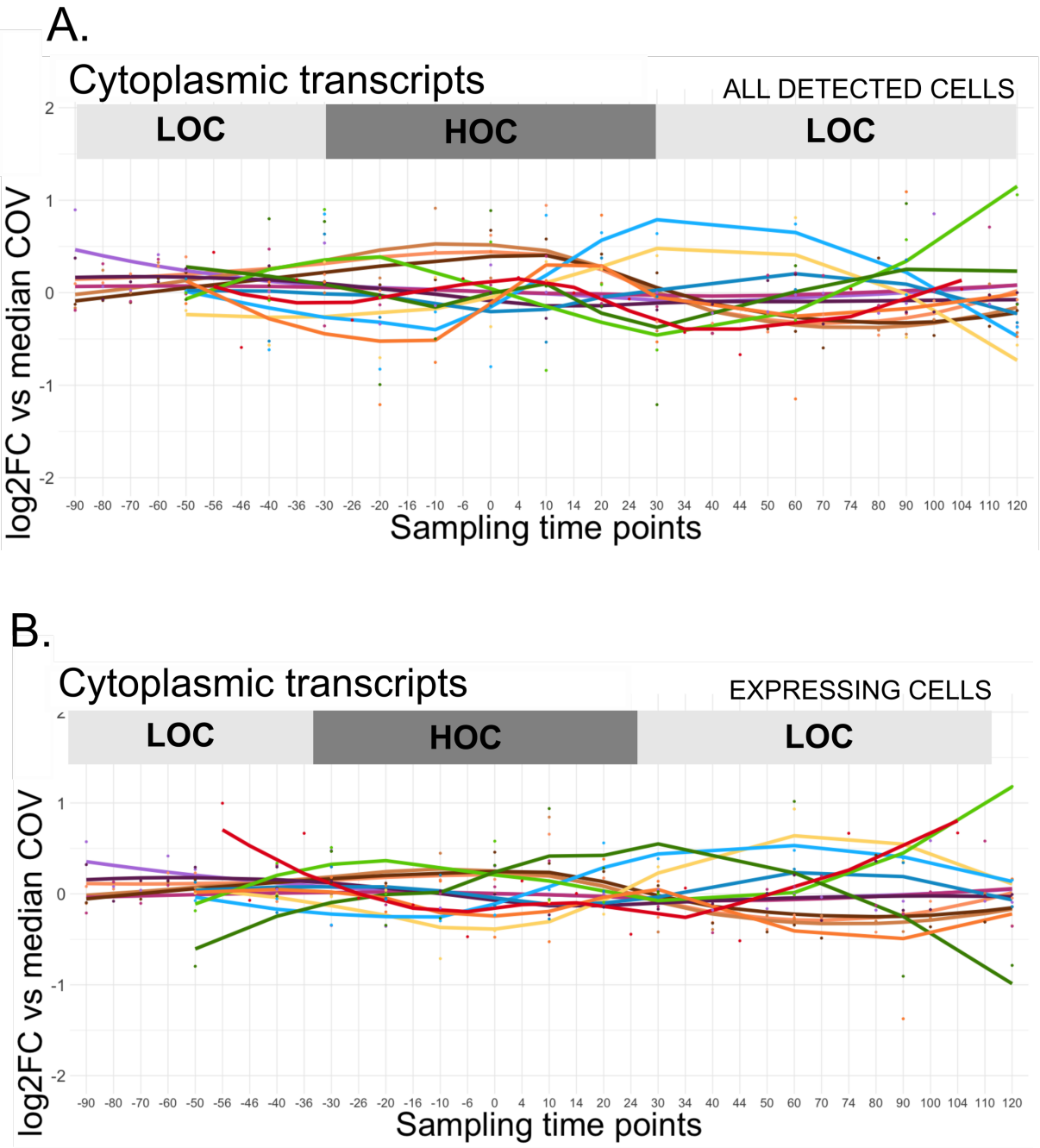
A.
Cytoplasmic transcripts
ALL DETECTED CELLS
LOC
HOC
LOC
log2FC vs median COV
Sampling time points
B.
Cytoplasmic transcripts
EXPRESSING CELLS
LOC
HOC
LOC
log2FC vs median COV
Sampling time points

Figure 5.13.2

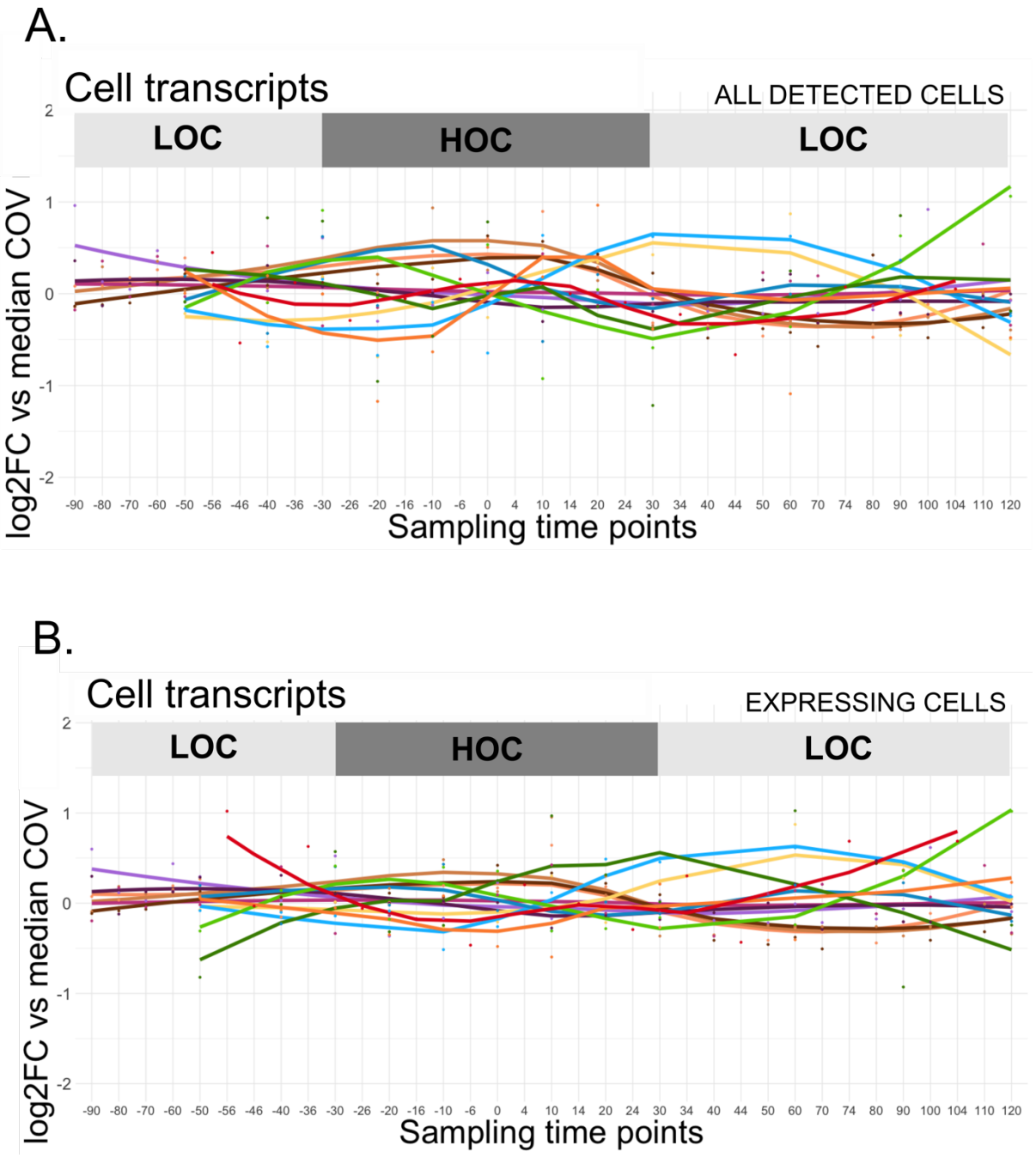

Figure 5.13.3

Figure 5.13.1,2 & 3 Overall noise levels cycle along the YMC.

Smoothed conditional means of the log_2 fold-change of the coefficient of variation for RNA numbers vs median COV for RNA number (LFCM) over the YMC. Time shown in minutes relative to the point of lowest dissolved oxygen levels in media (dO_2 %) found across the YMC, displayed as "0". ***A.*** *In all detected cells.* ***B.*** *In expressing cells only. For nuclear (1), cytoplasmic (2) and cell (3) transcripts. Colors indicate the different experimental repeats; ATO3 levels are in yellow, orange, red and shades of brown; SHM2 levels are in light and dark blue; IDH1 levels are in light and dark green and ACT1 levels are in shades of purple.*

Focusing on all the cells detected, noise increases as transcript levels decrease (Figure 5.9 & figure 5.13.A). Thus, as the proportion of non-expressing cells increases, gene expression heterogeneity rises. This is true for all target transcripts. By contrast, looking at expressing cells only (Figure 5.13.B), noise levels increase when transcript levels rise for *ATO3* and *IDH1,* but not so much for *SHM2*, for which noise level still increase when transcript levels decrease. Importantly, as opposed to the other transcripts, *ACT1* noise levels stay regular over the cycle, providing a good control for noise. It demonstrates that experimental noise for *ACT1* is kept low along the YMC, and validates observations and conclusions made for the other transcripts.

5.II.3 Conclusions

Accordingly, it implies that transcription of the target genes picked in this study and/or any mechanisms involved in nuclear transcripts regulation is noisy. This supports the hypothesis that noise levels differ through time and metabolic changes of the YMC for the different target genes and contradicts the hypothesis which suggests that single cells from synchronous population possess exact similar behaviour, transcript levels and transcription status. As global gene expression changes occur, the average expression levels does not change in a similar way in all individual cells from that synchronized population.

Finally, these results indicate that gene expression noise arises mostly from the proportion of non-expressing cells in the population. This means the “on-off status of cells” is the major source of noise identified here. However, gene expression in YMC populations is heterogeneous even when looking at “expressing cells only”. Indeed, the level of heterogeneity rises both at the point of transcription and with the transcript

levels in these cells, perhaps indicating other sources of noise, rising from processes that regulate transcription and transcripts.

5.II.4 Results

Previously, profiles of transcript levels of expressing cells were proved to be flatter than the ones for all detected cells (Figure 5.9). Indeed, a log2 fold-change of up to 3 or 4.5 is observed for all detected cells, compared to a log2 fold-change of up to 1.5 or 2 for expressing cells, when considering expression in-nucleus or in-cytoplasm respectively. As results show the effect of “non-expressing” cells on the amplitude of overall transcript levels detected over the YMC, **this leads to the question as to whether the proportion of cell expressing transcripts changes over the YMC and if so how.**

5.II.4.1 The fraction of expressing cells oscillates over the YMC

The proportion of expressing (in colour) or non-expressing (in light grey) cells of each YMC sampling timepoints, for each target transcripts or each replica are plotted in Figure 5.14, for nuclear, cytoplasmic and cell transcripts.

A.

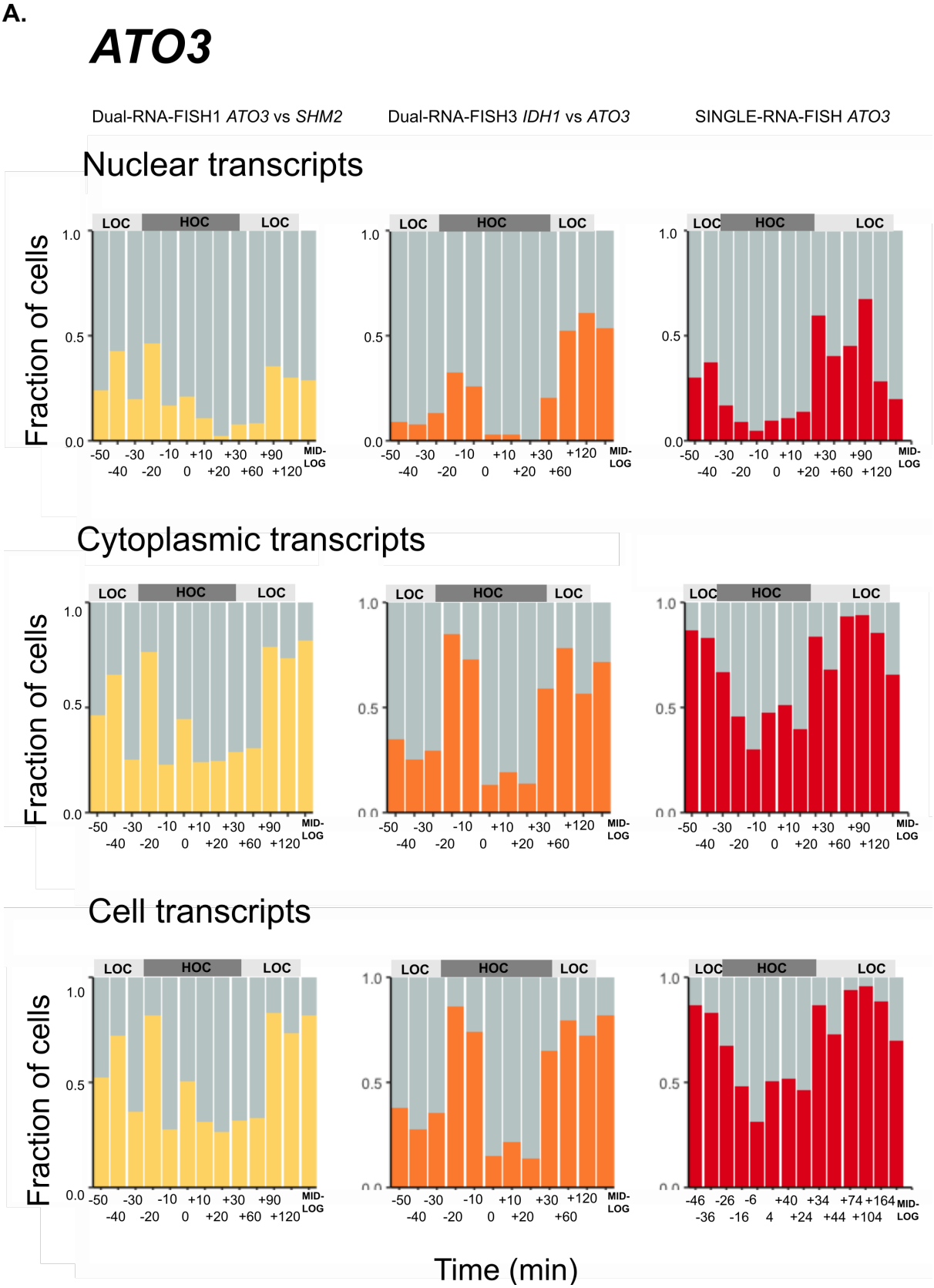

Figure 5.14.A.1

A.

SHM2

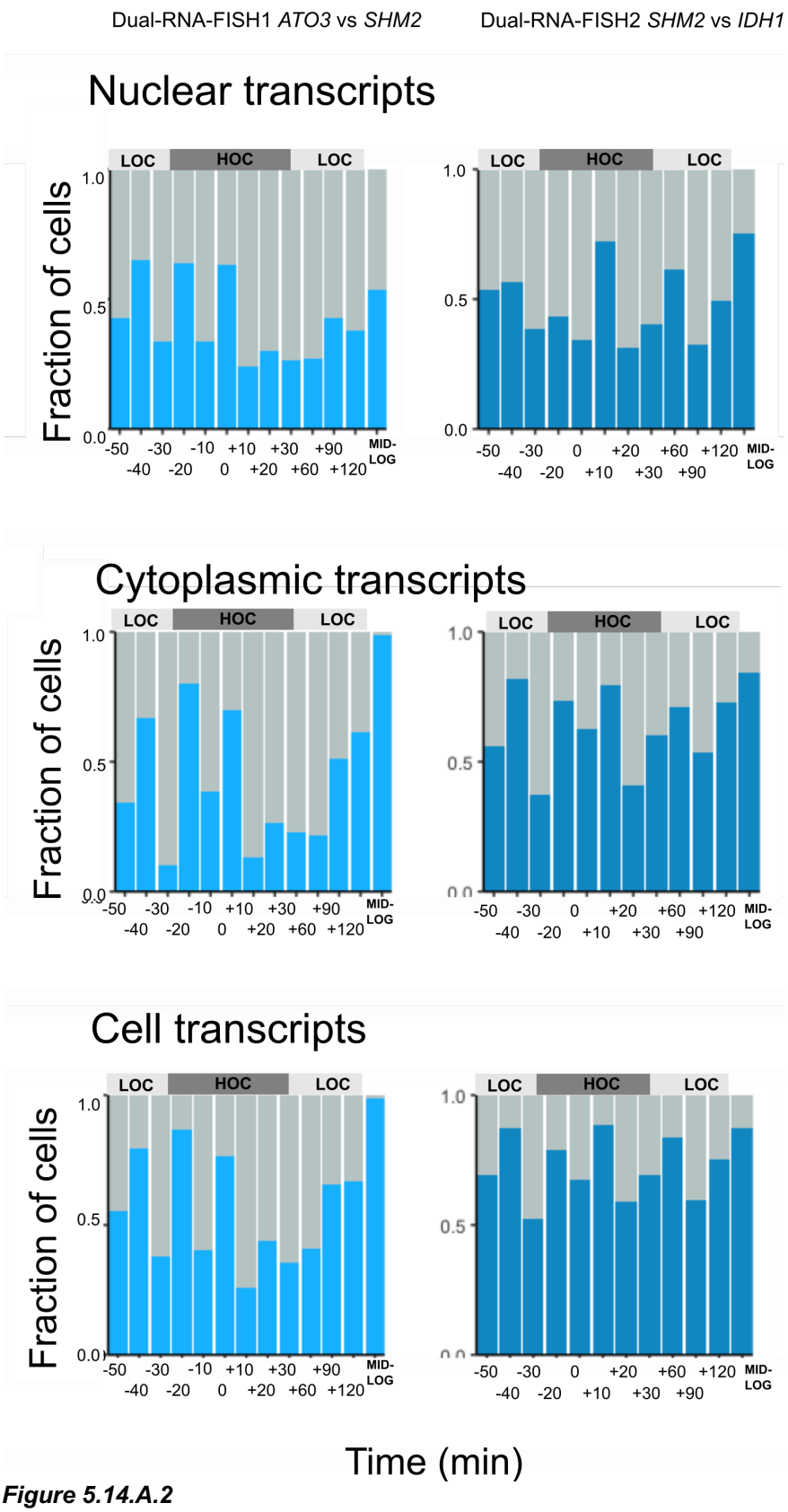

Figure 5.14.A.2

A.

IDH1

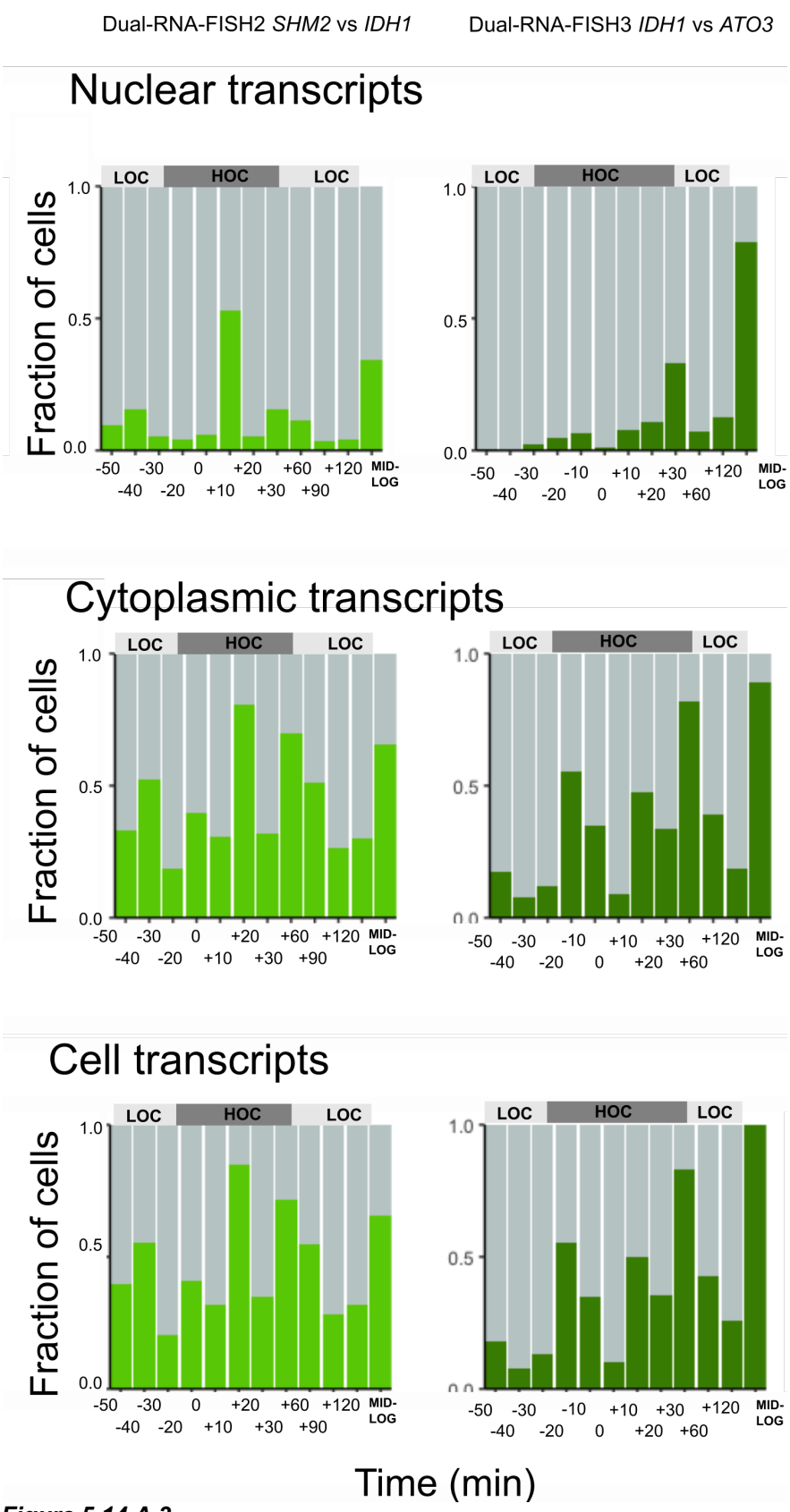

Figure 5.14.A.3

B.

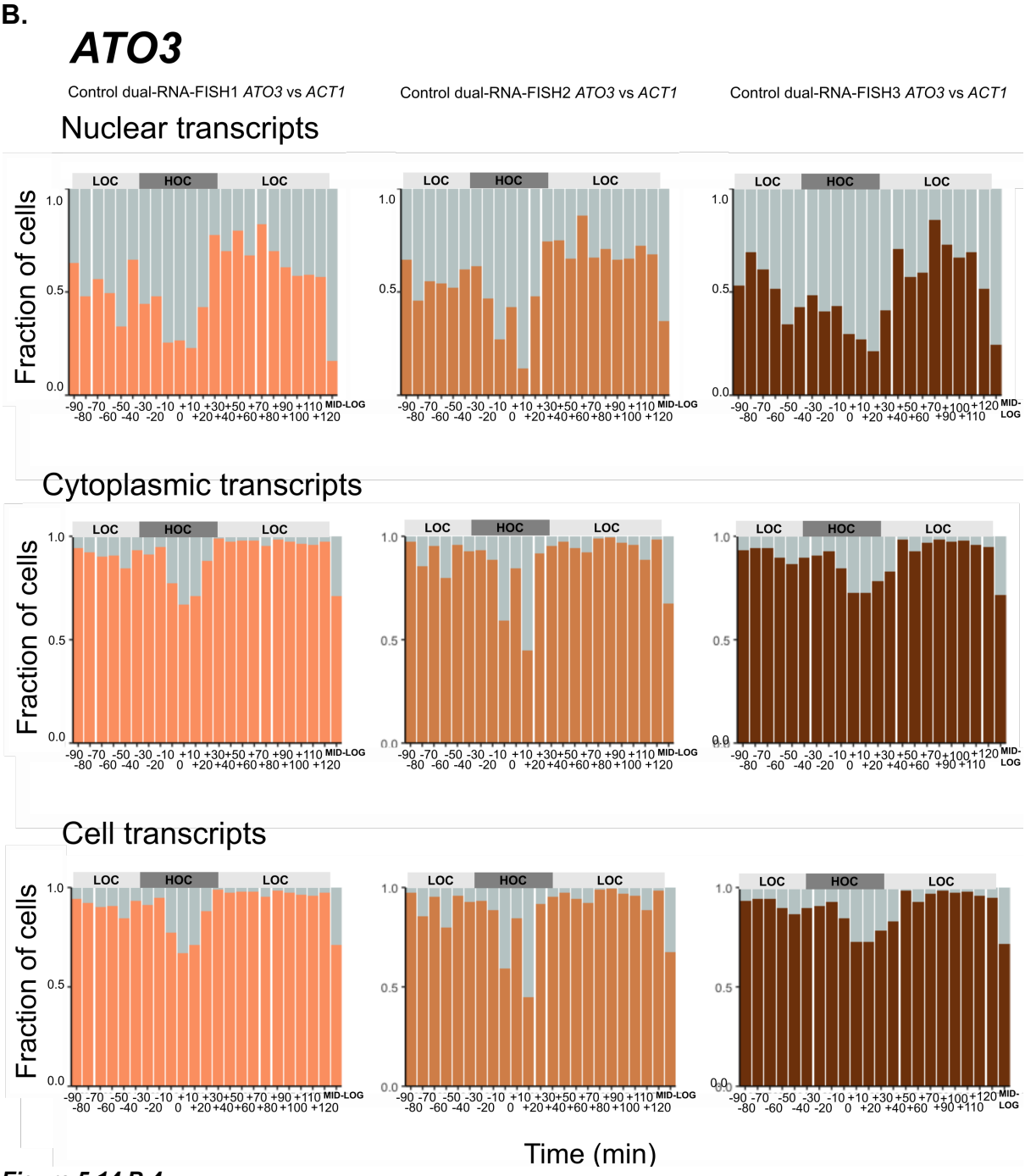

Figure 5.14.B.4

B.

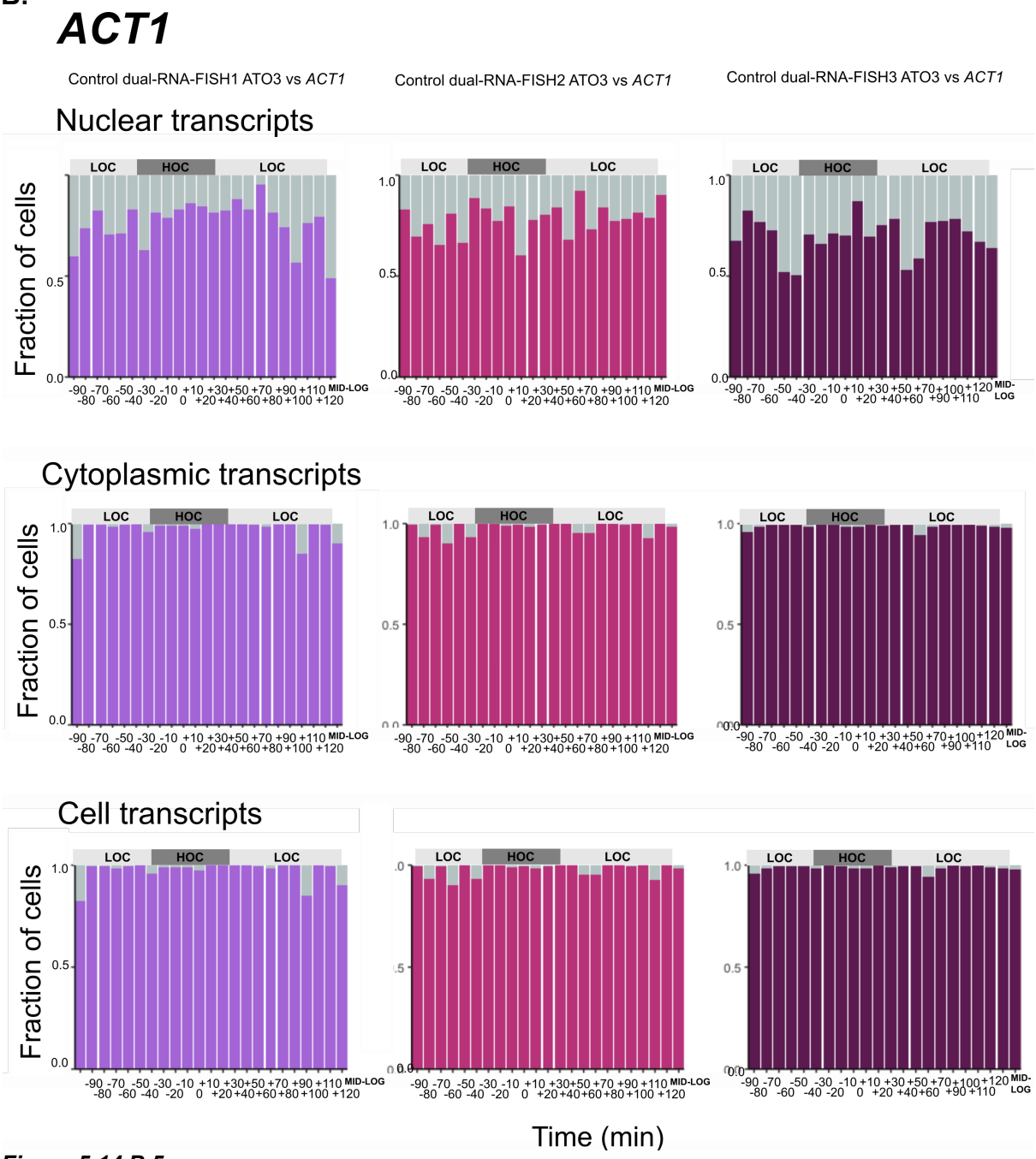

Figure 5.14.B.5

Figure 5.14.A.1,A.2,A.3,B.4 & B.5 The fraction of expressing cells oscillates over the YMC

Bar chart of the fraction of expressing (colour) or non-expressing (grey) cells for each sampling timepoint along the YMC and mid-log phase, of each replica of each target transcripts. For nuclear (1), cytoplasmic (2) and cell (3) transcripts. Colors indicate the different experimental repeats. ***A.*** *Single and dual-FISH experiments: (**5.14.1**) ATO3 levels are in yellow, orange, red. (**5.14.2**) SHM2 levels are in light and dark blue; (**5.14.3**) IDH1 levels are in light and dark green.* ***B.*** *Control dual-FISH experiments: (**5.14.4**) ATO3 levels are in shades of brown; and (**5.14.5**) ACT1 levels are in shades of purple. Upper panels indicate the phase of the YMC; HOC vs LOC. Time shown in minutes relative to the point of lowest dissolved oxygen levels in media (dO_2 %) found across the YMC, displayed as "0", "MID-LOG": Mid-logarithmic phase.*

Bar charts in Figure 5.14 indicate oscillation in the number of expressing cells over the YMC. There, similar oscillations of the fraction of expressing cells can be observed between FISH experiments for a same target transcript, while differences in exact proportions of expressing cells at specific timepoints are evident between replica due to experimental variability. The lowest minima and highest maxima between repeats, between the different timepoints of the YMC and between mid-log samples are indicated in Table 5.3.

First, it is notable that the majority of the mid-log cells express the *ACT1* transcript (shades of purple) in their cytoplasm, supporting the efficiency of the smRNA-FISH labelling procedure and giving confidence that cells lacking transcripts are real and not artifacts of poor probe penetration into the cells (Figure 5.14).

Next, the data obtained from mid-log cultures (Doubling time, DT = ˜2.08h) is compared with the samples obtained over the YMC (growth rate = 0.072h^{-1}, YMC period = 3h20min & DT = ˜9.62h).

Table. 5.3 Range of the percentage of cells expressing each target transcripts

A. *Between the different timepoints of the YMC.* ***B.*** *For mid-log samples. The lowest minima and highest maxima between repeats are shown.*

		Dual-RNA-FISH			Control dual-RNA-FISH	
Culture	**Expression**	**ATO3**	**SHM2**	**IDH1**	**ATO3**	**ACT1**
YMC	In-nucleus	1 – 67	17 – 72	0 – 53	13 – 87	50 – 95
	In-cytoplasm	14 – 94	2 – 82	0 – 80	45 – 99	82 – 100
	In-cell	15 – 96	18 – 89	3 – 85	47 – 99	83 – 100
Mid-log	In-nucleus	20 – 54	48 – 75	34 – 79	16 – 36	49 – 90
	In-cytoplasm	66 – 82	84 – 88	66 – 89	67 – 71	90 – 98
	In-cell	70 – 82	88	66 – 100	72 – 84	91 – 98

First, a recap of the data for the range of cells expressing individual transcripts in the nucleus or cytoplasm is shown in Table 5.3 for mid-log cells compared to YMC samples. In mid-log cultures, a high proportion of cells express *SHM2*, *IDH1* and *ACT1*, with minima of 48, 34 and 49% of cells expressing transcripts in-nucleus and 84, 66 and 90% of cells expressing transcripts in-cytoplasm. In the YMC, at timepoints for which the proportion of expressing cells is at their peak, similar or slightly higher proportions of cells expressing *SHM2* and *IDH1* are found compared to mid-log phase. The proportion of cells expressing *ACT1* is relatively similar in YMC and mid-log cultures. However, the proportion of cells expressing *ATO3* is higher (at times of optimal expression) in the LOC phase of the YMC than in mid-log cultures. These results are coherent with previous findings characterizing *ATO3* as a stationary phase transcript (Gash et al. 2000, Martinez et al. 2004, Radonjic et al. 2005) and for which the expression is higher in slow-growth culture, as opposed to *ACT1, SHM2 and IDH1* (to a lesser extent) for which expression is higher in high-growth than slow-growth cultures (Table 5.2.B vs C) (data from Holstege et al. 1998 vs Lahtvee et al. 2017).

The results in (Figure 5.14) support the following interpretation of events throughout the YMC. The fraction of cells expressing *ATO3* transcripts (shades of orange and brown, Fig.5.14), is lower in the HOC phase and higher in the LOC phase. The proportion of cells which contain *SHM2* nuclear and cytoplasmic transcripts (shades of blue, Fig.5.14) is at its peak during the HOC phase and lower, though still relatively high, in LOC phase. The first replica for *SHM2* shows a peak in early HOC phase, while the second replica for *SHM2* displays an increase in expressing cells in the late HOC phase. The number of cells presenting *IDH1* transcripts (shades of green, Fig.5.14) in-nucleus and in-cytoplasm, is high during the late HOC phase (particularly

in late HOC), and at low during the LOC phase of the YMC. Finally, the fraction of cells expressing *ACT1* transcript (shades of purple, Fig.5.14) is relatively constant over the YMC, providing proof of high labelling efficiency of smRNA-FISH probes and low experimental noise. These observations are applicable when considering the expression of transcript in-nucleus, in-cytoplasm and in cell, although trends are stronger for cytoplasmic and cell transcripts compared to nuclear transcripts, for which the fraction of expressing cells is more variable.

Finally, along the YMC and in mid-log phase samples, for all target transcripts, the fraction of cells containing cytoplasmic transcripts is most often equal or higher to the fraction of cells containing nuclear transcripts as observed in Figure 5.14. Notably there are exceptions, such as the behaviour of the *SHM2* transcripts and a few sampling timepoints where the opposite is found and nuclear transcript levels are higher. The maxima presented in Table 5.3 also indicate more cells show cytoplasmic than nuclear transcripts.

To give a few detailed examples, when comparing maxima of the fraction of expressing cells between repeats of the *ATO3* FISH experiments, up to 27% of cells possess *ATO3* nuclear transcripts in the second half of the HOC phase (+10) compared to up to 87% of cells in the LOC phase. Trends are similar when looking at the cytoplasmic transcripts, although more cells are found to possess transcripts; a maximum of 72% of cells are expressing in late HOC phase (+10) for up to 99% of cells in LOC phase.

The maximum percentage of cells showing *IDH1* in late HOC phase, is of 53% at +10 for the first replica and of 33% at +30 for the second when considering nuclear

transcripts. Accordingly, the maximum fraction of cells expressing cytoplasmic transcript at these timepoints is high and between 80 to 82%. The fraction of cells outside the late HOC is low and oscillate between 0 and 15% for transcripts in-nucleus and 0 to 55 % for transcripts in-cytoplasm.

The proportion of cells expressing *ACT1* stays relatively high and constant over the YMC, with the fraction of cells expressing nuclear transcripts shifting between 50 and 95%, and the fraction of cells expressing cytoplasmic transcripts changing between 82 and 100%.

For *SHM2* more variability was observed between the experimental repeats, making conclusion more challenging to draw. Depending on the repeat, a peak is observed in early or late HOC phase, with the fraction of expressing cells going up to 64 or 72% for nuclear transcripts. Meanwhile the percentage of cell with cytoplasmic transcripts is relatively high over the cycle with maxima of 79 or 80% in HOC. In the LOC phase of the cycle, levels stay relatively high with percentage oscillating between 17 and 65% for nuclear transcripts and between 10 and 82 % for cytoplasmic transcripts.

5.II.4.2 At all times during the YMC a small proportion of cells is detected without transcripts

Along the YMC, some cells miss transcripts (Figure 5.14, light grey bars). In fact, around a fifth of the population do not express oscillating and constant transcripts in-nucleus. Moreover, around a tenth (or less for *ACT1*) of the population do not contain oscillating transcripts in-cytoplasm along the YMC as opposed to mid-log phase samples for which almost all cells express cytoplasmic transcripts. (Figure S.7, in Appendix shows an example of an RNA-FISH image showing cells with low and no expression of transcripts). This leads to question why some cells do not express

transcripts in-nucleus and in-cytoplasm over the YMC. A few possibilities are considered here. First, perhaps the cells showing no cytoplasmic transcripts are dead. Second, it may be that they have sufficient protein product and are subject to feedback mechanisms to limit transcription. Third, it may be that these cells are incapable of expressing these transcripts in-nucleus or in-cytoplasm because they are newly born or due to their metabolic state. Finally, the detection of cells missing nuclear transcripts is possibly due to the combination of the stochastic nature of transcription, the 10 min time-course sampling along the YMC and the snap-shot microscopy technique employed here. Indeed, the detection of cells without transcripts was mentioned previously in studies using smRNA-FISH (Silverman et al. 2010, Brown et al. 2018) and is certainly a characteristic of single-cell techniques as methods including microscopy (Zenklunsen et al. 2008) or even single-cell RNA-Seq report a high frequency of zero observations for some genes characterized as noisy (Slovin et al. 2021).

5.II.5 Conclusions

In conclusion, differences in the proportion of expressing cells are notable between transcripts in YMC. Most importantly, variation in the fraction of expressing cells is observed along the YMC for all antagonist transcripts. These changes follow, to some extent, similar trends to global transcription and transcript levels (Figure 5.9). This suggests that the proportion of cells expressing or not a particular transcript in the population is at least, in part, responsible for the global transcript oscillations previously recorded in Tu et al. 2006, Kleveck et al. 2004 Kuang et al. 2014, Feltham et al. 2020.

5.II.6 Discussion

5.II.6.1 Fast changes of ON-OFF transcription state along the YMC

Clearly, if transcription events are rare, the probability of capturing cells with nuclear transcripts decreases. The counter arguments might also be true concerning the few timepoints for which more cells are detected expressing *SHM2* transcript in-nucleus compared to in-cytoplasm. With the use of a fixed microscopy technique such as RNA-FISH, the detection of transcription events is limited to the exact time at which the cells are sampled and fixed (Femino et al. 1998, Raj et al. 2008, Zenklunsen et al. 2008). In spite of this, results seem to indicate that transcription events are infrequent depending on the time and phases of the YMC in slow-growth synchronous populations but also in mid-log phase for *ATO3* (Figure 5.14).

First, as fewer cells are observed with nuclear transcripts than cytoplasmic transcripts, a greater variability is detected between repeats for the proportion of cells that contains transcripts in-nucleus compared to proportion of cells presenting transcripts in-cytoplasm. This for both YMC and mid-log samples. Second and conclusively, the fraction of non-expressing and expressing cells alternate rapidly during the YMC and between timepoints (10 min intervals). Indeed, big changes are observed in the proportion of non-expressing nuclei, meaning that the production of transcripts and the switch between an ON and an OFF transcription state is most likely a fast and dynamic process, in particular for *ATO3* and *IDH1* over the YMC.

5.II.6.2 Changing degradation rates are likely to be involved in the regulation of transcript levels over the YMC

The fact that higher proportions of cells are found to express transcripts in-cytoplasm compared to in-nucleus (Figure 5.14) could first and simply indicate that as transcription occur in cells, rapid export of transcripts to the cytoplasm follows, making it more likely to find more cells with cytoplasmic transcripts than nuclear, at times for which global target transcript levels are peaking. Accordingly, global transcripts levels are higher in-cytoplasm than in-nucleus (Figure 5.9) It could also indicate that mRNA decay is lower than the production rate of transcripts, leading to some accumulation of transcript in the cytoplasm. Nevertheless, cytoplasmic transcripts seem to undergo fast turnover rates, since the proportion of cells without cytoplasmic transcripts or transcript at all (in-cell) also alternate rapidly between low and high levels for some timepoints along the YMC (Figure 5.14). Therefore, degradation processes are expected to play an important role in the overall regulation of transcripts levels along the YMC.

In fact, it was proposed that the width and phase of the transcript peaks detected along the YMC showed direct proportionality to the transcript half-lives found in exponentially growing cultures (Soranzo et al. 2009), with early-HOC phase transcripts showing lower half-lives than transcripts peaking in late-HOC, in turn presenting lower half-lives than transcripts peaking in LOC (Soranzo et al. 2009). The data collected for the transcript picked for this study (Holstege et al. 1998, Geisberg et al. 2014) however do not seem to validate this postulate and show that some transcripts do not follow the trend described in Soranzo et al. 2009. Indeed, in one study transcripts half-lives are higher for *IDH1* compared to *ACT1* and for *ACT1* compared to both *ATO3* and *SHM2* (Table 5.1.B, Holstege et al. 1998). In the other study, both *SHM2* and *ACT1* show

higher half-lives than *IDH1*, itself showing a higher T1/2 compared to *ATO3* (Table 5.1.C, Geisberg et al. 2014).

Nonetheless, recent results from the lab (Part II student Noah Crook and Dr. Angel) using NET-Seq and RNA-Seq data from Dr. Xi (Feltham et al., 2020) agree with the RNA-FISH results and indicate changing degradation rates over the YMC for oscillating transcripts (Figures S8, Appendix).

5.II.7 Conclusions

In conclusion, here, results indicate fast changes in transcription rate (ON-OFF status of transcription in cells), but also that transcript turnover rates in slow-growing synchronous populations of the YMC might actually differ from the ones found for high-growth cultures since they most likely change along the metabolic cycle.

5.II.8 Results

Summary statistics revealed the presence of gene expression heterogeneity in “expressing” cells (RNA > 0) of YMC populations. Here, the distributions of transcripts in “expressing cells” were examined in detail to assess mRNA cell-to-cell variability in the population.

5.II.8.1 Individual cells possess a high degree of variability in levels of expression of individual transcripts

Previously, mean RNA numbers (Fig. 5.9, Figure S.6 appendix), as well as noise levels (Fi. 5.13) were shown to oscillate along the YMC. Accordingly, distributions of RNA numbers within the cell population must change across the cycle. The following analysis investigates whether this is the case or not.

RNA distributions were plotted for cells expressing transcripts in-nucleus, in-cytoplasm and in-cell, with histograms for details (Figure 5.15), and boxplots for ease of comparison (Figure 5.16).

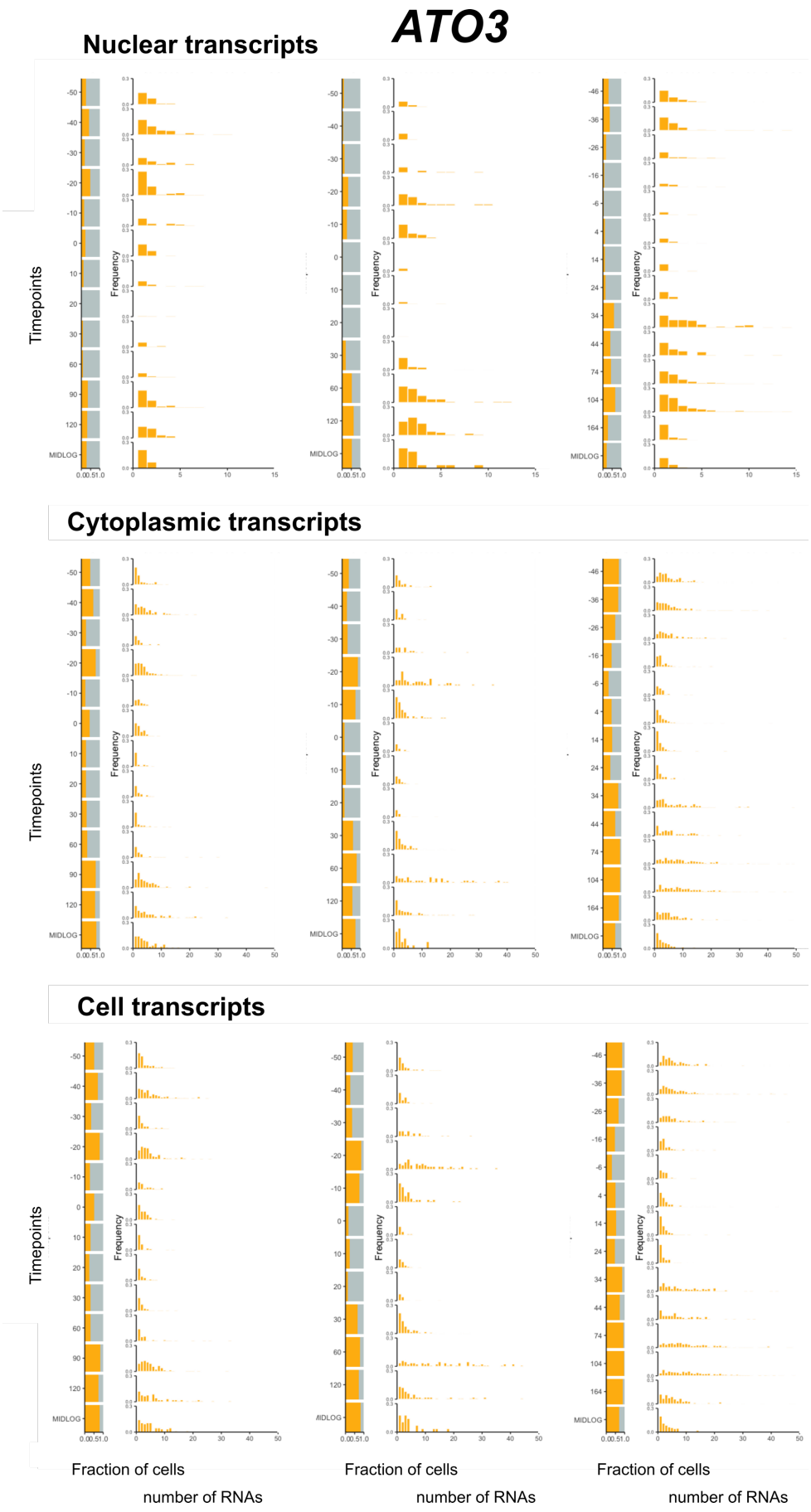

Figure 5.15. ATO3 (Single-RNA-FISH, type i & Dual-RNA-FISH, type iii)

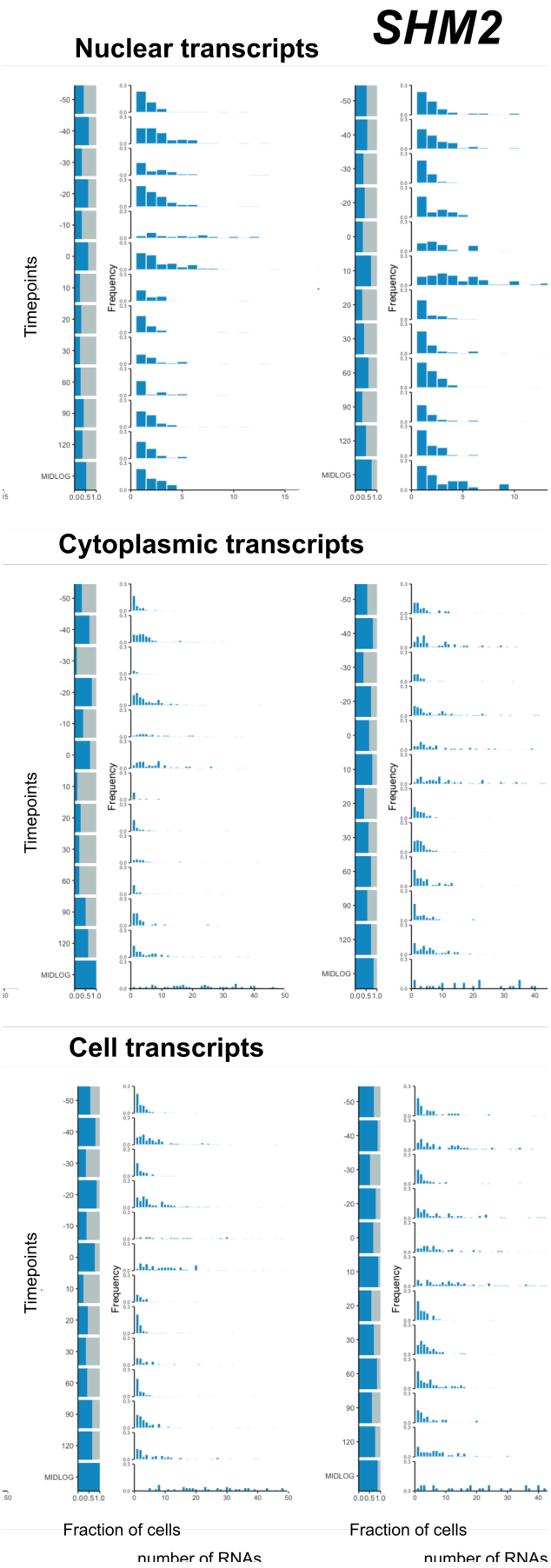

Figure 5.15. SHM2 (Dual-RNA-FISH, type iii)

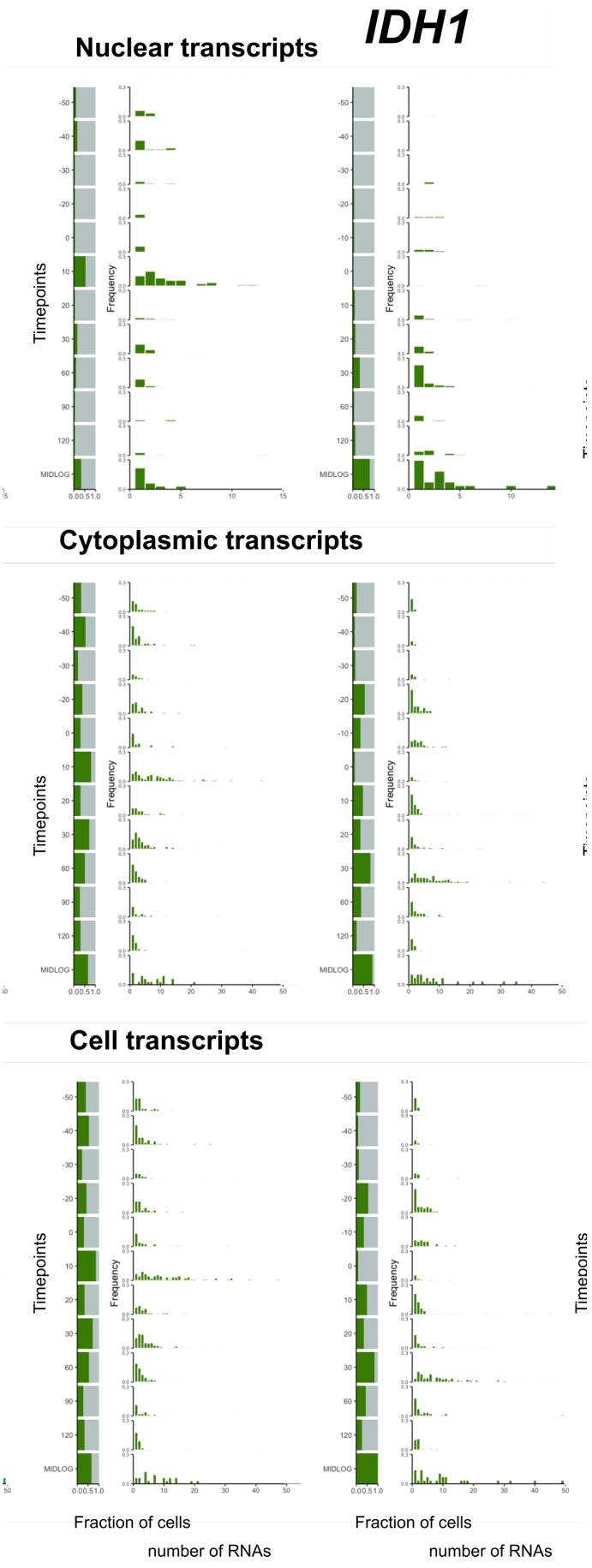

Figure 5.15. IDH1 (Dual-RNA-FISH, type iii)

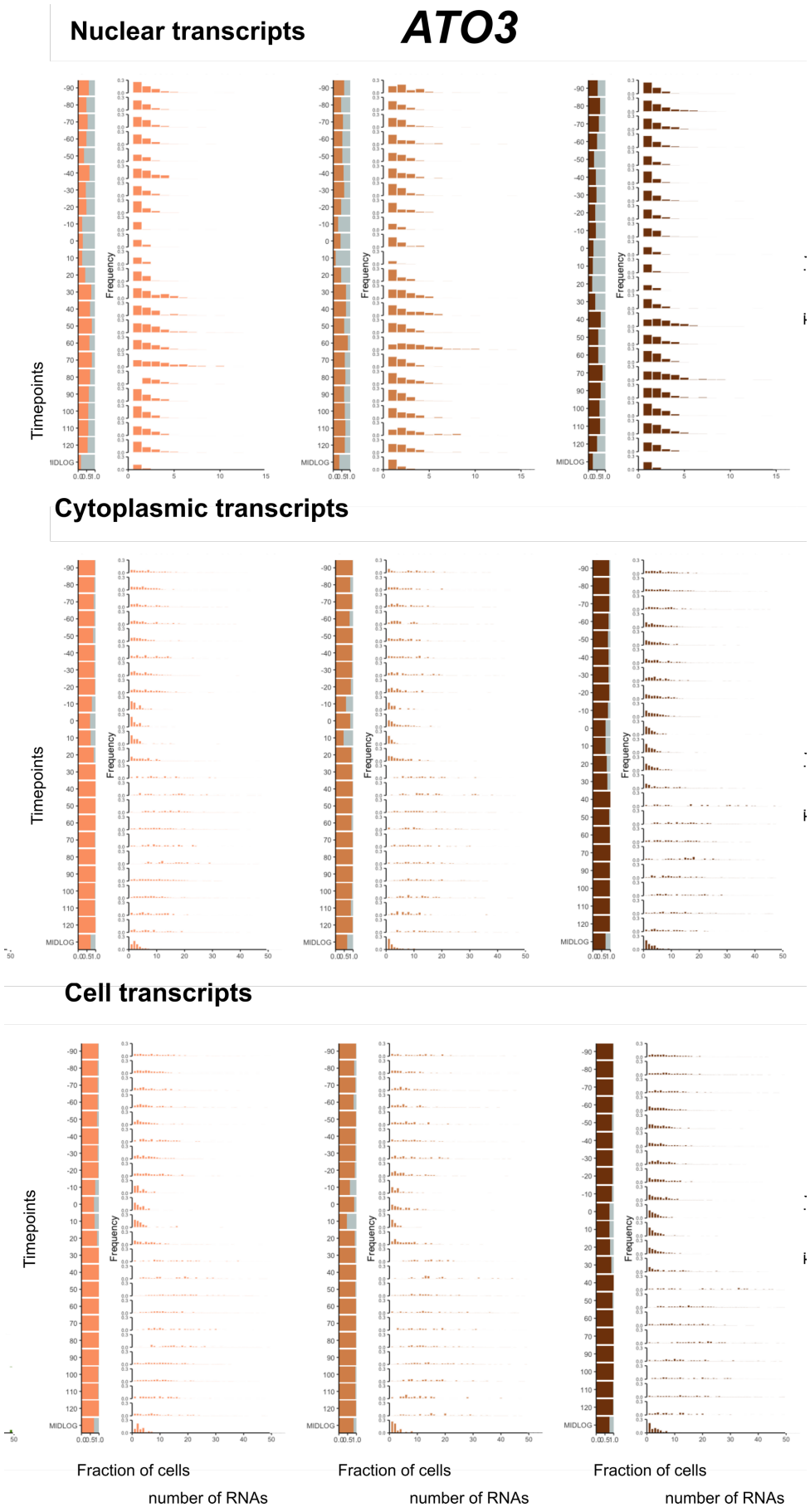

Figure 5.15. ATO3 (Control-Dual-RNA-FISH, type ii)

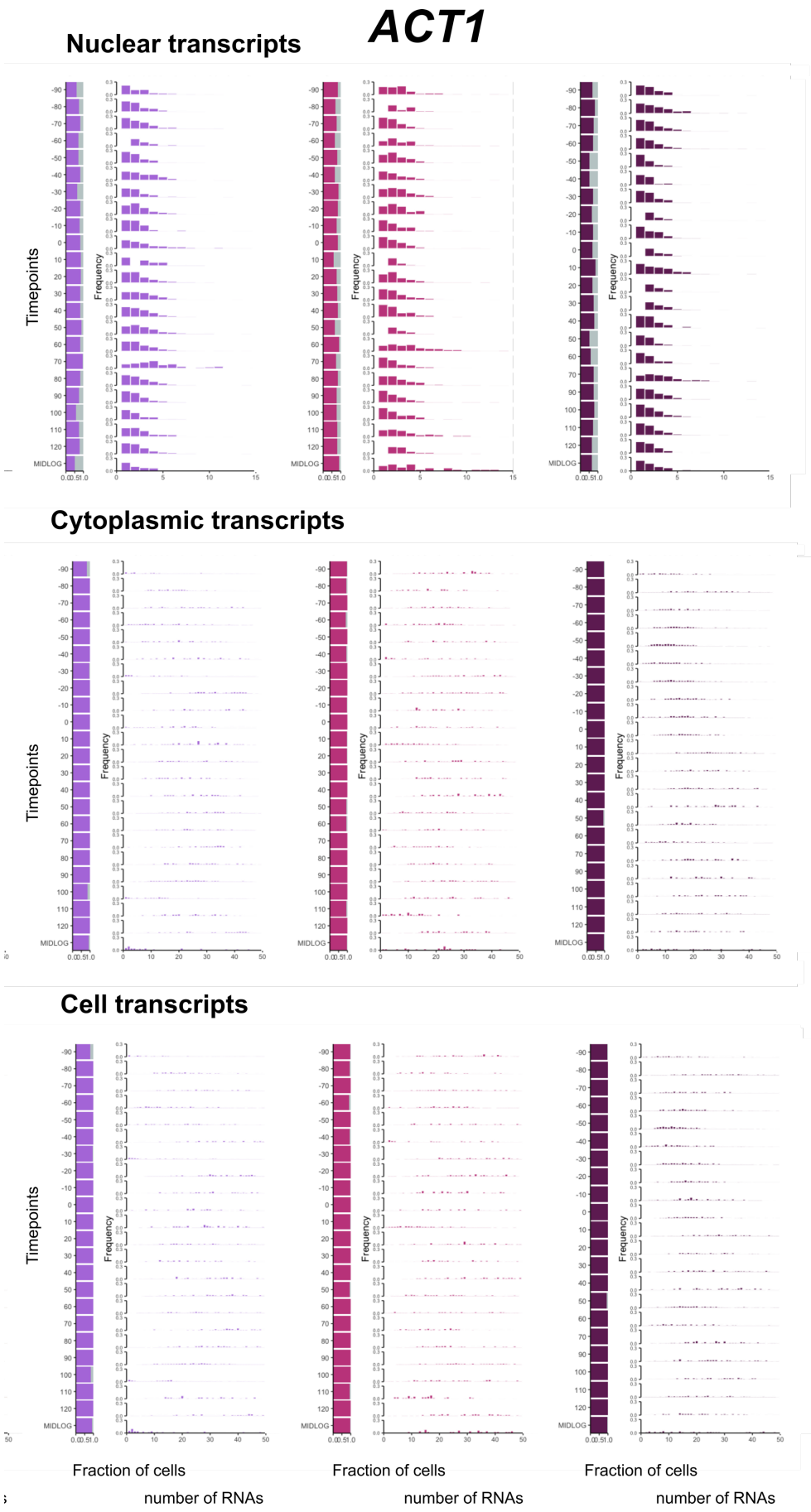

Figure 5.15. ACT1 (Control-Dual-RNA-FISH, type ii)

Figure 5.15 High degree of variability in levels of expression across the YMC

Histograms of RNA numbers for cells expressing in-nucleus (A), in-cytoplasm (B) or in-cell (C) (RNA number > 0). For each sampling timepoint along the YMC and mid-Log phase, of each replica (1,2,3) of each target transcripts (ATO3 in shades of orange and brown, SHM2 in shades of blue, IDH1 in shades of green and ACT1 in shades of purple). On the left of each histogram a barplot of the fraction of cells expressing (colour) or not (grey) transcripts is shown. Time shown in minutes relative to the point of lowest dissolved oxygen levels in media (dO_2 %) found across the YMC, displayed as "0", "MID-LOG": Mid-logarithmic phase.

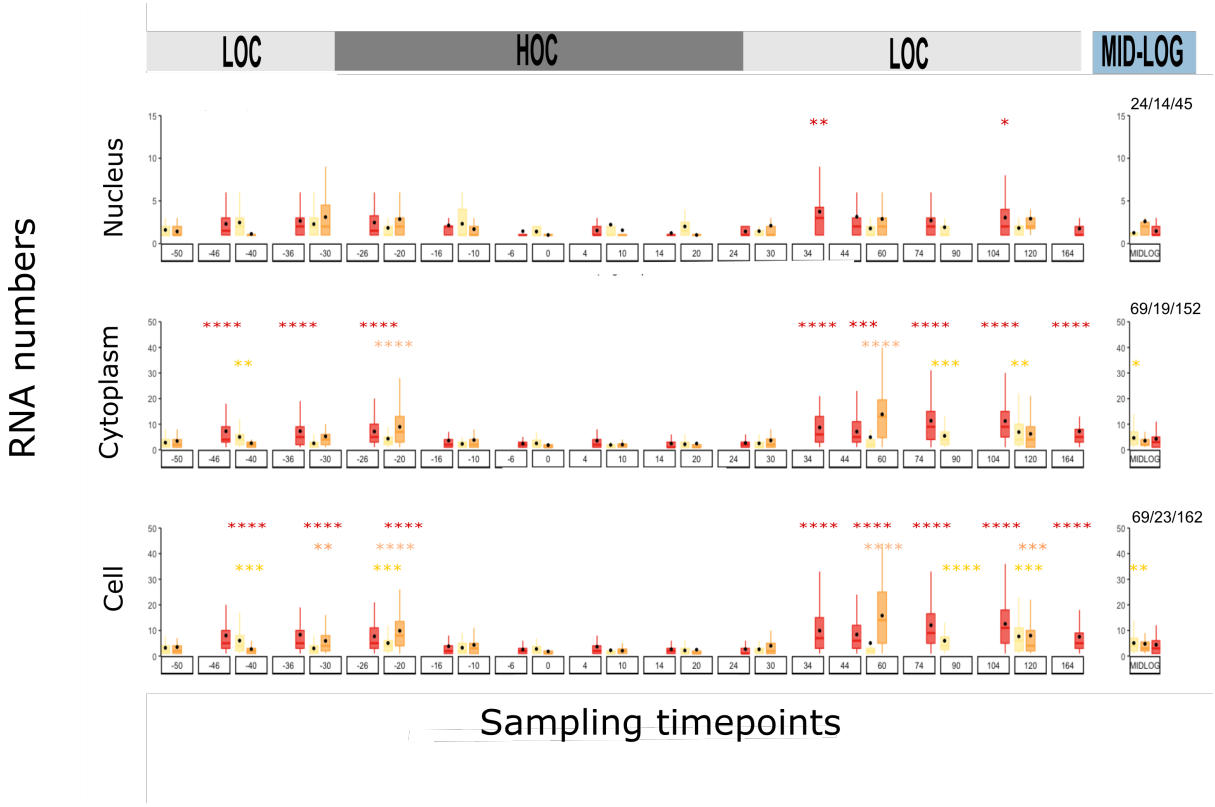

Figure 5.16. ATO3 (Single and Dual-RNA-FISH, type iii)

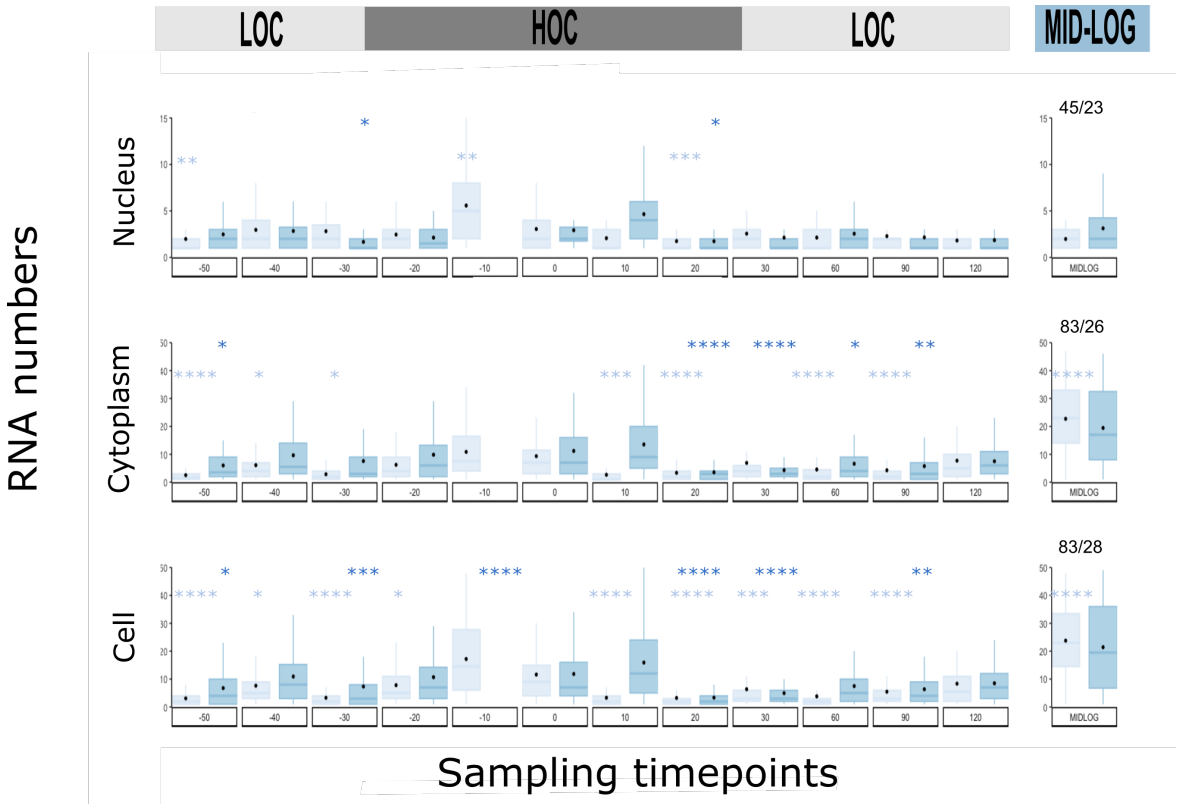

Figure 5.16. SHM2 (Dual-RNA-FISH, type iii)#

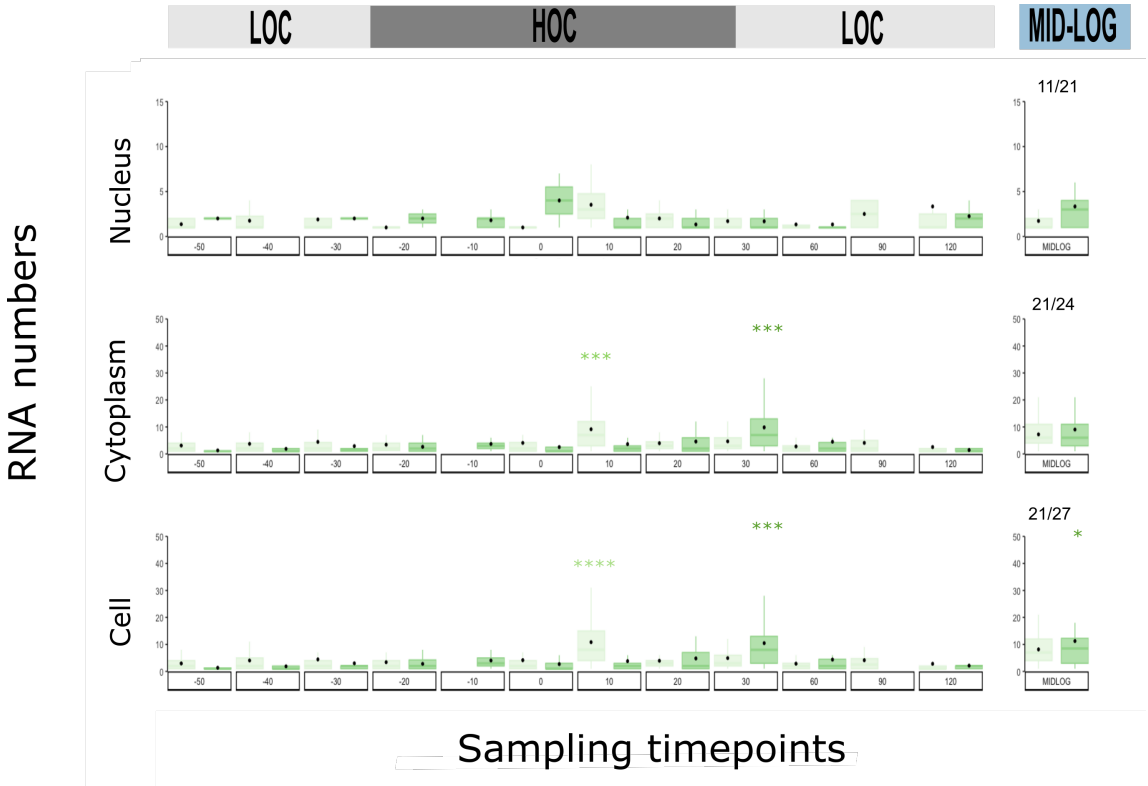

Figure 5.16. IDH1 (Dual-RNA-FISH, type iii)

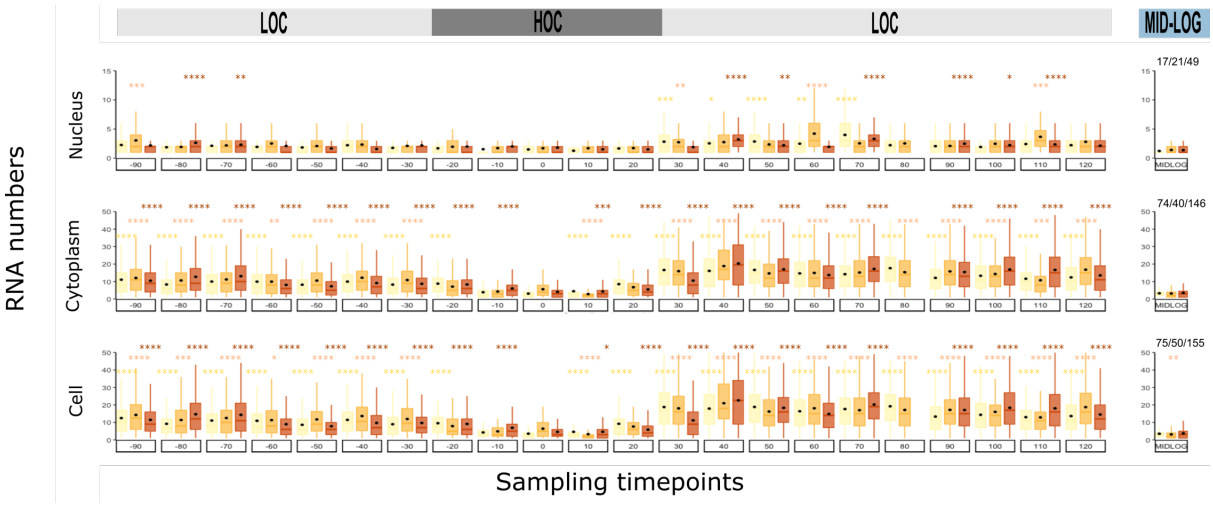

Figure 5.16. ATO3 (Control-Dual-RNA-FISH, type ii)

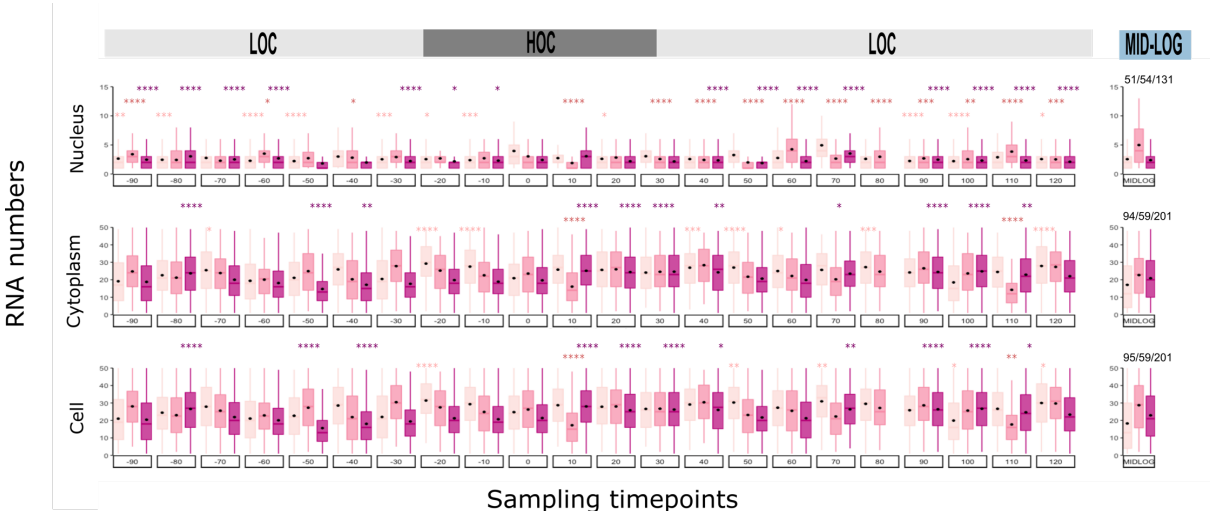

Figure 5.16. ACT1 (Control-Dual-RNA-FISH, type ii)

Figure 5.16 High degree of variability in levels of expression across the YMC

Boxplots showing distributions of RNA numbers from each cell, for each sampling timepoint along the YMC and mid-log phase. Time shown in minutes relative to the point of lowest dissolved oxygen levels in media (dO_2 %) found across the YMC, displayed as "0", "MID-LOG": Mid-logarithmic phase. This for each replica of each target transcripts A. ATO3 in yellow, orange and red, B. SHM2 in blue, C. IDH1 in green, D. ATO3 in brown and E. ACT1 in purple. The upper background indicates the phases of the YMC. Asterisks indicate time points for which RNA levels are significantly different than the point of lowest dO_2 % in the YMC, displayed as "0". (p-value<0.05, Wilcoxon rank sum tests, multiple pairwise-comparisons, Bonferroni p.adjust. method, H0: no difference in RNA numbers between samples). Note: Statistical tests could not be performed on nuclear RNA numbers for ATO3's second repeat (orange) and IDH1 repeats (green) due to the small sample size (low number of expressing cells along the cycle). Due to the low cell number captured in mid-Log phase, the number of cells detected with RNA (RNA number >0) is indicated above each boxplot for mid-Log samples.

First, histograms in Figure 5.15 show the distribution of RNA numbers within the cell population of each sampling timepoint taken throughout the YMC, for each target transcript, for “expressing” cells. Moreover, on the left side of each histogram, a bar plot indicates the fraction of expressing cells for each timepoint.

Along the YMC, for each target transcript, as the number of cells expressing in-nucleus, in-cytoplasm or in-cell increase, the distributions of RNA numbers expand and shift towards higher values (skewed distributions) indicating an increase in mean transcript levels. In other words, the increase in mean RNA levels follows the increase in numbers of expressing cells. This can be observed by comparing Figure 5.14 and 5.9. Most importantly, the histograms clearly show gene expression heterogeneity in yeast cell populations. A raise in heterogeneity is observed at timepoints for which RNA numbers increase, with cells showing a wider range of transcript numbers.

Second, boxplots in Figure 5.16 help observe changes in distributions widths along the YMC. Wilcoxon rank sum test (non-parametric equivalents of the t-test, working with unequal sample sizes) were used to work out multiple pairwise-comparisons between the timepoints. Results of statistical tests performed on distributions are indicated on plots to support the analysis and comparison of RNA levels between timepoints. Stars indicate samples for which distributions are significantly different than the RNA distribution found at the time of lowest oxygen level “0” recorded in mid-HOC phase of the YMC. It is notable that slight differences in nuclear transcripts are easily picked up by the statistical test thus clear trends can’t be determined for nuclear distributions.

All replica are plotted for the different target transcript in both Figure 5.15 and 5.16.

For ***ATO3*** (annotated LOC transcript; in yellow, orange and red for the data set and in

shades of brown for the control set) populations in LOC show a high proportion of expressing cells and wider RNA distributions compared to those of the population at the lowest oxygen level “0” or in HOC phase. LOC timepoints also show wider distribution ranges than mid-Log timepoints.

For ***SHM2*** (early HOC annotated transcript in shades of blue) trends are less clear as (i) higher RNA numbers are detected all along the YMC and (ii) the variability between repeats seems higher. Nevertheless, a high percentage of expressing cells as well as broader transcript distributions and higher RNA levels are observed in mid-HOC (-10 to +10). In late-HOC, fewer cells are expressing, narrower distributions are found and significantly lower RNA levels are present. In early to mid LOC, the percentage of cells expressing slightly increases with the distribution width and RNA levels in cytoplasm. In late LOC, the proportion of expressing cells, distributions and RNA levels are lower than in mid-HOC but higher than in early LOC. Mid-log samples display slightly narrower distributions for nuclear transcripts and broader distributions for cytoplasmic and cell transcripts than mid-HOC.

IDH1 (late HOC annotated transcript in shades of green) exhibit wider RNA distributions and higher RNA numbers in mid-HOC (0 and +10) for nuclear transcripts. Cytoplasmic RNA levels are significantly greater in late-HOC (+10 and +30). These corresponds to times for which the percentage of “expressing cells” is higher. Cells expressing RNA outside this window are rare. These cells show very low nuclear RNA number and low cytoplasmic RNA numbers. Similar or perhaps slightly higher distribution ranges are observed between late-HOC samples and mid-log ones.

Finally, ***ACT1*** (shades of purple) distributions are wide for both nuclear and cytoplasmic transcripts. *ACT1* shows wide variability between timepoints despite

presenting constant global metrics. Although nuclear RNA levels are relatively constant over the YMC (Figure 5.9), slight differences in nuclear transcripts are easily picked up by the statistical test, therefore showing differences (greater or lower levels) between different timepoints and the time of lowest oxygen level “0”. With the exception of the third repeat showing a slow increase in RNA levels in late-HOC, the proportion of cells expressing transcripts in-cytoplasm or in-cell, together with their distributions and RNA levels also stay relatively stable along the cycle.

Collectively, results indicate gene expression heterogeneity in cells expressing “periodic and flat transcripts” in-nucleus and in-cytoplasm (and thus in cells).

5.II.9 Discussion

5.II.9.1 Different modes of regulation of transcripts along the YMC

Rapid changes have been observed in the proportion of cells expressing transcripts and for mRNA distributions of periodic transcripts along the YMC. As shown in Figure 5.14 and Table 5.3, (i) the minimum and maximum proportions of expressing cells along the YMC varies between target transcripts. Moreover, the breadth of the distributions for RNA numbers contrasts between target transcripts (Figure 5.15). Together, these results indicate different modes of regulation of transcription and or transcript processes.

First, the proportion of expressing cells, in addition to the RNA distributions, of *ACT1* nuclear transcripts are high and relatively constant over the YMC. RNA numbers and distributions of *ACT1* are higher than they are for *ATO3*, *SHM2* and *IDH1*. Cytoplasmic levels follow similar trends, thus indicating perhaps a constant degradation rate over the YMC (Figure 5.14, 5.15 & 5.16). Clearly, high levels of *ACT1* are produced at all times along the YMC, with minimal noise levels (Figure 5.12 & 5.13). Therefore, *ACT1* seem to possess a more constitutive mode of transcription and a relatively high transcription rate.

Second, more cells express the *SHM2* transcript in-nucleus at all times, both throughout the YMC and in mid-log phase, than they do for *ATO3* or *IDH1* transcripts. Indeed, a minimum of 17% of cells are expressing *SHM2* nuclear transcript at all recorded times during the YMC, with still a relatively high proportion of expressing cells in the LOC phase (Fig.5.14), despite *SHM2* being described as a “HOC phase transcript” (Tu et al. 2005, sequencing data from Dr. Xi). *SHM2* also shows, higher nuclear RNA levels and broader distributions than *ATO3* or *IDH1* in mid-log samples, while RNA numbers and distributions are slightly lower and narrower than those of *ATO3*, but higher and wider than those of *IDH1* along the YMC (Fig.5.15 & 5.16). Finally, noise levels are lower for *SHM2* than for the other antagonist transcript (Figure 5.12 & 5.13). Thus, constitutive expression of *SHM2* is believed to take place in some cells at all times during the YMC, while an increase in transcription rate might happen in other cells in early to mid HOC phase (broader nuclear distributions). Finally, as cells are found with *SHM2* cytoplasmic transcripts outside of the HOC phase, it is possible that RNA degradation rates might be lower for *SHM2* than they are for *ACT1*, *ATO3* and *IDH1*.

As seen for WT budding yeast cells in exponential growing cultures (Table 5.1.B, Holstege et al. 1998), it seems that both *ACT1* and *SHM2* show higher transcriptional frequencies (mRNA/hr) than *ATO3* and *IDH1* even in slow-growing synchronized cultures of the YMC. Indeed, *IDH1* and *ATO3* show different changes in RNA distributions. On one hand, *IDH1* shows almost no expressing cells at times outside its peak, except during the late HOC phase (85% in-nucleus) (Figure 5.14), and if such cells exist they possess very low RNA numbers (Fig.5.15 & 5.16). This indicates a shorter time of expression for *IDH1*, agreeing with previous NET-Seq and RNA-Seq profiles for *IDH1*, showing a narrower window of expression for *IDH1* along the YMC (Figure 5.2, data from Dr. Xi). On the other hand, *ATO3* shows more cells expressing low levels of transcripts outside its peak time (LOC) compared to *IDH1*, but still less than *SHM2* (Figure 5.14). Indeed, *ATO3* shows low proportions of expressing cells in late HOC phase and high proportions of expressing cells at LOC phase. Furthermore, the peak expression of *ATO3* also spends over a larger time-window than *IDH1* (Figure 5.14).

Accordingly, in comparison to *SHM2* and *ACT1*, the proportion of expressing cells is mostly higher at the peak of global expression for *ATO3* and *IDH1*. This indicates that transcription is rapidly switched ON and OFF for these target transcripts, attributing a more noisy or “bursty” mode of transcription to *ATO3* and *IDH1* along the YMC.

Note that for all periodic transcripts examined here, cells expressing transcripts outside “their peaks” have a tendency to show narrower distributions, while cells expressing higher RNA numbers show broader distributions at the peak, perhaps indicating a difference in the mode of transcription for these cells.

Finally, both the proportions of cells expressing cytoplasmic transcripts together with the cytoplasmic RNA numbers quickly oscillate along the YMC, suggesting dynamic degradation rates for these transcripts as described previously.

Together these results demonstrate difference in gene expression heterogeneity levels between target transcripts and timepoints/phase of the YMC and support distinct mechanisms of regulation of transcript levels between model transcripts.

5.II.10 Conclusions

This work shows gene expression heterogeneity at the transcript level is detected in single cells from exponentially growing culture but most importantly in synchronized cultures showing metabolic oscillations, indicating that individual cells present different gene expression profiles and perhaps metabolic states despite global metabolic synchronisation at the population level.

First, low gene expression noise is discovered at the transcript level in synchronized populations, for genes transcribed by RNA Pol II. It is higher for *ATO3* and *IDH1* compared to *SHM2* and *ACT1*. These results are in accordance with transcriptional frequencies found for target transcripts in high-growth exponential phase (Holstege et al. 1998). Gene expression noise arises mainly from the ON-OFF transcription and transcript status of cells but is also detected in cells expressing transcripts. Finally, noise levels oscillate over the YMC.

Second, the fraction of expressing cells is found to oscillate for the different antagonist targets (*ATO3*, *SHM2* and *IDH1*), while it stays relatively even over the YMC for the

control transcript *ACT1*. As the proportions of cells expressing antagonist transcripts follow the trends of the population-averaged gene expression profiles, gene expression heterogeneity arising from the ON-OFF transcription status of cells seem to be responsible for overall transcription oscillation patterns. However, a high degree of variability in levels of expression of individual transcripts is also found in expressing cells and mean expression levels as well as noise levels also oscillate, at a lower amplitude, in expressing cells. For these cells a wide range of distributions of RNA numbers are detected along the YMC.

Third, as the proportion of cells expressing transcripts in-nucleus or in-cytoplasm changes rapidly, transcription rates and degradation rates seem to be highly regulated along the YMC and for the different target transcripts. Moreover, the different modes of transcription dynamics suggested are in line with gene expression noise results.

Thus, to conclude, global changes in transcript levels along the YMC correspond to oscillations in transcription and transcript levels within cells, together with a fluctuation in the number of cells within the population expressing these particular transcripts at variable levels. Here, 2 types of regulation seem to be in place within the cell population. The transcript status of cells in synchronous populations is proposed to be characterized by digital and analogue modes, a concept found in Antoniou-Kourounioti et al. 2020 biorxv. The digital mode is characterized by binary states, i.e. cells and their transcript status are either ON or OFF with fixed transcription rates. The analogue mode on the other hand, shows gradual and smooth increase or decrease in transcription rates (Munsky & Neuert. 2015). Figure 5.17, shows a cartoon of these mechanisms suggested to take place in synchronized cells of the YMC.

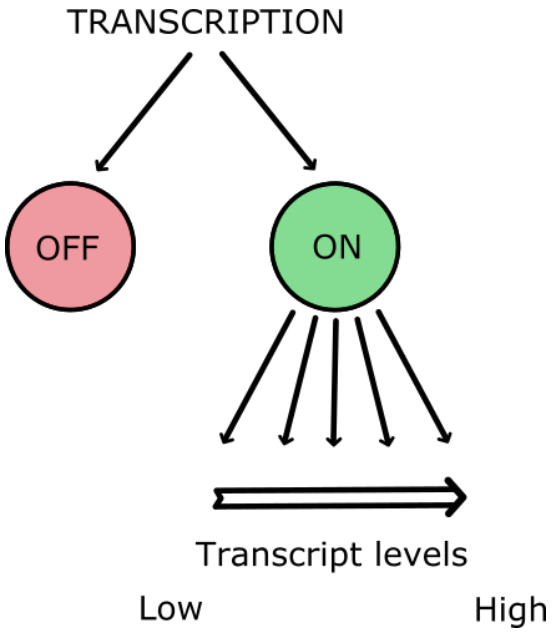

Figure 5.17 Cartoon of the Digital + Analogue switches in YMC populations

Transcription can switch from an ON to an OFF state. When tanscription is ON, transcription rates can smoothly increase or decrease. Concept from Antoniou-Kourounioti et al., 2020 biorxv.

In YMC populations, some cells are expressing a particular transcript, while others don't. The fraction of cells expressing this transcript fluctuates along the YMC. Thus, the transcription and transcript status of the cells are either ON or OFF (Figure 5.17). However, different levels of expression are observed for each transcript and transcript levels in single cells gradually increase and decrease, at various time over the YMC depending on the target transcript (Figures 5.15 & 5.16). Thus, gene expression of the synchronous yeast cell population seem to be regulated by the two modes (Figure 5.17).

Chapter 6

Transcription dynamics alter upon metabolic changes

The findings from chapter 5 revealed gene expression cell-to-cell heterogeneity in YMC cultures and differences in changes of RNA distributions along the metabolic cycle, between the oscillating transcripts picked for this work, suggesting different modes of regulation for these transcripts during the YMC. These lead to questions about which mechanisms and factors might be involved in such gene expression regulation and cell-to-cell heterogeneity.

6.1 Introduction

6.1.1 Sources of gene expression stochasticity

Understanding gene expression noise and its sources can enhance the comprehension of gene expression regulation. In the context of metabolic cycling, it is important to identify the relationships between key metabolic pathways and transcript levels regulation.

Both extrinsic and intrinsic noise contribute to gene expression stochasticity. While extrinsic factors affect multiple genes and their expression, intrinsic factors only affect a particular gene. A number of the extrinsic factors play a major role in stochasticity, including the position in the cell division cycle, cell size, the number of RNA polymerases or ribosomes and their availability in cells, but also other factors such as ageing and environmental factors (Perrez-Carrasco et al. 2020, Takhaveev & Heineman. 2018). Intrinsic noise on the contrary, emerges from intrinsic sources directly influencing a gene's transcription or a transcript's translation (Elowitz et al. 2002, Swain et al. 2002, Raser & O'Shea. 2004). In fact, a large proportion of gene expression noise arises from the process of translation (Ozbudak et al. 2002, Newman et al. 2006). Concerning transcriptional noise, typically the unique combination of

transcription factors, the particular promoter architecture and chromatin landscape can influence transcription stochasticity (Elowitz et al. 2002, Jones et al. 2015; Raj & van Oudenaarden. 2008).

As results from this study indicate the presence of both digital and analogue switches involved in the expression of antagonist transcripts, and averaged gene expression profiles of these targets over the YMC are shared by many other genes (gene clusters from Tu et al. 2006, Kleveck et al. 2004, Kuang et al. 2014, Feltham et al. 2020), it is likely that extrinsic factors are involved. Nevertheless, because gene expression noise fluctuates between target genes and over the YMC for each target, intrinsic factors might also be involved. Whether only one or the other or even both factors are responsible for the binary and the graded transcript status of cells remains to be determined.

In this study both extrinsic and intrinsic factors will be examined. In chapter 8, the effect of potential extrinsic factors on the transcript status of single cells will be explored, with the aim of characterising further sub-populations within the synchronous populations, and identifing key characteristics of metabolic HOC/LOC states. In this chapter, intrinsic factors will be investigated by exploring the transcription mode of periodic genes picked for this work over the YMC.

6.1.2 Modes of transcription

Typically, transcription in cells can be characterized by two modes; constitutive transcription and transcription bursts (Figure 6.1). For genes constitutively expressed, transcription initiation is always ON and transcription events are clearly separated in time. For genes expressed in bursts however, transcription initiation toggles from ON to OFF and transcription initiation events are clustered in time, separated by periods of transcription inactivity.

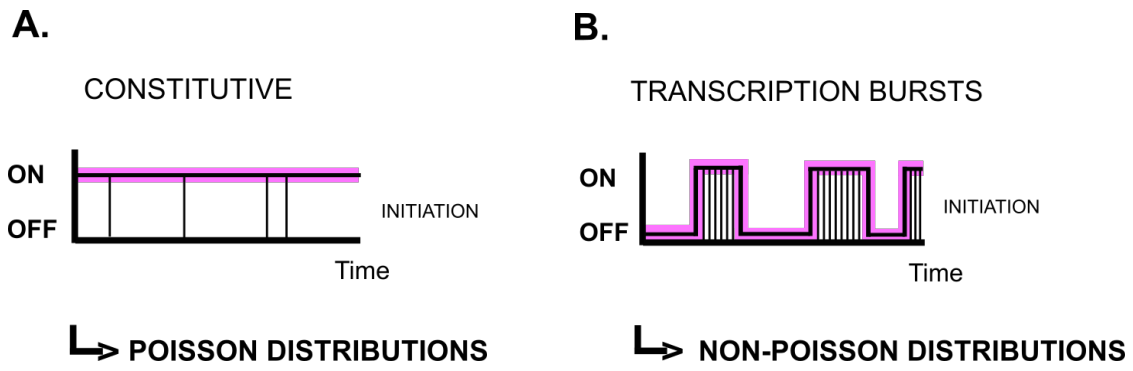

Figure 6.1 Transcription modes

A. *Constitutive mode of transcription,* ***B.*** *Transcription bursts. Vertical lines indicate transcription initiation events, horizontal lines indicate the time during which transcription initiation is ON or OFF. Adapted from Zenklusen et al, (2008).*

Thus as opposed to constitutive expression, during transcriptional bursts, many transcripts are produced within a short period of time (Zenklunsen et al. 2008, Brouwer & Lenstra. 2019). The presence of low noise in yeast when compare to complex eukaryotes (Golding et al. 2005; Sanchez et al. 2013) seemed to indicate that as opposed to mammalian cells (Raj et al. 2006), yeast cells mostly show constitutive expression of genes. Nevertheless, the existence of the two mode of expression were reported in *Saccharomyces cerevisiae* (Blake et al. 2003, Blake et al. 2006, Zenklusen et al. 2008, Lenstra et al. 2015) and transcriptional bursting is proposed to be the

primary cause of cell-to-cell variability (Raj et al. 2006, Raj & van Oudenaarden. 2008). It means that large differences in RNA numbers are observed between cells expressing transcripts in bursts.

Because in chapter 5 noise levels and RNA distributions were detected to change throughout the cycle for the different oscillating transcripts picked for this work, with higher levels of noise and wider RNA distributions at times, this lead to the question of whether noise, could result, in part, from transcriptional stochasticity/bursting. Aiming to identify the gene expression modes of the transcripts examined in this study during the YMC, the RNA-FISH data is examined using mathematical modelling, which can be used to make predictions about the mode of transcription.

6.2 Preliminary results

Simply, by comparing probability distributions (probability of occurrence of x number of transcripts) to RNA number distributions from RNA-FISH it is possible to identify gene expression modes (Zenklusen et al. 2008).

6.2.1. Poisson distributions do not fit cytoplasmic RNA distributions from the FISH data

Constitutive gene expression is characterized by a one-state mathematical model of transcription, in which transcription initiation is always ON. According to the one-state model, RNA distributions are expected to follow Poisson Distributions. Poisson Distributions are probability distributions that model the likelihood of an event occurring a given number of times in a given period of time (if the event has a constant rate). In this case the rate corresponds to the mean number of RNA. These distributions

depend on 1 parameter; the mean RNA number, which for constitutive gene expression is expected to be identical to the variance (Sanchez et al. 2013, Zenklunsen et al. 2008, Raj & van Oudenaarden. 2008).

Thus, in order to test whether antagonist transcripts analysed in chapter 5 showed constitutive gene expression or not, Poisson Distributions were fitted to cytoplasmic RNA distributions from the RNA-FISH experiments (chapter 5, Figure 5.15). An example of fit is presented at Figure 6.2. The black line represents the one-state model; i.e. the Poisson distribution expected for the mean RNA number of this sample. Blue bars are nuclear and cytoplasmic RNA distributions from the RNA-FISH experiment.

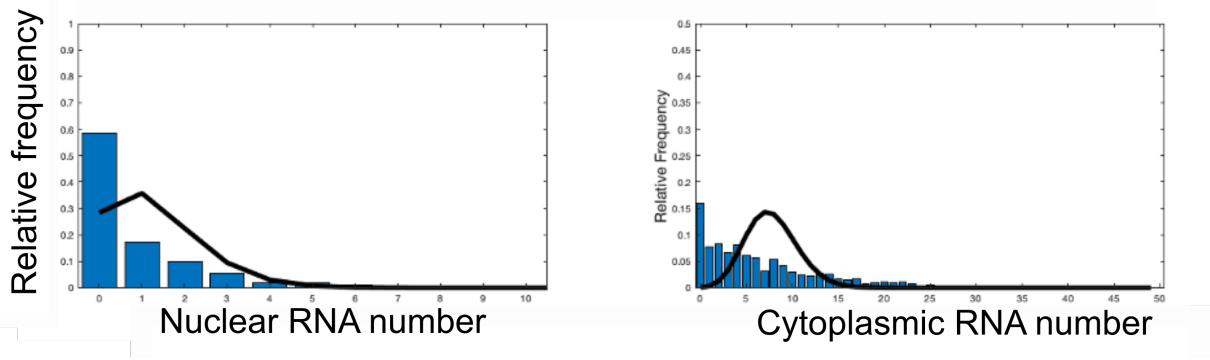

Figure 6.2 Example of Poisson Distribution fit to RNA-FISH distributions

In blue; nuclear and cytoplasmic RNA distributions, in black expected Poisson Distributions, for a sample taken during the YMC (-46min, in LOC phase), for the single label RNA-FISH experiment with ATO3.

Figure 6.3 shows fits for *ATO3*, *SHM2* and *IDH1* along the YMC and in mid-log phase. Kolmogorov-Smirnov (non-parametric) tests were computed to compare the RNA distributions from the RNA-FISH experiments and the probability distributions from the one-state mathematical model (assess the fit of the model to the data). All KS tests indicated the two distributions (model vs data) differed significantly for cytoplasmic RNA numbers (for the 3 transcripts, for the different repeats). i.e. the one-state model does not fit the cytoplasmic RNA distributions. Nevertheless some fits looked better than others indicating that perhaps statistical tests applied to the data are too strict. Therefore, future work might be necessary to validate the results. Additionally, similar fits might be applied to RNA distributions of *ACT1*, the “flat level” transcript.

6.3 Conclusions

In conclusion, periodic genes analysed in this study seem to be mainly 'bursty' in their mode of transcription in YMC cultures.

After all, some samples/RNA distributions along the YMC clearly show non-poisson distributions (deviation from the black line, Figure 6.3), suggesting that transcription occurs in a “bursty” mode for these target transcripts along the YMC and that the degree of burstiness change during the YMC for these transcripts. The results thus indicate that transcription dynamics alter upon metabolic changes. Accordingly, more investigation will be needed to determine whether fluctuating factors, such as histone PTMs (Cai et al. 2011, Shi & Tu. 2013) or other factors such as transcription factors (Rao & Pellegrini. 2011, Sanchez-Gaya et al. 2018) or nucleosome organisation and positions (Nocetti & Whitehouse. 2016) are responsible for such stochasticity of transcription.

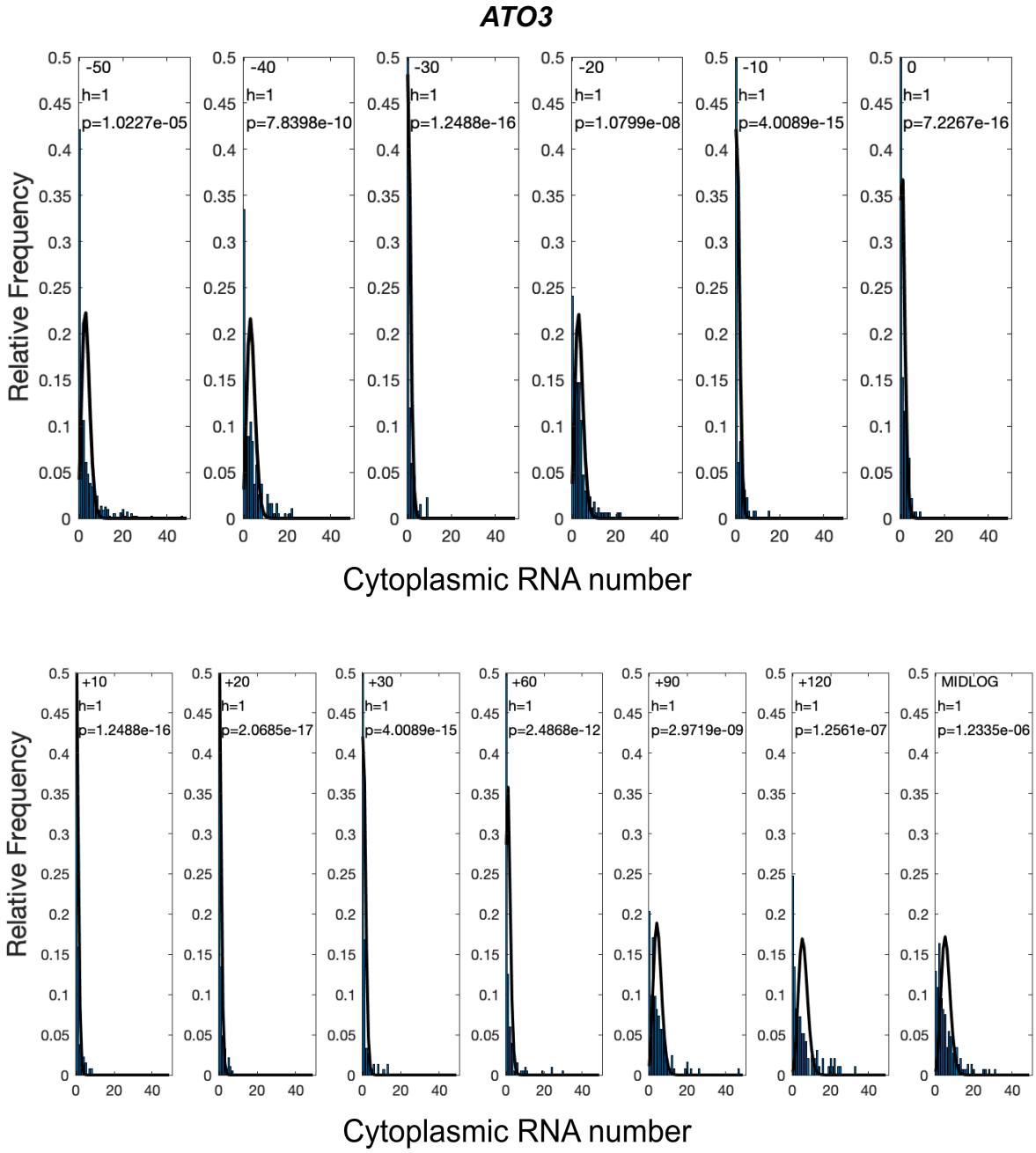
ATO3
-50
h=1
p=1.0227e-05
-40
h=1
p=7.8398e-10
-30
h=1
p=1.2488e-16
-20
h=1
p=1.0799e-08
-10
h=1
p=4.0089e-15
0
h=1
p=7.2267e-16
+10
h=1
p=1.2488e-16
+20
h=1
p=2.0685e-17
+30
h=1
p=4.0089e-15
+60
h=1
p=2.4868e-12
+90
h=1
p=2.9719e-09
+120
h=1
p=1.2561e-07
MIDLOG
h=1
p=1.2335e-06
Relative Frequency
Cytoplasmic RNA number

Figure 6.3.1

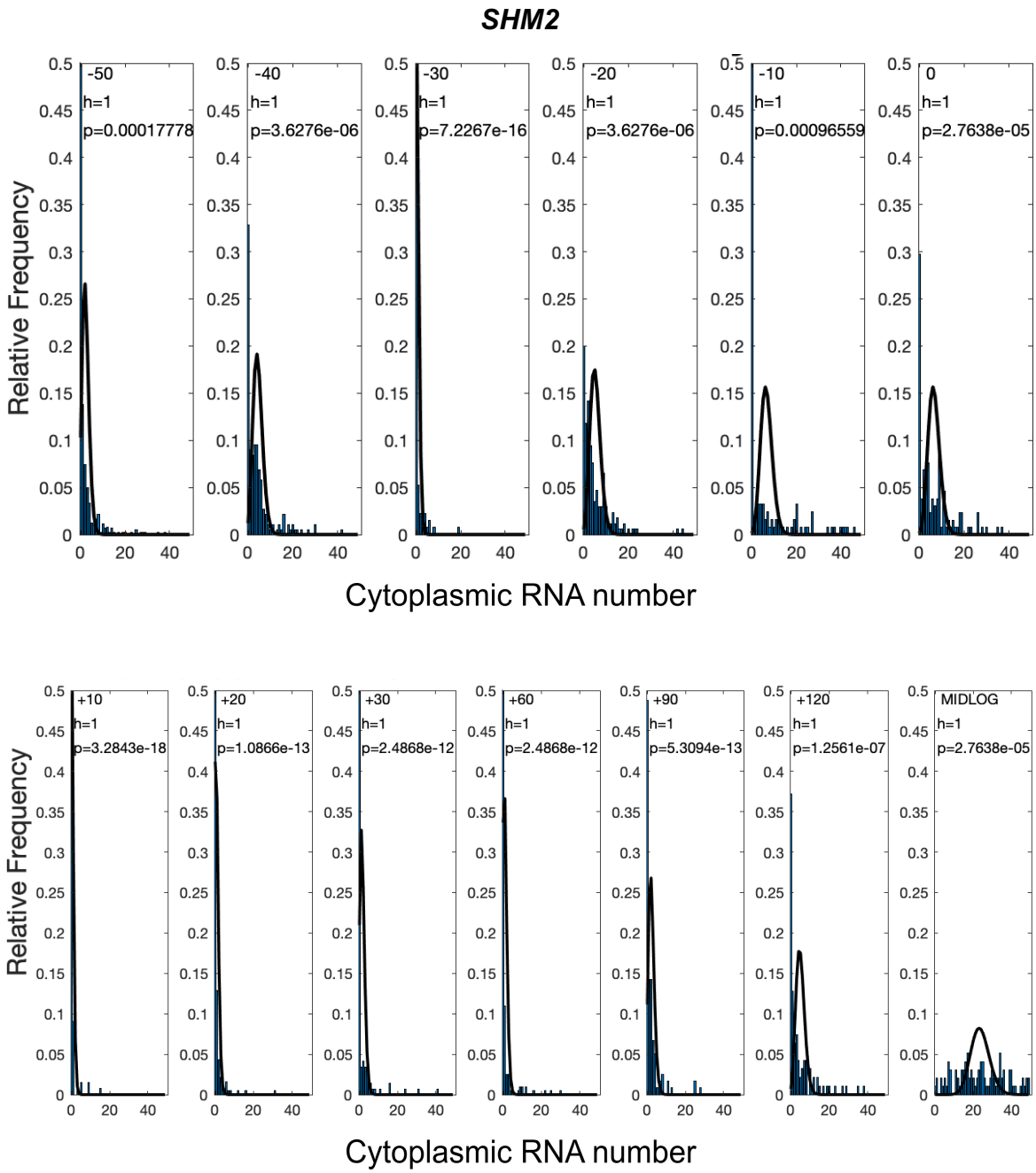
SHM2
-50
h=1
p=0.00017778
-40
h=1
p=3.6276e-06
-30
h=1
p=7.2267e-16
-20
h=1
p=3.6276e-06
-10
h=1
p=0.00096559
0
h=1
p=2.7638e-05
Relative Frequency
Cytoplasmic RNA number
+10
h=1
p=3.2843e-18
+20
h=1
p=1.0866e-13
+30
h=1
p=2.4868e-12
+60
h=1
p=2.4868e-12
+90
h=1
p=5.3094e-13
+120
h=1
p=1.2561e-07
MIDLOG
h=1
p=2.7638e-05
Relative Frequency
Cytoplasmic RNA number

Figure 6.3.2

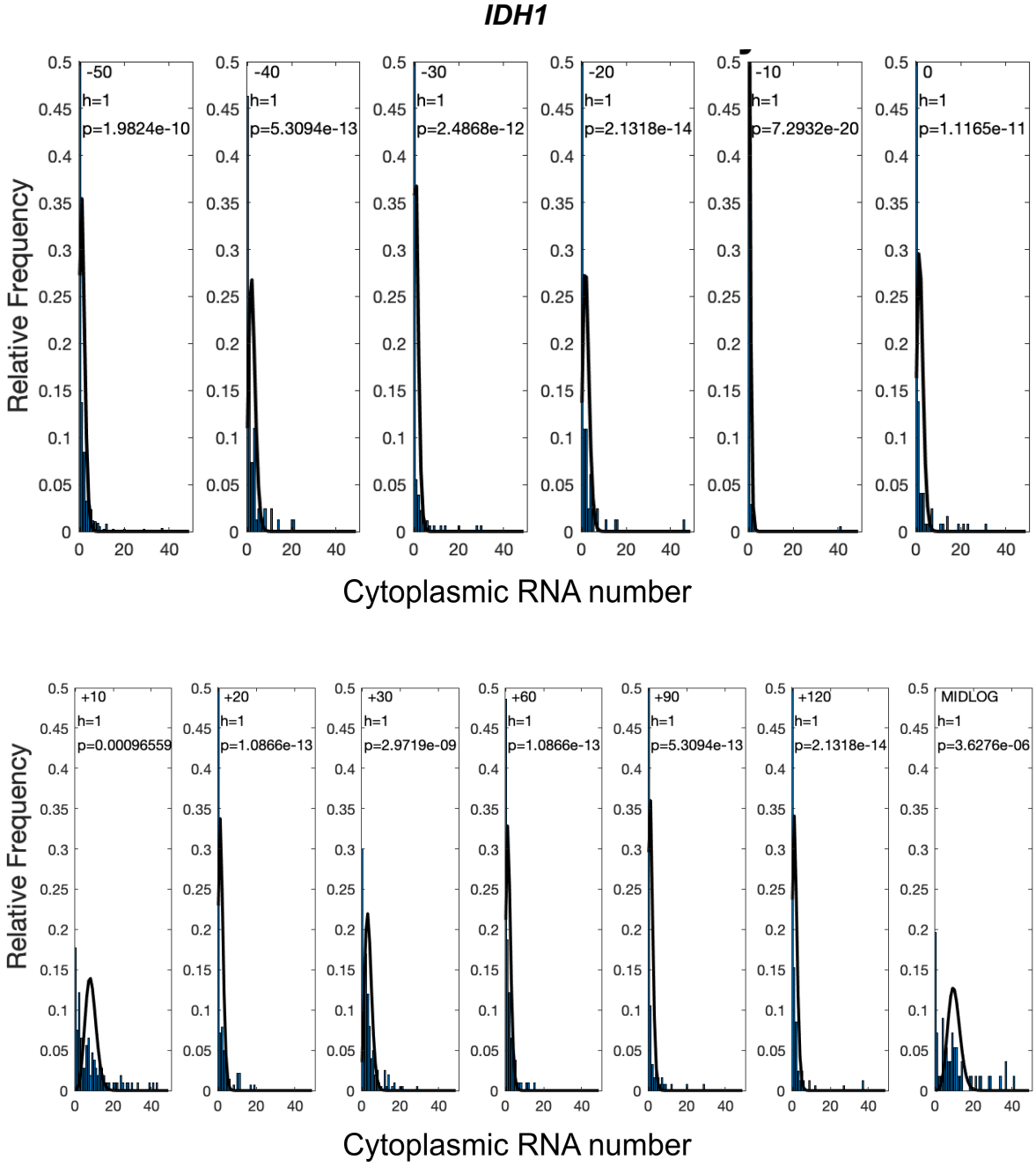

Figure 6.3.3

Figure 6.3.1,2 & 3 Example of Poisson Distribution fits to RNA-FISH distributions

*In blue; cytoplasmic RNA distributions, in black expected Poisson Distributions, for (**1**). ATO3 (dual-labelled FISH 1), for (**2**). SHM2 (dual-labelled FISH 1) and for (**3**) IDH1 (dual-labelled FISH 2). Results of KS tests are indicated on top of each distribution (H0:same distributions, h=1 indicates the null hypothesis is rejected with the p.value indicated). On top of each distribution, time is shown in minutes relative to the point of lowest dissolved oxygen levels in media (dO_2 %) found across the YMC, displayed as "0", "MID-LOG": Mid-logarithmic phase.*

6.4 Future directions

6.4.1 Using a two-state model of transcription

Next, because one-state models do not fit the data, the aim is to test whether a two-state model, characterising transcriptional bursting can. The two state model of transcription, also called the telegraph model (Zenklunsen et al. 2008, Sanchez et al. 2013, Choubey et al. 2015, Choubey et al. 2018) is presented at Figure 6.4. For this model, the promoter of a gene is ON or OFF, thus the transcription is ON or OFF. **a** indicates the rate of switching to the ON state. **b** indicates the rate of switching to the OFF state, **c** is the rate of initiation. **d** is the degradation rate of transcripts. **N** (not shown) is the distributions indicating the number of transcripts accepted. **a**, **b**, and **c** are free parameters while **d** and **N** are fixed.

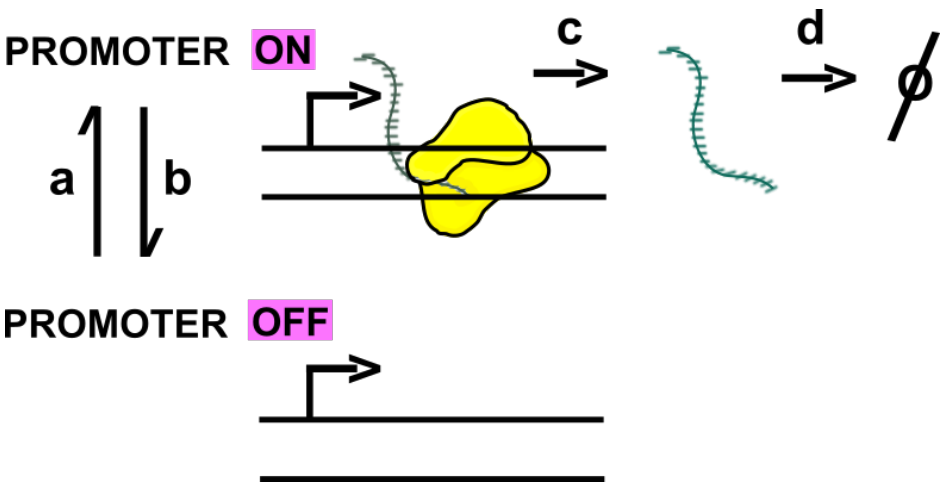

Figure 6.4 Two-state or telegraph model

*Mathematical model for transcription bursts. The promoter of the gene is ON or OFF. Free parameters; **a** = kON = rate of switching to the ON state, **b** = kOFF = rate of switching to the OFF state, **c** = kIN = rate of initiation (transcription while ON state). Fixed parameters; **d**= degradation rate, **N**= Distributions = all transcript numbers possible (0-50). Adapted from Zenklusen et al, (2008) and Brown et al., (2018).*

Importantly, Nascent transcript (NET-Seq) and RNA-Seq data (data from Dr. Xi, Feltham et al. 2020) were used to extract parameter values of the Degradation Rates along the YMC (these were obtained by Dr. Andrew Angel and Part II student Noah Crook). According to these predictions, degradation rates vary along the YMC and usually peak when transcripts levels go down (Figure S8 appendix).

These degradation rates were then used to parameterise the two-state mathematical model. In other words, changing degradation rates were used instead of a fixed degradation rate of transcripts (**d**). As this requires additional assumptions and fitting it greatly complexifies the process of mathematical modelling.

Using the analytical form of the steady state solution of the two-state model from Zenklunsen et al., (2008), a parameter sweep for **a**, **b** and **c** was performed, with changing degradation rates **d**. Finally, probability distributions characterizing transcriptional bursting were obtained.

The future directions for this project thus should involve the next steps; First, the solutions, i.e. probability distributions obtained should be fitted to the RNA distributions from the RNA-FISH experiments, then the fits should be assessed (KS test), finally best fits models could be used to extract the kinetics, i.e. parameters.

Chapter 7

Single cells from high-growth asynchronous mid-log cultures and slow-growth synchronous cultures possess an intrinsic metabolic clock and YMC cultures are organised in sub-populations

7.1 Introduction

7.1.1 Investigation of the concept of an intrinsic gene expression clock

This chapter addresses the question of whether an intrinsic gene expression clock reflecting metabolic states can be detected in YMC populations.

The aim of this work is to test the current ideas that the entire cell population cycles from LOC to HOC during the Yeast Metabolic Cycle, largely supported by the oscillating transcriptome (Tu et al. 2005, Kleveck et al. 2004 Kuang et al. 2014, Feltham et al. 2020) and the work of Silverman et al., who proposed the presence of an intrinsic metabolic clock in yeast single cells, from slow growing asynchronous cultures (growth rate of $0.1h^{-1}$ and doubling time/DT of ˜6.9h), using dual label smRNA-FISH (Silverman et al. 2010). In that work, transcripts whose expression show antagonistic (peaking in different phases of the YMC) or agonistic (both peaking in the same phase of the YMC, "YMC co-expressed") behaviour at the population level, as defined in the early transcriptome studies of the YMC from the McKnight lab (Tu et al. 2005), were proposed to show similar behaviour in single cells. The Silverman et al experiments reported that in asynchronous population under slow growth, many cells were; (i) detected without transcripts, (ii) found to co-express the agonistic transcripts, (iii) found to express one or the other transcript of an antagonist pair but not both.

It is important to point out that the work of Silverman et al. (2010) has some shortcomings. First, the proportion of non-expressing cells is mentioned as 'high' but the precise number or proportion is not stated. Next, they use correlation coefficients which describe how the global population behave but which do not represent the behaviour in single cells. The correlation coefficients from the FISH data are described as corresponding to the ones from the gene expression population-averaged data over the YMC from Tu et al. 2005. This argument is re-enforced (a) by a positive correlation-

of-correlations (0.65) between the 2 metrics (single-cell vs population) and (b) by a significant Wilcoxon rank sum test comparing the correlations of the group of co-expressing pair of transcripts to the group of antagonistically oscillating transcript. However, the smRNA-FISH data showed only weak positive or negative correlation coefficients. Furthermore, out of 11 pairs of antagonist transcripts, only 2 showed significant negative correlations (greatest r = -0.15, P ≤0.005) while 10 out of 11 pairs of "YMC-co-expressed" transcripts show a significant positive correlation (greatest r = 0.52, P ≤0.005). Instead, the range of Pearson correlation coefficients and heatmaps presenting the proportion of cells and their expression status (RNA numbers), displayed with the results, give a better appreciation of correlations at the single cell level. In fact, the single cell data shows that the transcript status in single cells in the slow-growth asynchronous cultures varies widely. Unfortunately, although Silverman et al., (2010) data shows a wide variability of gene expression profiles in single cells from asynchronous cell population, these results are not highlighted but this finding is crucial as it shows that although global trends follow the expected predictions made in the paper, this is not always present in single cells.

Next, based on literature, and predictions from Silverman et al., (2010), a hypothesis is formulated and tested in this chapter.

Similar to expectations for the asynchronous population (Silverman et al. 2010), for individual cells from synchronous populations in the YMC, a high proportion of cells co-expressing transcripts at high levels is expected if the transcript selected are in the "YMC co-expressed" class as defined by Tu et al. (2005), while most cells are expected to only express one transcript or the other when looking at pairs of antagonist transcripts. In fact, these assumptions should be stronger in synchronized populations

of the YMC compared to populations from slow-growth culture used Silverman et al., experiments, which are not synchronized and thus for which a variety of cell behaviours might be expected.

Here, only antagonist (*ATO3, SHM2 and IDH1*) or stable (*ACT1*) transcripts were picked for this study. Therefore, (**a**) most cells should only express one transcript or the other of an antagonist pair along the YMC, except at limited times when the expression of the transcript pairs are expected to overlap, (**b**) cells expressing only one transcript should possess higher transcript levels than cells co-expressing both antagonist transcripts.

7.2 Results

This hypothesis was tested taking advantage of the method of dual-labeling (multiplexing) of fluorescent probes. Dual-label smRNA-FISH data was carried out on YMC cultures as described in chapter 5 Part I, i.e. two labelled probes were added to the fixed cells allowing an evaluation of how two different transcripts behave in each cell over time in YMC cultures.

The data was analysed and the proportion of cells falling in each of the following cell category were plotted along the YMC as shown in Figure 7.1; (i) cells expressing no transcript (light grey), (ii) cells expressing only one transcript or the other (colour), (ii) cells co-expressing transcripts (dark grey).

This was done for all pairs of transcripts along the synchronous slow growing cultures of the YMC (growth rate of 0.072h^{-1}, YMC period of 3h20min and doubling time of ~9.62h) and in asynchronous fast growing mid-Log phase cultures (doubling time of ~2.08h) (Figure 7.1,last timepoint on the right of each plot).

The results are first presented and discussed for high-growth asynchronous mid-Log cultures then for slow-growth synchronous YMC cultures.

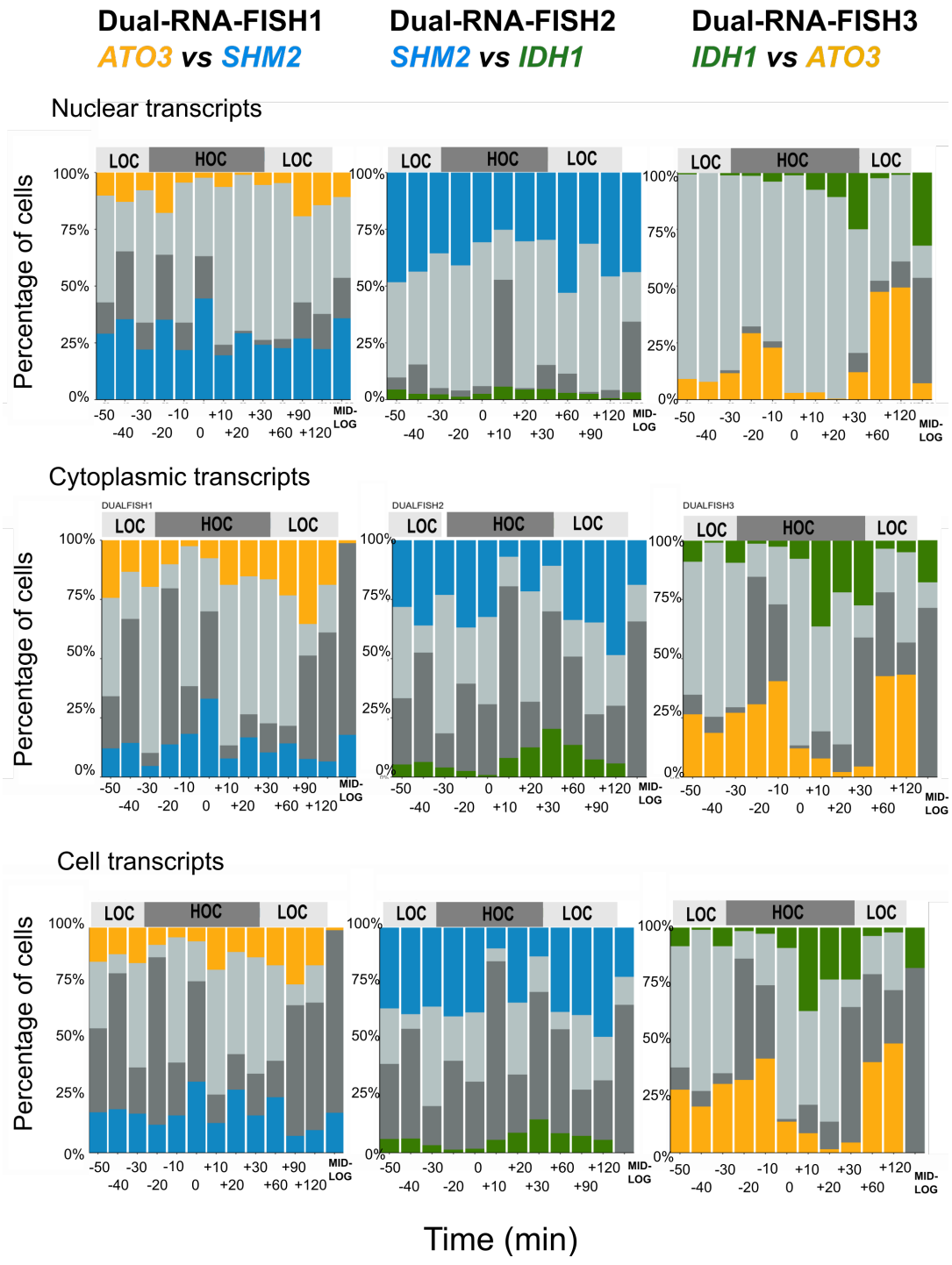

Figure 7.1.A Proportions of cells expressing both transcripts, only one or the other, or none. *Bar chart of the fraction of cells expressing transcript (top) in-nucleus, (middle) in-cytoplasm or (bottom) in-cell in each of the following subset; for cells expressing only in the first fluorescent channel (Cy5) (top colour), for cells expressing only in the second fluorescent channel (Cy3) (bottom colour), for cells expressing both transcripts (dark grey), for cells expressing no transcripts ("both non expressing") (light grey), for each sampling timepoint along the YMC and mid-log phase (last timepoint on the right). In yellow ATO3, in blue SHM2, in green IDH1. Upper panels indicate the YMC phases. Time is shown in minutes relative to the point of lowest dissolved oxygen levels in media (dO_2 %) found across the YMC, displayed as "0", "MID-LOG": Mid-logarithmic phase.*

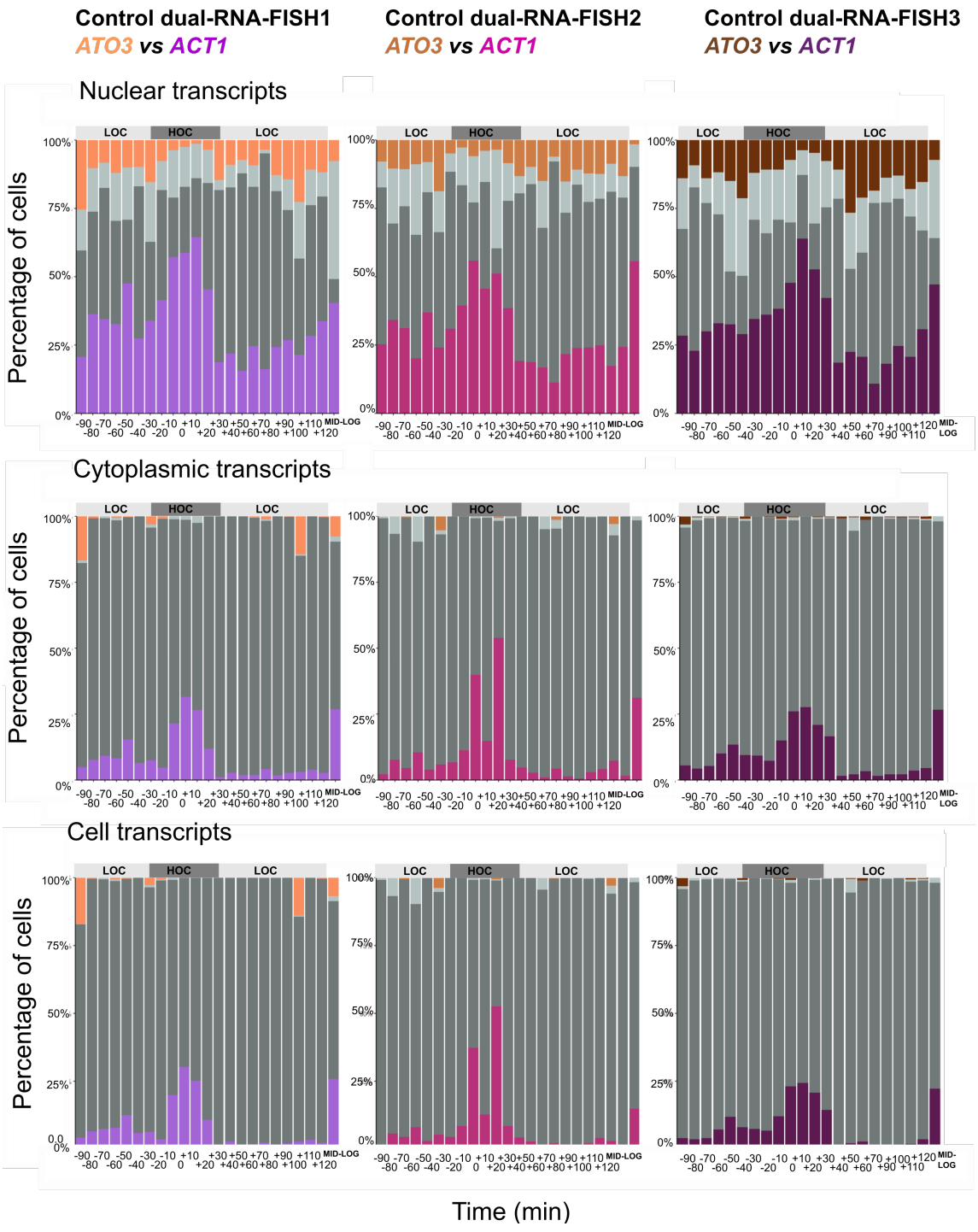

Figure 7.1.B Proportions of cells expressing both transcripts, only one or the other, or none. *Bar chart of the fraction of cells expressing transcript (top) in-nucleus, (middle) in-cytoplasm or (bottom) in-cell in each of the following subset; for cells expressing only in the first fluorescent channel (Cy5) (top colour), for cells expressing only in the second fluorescent channel (Cy3) (bottom colour), for cells expressing both transcripts (dark grey), for cells expressing no transcripts ("both non expressing") (light grey), for each sampling timepoint along the YMC and mid-log phase (last timepoint on the right). In shades of brown ATO3, in shades of purple ACT1. Upper panels indicate the YMC phases. Time is shown in minutes relative to the point of lowest dissolved oxygen levels in media (dO_2 %) found across the YMC, displayed as "0", "MID-LOG": Mid-logarithmic phase.*

7.3 High-growth asynchronous mid-log cultures

7.3.1 Cells co-express antagonist transcripts in high-growth asynchronous cell populations (mid-Log cells)

First, the effect of growth rate on patterns of expression is evaluated, comparing fast growing asynchronous mid-log cells (doubling time of ˜2.08h) with the Silverman et al., (2010) data using slow-growing asynchronous cells (growth rate of $0.1h^{-1}$ and doubling time of ˜6.9h).

In the mid-log phase samples of this study, cells show co-expression of cytoplasmic transcripts, despite being antagonistic in the YMC (Figure 7.1, last timepoint on the right). The percentage of cells expressing nuclear and cytoplasmic transcripts respectively is 18 and 81% for *ATO3* vs *SHM2*, 31 and 66% for *SHM2* vs *IDH1*, 46 and 71% for *IDH1* vs *ATO3* and 20 and 67% for the control pair *ATO3* vs *ACT1* (mean between 3 x control repeats). Results support relatively high proportions of cells co-expressing antagonist transcripts in the cytoplasm of cells from fast growing asynchronous cell populations. This is different to the prediction made by Silverman et al., (2010) on slow-growth asynchronous culture (DT=˜6.9h) in which not many cells are expected to co-express antagonist transcripts. In fact, this observation can be explained by the difference of growth rate of the cells (DT of˜ ˜2.08h for mid-log culture in this study and DT of ˜6.9h in Silverman study), consistent with the literature which shows that gene expression patterns associated with YMC phases become more pronounced at lower growth rate (Brauer et al. 2005). In addition, detailed gene expression profiles and transcriptional cascade occurring during the YMC can only be resolved at a lower feeding rate (Tu et al. 2005, Kuang et al. 2014) but not at a higher growth rate (Klevecz et al. 2004). Thus, at a higher growth rate, co-expression of antagonist transcripts increases in asynchronous culture, perhaps because many cells

possess an intermediate metabolic state, or perhaps because the switch between metabolic phases is too fast to be captured in asynchronous cell populations. Nevertheless, this is an important control as it means that any differences observed between slow-growth cultures can be distinguished from the effect of growth rate.

7.4 Discussion

7.4.1 The proportion of cells expressing only one transcript in asynchronous mid-log population returns the chronology of the transcriptional intrinsic clock

Remarkably, each pair of transcripts shows different proportions of cells presenting transcript exclusivity in mid-log phase samples. Figure 7.1 shows that cells that express only *ATO3* nuclear transcripts are rare when in pair with *IDH1* (7%) or *SHM2* (11%). Similarly, the proportion of cells expressing only nuclear *IDH1* is also low when in pair with *SHM2* at 3%, while it is higher when in pair with *ATO3* at 32%. The fraction of cells expressing only the *SHM2* transcript in-nucleus is high when in pair with *ATO3* at 36% and in pair with *IDH1* at 44%. Finally, for the control pair, the proportion of cells exclusively expressing *ATO3* nuclear transcript is low when in pair with *ACT1* with a mean* of 6%, while it is higher for the fraction only expressing *ACT1* when in pair with *ATO3* with a mean* of 48%. The proportion of cells expressing only one transcripts in-cytoplasm or in-cell falls below 3% for *ATO3* vs *SHM2*, *IDH1* or *ACT1* and for *IDH1* vs *SHM2*, while the fraction are higher when considering *SHM2* vs *ATO3* at 18%, *SHM2* vs *IDH1* at 19%, *IDH1* vs *ATO3* at 18% and *ACT1* with *ATO3* at 28%*.

*Mean between control replica.

These proportions are likely to reflect the nature of the transcription dynamics of these targets as fewer cells will be expected to show *ATO3* and *IDH1* transcripts if these are produced in bursts, compared to *SHM2* and *ACT1* if these are produced more constitutively (as described in chapter 5 & 6).

However, these finding may also suggest that in high-growth rate conditions, cells expressing *ATO3* can only do so after having expressed *IDH1, SHM2* and *ACT1*, because very few cells are found expressing *ATO3* only. This is again in agreement with the fact that *ATO3* is a transcript expressed at higher levels in stationary phase (Gash et al. 2000, Martinez et al. 2004, Radonjic et al. 2005, Lahtvee et al. 2017).

Similarly, *IDH1* expression itself seem to be only possible in cells after the expression of *SHM2*. By contrast, *ACT1* and *SHM2* are expressed in cells missing *ATO3*, and *ATO3* or *IDH1,* respectively, suggesting they are expressed more constitutively but perhaps also first in high-growth mid-log culture cells. Furthermore, in mid-log phase, the percentage of cells co-expressing nuclear transcripts is lower for *ATO3* vs *SHM2* (18%) and for the control pair *ATO3* vs *ACT1* (20%, mean between control repeats) than it is for *SHM2* and *IDH1* (31%) and *IDH1* vs *ATO3* (46 %), indicating perhaps that the period of time spent between the expression of the target transcripts, along the single cell metabolic clock, is greater between *ATO3* and *SHM2* or *ACT1* than between *SHM2* and *IDH1,* itself longer than the time between expression of *ATO3* and *IDH1* in single cells. This concept; i.e the chronology of the intrinsic clock described here is recapitulated at Figure.7.2.

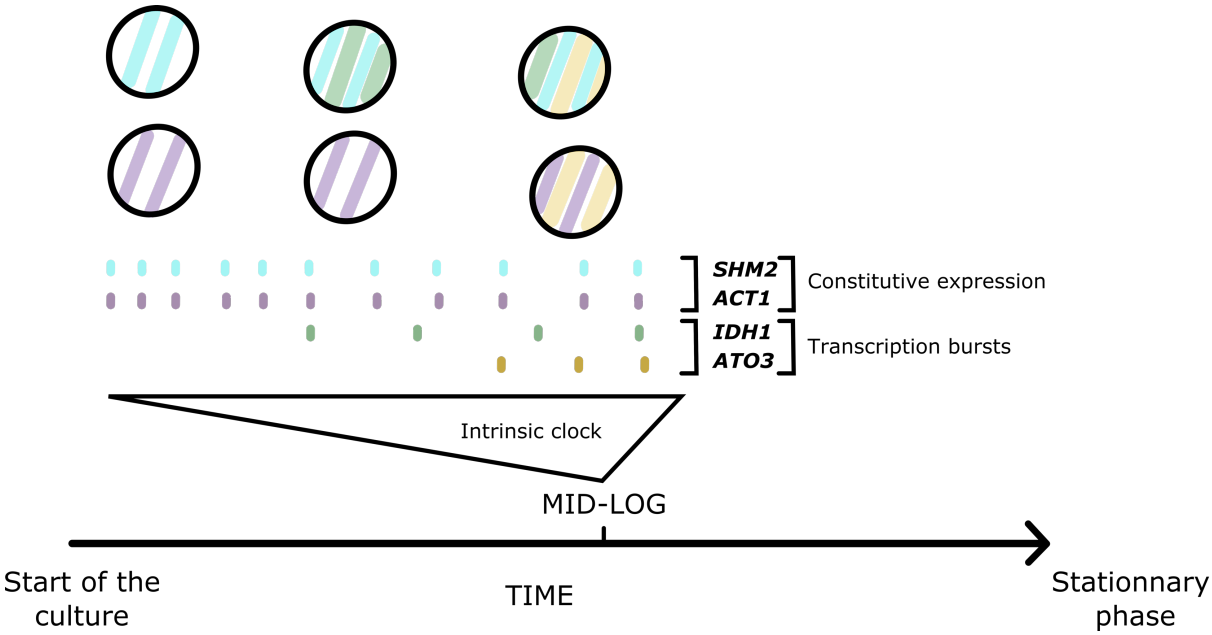

Figure 7.2 Chronology of the transcriptional intrinsic clock

Cartoon recapitulating the discussion made regarding mid-log cultures, the intrinsic gene expression clock in cells and how transcription dynamics might even be connected.

7.5 Conclusions

Here the proportion of cells expressing solely one or the other transcript of interest of a pair, is proposed to constitute a way to capture and recover the chronology of the intrinsic clock of cells in high-growth mid-log culture. The results thus support the idea of an intrinsic metabolic clock in single cells from asynchronous cultures, as suggested by different studies indicating that global transcript levels refer to the proportion of cells in a HOC or a LOC state (Silverman et al. 2010, Wyart et al. 2010, Slavov & Botstein. 2011, Slavov et al. 2011).

7.6 Slow-growth synchronous YMC cultures

Next batch asynchronous cultures from Silverman et al., and synchronized culture of the YMC from this study, which are both slow-grown (YMC DT =˜9.62h vs Asynchronous DT=˜6.9h) are compared. According to previous results, (6.2.1) no effect of growth is expected.

7.6.1 Antagonistically oscillating transcripts are co-expressed in single cells of the synchronized YMC population

Next the distribution of pairs of 'antagonistic' transcripts in the nucleus and cytoplasm of cells is examined throughout the YMC.

7.6.1.1 Nuclear expression

The proportion of cells that simultaneously express two antagonistically oscillating transcripts in their nucleus is low through most of the YMC, as predicted. The percentage of cells expressing both transcripts in-nucleus (for *ATO3* vs *SHM2*, *SHM2* vs *IDH1*, and *IDH1* vs *ATO3)* reaches maxima of 29, 47 and 11% for each pair respectively in the YMC. At specific timepoints for which global levels of target transcript are expected to crossover (Fig. 5.2 & Fig. 5.9), the percentage of cells expressing both transcripts increases, as predicted.

Indeed, Figure 7.1.A shows this happening;

(i) in late LOC to early-HOC and early LOC for the pair of *ATO3* (RNA peak in LOC) vs *SHM2* (RNA peak in early HOC),

(ii) in mid and late HOC for *SHM2* (RNA peak in early HOC) vs *IDH1* (RNA peak in late HOC),

(iii) in late-HOC to early-LOC for *IDH1* (RNA peak in late HOC) vs *ATO3* (RNA peak in LOC),

(iv) while control experiments featuring *ATO3* (LOC) vs *ACT1* (non-cycling) show higher proportions of cells co-expressing transcripts compare to antagonist pairs in the nucleus. Indeed, the fraction of cells reaches maxima of 81% for nuclear transcripts in early LOC (+60, +70) (Figure 7.1.B).

7.6.1.2 Cytoplasmic expression

Trends are similar for cytoplasmic transcripts, though higher proportions of cells express both antagonist transcripts in-cytoplasm compared to in-nucleus. The maxima ranging from 66, 72 and 54% for the *ATO3*/*SHM2* pair, *SHM2*/*IDH1* and *IDH1*/*ATO3* respectively. As predicted by the hypothesis, at the crossover points, more cells are found co-expressing *SHM2* and *IDH1*, both considered as HOC-phase transcripts (Tu et al. 2005, data from Dr. Xi), compared to the other pairs of transcripts. Similarly, control experiments assessing co-expression of *ATO3* vs *ACT1* show higher proportions of cells co-expressing transcripts compare to antagonist pairs. Indeed, the fraction of cells reach maxima of 99% for cytoplasmic transcripts in early LOC (+60, +70) (Figure 7.1.B).

Figure 7.3 shows an example of co-expression of *SHM2* and *IDH1* while Figure 7.4 shows an example of co-expression of *ATO3* and *ACT1* in yeast cells from YMC population as detected by fluorescence microscopy.

In summary, these results indicate that more cells express both antagonist transcripts at crossover points compare to other timepoints along the YMC, in accordance with the expectations derived previously with the hypothesis.

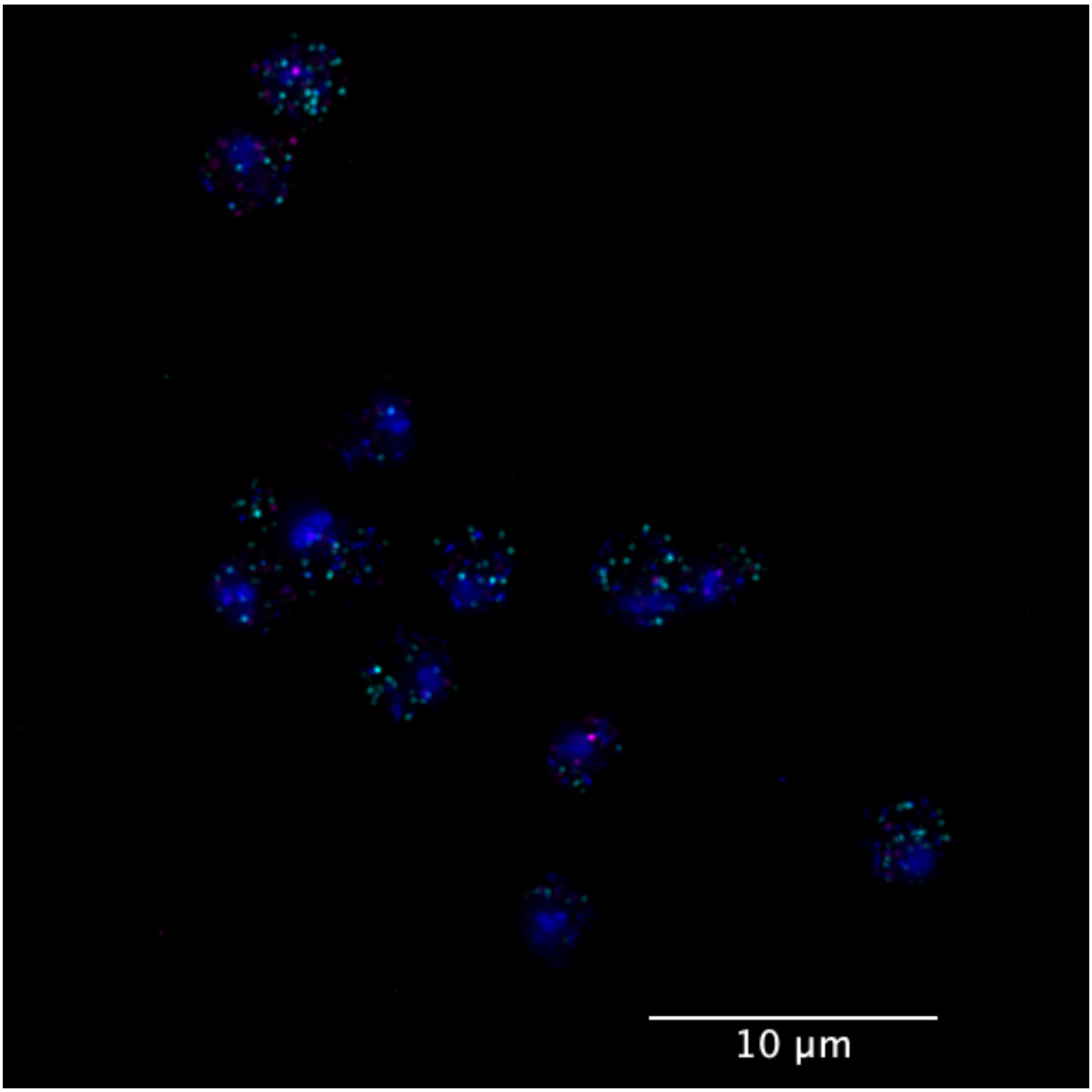

Figure 7.3 Examples of co-expression of SHM2 and IDH1

Example of an entire field of view, yeast cells from YMC timepoint (Tp +30, late-HOC), SHM2 is labelled in Cy5, IDH1 in Cy3, DNA is stained with DAPI.

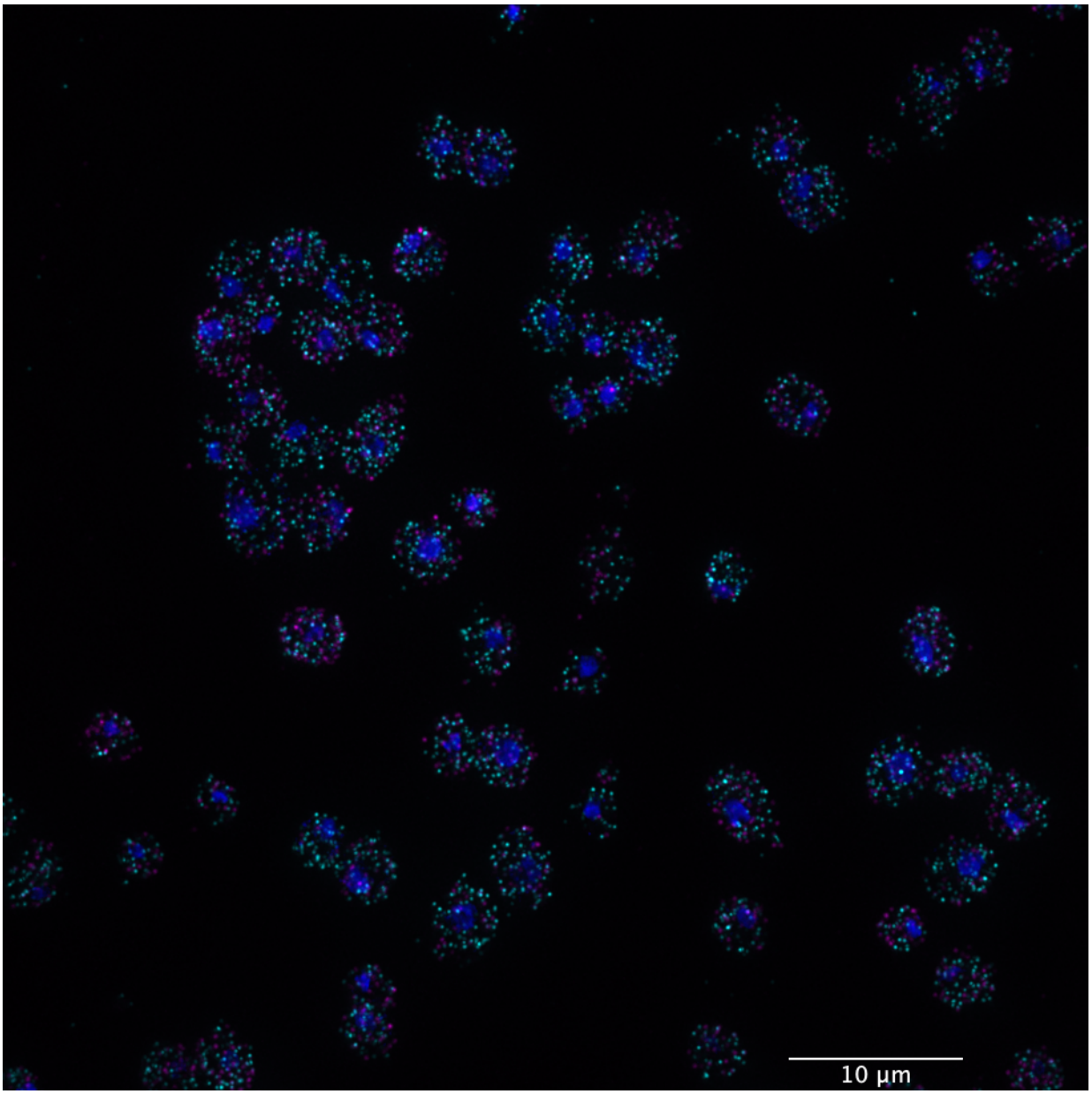

Figure 7.4 Example of a microscopy image gathered for this study.

Example of an entire field of view. Yeast cells from YMC timepoint (Tp +50), ATO3 is labelled in Cy5, ACT1 in Cy3, DNA is stained with DAPI. Cells co-express these transcripts, but ACT1 levels are higher than those of ATO3.

7.6.2 Transcript exclusivity rises as global transcript levels of antagonist drops

Figure 7.1 displays the proportion of cells expressing only one transcript of a pair in different shades of colour for the different transcripts; in yellow or brown (control) for *ATO3*, in blue for *SHM2*, in green for *IDH1* and in purple for *ACT1*. Concordant to Silverman's hypotheses, the proportion of cells expressing only one target transcript is at its peak when the global transcript levels of the antagonist target decline. First for the pair of ***ATO3* vs *SHM2***, the percentage of cells expressing *ATO3* nuclear RNA only ranges from 1% in late HOC to 19% in late and middle LOC. More cells express the *SHM2* transcript only, with values of 20% in LOC to 45% in HOC throughout the YMC. Second, for the ***SHM2* vs *IDH1*** pair, 16% of cells express only *SHM2* nuclear transcripts in mid HOC compared to 53% in early LOC. The proportion of cells expressing *IDH1* RNAs only is very low with 1% of cells expressing nuclear transcripts across the YMC to 6% in mid-HOC. Again, while more cells are found to co-express these transcripts, fewer are found to only express *IDH1*, as both *SHM2* and *IDH1* peak in the HOC phase of the cycle (YMC co-expressed). Third, for the ***IDH1* vs *ATO3*** pair, the percentage of cells expressing nuclear transcripts ranges from 0% along most of the YMC to 25% in late HOC for *IDH1*. It goes from 1% in mid HOC to 48% in LOC for *ATO3*. For all antagonist pairs looked at along the YMC, similar ranges as the ones described for nuclear transcripts are detected for cytoplasmic and cell transcripts.

Finally, the control set of ***ATO3* vs *ACT1*** also follows the Silverman et al. hypotheses, as at times of high global expression of *ATO3* (in LOC), many cells co-express these transcripts, while fewer cells co-express these transcripts and more cells express *ACT1* only when *ATO3* global levels plummet in HOC phase. Indeed, the *ATO3* vs *ACT1* pair shows 1 to 27% of cells express only *ATO3* nuclear transcripts in HOC and LOC, respectively, while higher fractions of cells express only *ACT1* in-nucleus with

percentage oscillating between 11% in LOC and 65% in HOC. It is worth noting, the proportion of cells expressing only *ATO3* is almost null when cytoplasmic transcripts are considered, indicating that all cells expressing *ATO3* in-cytoplasm also express the *ACT1* transcripts.

7.7 Conclusions

Although these results to a large extent confirm the hypotheses made by Silverman et al., (modified here in one hypothesis for synchronous YMC cultures), they also indicate that these assumptions do not constitute rigid rules. In particular, co-expression of antagonist transcripts is found in YMC and mid-log cultures, at cross-over points of global transcript oscillations but also outside of these crossover points, although to a lesser extent. This demonstrates that at the population level, the anti-phase oscillations of antagonist transcripts is simply accentuated by population-averaged techniques that buffer gene expression heterogeneity. In addition, the presentation of the phases as being strictly temporally compartmentalised gives a false impression, as this is often looser, at least in some cells.

7.8 Discussion

7.8.1 The proportion of cells expressing target transcripts in the YMC synchronous population indicate an organisation in sub-populations

Within the context of this research project, transcripts were picked to represent distinct transcript clusters and profiles found along the YMC at the global level (Tu et al. 2005, Kuang et al. 2014, Feltham et al. 2020, Xi. DPhil thesis. 2019). *ATO3* represents LOC transcripts, *SHM2* depicts early to mid-HOC transcripts, *IDH1* serves as model for the study of late-HOC transcripts while *ACT1* performs as a control and exhibit constant

transcripts behaviour. The transcripts picked for this work should thus inform the metabolic state (HOC-state vs LOC-state) of individual cells along the YMC.

Results from this chapter and chapter 5 show the fraction of cells expressing HOC and LOC transcripts indeed vary between phases of the YMC as expected (Wyart et al. 2010., Slavov et al. 2011). However, some cells are found to express LOC transcripts in HOC and some cells show HOC transcripts in HOC suggesting some cells behave differently or are in a different metabolic state than expected along the metabolic cycle.

Thus, next, the idea that the YMC population is organised into sub-populations of cells with different metabolic states is investigated.

7.8.2 A proportion of cells remains in the LOC state during the HOC phase

First, results indicate that only a proportion of the population transition from LOC to HOC, while another proportion stays in a constant LOC state over the YMC. Indeed, the proportion of cells expressing *ATO3* (a LOC transcript) decrease in HOC, but some cells still express *ATO3* in-nucleus and in-cytoplasm during the HOC phase. This result is particularly striking for the control data set (dual labelling for *ACT1* and *ATO3*) for which more cells were collected for the experiments, increasing the level of confidence that can be applied to the data. While the fraction of cells expressing nuclear transcripts stays constant over the cycle for *ACT1*, it drops (by ˜50%) in HOC phase for *ATO3*. Most importantly some cells (13% or more) still express *ATO3* in the HOC phase (Figure 7.1.B). Accordingly, the proportion of cells co-expressing *ACT1* and *ATO3* clearly drops in mid HOC phase to show an increase (˜25 to 50% depending on the repeat) in the proportion of cells expressing *ATC1* only (Figure 7.1.B).

Thus, these results indicate that not all cells transition from a LOC to a HOC state in HOC phase, but rather that only a proportion of cells will do so.

This model for which only a fraction of the population metabolically cycle while another fraction is arrested in a LOC state, is supported by previous observations described in the supplementary data of Slavov et al., 2011. Indeed, microarrays results revealed that average levels of LOC transcripts are higher in YMC cultures (LOC phase included) compared to exponentially growing ones. On the contrary, population levels of HOC transcripts are lower in synchronized YMC populations (HOC phase included) compared to mid-log phase asynchronous cultures. This would indicate that the proportion of cells in a LOC state is lower in mid-log phase than in LOC phase of the YMC, while the proportion of cells in a HOC state is higher in mid-log phase than in HOC phase of the YMC. Thus, one further conclusion is that some cells stay in a LOC state at all times during the YMC (Slavov et al. 2011).

Mean expression levels computed for this study confirm this hypothesis. When comparing YMC to mid-log phase samples, *ATO3* shows higher levels in LOC phase of the YMC, *SHM2* shows lower levels in HOC phase of the YMC, *IDH1* shows similar levels in both the HOC phase of the YMC and in mid-log phase, while *ACT1* also presents relatively identical levels in both cultures (Table 5.2, Figure S6, appendix).

Most importantly, the proportion of cells expressing transcripts presented at Figure 7.1.B clearly indicate that only a proportion of the population transitions to HOC at each cycle while another proportion of the population (perhaps varying between repeats) stays in a LOC state.

7.8.3. A proportion of cells stay in a HOC state at all times during the YMC

Next, although some cells do not express target transcripts at all (as seen for all transcripts, including *ACT1*), a large proportion of cells that do not contain *ATO3* nuclear transcripts, at all times along the YMC seem to be represented by a sub-population of cells expressing *SHM2* and/or *ACT1* nuclear transcripts only (Figure 7.1.A & B). Many cells are found to express *SHM2* nuclear transcript outside of the HOC phase. Around 20 to 25% of cells express solely *SHM2* nuclear transcripts at all times during the cycle, i.e. without co-expression of other transcripts (Figure 7.1.A). Similarly, around 15 to 25% of cells show *ACT1* nuclear transcripts at all times over the YMC without co-expression of *ATO3*, the LOC transcript (Figure 7.1.B). Thus, it seems that a proportion of the population also remains in a HOC state at all times during the YMC. In these cells, fewer cells express *IDH1* nuclear transcripts, perhaps because *IDH1* is expressed less constitutively than *SHM2* and *ACT1*, or perhaps because this metabolic state is more similar to an early HOC state.

Finally, this leads to the question as to which cells cycle metabolically over time.

7.8.4 Only a proportion of cells transition to a HOC state in HOC phase

The cells transitioning to the HOC state in the HOC phase must express HOC transcripts. This population of cells are expected to express *SHM2* in the nucleus at early HOC and *IDH1* in the nucleus in mid to late HOC. Accordingly, cells which transitioned into a HOC state should show co-expression of *SHM2* and *IDH1* in mid HOC. Surprisingly, cells that transition to an HOC state in the HOC phase seem to show co-expression of *SHM2* and *ATO3*. Indeed, the fraction of cells co-expressing *SHM2* with *ATO3* is higher in late LOC to early HOC phase and in mid LOC phase compared to late HOC for which only 25 to 40% express *SHM2* (Figure 7.1.A.).

Similarly, the proportion of cells expressing both *ACT1* and *ATO3* in-nucleus is also higher in late LOC to early HOC than in mid to late HOC. This perhaps indicates transitions from a LOC state to a HOC state and then from a HOC to a LOC state of some cells which thus would show mixed gene expression status.

7.9 Results

Next, in order to identify gene expression profiles of cells co-expressing transcripts, a threshold was applied on the data to separate cells with low expression from cells showing high expression levels, within the category of cells expressing both transcripts of a pair.

7.9.1 Cells that co-express HOC and LOC transcripts in HOC phase of the YMC show high expression levels of HOC transcripts and low expression levels of LOC transcripts

First, distributions of RNA numbers were plotted for cells expressing only one transcript or both antagonist transcripts. No striking difference or "typical distributions" could be identified between these two categories although the distributions varied (data not shown). Thus, in order to split cells with low or high expression, an arbitrary threshold of 5 RNAs was set based on skewed RNA distributions observed at Figure 5.15. This number was picked as the fraction of cells expressing more than 5 transcripts per cell in-cytoplasm is observed to greatly decrease compared to the fraction of cells expressing transcript numbers between 1 and 4, for all target transcripts. Therefore, here "low expression" of transcripts means the sum of RNA numbers detected in cells is strictly below 5 RNA molecules, while "high expression" of transcripts means the sum of RNA numbers detected in cells in equal or higher to 5 RNA molecules.

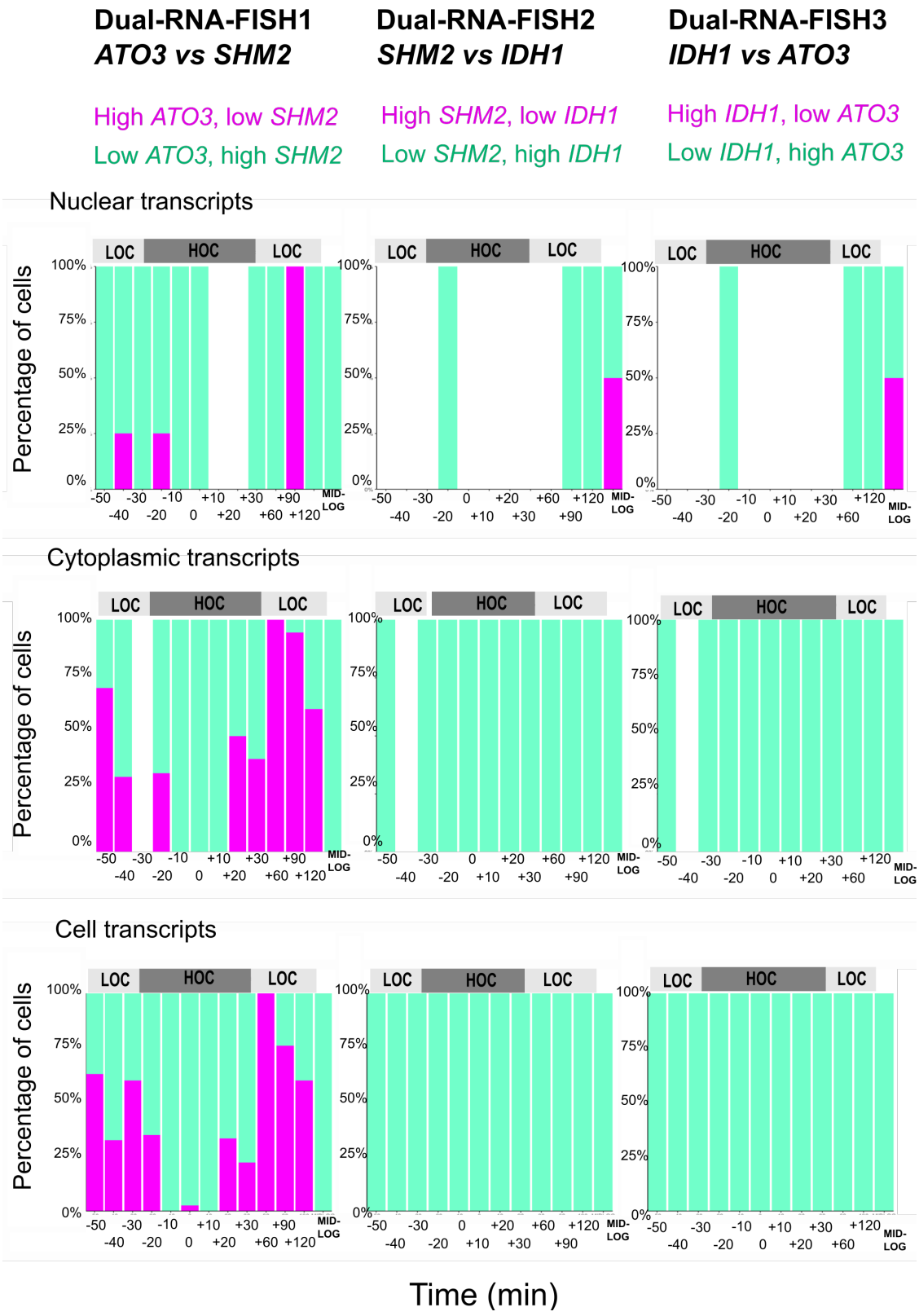

Figure 7.5.A Proportions of cells expressing both transcripts at low or high levels

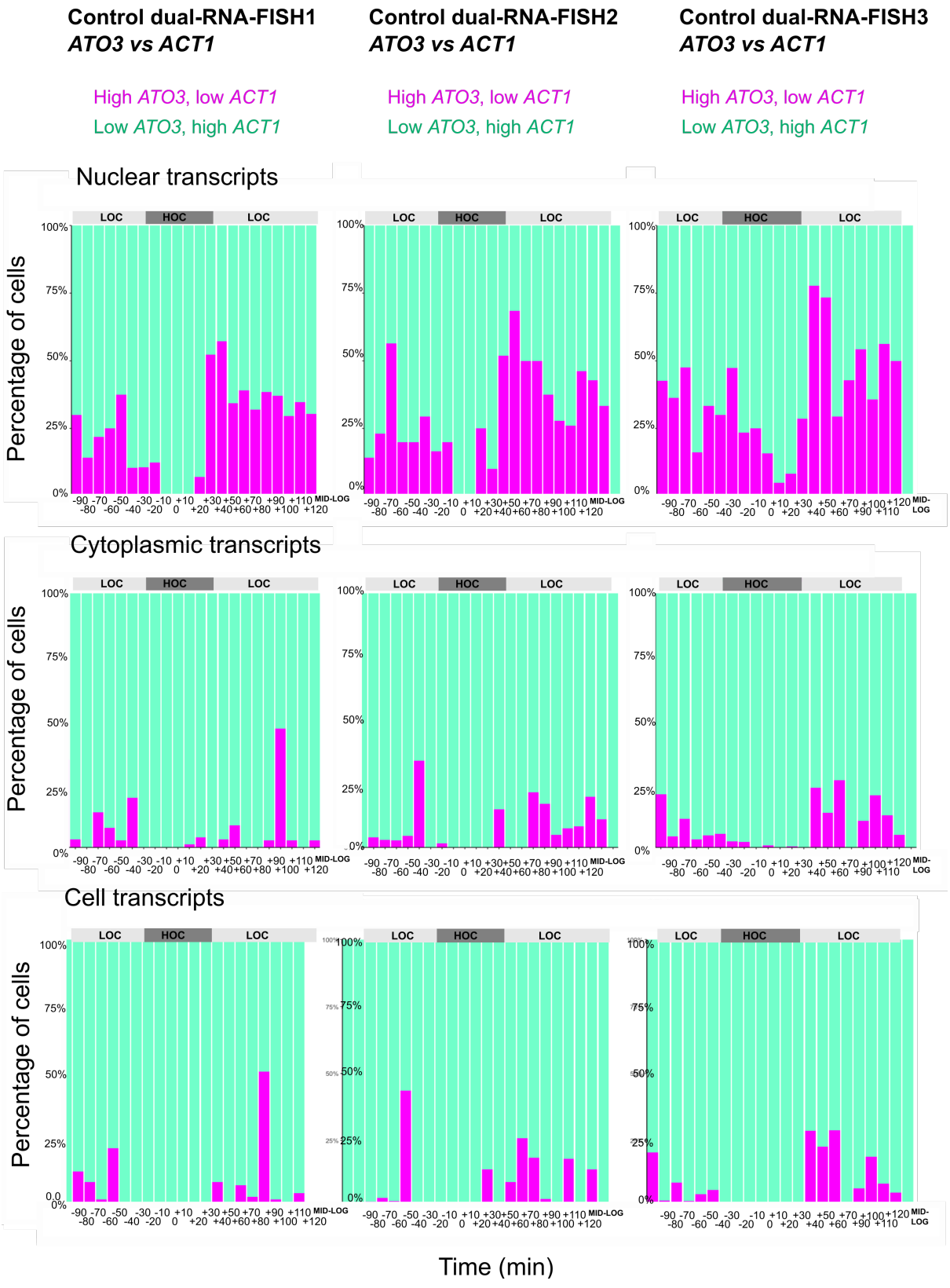

Figure 7.5.B Proportions of cells expressing both transcripts at low or high levels

Bar chart of the fraction of cells expressing both transcripts for each sampling timepoint along the YMC and mid-log phase, for the 6 dual-FISH experiments. Time is shown in minutes relative to the point of lowest dissolved oxygen levels in media (dO_2 %) found across the YMC, displayed as "0", "MID-LOG":

Mid-logarithmic phase. ***A. Dual-FISH data****: 1. ATO3 vs SHM2, 2. SHM2 vs IDH1, 3. IDH1 vs ATO3.* ***B. Control dual-FISH****: 1,2,3 ATO3 vs ACT1. One of the transcripts of a pair shows high levels while the other transcript shows low levels or vice versa. The proportion of the population that expresses high levels of transcript in the first fluorescent channel and low levels of transcript in the second fluorescent channel is represented in magenta. The fraction of cells with low levels of transcript in the first fluorescent channel and high levels of transcript in the second fluorescent channel is in cyan. The fluorescent channel and corresponding target transcript is indicated on top of each plot. High levels: x>=5, low levels: x<5, with x = RNA numbers in-nucleus, in-cytoplasm, or in-cell, per cell. Upper panels indicate the YMC phases.*

The bar charts at Figure 7.5.A & B present the fractions of cells expressing both transcripts of a pair, for all dual-fish experiments, for the sampling timepoints over the YMC, in-nucleus, in-cytoplasm and in-cell. Bars in magenta show the fraction of cells for which expression levels are high in the first fluorescent channel (x>=5) but low in the second fluorescent channel for the other target transcript (x<5). Bars in cyan show the opposite, i.e. the fraction of cells for which expression levels are low in the first fluorescent channel (x<5) but high in the second fluorescent channel for the other target transcript (x>=5). The fluorescent channel and corresponding target transcript is indicated on top of each plot.

During the YMC, among the proportion of cells found to co-express transcripts, the proportion of cells expressing high LOC transcript levels (*ATO3*) but low HOC transcript levels (*SHM2* & *IDH1*) is higher during LOC phase and lower during HOC phase. By contrast, the proportion of cells expressing high HOC transcript levels (*SHM2* & *IDH1*) but low LOC transcript levels (*ATO3*), is lower in LOC phase and increases in HOC phase to reach 100% of population of cells showing co-expression of antagonist transcripts. Similarly, the proportion of cells co-expressing *ATO3* and *ACT1* also shows higher levels of *ATO3* and lower levels of *ACT1* in LOC phase, as

opposed to lower levels of *ATO3* and higher levels of *ACT1* in HOC phase (see appendix for a more detailed description).

Therefore, it seems that only a proportion of cells transition from a LOC to a HOC state during the HOC phase of the YMC. This proportion of cells is characterized by high levels of expression of LOC transcripts and low levels of expression of HOC transcripts in LOC phase and by high levels of expression of HOC transcripts and low levels of/ or no expression of LOC transcripts in HOC phase.

7.10 Conclusions

This work reveals that different proportions of YMC cells can be grouped into different categories or sub-populations according to their transcript status in synchronous cultures.

7.10.1 A three-state population model for the YMC

A.

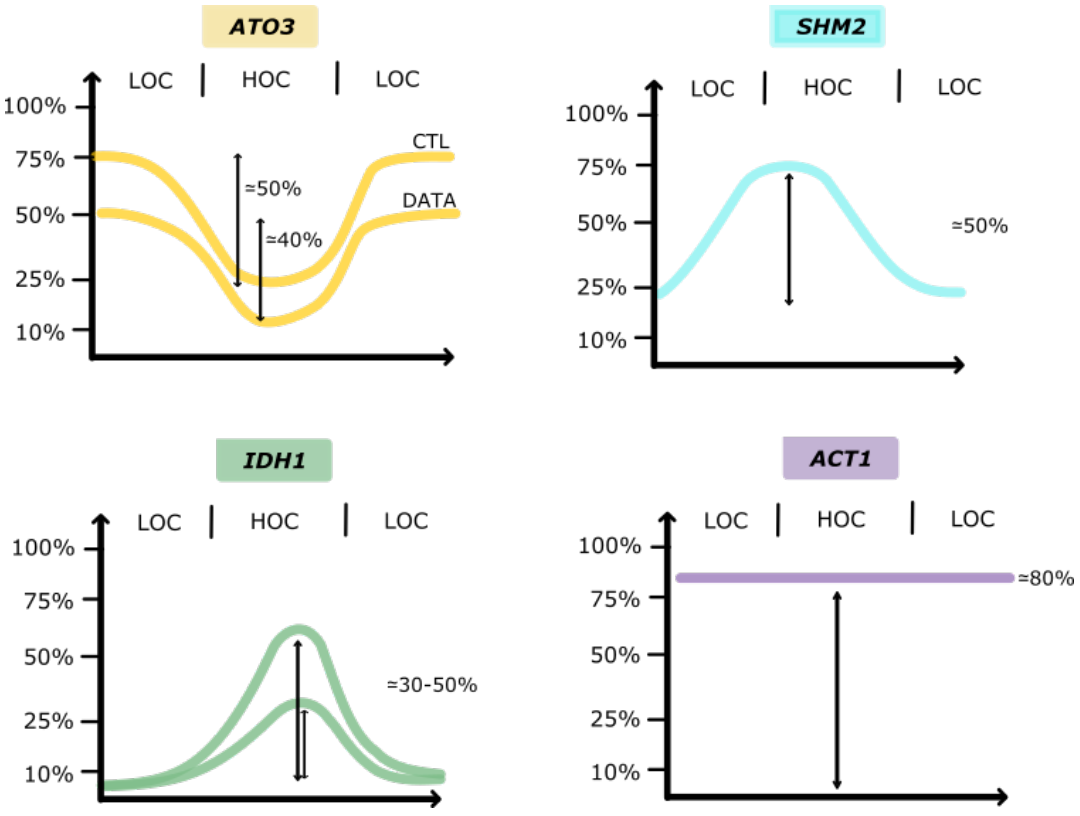

B.

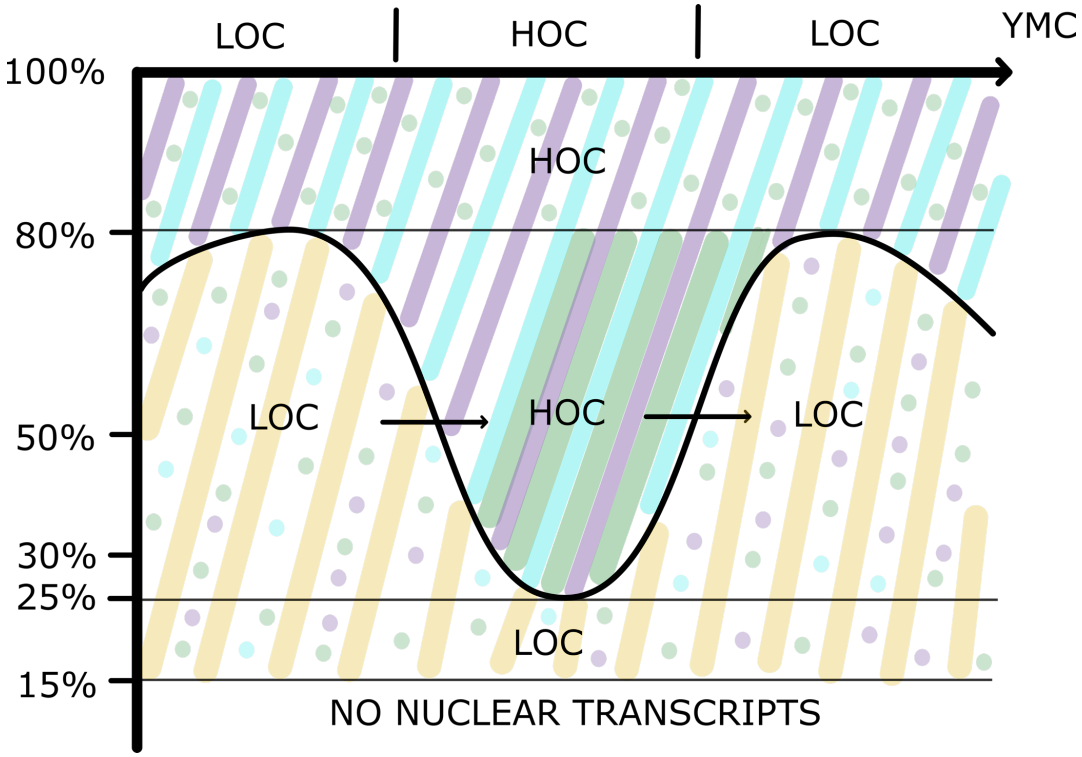

Figure 7.6 Sub-populations of the YMC; a three-state model

A. *Schematic of the fraction of cells expressing target transcripts in-nucleus based on results at Figure 5.14 , for all target transcripts, taking into account variability between repeats. 30 to 50% of the YMC cells cycle metabolically.* ***B.*** *Cartoon of the model of sub-populations suggested to compose synchronous population under slow growth. The fraction of cells in a particular state is presented over the YMC. LOC state; stationary-like state in which cells show high levels of LOC transcripts and no to low levels of HOC transcripts. HOC state: growth-like state in which cells show high levels of HOC transcripts and no to low levels of LOC transcripts. The expression of target transcripts are represented in colour: ATO3 in yellow, SHM2 in blue, IDH1 in green and ACT1 in purple. At all times, around 20% of the cells are in a HOC state, 10 to 25% are in a LOC state, and 5 to 15% of cells are expressing no nuclear transcripts, while 30 to 50% of the cell population cycle metabolically.*

Figure 7.6 shows in A. a schematic of the fraction of cells expressing target transcripts in-nucleus, and in B. a cartoon of the 3-state model of sub-populations suggested to comprise a synchronous population under slow growth. A LOC state is similar to a stationary-like state while a HOC state is characterized by a growth and proliferative state. A cell in a LOC state is expected to show high levels of LOC transcripts and no

to low levels of HOC transcripts. A cell in a HOC state is expected to show the opposite, i.e. high levels of HOC transcripts and no to low levels of LOC transcripts.

Here, results strongly supports the hypothesis that the YMC is made up of subpopulations of cells. Only a proportion of cells (˜30 to 50%) synchronously transition from a LOC state into a HOC state during HOC phase and then back to a LOC state in LOC phase, while another proportion of cells (˜10 to 25%) stays in a LOC state over time and along the YMC even in HOC phase and another part of the population (˜20%) stays in a growth-like or HOC state even in LOC phase of the YMC. Finally, a small fraction of cells also miss nuclear transcripts (˜5 to 15%).

In conclusion, using the single-cell technique of smRNA-FISH, reveals the presence of sub-populations of cells showing different gene expression status and thus most likely metabolic states along the Yeast Metabolic Cycle. Most importantly, more states were found across the YMC than the 2-states (transition from a LOC state to a HOC state in HOC phase of the YMC) predicted by Silverman et al., and Wyart et al., (2010) and by the 2-state “push-pull” mathematical model from Krishna & Laxman., (2018), thus indicating a more complex organisation of the YMC population.

Chapter 8

Coordination of growth, proliferation and gene expression delineates distinct sub-populations in mid-Log and YMC cultures

In this chapter the possible identity of the sub-populations of cells in the YMC is addressed, in particular their metabolic state, growth, size, quiescence, and cell cycle progression.

In this work, “Quiescence“ is referred as the reversible non-proliferative state. It characterises less metabolically active cells arrested in G0/G1 but capable of re-entering the cell division cycle (Werner-Washburne et al. 1993, Aragon et al. 2008).

8.1 Introduction

8.1.1 Coordination between Growth and CDC through Start

In order to proliferate in a sustainable manner, cells need to divide but only when sufficient biomass has accumulated and they have replicated cell basic units (cell membrane, cell wall, nucleus including DNA, cytoplasm, mitochondria, ribosomes). Therefore, some coordination is required between growth and cell division.

Although the process of growth and cell division are thought to be largely independent, notably because cell sizes continue to increase even when the cell cycle progression stops (Johnston et al. 1977, Saucedo & Edgard. 2002, Jorgensen et al. 2004) a checkpoint control coordinates the two. Ensuring a balance between growth and division, cells need to have access to enough nutrient, reach a critical cell size and a critical translation rate in order to pass the first checkpoint of Start (Hartwell et al. 1974, Johnston et al. 1977, Hartwell & Unger. 1977, Moore. 1988, Futcher. 1996, Jorgensen et al. 2004, Polymenis & Aramayo. 2015). Thus, the Start checkpoint coordinates cell division with growth and further with the environmental resources through a critical cell size threshold and various signalling pathways.

8.1.2 Cell size control and homeostasis

In order to transition from G1 into S-phase with replication of the DNA, budding yeast cells need to reach a critical size threshold, acting as an indicator of growth (Hartwell et al. 1974). Many factors are implicated in the regulation of cell size. Among the most important are the cyclin 3 and the factors Sfp1, Sch9, Whi5 (but also Cdh1 and Prs3) (Jorgensen et al. 2002). Whi5 has long been described as a cell size regulator or "sizer", blocking the transcription of G1/S genes during G1. In late G1, Whi5 is phosphorylated by Cln3/Cdc28 and re-localises to the cytoplasm. This allows the de-repression of the SBF and MBF complexes and the transcription of G1/S genes. Cln1,2 also inhibit Whi5, ensuring it only re-accumulate in the nucleus at the end of mitosis (Costanzo et al. 2004, Qu et al. 2019). Therefore, the transition to Start is highly dependent on Cln3 (de Bruin et al. 2004), particularly Cln3 mRNA translation (Polymenis & Schmidt. 1997), but also through its regulation by Whi3 (Wang et al. 2004, Cai & Futcher. 2013). Indeed, Cln3 protein abundance is believed to reflect the cell's translation rate, as it is unstable and subject to a high turnover rate. Finally, it was recently argued that protein synthesis increases more than cell size, leading to accumulation of Cln3 in cells in G1 leading to Start (Litsios et al. 2019).

8.1.3 Cell size acts as a proxy for growth and proliferative states of cells

Cell size is intrinsically linked to the cell cycle progression and growth. Cln3 is considered as a mechanism to sense critical translation rates, acting as a sensor downstream of protein synthesis and signalling pathways regulating it such as TORC1 and PKA (Barbet et al. 1996, Goranov et al. 2009). Accordingly, Cln3 was suggested to act as a sizer, as bigger cells are excepted to synthesise more Cln3 than smaller cells (Elliot & McLaughlin. 1978, Futcher. 1996, Hall et al. 1998). Cell size is also

connected to ribosome biogenesis via Sfp1 and Sch9. Nuclear localization of Sfp1 and the abundance and phosphorylation status of Sch9 promote RiBi and RP transcription and are necessary for a WT cell size increase, while down-regulation of these factors lead to a decrease in cell size and arrest of more cells in G1. Finally in absence of Sfp1 or Sch9 (which both reflect nutrient signals) cells adopt a minimal critical cell size threshold for the transition to start. Therefore, Sfp1 and Sch9 are believed to link nutrient signals to critical cell size threshold. Sfp1 is regulated by Ras/PKA and TORC1 and Sch9 by TORC1 (Jorgensen et al. 2002) and activation of the Ras/PKA pathway by cAMP is necessary to pass the Start checkpoint (Thevelein. 1992, Muller et al. 2003). The Pho85 kinase regulates the Gcn4 TF acting on different targets involved in the CDC such as Whi5 and Sic1 (Huang et al. 2007).

Many studies have investigated the molecular mechanisms by which cell size coordinates Start; while some claim it might relate to protein abundance of a yet unknown protein, others describe a way through the titration of the SBF/MBF binding sites (Heldt et al. 2018, Dorsey et al. 2018), the dilution of cyclin inhibitors (Schmoller et al. 2015, Barber et al. 2020) or a difference between cyclin activators and inhibitors accumulation rate and cell size increase (Chen & Futcher. 2020). Nevertheless, together, these findings indicate that cell size depends to a certain extent on growth, is regulated through nutrient signalling pathways, and cell growth and the progression to the cell cycle are linked (Jorgensen et al. 2004).

8.1.4 Cell size and a critical size threshold in nutrient limiting conditions

The critical cell size at which cells transition to Start is regulated by ploidy (diploids need to reach higher cell size), but also by growth outputs such as ribosome biogenesis and translation rates (Jorgensen & Tyers. 2004).

Under nutrient limitation, the proportion of cells in G1 increases linearly with a decreasing growth rate as cells growing slowly spend more time in the G1 phase (Brauer et al. 2008, Beck & von Meyenburg. 1968, Unger & Hartwell. 1976, Lorincz & Carter. 1979). Moreover, most stationary phase cells are in G0 or G1 (Hartwell et al. 1974, Miles et al. 2020).

Importantly, depending on the conditions, the critical cell size at which cells transition to Start varies (Jorgensen et al. 2004). Indeed, it was found to be higher in rich medium (~35 um^3 or higher) (Futcher. 1996) than in poor medium. However, the relationship between feeding rate and critical cell size was shown to be lost at lower feeding rate (0.23h^{-1}), pointing to a minimal critical cell size threshold independent of growth rate. A median cell size volume between 27.8-31.5 μm^3 characterizes this minimal critical volume (haploid C4.2 strain) (Johnston et al. 1979). Moreover, when cells were transferred from a low growth rate to a high growth rate carbon-sourced medium, cells adapted to the new conditions and needed to reach the critical cell size threshold of the fresh media they were transferred to, in order to restart the CDC (except for some cells for which cell size was too close to the 1st medium cell size threshold) (Lorincz & Carter. 1979).

8.2 Discussing the organisation of YMC population

Next models aiming to describe the relationship between growth and cell proliferation in YMC cultures are presented and discussed.

8.2.1 Organisation of yeast cells in synchronous population

A few hypotheses were made concerning the organisation of YMC sub-populations. These were based first on the detection of at least 2 sub-populations within YMC cultures; a proportion of the population that synchronously divide in late HOC phase

and another fraction that is arrested in G0/G1 (Klevecz et al. 2004, Tu et al. 2005, Laxman et al. 2010, Slavov & Botstein. 2011, Burnetti et al. 2016, Feltham et al. 2020). Models described in the literature are based on growth, cell sizes and quiescence to some extent and aim to explain why some cells divide and other don't during metabolic cycles. These are presented and discussed here.

8.2.1 Growth models

8.2.1.1 Asynchronous growth model

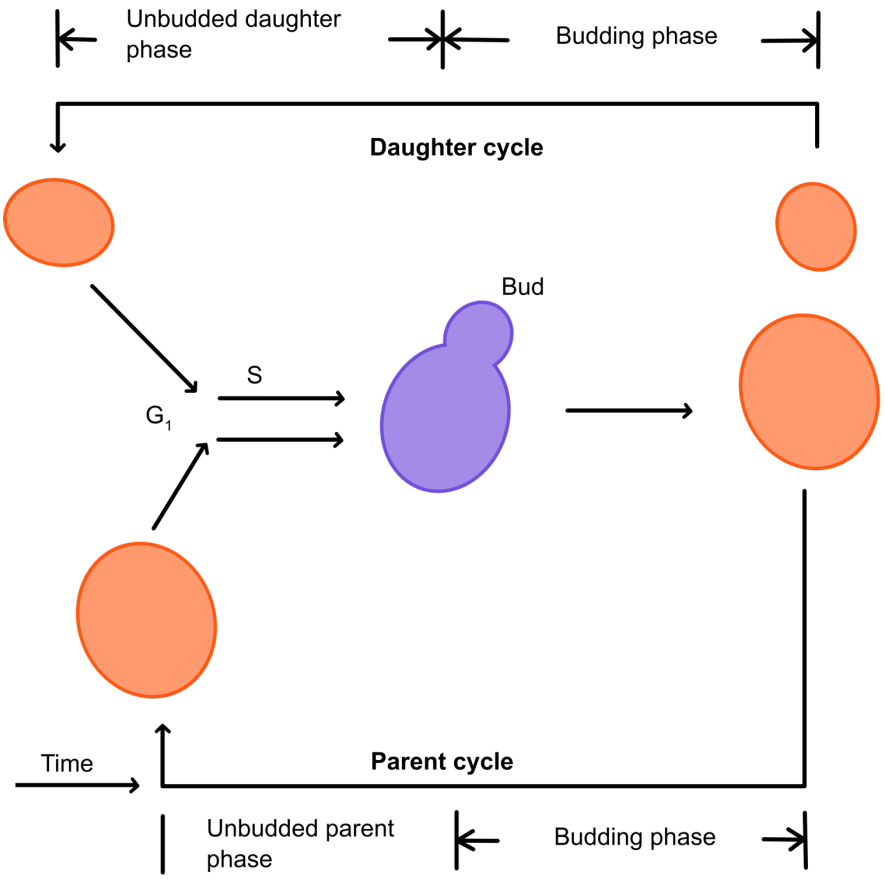

Figure 8.1 Asymmetric budding of Saccharomyces cerevisiae

Daughter cells are expected to go through longer unbudded phase before transitioning to S-phase, compared to mother cells. Modified from Patnaik. 2003 (already modified and based on models described in Chen & McDonald. 1990, Bellgardt. 1994, Hjortso,.1996).

A first model was suggested based on the asynchronous growth of mother and daughter cells (Patnaik. 2003, Burnetti et al. 2016). Under exponential growth, daughter cells spend more time in G1 and show longer unbudded phase compare to their mothers as they need to acquire sufficient resources, grow and reach a critical cell size before being able to transition and commit to CDC while mothers do not because they already are large (Hartwell et al.m1974, Hartwell & Unger. 1977, Bellgardt. 1994, Laabs et al. 2003, Jorgensen et al. 2004).

Thus, the cell size asymmetry and the difference in growth status between mother and daughter cells was suggested to be responsible for the partitioning of the YMC population (Roberston et al. 2008, Burnetti et al. 2016, Krishna & Laxman. 2018). The idea followed here was that mother cells could transition more easily to HOC and commit to CDC at each or most cycles, while daughter cells would stay in a non-proliferative state for many cycles and would thus need multiple cycles to grow slowly in order to transition to S phase. According to this model cell-to-cell communication would be responsible for the recruitment of more and more cells in a HOC-state (Roberston et al. 2008, Burnetti et al. 2016, Krishna & Laxman. 2018). Nevertheless, if metabolic cycles can be sustained indefinitely (Tu et al. 2005), some daughter cells will eventually divide because mother cells will either die due to their replicative lifespan, around 24 cycles in WT budding yeasts (Mortimer & Johnston. 1959, Steffen et al. 2009) or be discarded through the harvest pump. Moreover, it has also been argued that a mother cell who had just divided and used its resources to do so was probably less likely to re-enter the next metabolic cycle (Krishna & Laxman. 2018).

8.2.2 Alternating growth model

Accordingly, it was also proposed that cells would undergo one to several metabolic cycles in order to grow sufficiently before being able to replicate their DNA (Slavov et al. 2011). Some even suggested the presence of 2 populations of cells dividing in an antagonistic manner, each population dividing every 2 YMC (Porro et al. 1988, Robertson et al. 2008, Chen et al. 2007, Stowers et al. 2011, Morgan, Moses & Young. 2018). However, so far no convincing evidence could be collected to answer the question of whether different cells transition to HOC and commit to CDC each cycle or if the same cells do so.

8.2.3 The need for a model considering both growth and quiescence

Most importantly, the models described formerly present other issues as these focus on growth status but do not consider quiescence *per se*. However, after the period of starvation of the high-density batch culture required to start metabolic cycles (Figure 1.1) (Klevecz et al. 2004, Tu et al. 2005, Feltham et al. 2020), it is likely that some cells are in an early stationary phase state, meaning that some of the cells might be quiescents. Indeed, prior to synchonisation and entry into the YMC, batch culture cells are starved for short periods only (less than 24h) (chapter 2, Feltham et al. 2020), and thus do not reach stationary phase *per se* (definition >7days, De Virgilio. 2012) before transitioning to the metabolic cycle. Nevertheless, slow growth conditions have been argued to induce early physiological properties of quiescent cells (Klosinska et al. 2011) and YMC cultures share many characteristics with quiescent cells (chapter 1). Increases in cell densities, trehalose levels (Li et al. 2013, Shi et al. 2010, Tu et al.,2007, O'Neill et al. 2020) as well as in histone lysine deacetylation levels occur in quiescent cells as well as in cells from YMC populations in LOC phase (Friis et al.

2009, Mews et al. 2014, Cai et al. 2011, Kuang et al. 2011). Next, the liquidation and usage of carbohydrate stores, known to be coordinated to the passage through Start (Lillie & Pringle. 1980) occurs in stationary phase upon quiescence exit through the action of trehalase and glycogen phosphorylase (Werner-Washburne. 1993, Shi et al. 2010). Again, similar dynamics of carbohydrate store breakdown are believed to take place in cells during the HOC phase of the YMC (O'Neil et al. 2020, Feltham et al. 2020).

Most importantly exit from quiescence or G0/G1 is time regulated in daughters/quiescent cells as they divide synchronously, while mother/non-quiescent cells divide asynchronously upon addition of fresh media (Allen et al. 2006). Reminiscent of the singular behaviour of quiescent cells, synchronous cell divisions of 10 to 50% of cells occur in mid to late HOC phase of the YMC (for CEN. PK) (Tu et al. 2005, Klevecz et al. 2004, Robertson et al. 2008, Laxman et al. 2010, Slavov & Botstein. 2011, Burnetti et al. 2016, Feltham et al. 2019).

In light of these findings, growth models do not seem sufficient to explain the organization of YMC cell cultures. While the growth models explain synchronization and cell recruitment into HOC phase by cell-to-cell communication, a model considering growth as well as quiescence seems more convincing with respect to cell cycle synchronization.

8.2.4 Quiescence models

Several other models are conceivable when considering growth and quiescence. Next, follows an overview of these models.

As YMC cells show characteristics of quiescence but do not enter a long stationary phase, as opposed to quiescent cells (Allen et al. 2006, De Virgilio. 2012), before entering the yeast metabolic cycle, and only show some marks of quiescence, one of the metabolic states of cells in YMC populations is often referred as “quiescent-like“ as opposed to “growth-like“ (Krishna & Laxman. 2018).

8.2.4.1 All cells transition between quiescence and growth

First, a two-state model of quiescent-like versus growth-like states was suggested. Previous studies argued that “quiescence exit” depended on the metabolic status of the cells and that all cells enter a quiescence-like state upon stationary phase and thus cycle metabolically (Tu et al. 2005, Shi et al. 2010).

8.2.4.2 All cells enter quiescence, some only escape it

Second, the very fact that not all cells divide at each cycle indicate that only a proportion of cells can transition out of a G1 state (Burnetti et al. 2016, Slavov & Botstein. 2011). Furthermore, recent mathematical models, able to reproduce the typical dip in dissolved oxygen levels, predicted cells exist in at least two metabolic states and that some cells only, but not all, transition out from a “quiescent-like” state to a “growth-like” state and re-enter the cell cycle, upon intra or extra cellular signals (Krishna & Laxman. 2018). Finally, only a proportion of cells was detected to transition to lighter densities by breaking down their carbohydrates stores during HOC phase of

the YMC (Shi et al. 2010). Therefore, previous findings and models seem to argue that although all cells enter a quiescent-like state, only a fraction of cells escape it at each HOC phase.

Nevertheless, these models do not examine the possibility that some cells do not enter quiescence at all during the starvation phase of growth, despite the detection of a proportion of cells in a non-quiescent state in stationary phase (Allen et al. 2006, Werner-Washburne et al. 2012). Therefore, current models miss crucial information on the organisation of sub-populations of cells, such as the ones described in Miles et al. (2020), in which stationary phase cells were detected to present 3 to 4 sub-populations of cells as opposed to 2 based on the canonical view of a separation of the stationary phase culture into 50/50 large non-quiescent mothers vs small quiescent daughters (Werner-Washburn et al. 1993, Gray et al. 2004, Allen et al. 2006, Aragon et al. 2008, Davidson et al. 2011, Werner-Washburne et al. 2012). In their paper Miles et al., (2020) showed stationary phase cultures include more sub-populations of cells, with mothers and daughters with different sizes, cell densities, cell wall thickness and proliferative status.

8.3 Investigation of the relationship between cell cycle progression, cell size and gene expression in single cells of yeast cultures

Based on literature about the relationship between growth, quiescence, proliferation and cell size in budding yeast, models of the organization of YMC population might miss some information.

Because this project previously highlighted the presence of sub-populations of cells with different gene expression status in YMC cultures (chapter 7) and suggested the presence of at least 3 sub-populations, the aim of this chapter is to investigate whether some phenotypic traits characterizing the metabolism of the cells can be identified for cells with different gene expression profiles to add to the understanding of the organization of YMC populations.

Next, cell cycle progression states together with cell size are investigated in single cells from mid-Log and YMC cultures. Again, the three antagonistically oscillating transcripts, picked according to their global NET-Seq and RNA-Seq profiles, mark different metabolic phases and states of the YMC. *ATO3*, the transcript peaking during the Low Oxygen Consumption (LOC) phase marked the less metabolically active state or LOC-state in cells, while *SHM2* and *IDH1* peaking one after the other during the High Oxygen Consumption (HOC) phase of the YMC, marked a more metabolically active state or HOC-state in cells. Finally, *ACT1*, the transcript for actin, which shows global constant levels along the YMC was used as a control to ensure the RNA-FISH probe incorporation in cells.

Finally, the question of whether transcript levels and metabolic states correlate with these factors in cells is addressed by examining single cells collected for the RNA-FISH experiments previously reported.

8.4 Experimental design and method development

8.4.1 Identification of budded cells in YMC cultures

The different stages of the cell division cycle have been visualized in single cells detected in YMC cultures (Figure 8.1).

Quantification of budded cell through visual assessment of brightfield microscopy images is often used to identify S/G2/M phase cells, as the bud emergence starts at the same time of DNA replication (Hartwell et al. 1974, Cvrckova & Nasmyth. 1993, Ball et al. 2011). From the replication phase until cytokinesis, cells will thus present a bud. Thus, cells in S, G2 or M are budded while cells in G0/G1 are not. However, this time-consuming technique perhaps lack some accuracy, as it relies on visualization of buds, which can be small and sometimes difficult to detect. Further work would be needed to create an in-house pipeline enabling to; annotate cells (manually or using A.I.) and record their state throughout the RNA-FISH pipeline.

8.4.2 DAPI intensities in-nucleus accounts for the nuclear DNA content

Here, in order to discriminate the proliferative status of cells, the nuclear DNA content was computed in single cells from the YMC and mid-log cultures, using the intensity of the DAPI stain in the nucleus.

As the DNA content is replicated in cells during the S phase and has doubled in cells in G2/M, the DAPI intensities in these cells are expected to be higher than in G0/G1 cells and, like FACS using propidium iodide or Cytox Green to stain the DNA content (Tu et al. 2005, Klevecz et al. 2004, Feltham et al. Laxman et al. 2010, Slavov & Botstein. 2011, Burnetti et al. 2016), DAPI staining can be used to monitor the proportion of cells in the distinct phases of the cell division cycle.

The further refinement of using DAPI and imaging is that the buds attached to mother cells can be assigned as individual cells with fully replicated and segregated nuclei, and distinguished from those with lower DAPI intensities resulting from mitochondrial DNA staining. The outlining pipeline used in the data analysis detects buds attached to mother cells as one cell, unless the DAPI centre has a high enough intensity to be determined as a nucleus when the pipeline will separate the bud and mother cell into two separate cells (Figure 8.1). Thus the DAPI discrimination is important to distinguish cell cycle stage as well as the number of fully replicated cells. The experiments to quantify the nuclear DNA content were done from the "control" set in which dual labelling smRNA-FISH was used to label *ATO3* and *ACT1*. The 3 experimental repeats were merged to increase the cell numbers for this analysis (details in chapter 2).

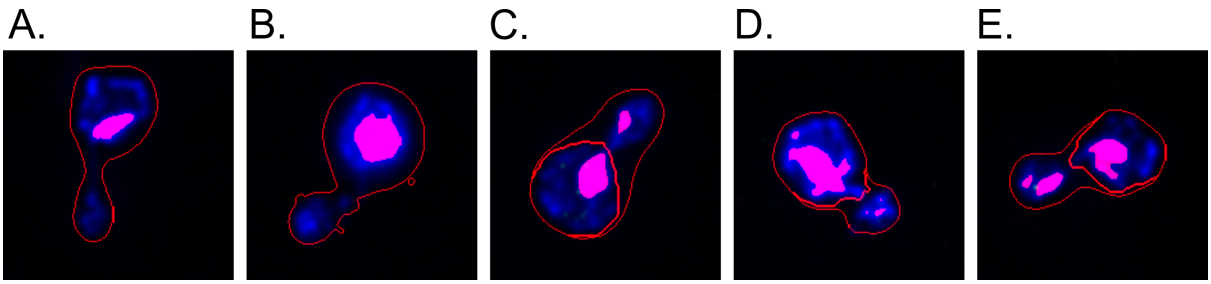

Figure 8.1 Examples of budded cells visualised in YMC samples

The images show the automated detection and outlining of cells (red line) and nuclei (pink centers). DNA is stained with DAPI (dark blue). Microscopy images were cropped and enlarged. Note: the DAPI signal is enhanced at this stage of the RNA-FISH quantification pipeline for the detection and outlining of nuclei and cells. Buds are only detected as individual cells when they present a DAPI center with high enough intensity to be determined as a nucleus as it is the case for ***C, D*** *and* ***E.*** *but not for* ***A*** *and* ***B*** *which show low DAPI intensities from mitochondrial DNA staining.*

8.4.3 Cell size distributions during the YMC

The size of single cells (in microns) was computed and analysed using the fluorescent and brightfield signal detected in cells of YMC and mid-log samples (details in chapter 2). Cell size is used (i) to compare growth between cells with different gene expression status, as a reflection of metabolic status and environmental conditions and (ii) to discriminate replicating cells from others, as cell size plays an essential role in cells exit from a vegetative (G1) state to a proliferative state, notably through the passage of a critical cell size threshold for Start (Hartwell et al. 1974). The distributions of cell size can be used to identify G1 from S/G2/M cells (Slavov & Botstein. 2011 supp data), as typically cell sizes are higher in M, than G2, than S, than G1 phase (Uchida et al. 2011).

8.4.4 Mitochondrial DNA as a proxy for cell cycle progression

Bright DAPI mitochondrial DNA nucleoids can be visualized in cells as fluorescent foci that line up on the mitochondrial network (Williamson & Fennel. 1975, Miyakawa et al. 1984, Chen & Butow. 2005). These were visualized in the cytoplasm of single cells of mid-Log phase cells or cells of the YMC population to examine whether there are differences or changes during the different growth conditions. Mitochondrial/mtDNA is compacted into nucleoids, DNA-protein complexes tethered to the mitochondrial membrane and bound to the actin skeleton (Chen & Butow. 2005, Lang et al. 2006). Haploid yeast in mid-log typically present 40 to 50 copies of mtDNA (Grimes et al. 1974) with 1 to two copies of mtDNA per mitochondria (Chen & Butow. 2005). Mitochondria are inherited from mothers to daughters in an active process (Yaffe. 1999), requiring actin cables to form in the mother to bud axis, and movement of mitochondria from mother to the forming bud starting at the G1/S transition (Boldogh

et al. 2005). The mitochondria to cell volume ratio in mid-log yeast is found relatively constant between the G1, S, G2 and M phases of the YMC (Uchida et al. 2011). Mitochondrial DNA copies are replicated in cells by Mip1, the mitochondrial DNA polymerase, to allow equal partitioning between mothers and daughters (Genga et al. 1986, Young et al. 2006).

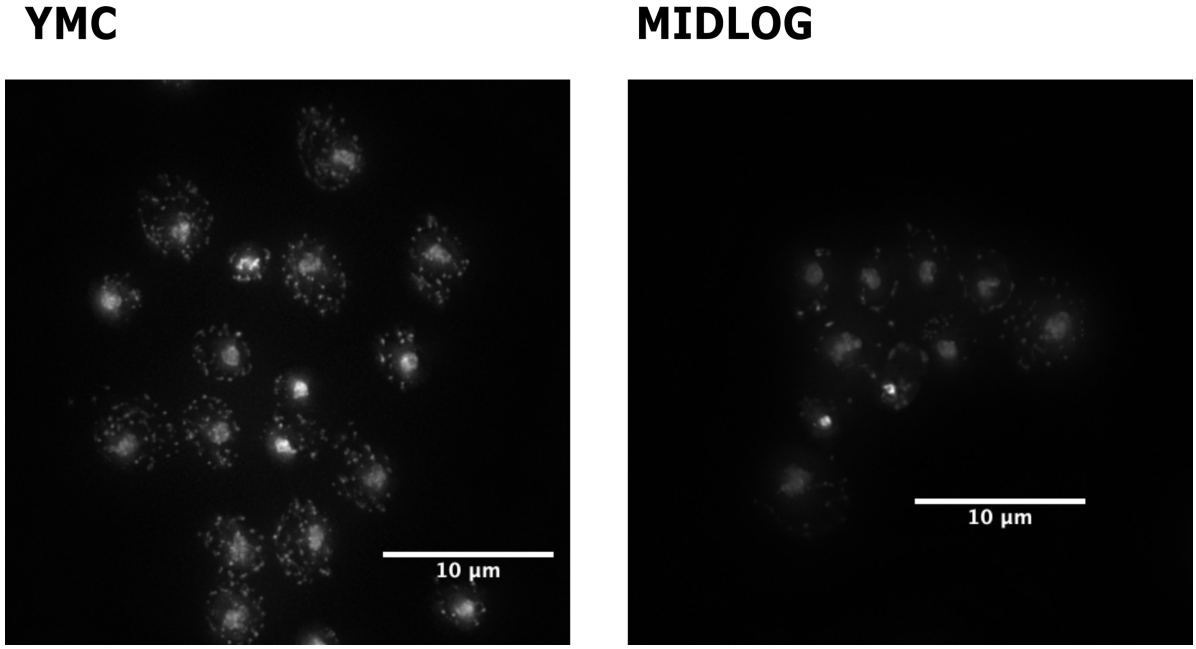

Figure 8.2. Detection of mitochondrial DNA

Example of microscopy image of yeast *samples taken along the YMC and in mid-Log phase. Microscopy images were cropped and enlarged. DNA is stained with DAPI (gray scale).*

The RNA-quantification pipeline was applied to the cytoplasmic DAPI signal in order to detect DAPI foci, quantify them and compute the sum of the cytoplasmic DAPI foci intensities in single cells (Figure 8.2). Samples of different timepoints along the YMC were grouped together according to the phases of the YMC; late LOC, early HOC, mid-HOC, late HOC and early LOC, in order to increase the number of cells detected per sample and also clarify the interpretation of results.

8.5 Results

Next, DNA content and cell diameters are analyzed in YMC and mid-Log cultures.

8.5.1 Nuclear and mitochondrial DNA content in single cells

Boxplots show the distributions of the nuclear and mitochondrial DNA DAPI intensities per cell in the different phases of the YMC and for mid-Log samples (Figure 8.3). Statistical tests were used to compare differences between the samples and indicate that the nuclear and mtDNA total content per cell is higher in mid-log phase than during the YMC when pooled (darker blue) or in different phases of the YMC (Figure 8.3.A-B. 1 & 2). This is likely to reflect more mid-Log cells replicating their DNA. In the different phases of the YMC, nuclear and mtDNA total content also differ, being highest in mid-HOC > early LOC > early HOC and late HOC > late LOC. This indicates that there is no simple relationship between temporal progression though the YMC and DNA content but that DNA replication is likely to occur in mid-HOC.

The distribution of the DNA content in mid-log cells shows a bimodal distribution. Such a bimodal distribution is typically detected when staining cells with propidium iodide or Cytox Green and sorting cells with FACS discriminating G1 from G2/M cells, with cells found in S-phase in between these 2 peaks (Tu et al. 2005, Miles et al. 2020).

Nuclear DNA content

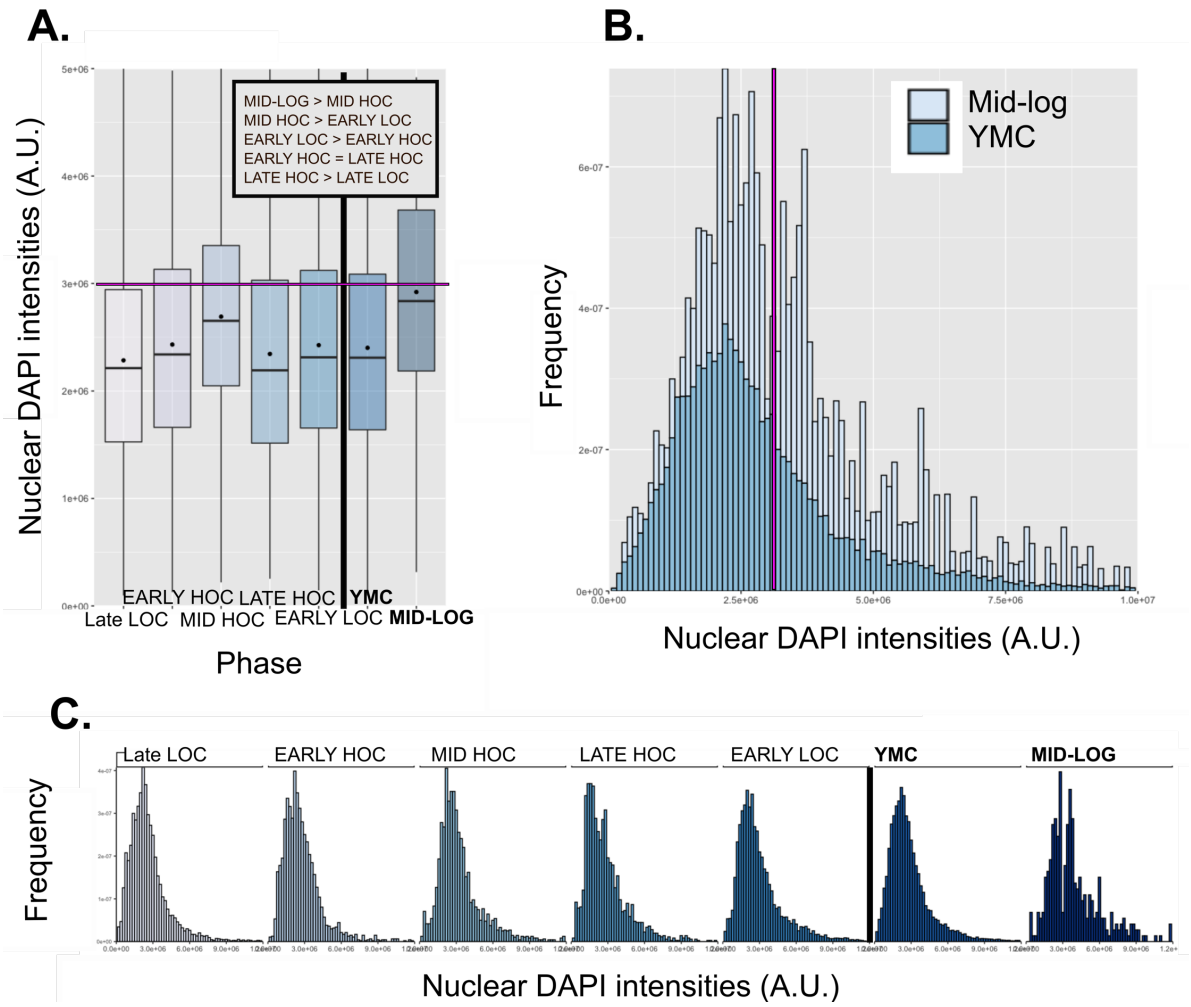

Figure 8.3.1

Mitochondrial DNA content

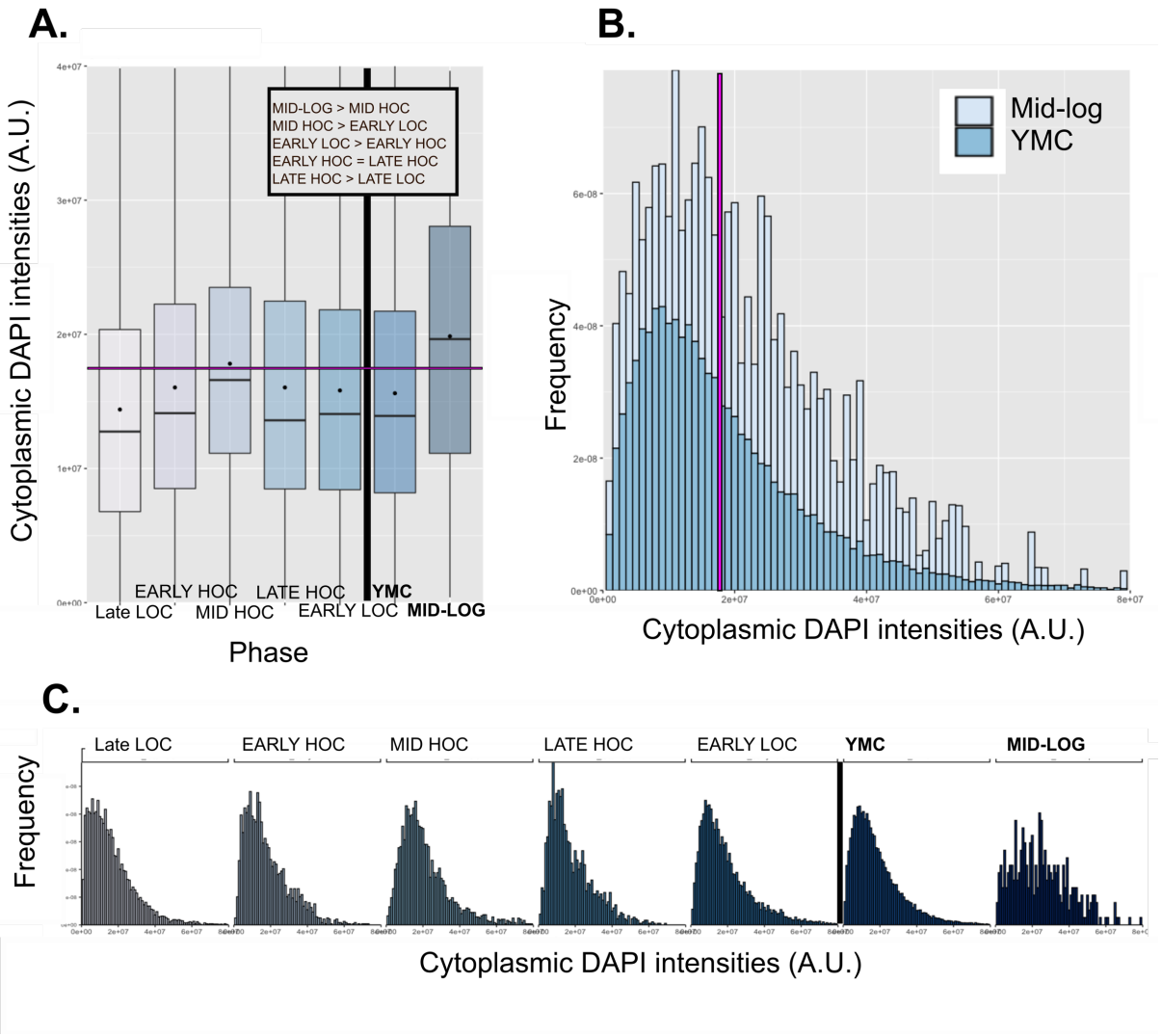

Figure 8.3.2

Figure 8.3. 1 & 2 Nuclear and mitochondrial DNA content is at its highest in mid-HOC phase of the YMC

1. *Sum of DAPI intensities in-nucleus.* ***2.*** *Sum of the total DAPI foci intensities in-cytoplasm per cell. The 3 repeats realised for the control set (ATO3 – ACT1) were merged.* ***A.*** *Boxplots showing distributions for YMC and Mid-log phase samples, but also for late LOC, early HOC, mid-HOC, late HOC and early LOC phases of the YMC. Black dots indicates means, while black horizonal bars indicate the medians. Samples from the different phases are ordered according to their distributions as determined by Wilcoxon tests (p-value<0.05).* ***B.*** *Histograms of the sum of DAPI intensities in-nucleus (1) or in-cytoplasm (2), for all YMC samples pulled together (dark blue) and mid-log phase samples (light blue). A purple line indicates a threshold between cells with low or high DNA content at plot A and B.* ***C.*** *Histograms of the sum of DAPI intensities in-nucleus (1) or in-cytoplasm (2) for late LOC, early HOC, mid-HOC, late HOC and early LOC phases of the YMC, all YMC samples together and mid-log phase.*

Bimodal distributions in the histograms of nuclear and mtDNA content are more difficult to detect for samples of the YMC, most likely because fewer cells are found outside the G1 phase of the YMC (DT ˜9h) compared to cells from mid-Log cutlures (DT ˜2h) (Figure 8.3.C. 1 & 2). However, there is evidence of a slight shift to the right depending on the phase of the YMC indicating the increase in DNA content presumably linked to entry into CDC.

Next, a threshold (3e+06 A.U, purple line) was set between these 2 distributions of nuclear DNA content in mid-Log phase samples to discriminate G1 from S/G2/M cells and separate cells with lower or higher nuclear DNA content (Figure 8.3.A.1). Boxplots of mtDNA DAPI intensities of cells with high and low nuclear DAPI intensities (Figure 8.4.A), indicate cells with higher nuclear DNA content also show higher mtDNA content. Remarkably, this effect is stronger for YMC samples than it is for mid-log phase samples. This is likely to reflect the increased oxygen consumption, perhaps a function of increased mitochondrial activity in the HOC phase together with cells entering the CDC. Thus, a second threshold (1.75e+07 A.U) was set to separate cells with lower or higher mtDNA content (Figure 8.3.A.2), using boxplots at Figure 8.4.A as guides.

Next, these nuclear and mtDNA thresholds were used to divide cells with high or low DNA content, and the relationship to cell size was examined for the different YMC phases and mid-log samples. Median cell diameters are reported in the text, while corresponding median cell volumes are found in parenthesis.

8.5.2 Cell size correlates with DNA content in the YMC and mid-log cultures

Cells with higher nuclear DNA content are larger with median cell diameters of 4.44μm & 4.63μm (45.83 & 51.97μm^3) compared to cells with lower nuclear DNA content with median cell diameters of 3.71μm & 3.47μm (21.88 & 26.74μm^3) (Figure 8.4.B & C). Boxplots of cell diameters overlap for cells with lower or higher nuclear DNA content (Figure 8.4.B), but not for cells with lower or higher mitochondrial DNA content (Figure 8.4.C), perhaps reflecting an increase in cytoplasmic volume compare to nuclear volume of cells during growth and progression through the cell division cycle. Most importantly, these results suggest the existence of a cell size threshold between cells with low DNA content, i.e. in G1 or late M phase (after anaphase) and cells in S/G2 and M phase (before anaphase). In order to find this cell size threshold, the nucleus and cell diameters of cells from YMC and mid-log population was studied next.

8.5.3 Cells from mid-log phase cultures are larger than YMC cells

Cell diameters are higher in mid-log phase than they are in YMC populations, in particular when compared to late LOC phase samples (Figure 8.5.A). The median cell diameter of 4.07μm in mid-log phase cultures compares to 3.93μm for YMC cultures (all samples together) and 3.79μm for late LOC phase samples (cell volumes of 35.3, 31.78 & 28.5 μm^3 respectively). Mid-log cell populations comprise more cells that are larger than in YMC populations (Figure 8.5.B). This difference in cell size can be explained by the difference in feeding rate and thus growth rate between the two types of cultures (YMC = 0.072h^{-1} , mid-log = 0.333h^{-1}), because cells from slow-growing cultures show lower cell volumes than cells from high-growth rate cultures (Brauer et al. 2008).

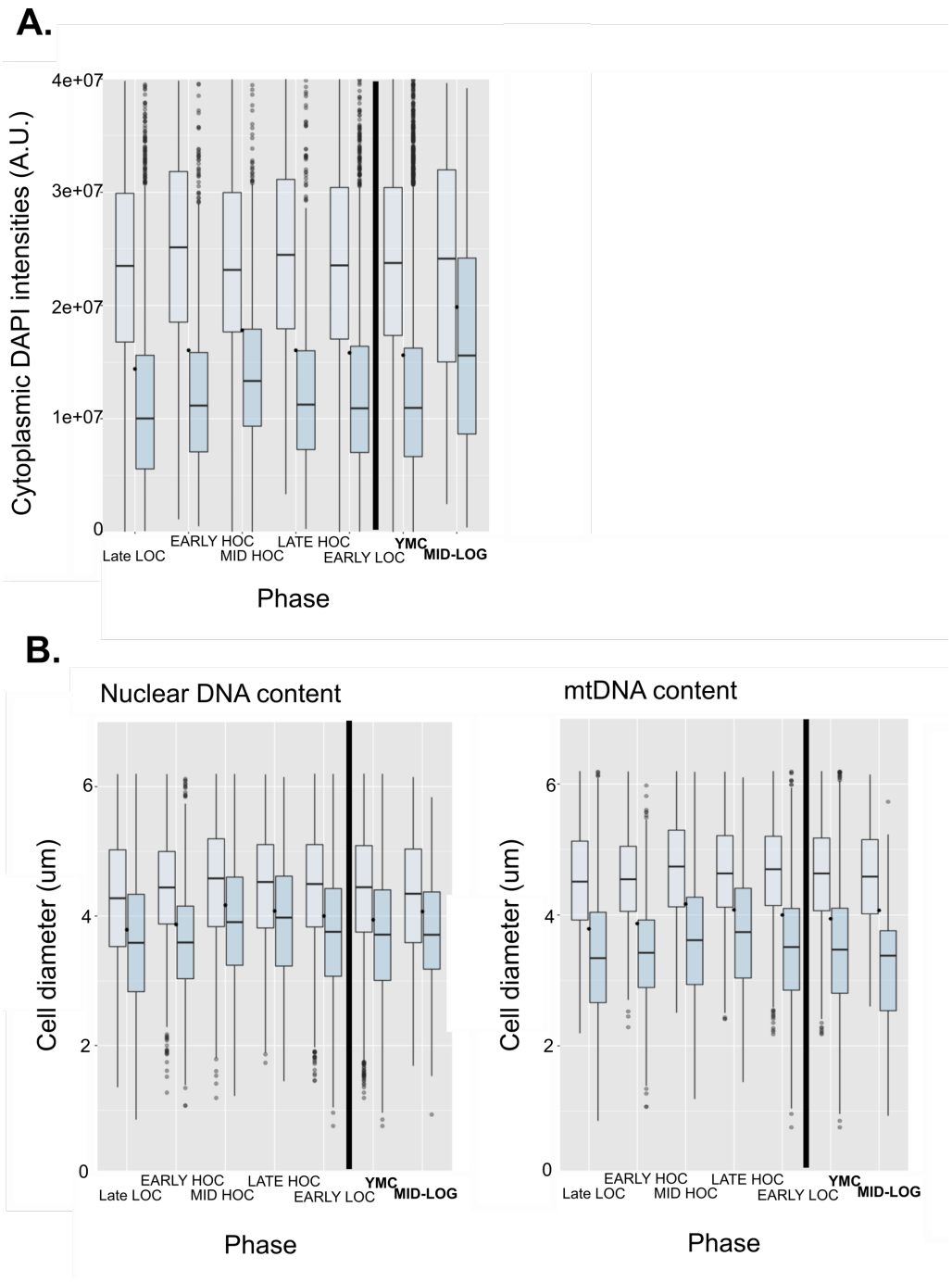

Figure 8.4 Cells with higher nuclear and mtDNA content are larger

A. *Boxplots of the mitochondrial DNA content (sum of DAPI intensities in-cytoplasm for cells showing nuclear DNA content (sum of DAPI intensities in-nucleus) under (dark blue) or above (light blue) the threshold set at Figure 8.3.1.B.* ***B.*** *Boxplots of the cell diameters (μm) distributions for YMC and Mid-log phase samples, but also for late LOC, early HOC, mid-HOC, late HOC and early LOC phases of the YMC. For cells showing* ***(1)*** *nuclear DNA content (sum of DAPI intensities in-nucleus)****, (2)*** *mtDNA content (sum of the total DAPI foci intensities) under (dark blue) or above (light blue) the threshold set at Figure 8.3.1 & 2.B. Black dots indicates means of the metrics, of all cells found for the specific phase, while black horizontal bars indicate the medians. The 3 repeats realised for the control set (ATO3 – ACT1) were merged.*

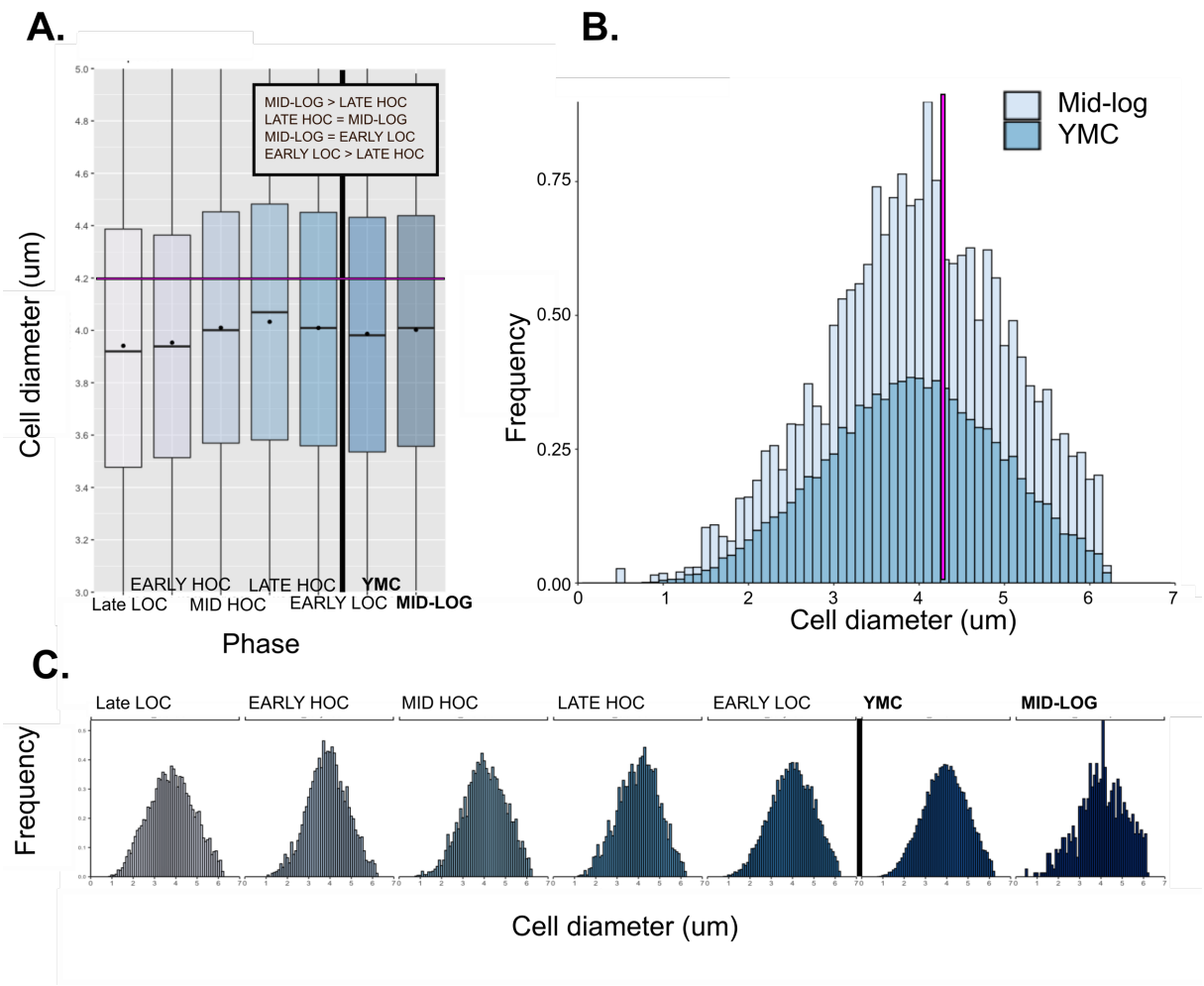

Figure 8.5 Nuclear and cell diameters vary along the YMC

A. *Boxplots showing distributions of cell diameters for YMC and mid-Log phase samples, but also for late LOC, early HOC, mid-HOC, late HOC and early LOC phases of the YMC. Black dots indicates means, while black horizontal bars indicate the medians. Samples from the different phases are ordered according to their distributions as determined by Wilcoxon tests (p-value<0.05).* ***B.*** *Histograms of the cell diameters for all YMC samples pulled together (dark blue) and mid-log phase samples (light blue). The purple line indicates a threshold between cells with low or high DNA content* ***C.*** *Histograms of the cell diameters for late LOC, early HOC, mid-HOC, late HOC and early LOC phases of the YMC, all YMC samples together and mid-log phase. All repeats were merged (Single-FISH:ATO3, Dual-FISH ATO3-SHM2, SHM2-IDH1, IDH1-ATO3, Control set: ATO3 – ACT1.*

8.5.4 A cell diameter threshold of ~4.2μm defines 2 sub-populations of cells in mid-log cultures

The control of cell size is related to ploidy and by the cell cycle progression (Jorgensen & Tyers. 2004, Hartwell et al. 1974). Distributions of cell size has been employed to determine whether or not cells are budded (Slavov & Botstein. 2011 supp data), as cells undergoing DNA replication or possessing 2 copies of DNA are bigger than cells in G1 with one DNA copy (Jorgensen & Tyers. 2004). Histograms of cell diameters for pooled YMC samples (darker blue) were compared to mid-log samples (lighter blue) and reveal a bimodal distribution in the mid-log phase histogram which is not obvious in the YMC histogram. In the mid-log phase, the drop in cell numbers between the two peaks occurs around a cell diameter of ˜4.2μm, corresponding to a cell volume of 38.8μm^3 (Figure 8.5.B). This threshold roughly corresponds to the median cell diameters found for cells with higher nuclear DNA content and differentiating cells with lower or higher mtDNA content (Figure 8.4.B & C). Taken together, these data support cells with diameters below the threshold of ˜4.2μm as unbudded (G1) while above this, cells are expected to be budded (S/G2/M). Therefore, ˜4.2μm and 38.8μm^3 are proposed to be the cell diameter and volume thresholds respectively for Start in mid-log phase samples under the conditions employed in this study.

8.5.5 The cell diameter of YMC cells increase in mid-HOC and peak in late HOC

The threshold of ˜4.2μm or 38.8μm^3 was applied to the YMC samples to define when cells pass Start into the CDC. It is important to point out that YMC cultures might possess a lower cell size threshold for passing start than mid-log phase cultures due to their different growth rate (Lorincz & Carter. 1979, Jorgensen et al. 2004). In fact, at a dilution rate of 0.072h^{-1}, the relationship between feeding rate and critical cell size is

expected to cease and cells are expected to bud at a minimal critical cell size threshold (volume of 27.8 - 31.5 μm^3 for the haploid C4.2 strain) according to previous studies (Johnston et al. 1979). YMC cultures might be more complex, as some cells might not consume nutrients which could increase nutrient availability for other cells and thus increase the critical cell size threshold for Start, as seen for cells transferred from poor to rich nutrients (Lorincz & Carter. 1979). In the YMC, cell diameters increase in early and mid-HOC, peak in late HOC and decrease in early LOC, with median cell diameters of 4.02μm in mid-HOC and 4.07μm in late HOC (corresponding to cell volumes of 34.01 & 35.3μm^3) (Figure 8.5.A). Although these values are below the thresholds defined for mid-log cells, they are above the minimal cell size threshold consistent with their growth rate in YMC cultures. Indeed, during the YMC, highest average cell volume were recorded at the time most cells were found budded (Porro et al. 1988).

Next, to resolve whether the larger cell in the YMC are just growing or have entered the CDC, cell diameter is related to the nuclear and mtDNA content.

8.5.6 The proportion of cells with higher cell sizes increases in mid-HOC phase of the YMC but does not scale up with the nuclear and mtDNA content

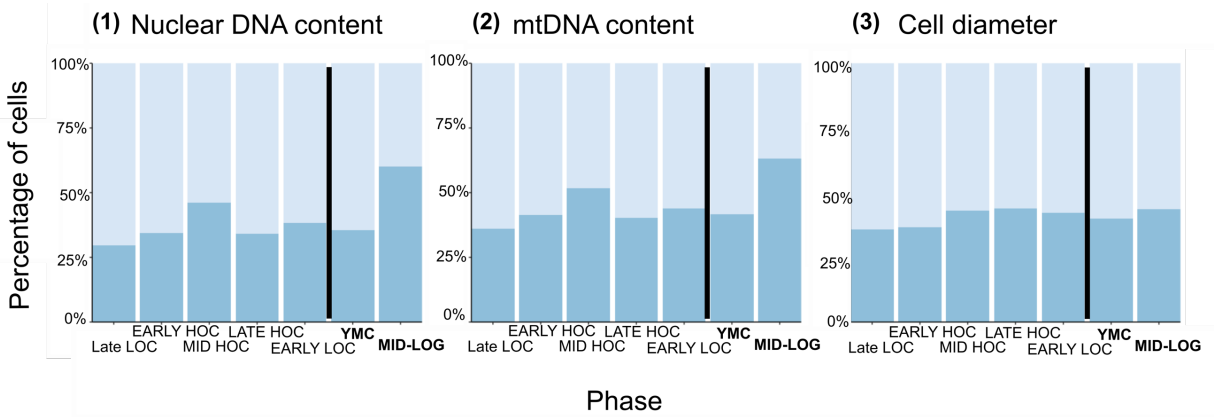

Figure 8.6. The proportion of cells with high nuclear DNA, mtDNA and cells size vary along the YMC

Fraction of cells with lower (light blue) or higher (dark blue) (1) nuclear DNA content (sum of DAPI intensities in-nucleus) (2) mitochondrial DNA content (sum of mtDNA DAPI foci intensities in-cytoplasm), (3) cell diameters (μm) for late LOC, early HOC, mid-HOC, late HOC and early LOC phases of the YMC, all YMC samples together and mid-log phase. Thresholds for dividing cells into the two classes are defined in Figures 8.3.1 & 2.B, 8.5.B. (1),(2)the 3 repeats for the control set (ATO3 – ACT1) were merged, (3) All repeats were merged.

The proportion of cells showing lower or higher nuclear DNA content, mtDNA content and cell diameter, relative to their respective thresholds, peaks in the mid-HOC phase of the YMC (Figure 8.6). In the YMC, there is only a slight increase (less than 10%) in the proportion of cells with higher cell diameters than the threshold (4.2um), between late LOC and mid-HOC phase (Figure 8.6). Moreover, between late LOC and late HOC the difference in cell diameter is up to 0.28um (Figure 8.5.A). Therefore, the results indicate that the cell size increase observed along the YMC is most likely connected to the progression of a proportion of cell through the CDC in mid-HOC phase of the YMC, with more cells transitioning out of a G1 phase, but this cell size increase does not scale perfectly to the progression of cells through the cell division cycle.

The proportion of cells with higher DNA content fluctuates along the YMC with ˜45 to 50% of the population in mid-HOC phase compared to ˜25 to 30% of the population showing higher levels in late LOC phase. This contrasts to mid-log cells with 65% of cells higher nuclear and mtDNA content.

Thus, the results show more cells are found with higher DNA content in mid-log phase than in YMC, in line with the fact that the proportion of cells progressing through the cell division cycle is expected to be higher in mid-log phase (DT ˜2h) than in YMC (DT ˜9h), with ˜62% of cells found in G2/M, ˜5% in S phase and ˜33% in G1 in mid-log cultures (Li et al. 2013) compare to ˜10 to 30% of cells found in in S/G2/M phase during each yeast metabolic cycle (Burnetti et al. 2016, Feltham et al. 2020). Results here indicate that 25 to 30% of cells are expected to be in S/G2/M phases of the cell division cycle throughout the YMC at all times and phases of the metabolic cycles as these cells present higher nuclear and mitochondrial DNA, indicating a higher proportion then the one reported by Robertson et al. 2010 and Burnetti et al. 2016 (˜10%).

8.6 Conclusions

In conclusion, results indicate (i) that 15 to 25% of cells leave the G1 state, pass the Start checkpoint and are in a S/G2/M phase in mid-HOC phase of the YMC (ii) ˜25 to 30% of the cells are in a S/G2/M phase at all times during the YMC (iii) the remaining cells (45 to 65%) stay in a G1 state throughout the YMC. These results thus suggest that some cells exit quiescence synchronously, while others divide asynchronously along the cycle, although most cells are found in quiescence.

Thus YMC cultures are composed of at least 3 sub-populations.

8.7 Introduction to mitochondrial biology

8.7.1 A proportion of cell show signs of respiratory growth in mid-HOC phase

Next, the results presented in Figure 8.7, show mitochondrial DNA nucleoid numbers increase in the HOC phase of the YMC. Importantly the number of mitochondrial DNA nucleoids (DAPI foci) but also the total mitochondrial DNA content might also refer to the metabolic state of cells with regards to respiratory growth.

Indeed, previous studies showed higher numbers of mtDNA nucleoids are found in aerobic cultures compare to anaerobic ones, indicating an increase in mtDNA nucleoids numbers in cells undergoing respiratory growth (Chen & Butow. 2005). Moreover, the morphology of the mitochondrial network also depends on environmental conditions, the type of growth and the metabolic status of cells, as post diauxic shift, under nutrient starvation and in old (chronological) cells, cells show a vesicular network (up to 50 vesicules), (Thorsness. 1992, Sagot et al. 2006, Klinger et al. 2010, Laporte et al. 2018), while under high growth and in proliferative cultures yeast cells present a tubular network (˜10 mitochondrial tubules) (Friedman and Nunnari. 2014). In fact, for yeast cells under starvation, the ability to perform respiratory growth seems critical for the establishment and exit from quiescence, as the rate of oxygen consumption was found to be six time higher in quiescent cells compare to non-quiescent cells (Davidson et al. 2011) and cells switching from fermentation to respiration were found more likely to exit quiescence (MacLean et al.,2001, Dhawan & Laxman. 2017). Similarly, respiration plays an important role in yeast metabolic cycles. During the YMC, the oxygen consumption through aerobic respiration, the CO_2 release and the H_2S production fluctuate (high in HOC, lower in LOC) (Murray, Haynes & Tomita. 2011). Accordingly, mitochondrial membrane potential also changes along the YMC, with polarization during HOC and

depolarisation during LOC (Llyoyd et al. 2002, Murray, Haynes & Tomita. 2011). Because of these results Davidson et al., described the yeast metabolic cycle as a system related to differentiation of a stationary phase population into quiescent and non-quiescent cells (Davidson et al. 2011).

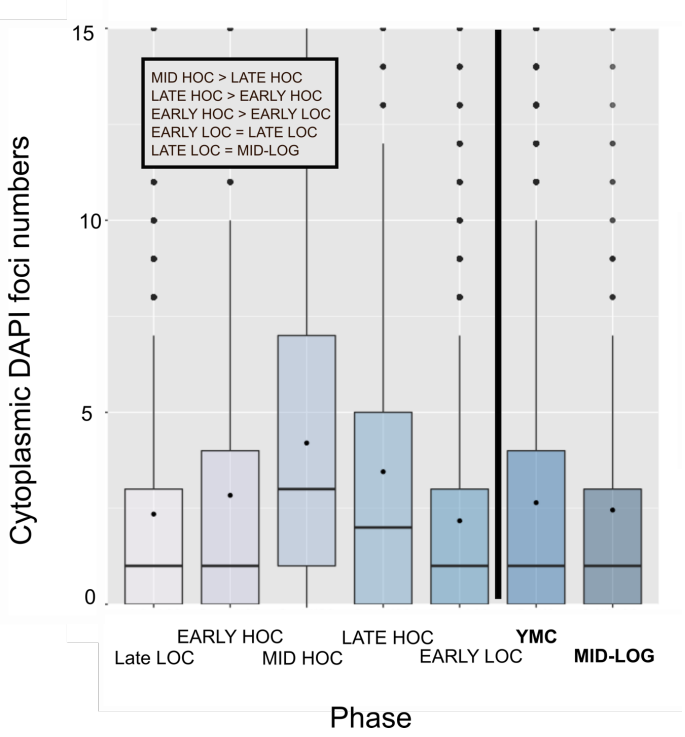

Figure 8.7 Mitochondrial DNA nucleoid numbers increase in mid-HOC phase of the YMC

Numbers of DAPI foci in-cytoplasm per cell. The 3 repeats realised for the control set (ATO3 – ACT1) were merged. Boxplots showing distributions for YMC and Mid-log phase samples, but also for late LOC, early HOC, mid-HOC, late HOC and early LOC phases of the YMC. Black dots indicates means, while black horizontal bars indicate the medians. Samples from the different phases are ordered according to their distributions as determined by Wilcoxon tests (p-value<0.05).

In light of these findings, the results presented in Figure 8.7 could indicate an increase in the proportion of cells undergoing respiratory growth in mid HOC. Nevertheless, this suggestion requires further investigations, as the relationship between the mitochondrial network, the number of mtDNA nucleoids and respiration seems more complex and the results indicate lower mtDNA nucleoid numbers than previously reported (Chen & Butow. 2005, Laporte et al. 2018).

8.8 Results

Next the relationship between gene expression, cell size and DNA content is investigated.

8.8.1 Transcript numbers poorly correlate with nuclear DNA, mtDNA content and cell size in the YMC and mid-log cultures

The relationships between nuclear DNA, mtDNA content, cell size and gene expression is investigated by calculating Spearman correlation coefficients between these factors with the aim of relating RNA numbers observed in single cells with lower or higher DNA content.

Spearman coefficients of correlations found between nuclear DNA content (Table 8.1.A), mtDNA content (Table 8.1.B) and transcript levels in cells (for the pooled control set: *ATO3* – *ACT1*) indicate low correlations between DNA content and total transcript numbers in cells from YMC (all timepoints pooled) and mid-log phase samples. Higher correlations are found between DNA content and gene expression for *ACT1* than for *ATO3*. Spearman coefficients of correlations between cell diameters and transcript levels in single cells from YMC or mid-log populations vary between repeats (Table 8.1). Slightly higher correlations are observed for *SHM2* and *IDH1* compared to *ATO3* and *ACT1* in mid-log phase samples, where the cells are larger. During the YMC, cells with higher nuclear and mtDNA content present higher levels (maximum of 1.4-fold) of *ATO3* and *ACT1* transcripts (Figure 8.8). In early LOC, a larger difference is observed in *ATO3* and *ACT1* RNA numbers between the DNA content categories (under or above the threshold) perhaps resulting from the higher proportion of cells leaving the G1 state, and transitioning through the cell division cycle at that time (Feltham et al. 2019, Burnetti et al. 2016). Similar trends are observed in mid-log phase, with a higher

difference in expression levels of *ACT1* detected between the cells with lower and higher DNA content (1.9-fold) , reflecting more cells with 2 copies of DNA in mid-Log samples.

Table 8.1 Gene expression is lowly correlated to DNA content and cell size in YMC cultures *Spearman correlation coefficients for YMC and mid-log phase cultures (all samples pooled) between* ***A.*** *Nuclear DNA content (sum of DAPI intensities in-nucleus) and transcript numbers in cells.* ***B.*** *Mitochondrial DNA content (sum of DAPI intensities in-cytoplasm) and transcript numbers in cells. The 3 repeats realised for the control set (ATO3 – ACT1) were merged and all YMC samples and mid-log samples pulled together respectively.* ***C.*** *Cell diameters and transcript numbers in cells. Range between all repeats (Single-FISH:ATO3, Dual-FISH ATO3-SHM2, SHM2-IDH1, IDH1-ATO3, Control set: ATO3 – ACT1), all YMC samples and mid-log samples pooled.*

A. Nuclear DNA content

Transcript	YMC	Mid-log
ATO3	0.12	0.18
ACT1	0.21	0.36

B. Mitochondrial DNA content

Transcript	YMC	Mid-log
ATO3	0.22	0.3
ACT1	0.34	0.43

C. Cell diameters

Transcript	YMC	Mid-log
ATO3	0.13 – 0.28	0.05 – 0.27
SHM2	0.15 – 0.32	0.28 – 0.68
IDH1	0.19 – 0.27	0.28 – 0.53
ACT1	0.4	0.24

Cells with diameters above the threshold (4.2μm) tend to show higher transcript levels along the YMC and in mid-log phase (Figure 8.9). For all transcripts, a bigger difference in gene expression levels between cells of lower or higher diameters is observed at phases of higher expression. This effect is particularly strong for *ACT1* transcripts in YMC and mid-log cultures, and for *SHM2* in mid-log phase cultures with 5.2 fold change differences compare to 1.2 fold change differences for *ATO3* and *IDH1*. These results thus suggest a stronger connection between cell size and *SHM2*

and *ACT1* transcripts. Together these results indicate target transcript expression only poorly correlates with the nuclear and mtDNA content, but also with cell size, indicating only a low global correlation between gene expression and cell growth.

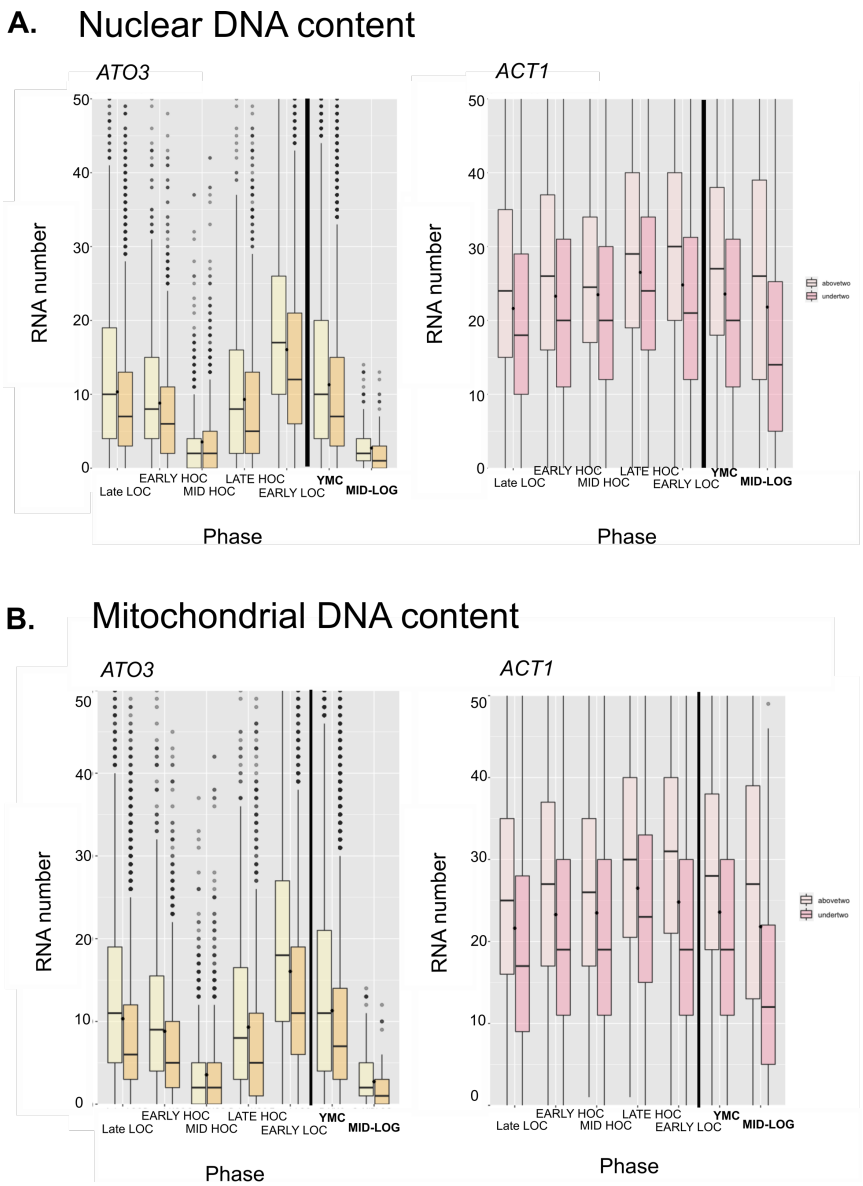

Figure 8.8 Cells with higher nuclear and mitochondrial DAPI intensities show higher transcript levels.

Boxplots of the distributions of RNA numbers for cells showing higher (light colour) or lower (dark colour) DAPI intensities in single cells. ***A.*** *for nuclear DAPI intensities, i.e. nuclear DNA content,* ***B.*** *For cytoplasmic DAPI intensities, i.e. mtDNA content. The 3 repeats realised for the control set (ATO3 – ACT1) were merged. Transcripts levels of ATO3 (yellow) and ACT1 (pink) are shown in late LOC, early HOC, mid-HOC, late HOC and early LOC phases of the YMC, as well as for all YMC samples together and all Mid-log samples. Black dots indicates means of the metrics, of all cells found for the specific phase, while black horizontal bars indicate the medians.*

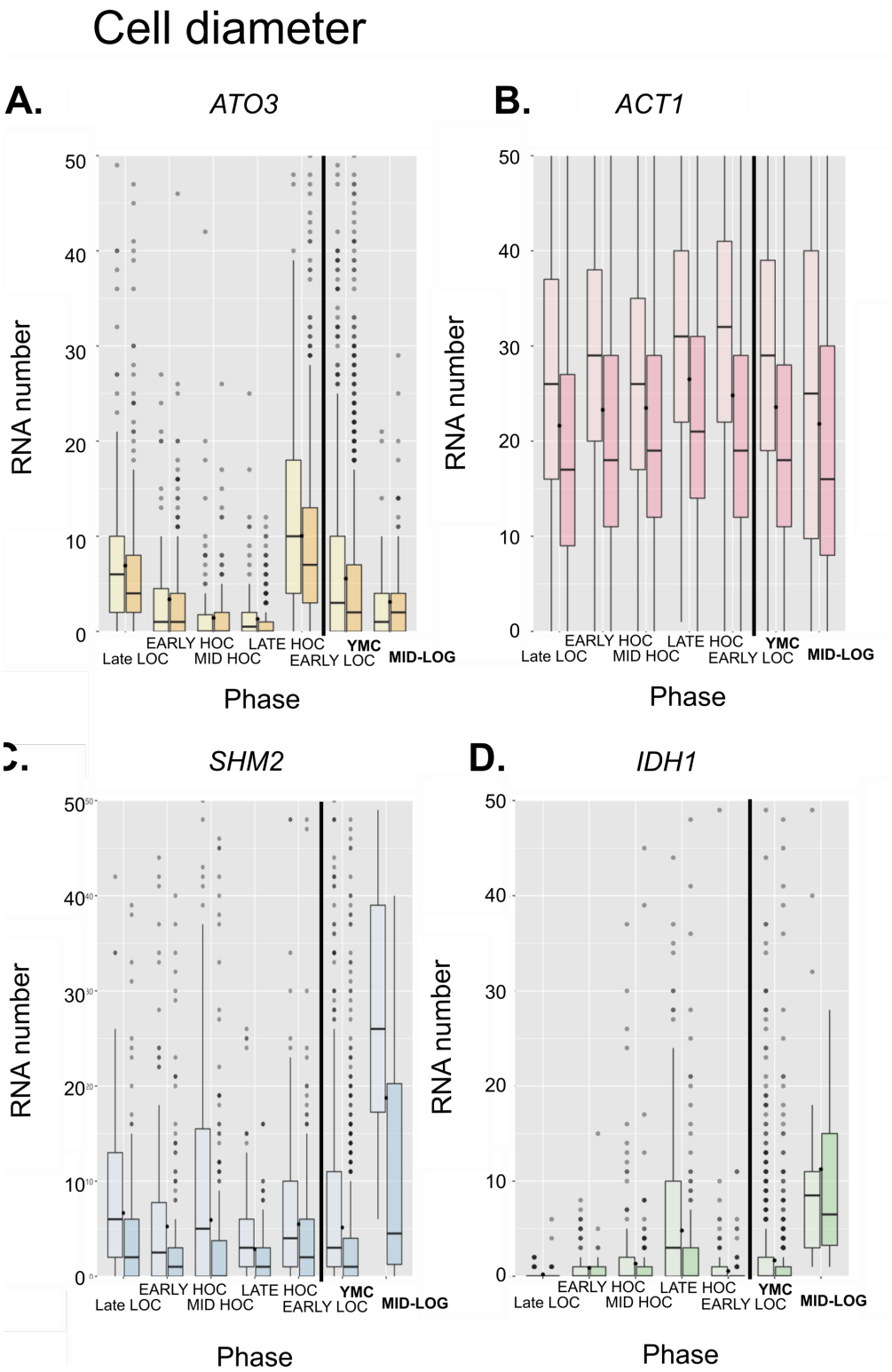

Figure 8.9 Larger cells tend to show higher transcript levels

Boxplots of the distributions of total RNA numbers for cells showing higher (light colour) or lower (dark colour) cell diameters than 4.2μm in single cells. ***A.*** *for ATO3 in yellow (Single-FISH)* ***B.*** *for ACT1 in pink (Control set)* ***C.*** *for SHM2 in blue (Dual-FISH2)* ***D.*** *for IDH1 in green (Dual-FISH3). Transcripts levels are shown in late LOC, early HOC, mid-HOC, late HOC and early LOC phases of the YMC, as well as for all YMC samples together and all Mid-log samples. Black dots indicates means of the metrics, of all cells found for the specific phase, while black horizontal bars indicate the medians.*

8.9 High-growth asynchronous mid-log cultures

8.9.1 Gene expression and cell size are coordinated in mid-log phase

The relationship between the growth and proliferative status of cells and their gene expression state is investigated first in mid-log phase cultures. Cell size is used as a proxy for growth and CDC progression. Distributions of cell diameters are compared between cells showing different gene expression state as determined by RNA-FISH; (i) for *ATO3* and *ACT1*, (ii) for *ATO3* and *SHM2*, (iii) for *SHM2* and *IDH1* and (iv) for *IDH1* and *ATO3.* Previously, the proportion of cells with different transcripts found in mid-log phase pointed to a certain chronology of transcriptional events based on the following observation.

- Most cells expressing *ATO3* co-express other transcripts.
- Only a few cells were found expressing *ATO3* alone.
- *IDH1* is usually co-expressed with *SHM2*.
- Cell co-expressing *ACT1* and *SHM2* were found to be expressed with or without *ATO3* or *IDH1*.

These results lead to a proposal that transcripts are produced in the following chronology: Early in their lifetime, cells constitutively transcribe *ACT1* and *SHM2. IDH1* is expressed transiently later in the lifetime of cells. *ATO3* is the final transcript to be expressed. This hypothesis can be validated by assessing cell size and relating this to the type of transcript(s) expressed. The data reveal that cells with different gene expression status show distinct cell size ranges (Figure 8.10).

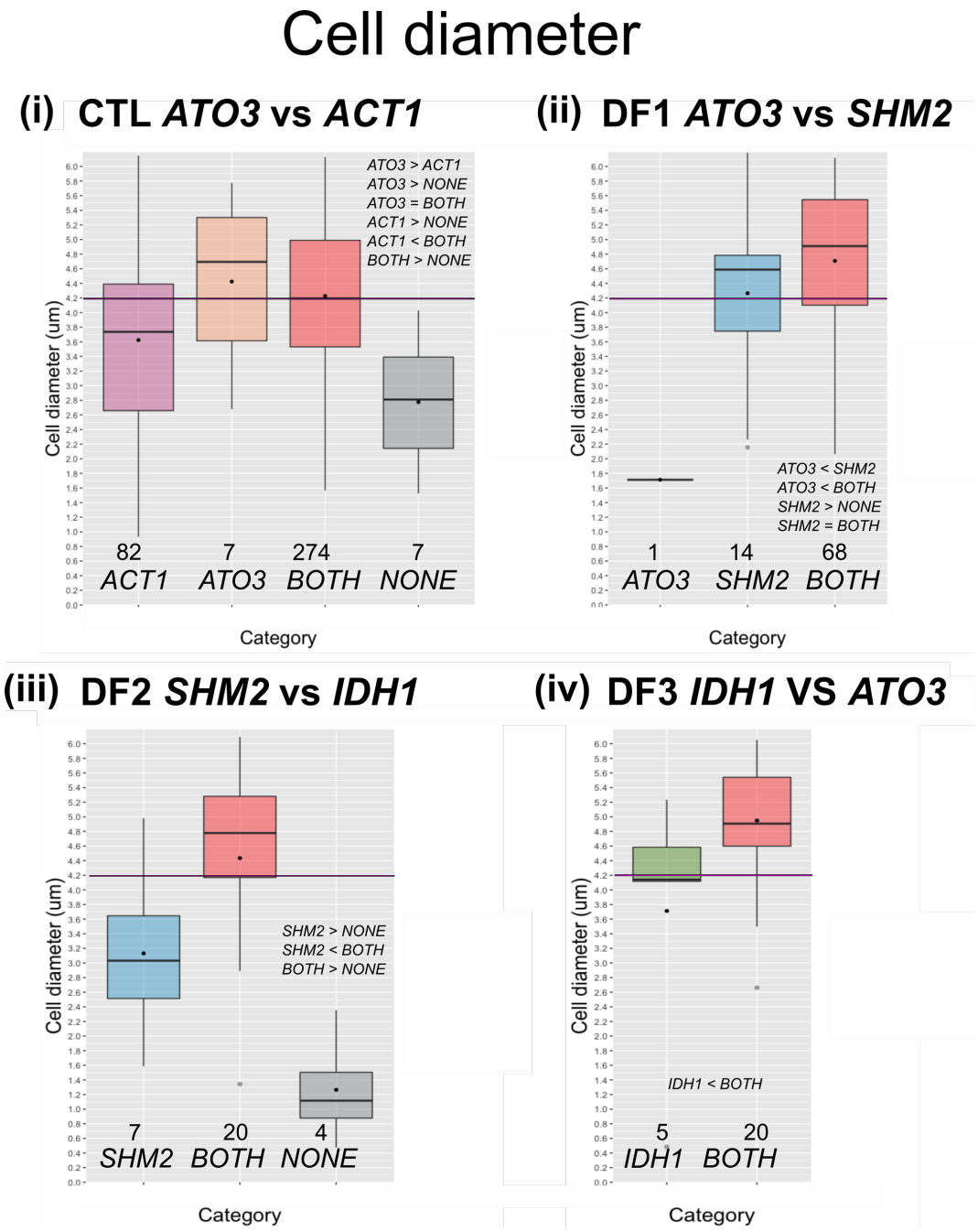

Figure 8.10 Cell size differs between cells of different gene expression status in mid-log phase cultures *Boxplots of the distributions of cell diameters for cells expressing transcripts in-cells; (a) only in the first fluorescent channel (Cy5), (b) for cells expressing only in the second fluorescent channel (Cy3), (c) for cells expressing both transcripts (red), (d) for cells expressing no transcripts (grey) in mid-log phase cultures.* ***(i).*** *for the Control set ACT1 in purple, ATO3 in orange* ***(ii).*** *For the 1st Dual-FISH ATO3 in yellow, SHM2 in blue,* ***(iii)*** *For the 2nd Dual-FISH SHM2 in blue, IDH1 in green.* ***(iv).*** *For the 3rd Dual-FISH IDH1 in green, ATO3 in yellow. Black dots indicate means, black horizontal bars indicate the medians. The horizontal line indicates a threshold between cells with low or high cell diameters. Samples from the different "expressing categories" phases are ordered according to their distributions as determined by Wilcoxon tests (p-value<0.05). Due to the low cell number captured in mid-Log phase, the number of cells detected in each category is indicated under each boxplot for mid-Log samples.*

Specifically, with median cell diameters reported in parenthesis:

(i) The few cells expressing *ATO3* without *ACT1* (orange, ˜4.7μm) show higher cell diameters then cells expressing *ATO3* with *ACT1* (red,˜4.2μm) while cells expressing *ACT1* only are smaller than any cell also expressing *ATO3* (purple,˜3.7μm). All cells expressing transcripts have higher cell diameters than cells without transcripts (grey,˜2.8μm).

(ii) Cells co-expressing *ATO3* and *SHM2* (red, ˜4.9μm) show higher cell sizes than cells expressing *SHM2* only (blue,˜4.6μm), while cells expressing *SHM2* with or without *ATO3* show higher cell sizes than cells expressing *ATO3* transcripts only (orange,˜1.7μm).

(iii) Cells expressing both *SHM2* and *IDH1* transcripts (red,˜4.8μm) present higher cells sizes than cells expressing *SHM2* only (blue,˜3μm), while cells expressing any of these transcripts show higher cell size than cells found with no transcripts (grey,˜1.1μm).

(iv) Cells co-expressing *IDH1* and *ATO3* (red,˜4.9μm) present a higher cell diameter than cells expressing *IDH1* only (green,˜4.2μm).

(v) Finally, cells co-expressing (red) *ATO3* and *SHM2* or *ATO3* and *IDH1* show slightly higher cell diameters (˜5μm) then cells co-expressing *SHM2* and *IDH1* (˜4.8μm) or cells co-expressing *ATO3* and *ACT1* (˜4.2μm).

8.10 Discussion

8.10.1 The cell size seems coordinated with the intrinsic metabolic clock

The model at Figure 8.11 aims to capture the relationship between cell size and the type of transcripts expressed in single cells of mid-log phase samples. In summary, cells expressing the stationary phase transcript *ATO3* tend to show higher cell diameters than cells that express *ACT1*, *SHM2* or *IDH1* only. Similarly, cells that express *IDH1* and cells that express *ACT1* are larger than cells expressing *SHM2* only. Finally cells expressing any of these transcripts are generally larger than cells found without any transcripts. Therefore, together these results indicate that in mid-log phase, cell size correlates with the intrinsic metabolic clock of cells described in chapter 7.

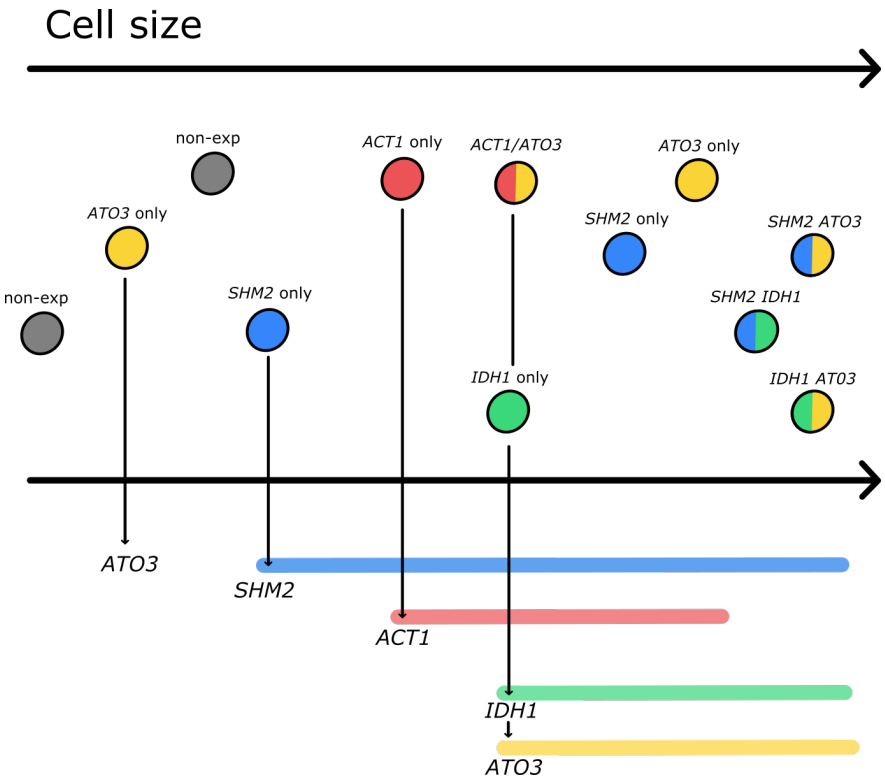

Figure 8.11 Cell size and gene expression coordination in mid-log phase cultures

Cells and their distinct gene expression profiles were classified by ascending cell sizes based on results from Figure 8.10. This model indicates a coordination between gene expression and cell sizes in mid-Log cultures.

8.10.2 Cells with quiescent stationary phase characteristics are found in mid-log cultures

Cell size is one of the characteristics that distinguishes stationary phase sub-populations. Typically, small daughter cells are characterized as quiescent and large mother cells are characterized as non-quiescent (Miles et al. 2020). *ATO3* (a LOC transcript in the YMC) is generally expressed in the stationary phase of batch grown cells while *SHM2* (a HOC transcript in the YMC) is highly expressed in mid-log phase cells. In this characterisation of transcripts and cell size in mid-log cells, those co-expressing *SHM2* and *ATO3* tend to be larger than cells expressing *SHM2* only, while the few small cells are found to express *ATO3* but not *SHM2* (Figure 8.10.ii). This is surprising as most cells expressing *ATO3* tend to be large but when they are large they also co-express *SHM2* or *IDH1* (normally HOC transcripts) (Figure 8.10.ii, iv). Thus, here the results suggest that cells co-expressing LOC (*ATO3*) and HOC (*SHM2* or *IDH1*) transcripts might be larger non-quiescent mother cells, while cells expressing LOC (*ATO3*) transcript only might be small quiescent daughter cells. This supports a relationship between transcripts and an intrinsic metabolic clock.

8.11 Slow-growth synchronous YMC cultures

8.11.1 In YMC cultures gene expression, cell growth and proliferation are coordinated

Next, the relationship between growth, cell cycle progression and gene expression state is examined over time in YMC cultures. Again cell size is used as a proxy for growth and together with nuclear and mitochondrial DNA content, these metrics indicate the CDC states of cells. The aim of this work is to characterize sub-populations within the synchronous YMC cultures. The results are interpreted in light of data obtained from mid-log cells and transcript distributions over the YMC:

(i) cells expressing high *ATO3* transcripts are expected to be in a LOC or less metabolically active state

(ii) cells expressing high *SHM2* and *IDH1* levels are expected to be in a HOC or more metabolically active state

(iii) cells that express high *ATO3* transcript levels during the HOC phase are likely to be stuck in an LOC metabolic state (less metabolically active state).

(iv) cells that do not express *ATO3* transcripts in the LOC phase are likely to be growing or in the CDC (more metabolically active state).

First, distributions of (i) cell diameters, (ii) nuclear DNA content and (iii) mitochondrial DNA content in late LOC, early HOC, mid-HOC, late HOC and early LOC are determined for cells expressing *ATO3* only (orange), *ACT1* only (purple), both transcripts (red), no transcript (grey) (Figure 8.12), high levels of *ATO3* and low levels of *ACT1* or vice versa (Figure 8.13). The thresholds for the different parameters are determined previously (Figure 8.3.1 & 2.B and 8.5.B) and are shown as horizontal purple lines.

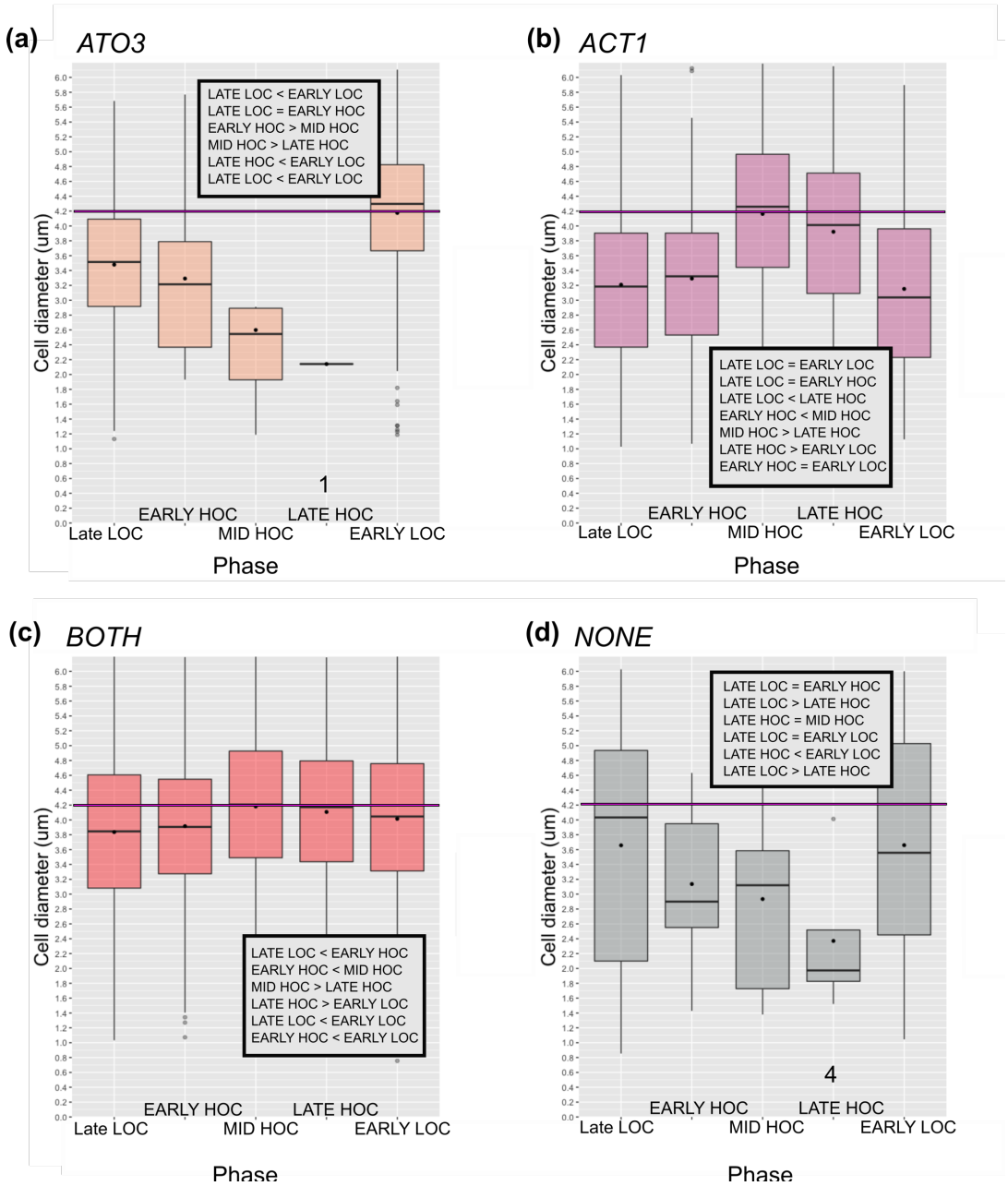

Figure 8.12 Cell diameters vary between cells of different gene expression status

Boxplots of the distributions of cell diameters for cells expressing transcripts in-cells; ***(a)*** *only in the first fluorescent channel (Cy5, ATO3 in orange),* ***(b)*** *for cells expressing only in the second fluorescent channel (Cy3, ACT1 in purple),* ***(c)*** *for cells expressing both transcripts (red),* ***(d)*** *for cells expressing no transcripts (grey) for the Control set. The 3 repeats realised for the control set (ATO3 – ACT1) were merged. Black dots indicate means, black horizontal bars indicate the medians. The horizontal line indicates a threshold between cells with low or high cell diameters. Samples from the different "expressing categories" phases are ordered according to their distributions as determined by Wilcoxon tests (p-value<0.05). When a low cell number is detected in a category, the number of cells detected is indicated under the boxplot of cell diameters.*

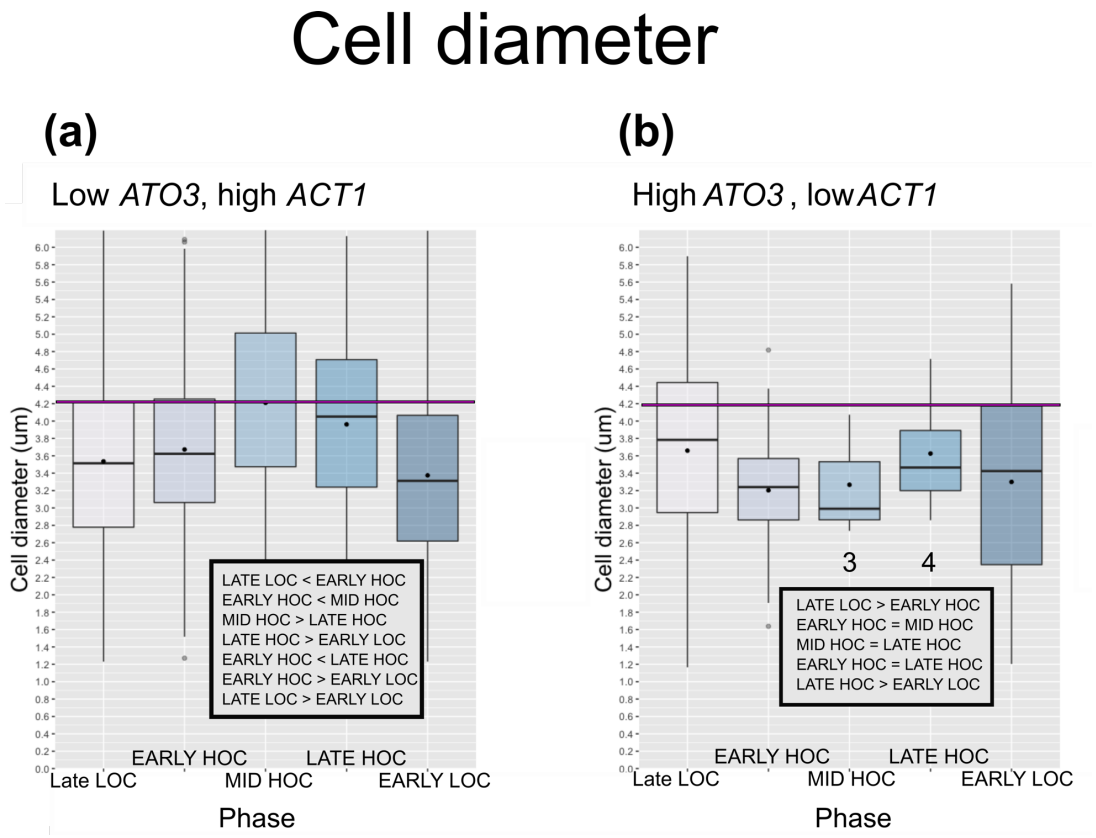

Figure 8.13 Cell diameters vary between cells expressing high or low levels of transcripts

Boxplots of the distributions of cell diameters for cells expressing ***(a)*** *low ATO3 levels and high ACT1 levels* ***(b)*** *high ATO3 levels and low ACT1 levels; in late LOC, early HOC, mid-HOC, late HOC and early LOC phases of the YMC as indicated by different levels of blue. High levels: x>=5, low levels: x<5, with x = RNA numbers in-cell. The 3 repeats realised for the control set (ATO3 – ACT1) were merged. Black dots indicate means, black horizontal bars indicate the medians. The horizontal line indicates a threshold between cells with low or high cell diameters. Samples from the different "expressing categories" phases are ordered according to their distributions as determined by Wilcoxon tests (p-value<0.05). When a low cell number is detected in a category, the number of cells detected is indicated under the boxplot of cell diameters.*

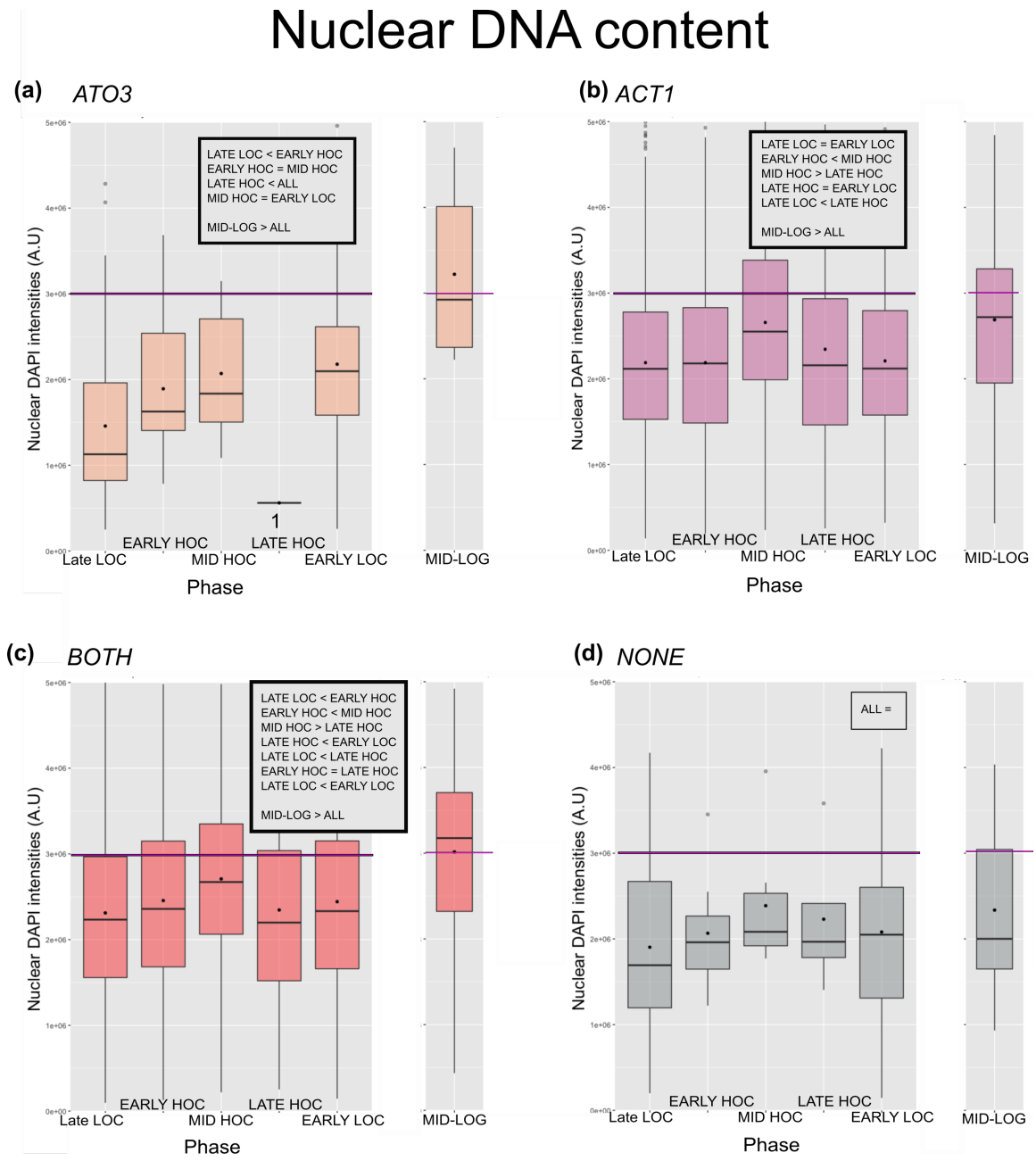

Figure 8.14 Nuclear DNA content vary between cells of different gene expression status

Boxplots of the distributions of nuclear DNA content (Sum of DAPI intensities in-nucleus) for cells expressing transcripts in-cells; ***(a)*** *only in the first fluorescent channel (Cy5, ATO3 in orange),* ***(b)*** *for cells expressing only in the second fluorescent channel (Cy3, ACT1 in purple),* ***(c)*** *for cells expressing both transcripts (red),* ***(d)*** *for cells expressing no transcripts (grey) for the Control set. For late LOC, early HOC, mid-HOC, late HOC and early LOC phases of the YMC and mid-Log samples. The 3 repeats realised for the control set (ATO3 – ACT1) were merged. Black dots indicate means, black horizontal bars indicate the medians. The horizontal line indicates a threshold between cells with low or high nuclear DNA content. Samples from the different "expressing categories" phases are ordered according to their distributions as determined by Wilcoxon tests (p-value<0.05). When a low cell number is detected in a category, the number of cells detected is indicated under the boxplot of nuclear DAPI intensities.*

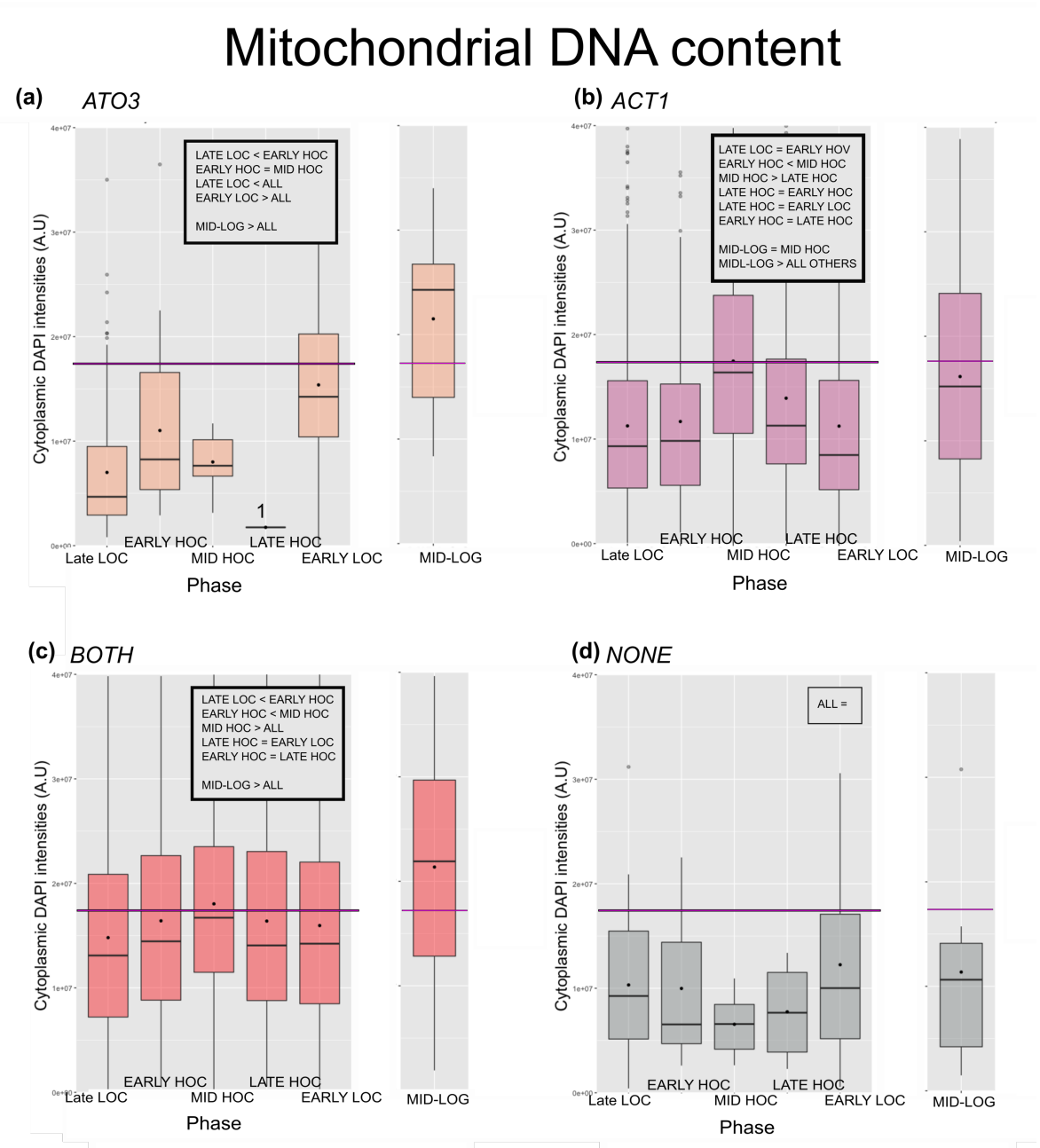

Figure 8.15 Mitochondrial DNA content vary between cells of different gene expression status

Boxplots of the distributions of mitochondrial DNA content (Sum of the total DAPI foci intensities in-cytoplasm per cell)) for cells expressing transcripts in-cells; ***(a)*** *only in the first fluorescent channel (Cy5, ATO3 in orange),* ***(b)*** *for cells expressing only in the second fluorescent channel (Cy3, ACT1 in purple),* ***(c)*** *for cells expressing both transcripts (red),* ***(d)*** *for cells expressing no transcripts (grey) for the Control set. For late LOC, early HOC, mid-HOC, late HOC and early LOC phases of the YMC and mid-Log samples. The 3 repeats realised for the control set (ATO3 – ACT1) were merged. Black dots indicate means, black horizontal bars indicate the medians. The horizontal line indicates a threshold between cells with low or high mtDNA content. Samples from the different "expressing categories" phases are ordered according to their distributions as determined by Wilcoxon tests (p-value<0.05). When a low cell number is detected in a category, the number of cells detected is indicated above the boxplot of cytoplasmic DAPI intensities.*

8.11.1.1 A small proportion of quiescent cells are found in HOC

The small proportion of cells expressing *ATO3* only (Figure 8.12,14,15 in orange) show a decrease in cell size in HOC relative to late LOC and early LOC (˜3.5 to 2.1 to 4.3μm) but an increase in nuclear and mtDNA content from late LOC to early LOC (˜2 fold increase). Similarly, the small proportion of cells expressing high *ATO3* and low *ACT1* transcript levels in HOC, shows lower cell sizes in HOC (Figure 8.13.B). These results also indicate that the small proportion of cells that express *ATO3* only (or *ATO3* at high levels and *ACT1* at low levels) are particularly small in HOC phase. Although these cells show higher DNA content in HOC than in early LOC, these cells still show low nuclear and mtDNA content (below the thresholds) in HOC. These results suggest that most of the cells expressing *ATO3* in HOC are small G1 cells.

In early LOC, the increase in cell size and DNA content is suggested to account for the increase in the proportion of cells expressing *ATO3* at this stage of the YMC, implying these compose another sub-population of cells, bigger mother cells.

Thus it seems that in HOC, a small proportion of cells are unable to transition out of a quiescent-like state. Cells expressing the stationary phase transcripts in HOC are particularly small (˜2.5μm, corresponding to a cell volume of ˜8.2μm^3), similar to the quiescent daughter cells reported in stationary phase cultures (14um^3 at birth, median cell volume of 20μm^3, Laporte et al. 2018). Finally, these results suggest that cells expressing the stationary phase transcript in HOC, that are too small, might not be able to pass Start. This results thus prompts the hypothesis that the ability of quiescent-like cells to exit quiescence and enter the cell cycle in YMC cultures (in

HOC) is size-dependent, similar to the discovery made for quiescent cells in stationary phase (Laporte et al. 2017).

8.11.1.2 Cells expressing high levels of *ATO3* in LOC and high levels of *ACT1* in HOC proceed to cell division in late HOC

Cells expressing *ACT1* without *ATO3* (in purple) show an increase in cell diameters in mid and late HOC (˜3.2 to 4.3μm), together with an increase in nuclear DNA content and mitochondrial DNA content in mid-HOC phase of the YMC. Increases in cell diameters, nuclear and mtDNA content are also observed in mid-HOC in cells co-expressing *ATO3* and *ACT1* (in red) (˜3.85 to 4.2μm). However, the changes are not as considerable as those for cells expressing *ACT1* only (purple). Moreover, the majority of the cells co-expressing *ATO3* and *ACT1* show high levels of *ACT1* and low levels of *ATO3* in HOC (chapter 7). These cells show an increase in cell diameters in mid HOC (Figure 8.12 & 13). These results indicate that in HOC some cells stop expressing the stationary phase transcripts *ATO3* (or express it lowly) but still express *ACT1*, increasing the proportion of cells with this gene expression status (purple). These cells become larger and see their nuclear and mtDNA content increase in mid-HOC, above the thresholds previously identified. Thus the results suggest that these cells pass the cell size threshold for Start between early and mid-HOC, leave the G1 state and are in a S/G2/M state in mid-HOC phase of the YMC. In late HOC, cells size and DNA content of these cells decrease to those similar levels in early LOC as those found in late LOC, suggesting that cell division occurs for these cells in late HOC phase of the YMC. Therefore, the results suggest that the cells exiting a quiescent-like state form a proportion of cells showing high *ATO3* levels in LOC, that transition out of a G1 state, i.e. exit quiescence in HOC, express *ACT1* but no or low expression of *ATO3* in

HOC, grow and progress through the CDC to divide in late HOC. These results thus agree with the model described in chapter 7 and indicate that cells that transition from a quiescent-like to a growth-like and proliferative state express the constant transcript but not the LOC transcript.

8.11.1.3 Characteristics of cells that do not express the LOC transcript *ATO3*

Cells that neither express *ATO3* nor *ACT1* (grey), which are rare among the YMC cultures, decrease in cell size from the late LOC phase to the late HOC phase, followed by an increase in early LOC (˜4 to 2 to 3.6μm), while nuclear and mtDNA content stay relatively constant and low in these cells across the cycle. The decrease in cell size observed for cells expressing neither *ATO3* nor *ACT1* transcripts in HOC (median volume of 4.2um^3) is thus proposed to result from the formation of newly buds (from Start to cell division in late HOC), as these might not show expression of *ACT1* at that stage. Thus, cells that express neither *ATO3* or *ACT1* may be small new born cells.

By contrast, cells expressing *ACT1* only but not *ATO3* (purple) at all times along the YMC show lower median nuclear and mtDNA content than the thresholds indicating that most of these cells are in G1. However, among cells that co-express *ACT1* and *ATO3* (red), in particular cells that express high levels of *ACT1* but low levels of *ATO3*, overall distributions of cell diameters, nuclear and mt DNA content show higher levels, while a small proportion of cells show higher cell size and mtDNA content than the thresholds all along the YMC. These results indicate perhaps that some of these cells are found in a G2/S/M phase and thus may be proliferative.

8.11.2 In YMC cultures sub-populations of cells show distinct gene expression, cell growth and proliferation profiles

Cell diameters of cells in late LOC, early HOC, mid-HOC, late HOC and early LOC, expressing only one or the other transcript of a pair (*ATO3* in orange, *SHM2* in blue and *IDH1* in green) and both transcripts of a pair (in red) are shown in boxplots (Figure 8.16,17,18). The results indicate a complex relation between growth, metabolism and gene expression in sub-populations of yeast cultures. For these experiments nuclear and mitochondrial DNA content were not assessed and thus only the cell size is used to infer growth and the proliferative status of cells.

8.11.2.1 Cells that express the LOC transcript *ATO3* in the HOC phase grow but do not divide.

Cells expressing *ATO3* but not *SHM2* (orange) show an increase in cell size from late LOC phase to the start of the next early LOC. The increase in size is greatest in HOC (˜3.4 to 4.1μm). Importantly, most of these cells show lower cell diameters than the cell size threshold in early and mid-HOC indicating that most of these cells likely are in G1. This suggests the small proportion of cells that express *ATO3* transcripts in HOC grow during the HOC phase of the cycle.

Cell diameter

(i) DF1 *ATO3* - *SHM2*

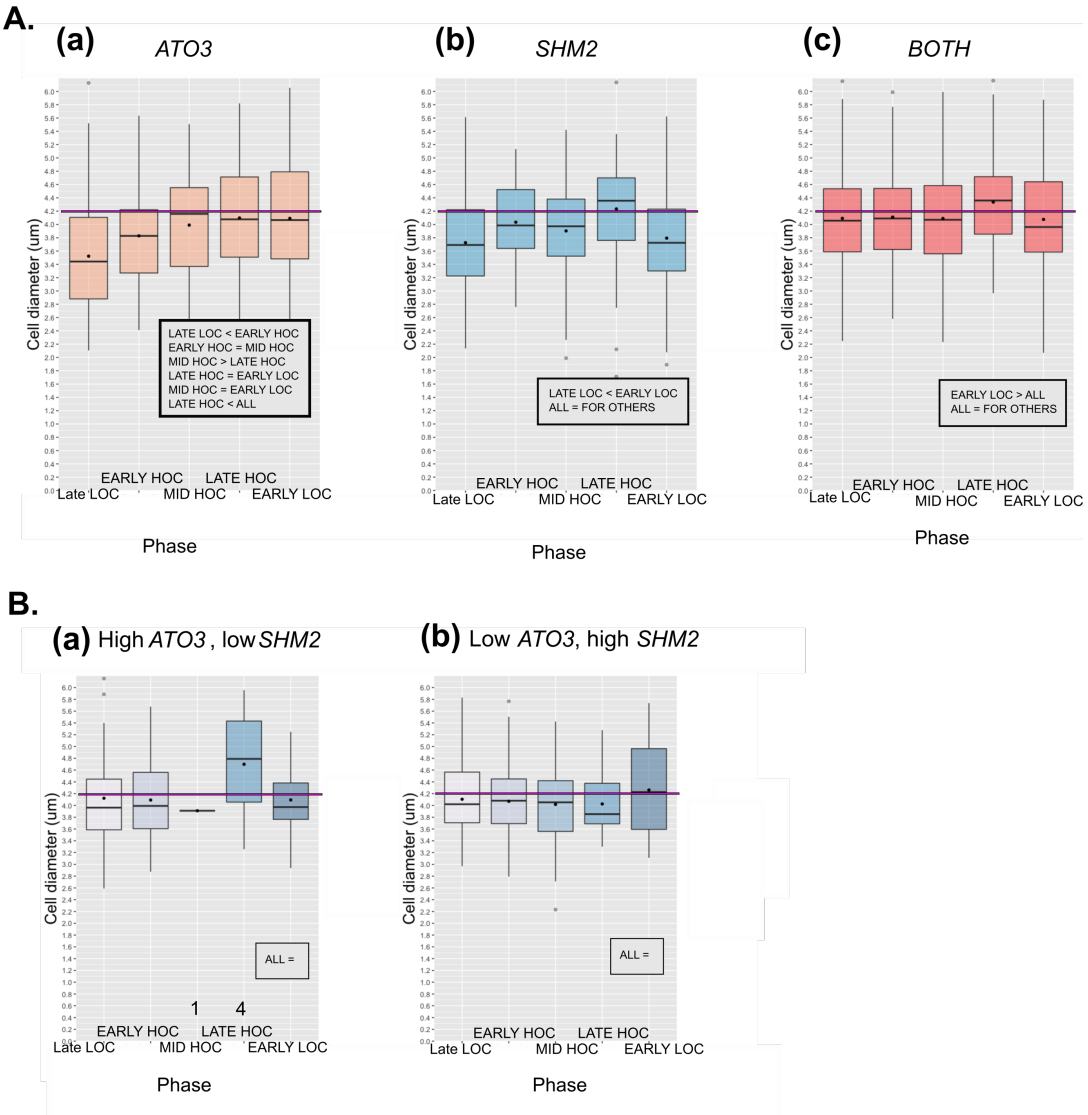

Figure 8.16 Cell diameters vary between cells of different gene expression status

A. *Boxplots of the distributions of cell diameters for cells expressing transcripts in-cells;* ***(a)*** *only in the first fluorescent channel (Cy5),* ***(b)*** *for cells expressing only in the second fluorescent channel (Cy3),* ***(c)*** *for cells expressing both transcripts (red). For the 1st Dual-FISH ATO3 in orange, SHM2 in blue.* ***B.*** *Boxplots of the distributions of cell diameters for cells expressing (**a**) high ATO3 levels and low SHM2 levels* ***(b)*** *low ATO3 levels and high SHM2 levels, In late LOC, early HOC, mid-HOC, late HOC and early LOC phases of the YMC, as indicated by different levels of blue. High levels: x>=5, low levels: x<5, with x = RNA numbers in-cell. Black dots indicate means, black horizontal bars indicate the medians. The horizontal line indicates a threshold between cells with low or high cell diameters. Samples from the different "expressing categories" phases are ordered according to their distributions as determined by Wilcoxon tests (p-value<0.05). When a low cell number is detected in a category, the number of cells detected is indicated under the boxplot of cell diameters.*

Cell diameter

(ii) DF2 *SHM2* - *IDH1*

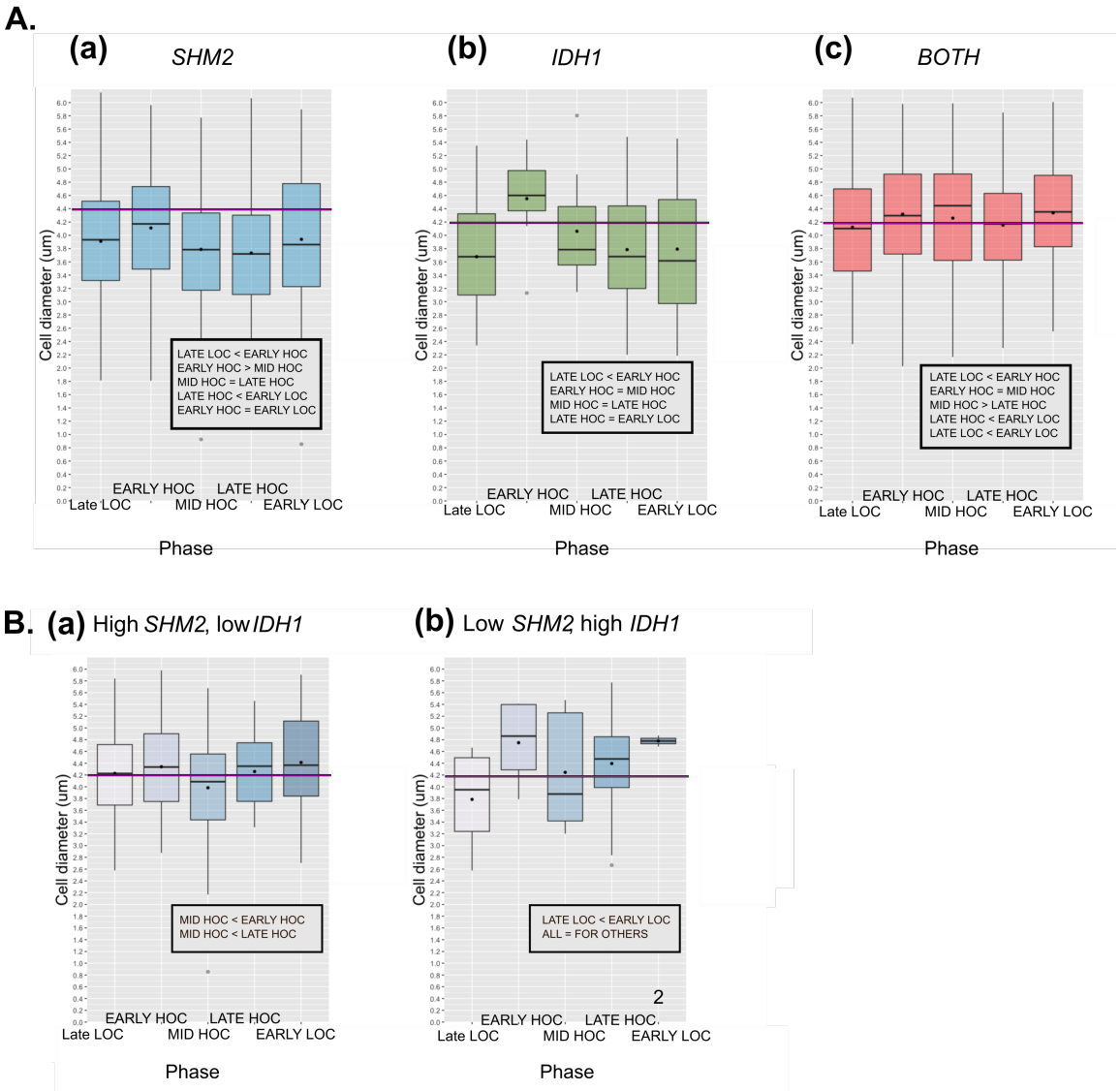

Figure 8.17 Cell diameters vary between cells of different gene expression status

A. *Boxplots of the distributions of cell diameters for cells expressing transcripts in-cells;* ***(a)*** *only in the first fluorescent channel (Cy5),* ***(b)*** *for cells expressing only in the second fluorescent channel (Cy3),* ***(c)*** *for cells expressing both transcripts (red), For the 2nd Dual-FISH SHM2 in blue, IDH1 in green.* ***B.*** *Boxplots of the distributions of cell diameters for cells expressing* ***(a)*** *high SHM2 levels and low IDH1 levels in blue* ***(b)*** *low SHM2 levels and high IDH1 levels, In late LOC, early HOC, mid-HOC, late HOC and early LOC phases of the YMC, as indicated by different levels of blue. High levels: x>=5, low levels: x<5, with x = RNA numbers in-cell. Black dots indicate means, black horizontal bars indicate the medians. . The horizontal line indicates a threshold between cells with low or high cell diameters. Samples from the different "expressing categories" phases are ordered according to their distributions as determined by Wilcoxon tests (p-value<0.05). When a low cell number is detected in a category, the number of cells detected is indicated under the boxplot of cell diameters.*

Cell diameter

(iii) DF3 *IDH1* - *ATO3*

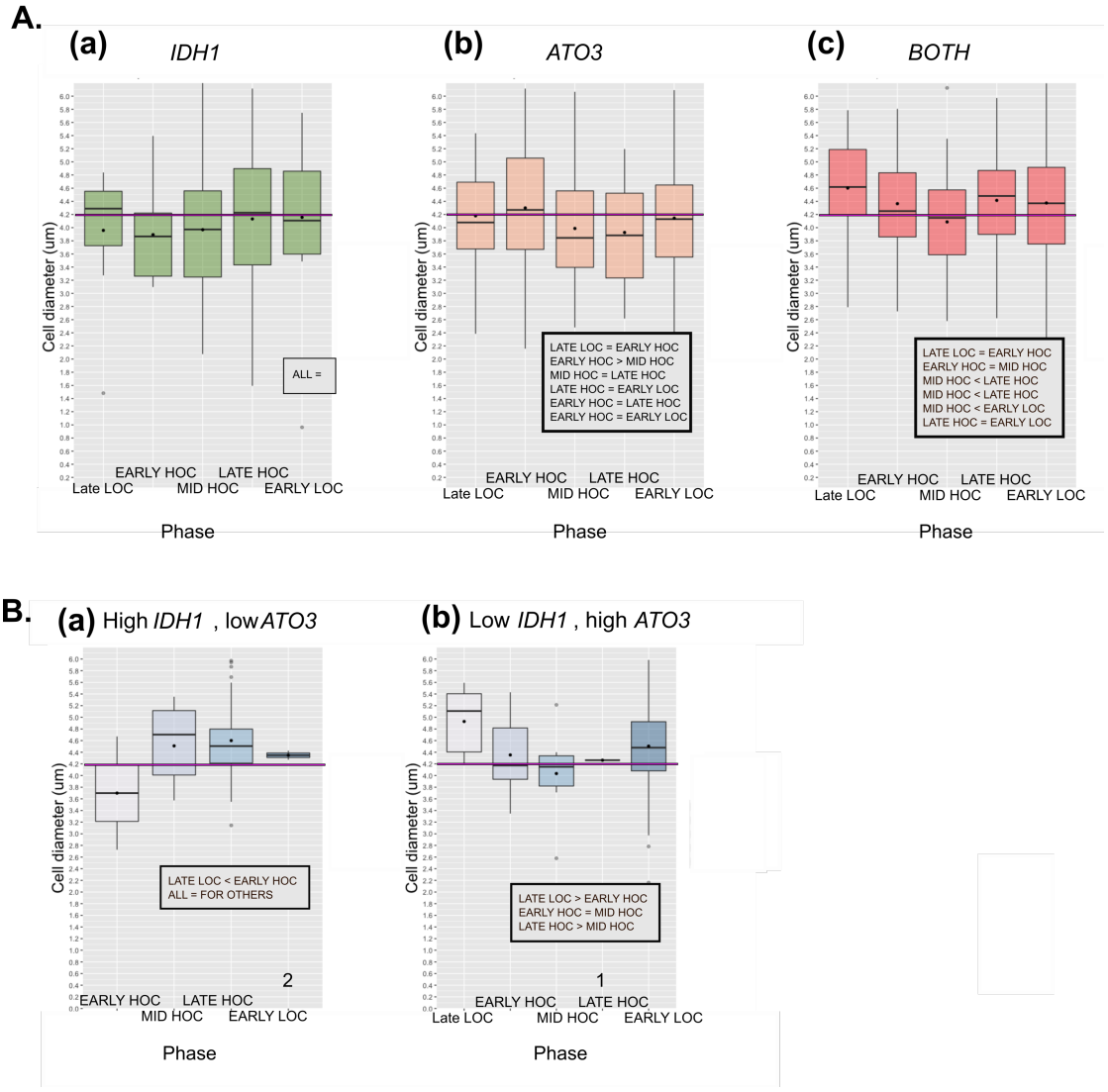

Figure 8.18 Cell diameters vary between cells of different gene expression status

A. *Boxplots of the distributions of cell diameters for cells expressing transcripts in-cells;* ***(a)*** *only in the first fluorescent channel (Cy5),* ***(b)*** *for cells expressing only in the second fluorescent channel (Cy3),* ***(c)*** *for cells expressing both transcripts (red), For the 3rd DUAL-FISH IDH1 in green, ATO3 in orange.* ***B.*** *Boxplots of the distributions of cell diameters for cells expressing* ***(a)*** *high IDH1 levels and low ATO3 levels* ***(b)*** *low IDH1 levels and high ATO3 levels. In late LOC, early HOC, mid-HOC, late HOC and early LOC phases of the YMC, as indicated by different levels of blue. High levels: x>=5, low levels: x<5, with x = RNA numbers in-cell. Black dots indicate means, black horizontal bars indicate the medians. . The horizontal line indicates a threshold between cells with low or high cell diameters. Samples from the different "expressing categories" phases are ordered according to their distributions as determined by Wilcoxon tests (p-value<0.05). When a low cell number is detected in a category, the number of cells detected is indicated under the boxplot of cell diameters.*

8.11.2.2 A proportion of cells express the HOC transcript *SHM2* and progress through Start in HOC phase of the YMC

Cells expressing *SHM2* but not *ATO3* (in blue, Figure 8.16.A), show an increase in cell diameters from the late LOC phase to the late HOC phase and a decrease in early LOC (˜3.7 to 4.4 to 3.7μm). The increase in cell diameter above the cell size threshold indicates some of the cells that express the HOC transcript *SHM2* transition to Start in HOC phase of the YMC.

8.11.2.3 Newborn cells might express the HOC transcript *SHM2* in early LOC

Cells expressing *SHM2* only show a decrease in cell size in early LOC, and lower cell size than cells co-expressing *ATO3* and *SHM2* (red) and cells expressing *ATO3* only (orange) (Figure 8.16.A) (3.7 vs 4.1μm). Because early LOC phase of the YMC is the time at which a proportion of the population is expected to divide, it is plausible that a proportion of the cells expressing *SHM2* only are newborn cells.

8.11.2.4 Cells expressing high levels of LOC transcript *ATO3* in LOC and high levels of HOC transcript *SHM2* in HOC most likely progress through the cell cycle

Cells co-expressing *ATO3* and *SHM2* (red) show an increase in cell diameters in late HOC (˜4.1 to 4.4μm). Most importantly, these cells (red) are larger than cells expressing *ATO3* or *SHM2* only (orange or blue) (Figue 8.16.A) (4.4 vs 4.1μm). Furthermore, cells that show high *ATO3* levels and low *SHM2* levels (Figure 8.16.B.a) show an increase in cell size in late HOC phase of the YMC. These results thus suggest that cells transitioning out of a quiescent-like state, highly express the *ATO3* transcript in late LOC before exiting quiescence and growing in HOC, at which stage

these cells show high expression of HOC transcripts (*SHM2*) and low expression of LOC transcripts (*ATO3*). After late HOC, perhaps after cell division, cells express high levels of *ATO3* while low levels of *SHM2* remain in cells. Because the cell diameters of these cells is above the cell size threshold in early LOC (Figure 8.16.B.a), the results suggest a proportion of these cells are larger, perhaps mother cells.

8.11.2.5 A small proportion of the cells expressing high levels of the HOC transcript *SHM2* in LOC might be proliferative

In LOC, cells that express *SHM2* only show lower median cell size than the thresholds (Figure 8.16.A) indicating that most of these cells are likely in G1. However, a small proportion of cells express *SHM2* at high levels and *ATO3* at low levels in LOC and these show higher cell size distribution in early LOC (Figure 8.16.B.b). As the distribution of cell diameters for these cells are slightly higher than the cell size threshold for Start, a few cells expressing high *SHM2* transcripts might be in a G2/S/M phase in LOC. These results together with the ones gathered for the *ATO3* and *ACT1* pair suggest that cells that do not express *ATO3* but express *SHM2* and *ACT1* at high levels might compose the population of asynchronously dividing cells along the YMC, described previously by Robertson et al. (2011).

8.11.2.6 Cells expressing HOC transcripts, *SHM2* and *IDH1* pass the Start cell size threshold in HOC and divide in late HOC phase of the YMC

Cells that express *SHM2* show a mild increase in cell size in early HOC, a decrease in mid and late HOC and an increase in late LOC (Figure 8.17.A) (4 to 4.2um to 3.8μm). Only a few cells express *IDH1* without *SHM2* (green) in early HOC, but show higher cell diameters than cells expressing both *IDH1* and *SHM2* or cells expressing *SHM2*

only (4.6um vs 4um) (Figure 8.17.A). This indicates that in early HOC, a global increase in cell size seem to occur in cells expressing HOC transcripts (*SHM2* and/or *IDH1*).

In mid-HOC, cells that co-express *SHM2* and *IDH1* (red) are bigger than cells that express *SHM2* only (blue) or *IDH1* only (green) (4.4um vs 3.8μm) and larger than the threshold for cells past Start. Cells that co-express *SHM2* and *IDH1*, show an increase in cell size in early and mid-HOC, a decrease in late HOC followed by an increase in early LOC (˜4.1 to 4.45μm). Among these cells, many express high levels of *IDH1* and low levels of *SHM2*. These cells show a great increase in cell size from mid-HOC to early LOC, at the time *IDH1* expression peak (Figure 8.17.B.b). Thus, these results suggest that cells expressing HOC transcripts grow in the HOC phase of the YMC. In particular cells expressing both *SHM2* and *IDH1* (at high levels) show median cell diameters above the cell size threshold determined for Start in early and mid-HOC phase of the cycle, a drop in cell diameters in late HOC and an increase again in early LOC suggesting that these cells divide in late HOC.

8.11.2.7 Cells grow prior to expression of the HOC transcripts *IDH1* in mid-HOC phase

Cells that express *ATO3* only without *IDH1* (orange) show a slight increase in cell size in early HOC followed by a decrease in mid and late HOC (˜ 4.3 to 3.8μm) (Figure 8.18.A). Cells co-expressing *IDH1* and *ATO3* (red), show a decrease in cell diameter in early HOC and mid-HOC followed by an increase in late HOC (˜4.6 to 4.2 to 4.5μm). Cells that co-express *ATO3* and *IDH1* are mostly composed of cells with high levels of ATO3 and low levels of *IDH1* and also show a cell size decrease in HOC (Figure 8.18.B.b). Thus it seems that in early HOC, when only a few cells express *IDH1* at low

levels, cells that do not express *IDH1* (or only at low levels) become larger perhaps reflecting the fact that a proportion of cell grow and transition out of a quiescent-like state prior to express *IDH1*, as suggested by the cell size increase in that phase for cells expressing *SHM2* but not *IDH1* (Figure 8.17.B). Finally, here the cell size drop in HOC for cells that do not express *IDH1* (or lowly) but show high *ATO3* levels suggests again that the small proportion of cells expressing the stationary transcripts *ATO3* in HOC is mainly composed of smaller cells.

8.11.2.8 Cells expressing high levels of HOC transcript *IDH1* grow in mid and late HOC phase of the YMC, some progress through the cell cycle

Cells that express *IDH1* without *ATO3* (green) show a slight decrease in early HOC and a greater increase in mid and late HOC, when *IDH1* expression peaks and cell diameter is between ˜3.8 to 4.2μm (Figure 8.18.A). This increase in cell size in mid and late HOC is also observed in cells with high *IDH1* levels and low *ATO3* levels (Figure 8.18.B.a). Because these cells show diameters above the cell size threshold suggested for Start and show no to low levels of stationary phase transcripts (*ATO3*), these cells are likely the cells transitioning synchronously out of quiescence into a S/G2/M state in HOC phase.

8.12 Conclusions

The results from this chapter corroborate previous findings about the organisation of cells in synchronized cultures of the YMC but also add on to the understanding of such organisation.

The main conclusion of this chapter is that there are three sub-population of cells in the YMC, derived from single cell analysis of DNA content, cell size and transcript status. Nuclear and mitochondrial DNA content together with cell sizes increase in 15 to 25 % cells of the YMC populations in mid to late HOC phase, backing up previous findings (˜10-50%) from Tu et al. 2005, Klevecz et al. 2004, Feltham et al. 2020, Laxman et al. 2010, Slavov & Botstein. 2011, Burnetti et al. 2016, while 25 to 30% of the YMC cells show high DNA content and larger cell size at all times throughout the YMC, indicating a higher proportion of cells divide asynchronously throughout the YMC than previously reported by Robertson et al. 2010 and Burnetti et al. 2016 (˜10%). Finally, the remaining 40 to 60% of cells show no change in cell size or DNA content. Therefore, 3 sub-populations of cells can be recovered using single cell analysis; a proportion of cell synchronously exiting quiescence and progressing through the cell division cycle in HOC, a proportion of cells asynchronously dividing at all times and a proportion of cells that stays in a vegetative state (G1).

When compared to YMC cells, mid-log cultures show higher proportions of cells in S/G2/M (˜65%) and bimodal distributions of cell sizes found for mid-log samples indicate a cell size threshold for Start of ˜4.2um (38.8μm^3). A similar size threshold seem to separate cells with high or low nuclear and mitochondrial DNA content along the YMC.

Gene expression from single cells only poorly correlate with DNA content and cell size in YMC and mid-log cultures, supporting more complex relationships for distinct target transcripts, underlying the basis of the three population model. However, gene expression and cell sizes are found to be coordinated through an intrinsic metabolic clock in both YMC and mid-log phase.

In particular, distinct sub-populations are identified in YMC cultures, with different gene expression statuses associated with different cell sizes, nuclear and mtDNA content. Cell size, mitochondrial and nuclear DNA content were looked at as means to estimate whether or not cells were big enough and would contain high enough DNA content to pass the Start threshold therefore, if some cells would be more prone to transition from a G1 state back into the cell division cycle. Again, oscillating transcripts were used as markers of metabolic states in cells.

Based on the distribution of transcripts, the results suggest sub-populations possess different metabolic states as depicted at figure 8.19.

Looking at cell sizes but also nuclear and mitochondrial DNA content (Figure 8.19.A), some cells expressing the LOC transcript *ATO3* were found in HOC. These are particularly small with low DNA content, while cells expressing zero to low levels of *ATO3* but high levels of *ACT1* in HOC phase of the YMC tend to be bigger and possess higher DNA content, making some of them more prone to re-enter the cell division cycle.

Focusing on the size of cells and as opposed to expectations (Figure 8.19.B);

In LOC phase of the YMC, a proportion of cells was found to express the HOC transcript *SHM2*, indicating a more metabolically active state. Some of these cells were found to be big enough to pass the Start threshold, therefore some of these cells

A.

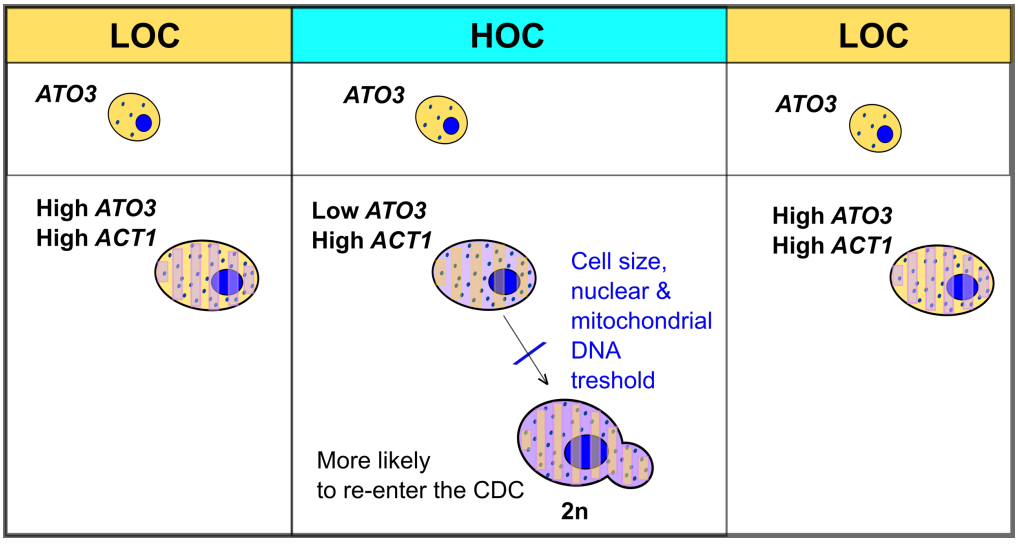

B.

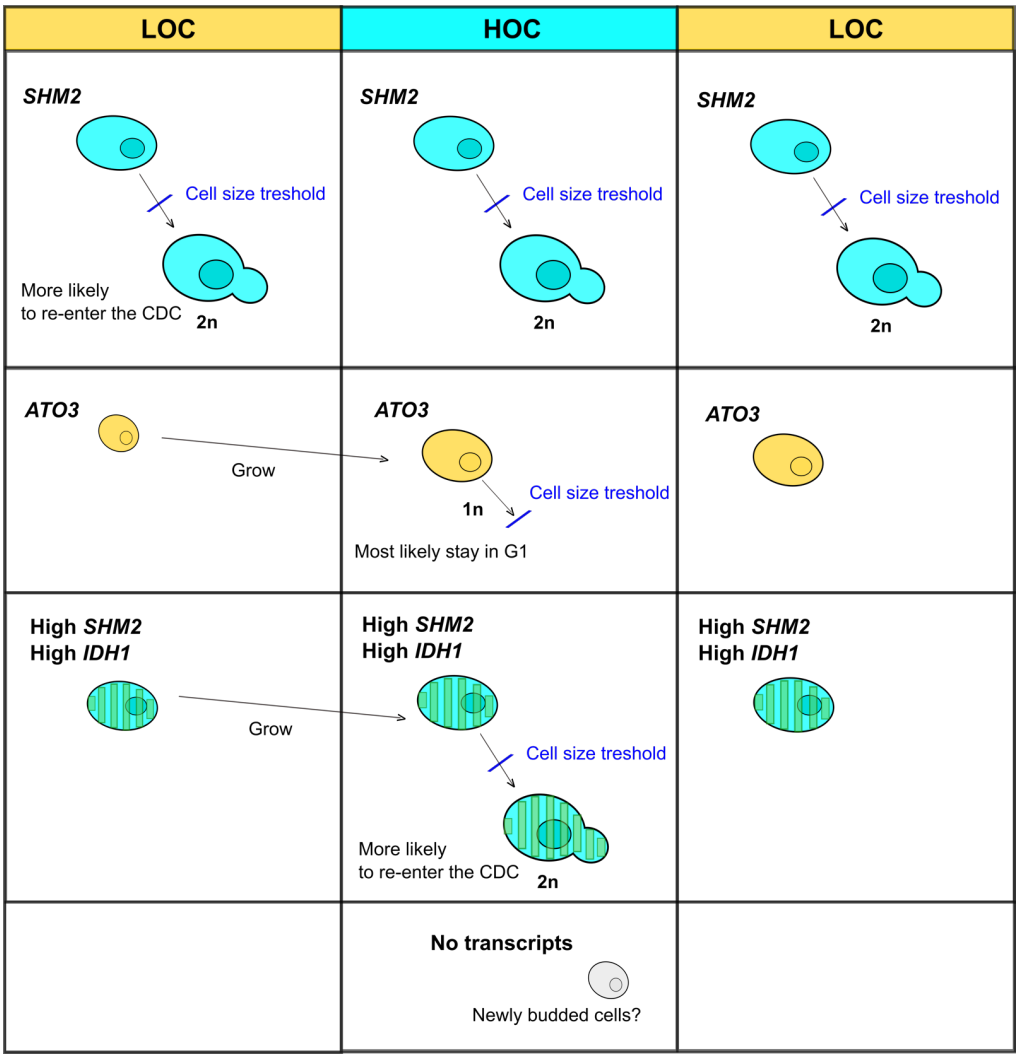

Figure 8.19 Synchronized YMC populations are organised in 3 or more sub-populations

Schematic of the different sub-populations of the YMC cultures; ***A.*** *According to cell size, mitochondrial DNA content, nuclear DNA content and transcript levels.* ***B.*** *According to cell size and transcript levels.*

might proceed to DNA replication.

In HOC phase of the YMC, a proportion of cell was found to express the LOC transcript *ATO3*, indicating a less metabolically active state. Despite the fact that these cells seem to grow during the HOC phase, they do not reach the cell size threshold for Start and therefore are likely in G1.

Next, in HOC, cells expressing high levels of HOC transcripts *SHM2* and *IDH1* are bigger than cells that do not express these transcript in HOC. Some of these more metabolically active cells reach the cell size threshold for Start, and are thus more prone to exit G1 and re-enter the cell division cycle.

Lastly, small cells without transcripts are detected in late HOC and these cells could potentially be new born cells.

Together these results suggest: (**i)** a proportion of cells remains in a quiescent-like, less metabolically active state in HOC, **(ii)** a proportion of cells exit this quiescent-like state and enter the cell division cycle in HOC, **(iii)** a proportion of cells is non-quiescent, more metabolically active in LOC as these cells do not express the stationary phase transcripts *ATO3* (some of these cells might even divide) **(iv)** and finally, a proportion of small non-expressing cells might be new born cells in late HOC. A cartoon aiming to recapitulate the organisation of the synchronized YMC culture in HOC and LOC phase is presented at figure 8.20.

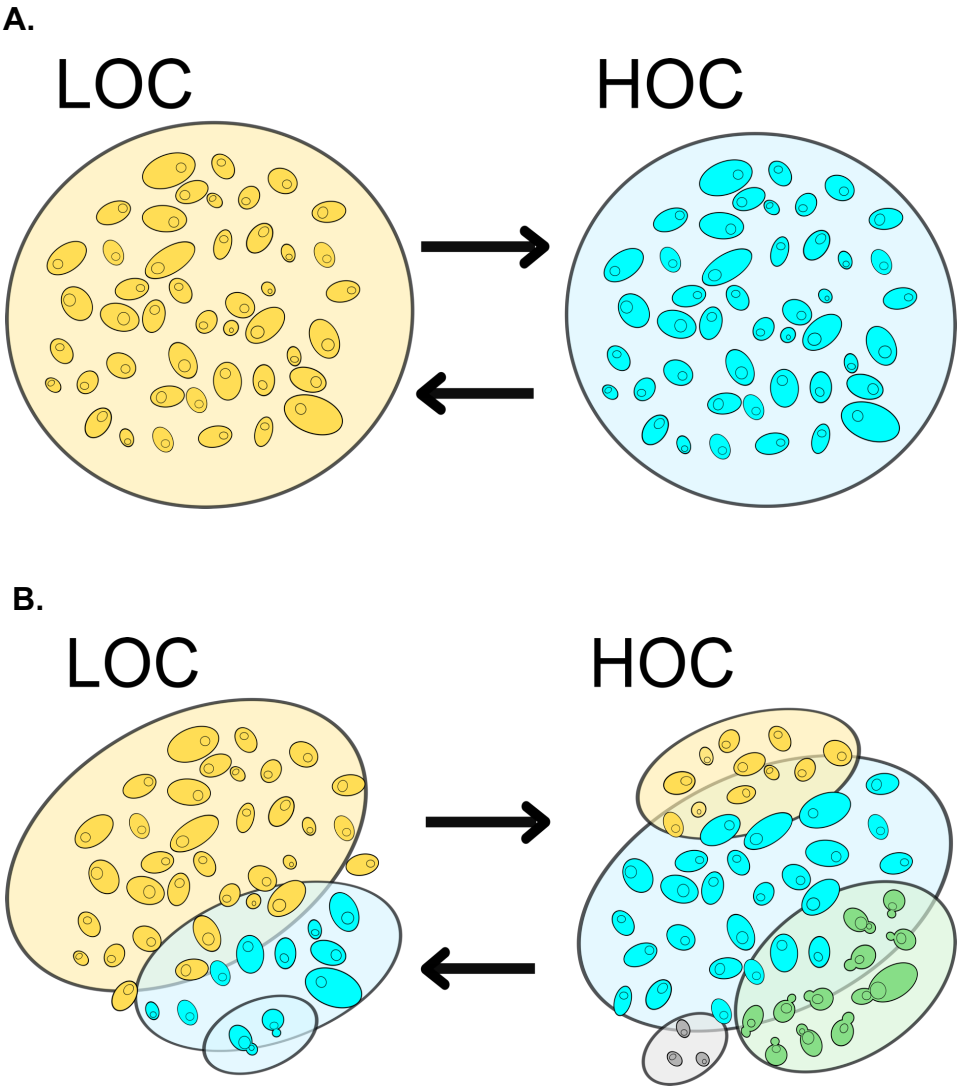

Figure 8.20 Sub-populations in LOC and HOC phase of the YMC

A more complex organisation of cells is detected in YMC cultures. ***A.*** *Composition of YMC cultures according to the current state of the field.* ***B.*** *Composition of YMC cultures according to the results from this work. Blue and green cells represent cells found with HOC transcripts SHM2 and IDH1 and are therefore considered to be in a more metabolically active state. Yellow cells represent cells found to express the LOC transcript ATO3 and are therefore considered to be in a less metabolically active state. Grey cells represent small cells found without transcripts. Some cells were found to show high DNA content and cell size suggesting these are able to exit G1 and re-enter the cell division cycle.*

8.13 Discussion

The results suggest that the ability of cells to exit a quiescent-like state in the HOC phase of the YMC cultures depends on growth and cell sizes. The results and analysis of cell size and gene expression for the different pairs of antagonist transcripts suggest that (i) a proportion of quiescent-like cells found in HOC still grow in that phase, (ii) a small proportion of cells that do not express stationary phase transcripts in LOC might be asynchronously dividing, (iii) the proportion of cells expressing high stationary phase transcript levels in LOC and high HOC transcript levels in HOC pass the cell size threshold for Start, exit the quiescent-like state and progress through the cell cycle in HOC, (iv) not all cells expressing the HOC transcripts in HOC reach high DNA content and cell size indicating that not all of these cells enter the cell division cycle.

Together, the results gathered in this work strongly support the “Finishing-kick to Start” hypothesis by Futcher., (2006), also supported by population-averaged results from (Slavov & Bostein. 2011, Burnetti et al. 2016, Papagiannakis et al. 2017, Fetham et al. 2020., O’Neill et al. 2020, Machne et al. 2021), as single cells expressing high HOC transcripts and low LOC transcripts in HOC phase of the YMC, indicating a “HOC or growth metabolic state”, show higher DNA content and cell size compare to cells expressing LOC transcripts during the HOC phase of the YMC. Therefore, a “gating of growth” is found in a proportion of individual cells of YMC populations.

Next, recent findings from studies on stationary phase cultures suggest that this relationship between growth and proliferation in single cells of YMC cultures might be regulated in quiescent cells but not in non-quiescent cells.

Indeed, the cell the volume was suggested to act as a checkpoint for rapid quiescence exit and re-entry into the cell cycle. Most importantly, this mechanism was proposed

to affect quiescent daughter cells only (Laporte et al. 2017). When stationary phase cells are fed with fresh glucose, cells re-enter the cell cycle. 80% of the mother cells do so asynchronously within 2 hours, while 40% of the daughter cells re-enter the cell cycle and do so synchronously. Remarkably, the initial cell size volume of daughter cells, at the time of transition into glucose media (median of ˜41+/- 16μm^3), regulate their ability to exit rapidly (<2h) their quiescent state and re-enter the cell cycle and bud at a median cell volume of 58+/-12μm^3. Most importantly, quiescent daughters cells with lower initial cell volume (<35μm^3) are unable to transition back to the CDC and need more time to do so and grow (>2h). Finally, the initial volume of large mothers (median of 101+/-29μm^3) nor their replicative age seems to matter for these cells to bud (Laporte et al. 2017).

Thus based on literature (Li et al. 2013, Miles et al. 2020, Breeden & Tsukiyama. 2022) and results from this work, (i) the proportion of cell that divide at all time during the YMC is proposed to consist of large non-quiescent-like mother cells, (ii) the proportion of cells re-entering synchronously the cell cycle at each metabolic cycle is proposed to mainly comprise “small” quiescent-like daughters cells, (iii) the proportion of cells that do not divide during the cycle is proposed to contain both non-quiescent-like and quiescent-like mother and daughter cells. Finally, under the chemostatic conditions of the YMC, i.e. the constant limiting concentration of glucose, cells that divide in late HOC-phase of the YMC are suggested to re-enter stationary phase and thus partition into non-quiescent and quiescent-like populations, as it was shown that slow growth conditions (in batch cultures) can induce early quiescence (Klosinska et al. 2011).

8.14 Future directions

The results for the different pairs of antagonist transcripts allow predictions to be made about the relationship between gene expression status and cell sizes but in the future, dedicated experiments will be required to verify these. Re-assessing DNA content, cell sizes and cell wall thickness along the YMC through FACS experiments might be necessary to get a full picture of the organization of YMC population, in light of the results presented in Li et al. 2013, Miles et al. 2020 on stationary phase cells. RNA-FISH experiments on yeast cultures after separation through cell density percoll gradient or centrifugal elutriation might constitute other options to investigate sub-populations of YMC cultures.

Chapter 9

Discussion

9.1 Summary of results

This thesis investigates the relationship between gene expression and metabolism in single cells of *Saccharomyces cerevisiae*.

First, an experimental approach was designed to assess single cell transcript levels across the Yeast Metabolic Cycle at a high temporal resolution. The technique of single-molecule RNA-FISH was optimized for YMC samples. In particular, adequate treatment of the samples and proper spheroplasting were developed, as the composition of the yeast cell walls most likely changes over the YMC and thus the ease with which it can be removed during spheroplasting. Single-molecule RNA-FISH probes were made in-house to reduce the experimental costs. Specific controls such as the use of RNAseA treatment and KO strains guaranteed detection of the target transcripts above noise signals. Slightly different versions of the analytical pipeline were tailored for the quantification of sum of RNA levels (pre-rRNA), discrete transcript levels in single cells (smRNA-FISH on antagonists), nuclear and mitochondrial DNA content and the computation of cell sizes. The pipeline and main modifications were designed by Dr. Andrew Angel. Finally, downstream analysis allowed the comparison of transcript levels and other metrics between mid-logarithmic and YMC cultures, and most importantly assessments of RNA levels along continuous metabolic changes in YMC populations.

Second, pre-ribosomal RNA levels were assessed in single cells of YMC cultures, using RNA-FISH along the YMC in order to record ribosomal production, reflecting synthesis and processing of the polycistronic 35S pre-rRNA by Rps6. Ribosomal RNA production was found to match the increase in phosphorylated isoforms of Rps6 in the middle of the HOC phase of the YMC. Because Rps6 protein levels were shown to

remain constant over the metabolic cycle, such coordination suggests phosphorylation of Rps6 during the YMC regulates its activity in processing the 35S pre-rRNA. Evidence of such regulation supports a role for protein post-translational modification rather than protein levels in the regulation and progression of the YMC. In particular this finding supports other studies which advocate the nutrient sensing TORC1 complex, downstream phosphorylation cascades and control of ribosome biogenesis as major regulators of the metabolic transition between states of quiescence and growth, at the LOC-HOC boundary in YMC populations. The analysis of the fraction of cells showing high ribosomal RNA production suggests at least 3 sub-populations compose the YMC cultures; a proportion of cells transitioning to a growth-state from LOC to HOC phase, a proportion of cells staying in a quiescent-state in HOC and a proportion of cells found in a growth-state at all time during the cycle. Finally, the results show cell-to-cell heterogeneity of pre-rRNA levels in YMC populations, indicating synchronous cell population in fact include cells with very different RNA Pol I gene expression status.

Third, an experimental plan was designed to obtain discrete transcript levels of genes transcribed by RNA polymerase II, in single cells from YMC cultures. Transcript were picked according to their population-averaged levels over the YMC. Nascent and steady state mRNA numbers of three antagonist oscillating transcripts (*ATO3*, *SHM2* and *IDH1*) and one constant transcript (*ACT1*) were assessed along the YMC using smRNA-FISH. Mean RNA numbers from the FISH data recapitulate global transcript profiles previously reported over the YMC, despite variability detected between experimental repeats, validating the experimental approach taken in this study. Transcript numbers for *ATO3* are high in LOC phase and low in HOC phase. For

SHM2 they are high in early and mid-HOC phase and low during the rest of the cycle. For *IDH1* they are high in late-HOC phase at the transition with the LOC phase and low otherwise, Finally for *ACT1* transcripts levels are high and rather constant over cycle. Besides, growth rate was found to affect transcript levels in asynchronous cell populations as higher RNA numbers were detected for *SHM2*, *IDH1* and *ACT1* when comparing high-growth to slow-growth asynchronous cultures. However, when comparing slow-growth YMC cultures with asynchronous cultures at slow or high-growth, the metabolic phase of the YMC (HOC vs LOC) rather than the growth rate affects transcript levels.

Fourth, low gene expression noise was detected in YMC populations. Noise levels were found to be higher for *ATO3* and *IDH1* when compared to *SHM2* and *ACT1*. Moreover, gene expression noise was found to fluctuate during the metabolic cycle. Accordingly, investigations of the proportion of cells expressing transcripts along the YMC revealed gene expression heterogeneity mainly emerges from a switch in transcription mode between ON and OFF states. The proportion of cells transcribing was thus found to be partly responsible for the global gene expression oscillation observed for the antagonistic transcripts over the YMC. RNA distributions corroborate these results, and indicate a difference in transcription modes between *ATO3* and *IDH1* versus *SHM2* and *ACT1*, which respectively show a more bursty expression mode and a more constitutive expression mode. RNA distributions in individual cells of YMC cultures show a high cell-to-cell variability in transcript numbers, suggesting a combination of analogue and digital switches of transcription along the YMC. Finally because the proportion of cells expressing transcripts in-cytoplasm greatly varies during the YMC (except for *ACT1*), post-transcriptional processes such as active degradation are likely to be involved in the regulation of steady state transcript levels.

Overall, the results clearly indicate that transcript levels vary between individual cells of the synchronous population of the YMC.

Fifth using the simple one-state mathematical model of transcription characterising the constitutive transcription mode, transcription dynamics of the three antagonist transcripts were investigated along the YMC. Preliminary results corroborated suggestions made in the previous chapter (chapter 5 part II). Poisson probability distributions do not fit the distributions of cytoplasmic RNA numbers of YMC cultures. Moreover, the degree of fit of the mathematical model for constitutive transcription to the RNA distributions seems to change over the cycle. Although further analysis using a less strict statistical test might be required, the results suggest a bursty mode of transcription across the YMC for all three antagonist transcripts picked for this study.

Sixth, the concept of intrinsic metabolic and gene expression clocks was investigated in mid-log phase cultures and over the YMC, using dual-label smRNA-FISH on different pairs of transcripts expected to be partially co-expressed (SHM2/IDH1, ATO3/ACT1) or antagonistically expressed (ATO3/SHM2, IDH1/ATO3) during the YMC, according to population-averaged data. In mid-log cultures, the study of the absence or presence of one or two transcripts of a pair in single cells revealed whether or not these transcripts are co-expressed and suggested a temporal organisation of gene expression. Accordingly, the results support the concept of a metabolic and gene expression intrinsic clock in single cells even in high-growth asynchronous cultures.
In synchronized populations of the YMC, the Silverman et al., hypotheses were confirmed in some cells. In particular more cells were found to express only one or the other transcript of a pair of antagonists at the time anti-phase expression was predicted by global gene expression levels, while co-expression of antagonists (and

agonists) was found in single cells at the times global transcript levels crossover. However, some cells did not follow the expected pattern of expression, suggesting that not all cells behave similarly/synchronously along to YMC. This led to the idea of sub-populations of cells with different gene expression and metabolism in YMC cultures. A proportion of cells was found to express the HOC transcripts at all time during the YMC including in LOC, while a proportion of cells was found to express the LOC transcript in HOC, and finally a proportion of cell showed high HOC transcript and low LOC transcript in HOC. The results thus suggest that some cells might not be synchronized with the rest of the cell population and that some might possess a growth-state along the YMC even in LOC, while other might possess a quiescent-state even in HOC. Therefore, the results support a three state population model of YMC cultures.

Seventh, cell diameters, nuclear and mitochondrial DNA content levels were used to assess the proliferative states of cells and their progression through the cell cycle. DNA content and cell diameter thresholds were employed to distinguish G1 from S/G2/M phase cells. An increase in all metrics, particularly a greater increase in DNA content than in cell diameter, was identified in mid-HOC and late-HOC, times at which a proportion of cells are expected to enter the cell cycle synchronously, transition into S-phase and then progress to G2/M.

In mid-log cultures, gene expression and cell diameters were shown to be chronologically coordinated, providing additional evidence of an intrinsic clock relating metabolism and gene expression in individual budding yeast cells. In the YMC, coordination between cell growth, proliferation and gene expression was found in individual cells throughout the YMC. Using the transcripts as metabolic indicators,

together with the information on cell size and DNA content in individual cells of YMC cultures, a three-state (or more) population model was developed.

A proportion of cells is proposed to exit the quiescent-state and enter the cell cycle in HOC with 15 - 25% of cells exiting G1 in HOC, passing the Start checkpoint in early HOC, progressing through the cell cycle in mid-HOC and dividing synchronously in late HOC.

A proportion of cells is not in a quiescent-state at all time during the YMC with 25 - 30% of the cells in a S/G2/M phase, progressing through the cell cycle over the metabolic cycle.

A proportion of cells stays in a quiescent-state at all times along the cycle with ˜50% of cells in G1 during the HOC phase of the YMC.

Such coordination implies that cell size and growth participate in the regulation of quiescence exit in individual cells of YMC populations, corroborating previous predictions.

9.2 The Yeast Metabolic Cycle in context of other biological systems

The concept of intrinsic metabolic clock in individual cells and how cells and clocks synchronize is of great interest in other biological systems too.

As referred previously (Introduction 1.3.2), this concept is studied within the context of circadian rhythms. Remarkably, circadian oscillations in mammalian cells, such as YMC oscillations in yeasts, might not be driven by transcription but might instead result from metabolic fluxes and protein post-translational modifications. Indeed, erythrocytes were shown to cycle metabolically as rhythmic post-transcriptional modifications of peroxiredoxins were detected in red blood cells deprived from their nucleus (O'Neill & Reddy. 2011). The presence of circadian oscillations despite the absence of transcription clearly indicates that metabolism is timely regulated by other mechanisms in individual human red blood cells and points that future studies could focus on single-cell metabolomics to fully grasp the metabolic/circadian life of single cells.

Understanding metabolic clocks and the complexity of “synchronized cell populations” seems also crucial in the field of therapeutics and in particular for cancer treatments. Indeed not only circadian clocks can be disrupted by cancers such as lung cancers (Pariollaud et al. 2022, Stincardini et al. 2023), but the targeting of the circadian clock can also help in cancer therapy, of glioblastomas for example (Chan, Rich, J& Kay. 2023). Finally some studies suggest chronochemotherapy for the treatment of colorectal and endometrial cancers, among others. Although this approach seems relevant, more systematic studies seem to be required for the scientific community to accord on this proposition (Sancar & Van Gelder. 2021, Yang et al. 2021).

Similarly, understanding the mechanisms and regulations of the metabolic clock in cells seems relevant for this field. The discovery of the cell-to-cell heterogeneity in the "synchronized cell populations" of the YMC clearly indicates that single cell transcription profile, metabolism and behaviour can greatly vary between cells of a synchronized culture. In particular, the presence of characteristics of intermediate transcriptional and metabolic states in some cells of the YMC population suggests an explanation as of why some cells can be less responsive to treatment, despite being determined as 'identical' or 'synchronized' according to bulk essays. This is of particular interest when some cells are found resistant to drugs in cancer chemotherapy (Wu et al. 2014), or even for the development of therapies within the context of multi-drug-resistant bacteria such as *Staphylococcus aureus* (WHO. 2012). Thus, this finding reaffirms the need of single cell studies, especially when testing drugs' assimilation and efficiency.

Ultimately, understanding what triggers and keeps the overall cell synchronization while allowing the cell diversity detected in YMC cultures can add to the comprehensive understanding of cell differentiation.

Major metabolic changes are recorded between pluripotent stem cells and differentiated cells. Oxygen consumption, for example, also drastically shifts between these two states (as in YMC cultures), with stem cells prioritising glycolysis over oxidative phosphorylation (Nishimura, Fukuda, & Hisatake. 2019, Tyurin-Kuzmin et al. 2020). Stem cells in that sense perhaps resemble the less metabolically active cells (in a LOC state) of the YMC. Therefore, experiments could be designed to test the conditions that initiate the YMC and to understand how these impact the cell population, its heterogeneity, and the proportion of cells with a specific metabolic state.

This could facilitate the global comprehension of what triggers cell differentiation and maintains cell fate.

9.3 Future directions

First, in order to get a detailed understanding of transcription dynamics, and obtain kinetics of transcription for the target transcripts along the YMC, future directions might include finding the best fits of the 2-state model of transcription (transcriptional burst) (Zenklunsen et al. 2008) to the data.

Second, the partition and organisation of sub-populations of cells along the YMC could be further investigated with regards to finding about the proportion of and characteristics of non-quiescent and quiescent cells. Findings by Li et al., & Miles et al., showed that the differentiation into quiescent and non-quiescent cells starts before the diauxic shift and that at least 3 to 4 sub-populations are present within stationary phase cultures, with dense and light mother and daughter cells. Indeed, in batch cultures after 24h, 20% of cells are small, daughters cells, of light densities and stuck in G1 (R1), 50% of cells are mainly composed of mothers, most of which are arrested in G1 though some are found in S/G2/M (R2), finally around 30% of the population is composed of small daughter cells (larger than R1), dense and stuck in G1 (Li et al. 2013, Miles et al. 2020). In light of these results, re-assessment of individual cells of YMC cultures through FACS experiments to collect information on DNA content, cell size and cell wall thickness are suggested. Key characteristics of sub-populations of cells under limiting nutrient conditions could also be revealed through the evaluation of gene expression status via sequencing and/or smRNA-FISH after centrifugal elutriation or cell density Percoll gradient experiments. Moreover, investigation of gene

expression profiles and metabolic status of cells from nutrient limited colonies (Palkova et al. 2002, Vachova & Palkova. 2005, Varahan et al. 2019), would provide a way to test spatial organization of gene expression in budding yeast. Finally, a focus on mitochondrial respiratory growth in single cells might be necessary to completely decipher sub-populations partition in YMC cultures because the function and morphology of the mitochondrial network highly depends on environmental conditions (Friedman and Nunnari. 2014), respiration plays a crucial role in quiescence exit (MacLean et al. 2001, Davidson et al. 2011 Dhawan & Laxman. 2017) and was suggested to regulate the ability of stationary phase cells to exit quiescence and re-enter the cell cycle (Laporte et al. 2018), and is undeniably a key component of the YMC.

Third, major histone post-transcriptional modifications take place during quiescence entry, maintenance and exit in stationary phase cultures, but also during the YMC. In particular, histone lysine acetylation levels are affected in both types of cultures. Rpd3L histone deacetylase induces a global decrease in HK acetylation levels in quiescent cells (McKnight et al. 2015., Miles & Breeden. 2016, Friis et al. 2009, Mews et al. 2014), leading to a more compact chromatin (Pinon et al. 1978, Swygert et al. 2021) while Gcn5 from the SAGA complex was reported to increase acetylation levels at histones lysines of growth genes (RNA peak in HOC) during the HOC phase of the metabolic cycle, suggesting the change in Acetyl-CoA levels along the YMC regulates gene expression via histone lysine acetylation (Cai et al. 2011, Kuang et al. 2011, Shi & Tu. 2013, Kuang et al. 2017, Sanchez-Gaya et al. 2018). Therefore, the relationship between metabolism and gene expression along the YMC might reside there, with H-PTMs acting as integrators of metabolic flux in cells. Thus, investigation of epigenetic

marks via the study of H-PTMs, chromatin remodellers and chromatin compaction levels might reveal the connection between metabolic and gene expression states in YMC cultures. Techniques such as micro-C (Hsieh et al. 2015, Hsieh et al. 2016) or the Oxford Biodynamics technology (Episwitch Explorer Array kits) could be employed on YMC populations to capture detailed chromatin organisation and identify chromosome interacting domains during metabolic changes. Nevertheless, because results from this study showed high cell-to-cell gene expression variability in YMC cultures, examination of H-PTMs and chromatin compaction in single cells also seems necessary.

For this work, attempts were made to combine indirect immunofluorescence and smRNA-FISH techniques with Super Resolution Microscopy (SRM) (Kaplan & Ewers. 2015, Schermelleh et al. 2019, Maiser et al. 2020) to examine H3Kac levels, cell division cycle state, DNA compaction and transcript levels in single cells from a YMC population (Figure 9.1) but further optimizations will be required to obtain quantitative data from this set of experiments.

Finally, a combination of single cell metabolomic, transcriptomic and proteomic experiments at key timepoints of the YMC might reveal a more detailed but also global view of sub-populations organisation in *Saccharomyces cerevisiae*.

A. **B.**

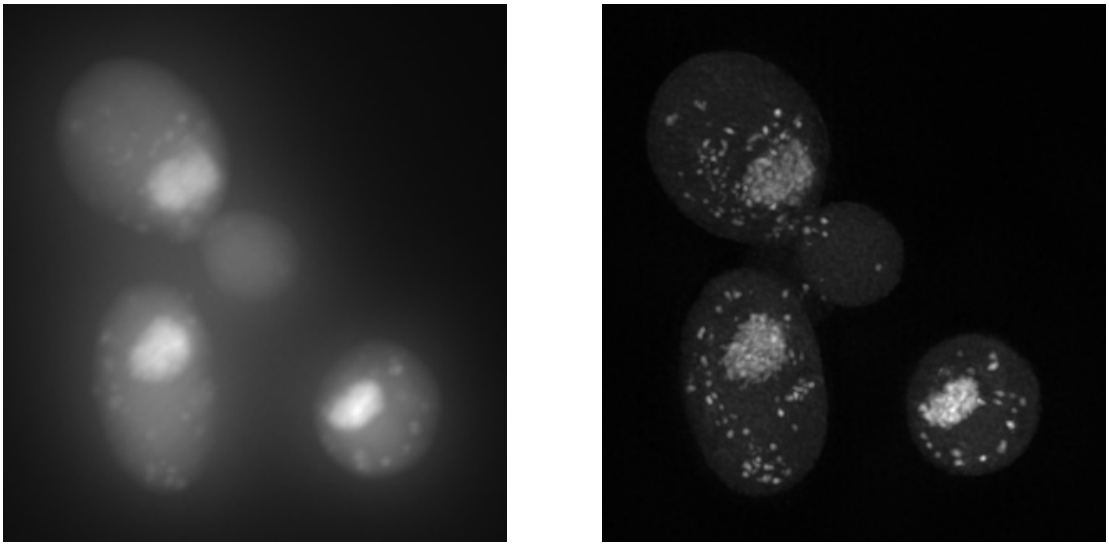

Figure 9.1 An example of microscopy images gathered within the context of this work of CENPK WT cells sampled in mid-log phase

Using; ***A.*** *Widefield fluorescence microscopy (without deconvolution).* ***B.*** *Super Resolution Microscopy. DNA is stained with DAPI. Mitochondrial DNA nucleoids, Nuclear DNA content and degree of compaction is apparent. The images are cropped and enlarged. The images were acquired with the help of Associate Professor Lothar Schermelleh with the 3D SIM microscope.*

9.4 Concluding remarks

This work investigates the relationship between metabolism and gene expression in *Saccharomyces cerevisiae*, addressing some of the gaps found in the literature. To do so, the Yeast Metabolic Cycle, a system of temporal organisation of cellular and metabolic processes is employed to set up, monitor and analyse rapidly-changing metabolic states. The technique of single-molecule RNA-FISH is performed along the YMC, at a high temporal resolution, allowing the detection and quantification of absolute transcript numbers in single cells from synchronous populations. Finally, quantitative analysis is applied to the gene expression data.

The first achievement of this study is the establishment of a detailed experimental plan including controls and a protocol for time-course smRNA-FISH experiments along the YMC. Five main discoveries are made in this study.

First, the detection of coordination in time during the YMC, between ribosomal RNA production and Rps6 phosphorylation indicates Rps6 activity is regulated by its phosphorylation along the cycle. This result further implies regulation of ribosome biogenesis by TORC1 in YMC cultures. It also supports the current idea that protein post-transcriptional modifications rather than protein levels drive the YMC progression (Feltham et al. 2020). **Second**, the analysis of pre-rRNA distributions and the mRNA distributions of 3 antagonist transcripts and one constant transcript along the YMC revealed high gene expression heterogeneity in YMC populations for genes transcribed by RNA Polymerase I and II, clearly indicating that individual cells from the synchronous population show different gene expression profiles. **Third**, the global oscillation in transcript profiles is found to result from the fast ON-OFF transcription changes but also from changes in transcript levels. In particular the results suggest

antagonist transcripts are produced via transcriptional bursts. **Fourth**, the concept of an intrinsic metabolic clock is supported by the single cell data acquired in both mid-log and YMC cultures. Mid-log populations show a chronological organisation of gene expression related to cell size while YMC cultures also show a temporal compartmentalisation of gene expression in single cells, but more complex coordination with cell size and DNA content. **Fifth**, although most cells of YMC cultures follow predictions under the intrinsic clock concept, some cells of YMC cultures do not. These cells indicate the presence of sub-populations of cells in YMC cultures behaving differently than predicted by the literature (Silverman et al. 2010). Combining results from the literature and this study on the coordination between growth, cell proliferation and gene expression, a three-state model is proposed for the organisation of YMC population, indicating a partition of the population between cells remaining in a quiescent-like state along the cycle, cells remaining in a growth-like state along the cycle and cells transitioning between the two states and proliferating in HOC.

This work thus contributes to the detailed understanding of gene expression regulation in link with metabolism in YMC populations.

Chapter 10

Appendix

OX

EARLY HOC

Ribosome synthesis

1.
- Ribosome biogenesis (ribis)
- rRNA processing
- RNA metabolism: small nuclear RNAs, RNA processing, RNA splicing
- Sulfur metabolism: sulfate uptake, methionine synthesis
- Nucleolus architecture
- RNA Pol I and Pol III
- Methyltransferase activity

2.
- Amino-acid biosynthetic process, metabolism and transport
- Ribosomal proteins (RP)
- Cytoplasmic translation initiation and regulation, Protein de novo
- tRNA and snoRNA processing, RNA modification

- Glycolysis and gluconeogenesis
- Re-folding actin cap
- Plasma membrane
- Purine synthesis
- Allantoin catabolic process
- Nitrogen utilization
- ADH1: alcohol dehydrogenase 1 peaks just before EtOH towards the end of Ox beginning of RB

S.1.A

RB

Middle HOC

- Cell division cycle: DNA replication, Replication fork, including alpha-DNA-polymerase complex, DNA repair.
- Mitochondria functions and biogenesis: Nuclear encoded mitochondrial proteins affecting mitochondrial DNA replication, respiration, protein import
- Glutamate biosynthesis process
- Citrate metabolic process
- Tricarboxylic acid cycle
- Glyoxylate cycle
- Respiratory chain complex
- ATP synthesis with proton transport

Late-HOC

- Mitochondrial ribosomal proteins and translation
- Mitochondrion organization
- Histones
- Septin complex, Spindle pole components, Kinetochore microtubules

Transition late HOC to early LOC

- Mitochondrial matrix and envelope
- Aerobic respiration, Respiratory chain complex, mitochondrial proton-transporting ATP synthase complex assembly
- Generation of precursor metabolites and energy
- Cytokinesis, cell bud

- Peroxisomal matrix
- Arginine biosynthetic process
- Proline catabolic process
- **Ammonium transport**
- Siderophore transport
- Heme binding
- Carnitine and propionate metabolic process
- Gluconeogenesis
- Cell wall

S.1.B

S.1.C

Figure S.1.A, B and C Detailed view of GO terms

GO terms found for the 3 gene expression clusters OX, RB and RC and for the two HOC and LOC gene expression clusters (Modified from Klevecz et al. 2004, Li & Klevecz. 2006, Tu et al. 2005, Soranzo et al. 2009, Machne & Murray. 2012, Kuang et al. 2014, Feltham et al. 2020).

List of oligos used to make smRNA-FISH probes.

Table S.1 Pre rRNA-FISH probes; complementary sequences of the external and internal transcribed spacers regions of the 35S rRNA

Probe Name	Sequence (5'-3')
pre-rRNA tsr_1	cttgtcttcaactgctttcg
pre-rRNA tsr_2	tcgtttccaaactcttttcg
pre-rRNA tsr_3	acgaacgacaagcctactcg
pre-rRNA tsr_4	tttgacgaggccatttacaa
pre-rRNA tsr_5	gatcacctagcgactctctc
pre-rRNA tsr_6	atagagactaggcagatctg
pre-rRNA tsr_7	cccatgtcaattaaacacgc
pre-rRNA tsr_8	tgtatctctcaatacgcatc
pre-rRNA tsr_9	cacactctgggaatttcttc
pre-rRNA tsr_10	acgatgagactgttcaggtt
pre-rRNA tsr_11	ccaatggaatcgcaagatgc
pre-rRNA tsr_12	ctagtaatccaccaaatcct
pre-rRNA tsr_13	cccaagtttgaattctttga
pre-rRNA tsr_14	cggctattcaacaaggcatt
pre-rRNA tsr_15	tgaagaatcacagtcttgcg
pre-rRNA tsr_16	atcgctgatttgagaggagg
pre-rRNA tsr_17	gtttcacggaatggtacgtt
pre-rRNA tsr_18	ggttccaccaaacagatacc
pre-rRNA tsr_19	ctctttgagtttcctctaat
pre-rRNA tsr_20	actccgtcaccataccatag
pre-rRNA tsr_21	gcttttacactcttgaccag
pre-rRNA tsr_22	cggaaatgctctctgttcaa
pre-rRNA tsr_23	aattgctttttcaggtctct
pre-rRNA tsr_24	ttgagtttggaaacagctga
pre-rRNA tsr_25	ttccctcttgctagaagata
pre-rRNA tsr_26	tctctttttttttttcccac
pre-rRNA tsr_27	tctcatgctcttgccaaaac
pre-rRNA tsr_28	tgtcttcttgcccagtaaaa
pre-rRNA tsr_29	ttacaagcctagcaagaccg
pre-rRNA tsr_30	ctcaccgtttggaatagcaa
pre-rRNA tsr_31	acggttttaattgtcctata
pre-rRNA tsr_32	aactccacagtgtgttgtat
pre-rRNA tsr_33	ttgctcgaatgcccaaagaa
pre-rRNA tsr_34	ttgtttgtgtttgttacctc
pre-rRNA tsr_35	agagtatcactcactaccaa
pre-rRNA tsr_36	aggccagcaatttcaagtta
pre-rRNA tsr_37	cgcagagaaacctctctttg
pre-rRNA tsr_38	cgtacttgcattatacctca
pre-rRNA tsr_39	ccgcagttggtaaaacctaa
pre-rRNA tsr_40	gttccaatacgctcagtata
pre-rRNA tsr_41	acgctctcttcttatcgata
pre-rRNA tsr_42	ccagtacccacttagaaaga
pre-rRNA tsr_43	ttgttcagtctacttctctc
pre-rRNA tsr_44	acccggatcatagaattctt
pre-rRNA tsr_45	catcctcatcgtatattata
pre-rRNA tsr_46	atggtacactcttacacact

Table S.2 Multiplex (dual-labelled) smRNA-FISH probes; complementary sequences of ATO3 and SHM2 mRNAs.

ATO3		SHM2	
Probe number	**Sequence (5'- 3')**	**Probe number**	**Sequence (5'- 3')**
1	ggagaagaagcagacgatgt	1	gagcgtcggatagagtgtaa
2	ttcacacccttttccaaatc	2	ccaccaaatgagaggtgatc
3	gggagcgtctcaatattttc	3	atccttgataatggagtcca
4	gaaacgcctgcaatcgaacc	4	atggagtgcttttgtctttc
5	ttgaatattagggaagccct	5	ggcatcgaaaacggaggttg
6	agtctctgtcggagtatatc	6	tgttggacaatggagttcca
7	gtggaggatcctagagtaat	7	cctggataaccttcagagta
8	ctgtctagtgcattgagcaa	8	attaccaccgtagtaacgag
9	cggagtatactttgcacagt	9	tttccattctgtcaatgtgt
10	gaaccggattagcgaactgg	10	gctttcaaagctctttgttg
11	agaaaacgatgcgagaccca	11	aagtttggacgttaacaccc
12	gcgacagaactagacatgac	12	tgcaagttagcaggagaacc
13	ccgcgaacgttcgcattaat	13	gaggcttcataatagcttga
14	aacaaacttagcgcccattt	14	aggtatagacccatcaatct
15	caattcaatggcaccaccaa	15	cgtgagacaaatgaccacca
16	caaaacacaataacccggca	16	ttttctgttttcagtagcgt
17	acacagtcatggcgtatgtg	17	tgggttaactctgtatggga
18	cagaacccgccgaaagaact	18	tcgtagtcgataataccggt
19	tatctgttagcccataaccg	19	gtctatataggatggcgttc
20	tagccgctgaccaaattatc	20	gtatgctgaagtaccagcaa
21	gttcaacattgtgggatcgg	21	tctctcattctcttgtagtc
22	gcaaggaagaacccaatgac	22	agtaagcaccacatttgtcg
23	gaaggtgaaaacggtccagc	23	aaaccagaaatgtgggccat
24	gctcttcaatgtacacatca	24	aaggagatgggatgacacct
25	atagtaagaacaaaccccac	25	gtggtggtggtaacgatatc
26	gtagtaggaaggtaagatcc	26	tggacctctcaaagacttgt
27	gtcaatgaaggtgccgatac	27	gttgatagatctcacacctc
28	aattccaaaatagccaccgg	28	tatagaacttccttaccggt
29	aataccaaccgcagcaacta	29	gttaattgggttttccaagt
30	ggactcaccacagaacagta	30	cttggtgacctgggaaaaca
31	cgccctgaaggctaaataag	31	caatggtatggttgtgtgga
32	aaggagcatttggcattgtg	32	cttcaaagcagtggccaaag
		33	cttgaattctggagtggcag
		34	cttcaagacttgagtttggt
		35	ttcactttccaaagccttag
		36	aactaatctgtagcccaagt
		37	atgtgagaatcggtaccgtt
		38	ccttttctctcaaggatact
		39	tcaacacgagcaccatcaac
		40	gtcacctggaatagagtttt
		41	cacctggaaccaaagcagat
		42	tggaaatcttcttcacccat
		43	cgaattctacagccttgtta
		44	tacaagcatcctttggcaag
		45	cttggctttgaagtccttta
		46	aaacatcagagccttcgtcg
		47	ccagtcgtaaatttccttt
		48	tacacagccaatgggtattc

Table S.3 Multiplex (dual-labelled) smRNA-FISH probes; complementary sequences of IDH1 and ACT1 mRNAs.

IDH1		ACT1	
Probe number	**Sequence (5'- 3')**	**Probe number**	**Sequence (5'- 3')**
1	ctcttagcaattgttctgtt	1	agaaccgttatcaataacca
2	ctgagcggcagtggctaaag	2	gcaaaaccggctttacacat
3	tacttcttgggtagggtgcg	3	aagacagcacgaggagcgtc
4	agtgacggtgaaacgaccgc	4	tggtctaccgacgatagatg
5	caacaccgtcaccaggtatc	5	cgaccatgataccttggtgt
6	ggttctcactgaatcagtga	6	taggagtctttttgacccat
7	gggatattttcagcctcaaa	7	ggattgagcttcatcaccaa
8	tgtttatagtttcccagtcg	8	cgtaaagtcaagatacctct
9	tccttatgatctgtttgctt	9	aataccgtgttcaattgggt
10	ctcaacagcttcatagacgc	10	tttccatatcgtcccagttg
11	gaccaatcttatttctcttt	11	gtagaaggtatgatgccaga
12	tcagcaggagtgtgccatag	12	ttctggggcaactctcaatt
13	tagtgaaccgtgacctgttt	13	cagtcaaaagaacagggtgt
14	gttgtttacgcaaagcaacg	14	gatttagggttcattggagc
15	gccacattggcgtagatatc	15	ttgagtcatcttttctctgt
16	tgacacccttcaaggatttg	16	cgtagaaggctggaacgttg
17	tctatgtctggaattctagt	17	gacaaaacggcttggatgga
18	ctccgtgttttctctaatga	18	agttctaccggaagagtaca
19	catgttccaggcctgagaac	19	ccggaatccaaaacaatacc
20	aaagattccactacaccagg	20	ggaacgacgtgagtaacacc
21	cttaggtctagtcataactt	21	ggtagagagaaaccagcgta
22	caaatctggcgatcctttct	22	atcgattctcaaaatggcgt
23	tgtatttcttggcgaagtca	23	agtcagtcaaatctctaccg
24	cacagctgtgacagactttc	24	ccacgttcactcaagatctt
25	acttcatgatatttgcctta	25	agcagtggtggagaaagagt
26	atttctgaacagaccgtcac	26	tgtcacggacaatttctctt
27	ctttttggccaatttcagtt	27	gacgtaacatagtttttcct
28	tggacgatacgtcaatatca	28	tttcttgttcgaagtccaag
29	atggaggcattgtcgacaat	29	gaagattgagcagcggtttg
30	aattgatgaggtttggccac	30	gttcgtaggatttttcaatt
31	cgtacattgaaggggtaact	31	gtgatgacttgaccatctgg
32	ccaatgttgcctaagatggt	32	tctgaatctttcgttaccaa
33	tggaccaccgatcaaagcag	33	gatggaacaaagcttctggg
34	ttcgaagacagcatagtccc	34	gattccaaacccaaaacaga
35	aaccaacatgtctggaacct	35	agtagtttggtcaataccgg
36	ccacattttggcctttaata	36	cacacttcatgatggagttg
37	aaaggatcatggcagttggg	37	aattccttacggacatcgac
38	tggttcaacattaacgtgga	38	ggacataacgatgttaccgt
39	agcatattcattcaaaccca	39	ctgggaacatggtggtacca
40	tgaactgcctttgagattct	40	ttttgcattctttcggcaat
41	tatgcttaccttctgcgatc	41	atggagccaaagcggtgatt
42	gaggaaccaccaatatctct	42	atgatcttgaccttcatgga
43	tcattcgtgaagtcagtagt	43	gtactttctttctggaggag
		44	tagaaccaccaatccagacg
		45	gaaggtagtcaaagaagcca
		46	gttttgagatccacatttgt
		47	ggaccactttcgtcgtattc
		48	acacttgtggtgaacgatag

1.

A.

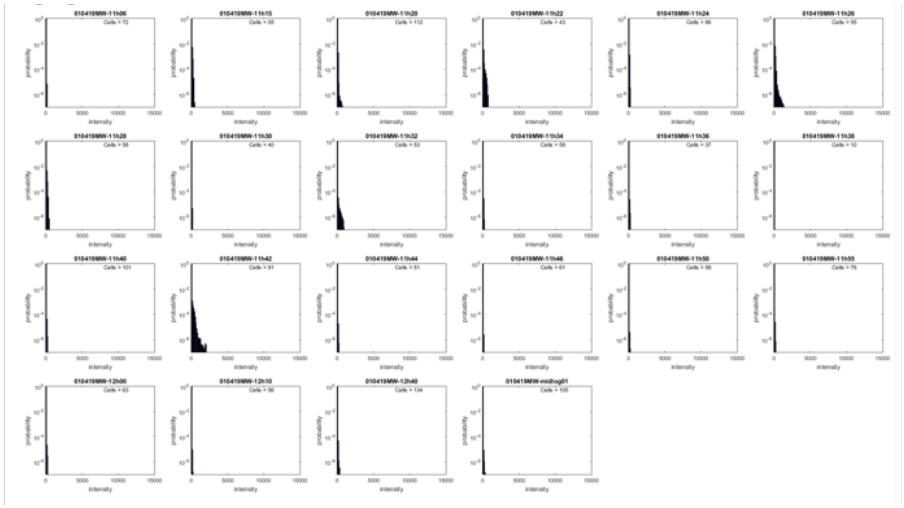

B.

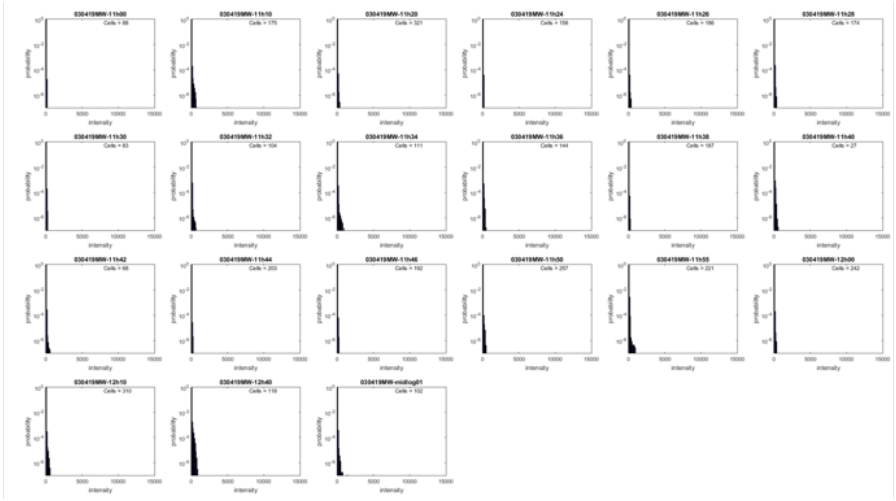

C.

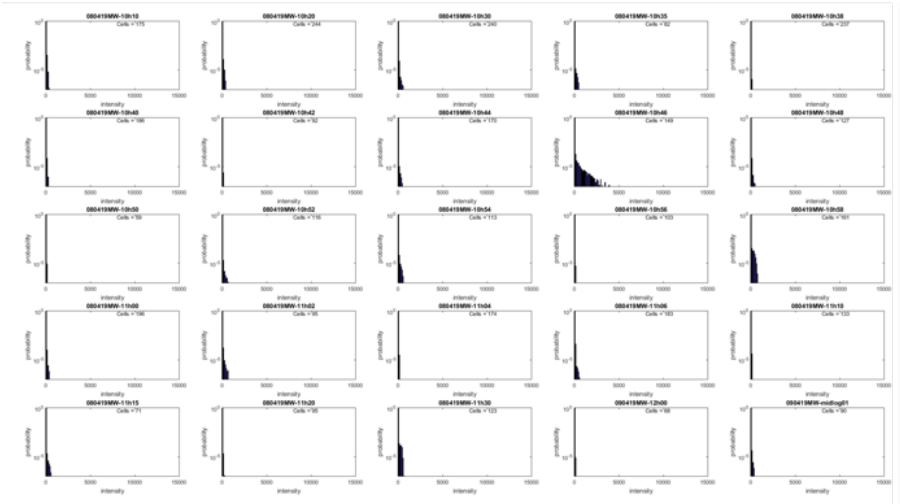

Figure S.2.A

2.

A.

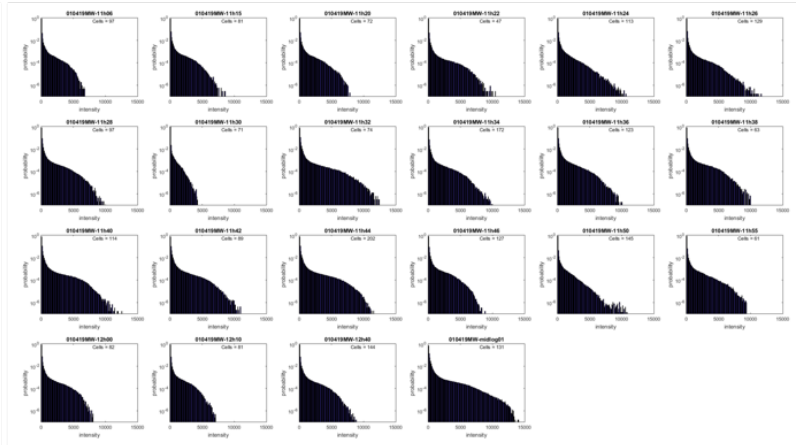

B.

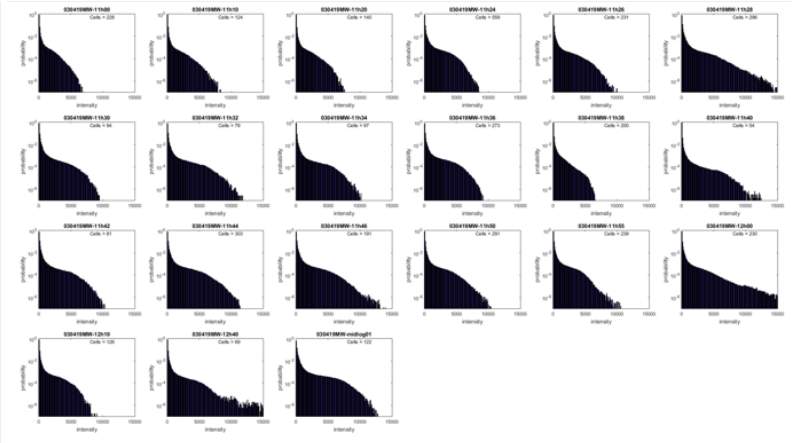

C.

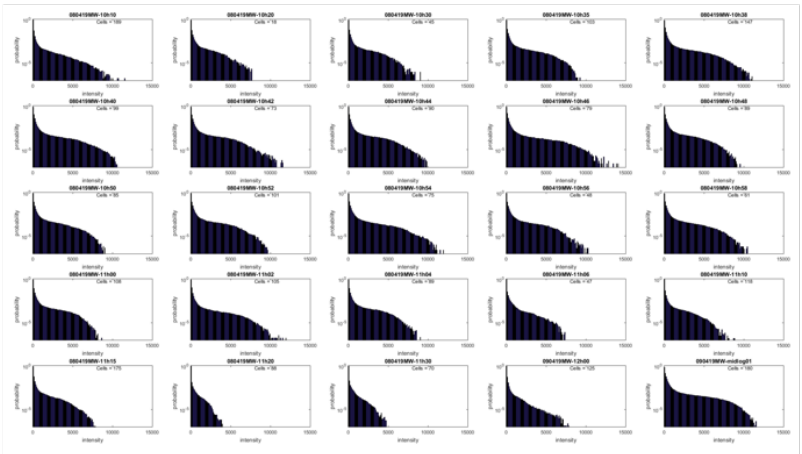

Figure S.2.B

Figure S.2. Histograms of the fluorescent signal intensities of the data vs control for the pre-ribosomal RNA-FISH experiments.

*Number of detected pixels against the pixel intensities of the fluorescent signal **1.** for RNAseA treated cells (control), **2.** for WT cells (data); hybridized with pre-rRNA TSRs RNA-FISH probes, for each sampling timepoint taken along the YMC and in mid-log phase, for the 3 biological replica (A,B,C).*

Figure S.3. Histograms of the fluorescent signal intensities of the data vs control for the single-label and dual RNA-FISH experiments on antagonist transcripts

Number of detected pixels against the pixel intensities of the fluorescent signal for the different target transcripts in Cy5 (atto633 fluorophore) or Cy3/TRITC (atto565 fluorophore) channel. The colours indicate data from WT yeast cells (blue) or from KO cells/controls (brown) for each sampling timepoint taken along the YMC and in mid-log phase. ***(1)*** *Single- label RNA-FISH: ATO3 in Cy3, (n=1).* ***(2)*** *Dual-RNA-FISH: ATO3 in Cy5 vs SHM2 in Cy3,* ***(3)*** *Dual-RNA-FISH: SHM2 in Cy5 vs IDH1 in Cy3,* ***(4)*** *Dual-RNA-FISH: IDH1 in Cy5 vs ATO3 in Cy3, (n=2 for each transcript).*

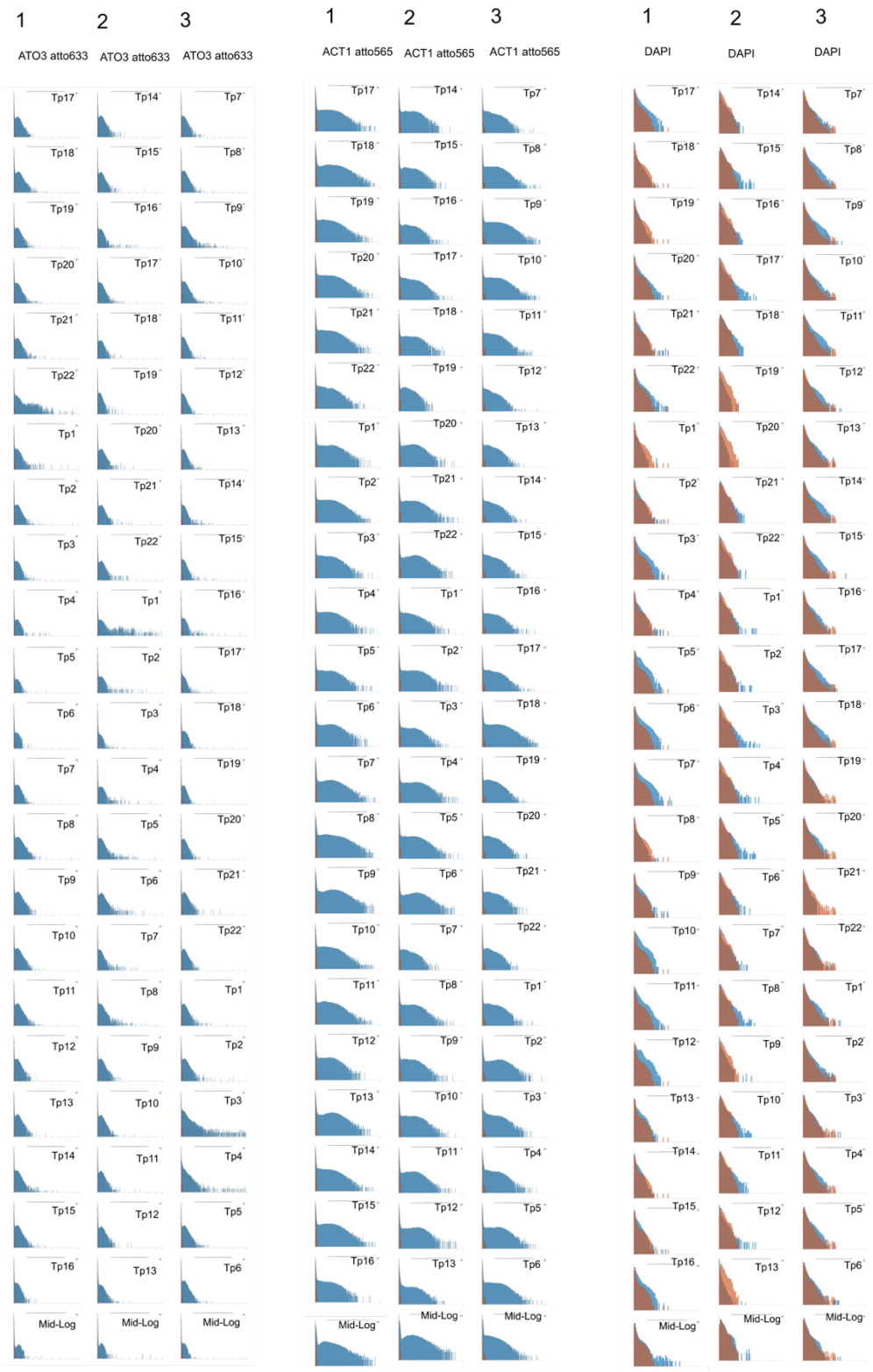

Figure S.4. Histograms of the fluorescent signal intensities of the data vs control for control dual-RNA-FISH *Number of detected pixels against the pixel intensities of the fluorescent signal for the different target transcripts in Cy5 (atto633 fluorophore) or Cy3/TRITC (atto565 fluorophore) channel. The colours indicate data from WT yeast cells (blue) or from KO cells/controls (brown) for each sampling timepoint taken along the YMC and in mid-log phase. Control dual-RNA-FISH: ATO3 in Cy5 vs ACT1 in Cy3, (n=3), (**1,2,3** indicate the different replica).*

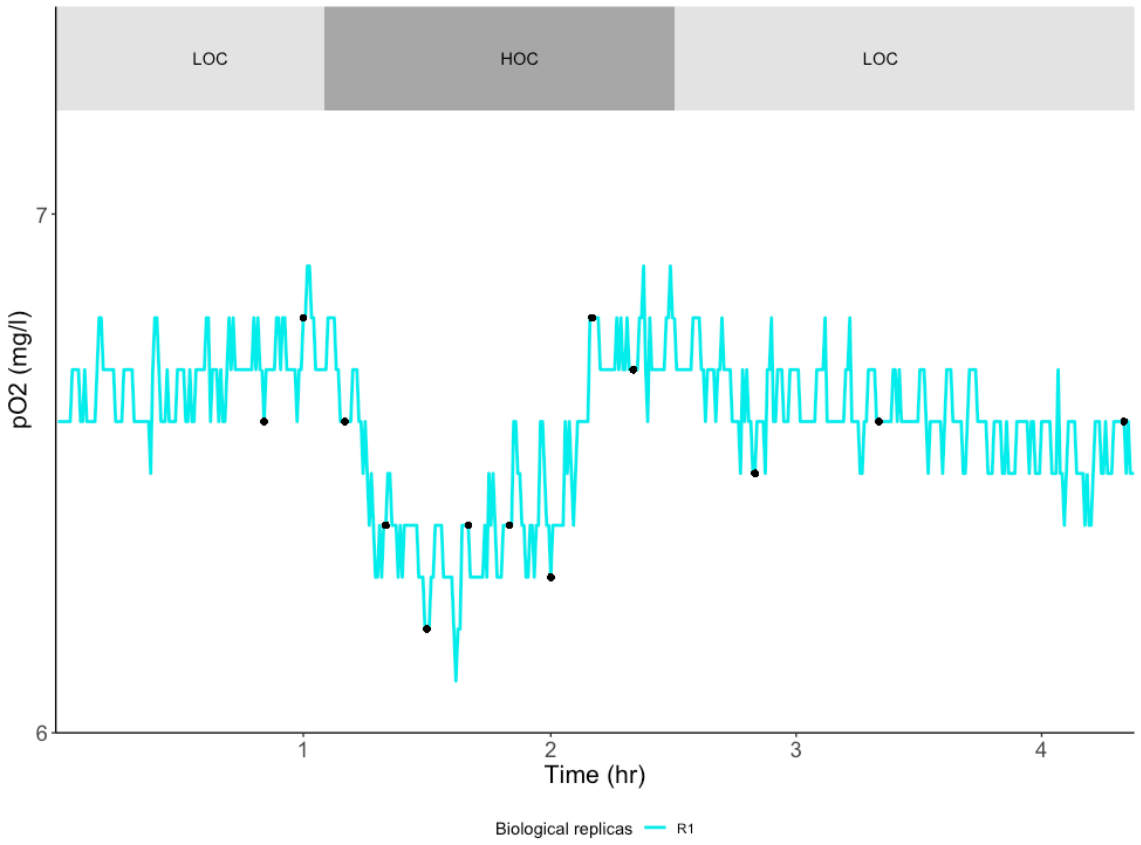

(i) Figure S.5.A

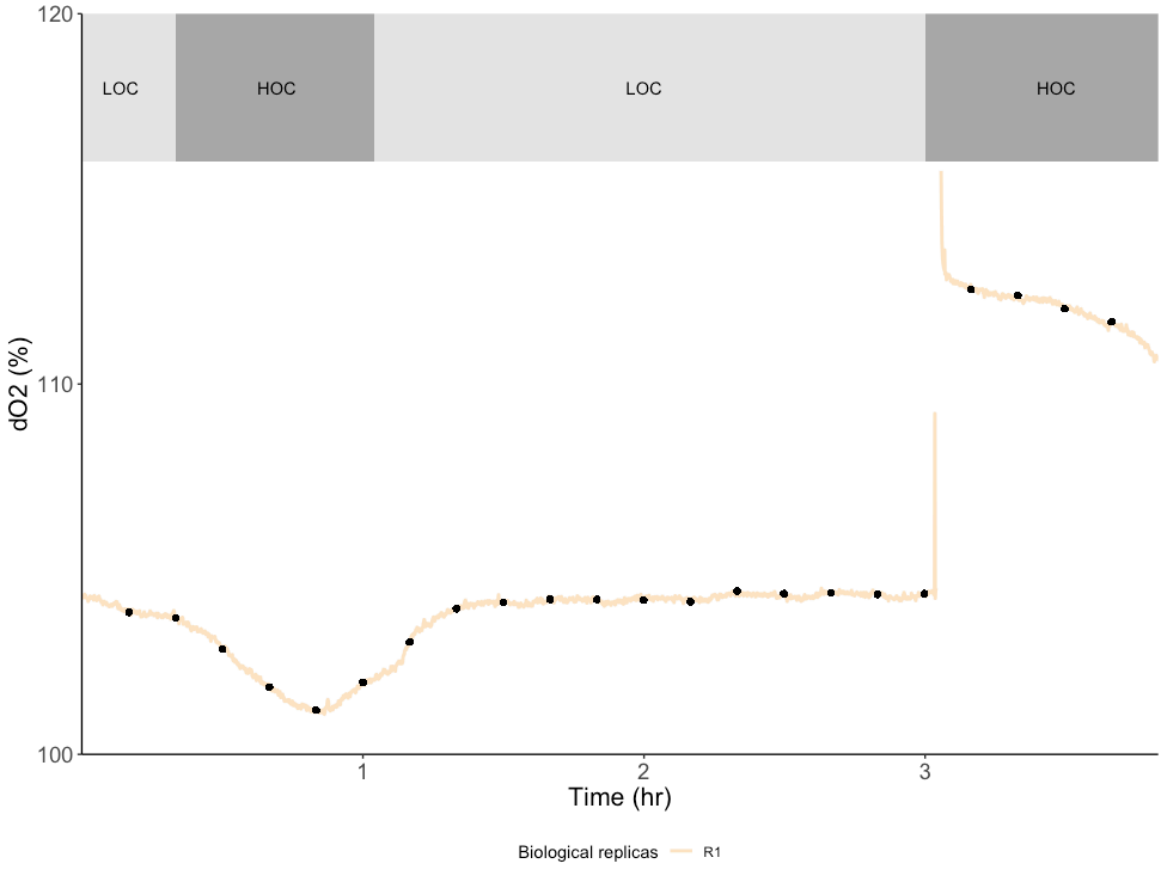

(ii) Figure S.5.B.1

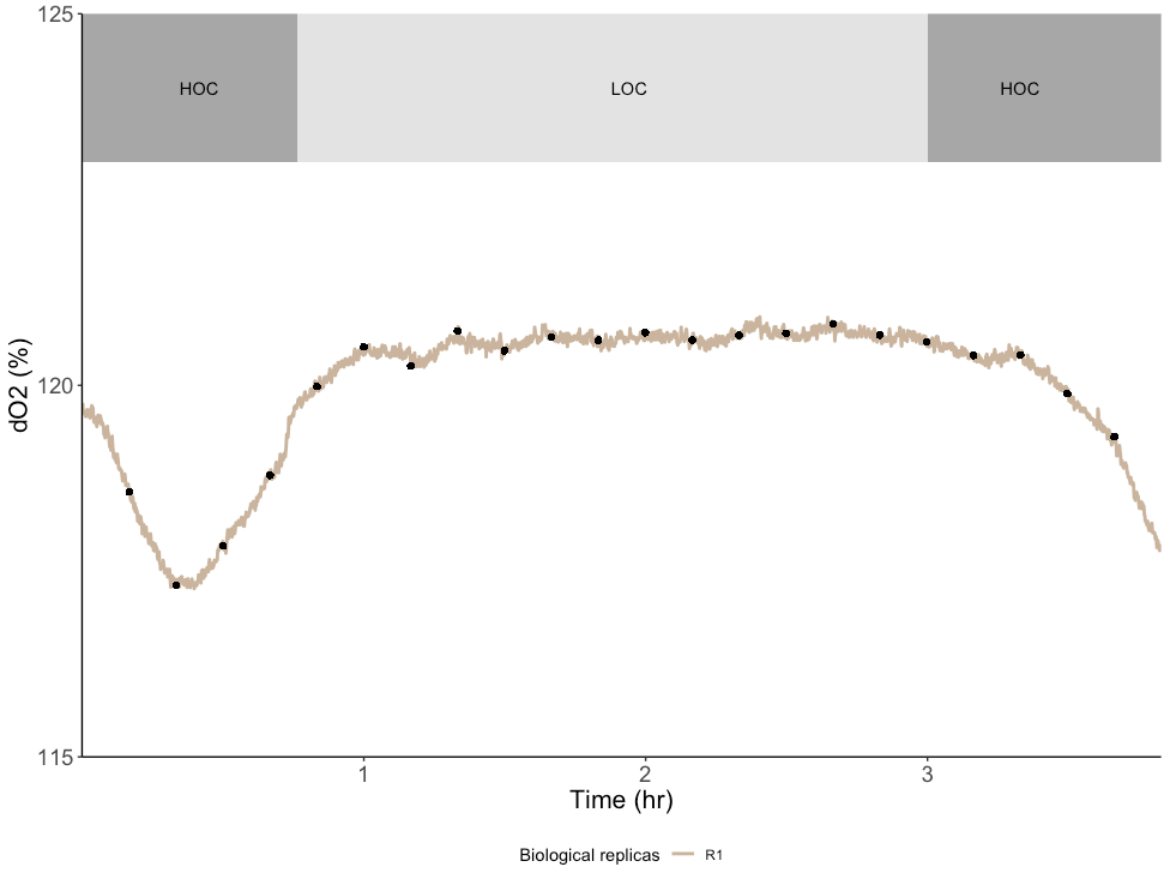

(ii) Figure S.5.B.2

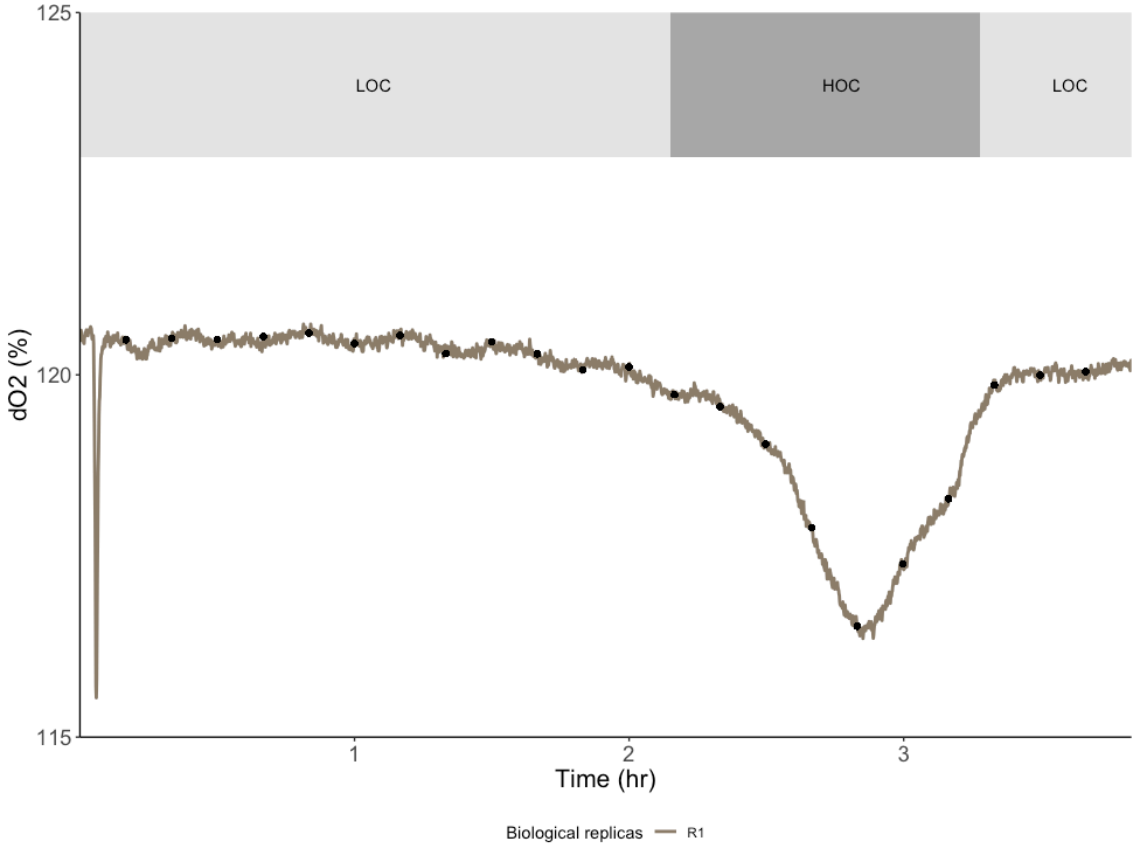

(ii) Figure S.5.B.3

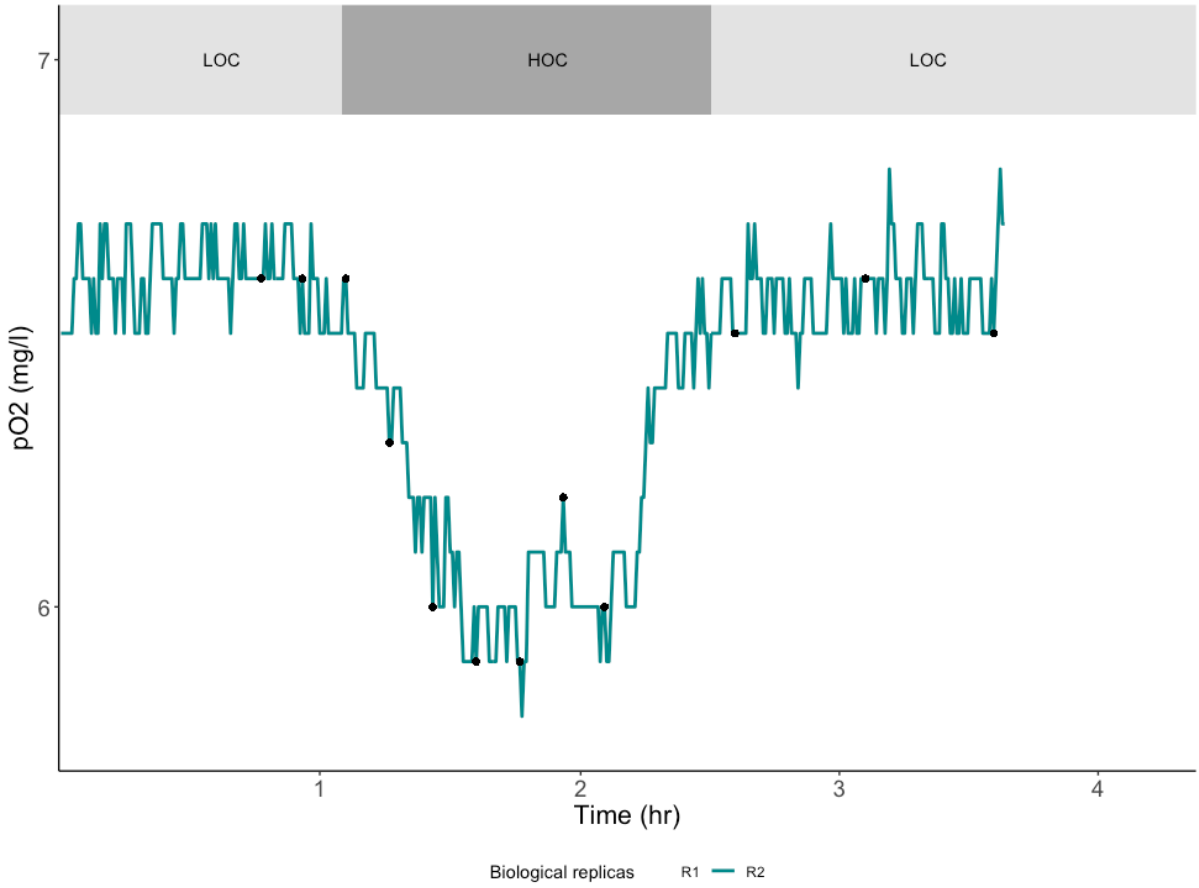

(iii) Figure S.5.C

Figure S5 (5.3.BIS) Outline of the design of the three smRNA-FISH experiments

Dissolved oxygen levels fermenter traces, sampling time points (time shown in hour) and biological replicates of the different FISH experiments.

(i). Figure S.5.A: Single- label RNA-FISH; *Minifor dO_2 traces, **ATO3** in Cy3, (n=1; 1 biological repeat or YMC sampling and 1 technical repeat or smRNA-FISH experiment).*

(ii) Figure S.5.B: Control dual-RNA-FISH; *Bioflo320 dO_2 traces, **ATO3** in Cy5 vs **ACT1** in Cy3, (n=3; 3 biological repeats (**S.5.B.1,2,3**) or YMC sampling and 3 technical repeats or smRNA-FISH experiments).*

(iii) Figure S.5.C: Dual-RNA-FISH; *Minifor dO_2 traces, **ATO3** in Cy5 vs **SHM2** in Cy3, **SHM2** in Cy5 vs **IDH1** in Cy3, **IDH1** in Cy5 vs **ATO3** in Cy3, (n=2; 1 biological repeat or YMC sampling, 3 technical repeats or smRNA-FISH experiments, 2 technical repeats for each transcript).*

1.

A.

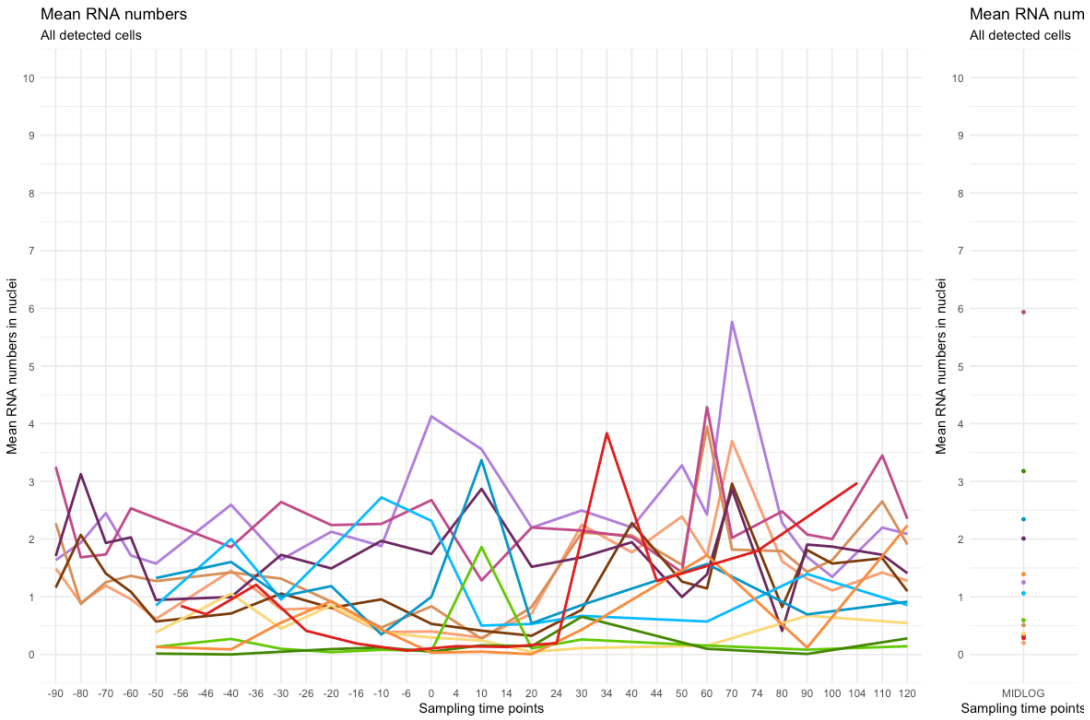

B.

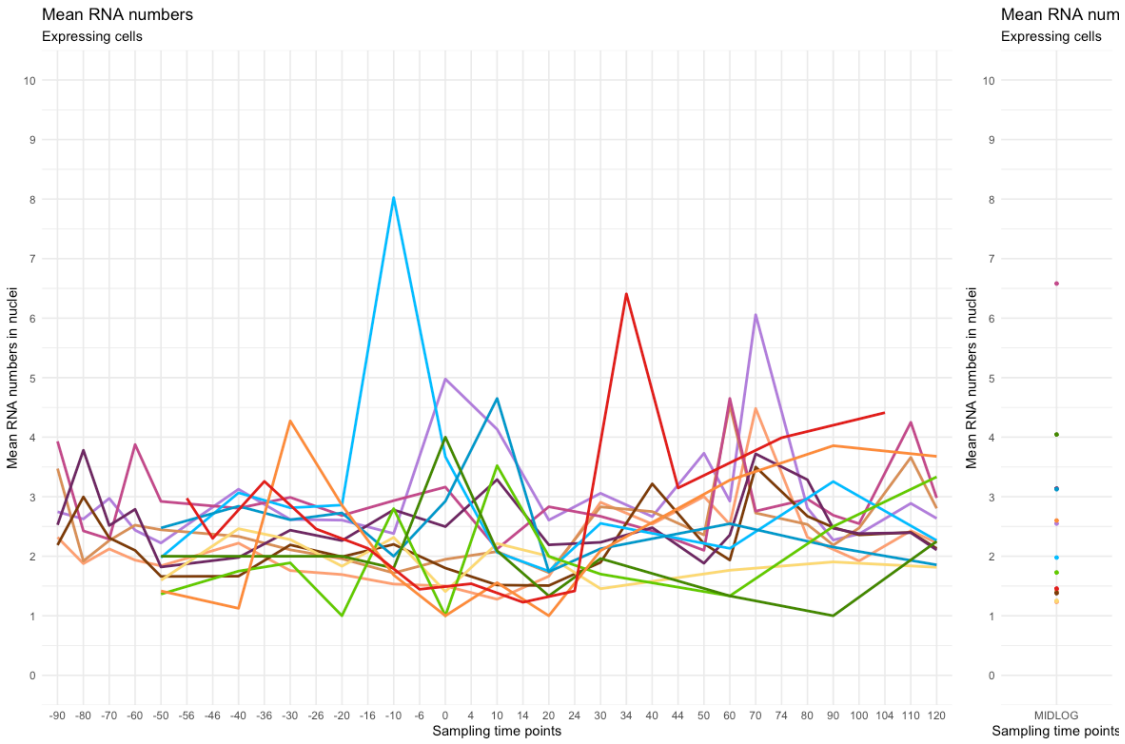

Figure S.6.1

2.

A.

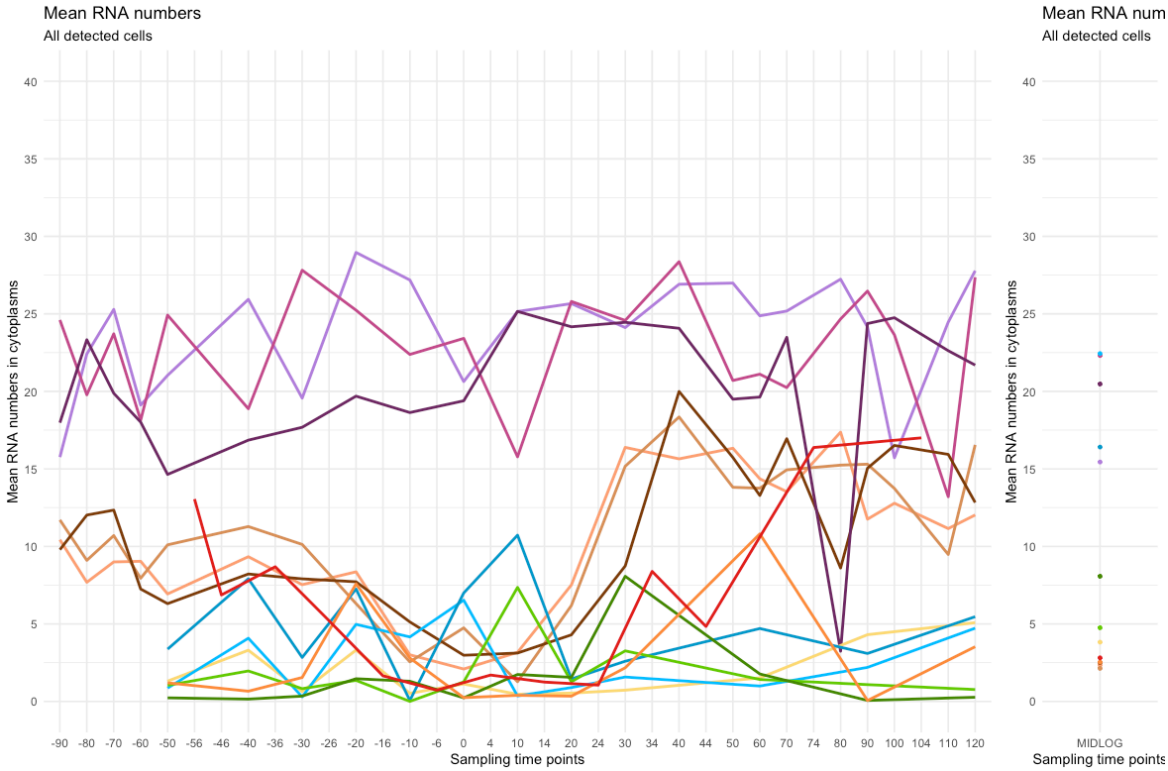

B.

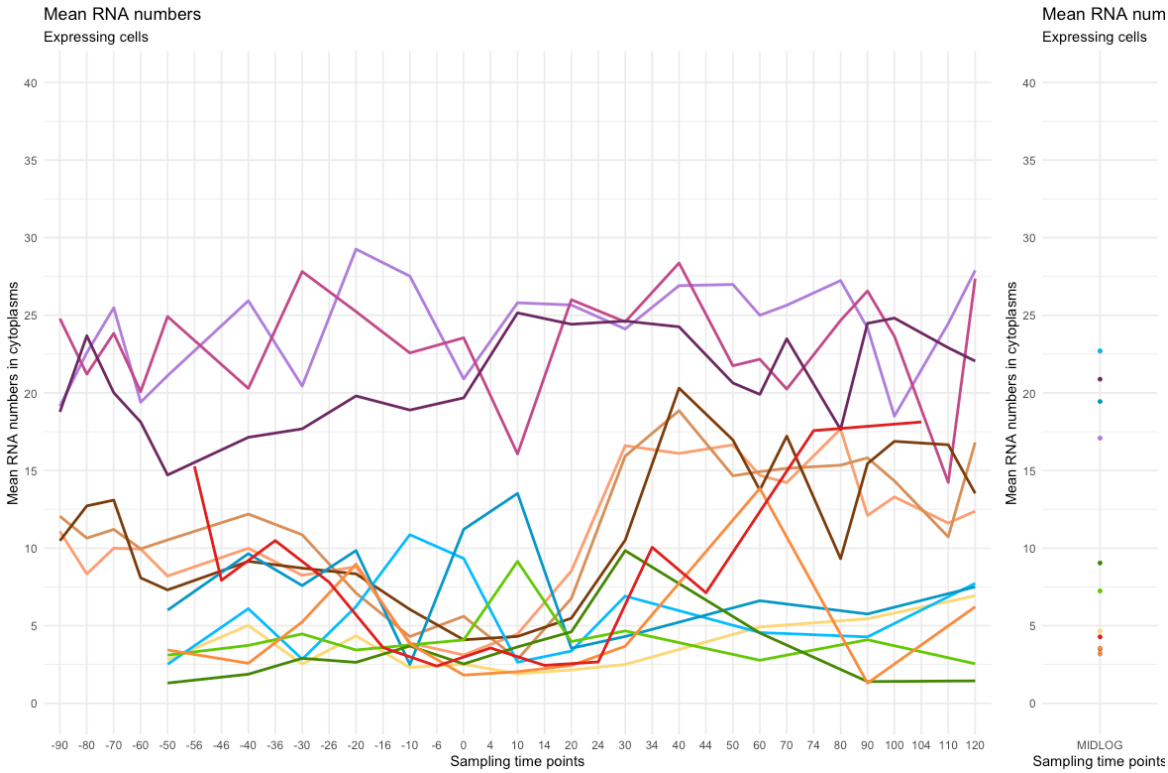

Figure S.6.2

3.

A.

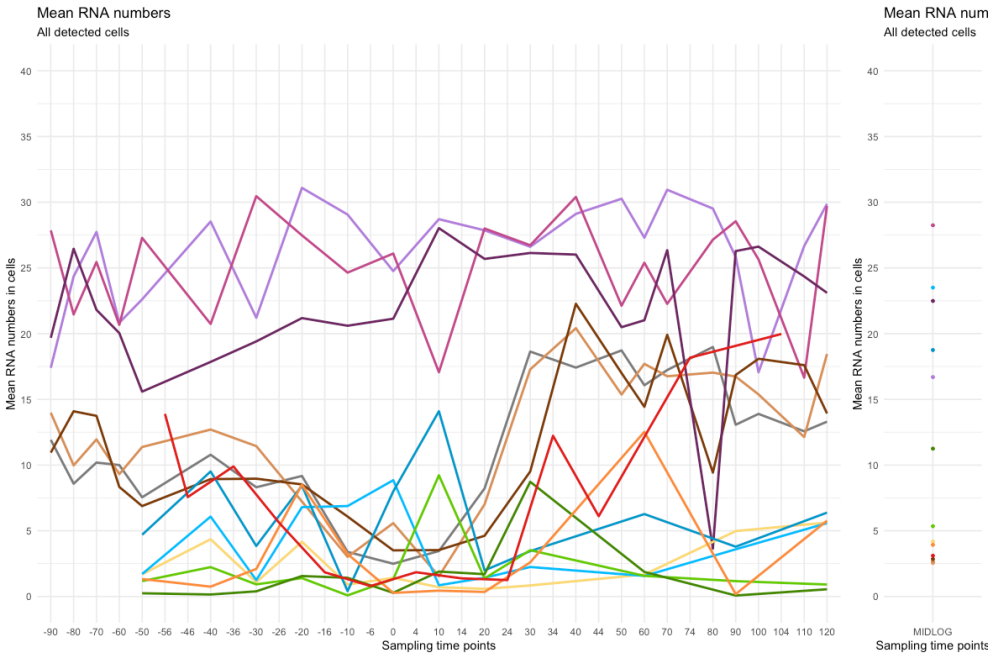

B.

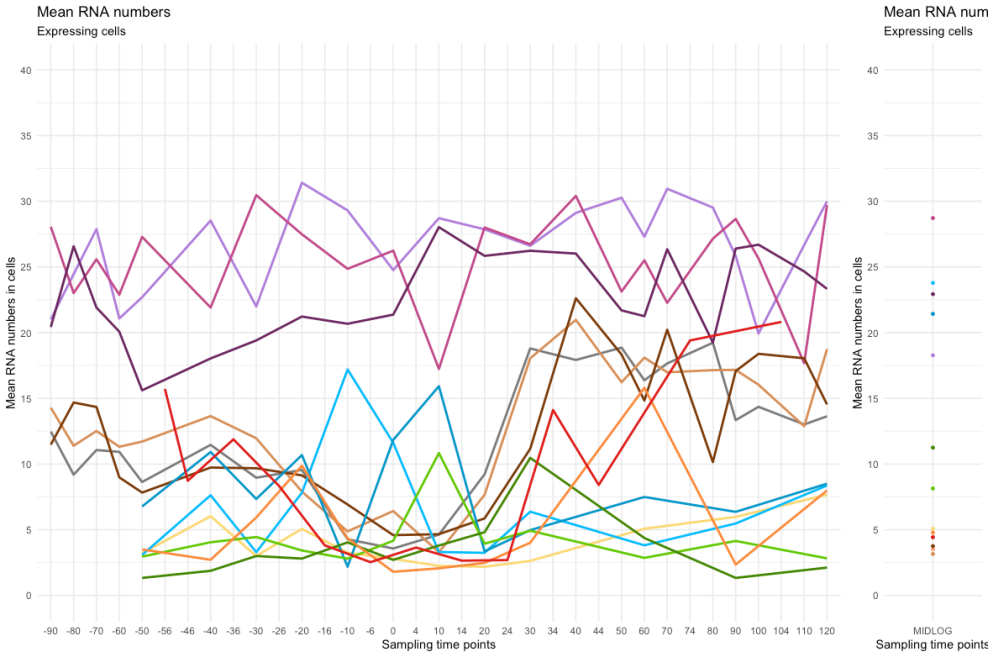

Figure S.6.3

Figure S.6 Overall transcript levels cycle along the YMC.

Mean RNA numbers over the YMC. ***A.*** *In all detected cells.* ***B.*** *In expressing cells only. For nuclear* ***(1)****, cytoplasmic* ***(2)*** *and cell* ***(3)*** *transcripts. Colors indicate the different experimental repeats; ATO3 levels are in yellow, orange, red and brown; SHM2 levels are in light and dark blue; IDH1 levels are in light and dark green and ACT1 levels are in purple. Time is shown in minutes relative to the point of lowest dissolved oxygen levels in media (dO_2 %) found across the YMC, displayed as "0", "MID-LOG": Mid-Logarithmic phase.*

ATO3 vs SHM2

YMC Tp +10 Low/No expression

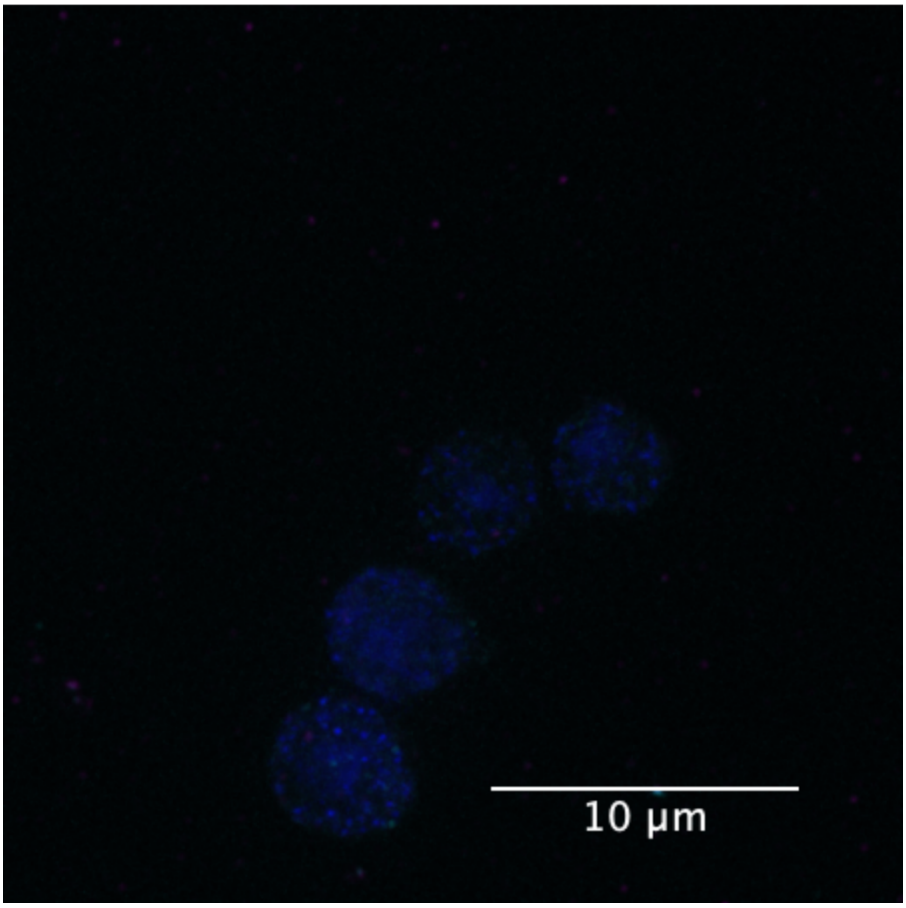

Figure S.7. Example of cells with low to no expression of transcripts

*Yeast cells from YMC timepoint (Tp +10), ATO3 is labelled in Cy5, SHM2 in Cy3 (**field of view from a type ii dual label** RNA-FISH). DNA is stained with DAPI.*

Detailed description of Figure 7.5.A & B from chapter 7

Proportions of cells expressing both transcripts**.**

ATO3/SHM2

Over the YMC, the percentage of cells expressing *ATO3* at high levels and *SHM2* at low levels (cyan) is high (65%) in-cells, in late LOC phase. It decreases in HOC (0%) and re-increase in late HOC and is highest in early LOC (100%), while it decreases again slightly in mid-LOC phase. On the opposite, the fraction of cells expressing *SHM2* at high levels and *ATO3* at low levels (magenta) is low (35%) in late LOC phase, increases in HOC (100%), decreases in late HOC to its lowest in early LOC (0%), while it increases again slightly in mid-LOC phase. Finally, the fraction of cells expressing both ATO3 and SHM2 at high levels, increases in early HOC decreases in mid to late HOC and re-increases in LOC.

SHM2/IDH1

In-nucleus, cells co-expressing show high levels of *SHM2* compare to low levels of *IDH1*. Similarly, the fraction of cells with this transcript status is high along the cycle for cytoplasmic and cell transcripts, though in late HOC only the fraction of cells expressing higher levels of *IDH1* increases up to 50% (magenta). Finally, the fraction of cells expressing both transcripts at high levels is already high in late LOC, increases in mid to late HOC and decreases in LOC.

ATO3/IDH1

Not many cells are found with both nuclear transcripts of the *ATO3* and *IDH1* pair. Next, the percentage of cells showing high levels of *ATO3* and low levels of *IDH1* (magenta) is at its maximum (100%) in late LOC, after what the fraction of cells showing high *IDH1* levels and low *ATO3* levels increases in early HOC to reach 100%

in mid-late HOC, then in early LOC, the transition is abrupt with all cells showing again high levels of *ATO3* and low levels of *IDH1*. Again in-nucleus, more cells express both transcript at low levels rather than at high levels. In-cytoplasm and in-cell, the fraction of cells expressing both transcripts at high levels increases in early HOC and then again in early LOC (50%) to fully decrease to 0% in mid LOC phase.

ATO3/ACT1

Along the YMC, the percentage of cells with high *ATO3* and low *ACT1* levels is low. Nevertheless, it is higher in LOC when considering transcript numbers in nucleus, with around 25 % of the cells showing such status in LOC with up to 50-75% of cells showing high *ATO3* and low *ACT1* levels at the transition point between late HOC and LOC. Looking at numbers in-cytoplasm and in cells, almost all cells show high levels of *ACT1* and low levels of *ATO3* (magenta), while 25 to 50% of the cells show the opposite in LOC phase only. Finally, the fraction of cells expressing both ATO3 and ACT1 at low levels, is high all along the YMC (100%) and decrease by around 30% only in early LOC phase, indicating a peak of transcription of both transcripts at that time. Cytoplasmic and cell RNA numbers are high for both transcript along the YMC.

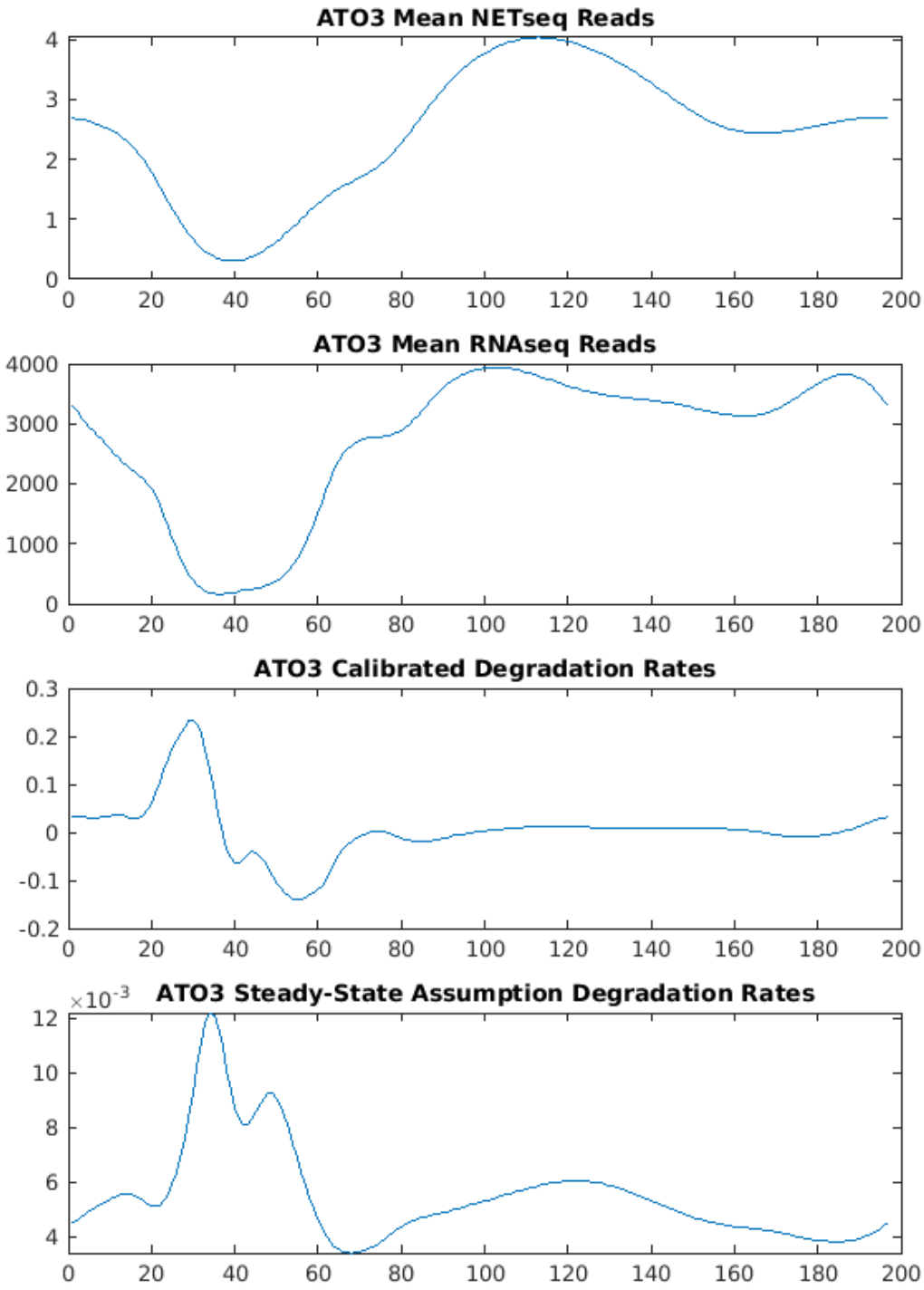
ATO3 Mean NETseq Reads
ATO3 Mean RNAseq Reads
ATO3 Calibrated Degradation Rates
ATO3 Steady-State Assumption Degradation Rates
×10^-3

Figure S8.1

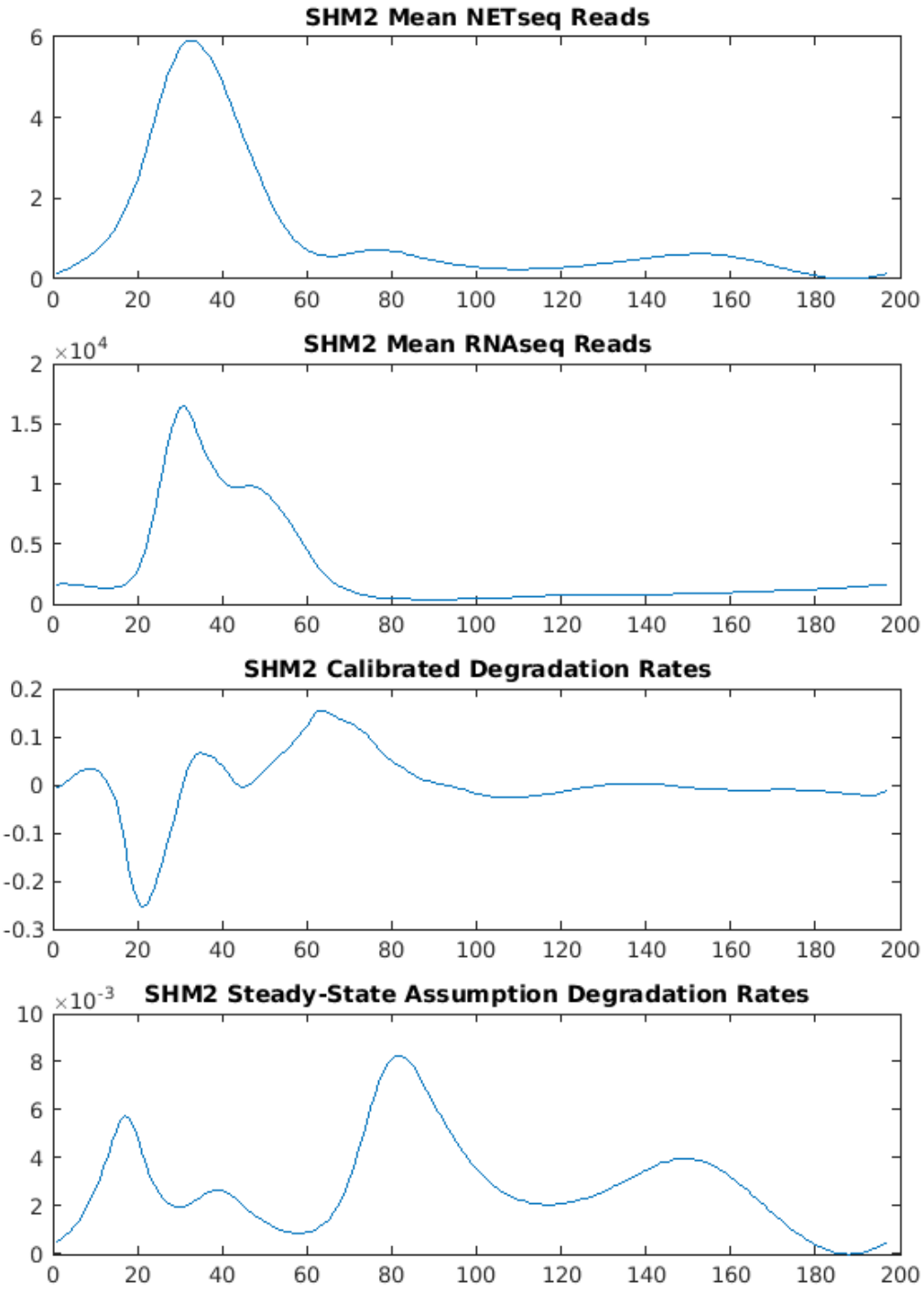
SHM2 Mean NETseq Reads
SHM2 Mean RNAseq Reads
×10^4
SHM2 Calibrated Degradation Rates
SHM2 Steady-State Assumption Degradation Rates
×10^-3

Figure S8.2

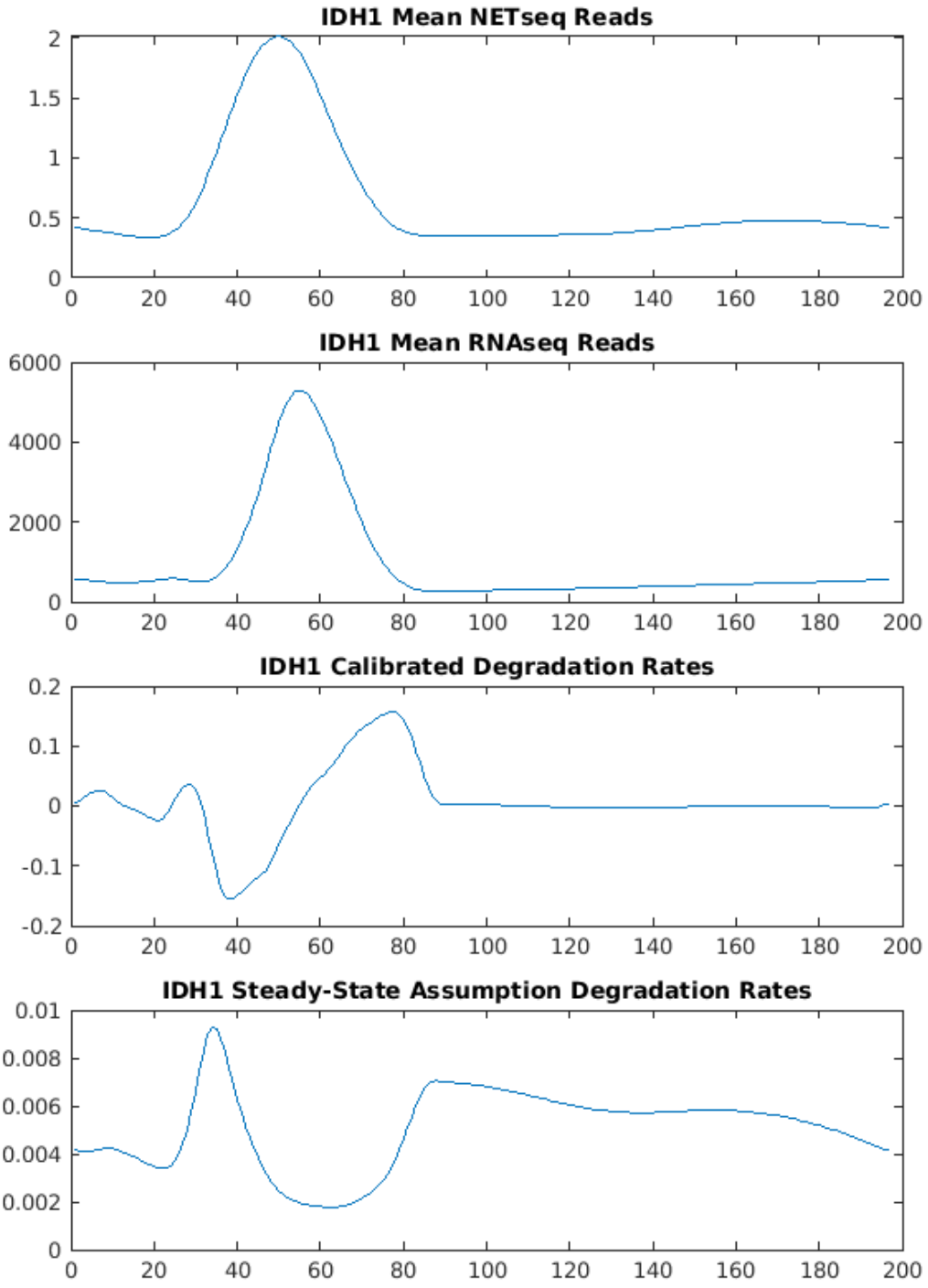
IDH1 Mean NETseq Reads
IDH1 Mean RNAseq Reads
IDH1 Calibrated Degradation Rates
IDH1 Steady-State Assumption Degradation Rates

Figure S8.3

Figure S8 The degradation rates of oscillating transcripts vary over the YMC

A. *Spline-smoothing fit NET-seq average read number over the YMC in Arbitrary Units (A.U).*

B. *Spline-smoothing fit of the RNA-seq average read number over the YMC (A.U). The average read number is the average number of sense reads per bp within a 300 bp window placed immediately downstream of the Transcription Start Site. Data from Dr. Shidong Xi (Xi. DPhil thesis. 2019).*

C. *Degradation rates per minute. Degradation rates were calculated by assuming that the rate of change of RNA is proportional to the production rate (itself assumed proportional to the mean NETseq level at a given time) minus the product of the RNA level and the degradation rate. Due to the unknown proportionalities between NETseq and production, and RNAseq and RNA numbers, the degradation rates were calibrated such that the mean half-life of RNA is as measured in Geisberg et al. 2014 (32min).*

D. *Approximation of the degradation rates per min. As the calculation in the third panel produced apparent negative degradation rates, another (adiabatic) approximation was used - the degradation rate is proportional to the ratio of production to level. This was similarly calibrated to the mean RNA half-life as for the third panel.*

The calculation of the degradation rates, as well as these figures were produced by Dr. Andrew Angel.

References

Aguilaniu, H., Gustafsson, L., Rigoulet, M., & Nyström, T. (2003). Asymmetric inheritance of oxidatively damaged proteins during cytokinesis. *Science (New York, N.Y.)*, *299*(5613), 1751–1753. https://doi.org/10.1126/science.1080418

Alfatah, M., Wong, J. H., Krishnan, V. G., Lee, Y. C., Sin, Q. F., Goh, C. J. H., Kong, K. W., Lee, W. T., Lewis, J., Hoon, S., & Arumugam, P. (2021). TORC1 regulates the transcriptional response to glucose and developmental cycle via the Tap42-Sit4-Rrd1/2 pathway in Saccharomyces cerevisiae. *BMC biology*, *19*(1), 95. https://doi.org/10.1186/s12915-021-01030-3

Allen, C., Büttner, S., Aragon, A. D., Thomas, J. A., Meirelles, O., Jaetao, J. E., Benn, D., Ruby, S. W., Veenhuis, M., Madeo, F., & Werner-Washburne, M. (2006). Isolation of quiescent and nonquiescent cells from yeast stationary-phase cultures. *The Journal of cell biology*, *174*(1), 89–100. https://doi.org/10.1083/jcb.200604072

Alvers, A. L., Wood, M. S., Hu, D., Kaywell, A. C., Dunn, W. A., Jr, & Aris, J. P. (2009). Autophagy is required for extension of yeast chronological life span by rapamycin. *Autophagy*, *5*(6), 847–849. https://doi.org/10.4161/auto.8824

Amponsah, P. S., Yahya, G., Zimmermann, J., Mai, M., Mergel, S., Mühlhaus, T., Storchova, Z., & Morgan, B. (2021). Peroxiredoxins couple metabolism and cell division in an ultradian cycle. *Nature chemical biology*, *17*(4), 477–484. https://doi.org/10.1038/s41589-020-00728-9

Antoniou-Kourounioti, R. L., Meschichi, A., Reeck, S., Berry, S., Menon, G., Zhao, Y., Fozard, J. A., Holmes, T. L., Wang, H., Hartley, M., Dean, C., Rosa, S., & Howard, M. (2022). Integrating analog and digital modes of gene expression at Arabidopsis FLC *BioRxiv*, 2022.07.04.498694. https://doi.org/10.1101/2022.07.04.498694

Aon, M. A., Cortassa, S., Lemar, K. M., Hayes, A. J., & Lloyd, D. (2007). Single and cell population respiratory oscillations in yeast: a 2-photon scanning laser microscopy study. *FEBS letters*, *581*(1), 8–14. https://doi.org/10.1016/j.febslet.2006.11.068

Aragon, A. D., Rodriguez, A. L., Meirelles, O., Roy, S., Davidson, G. S., Tapia, P. H., Allen, C., Joe, R., Benn, D., & Werner-Washburne, M. (2008). Characterization of differentiated quiescent and nonquiescent cells in yeast stationary-phase cultures. *Molecular biology of the cell*, *19*(3), 1271–1280. https://doi.org/10.1091/mbc.e07-07-0666

Ball, D. A., Ahn, T. H., Wang, P., Chen, K. C., Cao, Y., Tyson, J. J., Peccoud, J., & Baumann, W. T. (2011). Stochastic exit from mitosis in budding yeast: model predictions and experimental observations. *Cell cycle (Georgetown, Tex.)*, *10*(6), 999–1009. https://doi.org/10.4161/cc.10.6.14966

Barber, F., Amir, A., & Murray, A. W. (2020). Cell-size regulation in budding yeast does not depend on linear accumulation of Whi5. *Proceedings of the National Academy of Sciences of the United States of America*, *117*(25), 14243–14250. https://doi.org/10.1073/pnas.2001255117

Barbet, N. C., Schneider, U., Helliwell, S. B., Stansfield, I., Tuite, M. F., & Hall, M. N. (1996). TOR controls translation initiation and early G1 progression in yeast. *Molecular biology of the cell*, *7*(1), 25–42. https://doi.org/10.1091/mbc.7.1.25

Bartholomai, B. M., Gladfelter, A. S., Loros, J. J., & Dunlap, J. C. (2022). PRD-2 mediates clock-regulated perinuclear localization of clock gene RNAs within the circadian cycle of *Neurospora*. *Proceedings of the National Academy of Sciences of the United States of America*, *119*(31), e2203078119. https://doi.org/10.1073/pnas.2203078119

Baumgartner, B. L., O'Laughlin, R., Jin, M., Tsimring, L. S., Hao, N., & Hasty, J. (2018). Flavin-based metabolic cycles are integral features of growth and division in single yeast cells. *Scientific reports*, *8*(1), 18045. https://doi.org/10.1038/s41598-018-35936-w

Beck, C., & von Meyenburg, H. K. (1968). Enzyme pattern and aerobic growth of Saccharomyces cerevisiae under various degrees of glucose limitation. *Journal of bacteriology*, *96*(2), 479–486. https://doi.org/10.1128/jb.96.2.479-486.1968

Bellgardt, K.-H. (1994). Analysis of synchronous growth of baker's yeast. Part II: Comparison of model prediction and experimental data. *Journal of Biotechnology*, *35*(1), 35–49. https://doi.org/https://doi.org/10.1016/0168-1656(94)90188-0

Blake, W. J., Balázsi, G., Kohanski, M. A., Isaacs, F. J., Murphy, K. F., Kuang, Y., Cantor, C. R., Walt, D. R., & Collins, J. J. (2006). Phenotypic consequences of promoter-mediated transcriptional noise. *Molecular cell*, *24*(6), 853–865. https://doi.org/10.1016/j.molcel.2006.11.003

Blake, W. J., KAErn, M., Cantor, C. R., & Collins, J. J. (2003). Noise in eukaryotic gene expressi Keren L, van Dijk D, Weingarten-Gabbay S, Davidi D, Jona G, Weinberger A, Milo R, Segal E. Noise in gene expression is coupled to growth rate. Genome Res. 2015 Dec;25(12):1893-902. doi: 10.1101/gr.191635.115. Epub 2015 Sep 9. PMID: 26355006; PMCID: PMC4665010.on. *Nature*, *422*(6932), 633–637. https://doi.org/10.1038/nature01546

Boczko, E. M., Gedeon, T., Stowers, C. C., & Young, T. R. (2010). ODE, RDE and SDE models of cell cycle dynamics and clustering in yeast. *Journal of biological dynamics*, *4*(4), 328–345. https://doi.org/10.1080/17513750903288003

Boldogh, I. R., Fehrenbacher, K. L., Yang, H. C., & Pon, L. A. (2005). Mitochondrial movement and inheritance in budding yeast. *Gene*, *354*, 28–36. https://doi.org/10.1016/j.gene.2005.03.049

Borzani, W.; Gregori, R. E. and Vairo, M. L. R. (1977), Some observations on oscillatory changes in the growth rate of Saccharomyces cerevisiae in aerobic continuous undisturbed culture. Biotechnol. Bioeng., 19, 1363-1374.

Boucherie H. (1985). Protein synthesis during transition and stationary phases under glucose limitation in Saccharomyces cerevisiae. *Journal of bacteriology*, *161*(1), 385–392. https://doi.org/10.1128/jb.161.1.385-392.1985

Boy-Marcotte, E., Ikonomi, P., & Jacquet, M. (1996). SDC25, a dispensable Ras guanine nucleotide exchange factor of Saccharomyces cerevisiae differs from CDC25 by its regulation. *Molecular biology of the cell*, *7*(4), 529–539. https://doi.org/10.1091/mbc.7.4.529

Brauer, M. J., Huttenhower, C., Airoldi, E. M., Rosenstein, R., Matese, J. C., Gresham, D., Boer, V. M., Troyanskaya, O. G., & Botstein, D. (2008). Coordination of growth rate, cell cycle, stress response, and metabolic activity in yeast. *Molecular biology of the cell*, *19*(1), 352–367. https://doi.org/10.1091/mbc.e07-08-0779

Brauer, M. J., Saldanha, A. J., Dolinski, K., & Botstein, D. (2005). Homeostatic adjustment and metabolic remodeling in glucose-limited yeast cultures. *Molecular biology of the cell*, *16*(5), 2503–2517. https://doi.org/10.1091/mbc.e04-11-0968

Breeden, L. L., & Tsukiyama, T. (2022). Quiescence in *Saccharomyces cerevisiae*. *Annual review of genetics*, *56*, 253–278. https://doi.org/10.1146/annurev-genet-080320-023632

Brouwer, I., & Lenstra, T. L. (2019). Visualizing transcription: key to understanding gene expression dynamics. *Current opinion in chemical biology*, *51*, 122–129. https://doi.org/10.1016/j.cbpa.2019.05.031

Brown, T., Howe, F. S., Murray, S. C., Wouters, M., Lorenz, P., Seward, E., Rata, S., Angel, A., & Mellor, J. (2018). Antisense transcription-dependent chromatin signature modulates sense transcript dynamics. *Molecular systems biology*, *14*(2), e8007. https://doi.org/10.15252/msb.20178007

Budovskaya, Y. V., Stephan, J. S., Reggiori, F., Klionsky, D. J., & Herman, P. K. (2004). The Ras/cAMP-dependent protein kinase signaling pathway regulates an early step of the autophagy process in Saccharomyces cerevisiae. *The Journal of biological chemistry*, *279*(20), 20663–20671. https://doi.org/10.1074/jbc.M400272200

Burnetti, A. J., Aydin, M., & Buchler, N. E. (2016). Cell cycle Start is coupled to entry into the yeast metabolic cycle across diverse strains and growth rates. *Molecular biology of the cell*, *27*(1), 64–74. https://doi.org/10.1091/mbc.E15-07-0454

Cai, L., & Tu, B. P. (2011). Acetyl-CoA drives the transcriptional growth program in yeast. *Cell cycle (Georgetown, Tex.)*, *10*(18), 3045–3046. https://doi.org/10.4161/cc.10.18.17000

Cai, L., & Tu, B. P. (2012). Driving the cell cycle through metabolism. *Annual review of cell and developmental biology*, *28*, 59–87. https://doi.org/10.1146/annurev-cellbio-092910-154010

Cai, Y., & Futcher, B. (2013). Effects of the yeast RNA-binding protein Whi3 on the half-life and abundance of CLN3 mRNA and other targets. *PloS one*, *8*(12), e84630. https://doi.org/10.1371/journal.pone.0084630

Carpenter, A. E., Jones, T. R., Lamprecht, M. R., Clarke, C., Kang, I. H., Friman, O., Guertin, D. A., Chang, J. H., Lindquist, R. A., Moffat, J., Golland, P., & Sabatini, D. M. (2006). CellProfiler: image analysis software for identifying and quantifying cell phenotypes. *Genome biology*, *7*(10), R100. https://doi.org/10.1186/gb-2006-7-10-r100

Castrillo, J. I., Zeef, L. A., Hoyle, D. C., Zhang, N., Hayes, A., Gardner, D. C., Cornell, M. J., Petty, J., Hakes, L., Wardleworth, L., Rash, B., Brown, M., Dunn, W. B., Broadhurst, D., O'Donoghue, K., Hester, S. S., Dunkley, T. P., Hart, S. R., Swainston, N., Li, P., … Oliver, S. G. (2007). Growth control of the eukaryote cell: a systems biology study in yeast. *Journal of biology*, *6*(2), 4. https://doi.org/10.1186/jbiol54

Causton, H. C., Feeney, K. A., Ziegler, C. A., & O'Neill, J. S. (2015). Metabolic Cycles in Yeast Share Features Conserved among Circadian Rhythms. *Current biology : CB*, *25*(8), 1056–1062. https://doi.org/10.1016/j.cub.2015.02.035

Causton, H. C., Ren, B., Koh, S. S., Harbison, C. T., Kanin, E., Jennings, E. G., Lee, T. I., True, H. L., Lander, E. S., & Young, R. A. (2001). Remodeling of yeast genome expression in response to environmental changes. *Molecular biology of the cell*, *12*(2), 323–337. https://doi.org/10.1091/mbc.12.2.323

Chan, P., Rich, J. N., & Kay, S. A. (2023). Watching the Clock in Glioblastoma. *Neuro-oncology*, noad107. Advance online publication. https://doi.org/10.1093/neuonc/noad107

Chen, C. I., McDonald, K. A., & Bisson, L. (1990). Oscillatory behavior of Saccharomyces cerevisiae in continuous culture: I. Effects of pH and nitrogen levels. *Biotechnology and bioengineering*, *36*(1), 19–27. https://doi.org/10.1002/bit.260360104

Chen, Y., Zhao, G., Zahumensky, J., Honey, S., & Futcher, B. (2020). Differential Scaling of Gene Expression with Cell Size May Explain Size Control in Budding Yeast. *Molecular cell*, *78*(2), 359–370.e6. https://doi.org/10.1016/j.molcel.2020.03.012

Chen, Z., Odstrcil, E. A., Tu, B. P., & McKnight, S. L. (2007). Restriction of DNA replication to the reductive phase of the metabolic cycle protects genome integrity. *Science (New York, N.Y.)*, *316*(5833), 1916–1919. https://doi.org/10.1126/science.1140958

Cho, R. J., Campbell, M. J., Winzeler, E. A., Steinmetz, L., Conway, A., Wodicka, L., Wolfsberg, T. G., Gabrielian, A. E., Landsman, D., Lockhart, D. J., & Davis, R. W.

(1998). A genome-wide transcriptional analysis of the mitotic cell cycle. *Molecular cell*, *2*(1), 65–73. https://doi.org/10.1016/s1097-2765(00)80114-8

Choder M. (1991). A general topoisomerase I-dependent transcriptional repression in the stationary phase in yeast. *Genes & development*, *5*(12A), 2315–2326. https://doi.org/10.1101/gad.5.12a.2315

Choubey, S., Kondev, J., & Sanchez, A. (2015). Deciphering Transcriptional Dynamics In Vivo by Counting Nascent RNA Molecules. *PLoS computational biology*, *11*(11), e1004345. https://doi.org/10.1371/journal.pcbi.1004345

Choubey, S., Kondev, J., & Sanchez, A. (2018). Distribution of Initiation Times Reveals Mechanisms of Transcriptional Regulation in Single Cells. *Biophysical journal*, *114*(9), 2072–2082. https://doi.org/10.1016/j.bpj.2018.03.031

Churchman, L. S., & Weissman, J. S. (2011). Nascent transcript sequencing visualizes transcription at nucleotide resolution. *Nature*, *469*(7330), 368–373. https://doi.org/10.1038/nature09652

Cohen, S. E., & Golden, S. S. (2015). Circadian Rhythms in Cyanobacteria. *Microbiology and molecular biology reviews : MMBR*, *79*(4), 373–385. https://doi.org/10.1128/MMBR.00036-15

Costanzo, M., Nishikawa, J. L., Tang, X., Millman, J. S., Schub, O., Breitkreuz, K., Dewar, D., Rupes, I., Andrews, B., & Tyers, M. (2004). CDK activity antagonizes Whi5, an inhibitor of G1/S transcription in yeast. *Cell*, *117*(7), 899–913. https://doi.org/10.1016/j.cell.2004.05.024

Courel, M., Bénard, M., Ernoult-Lange, M., Chouaib, R., Hubstenberger, A., Kress, M., & Weil, D. (2018). Les P-bodies - Des gouttelettes microscopiques pour stocker les messagers de protéines régulatrices [P-bodies: microscopic droplets to store mRNAs encoding regulatory proteins]. *Medecine sciences : M/S*, *34*(4), 306–308. https://doi.org/10.1051/medsci/20183404009

Craggs T. D. (2009). Green fluorescent protein: structure, folding and chromophore maturation. *Chemical Society reviews*, *38*(10), 2865–2875. https://doi.org/10.1039/b903641p

Cucinotta, C. E., Dell, R. H., Braceros, K. C., & Tsukiyama, T. (2021). RSC primes the quiescent genome for hypertranscription upon cell-cycle re-entry. *eLife*, *10*, e67033. https://doi.org/10.7554/eLife.67033

Cupp, J. R., & McAlister-Henn, L. (1992). Cloning and characterization of the gene encoding the IDH1 subunit of NAD(+)-dependent isocitrate dehydrogenase from Saccharomyces cerevisiae. *The Journal of biological chemistry*, *267*(23), 16417–16423.

Cvrcková, F., & Nasmyth, K. (1993). Yeast G1 cyclins CLN1 and CLN2 and a GAP-like protein have a role in bud formation. *The EMBO journal*, *12*(13), 5277–5286. https://doi.org/10.1002/j.1460-2075.1993.tb06223.x

Dammann, R., Lucchini, R., Koller, T., & Sogo, J. M. (1993). Chromatin structures and transcription of rDNA in yeast Saccharomyces cerevisiae. *Nucleic acids research*, *21*(10), 2331–2338. https://doi.org/10.1093/nar/21.10.2331

Davidson, G. S., Joe, R. M., Roy, S., Meirelles, O., Allen, C. P., Wilson, M. R., Tapia, P. H., Manzanilla, E. E., Dodson, A. E., Chakraborty, S., Carter, M., Young, S., Edwards, B., Sklar, L., & Werner-Washburne, M. (2011). The proteomics of quiescent and nonquiescent cell differentiation in yeast stationary-phase cultures. *Molecular biology of the cell*, *22*(7), 988–998. https://doi.org/10.1091/mbc.E10-06-0499

de Beer, M. A., & Giepmans, B. N. G. (2020). Nanobody-Based Probes for Subcellular Protein Identification and Visualization. *Frontiers in cellular neuroscience*, *14*, 573278. https://doi.org/10.3389/fncel.2020.573278

de Bruin, L. M., de Kreuk, M. K., van der Roest, H. F., Uijterlinde, C., & van Loosdrecht, M. C. (2004). Aerobic granular sludge technology: an alternative to activated sludge?. *Water science and technology : a journal of the International Association on Water Pollution Research*, *49*(11-12), 1–7.

De Virgilio C. (2012). The essence of yeast quiescence. *FEMS microbiology reviews*, *36*(2), 306–339. https://doi.org/10.1111/j.1574-6976.2011.00287.x

De Virgilio, C., & Loewith, R. (2006). The TOR signalling network from yeast to man. *The international journal of biochemistry & cell biology*, *38*(9), 1476–1481. https://doi.org/10.1016/j.biocel.2006.02.013

Delarue, M., Brittingham, G. P., Pfeffer, S., Surovtsev, I. V., Pinglay, S., Kennedy, K. J., Schaffer, M., Gutierrez, J. I., Sang, D., Poterewicz, G., Chung, J. K., Plitzko, J. M., Groves, J. T., Jacobs-Wagner, C., Engel, B. D., & Holt, L. J. (2018). mTORC1 Controls Phase Separation and the Biophysical Properties of the Cytoplasm by Tuning Crowding. *Cell*, *174*(2), 338–349.e20. https://doi.org/10.1016/j.cell.2018.05.042

Denis, V., & Daignan-Fornier, B. (1998). Synthesis of glutamine, glycine and 10-formyl tetrahydrofolate is coregulated with purine biosynthesis in Saccharomyces cerevisiae. *Molecular & general genetics : MGG*, *259*(3), 246–255. https://doi.org/10.1007/s004380050810

Deprez, M. A., Eskes, E., Winderickx, J., & Wilms, T. (2018). The TORC1-Sch9 pathway as a crucial mediator of chronological lifespan in the yeast Saccharomyces cerevisiae. *FEMS yeast research*, *18*(5), 10.1093/femsyr/foy048. https://doi.org/10.1093/femsyr/foy048

DeRisi, J. L., Iyer, V. R., & Brown, P. O. (1997). Exploring the metabolic and genetic control of gene expression on a genomic scale. *Science (New York, N.Y.)*, *278*(5338), 680–686. https://doi.org/10.1126/science.278.5338.680

Dhawan J, Laxman S. Decoding the stem cell quiescence cycle--lessons from yeast for regenerative biology. J Cell Sci. 2015 Dec 15;128(24):4467-74. doi: 10.1242/jcs.177758. PMID: 26672015; PMCID: PMC5695657.

Dickinson, J. R., & Schweizer, L. M. (1999). *The metabolism & molecular physiology of Saccharomyces cerevisiae*. Taylor & Francis.

Dodd, B. J. T., & Kralj, J. M. (2017). Live Cell Imaging Reveals pH Oscillations in Saccharomyces cerevisiae During Metabolic Transitions. *Scientific reports*, *7*(1), 13922. https://doi.org/10.1038/s41598-017-14382-0

Dorsey, S., Tollis, S., Cheng, J., Black, L., Notley, S., Tyers, M., & Royer, C. A. (2018). G1/S Transcription Factor Copy Number Is a Growth-Dependent Determinant of Cell Cycle Commitment in Yeast. *Cell systems*, *6*(5), 539–554.e11. https://doi.org/10.1016/j.cels.2018.04.012

Dunlap J. C. (1999). Molecular bases for circadian clocks. *Cell*, *96*(2), 271–290. https://doi.org/10.1016/s0092-8674(00)80566-8

Elliott, S. G., & McLaughlin, C. S. (1978). Rate of macromolecular synthesis through the cell cycle of the yeast Saccharomyces cerevisiae. *Proceedings of the National Academy of Sciences of the United States of America*, *75*(9), 4384–4388. https://doi.org/10.1073/pnas.75.9.4384

Elowitz, M. B., Levine, A. J., Siggia, E. D., & Swain, P. S. (2002). Stochastic gene expression in a single cell. *Science (New York, N.Y.)*, *297*(5584), 1183–1186. https://doi.org/10.1126/science.1070919

Espinet, C., de la Torre, M. A., Aldea, M., & Herrero, E. (1995). An efficient method to isolate yeast genes causing overexpression-mediated growth arrest. *Yeast (Chichester, England)*, *11*(1), 25–32. https://doi.org/10.1002/yea.320110104

Evangelista, M., Pruyne, D., Amberg, D. C., Boone, C., & Bretscher, A. (2002). Formins direct Arp2/3-independent actin filament assembly to polarize cell growth in yeast. *Nature cell biology*, *4*(1), 32–41. https://doi.org/10.1038/ncb718

Fabrizio, P., Battistella, L., Vardavas, R., Gattazzo, C., Liou, L. L., Diaspro, A., Dossen, J. W., Gralla, E. B., & Longo, V. D. (2004). Superoxide is a mediator of an altruistic aging program in Saccharomyces cerevisiae. *The Journal of cell biology*, *166*(7), 1055–1067. https://doi.org/10.1083/jcb.200404002

Feltham, J. (2018). *Gene Expression & Regulation in the Yeast Metabolic Cycle*. [PhD thesis]. University of Oxford.

Feltham, J. E., Xi, S., Murray, S. C., Wouters, M., Urdiain-Arraiza, J., Heilig, R., George, C., Townley, A. F., Roberts, E., Kessler, B. M., Liberatori, S., Charles, P. D., Angel, A., Fischer, R., & Mellor, J. (2020). Transcriptional changes are regulated by metabolic pathway dynamics but decoupled from protein levels. *BioRxiv*, 833921. https://doi.org/10.1101/833921

Femino, A. M., Fay, F. S., Fogarty, K., & Singer, R. H. (1998). Visualization of single RNA transcripts in situ. *Science (New York, N.Y.)*, *280*(5363), 585–590. https://doi.org/10.1126/science.280.5363.585

Foat, B. C., Houshmandi, S. S., Olivas, W. M., & Bussemaker, H. J. (2005). Profiling condition-specific, genome-wide regulation of mRNA stability in yeast. *Proceedings of the National Academy of Sciences of the United States of America*, *102*(49), 17675–17680. https://doi.org/10.1073/pnas.0503803102

Fridy, P. C., Li, Y., Keegan, S., Thompson, M. K., Nudelman, I., Scheid, J. F., Oeffinger, M., Nussenzweig, M. C., Fenyö, D., Chait, B. T., & Rout, M. P. (2014). A robust pipeline for rapid production of versatile nanobody repertoires. *Nature methods*, *11*(12), 1253–1260. https://doi.org/10.1038/nmeth.3170

Friedman, J. R., & Nunnari, J. (2014). Mitochondrial form and function. *Nature*, *505*(7483), 335–343. https://doi.org/10.1038/nature12985Friis, R. M., Wu, B. P., Reinke, S. N., Hockman, D. J., Sykes, B. D., & Schultz, M. C. (2009). A glycolytic burst drives glucose induction of global histone acetylation by picNuA4 and SAGA. *Nucleic acids research*, *37*(12), 3969–3980. https://doi.org/10.1093/nar/gkp270

Fuge, E. K., Braun, E. L., & Werner-Washburne, M. (1994). Protein synthesis in long-term stationary-phase cultures of Saccharomyces cerevisiae. *Journal of bacteriology*, *176*(18), 5802–5813. https://doi.org/10.1128/jb.176.18.5802-5813.1994

Furuta, S., Hidaka, E., Ogata, A., Yokota, S., & Kamata, T. (2004). Ras is involved in the negative control of autophagy through the class I PI3-kinase. *Oncogene*, *23*(22), 3898–3904. https://doi.org/10.1038/sj.onc.1207539

Futcher B. (1996). Cyclins and the wiring of the yeast cell cycle. *Yeast (Chichester, England)*, *12*(16), 1635–1646. https://doi.org/10.1002/(SICI)1097-0061(199612)12:16%3C1635::AID-YEA83%3E3.0.CO;2-O

Futcher B. (2006). Metabolic cycle, cell cycle, and the finishing kick to Start. *Genome biology*, *7*(4), 107. https://doi.org/10.1186/gb-2006-7-4-107

Gallwitz, D., & Seidel, R. (1980). Molecular cloning of the actin gene from yeast Saccharomyces cerevisiae. *Nucleic acids research*, *8*(5), 1043–1059. https://doi.org/10.1093/nar/8.5.1043

García-Martínez, J., Aranda, A., & Pérez-Ortín, J. E. (2004). Genomic run-on evaluates transcription rates for all yeast genes and identifies gene regulatory mechanisms. *Molecular cell*, *15*(2), 303–313. https://doi.org/10.1016/j.molcel.2004.06.004

Gasch, A. P., & Werner-Washburne, M. (2002). The genomics of yeast responses to environmental stress and starvation. *Functional & integrative genomics*, *2*(4-5), 181–192. https://doi.org/10.1007/s10142-002-0058-2

Gasch, A. P., Spellman, P. T., Kao, C. M., Carmel-Harel, O., Eisen, M. B., Storz, G., Botstein, D., & Brown, P. O. (2000). Genomic expression programs in the response of yeast cells to environmental changes. *Molecular biology of the cell*, *11*(12), 4241–4257. https://doi.org/10.1091/mbc.11.12.4241

Gaspar, I., Wippich, F., & Ephrussi, A. (2017). Enzymatic production of single-molecule FISH and RNA capture probes. *RNA (New York, N.Y.)*, *23*(10), 1582–1591. https://doi.org/10.1261/rna.061184.117

Geisberg, J. V., Moqtaderi, Z., Fan, X., Ozsolak, F., & Struhl, K. (2014). Global analysis of mRNA isoform half-lives reveals stabilizing and destabilizing elements in yeast. *Cell*, *156*(4), 812–824. https://doi.org/10.1016/j.cell.2013.12.026

Genga, A., Bianchi, L., & Foury, F. (1986). A nuclear mutant of Saccharomyces cerevisiae deficient in mitochondrial DNA replication and polymerase activity. *The Journal of biological chemistry*, *261*(20), 9328–9332.

Gerber, A. P., Herschlag, D., & Brown, P. O. (2004). Extensive association of functionally and cytotopically related mRNAs with Puf family RNA-binding proteins in yeast. *PLoS biology*, *2*(3), E79. https://doi.org/10.1371/journal.pbio.0020079

Giepmans, B. N., Adams, S. R., Ellisman, M. H., & Tsien, R. Y. (2006). The fluorescent toolbox for assessing protein location and function. *Science (New York, N.Y.)*, *312*(5771), 217–224. https://doi.org/10.1126/science.1124618

Golden, S. S., Ishiura, M., Johnson, C. H., & Kondo, T. (1997). CYANOBACTERIAL CIRCADIAN RHYTHMS. *Annual review of plant physiology and plant molecular biology*, *48*, 327–354. https://doi.org/10.1146/annurev.arplant.48.1.327

Golding, I., Paulsson, J., Zawilski, S. M., & Cox, E. C. (2005). Real-time kinetics of gene activity in individual bacteria. *Cell*, *123*(6), 1025–1036. https://doi.org/10.1016/j.cell.2005.09.031

González A, Hall MN. Nutrient sensing and TOR signaling in yeast and mammals. EMBO J. 2017 Feb 15;36(4):397-408. doi: 10.15252/embj.201696010. Epub 2017 Jan 17. PMID: 28096180; PMCID: PMC5694944.

Goranov AI, Gulati A, Dephoure N, Takahara T, Maeda T, Gygi SP, Manalis S, Amon A. Changes in cell morphology are coordinated with cell growth through the TORC1 pathway. Curr Biol. 2013 Jul 22;23(14):1269-79. doi: 10.1016/j.cub.2013.05.035. Epub 2013 Jun 27. PMID: 23810534; PMCID: PMC3880154.

Gray, J. V., Petsko, G. A., Johnston, G. C., Ringe, D., Singer, R. A., & Werner-Washburne, M. (2004). "Sleeping beauty": quiescence in Saccharomyces cerevisiae. *Microbiology and molecular biology reviews : MMBR*, *68*(2), 187–206. https://doi.org/10.1128/MMBR.68.2.187-206.2004

Grigull, J., Mnaimneh, S., Pootoolal, J., Robinson, M. D., & Hughes, T. R. (2004). Genome-wide analysis of mRNA stability using transcription inhibitors and microarrays reveals posttranscriptional control of ribosome biogenesis factors. *Molecular and cellular biology*, *24*(12), 5534–5547. https://doi.org/10.1128/MCB.24.12.5534-5547.2004

Grimes, G. W., Mahler, H. R., & Perlman, P. S. (1974). Letter: Mitochondrial morphology. *Science (New York, N.Y.)*, *185*(4151), 630–631. https://doi.org/10.1126/science.185.4151.630

Grimm, J. B., English, B. P., Chen, J., Slaughter, J. P., Zhang, Z., Revyakin, A., Patel, R., Macklin, J. J., Normanno, D., Singer, R. H., Lionnet, T., & Lavis, L. D. (2015). A general method to improve fluorophores for live-cell and single-molecule microscopy. *Nature methods*, *12*(3), 244–250. https://doi.org/10.1038/nmeth.3256

Guaragnella, N., & Butow, R. A. (2003). ATO3 encoding a putative outward ammonium transporter is an RTG-independent retrograde responsive gene regulated by GCN4 and the Ssy1-Ptr3-Ssy5 amino acid sensor system. *The Journal of biological chemistry*, *278*(46), 45882–45887. https://doi.org/10.1074/jbc.M309301200

Hall, D. D., Markwardt, D. D., Parviz, F., & Heideman, W. (1998). Regulation of the Cln3-Cdc28 kinase by cAMP in Saccharomyces cerevisiae. *The EMBO journal*, *17*(15), 4370–4378. https://doi.org/10.1093/emboj/17.15.4370

Hameed, A., Hussain, S. A., Ijaz, M. U., & Umer, M. (2020). Deletions of the Idh1, Eco1, Rom2, and Taf10 Genes Differently Control the Hyphal Growth, Drug Tolerance, and Virulence of Candida albicans. *Folia biologica*, *66*(3), 91–103.

Hanisch, D., Zien, A., Zimmer, R., & Lengauer, T. (2002). Co-clustering of biological networks and gene expression data. *Bioinformatics (Oxford, England)*, *18 Suppl 1*, S145–S154. https://doi.org/10.1093/bioinformatics/18.suppl_1.s145

Hartwell, L. H., & Unger, M. W. (1977). Unequal division in Saccharomyces cerevisiae and its implications for the control of cell division. *The Journal of cell biology*, *75*(2 Pt 1), 422–435. https://doi.org/10.1083/jcb.75.2.422

Hartwell, L. H., Culotti, J., Pringle, J. R., & Reid, B. J. (1974). Genetic control of the cell division cycle in yeast. *Science (New York, N.Y.)*, *183*(4120), 46–51. https://doi.org/10.1126/science.183.4120.46

Hastings, M. H., Maywood, E. S., & Brancaccio, M. (2019). The Mammalian Circadian Timing System and the Suprachiasmatic Nucleus as Its Pacemaker. *Biology*, *8*(1), 13. https://doi.org/10.3390/biology8010013

HATHAWAY, J. A., & ATKINSON, D. E. (1963). THE EFFECT OF ADENYLIC ACID ON YEAST NICOTINAMIDE ADENINE DINUCLEOTIDE ISOCITRATE DEHYDROGENASE, A POSSIBLE METABOLIC CONTROL MECHANISM. *The Journal of biological chemistry*, *238*, 2875–2881.

Heitman, J., Movva, N. R., & Hall, M. N. (1991). Targets for cell cycle arrest by the immunosuppressant rapamycin in yeast. *Science (New York, N.Y.)*, *253*(5022), 905–909. https://doi.org/10.1126/science.1715094

Heldt, F. S., Barr, A. R., Cooper, S., Bakal, C., & Novák, B. (2018). A comprehensive model for the proliferation-quiescence decision in response to endogenous DNA damage in human cells. *Proceedings of the National Academy of Sciences of the*

United States of America, *115*(10), 2532–2537. https://doi.org/10.1073/pnas.1715345115

Henson M. A. (2004). Modeling the synchronization of yeast respiratory oscillations. *Journal of theoretical biology*, *231*(3), 443–458. https://doi.org/10.1016/j.jtbi.2004.07.009

Herker, E., Jungwirth, H., Lehmann, K. A., Maldener, C., Fröhlich, K. U., Wissing, S., Büttner, S., Fehr, M., Sigrist, S., & Madeo, F. (2004). Chronological aging leads to apoptosis in yeast. *The Journal of cell biology*, *164*(4), 501–507. https://doi.org/10.1083/jcb.200310014

Herman P. K. (2002). Stationary phase in yeast. *Current opinion in microbiology*, *5*(6), 602–607. https://doi.org/10.1016/s1369-5274(02)00377-6

Herzog, R. W., & High, K. A. (1998). Problems and prospects in gene therapy for hemophilia. *Current opinion in hematology*, *5*(5), 321–326. https://doi.org/10.1097/00062752-199809000-00003

Hinnebusch A (1992) "General and Pathway-specific Regulatory Mechanisms Controlling the Synthesis of Amino Acid Biosynthetic Enzymes in Saccharomyces cerevisiae". Pp. 319-414 in The Molecular and Cellular Biology of the Yeast Saccharomyces: Gene Expression, edited by Jones EW, Pringle JR and Broach JR. Cold Spring Harbor, NY: Cold Spring Harbor Laboratory Press

Hocine, S., Raymond, P., Zenklusen, D., Chao, J. A., & Singer, R. H. (2013). Single-molecule analysis of gene expression using two-color RNA labeling in live yeast. *Nature methods*, *10*(2), 119–121. https://doi.org/10.1038/nmeth.2305

Holstege, F. C., Jennings, E. G., Wyrick, J. J., Lee, T. I., Hengartner, C. J., Green, M. R., Golub, T. R., Lander, E. S., & Young, R. A. (1998). Dissecting the regulatory circuitry of a eukaryotic genome. *Cell*, *95*(5), 717–728. https://doi.org/10.1016/s0092-8674(00)81641-4

Honma Y, Kitamura A, Shioda R, Maruyama H, Ozaki K, Oda Y, Mini T, Jenö P, Maki Y, Yonezawa K, Hurt E, Ueno M, Uritani M, Hall MN, Ushimaru T. TOR regulates late steps of ribosome maturation in the nucleoplasm via Nog1 in response to nutrients. EMBO J. 2006 Aug 23;25(16):3832-42. doi: 10.1038/sj.emboj.7601262. Epub 2006 Aug 3. PMID: 16888624; PMCID: PMC1553199.

Hsieh, T. H., Weiner, A., Lajoie, B., Dekker, J., Friedman, N., & Rando, O. J. (2015). Mapping Nucleosome Resolution Chromosome Folding in Yeast by Micro-C. *Cell*, *162*(1), 108–119. https://doi.org/10.1016/j.cell.2015.05.048

Hsieh, TH., Fudenberg, G., Goloborodko, A. *et al.* Micro-C XL: assaying chromosome conformation from the nucleosome to the entire genome. *Nat Methods* **13**, 1009–1011 (2016). https://doi.org/10.1038/nmeth.4025

Huang, D., Friesen, H., & Andrews, B. (2007). Pho85, a multifunctional cyclin-dependent protein kinase in budding yeast. *Molecular microbiology*, *66*(2), 303–314. https://doi.org/10.1111/j.1365-2958.2007.05914.x

Huang, R., Xu, Y., Wan, W., Shou, X., Qian, J., You, Z., Liu, B., Chang, C., Zhou, T., Lippincott-Schwartz, J., & Liu, W. (2015). Deacetylation of nuclear LC3 drives autophagy initiation under starvation. *Molecular cell*, *57*(3), 456–466. https://doi.org/10.1016/j.molcel.2014.12.013

Hughes Hallett, J. E., Luo, X., & Capaldi, A. P. (2014). State transitions in the TORC1 signaling pathway and information processing in Saccharomyces cerevisiae. *Genetics*, *198*(2), 773–786. https://doi.org/10.1534/genetics.114.168369

Hurley, J. M., Dasgupta, A., Emerson, J. M., Zhou, X., Ringelberg, C. S., Knabe, N., Lipzen, A. M., Lindquist, E. A., Daum, C. G., Barry, K. W., Grigoriev, I. V., Smith, K. M., Galagan, J. E., Bell-Pedersen, D., Freitag, M., Cheng, C., Loros, J. J., & Dunlap, J. C. (2014). Analysis of clock-regulated genes in Neurospora reveals widespread posttranscriptional control of metabolic potential. *Proceedings of the National Academy of Sciences of the United States of America*, *111*(48), 16995–17002. https://doi.org/10.1073/pnas.1418963111

Imbert, A., Ouyang, W., Safieddine, A., Coleno, E., Zimmer, C., Bertrand, E., Walter, T., & Mueller, F. (2021). FISH-quant v2: a scalable and modular analysis tool for smFISH image analysis. *BioRxiv*, 2021.07.20.453024. https://doi.org/10.1101/2021.07.20.453024

Johnson, L. N., & Barford, D. (1993). The effects of phosphorylation on the structure and function of proteins. *Annual review of biophysics and biomolecular structure*, *22*, 199–232. https://doi.org/10.1146/annurev.bb.22.060193.001215

Johnston M. (1999). Feasting, fasting and fermenting. Glucose sensing in yeast and other cells. *Trends in genetics : TIG*, *15*(1), 29–33. https://doi.org/10.1016/s0168-9525(98)01637-0

Johnston, G. C., Ehrhardt, C. W., Lorincz, A., & Carter, B. L. (1979). Regulation of cell size in the yeast Saccharomyces cerevisiae. *Journal of bacteriology*, *137*(1), 1–5. https://doi.org/10.1128/jb.137.1.1-5.1979

Johnston, G. C., Pringle, J. R., & Hartwell, L. H. (1977). Coordination of growth with cell division in the yeast Saccharomyces cerevisiae. *Experimental cell research*, *105*(1), 79–98. https://doi.org/10.1016/0014-4827(77)90154-9

Jona, G., Choder, M., & Gileadi, O. (2000). Glucose starvation induces a drastic reduction in the rates of both transcription and degradation of mRNA in yeast. *Biochimica et biophysica acta*, *1491*(1-3), 37–48. https://doi.org/10.1016/s0167-4781(00)00016-6

Jones, R. N., Rosenberg, A. L., Morris, J. N., Allaire, J. C., McCoy, K. J., Marsiske, M., Kleinman, K. P., Rebok, G. W., & Malloy, P. F. (2005). A growth curve model of

learning acquisition among cognitively normal older adults. *Experimental aging research*, *31*(3), 291–312. https://doi.org/10.1080/03610730590948195

Jorgensen, P., & Tyers, M. (2004). How cells coordinate growth and division. *Current biology : CB*, *14*(23), R1014–R1027. https://doi.org/10.1016/j.cub.2004.11.027

Jorgensen, P., Nishikawa, J. L., Breitkreutz, B. J., & Tyers, M. (2002). Systematic identification of pathways that couple cell growth and division in yeast. *Science (New York, N.Y.)*, *297*(5580), 395–400. https://doi.org/10.1126/science.1070850

Kaeberlein, M., McDonagh, T., Heltweg, B., Hixon, J., Westman, E. A., Caldwell, S. D., Napper, A., Curtis, R., DiStefano, P. S., Fields, S., Bedalov, A., & Kennedy, B. K. (2005). Substrate-specific activation of sirtuins by resveratrol. *The Journal of biological chemistry*, *280*(17), 17038–17045. https://doi.org/10.1074/jbc.M500655200

Kamada, Y., Sekito, T., & Ohsumi, Y. (2004). Autophagy in yeast: a TOR-mediated response to nutrient starvation. *Current topics in microbiology and immunology*, *279*, 73–84. https://doi.org/10.1007/978-3-642-18930-2_5

Kaplan, C., & Ewers, H. (2015). Optimized sample preparation for single-molecule localization-based superresolution microscopy in yeast. *Nature protocols*, *10*(7), 1007–1021. https://doi.org/10.1038/nprot.2015.060

Kapoor, P., Chen, M., Winkler, D. D., Luger, K., & Shen, X. (2013). Evidence for monomeric actin function in INO80 chromatin remodeling. *Nature structural & molecular biology*, *20*(4), 426–432. https://doi.org/10.1038/nsmb.2529

Keulers, M., Suzuki, T., Satroutdinov, A. D., & Kuriyama, H. (1996). Autonomous metabolic oscillation in continuous culture of Saccharomyces cerevisiae grown on ethanol. *FEMS microbiology letters*, *142*(2-3), 253–258. https://doi.org/10.1111/j.1574-6968.1996.tb08439.x

Khong, A., Matheny, T., Jain, S., Mitchell, S. F., Wheeler, J. R., & Parker, R. (2017). The Stress Granule Transcriptome Reveals Principles of mRNA Accumulation in Stress Granules. *Molecular cell*, *68*(4), 808–820.e5. https://doi.org/10.1016/j.molcel.2017.10.015

Kief, D. R., & Warner, J. R. (1981). Coordinate control of syntheses of ribosomal ribonucleic acid and ribosomal proteins during nutritional shift-up in Saccharomyces cerevisiae. *Molecular and cellular biology*, *1*(11), 1007–1015. https://doi.org/10.1128/mcb.1.11.1007-1015.1981

Kilmartin, J. V., & Adams, A. E. (1984). Structural rearrangements of tubulin and actin during the cell cycle of the yeast Saccharomyces. *The Journal of cell biology*, *98*(3), 922–933. https://doi.org/10.1083/jcb.98.3.922 Ayscough, K. R., Stryker, J., Pokala, N., Sanders, M., Crews, P., & Drubin, D. G. (1997). High rates of actin filament turnover in budding yeast and roles for actin in establishment and maintenance of cell polarity revealed using the actin inhibitor latrunculin-A. *The Journal of cell biology*, *137*(2), 399–416. https://doi.org/10.1083/jcb.137.2.399

Kim, K. S., Rosenkrantz, M. S., & Guarente, L. (1986). Saccharomyces cerevisiae contains two functional citrate synthase genes. *Molecular and cellular biology*, *6*(6), 1936–1942. https://doi.org/10.1128/mcb.6.6.1936-1942.1986

Klevecz, R. R., Bolen, J., Forrest, G., & Murray, D. B. (2004). A genomewide oscillation in transcription gates DNA replication and cell cycle. *Proceedings of the National Academy of Sciences of the United States of America*, *101*(5), 1200–1205. https://doi.org/10.1073/pnas.0306490101

Klinger, H., Rinnerthaler, M., Lam, Y. T., Laun, P., Heeren, G., Klocker, A., Simon-Nobbe, B., Dickinson, J. R., Dawes, I. W., & Breitenbach, M. (2010). Quantitation of (a)symmetric inheritance of functional and of oxidatively damaged mitochondrial aconitase in the cell division of old yeast mother cells. *Experimental gerontology*, *45*(7-8), 533–542. https://doi.org/10.1016/j.exger.2010.03.016

Klosinska, M. M., Crutchfield, C. A., Bradley, P. H., Rabinowitz, J. D., & Broach, J. R. (2011). Yeast cells can access distinct quiescent states. *Genes & development*, *25*(4), 336–349. https://doi.org/10.1101/gad.2011311

Krishna, S., & Laxman, S. (2018). A minimal "push-pull" bistability model explains oscillations between quiescent and proliferative cell states. *Molecular biology of the cell*, *29*(19), 2243–2258. https://doi.org/10.1091/mbc.E18-01-0017

Kuai, L., Das, B., & Sherman, F. (2005). A nuclear degradation pathway controls the abundance of normal mRNAs in Saccharomyces cerevisiae. *Proceedings of the National Academy of Sciences of the United States of America*, *102*(39), 13962–13967. https://doi.org/10.1073/pnas.0506518102

Kuang, Z., Cai, L., Zhang, X., Ji, H., Tu, B. P., & Boeke, J. D. (2014). High-temporal-resolution view of transcription and chromatin states across distinct metabolic states in budding yeast. *Nature structural & molecular biology*, *21*(10), 854–863. https://doi.org/10.1038/nsmb.2881

Kuang, Z., Pinglay, S., Ji, H., & Boeke, J. D. (2017). Msn2/4 regulate expression of glycolytic enzymes and control transition from quiescence to growth. *eLife*, *6*, e29938. https://doi.org/10.7554/eLife.29938

Laabs, T. L., Markwardt, D. D., Slattery, M. G., Newcomb, L. L., Stillman, D. J., & Heideman, W. (2003). ACE2 is required for daughter cell-specific G1 delay in Saccharomyces cerevisiae. *Proceedings of the National Academy of Sciences of the United States of America*, *100*(18), 10275–10280. https://doi.org/10.1073/pnas.1833999100

Lahtvee, P. J., Sánchez, B. J., Smialowska, A., Kasvandik, S., Elsemman, I. E., Gatto, F., & Nielsen, J. (2017). Absolute Quantification of Protein and mRNA Abundances Demonstrate Variability in Gene-Specific Translation Efficiency in Yeast. *Cell systems*, *4*(5), 495–504.e5. https://doi.org/10.1016/j.cels.2017.03.003

Lai, C. Y., Jaruga, E., Borghouts, C., & Jazwinski, S. M. (2002). A mutation in the ATP2 gene abrogates the age asymmetry between mother and daughter cells of the yeast

Saccharomyces cerevisiae. *Genetics*, *162*(1), 73–87. https://doi.org/10.1093/genetics/162.1.73

Laporte, D., Gouleme, L., Jimenez, L., Khemiri, I., & Sagot, I. (2018). Mitochondria reorganization upon proliferation arrest predicts individual yeast cell fate. *eLife*, *7*, e35685. https://doi.org/10.7554/eLife.35685

Laporte, D., Jimenez, L., Gouleme, L., & Sagot, I. (2017). Yeast quiescence exit swiftness is influenced by cell volume and chronological age. *Microbial cell (Graz, Austria)*, *5*(2), 104–111. https://doi.org/10.15698/mic2018.02.615

LaPorte, S. L., Juo, Z. S., Vaclavikova, J., Colf, L. A., Qi, X., Heller, N. M., Keegan, A. D., & Garcia, K. C. (2008). Molecular and structural basis of cytokine receptor pleiotropy in the interleukin-4/13 system. *Cell*, *132*(2), 259–272. https://doi.org/10.1016/j.cell.2007.12.030

Laxman, S., Sutter, B. M., & Tu, B. P. (2010). Behavior of a metabolic cycling population at the single cell level as visualized by fluorescent gene expression reporters. *PloS one*, *5*(9), e12595. https://doi.org/10.1371/journal.pone.0012595

Lecompte, O., Ripp, R., Thierry, J. C., Moras, D., & Poch, O. (2002). Comparative analysis of ribosomal proteins in complete genomes: an example of reductive evolution at the domain scale. Nucleic acids research, 30(24), 5382–5390.

Lenstra, T. L., Coulon, A., Chow, C. C., & Larson, D. R. (2015). Single-Molecule Imaging Reveals a Switch between Spurious and Functional ncRNA Transcription. *Molecular cell*, *60*(4), 597–610. https://doi.org/10.1016/j.molcel.2015.09.028

Lesage, G., & Bussey, H. (2006). Cell wall assembly in Saccharomyces cerevisiae. *Microbiology and molecular biology reviews : MMBR*, *70*(2), 317–343. https://doi.org/10.1128/MMBR.00038-05

Li L, Miles S, Melville Z, Prasad A, Bradley G, Breeden LL. Key events during the transition from rapid growth to quiescence in budding yeast require posttranscriptional regulators. Mol Biol Cell. 2013 Dec;24(23):3697-709. doi: 10.1091/mbc.E13-05-0241. Epub 2013 Oct 2. PMID: 24088570; PMCID: PMC3842996.

Li, C. M., & Klevecz, R. R. (2006). A rapid genome-scale response of the transcriptional oscillator to perturbation reveals a period-doubling path to phenotypic change. *Proceedings of the National Academy of Sciences of the United States of America*, *103*(44), 16254–16259. https://doi.org/10.1073/pnas.0604860103

Li, L., Kaplan, J., & Ward, D. M. (2017). The glucose sensor Snf1 and the transcription factors Msn2 and Msn4 regulate transcription of the vacuolar iron importer gene *CCC1* and iron resistance in yeast. *The Journal of biological chemistry*, *292*(37), 15577–15586. https://doi.org/10.1074/jbc.M117.802504

Li, L., Miles, S., & Breeden, L. L. (2015). A Genetic Screen for Saccharomyces cerevisiae Mutants That Fail to Enter Quiescence. *G3 (Bethesda, Md.)*, *5*(8), 1783–1795. https://doi.org/10.1534/g3.115.019091

Lillie, S. H., & Pringle, J. R. (1980). Reserve carbohydrate metabolism in Saccharomyces cerevisiae: responses to nutrient limitation. *Journal of bacteriology*, *143*(3), 1384–1394. https://doi.org/10.1128/jb.143.3.1384-1394.1980

Lipson, D., Raz, T., Kieu, A., Jones, D. R., Giladi, E., Thayer, E., Thompson, J. F., Letovsky, S., Milos, P., & Causey, M. (2009). Quantification of the yeast transcriptome by single-molecule sequencing. *Nature biotechnology*, *27*(7), 652–658. https://doi.org/10.1038/nbt.1551

Litsios, A., Huberts, D. H. E. W., Terpstra, H. M., Guerra, P., Schmidt, A., Buczak, K., Papagiannakis, A., Rovetta, M., Hekelaar, J., Hubmann, G., Exterkate, M., Milias-Argeitis, A., & Heinemann, M. (2019). Differential scaling between G1 protein production and cell size dynamics promotes commitment to the cell division cycle in budding yeast. *Nature cell biology*, *21*(11), 1382–1392. https://doi.org/10.1038/s41556-019-0413-3

Liu, Z., & Butow, R. A. (2006). Mitochondrial retrograde signaling. *Annual review of genetics*, *40*, 159–185. https://doi.org/10.1146/annurev.genet.40.110405.090613

Lloyd, D., Salgado, L. E. J., Turner, M. P., Suller, M. T. E., & Murray, D. (2002). Cycles of mitochondrial energization driven by the ultradian clock in a continuous culture of Saccharomyces cerevisiae. *Microbiology (Reading, England)*, *148*(Pt 11), 3715–3724. https://doi.org/10.1099/00221287-148-11-3715

Loewith, R., & Hall, M. N. (2011). Target of rapamycin (TOR) in nutrient signaling and growth control. *Genetics*, *189*(4), 1177–1201. https://doi.org/10.1534/genetics.111.133363

Longtine, M. S., Fares, H., & Pringle, J. R. (1998). Role of the yeast Gin4p protein kinase in septin assembly and the relationship between septin assembly and septin function. *The Journal of cell biology*, *143*(3), 719–736. https://doi.org/10.1083/jcb.143.3.719

Lorenz, M. C., & Fink, G. R. (2001). The glyoxylate cycle is required for fungal virulence. *Nature*, *412*(6842), 83–86. https://doi.org/10.1038/35083594 M R A Chance, 'Population size and variation in small populations', *Proc. R. Soc. Med.*, 1964, **57**: 174.

Maaloe, O. (1979). Regulation of the protein-synthesizing machinery, ribosomes, tRNA, factors and so on. In: Biological regulation and development, ed. Goldberger, R.F., Plenum Press, New York, pp. 487–542.

Machné, R., & Murray, D. B. (2012). The yin and yang of yeast transcription: elements of a global feedback system between metabolism and chromatin. *PloS one*, *7*(6), e37906. https://doi.org/10.1371/journal.pone.0037906

MacLean, M., Harris, N., & Piper, P. W. (2001). Chronological lifespan of stationary phase yeast cells; a model for investigating the factors that might influence the ageing of postmitotic tissues in higher organisms. *Yeast (Chichester, England)*, *18*(6), 499–509. https://doi.org/10.1002/yea.701

Magalhães, R. S. S., Popova, B., Braus, G. H., Outeiro, T. F., & Eleutherio, E. C. A. (2018). The trehalose protective mechanism during thermal stress in Saccharomyces cerevisiae: the roles of Ath1 and Agt1. *FEMS yeast research*, *18*(6), 10.1093/femsyr/foy066. https://doi.org/10.1093/femsyr/foy066

Magnuson, B., Ekim, B., & Fingar, D. C. (2011). Regulation and function of ribosomal protein S6 kinase (S6K) within mTOR signalling networks. Biochemical Journal, 441(1), 1–21.

Maiser, A., Dillinger, S., Längst, G. *et al.* Super-resolution *in situ* analysis of active ribosomal DNA chromatin organization in the nucleolus. *Sci Rep* **10**, 7462 (2020). https://doi.org/10.1038/s41598-020-64589-x

Martin, D. E., & Hall, M. N. (2005). The expanding TOR signaling network. *Current opinion in cell biology*, *17*(2), 158–166. https://doi.org/10.1016/j.ceb.2005.02.008

Martinez, M. J., Roy, S., Archuletta, A. B., Wentzell, P. D., Anna-Arriola, S. S., Rodriguez, A. L., Aragon, A. D., Quiñones, G. A., Allen, C., & Werner-Washburne, M. (2004). Genomic analysis of stationary-phase and exit in Saccharomyces cerevisiae: gene expression and identification of novel essential genes. *Molecular biology of the cell*, *15*(12), 5295–5305. https://doi.org/10.1091/mbc.e03-11-0856

Mateus, C., & Avery, S. V. (2000). Destabilized green fluorescent protein for monitoring dynamic changes in yeast gene expression with flow cytometry. *Yeast (Chichester, England)*, *16*(14), 1313–1323. https://doi.org/10.1002/1097-0061(200010)16:14<1313::AID-YEA626>3.0.CO;2-O

May, J. L., Kouri, F. M., Hurley, L. A., Liu, J., Tommasini-Ghelfi, S., Ji, Y., Gao, P., Calvert, A. E., Lee, A., Chandel, N. S., Davuluri, R. V., Horbinski, C. M., Locasale, J. W., & Stegh, A. H. (2019). IDH3α regulates one-carbon metabolism in glioblastoma. *Science advances*, *5*(1), eaat0456. https://doi.org/10.1126/sciadv.aat0456

Mayer, C., & Grummt, I. (2006). Ribosome biogenesis and cell growth: mTOR coordinates transcription by all three classes of nuclear RNA polymerases. *Oncogene*, *25*(48), 6384–6391. https://doi.org/10.1038/sj.onc.1209883

McKnight, J. N., Boerma, J. W., Breeden, L. L., & Tsukiyama, T. (2015). Global Promoter Targeting of a Conserved Lysine Deacetylase for Transcriptional Shutoff during Quiescence Entry. *Molecular cell*, *59*(5), 732–743. https://doi.org/10.1016/j.molcel.2015.07.014

McNeil, J. B., McIntosh, E. M., Taylor, B. V., Zhang, F. R., Tang, S., & Bognar, A. L. (1994). Cloning and molecular characterization of three genes, including two genes encoding serine hydroxymethyltransferases, whose inactivation is required to render

yeast auxotrophic for glycine. *The Journal of biological chemistry*, *269*(12), 9155–9165.

Mellor J. (2016). The molecular basis of metabolic cycles and their relationship to circadian rhythms. *Nature structural & molecular biology*, *23*(12), 1035–1044. https://doi.org/10.1038/nsmb.3311

Mews, P., Zee, B. M., Liu, S., Donahue, G., Garcia, B. A., & Berger, S. L. (2014). Histone methylation has dynamics distinct from those of histone acetylation in cell cycle reentry from quiescence. *Molecular and cellular biology*, *34*(21), 3968–3980. https://doi.org/10.1128/MCB.00763-14

Meyuhas O. (2008). Physiological roles of ribosomal protein S6: one of its kind. *International review of cell and molecular biology*, *268*, 1–37. https://doi.org/10.1016/S1937-6448(08)00801-0

Miles, S., Bradley, G. T., & Breeden, L. L. (2021). The budding yeast transition to quiescence. *Yeast (Chichester, England)*, *38*(1), 30–38. https://doi.org/10.1002/yea.3546

Miles, S., Li, L., Davison, J., & Breeden, L. L. (2013). Xbp1 directs global repression of budding yeast transcription during the transition to quiescence and is important for the longevity and reversibility of the quiescent state. *PLoS genetics*, *9*(10), e1003854. https://doi.org/10.1371/journal.pgen.1003854

Miura, F., Kawaguchi, N., Yoshida, M., Uematsu, C., Kito, K., Sakaki, Y., & Ito, T. (2008). Absolute quantification of the budding yeast transcriptome by means of competitive PCR between genomic and complementary DNAs. *BMC genomics*, *9*, 574. https://doi.org/10.1186/1471-2164-9-574

Miyakawa, I., Aoi, H., Sando, N., & Kuroiwa, T. (1984). Fluorescence microscopic studies of mitochondrial nucleoids during meiosis and sporulation in the yeast, Saccharomyces cerevisiae. *Journal of Cell Science*, *66*(1), 21–38. https://doi.org/10.1242/jcs.66.1.21

MONOD, J., & TORRIANI, A. M. (1950). De l'amylomaltase d'Escherichia coli [Amylomaltase of Escherichia coli]. *Annales de l'Institut Pasteur*, *78*(1), 65–77.

Moore P. B. (1988). The ribosome returns. *Nature*, *331*(6153), 223–227. https://doi.org/10.1038/331223a0

Morgan, J. T., Fink, G. R., & Bartel, D. P. (2019). Excised linear introns regulate growth in yeast. *Nature*, *565*(7741), 606–611. https://doi.org/10.1038/s41586-018-0828-1

MorganL., MosesG., & YoungT. (2018). Coupling of the cell cycle and metabolism in yeast cell-cycle-related oscillations via resource criticality and checkpoint gating. *Letters in Biomathematics*, *5*(1), 113-128. https://doi.org/10.30707/LiB5.1Morgana

MORTIMER, R. K., & JOHNSTON, J. R. (1959). Life span of individual yeast cells. *Nature*, *183*(4677), 1751–1752. https://doi.org/10.1038/1831751a0

Mueller, F., Senecal, A., Tantale, K., Marie-Nelly, H., Ly, N., Collin, O., Basyuk, E., Bertrand, E., Darzacq, X., & Zimmer, C. (2013). FISH-quant: automatic counting of transcripts in 3D FISH images. *Nature methods*, *10*(4), 277–278. https://doi.org/10.1038/nmeth.2406

Müller, D., Exler, S., Aguilera-Vázquez, L., Guerrero-Martín, E., & Reuss, M. (2003). Cyclic AMP mediates the cell cycle dynamics of energy metabolism in Saccharomyces cerevisiae. *Yeast (Chichester, England)*, *20*(4), 351–367. https://doi.org/10.1002/yea.967

Münch, T., Sonnleitner, B., & Fiechter, A. (1992). The decisive role of the Saccharomyces cerevisiae cell cycle behaviour for dynamic growth characterization. *Journal of biotechnology*, *22*(3), 329–351. https://doi.org/10.1016/0168-1656(92)90150-8

Munns R. (2002). Comparative physiology of salt and water stress. *Plant, cell & environment*, *25*(2), 239–250. https://doi.org/10.1046/j.0016-8025.2001.00808.x

Munsky, B., & Neuert, G. (2015). From analog to digital models of gene regulation. *Physical biology*, *12*(4), 045004. https://doi.org/10.1088/1478-3975/12/4/045004

Murphy M. P. (2009). How mitochondria produce reactive oxygen species. *The Biochemical journal*, *417*(1), 1–13. https://doi.org/10.1042/BJ20081386

Murphy, J. P., Stepanova, E., Everley, R. A., Paulo, J. A., & Gygi, S. P. (2015). Comprehensive Temporal Protein Dynamics during the Diauxic Shift in Saccharomyces cerevisiae. *Molecular & cellular proteomics : MCP*, *14*(9), 2454–2465. https://doi.org/10.1074/mcp.M114.045849

Murray, D. B., & Lloyd, D. (2021). Multiple Rediscoveries and Misconceptions; the Yeast Metabolic Oscillation. *Function (Oxford, England)*, *2*(5), zqab039. https://doi.org/10.1093/function/zqab039

Murray, D. B., Beckmann, M., & Kitano, H. (2007). Regulation of yeast oscillatory dynamics. *Proceedings of the National Academy of Sciences of the United States of America*, *104*(7), 2241–2246. https://doi.org/10.1073/pnas.0606677104

Murray, D. B., Engelen, F., Lloyd, D., & Kuriyama, H. (1999). Involvement of glutathione in the regulation of respiratory oscillation during a continuous culture of Saccharomyces cerevisiae. *Microbiology (Reading, England)*, *145 (Pt 10)*, 2739–2745. https://doi.org/10.1099/00221287-145-10-2739

Murray, D. B., Haynes, K., & Tomita, M. (2011). Redox regulation in respiring Saccharomyces cerevisiae. *Biochimica et biophysica acta*, *1810*(10), 945–958. https://doi.org/10.1016/j.bbagen.2011.04.005

Murray, D. B., Klevecz, R. R., & Lloyd, D. (2003). Generation and maintenance of synchrony in Saccharomyces cerevisiae continuous culture. *Experimental cell research*, *287*(1), 10–15. https://doi.org/10.1016/s0014-4827(03)00068-5

Newman JR, Ghaemmaghami S, Ihmels J, Breslow DK, Noble M, DeRisi JL, Weissman JS. Single-cell proteomic analysis of S. cerevisiae reveals the architecture of biological noise. Nature. 2006 Jun 15;441(7095):840-6. doi: 10.1038/nature04785. Epub 2006 May 14. PMID: 16699522.

Ng, R., & Abelson, J. (1980). Isolation and sequence of the gene for actin in Saccharomyces cerevisiae. *Proceedings of the National Academy of Sciences of the United States of America*, *77*(7), 3912–3916. https://doi.org/10.1073/pnas.77.7.3912

Nishimura, K., Fukuda, A., & Hisatake, K. (2019). Mechanisms of the Metabolic Shift during Somatic Cell Reprogramming. *International journal of molecular sciences*, *20*(9), 2254. https://doi.org/10.3390/ijms20092254

Nocetti, N., & Whitehouse, I. (2016). Nucleosome repositioning underlies dynamic gene expression. *Genes & development*, *30*(6), 660–672. https://doi.org/10.1101/gad.274910.115

Nojima, T., Gomes, T., Grosso, A. R. F., Kimura, H., Dye, M. J., Dhir, S., Carmo-Fonseca, M., & Proudfoot, N. J. (2015). Mammalian NET-Seq Reveals Genome-wide Nascent Transcription Coupled to RNA Processing. *Cell*, *161*(3), 526–540. https://doi.org/10.1016/j.cell.2015.03.027

NOVICK, A., & SZILARD, L. (1950). Experiments with the Chemostat on spontaneous mutations of bacteria. *Proceedings of the National Academy of Sciences of the United States of America*, *36*(12), 708–719. https://doi.org/10.1073/pnas.36.12.708

Novick, A., & Weiner, M. (1957). ENZYME INDUCTION AS AN ALL-OR-NONE PHENOMENON. *Proceedings of the National Academy of Sciences of the United States of America*, *43*(7), 553–566. https://doi.org/10.1073/pnas.43.7.553

O'Neill, J. S., & Reddy, A. B. (2011). Circadian clocks in human red blood cells. *Nature*, *469*(7331), 498–503. https://doi.org/10.1038/nature09702

O'Neill, J. S., Hoyle, N. P., Robertson, J. B., Edgar, R. S., Beale, A. D., Peak-Chew, S. Y., Day, J., Costa, A. S. H., Frezza, C., & Causton, H. C. (2020). Eukaryotic cell biology is temporally coordinated to support the energetic demands of protein homeostasis. *Nature communications*, *11*(1), 4706. https://doi.org/10.1038/s41467-020-18330-x

Okada, H., Kono, K., Neiman, A. M., & Ohya, Y. (2016). Examination and Disruption of the Yeast Cell Wall. *Cold Spring Harbor protocols*, *2016*(8), 10.1101/pdb.top078659. https://doi.org/10.1101/pdb.top078659

Orlean P. (2012). Architecture and biosynthesis of the Saccharomyces cerevisiae cell wall. *Genetics*, *192*(3), 775–818. https://doi.org/10.1534/genetics.112.144485

Ozbudak, E. M., Thattai, M., Kurtser, I., Grossman, A. D., & van Oudenaarden, A. (2002). Regulation of noise in the expression of a single gene. *Nature genetics*, *31*(1), 69–73. https://doi.org/10.1038/ng869

Özsezen, S., Papagiannakis, A., Chen, H., Niebel, B., Milias-Argeitis, A., & Heinemann, M. (2019). Inference of the High-Level Interaction Topology between the Metabolic and Cell-Cycle Oscillators from Single-Cell Dynamics. *Cell systems*, *9*(4), 354–365.e6. https://doi.org/10.1016/j.cels.2019.09.003

Palková, Z., Devaux, F., Icicová, M., Mináriková, L., Le Crom, S., & Jacq, C. (2002). Ammonia pulses and metabolic oscillations guide yeast colony development. *Molecular biology of the cell*, *13*(11), 3901–3914. https://doi.org/10.1091/mbc.e01-12-0149

Panisko, E. A., & McAlister-Henn, L. (2001). Subunit interactions of yeast NAD+-specific isocitrate dehydrogenase. *The Journal of biological chemistry*, *276*(2), 1204–1210. https://doi.org/10.1074/jbc.M005056200

Papagiannakis, A., Niebel, B., Wit, E. C., & Heinemann, M. (2017). Autonomous Metabolic Oscillations Robustly Gate the Early and Late Cell Cycle. *Molecular cell*, *65*(2), 285–295. https://doi.org/10.1016/j.molcel.2016.11.018

Parelukar S. J., Semones G. B., Rolf M. J., Lievense J. C., Lim H. C. 1986; Induction and elimination of oscillations in continuous cultures of *Saccharomyces cerevisiae* . *Biotechnol Bioeng* 28:700–710

Parker, D. M., Winkenbach, L. P., & Osborne Nishimura, E. (2022). It's Just a Phase: Exploring the Relationship Between mRNA, Biomolecular Condensates, and Translational Control. *Frontiers in genetics*, *13*, 931220. https://doi.org/10.3389/fgene.2022.931220

Pariollaud, M., Ibrahim, L. H., Irizarry, E., Mello, R. M., Chan, A. B., Altman, B. J., Shaw, R. J., Bollong, M. J., Wiseman, R. L., & Lamia, K. A. (2022). Circadian disruption enhances HSF1 signaling and tumorigenesis in *Kras*-driven lung cancer. *Science advances*, *8*(39), eabo1123. https://doi.org/10.1126/sciadv.abo1123

Patnaik P. R. (2003). Oscillatory metabolism of Saccharomyces cerevisiae: an overview of mechanisms and models. *Biotechnology advances*, *21*(3), 183–192. https://doi.org/10.1016/s0734-9750(03)00022-3

Pawson, C. T., & Scott, J. D. (2010). Signal integration through blending, bolstering and bifurcating of intracellular information. *Nature structural & molecular biology*, *17*(6), 653–658. https://doi.org/10.1038/nsmb.1843

Pearce, L. R., Komander, D., & Alessi, D. R. (2010). The nuts and bolts of AGC protein kinases. *Nature reviews. Molecular cell biology*, *11*(1), 9–22. https://doi.org/10.1038/nrm2822

Perez-Carrasco, R., Guerrero, P., Briscoe, J., & Page, K. M. (2016). Intrinsic Noise Profoundly Alters the Dynamics and Steady State of Morphogen-Controlled Bistable

Genetic Switches. *PLoS computational biology*, *12*(10), e1005154. https://doi.org/10.1371/journal.pcbi.1005154

Pfeiffer, T., & Morley, A. (2014). An evolutionary perspective on the Crabtree effect. *Frontiers in molecular biosciences*, *1*, 17. https://doi.org/10.3389/fmolb.2014.00017

Phipps, A. I., Chlebowski, R. T., Prentice, R., McTiernan, A., Wactawski-Wende, J., Kuller, L. H., Adams-Campbell, L. L., Lane, D., Stefanick, M. L., Vitolins, M., Kabat, G. C., Rohan, T. E., & Li, C. I. (2011). Reproductive history and oral contraceptive use in relation to risk of triple-negative breast cancer. *Journal of the National Cancer Institute*, *103*(6), 470–477. https://doi.org/10.1093/jnci/djr030

Piñon R. (1978). Folded chromosomes in non-cycling yeast cells: evidence for a characteristic g0 form. *Chromosoma*, *67*(3), 263–274. https://doi.org/10.1007/BF02569039

Planta, R. J., & Mager, W. H. (1998). The list of cytoplasmic ribosomal proteins of Saccharomyces cerevisiae. Yeast (Chichester, England), 14(5), 471–477.

Polymenis, M., & Aramayo, R. (2015). Translate to divide: control of the cell cycle by protein synthesis. *Microbial cell (Graz, Austria)*, *2*(4), 94–104. https://doi.org/10.15698/mic2015.04.198

Polymenis, M., & Schmidt, E. V. (1997). Coupling of cell division to cell growth by translational control of the G1 cyclin CLN3 in yeast. *Genes & development*, *11*(19), 2522–2531. https://doi.org/10.1101/gad.11.19.2522

Porro, D., Martegani, E., Ranzi, B. M., & Alberghina, L. (1988). Oscillations in continuous cultures of budding yeast: a segregated parameter analysis. *Biotechnology and Bioengineering*, *32*(4), 411–417. https://doi.org/10.1002/bit.260320402

Powers, T., & Walter, P. (1999). Regulation of ribosome biogenesis by the rapamycin-sensitive TOR-signaling pathway in Saccharomyces cerevisiae. *Molecular biology of the cell*, *10*(4), 987–1000. https://doi.org/10.1091/mbc.10.4.987

Prakash, K., Diederich, B., Heintzmann, R., & Schermelleh, L. (2022). Super-resolution microscopy: a brief history and new avenues. *Philosophical transactions. Series A, Mathematical, physical, and engineering sciences*, *380*(2220), 20210110. https://doi.org/10.1098/rsta.2021.0110

Pruyne, D., & Bretscher, A. (2000). Polarization of cell growth in yeast. *Journal of cell science*, *113 (Pt 4)*, 571–585. https://doi.org/10.1242/jcs.113.4.571

Puig, S., & Pérez-Ortín, J. E. (2000). Stress response and expression patterns in wine fermentations of yeast genes induced at the diauxic shift. *Yeast (Chichester, England)*, *16*(2), 139–148. https://doi.org/10.1002/(SICI)1097-0061(20000130)16:2<139::AID-YEA512>3.0.CO;2-J

Qu, Y., Jiang, J., Liu, X., Wei, P., Yang, X., & Tang, C. (2019). Cell Cycle Inhibitor Whi5 Records Environmental Information to Coordinate Growth and Division in Yeast. *Cell reports*, *29*(4), 987–994.e5. https://doi.org/10.1016/j.celrep.2019.09.030

Rabani, M., Raychowdhury, R., Jovanovic, M., Rooney, M., Stumpo, D. J., Pauli, A., Hacohen, N., Schier, A. F., Blackshear, P. J., Friedman, N., Amit, I., & Regev, A. (2014). High-resolution sequencing and modeling identifies distinct dynamic RNA regulatory strategies. *Cell*, *159*(7), 1698–1710. https://doi.org/10.1016/j.cell.2014.11.015

Radonjic, M., Andrau, J. C., Lijnzaad, P., Kemmeren, P., Kockelkorn, T. T., van Leenen, D., van Berkum, N. L., & Holstege, F. C. (2005). Genome-wide analyses reveal RNA polymerase II located upstream of genes poised for rapid response upon S. cerevisiae stationary phase exit. *Molecular cell*, *18*(2), 171–183. https://doi.org/10.1016/j.molcel.2005.03.010

Raj, A., & van Oudenaarden, A. (2008). Nature, nurture, or chance: stochastic gene expression and its consequences. *Cell*, *135*(2), 216–226. https://doi.org/10.1016/j.cell.2008.09.050

Raj, A., Peskin, C. S., Tranchina, D., Vargas, D. Y., & Tyagi, S. (2006). Stochastic mRNA synthesis in mammalian cells. *PLoS biology*, *4*(10), e309. https://doi.org/10.1371/journal.pbio.0040309

Raj, A., van den Bogaard, P., Rifkin, S. A., van Oudenaarden, A., & Tyagi, S. (2008). Imaging individual mRNA molecules using multiple singly labeled probes. *Nature methods*, *5*(10), 877–879. https://doi.org/10.1038/nmeth.1253

Rao, A. R., & Pellegrini, M. (2011). Regulation of the yeast metabolic cycle by transcription factors with periodic activities. *BMC systems biology*, *5*, 160. https://doi.org/10.1186/1752-0509-5-160

Raser, J. M., & O'Shea, E. K. (2005). Noise in gene expression: origins, consequences, and control. *Science (New York, N.Y.)*, *309*(5743), 2010–2013. https://doi.org/10.1126/science.1105891

Reinders, J., Wagner, K., Zahedi, R. P., Stojanovski, D., Eyrich, B., van der Laan, M., Rehling, P., Sickmann, A., Pfanner, N., & Meisinger, C. (2007). Profiling phosphoproteins of yeast mitochondria reveals a role of phosphorylation in assembly of the ATP synthase. *Molecular & cellular proteomics : MCP*, *6*(11), 1896–1906. https://doi.org/10.1074/mcp.M700098-MCP200

Reinke, H., & Gatfield, D. (2006). Genome-wide oscillation of transcription in yeast. *Trends in biochemical sciences*, *31*(4), 189–191. https://doi.org/10.1016/j.tibs.2006.02.001

Robertson, J. B., Stowers, C. C., Boczko, E., & Johnson, C. H. (2008). Real-time luminescence monitoring of cell-cycle and respiratory oscillations in yeast. *Proceedings of the National Academy of Sciences of the United States of America*, *105*(46), 17988–17993. https://doi.org/10.1073/pnas.0809482105

Roden, C., & Gladfelter, A. S. (2021). RNA contributions to the form and function of biomolecular condensates. *Nature reviews. Molecular cell biology*, *22*(3), 183–195. https://doi.org/10.1038/s41580-020-0264-6

Ron Padilla, Suleiman A. Igdoura, Dysfunctional autophagy impairs muscle regeneration in lysosomal diseases, Molecular Genetics and Metabolism,volume 126, Issue 2, 2019,

Sagot, I., Rodal, A. A., Moseley, J., Goode, B. L., & Pellman, D. (2002). An actin nucleation mechanism mediated by Bni1 and profilin. *Nature cell biology*, *4*(8), 626–631.

Sancar, A., & Van Gelder, R. N. (2021). Clocks, cancer, and chronochemotherapy. *Science (New York, N.Y.)*, *371*(6524), eabb0738. https://doi.org/10.1126/science.abb0738

Sánchez-Gaya, V., Casaní-Galdón, S., Ugidos, M., Kuang, Z., Mellor, J., Conesa, A., & Tarazona, S. (2018). Elucidating the Role of Chromatin State and Transcription Factors on the Regulation of the Yeast Metabolic Cycle: A Multi-Omic Integrative Approach. *Frontiers in genetics*, *9*, 578. https://doi.org/10.3389/fgene.2018.00578

Sanchez, A., Choubey, S., & Kondev, J. (2013). Regulation of noise in gene expression. *Annual review of biophysics*, *42*, 469–491. https://doi.org/10.1146/annurev-biophys-083012-130401

Saqcena, M., Menon, D., Patel, D., Mukhopadhyay, S., Chow, V., & Foster, D. A. (2013). Amino acids and mTOR mediate distinct metabolic checkpoints in mammalian G1 cell cycle. *PloS one*, *8*(8), e74157. https://doi.org/10.1371/journal.pone.0074157

Satroutdinov, A. D., Kuriyama, H., & Kobayashi, H. (1992). Oscillatory metabolism of Saccharomyces cerevisiae in continuous culture. *FEMS microbiology letters*, *77*(1-3), 261–267. https://doi.org/10.1016/0378-1097(92)90167-m

Saucedo, L. J., & Edgar, B. A. (2002). Why size matters: altering cell size. *Current opinion in genetics & development*, *12*(5), 565–571. https://doi.org/10.1016/s0959-437x(02)00341-6

Schermelleh, L., Ferrand, A., Huser, T. *et al.* Super-resolution microscopy demystified. *Nat Cell Biol* **21**, 72–84 (2019). https://doi.org/10.1038/s41556-018-0251-8

Schmoller, K. M., Turner, J. J., Kõivomägi, M., & Skotheim, J. M. (2015). Dilution of the cell cycle inhibitor Whi5 controls budding-yeast cell size. *Nature*, *526*(7572), 268–272. https://doi.org/10.1038/nature14908

Schott, D., Huffaker, T., & Bretscher, A. (2002). Microfilaments and microtubules: the news from yeast. *Current opinion in microbiology*, *5*(6), 564–574. https://doi.org/10.1016/s1369-5274(02)00369-7

Shah, K. H., Nostramo, R., Zhang, B., Varia, S. N., Klett, B. M., & Herman, P. K. (2014). Protein kinases are associated with multiple, distinct cytoplasmic granules in quiescent yeast cells. *Genetics*, *198*(4), 1495–1512. https://doi.org/10.1534/genetics.114.172031

Shi, L., & Tu, B. P. (2013). Acetyl-CoA induces transcription of the key G1 cyclin CLN3 to promote entry into the cell division cycle in Saccharomyces cerevisiae. *Proceedings of the National Academy of Sciences of the United States of America*, *110*(18), 7318–7323. https://doi.org/10.1073/pnas.1302490110

Shi, L., Sutter, B. M., Ye, X., & Tu, B. P. (2010). Trehalose is a key determinant of the quiescent metabolic state that fuels cell cycle progression upon return to growth. *Molecular biology of the cell*, *21*(12), 1982–1990. https://doi.org/10.1091/mbc.e10-01-0056

Silverman, S. J., Petti, A. A., Slavov, N., Parsons, L., Briehof, R., Thiberge, S. Y., Zenklusen, D., Gandhi, S. J., Larson, D. R., Singer, R. H., & Botstein, D. (2010). Metabolic cycling in single yeast cells from unsynchronized steady-state populations limited on glucose or phosphate. *Proceedings of the National Academy of Sciences of the United States of America*, *107*(15), 6946–6951. https://doi.org/10.1073/pnas.1002422107

Slattery, M. G., Liko, D., & Heideman, W. (2008). Protein kinase A, TOR, and glucose transport control the response to nutrient repletion in Saccharomyces cerevisiae. *Eukaryotic cell*, *7*(2), 358–367. https://doi.org/10.1128/EC.00334-07

Slavov, N., & Botstein, D. (2011). Coupling among growth rate response, metabolic cycle, and cell division cycle in yeast. *Molecular biology of the cell*, *22*(12), 1997–2009. https://doi.org/10.1091/mbc.E11-02-0132

Slavov, N., Macinskas, J., Caudy, A., & Botstein, D. (2011). Metabolic cycling without cell division cycling in respiring yeast. *Proceedings of the National Academy of Sciences of the United States of America*, *108*(47), 19090–19095. https://doi.org/10.1073/pnas.1116998108

Sohn, H. Y., Murray, D. B., & Kuriyama, H. (2000). Ultradian oscillation of Saccharomyces cerevisiae during aerobic continuous culture: hydrogen sulphide mediates population synchrony. *Yeast (Chichester, England)*, *16*(13), 1185–1190. https://doi.org/10.1002/1097-0061(20000930)16:13<1185::AID-YEA619>3.0.CO;2-W

Sohn, H., & Kuriyama, H. (2001). Ultradian metabolic oscillation of Saccharomyces cerevisiae during aerobic continuous culture: hydrogen sulphide, a population synchronizer, is produced by sulphite reductase. *Yeast (Chichester, England)*, *18*(2), 125–135. https://doi.org/10.1002/1097-0061(20010130)18:2<125::AID-YEA655>3.0.CO;2-9

Soranzo, N., Zampieri, M., Farina, L., & Altafini, C. (2009). mRNA stability and the unfolding of gene expression in the long-period yeast metabolic cycle. *BMC systems biology*, *3*, 18. https://doi.org/10.1186/1752-0509-3-18

Steffen, K. K., Kennedy, B. K., & Kaeberlein, M. (2009). Measuring replicative life span in the budding yeast. *Journal of visualized experiments : JoVE*, (28), 1209. https://doi.org/10.3791/1209

Stincardini, C., Pariano, M., D'Onofrio, F., Renga, G., Orecchini, E., Orabona, C., Nunzi, E., Gargaro, M., Fallarino, F., Chun, S. K., Fortin, B. M., Masri, S., Brancorsini, S., Romani, L., Costantini, C., & Bellet, M. M. (2023). The circadian control of tryptophan metabolism regulates the host response to pulmonary fungal infections. *PNAS nexus*, *2*(3), pgad036. https://doi.org/10.1093/pnasnexus/pgad036

Suzuki, T., & Inoki, K. (2011). Spatial regulation of the mTORC1 system in amino acids sensing pathway. *Acta biochimica et biophysica Sinica*, *43*(9), 671–679. https://doi.org/10.1093/abbs/gmr066

Swain, P. S., Elowitz, M. B., & Siggia, E. D. (2002). Intrinsic and extrinsic contributions to stochasticity in gene expression. *Proceedings of the National Academy of Sciences of the United States of America*, *99*(20), 12795–12800. https://doi.org/10.1073/pnas.162041399

Swygert, S. G., Lin, D., Portillo-Ledesma, S., Lin, P. Y., Hunt, D. R., Kao, C. F., Schlick, T., Noble, W. S., & Tsukiyama, T. (2021). Local chromatin fiber folding represses transcription and loop extrusion in quiescent cells. *eLife*, *10*, e72062. https://doi.org/10.7554/eLife.72062

Takhaveev V, Özsezen S, Smith EN, Zylstra A, Chaillet ML, Chen H, Papagiannakis A, Milias-Argeitis A, Heinemann M. Temporal segregation of biosynthetic processes is responsible for metabolic oscillations during the budding yeast cell cycle. Nat Metab. 2023 Feb;5(2):294-313. doi: 10.1038/s42255-023-00741-x. Epub 2023 Feb 27. PMID: 36849832; PMCID: PMC9970877.

Takhaveev, V., & Heinemann, M. (2018). Metabolic heterogeneity in clonal microbial populations. *Current opinion in microbiology*, *45*, 30–38. https://doi.org/10.1016/j.mib.2018.02.004

Takubo, K., Nagamatsu, G., Kobayashi, C. I., Nakamura-Ishizu, A., Kobayashi, H., Ikeda, E., Goda, N., Rahimi, Y., Johnson, R. S., Soga, T., Hirao, A., Suematsu, M., & Suda, T. (2013). Regulation of glycolysis by Pdk functions as a metabolic checkpoint for cell cycle quiescence in hematopoietic stem cells. *Cell stem cell*, *12*(1), 49–61. https://doi.org/10.1016/j.stem.2012.10.011

Tao, R., Zhao, Y., Chu, H., Wang, A., Zhu, J., Chen, X., Zou, Y., Shi, M., Liu, R., Su, N., Du, J., Zhou, H. M., Zhu, L., Qian, X., Liu, H., Loscalzo, J., & Yang, Y. (2017). Genetically encoded fluorescent sensors reveal dynamic regulation of NADPH metabolism. *Nature methods*, *14*(7), 720–728. https://doi.org/10.1038/nmeth.4306

Tate, J. J., & Cooper, T. G. (2003). Tor1/2 regulation of retrograde gene expression in Saccharomyces cerevisiae derives indirectly as a consequence of alterations in ammonia metabolism. *The Journal of biological chemistry*, *278*(38), 36924–36933. https://doi.org/10.1074/jbc.M301829200

Terzi, M. Y., Izmirli, M., & Gogebakan, B. (2016). The cell fate: senescence or quiescence. *Molecular biology reports*, *43*(11), 1213–1220. https://doi.org/10.1007/s11033-016-4065-0

Thattai, M., & van Oudenaarden, A. (2001). Intrinsic noise in gene regulatory networks. *Proceedings of the National Academy of Sciences of the United States of America*, *98*(15), 8614–8619. https://doi.org/10.1073/pnas.151588598

Thevelein J. M. (1992). The RAS-adenylate cyclase pathway and cell cycle control in Saccharomyces cerevisiae. *Antonie van Leeuwenhoek*, *62*(1-2), 109–130. https://doi.org/10.1007/BF00584466

Thorsness P. E. (1992). Structural dynamics of the mitochondrial compartment. *Mutation research*, *275*(3-6), 237–241. https://doi.org/10.1016/0921-8734(92)90027-m

Tolliday, N., Bouquin, N., & Li, R. (2001). Assembly and regulation of the cytokinetic apparatus in budding yeast. *Current opinion in microbiology*, *4*(6), 690–695. https://doi.org/10.1016/s1369-5274(01)00270-3

Traenkle, B., & Rothbauer, U. (2017). Under the Microscope: Single-Domain Antibodies for Live-Cell Imaging and Super-Resolution Microscopy. *Frontiers in immunology*, *8*, 1030. https://doi.org/10.3389/fimmu.2017.01030

Trcek, T., Larson, D. R., Moldón, A., Query, C. C., & Singer, R. H. (2011). Single-molecule mRNA decay measurements reveal promoter- regulated mRNA stability in yeast. *Cell*, *147*(7), 1484–1497. https://doi.org/10.1016/j.cell.2011.11.051

Tu, B. P., Kudlicki, A., Rowicka, M., & McKnight, S. L. (2005). Logic of the yeast metabolic cycle: temporal compartmentalization of cellular processes. *Science (New York, N.Y.)*, *310*(5751), 1152–1158. https://doi.org/10.1126/science.1120499

Tu, B. P., & McKnight, S. L. (2006). Metabolic cycles as an underlying basis of biological oscillations. *Nature reviews. Molecular cell biology*, *7*(9), 696–701. https://doi.org/10.1038/nrm1980

Tu, B. P., & McKnight, S. L. (2007). The yeast metabolic cycle: insights into the life of a eukaryotic cell. *Cold Spring Harbor symposia on quantitative biology*, *72*, 339–343. https://doi.org/10.1101/sqb.2007.72.019

Tu, B. P., & McKnight, S. L. (2009). Evidence of carbon monoxide-mediated phase advancement of the yeast metabolic cycle. *Proceedings of the National Academy of Sciences of the United States of America*, *106*(34), 14293–14296. https://doi.org/10.1073/pnas.0907786106

Tyurin-Kuzmin, P. A., Molchanov, A. Y., Chechekhin, V. I., Ivanova, A. M., & Kulebyakin, K. Y. (2020). Metabolic Regulation of Mammalian Stem Cell Differentiation. *Biochemistry. Biokhimiia*, *85*(3), 264–278. https://doi.org/10.1134/S0006297920030025

Uchida M, Sun Y, McDermott G, Knoechel C, Le Gros MA, Parkinson D, Drubin DG, Larabell CA. Quantitative analysis of yeast internal architecture using soft X-ray tomography. Yeast. 2011 Mar;28(3):227-36. doi: 10.1002/yea.1834. Epub 2010 Dec 22. PMID: 21360734; PMCID: PMC3404734.

Urdiain-Arraiza, J. (2019). *Investigating the conditions and the function of Rps6 and Nth1 phosphorylation using the Yeast Metabolic Cycle.* [Master's thesis]. UCLouvain, [Master's internship]. University of Oxford.

Váchová, L., & Palková, Z. (2005). Physiological regulation of yeast cell death in multicellular colonies is triggered by ammonia. *The Journal of cell biology*, *169*(5), 711–717. https://doi.org/10.1083/jcb.200410064

Valcourt, J. R., Lemons, J. M., Haley, E. M., Kojima, M., Demuren, O. O., & Coller, H. A. (2012). Staying alive: metabolic adaptations to quiescence. *Cell cycle (Georgetown, Tex.)*, *11*(9), 1680–1696. https://doi.org/10.4161/cc.19879

Varahan, S., Walvekar, A., Sinha, V., Krishna, S., & Laxman, S. (2019). Metabolic constraints drive self-organization of specialized cell groups. *eLife*, *8*, e46735. https://doi.org/10.7554/eLife.46735

Vlastaridis, P., Papakyriakou, A., Chaliotis, A., Stratikos, E., Oliver, S. G., & Amoutzias, G. D. (2017). The Pivotal Role of Protein Phosphorylation in the Control of Yeast Central Metabolism. *G3 (Bethesda, Md.)*, *7*(4), 1239–1249. https://doi.org/10.1534/g3.116.037218

Vogel, C., & Marcotte, E. M. (2012). Insights into the regulation of protein abundance from proteomic and transcriptomic analyses. *Nature reviews. Genetics*, *13*(4), 227–232. https://doi.org/10.1038/nrg3185

von Meyenburg K. (1969). Control of respiration and aerobic fermentation in Saccharomyces cerevisiae. *Antonie van Leeuwenhoek*, *35*, G19–G20.

Waite, K. A., De-La Mota-Peynado, A., Vontz, G., & Roelofs, J. (2016). Starvation Induces Proteasome Autophagy with Different Pathways for Core and Regulatory Particles. *The Journal of biological chemistry*, *291*(7), 3239–3253. https://doi.org/10.1074/jbc.M115.699124

Walvekar, A., Rashida, Z., Maddali, H., & Laxman, S. (2018). A versatile LC-MS/MS approach for comprehensive, quantitative analysis of central metabolic pathways. *Wellcome open research*, *3*, 122. https://doi.org/10.12688/wellcomeopenres.14832.1

Wang, B., Kettenbach, A. N., Zhou, X., Loros, J. J., & Dunlap, J. C. (2019). The Phospho-Code Determining Circadian Feedback Loop Closure and Output in Neurospora. *Molecular cell*, *74*(4), 771–784.e3. https://doi.org/10.1016/j.molcel.2019.03.003

Wang, M., Ogé, L., Perez-Garcia, M. D., Hamama, L., & Sakr, S. (2018). The PUF Protein Family: Overview on PUF RNA Targets, Biological Functions, and Post

Transcriptional Regulation. *International journal of molecular sciences*, *19*(2), 410. https://doi.org/10.3390/ijms19020410

Wang, X., Wang, W., Li, L., Perry, G., Lee, H. G., & Zhu, X. (2014). Oxidative stress and mitochondrial dysfunction in Alzheimer's disease. *Biochimica et biophysica acta*, *1842*(8), 1240–1247. https://doi.org/10.1016/j.bbadis.2013.10.015

Warner J. R. (1999). The economics of ribosome biosynthesis in yeast. *Trends in biochemical sciences*, *24*(11), 437–440. https://doi.org/10.1016/s0968-0004(99)01460-7

Warner J. R. (2001). Nascent ribosomes. *Cell*, *107*(2), 133–136. https://doi.org/10.1016/s0092-8674(01)00531-1

Wells WA. Metabolism as a production line. J Cell Biol. 2004 May 24;165(4):457. doi: 10.1083/jcb1654rr4. PMCID: PMC2249970.

Welsh, D. K., Logothetis, D. E., Meister, M., & Reppert, S. M. (1995). Individual neurons dissociated from rat suprachiasmatic nucleus express independently phased circadian firing rhythms. *Neuron*, *14*(4), 697–706. https://doi.org/10.1016/0896-6273(95)90214-7

Werner-Washburne, M., Braun, E., Johnston, G. C., & Singer, R. A. (1993). Stationary phase in the yeast Saccharomyces cerevisiae. *Microbiological reviews*, *57*(2), 383–401. https://doi.org/10.1128/mr.57.2.383-401.1993

Werner-Washburne, M., Roy, S., & Davidson, G. S. (2012). Aging and the survival of quiescent and non-quiescent cells in yeast stationary-phase cultures. *Sub-cellular biochemistry*, *57*, 123–143. https://doi.org/10.1007/978-94-007-2561-4_6

WHO Antimicrobial Resistance in the European Union and the World. 2012. [(accessed on 15 June 2022)]. Available online: https://www.who.int/director-general/speeches/detail/antimicrobial-resistance-in-the-european-union-and-the-world

WILLIAMSON, D. K., AND D. J. FENNELL. 1975. The use of fluorescent DNA-binding agent for detecting and separating yeast mitochondrial DNA, p. 335-354. Zn D. M. Prescott [ed.], Methods in cell biology, v. 12. Academic

Winter, D., Podtelejnikov, A. V., Mann, M., & Li, R. (1997). The complex containing actin-related proteins Arp2 and Arp3 is required for the motility and integrity of yeast actin patches. *Current biology : CB*, *7*(7), 519–529. https://doi.org/10.1016/s0960-9822(06)00223-5

Wolf, J., Sohn, H., Heinrich, R., & Kuriyama, H. (2001). Mathematical analysis of a mechanism for autonomous metabolic oscillations in continuous culture of Saccharomyces cerevisiae. *FEBS letters*, *499*(3), 230–234. https://doi.org/10.1016/s0014-5793(01)02562-5

Wouters, M. (2017). *Investigating the influence of H3K4methylation on mRNA noise.* [Master's thesis]. UCLouvain, [Master's internship]. University of Oxford.

Wu, Q., Yang, Z., Nie, Y., Shi, Y., & Fan, D. (2014). Multi-drug resistance in cancer chemotherapeutics: mechanisms and lab approaches. *Cancer letters*, *347*(2), 159–166. https://doi.org/10.1016/j.canlet.2014.03.013

Wullschleger, S., Loewith, R., & Hall, M. N. (2006). TOR signaling in growth and metabolism. *Cell*, *124*(3), 471–484. https://doi.org/10.1016/j.cell.2006.01.016

Wyart, M., Botstein, D., & Wingreen, N. S. (2010). Evaluating gene expression dynamics using pairwise RNA FISH data. *PLoS computational biology*, *6*(11), e1000979. https://doi.org/10.1371/journal.pcbi.1000979

Xi, S. (2019). *Multiomic Investigation on the Relationship between Metabolism and Gene Expression*. [PhD thesis]. University of Oxford.

Yaffe M. P. (1999). Dynamic mitochondria. *Nature cell biology*, *1*(6), E149–E150. https://doi.org/10.1038/14101

Yang, Y., Lindsey-Boltz, L. A., Vaughn, C. M., Selby, C. P., Cao, X., Liu, Z., Hsu, D. S., & Sancar, A. (2021). Circadian clock, carcinogenesis, chronochemotherapy connections. *The Journal of biological chemistry*, *297*(3), 101068. https://doi.org/10.1016/j.jbc.2021.101068

Ye, L., Berden, J. A., van Dam, K., & Kruckeberg, A. L. (2001). Expression and activity of the Hxt7 high-affinity hexose transporter of Saccharomyces cerevisiae. *Yeast (Chichester, England)*, *18*(13), 1257–1267. https://doi.org/10.1002/yea.771

Yerlikaya, S., Meusburger, M., Kumari, R., Huber, A., Anrather, D., Costanzo, M., Boone, C., Ammerer, G., Baranov, P. V., & Loewith, R. (2016). TORC1 and TORC2 work together to regulate ribosomal protein S6 phosphorylation in Saccharomyces cerevisiae. *Molecular biology of the cell*, *27*(2), 397–409. https://doi.org/10.1091/mbc.E15-08-0594

Youk, H., & van Oudenaarden, A. (2009). Growth landscape formed by perception and import of glucose in yeast. *Nature*, *462*(7275), 875–879. https://doi.org/10.1038/nature08653

Young, E. T., Zhang, C., Shokat, K. M., Parua, P. K., & Braun, K. A. (2012). The AMP-activated protein kinase Snf1 regulates transcription factor binding, RNA polymerase II activity, and mRNA stability of glucose-repressed genes in Saccharomyces cerevisiae. *The Journal of biological chemistry*, *287*(34), 29021–29034. https://doi.org/10.1074/jbc.M112.380147

Young, M. J., Theriault, S. S., Li, M., & Court, D. A. (2006). The carboxyl-terminal extension on fungal mitochondrial DNA polymerases: identification of a critical region of the enzyme from Saccharomyces cerevisiae. *Yeast (Chichester, England)*, *23*(2), 101–116. https://doi.org/10.1002/yea.1344

Zampar, G. G., Kümmel, A., Ewald, J., Jol, S., Niebel, B., Picotti, P., Aebersold, R., Sauer, U., Zamboni, N., & Heinemann, M. (2013). Temporal system-level organization of the switch from glycolytic to gluconeogenic operation in yeast. *Molecular systems biology*, *9*, 651. https://doi.org/10.1038/msb.2013.11

Zenklusen, D., & Singer, R. H. (2010). Analyzing mRNA expression using single mRNA resolution fluorescent in situ hybridization. *Methods in enzymology*, *470*, 641–659. https://doi.org/10.1016/S0076-6879(10)70026-4

Zenklusen, D., Larson, D. R., & Singer, R. H. (2008). Single-RNA counting reveals alternative modes of gene expression in yeast. *Nature structural & molecular biology*, *15*(12), 1263–1271. https://doi.org/10.1038/nsmb.1514